NASA CR-178,060

NASA Contractor Report 178060

NASA-CR-178060
19860020405

Near-Field Testing of the 15-Meter Model of the Hoop Column Antenna

Volume II— Near- and Far-Field Plots for the LaRC Feeds Final Report

Martin Marietta Denver Aerospace
Denver, CO 80201

Contract NAS1-18016
March 1986

National Aeronautics and
Space Administration

Langley Research Center
Hampton, Virginia 23665

MCR-85-640
Contract No. NAS1-18016

Volume II

Final
Report

March 1986

Near- and Far-Field Plots
for the LaRC Feeds

NEAR-FIELD TESTING OF THE 15-METER MODEL OF THE HOOP COLUMN ANTENNA

To

NASA Langley Research Center
Antenna and Microwave Research Branch

Authors:

John Hoover
Neill Kefauver
Tom Cencich

Jim Osborn
Program Manager and Author

Joe Osmanski
Manager
Environmental & Test Technologies

MARTIN MARIETTA
DENVER AEROSPACE
P.O. Box 179
Denver, Colorado 80201

FOREWORD

This report, prepared by Margin Marietta Denver Aerospace, is submitted to the NASA Langley Research Center Antenna and Microwave Research Branch, in response to Contract NAS1-18016, Near-Field Testing of the 15-Meter Model of the Hoop Column Antenna, CDRL Line Item I.D. Our report consists of three volumes:

Volume I Technical Report

Volume II Near- and Far-Field Plots for the LaRC Feeds

Volume III Near- and Far-Field Plots for the JPL Feed

CONTENTS

		Page
	GLOSSARY	v
1.0	INTRODUCTION	1
2.0	TEST PLAN	3
3.0	ANTENNA DEPLOYMENT IN THE NEAR-FIELD LAB	7
4.0	NEAR- AND FAR-FIELD PATTERN PLOTS	15
4.1	Tests 1, 2 and 3 (7.73 GHz)	18
4.2	Test 4 (11.60 GHz)	20
4.3	Tests 5, 6, and 7 (2.27 GHz)	20
4.4	Tests 12-17 (4.26 GHz)	21
4.5	Tests 18-26 (Abbreviated Scans)	22
5.0	ANTENNA GAIN/BEAMWIDTH	273
6.0	SUMMARY AND CONCLUSIONS	275

Figure

1	Test Positions of Feeds	4
1a	Test Positions for 7.73- and 4.26-GHz Feeds	4
1b	Test Positions for 2.27-GHz Feed	4
2	HCA During Deployment	8
3	HCA Free Standing Ready for Test	9
4	LaRC 7.73-GHz Feed	11
5	LaRC 11.60-GHz Feed	11
6	LaRC 2.27-GHz Feed	12
7	LaRC 4.26-GHz Feed	13
8	Far-Field Coordinate System	16
9-19	Test 1 Pattern Plots	25-36
20-24	Test 2 Pattern Plots	37-41
25-35	Test 3 Pattern Plots	42-54
36-46	Test 4 Pattern Plots	55-66
47-57	Test 5 Pattern Plots	67-78
58-62	Test 6 Pattern Plots	79-83
63-73	Test 7 Pattern Plots	84-96
74-84	Test 12 Pattern Plots	97-108
85-95	Test 13 Pattern Plots	109-120
96-106	Test 14 Pattern Plots	121-132
107-117	Test 15 Pattern Plots	133-144
118-128	Test 16 Pattern Plots	145-156
129-139	Test 17 Pattern Plots	157-168

		Page
140-150	Test 18 Pattern Plots	169-180
151-161	Test 19 Pattern Plots	181-192
162-171	Test 20 Pattern Plots	193-204
172-181	Test 21 Pattern Plots	205-216
182-191	Test 22 Pattern Plots	217-228
192-202	Test 23 Pattern Plots	229-239
203-212	Test 24 Pattern Plots	240-250
213-223	Test 25 Pattern Plots	251-262
224-232	Test 26 Pattern Plots	263-271

Table		
2-1	LaRC Test Plan	3
4-1	Plotting Formats	17
4-1(a)	Co-Polarized Plotting Formats	17
4-1(b)	Cross-Polarized Plotting Formats	17
5-1	Antenna Gain and Maximum First Sidelobe Level for Each Test	274
5-2	Antenna Gain and Beamwidth for Each Test Frequency	274

GLOSSARY

HCA	Hoop Column Antenna
JPL	Jet Propulsion Laboratory
LaRC	NASA Langley Research Center
NFTL	Near-Field Test Laboratory

1.0 INTRODUCTION

This report is Volume II in a three-volume final report for Contract NAS1-18016 between NASA Langley Research Center and Martin Marietta Denver Aerospace. The contract, "Near-Field Testing of the 15-Meter Model of the Hoop Column Antenna," calls for a series of tests on this antenna based on a predetermined test plan. The contract had two objectives: to demonstrate that high-performance space-deployable antennas can be built, and to demonstrate that antenna performance can be accurately measured. Data contained in the report show that these objectives have been achieved.

Because the program generated extensive data, the reporting has been divided into three volumes. During the tests, NASA Langley Research Center (LaRC) and the Jet Propulsion Laboratory (JPL) supplied feed systems for the antenna, the basis for dividing the report. Volume I, a technical summary, contains information essential to the two program objectives; Volume II contains a complete set of graphical data using the LaRC feeds; Volume III contains corresponding data using the JPL feed.

Many types of tests were performed on the antenna in the Near-Field Test Laboratory (NFTL), including optical/electrical measurements of reflector surface trueness, mechanical measurements of structural stability, and electrical measurements of antenna performance. This volume includes the electrical tests using the LaRC feeds. In the test plan, the far-field antenna radiation patterns and gain (based on near-field measurements) were determined at four frequencies (2.27, 4.26, 7.73, and 11.6 GHz), a separate feed system used for each frequency. All feeds are linearly polarized, and both co-polarized and cross-polarized measurements were made.

This report follows the test plan chronologically. The data analysis emphasizes the changes in antenna performance caused by frequency. The analysis shows conclusively that the factors most affecting antenna performance are reflector surface trueness and aperture illumination; i.e., feed design and surface control are the factors most critical to electrical performance for this antenna.

This Page Intentionally Left Blank

2.0 TEST PLAN

Table 2-1 lists the near-field tests performed on the Hoop Column Antenna (HCA). The list contains a total of 22 tests. For the near- and far-field pattern plots contained in this report, the beginning page number of the set of plots corresponding to each test is listed adjacent to the test number in Table 2-1. This table serves as the index for locating the plots for each test and will be referenced repeatedly. For the LaRC series there are four test frequencies and four separate feed systems. Each frequency required the installation of a separate feed system in the antenna. The 7.73- and 11.60-GHz tests used conical feed horns; at 4.26 and 2.27 GHz the feeds were patch subarrays installed in a panel capable of supporting an array of up to 11 subarrays. "Feed Position" in Table 2-1 identifies the position of the feed for beam-steering purposes. Actual position of the feed on the mount is shown in Figure 1 (A and B). "Far-Field Polarization" in Table 2-1 depends on the test antenna geometry. The final column lists the number of far-field beamwidths scanned for each test.

Table 2-1 LaRC Test Plan

Test	Page No.	Freq, GHz	Feed Pos.	Far-Field Polarization	Illum Quad.	Beamscan, Beamwidths
1	25-36	7.73	1	Co	4	0
2	37-41	7.73	1	Cross	4	0
3	42-54	7.73	11	Co	4	6
4	55-66	11.60	1	Co	4	0
5	67-78	2.27	1	Co	4	0
6	79-83	2.27	1	Cross	4	0
7	84-96	2.27	2	Co	2	1
12	97-108	4.26	1	Co	4	0
13	109-120	4.26	8	Co	2	2
14	121-132	4.26	11	Co	4	6
15	133-144	4.26	1	Co	2	0
16	145-156	4.26	2	Co	2	1
17	157-168	4.26	3	Co	2	-1
18	169-180	7.73	1	Co	4	0
19*	181-192	7.73	1	Co	4	0
20*	193-204	7.73	1	Co	2	0
21*	205-216	7.73	1	Co	3	0
22*	217-228	7.73	1	Co	1	0
23*	229-239	7.73	1	Cross	4	0
24*	240-250	7.73	1	Co	4	0
25*	251-262	11.60	1	Co	4	0
26*	263-271	11.60	1	Cross	4	0

*Abbreviated Scans after Final 33 Cord Adjustment

(A) TEST POSITIONS FOR 7.73- & 4.26-GHZ FEEDS

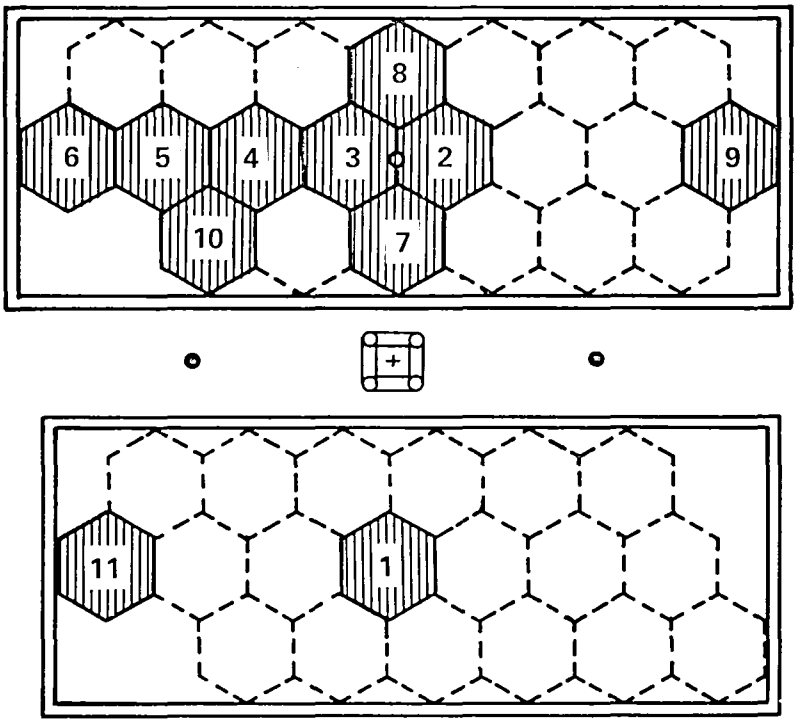

(B) TEST POSITIONS FOR 2.27-GHZ FEED

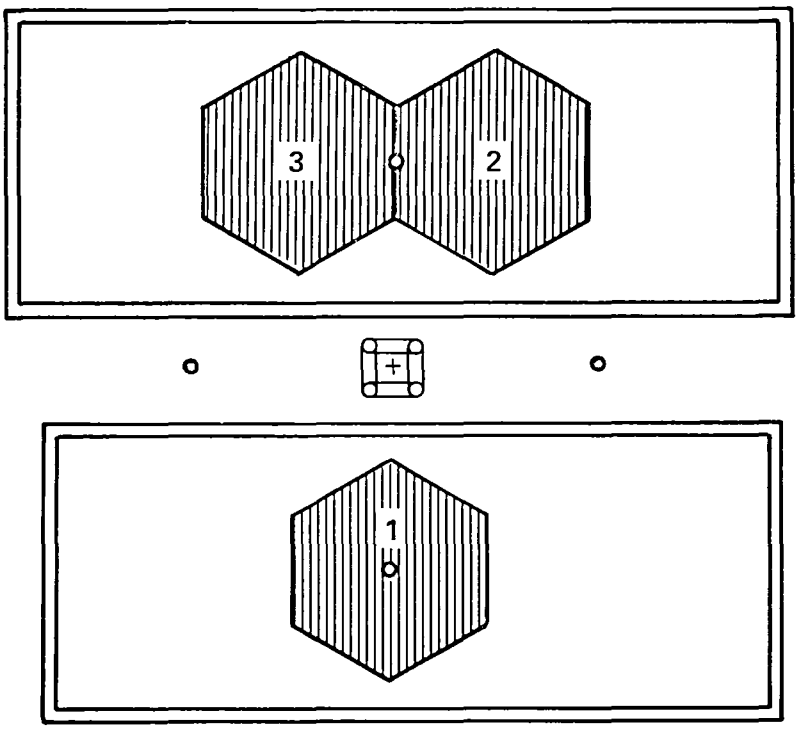

Figure 1 Test Positions of Feeds

The tests began at 7.73 GHz, predicted to be the maximum frequency for which high performance could reasonably be expected from the antenna. The next frequency (11.6 GHz) was expected to show far-field pattern deterioration as the frequency increased beyond 7.73 GHz. The lower frequencies, tested last, were selected in order of operational usefulness.

The test program used two scan modes, referred to as (1) quadrant scan and (2) abbreviated scan. In the quadrant mode (not to be confused with the quad apertures in the antenna) the scan plane was divided into four equal parts that were later combined in the processing with an algorithm named "reformat." The quadrant mode included all four antenna apertures in the near-field scan. Certain tests (refer to Table 2-1) used an abbreviated scan mode to reduce scan time. This mode included only the active quadrant of the antenna in the near-field scan. Using the abbreviated scan mode reduced the maximum valid far-field spatial angles and excluded from the patterns radiation from the other three quadrants. Abbreviated scans were used when far-field pattern information was desired over small angles that typically included the main beam and first few sidelobes.

This Page Intentionally Left Blank

3.0 ANTENNA DEPLOYMENT IN THE NEAR-FIELD LAB

The antenna has been named "Hoop Column" after its dominant structural members; a central column supporting a coaxial ring (or hoop). Both the column and the hoop are furlable, so the antenna can be stowed in a minimal configuration. In the deployed configuration, quartz cords, attached to the column at the top of the telescoping section, support the hoop. The reflecting surface (gold-plated molybdenum wire mesh) is controlled by fabric ribbing and a graphite cord system.

It is important to realize that the reflector is a quad aperture design, not a single paraboloid. This design contours the reflector to form four parabolic sections with four focal points offset from the axis of the column. The purpose of the quad aperture configuration is to generate four interleaving beams for use in multiple beam applications. In the reflector's full operational configuration, each focal point has multiple switched feeds, generating many beams, possibly over 100. The use of multiple feeds on one aperture requires beam steering, which creates the inherent problem of coma lobing when the feed is displaced on a parabolic reflector. To reduce the effects of coma lobing, a large f/d of active aperture (approximately 1.2) was used.

Figures 2 and 3 show the HCA antenna in the two most significant stages of deployment in the near-field lab. Figure 2 shows the antenna deployed with the deployment fixture in place; in Figure 3 it is free-standing, ready for near-field measurements. LaRC provided the conical feeds shown in Figures 4 and 5. Figures 6 and 7 show the patch subarrays.

Figure 2 HCA During Deployment

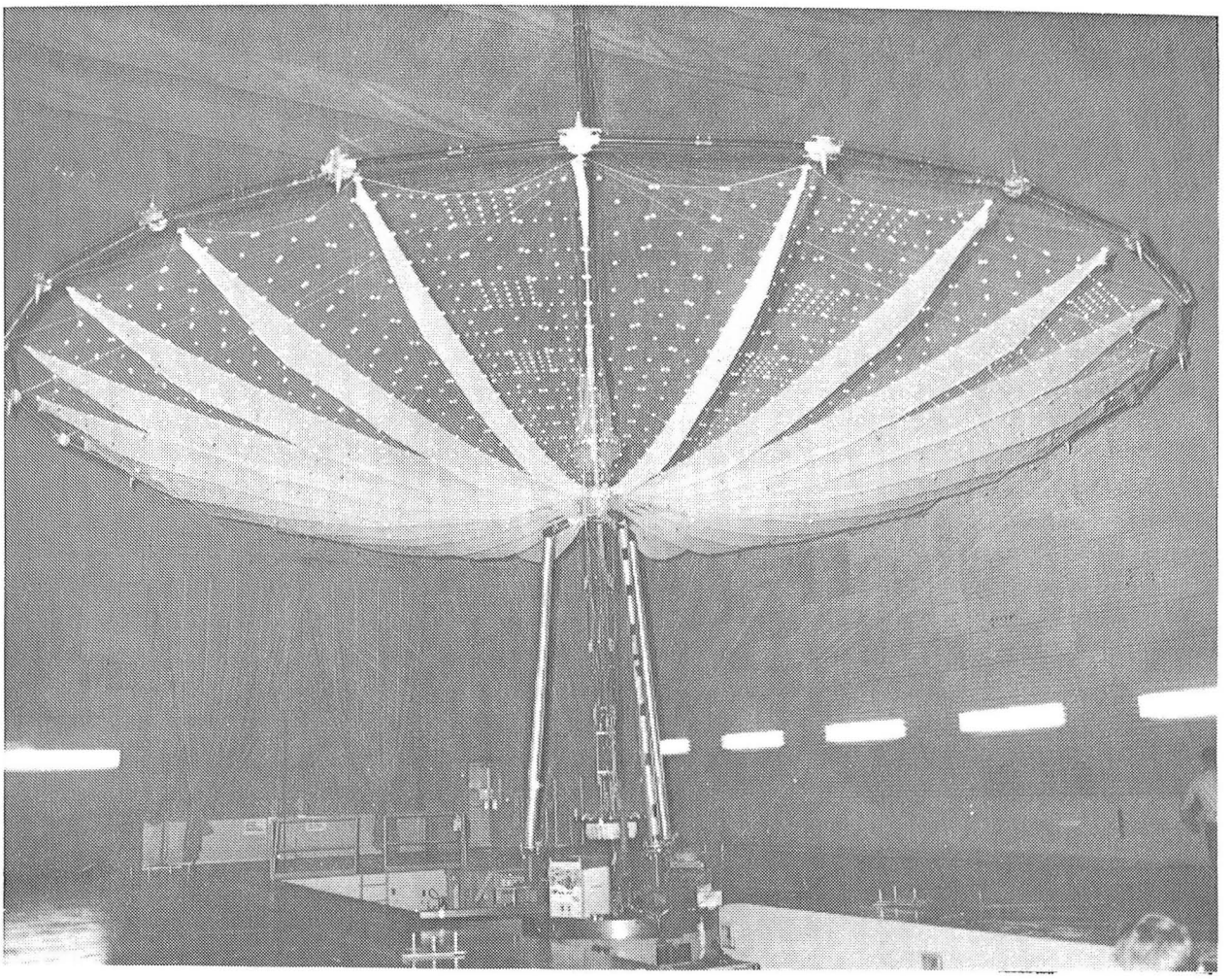

Figure 3 HCA Free Standing Ready for Test

This Page Intentionally Left Blank

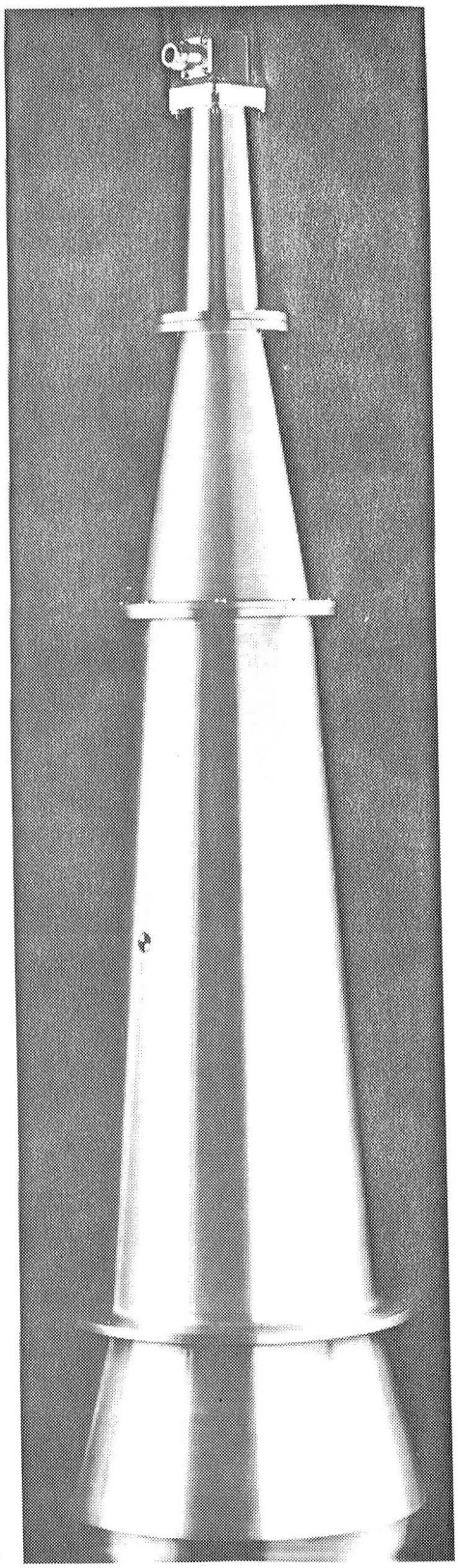

Figure 4 LaRC 7.73-GHz Feed

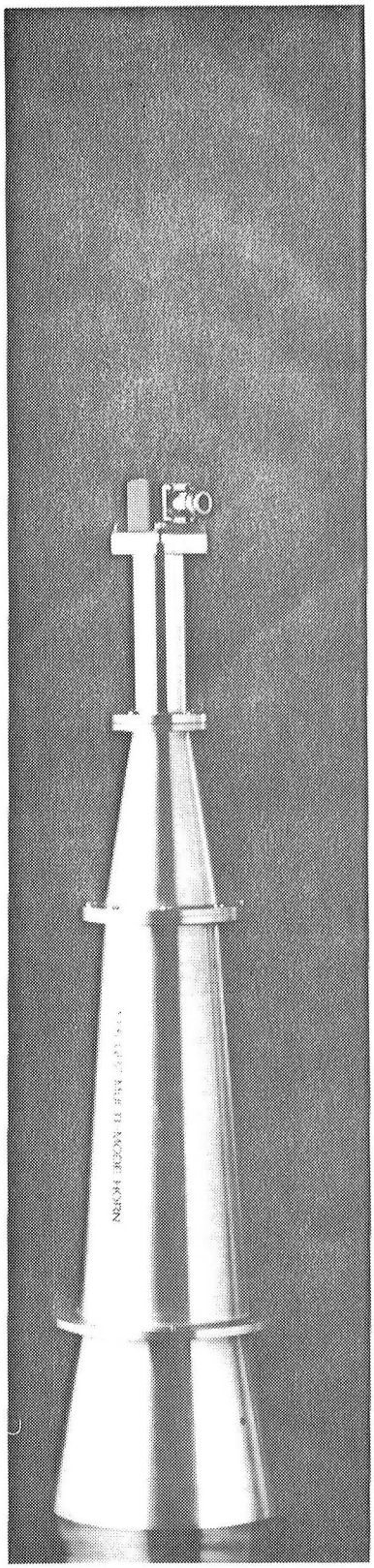

Figure 5 LaRC 11.60-GHz Feed

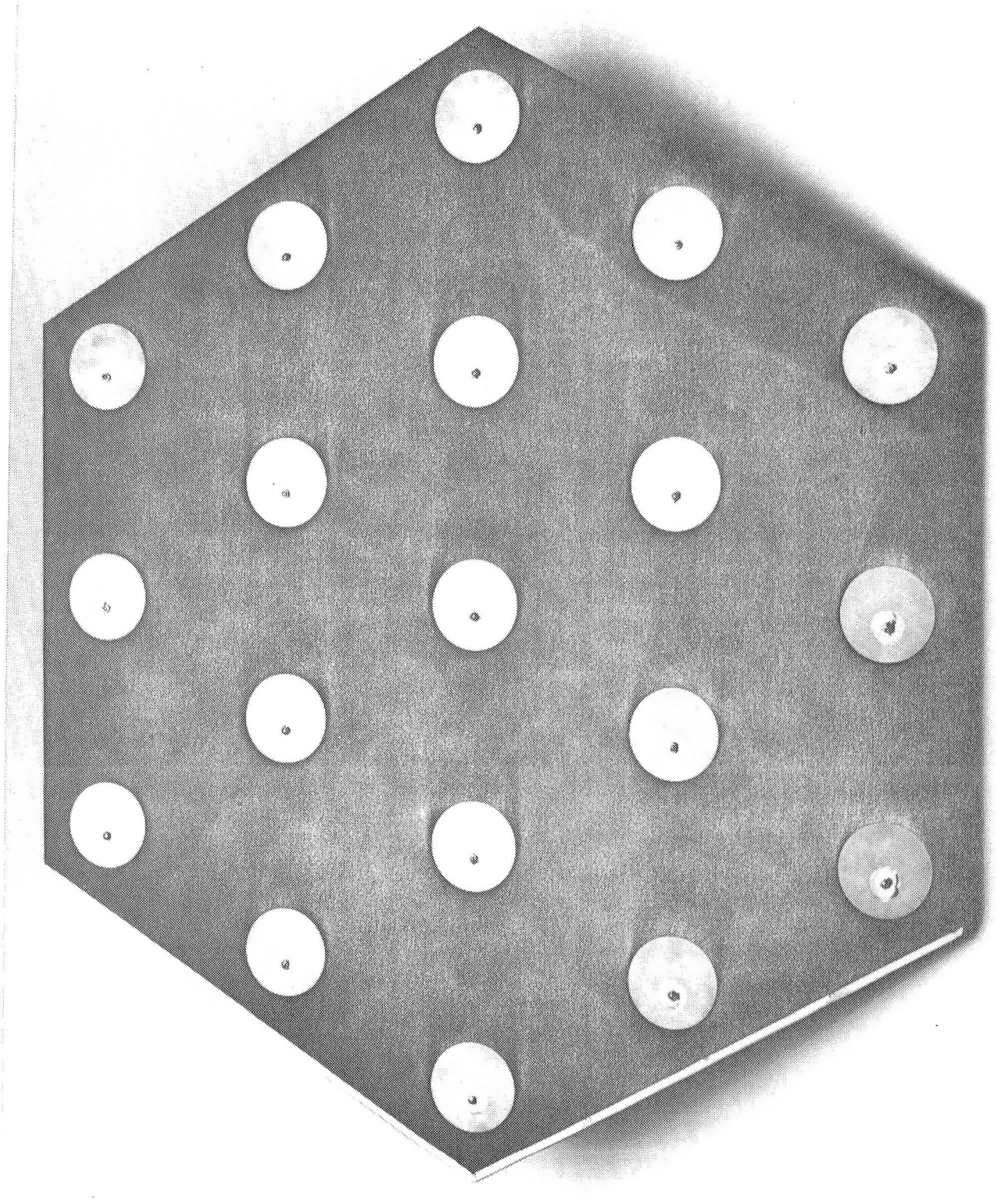

Figure 6 LaRC 2.27-GHz Feed

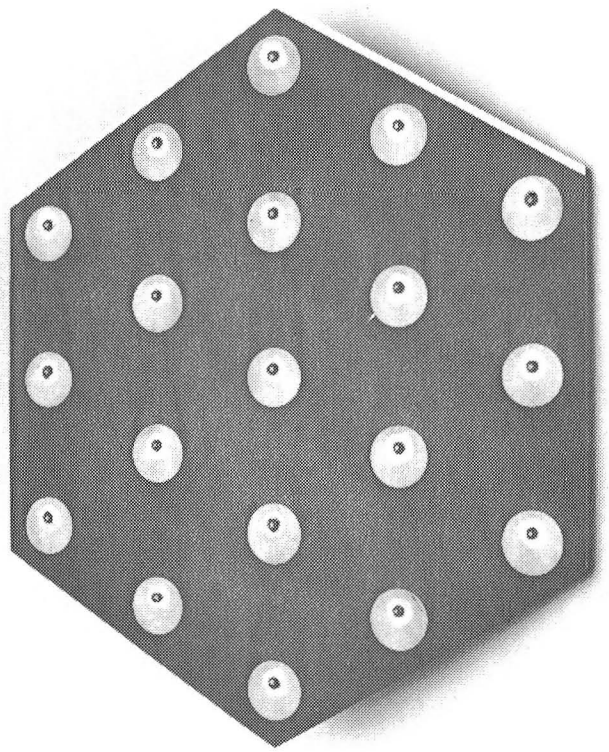

Figure 7 LaRC 4.26-GHz Feed

This Page Intentionally Left Blank

4.0 NEAR- AND FAR-FIELD PATTERN PLOTS

Both the near- and far-field plots in this report are organized in sequence with the test plan. Each test includes a set of plots, using a similar organization where possible, so that comparisons can be made on a test-to-test basis. The near-field plots used exclusively two-dimensional plots through the center of the active aperture. The far-field plots used three formats: 2-dimensional, contour, and 3-dimensional. All plots selected show the most relevant aspects of antenna performance, emphasizing parameters such as beam pointing angle, beamwidth, sidelobe level, level of cross-polarization, and distortion versus beam steering.

Table 4-1 shows the organization used for sets of plots. In Table 4-1(a) type designations 1-7 identify the co-polarized far-field plots; designations 9-11 identify near-field plots. In Table 4-1(b), designations 12-16 identify the far-field cross-polarized plots. The numbers designated are used on each plot in this report to minimize title length. The plots are labeled by test number, test frequency, plot type, and polarization.

Figure 8 shows the geometry used to plot the far-field data. There is a direct trigonometric relationship between the plane wave spectrum generated by the data processing and the azimuth elevation coordinate system. The antenna is aligned with the center radial of the illuminated aperture parallel to the negative x axis in Figure 8. To align antenna polarization relative to the scanner, the feed was first centered on the column using the remote feed positioning system. Next the feed was aligned with an optical target in the center of the active quadrant. Finally, the antenna was aligned co-polarized with the probes. This was done by making theodolite sightings through the vertical plane containing the four scanner probes, Hoop Point 19, and the cord along this joint.

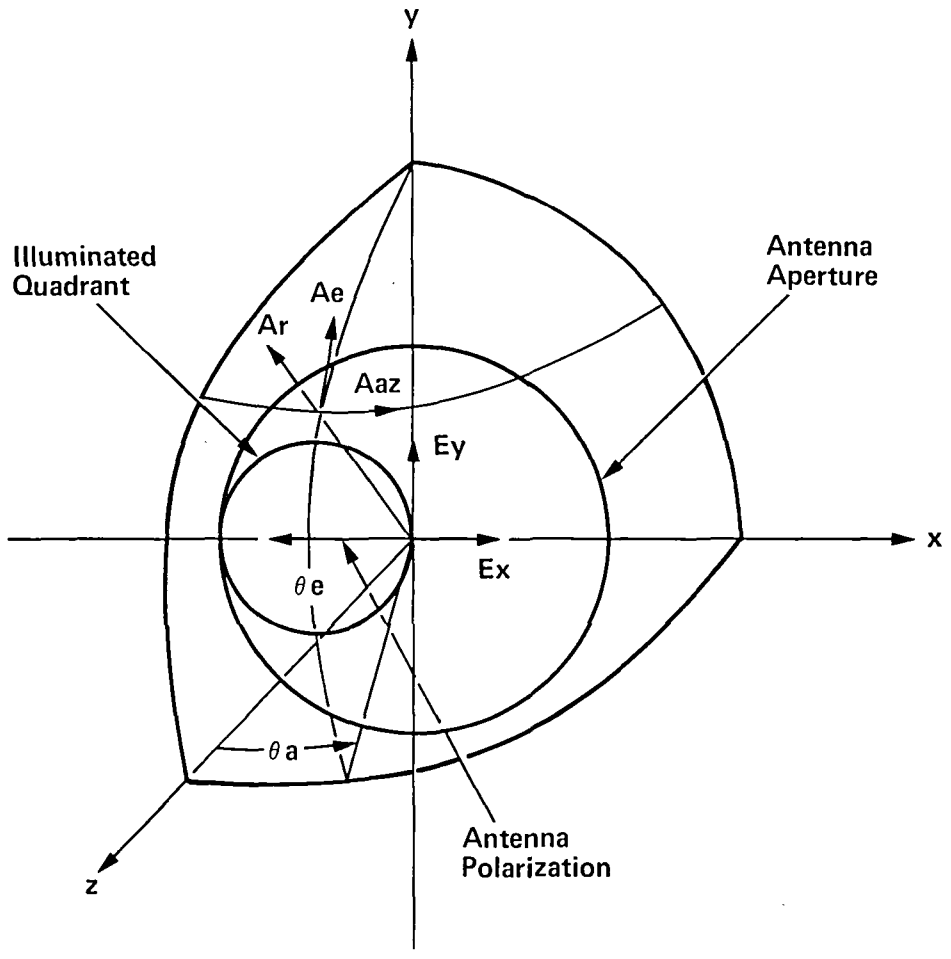

Figure 8 Far-Field Coordinate System

Table 4-1 Plotting Formats

(a) Co-Polarized Plotting Formats

Type	Far-Field Plot	Dynamic Range, dB	Far-Field Angle,°
1	E-Plane	-80 to 0	-30 to 30
2	H-Plane	-80 to 0	-30 to 30
3	E-Plane	-60 to 0	-10 to 10
4	H-Plane	-60 to 0	-10 to 10
5	Contour	-40,-30,-20,-10	-6 to 6
6	Contour	-30,-20,-10,-3	-3 to 3
7	Three Dimensional Plot	-40 to 0	-5 to 5
	Near-Field Plot	Dynamic Range, dB	Length of Plot
8	H-Plane	-80 to 0	Entire Aperture
9	E-Plane	-80 to 0	Entire Aperture
10	H-Plane	-80 to 0	Active Quadrant
11	E-Plane	-80 to 0	Active Quadrant

(b) Cross-Polarized Plotting Formats

Type	Far-Field Plot	Dynamic Range, dB	Far-Field Angle, °
12	E-Plane Overlay with Co-Pol	-80 to 0	-30 to 30
13	H-Plane Overlay with Co-Pol	-80 to 0	-30 to 30
14	E-Plane	-80 to 0	-30 to 30
15	H-Plane	-80 to 0	-30 to 30
16	Contour	-50,-40,-30	Determined by Sidelobe Structure

For all pattern plots, the far-field components and angles were referenced to the coordinate system shown in Figure 8. This figure identifies the near-field components by two vectors, E_x and E_y. After transformation into the far-field, the components are identified as A_{az} and A_{el} on a sphere defined by an azimuth and elevation coordinate system. A plane of constant elevation angle (E) will be parallel to this radial in the near-field. A plane of constant azimuth angle (A) will be parallel to the principal chord of the quadrant, which is parallel to the y axis of Figure 8, but offset from the center of rotation. Future references to a position in azimuth elevation coordinates will be written "(A,E)". Boresight for the antenna is "(0,0)". Principal planes will be plotted through the main beam of the antenna when it is steered off boresight. In the far-field pattern plots that follow, the E-plane and H-plane correspond to azimuth and elevation, respectively.

Immediately after antenna deployment, the reflector surface was fine adjusted by making small length changes in the control cords located on the back of the reflector. The adjustments were based on metric camera measurements taken before the antenna arrived at the NFTL. Following this adjustment, metric photos were taken to measure surface trueness. After the 7.73-GHz feed was installed and aligned using near-field focusing techniques, Test 1 began. Single near-field scans through the center of the aperture and near-field phase maps discussed in Volume I determined that the surface needed further adjustment. A cord had been improperly adjusted in the above sequence. Concurrently, results from the metric camera measurements reached the same conclusion. With information from the metric camera analysis the surface was again adjusted. The lengths of a total of 10 cords were changed. After this adjustment (referred to as the 10-cord adjustment) near-field scans showed the surface was acceptable for testing. Therefore, this was the final adjustment for Tests 1 through 18. Feed changes and alignments were made during the tests, but no surface adjustments were made. After Test 18 a final adjustment was made, and the surface was again photographed. The objective of this final adjustment was to refine the surface to its best possible state for this antenna. The test data supporting this improvement are shown below.

4.1 TESTS 1, 2, AND 3 (7.73 GHz)

The tests for 7.73 GHz (1, 2, and 3) were given first priority, because 7.73 GHz was the predicted upper frequency limit of high performance from the antenna. Figures 9-35 show the data obtained from these tests. Above this frequency, transmission through the mesh and surface tolerance of the mesh were expected to degrade antenna performance. For Tests 1-3, the entire antenna was scanned using the NFTL quadrant scan mode. The Test Plan in Table 2-1 shows that the tests, in sequence, measured the co-polarized, cross-polarized, and scanned co-polarized field components. The 7.73-GHz test analysis began with examination of the far-field performance of the HCA.

Figures 9-12 show that the co-pol far-field was plotted for the two principal planes. The first two sidelobes appeared slightly more than 20 dB below the peak of the main beam. (All dB references are to the main beam peak.) However, closer observation showed that the first sidelobe maximum did not occur in the principal planes but on a plane defined by both azimuth and elevation angles equal to 45° (referred to as a diagonal plane). On the diagonal, the first sidelobe level was -15.8 dB, and all other sidelobes were lower.

Only three major sidelobes were caused by sources other than surface errors. These sidelobes were located at approximately (2.5,2.5), (2.5,-2.5) and (5,0) (Fig. 13). These sidelobes were caused by illuminating the two adjacent and back apertures.

The surface errors caused the remaining sidelobe envelope above -40 dB. These errors were of two types: hardpoint mispositioning and surface pillowing. Hardpoint mispositioning is the hardpoint position's departure from the true paraboloid. This error was improved considerably as demonstrated in Test 19. The sidelobes caused by pillowing form a ring approximately 4.6° off boresight. This ring comes from a surface ripple across the aperture of 19 in./cycle, the approximate spacing of the mesh tie points. All the energy outside of 6° from boresight was caused by the amplitude taper of the aperture and by diffractions from the antenna. These effects were at extremely low levels, showing that illumination of the hoop, mast, and control cords caused minimal pattern degradation.

However, the cross-pol has different factors limiting accurate performance measurement, especially near boresight. A cross-pol is defined on boresight as the maximum axial ratio. The two components of the field at boresight should be 90° out-of-phase and at widely different levels for a linearly polarized antenna, the cross-pol actually corresponding to the circularly polarized component of the antenna. Rapid measurement in real time can determine the cross-pol for far-field ranges, but a near-field range must use one of two methods. The simpler method used by the NFTL for the initial tests was to align the antenna according to its physical geometry. The more accurate measurement method is a full compensation of the plane wave spectrum according to the far-field component rotation at boresight, optimizing the antenna axial ratio. Test 2 used the first method, and it was assumed to have sufficient accuracy to measure the cross-pol envelope.

Figure 24, a contour plot of the far-field level of the cross-pol, shows the dominant features of the cross-pol near boresight. Because the feed was a horn, the antenna should have had a well-defined null near boresight with the lobes on either side in balance. The pattern in Figure 24 shows a possible polarization misalignment which could change the cross-pol response slightly. Because each new feed will have a different polarization, and because the errors induced in using the geometric cross-pol of the antenna are very minor, the initial alignment of the antenna was maintained until Test 23.

To steer the antenna in Test 3, the feed was displaced on the feed mount 17.5 in. in the H-plane and tilted 8.6° in the E-plane to point the feed boresight to the center of the illuminated aperture. This steered the beam 2.6°, or approximately 6 beamwidths. The pattern showed no significant degradation such as coma lobing; the surface and aperture sidelobe structure steer with the main beam, generating no new sidelobes and preserving the pattern seen on boresight. The steering better defined the main beam because the first sidelobes were now cleanly separated from the main beam. The gain of the antenna improved slightly, possibly due to this improvement in the main beam structure.

The initial 7.73-GHz test sequence defined several of the controlling parameters on the antenna performance. The measurements showed that the antenna performance was limited by the surface accuracy at this frequency. The only observed limits to measurement accuracy during these tests were the system long-term phase stability, which could be processed out of the data; and the constant antenna oscillations, which introduced a far-field measurement floor of -65 dB.

4.2 TEST 4 (11.60 GHz)

Test 4 attempted to establish the upper frequency limit for the HCA. Figures 36-46 show data from this test. The trueness of the mesh surface reduced the antenna performance at 11.60 GHz much more than at 7.73 GHz. While the highest sidelobe caused by surface errors at 7.73 GHz was below -15 dB, at 11.60 GHz this sidelobe had risen to -12 dB. Figure 40 shows that the sidelobes more than 4.5° off boresight have all decreased and that those inside this ring have increased. The pillowing lobes, which are a very predictable structure, have scaled by frequency both in position and magnitude. The peak of these pillowing lobes is -24 dB at 3.0° off boresight, as shown in Figure 39.

The sidelobes generated by the unused apertures decrease in amplitude but do not change position. The amplitude reduction is caused by the 3.5-dB increase in the main aperture gain, which increase, because of amplitude taper, did not occur to the sidelobes generated by the other apertures. This effect suggests that increasing the aperture size may help decrease the sidelobes related to the other apertures.

4.3 TESTS 5, 6, AND 7 (2.27 GHz)

The feed used for the 2.27-GHz tests was an array of off-center feed circular microstrip patches. The off-center feed in the patch was used to excite linear polarization. It was important that this feed design had good impedance matches to reduce reflections inside the feed. The test data are compiled in Figures 47-73.

The feed was focused using near-field centerlines. Figures 56 and 57 show that the aperture phase front improved significantly, mainly due to the frequency scaling of the surface errors. The interference pattern in Figure 56 suggests that the effect of the adjacent apertures will be more significant in the far-field at this frequency.

Figure 51 shows that the surface effects have scaled because the -30-dB contour at 7.73 GHz corresponded approximately to the -40-dB contour at 2.27 GHz when the angles were neglected. However, almost all of the surface pillowing lobes are below the -40-dB contour because of the lower frequency, though one sidelobe did appear at 16° off boresight in the H-plane.

At 2.27 GHz, the surface errors had a minimal effect near the antenna boresight, due to two factors. The sidelobes caused by surface errors had decreased 10 dB over the entire far-field envelope, and the increased beamwidth had moved the sidelobes caused by the apertures in close to the main beam. Therefore, sidelobes due to the other apertures combined with the edge diffractions of the illuminated aperture to dominate the antenna pattern inside of 5°, causing the sidelobe structure near boresight and asymmetry of the main beam at -20 dB. Because these sources were the main cause of pattern degradation, reflector performance at this frequency could only be improved by changing the feed illumination.

The cross-pol measurement demonstrated that the patch elements used had a good, practical cross-pol level. However, as Figure 62 shows, the cross-pol itself did not have a well-defined predictable structure because it represented the cross-pol of an array of elements, not of a single horn. Although the cross-pol does not significantly affect the co-pol performance, it did degrade the null that is often used to block the reception of cross-pol signals. Unlike the cross-pol measurement at 7.73 GHz, the effects of the other apertures could not be isolated with this feed without further processing. These other apertures may also have caused some of the multiple peaks in the cross-pol pattern.

When this feed was steered one beamwidth in the H-plane, it was also placed over Quadrant 2, thus rotating 180° the far-field effects of the apertures. The major change in the pattern due to steering was an increase in the sidelobes along the H-plane. The increased sidelobe at (4,0) was due to the reflector surface in Quadrant 2. This was verified in the later Tests 13, 15, 16, 17, and 20. Once the rotation of the feed is accounted for in Test 5, the rest of the sidelobes remain unchanged.

These tests demonstrated that at this frequency, while the reflector surface performs very well, the antenna design has minor problems. These problems are due to a combination of factors: the reduced aperture size (in wavelength), the quad aperture geometry, and the aperture illumination. Use of an array illumination more closely matching the aperture geometry could greatly reduce the aperture sidelobes, and the aperture efficiency may improve as well. While the quad aperture design degrades the antenna performance, this degradation occurs below -20 dB.

4.4 TESTS 12-17 (4.26 GHz)

The feed used for the 4.26-GHz tests was a scaled version of the 2.27-GHz feed with the same aperture illumination and hexagonal geometry. In this series of tests the feed was located in several positions and used to illuminate both Quadrants 2 and 4. The cross-pol was not measured at this frequency because the performance should be similar to that of the 2.27-GHz feed. Data for these tests (12-17) are compiled in Figures 74-139.

The co-pol pattern of the antenna had a gain of 45.57 dB and first sidelobe levels at -18.4 dB. The pillowing lobes for this frequency occurred as a ring of sidelobes at 8.4° with a peak sidelobe of -33.3 dB--the position and amplitude predicted based on the previous tests. The effects of the other apertures were on the same level with those due to surface errors; therefore, they tended to interfere constructively or destructively depending on angular position from boresight. The far-field pattern at 4.26 GHz represented the crossover point between the spatially isolated error sources at 7.73 GHz and the complete overlap of these sources at 2.27 GHz.

The other apertures did not dominate the first sidelobe pattern at this frequency as they did at 2.27 GHz. In fact, at this frequency, aperture effects were difficult to isolate from the interfering sidelobe source of surface errors. It was obvious, even in these collections, that the sidelobes due to the other apertures still maintained their geometric position.

Tests 13, 14, 16, and 17 show steering of the antenna by moving the patch array to different positions on the panel. In all the collections except Test 14 the patterns remained virtually unaffected either in gain or sidelobe pattern. In Test 14 the beam was steered three times as far as any other collection, causing a significant increase in some sidelobes (Fig. 100). This result was not too surprising, since no attempt was made to refocus the antenna in this steered position. The feed had been displaced in the H-plane along a straight line instead of following focal curve. This straight-line displacement could easily defocus the feed. From the data collected on steering the antenna, especially at 4.26 GHz, it seems that either the beam should not be steered more than 3° or that the feed panel should conform to the locus of the reflector focal points to prevent this coma lobing.

4.5 TESTS 18-26 (ABBREVIATED SCANS)

After the completion of all the originally scheduled tests and the optional tests (12-17), a final surface control cord adjustment was made to improve the antenna performance at 7.73 GHz. To optimize the use of the remaining collection time, abbreviated scans were used to acquire data. Taking a quarter of the time to collect, abbreviated scans yield only a minor degradation in pattern accuracy, and this error was localized in the 7.73-GHz collections to the sidelobes at (2.5, 2.5), (2.5, -2.5), (5.0, 0.0). Since these sidelobes were created by the other apertures, which were not completely scanned, they no longer appeared well above the envelope as they did in Test 1.

Three tasks were done in this set of abbreviated scans. First, Tests 18 and 19 showed the improvement of antenna performance that could be achieved by adjusting the surface cords based on the finite elements model of the antenna. These results are shown in Figures 140-161. Second, the patterns of the other three quadrants were measured for comparison to Quadrant 4. Third, an attempt was made to optimize the cross-pol measurement at 7.73 GHz using near-field measurements.

Test 18 showed mild surface degradation (compare Figures 13 and 14 to 144 and 145) 48 days after the previous cord adjustments. This is not a surprising result considering the constant flexing of the antenna due to air currents and testing of over 600 hours that involved large scale translation and rotation of the structure. Because only the first sidelobes were affected by this long-term pattern degradation, these sidelobes were expected to be lowered by the final cord adjustment. As Figure 155 shows, there was significant improvement in the first sidelobe levels, a drop of 4 dB. The highest sidelobe remaining was now only -19.7 dB. This cord adjustment also reduced the total region of the sidelobe envelope above -30 dB. As expected, only one of the adjacent sidelobes appeared. This sidelobe was generated by the aperture which was partially inside of the rectangular scan area. Interestingly, the -40 dB contours for all the 7.73-GHz tests were virtually the same. This feature suggests that while sidelobes near boresight can be minimized by surface adjustment, the actual envelope of the far-field pattern can only be improved at this frequency by an increase in the number of surface adjustment chords.

Tests 20, 21, and 22 measured the far-field patterns of Quadrants 2, 3, and 1, respectively. The data from these abbreviated scans are shown in Figures 162-191. Test 20 on Quadrant 2 demonstrated that this quadrant, already used in Tests 7, 13, 15, 16, and 17, had only one sidelobe above -20 dB and had a well-defined main beam. In fact, with a peak sidelobe of -16.5 dB, Quadrant 2 had a better pattern after the adjustment than did Quadrant 4 before the final adjustment. Quadrant 3 performed better than Quadrant 2 (highest sidelobe -18 dB), although it had a larger -30-dB contour than either Quadrant 2 or Quadrant 4. Quadrant 1 had the worst performance of any of the quadrants for all characteristics of the far-field: sidelobe envelope, first and second sidelobes, and main beam definition. If this antenna is adjusted again, emphasis should be placed on correcting the surface of Quadrant 1. However, all the quadrant apertures performed well.

To optimize the cross-pol measurement, which became a concern after examining the Test 2 results, another approach to determine the true cross-pol was tried. Figures 192-212 show the results of this optimization. Near-field centerlines were taken of the cross-pol; and, because it was a horn feed, there was a well-defined null in the center of the scan with an associated 180° phase flip. To obtain a better cross-pol measurement the antenna was rotated for maximum phase slope along the centerline null. The resulting far-field patterns showed a more symmetric pattern than that in Test 2. However, the cross-pol peak was not on boresight, so Figures 201 and 202 were included to show that the antenna cross-pol measurement was accurate. In fact, after sufficient resolution of the data, the misalignment from true cross-pol on boresight can be determined as less than 0.1° of rotation resulting in an error of less than 0.2 dB in amplitude on an axial ratio of 38.6 dB, which error is well within other sources of measurement error for the cross-pol pattern.

Tests 25 and 26 (Fig. 213-232) demonstrated that each feed used will have a slightly different polarization. Using the same position as the 7.73 GHz tests (23 and 24) the cross-pol was still rotated slightly for the 11.60-GHz feed. Figure 232 shows that the cross-pol difference beams were no longer balanced, nor the null as deep, even though the 11.60-GHz feed was very similar in design. This series of cross-pol tests demonstrates that while the cross-pol sidelobe envelope was not changed by minor polarization misalignments, the peak cross-pol level and the axial ratio were extremely sensitive to this effect.

Test 24 can be considered a repeatability measurement of the surface adjustments. After 60 hours of testing there appeared to be no significant pattern degradation from patterns seen in Test 19. This implies that changes observed in Test 18 from Test 1 were due to the longer test period.

The changes in the sidelobe structure at 11.60 GHz due to the surface adjustment were only observable in the 3-D plots of Tests 4 and 25. These figures, 42 and 219, show a drop in the first sidelobes of approximately 4 dB, just as in the first sidelobes of the 7.73-GHz collection. The remainder of the sidelobe envelope was almost unchanged by the adjustment.

For this antenna the abbreviated scans were the more efficient means of obtaining information about the antenna at high frequencies. This method would not work as well for the lower frequencies, since at these frequencies the other apertures greatly affected the narrow angle response. At the higher frequencies the surface had the dominant effect near the main beam, because the other apertures' sidelobes were isolated by position. This allowed accurate data to be acquired with a 75% reduction in scan time.

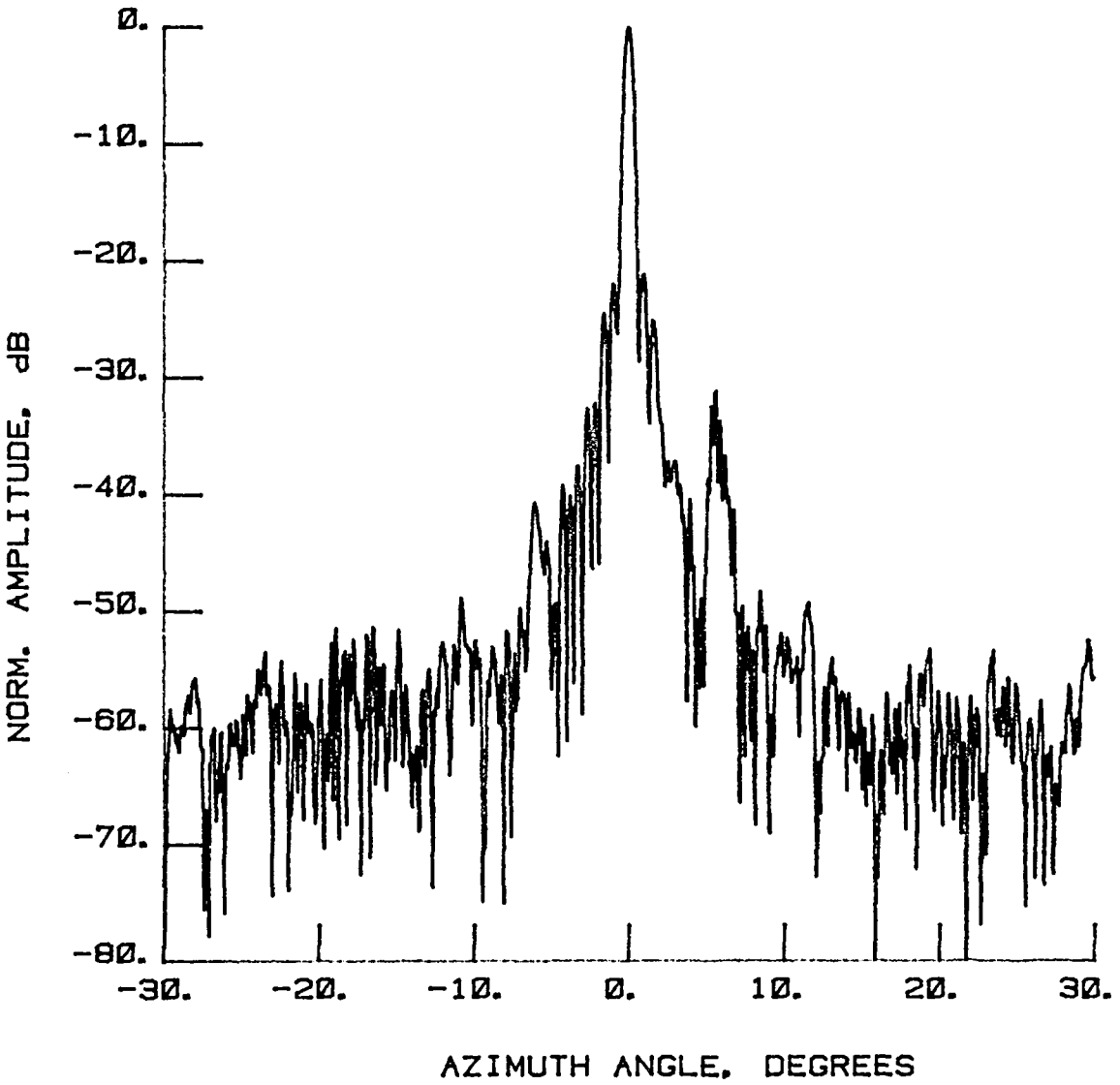

Figure 9 Test 1, 7.73 GHz, Co-Pol, E-Plane, Type 1

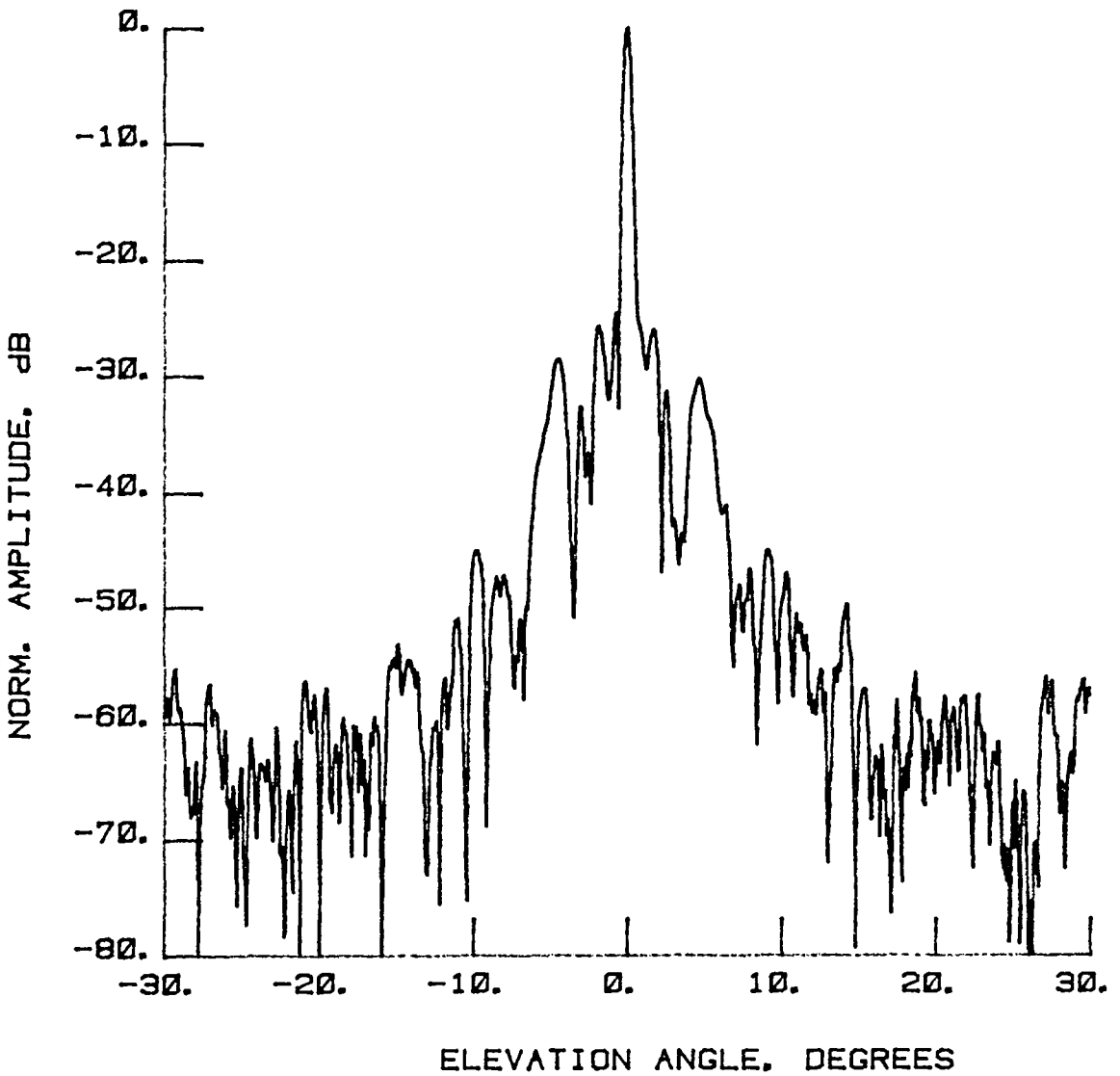

Figure 10 Test 1, 7.73 GHz, Co-Pol, H-Plane, Type 2

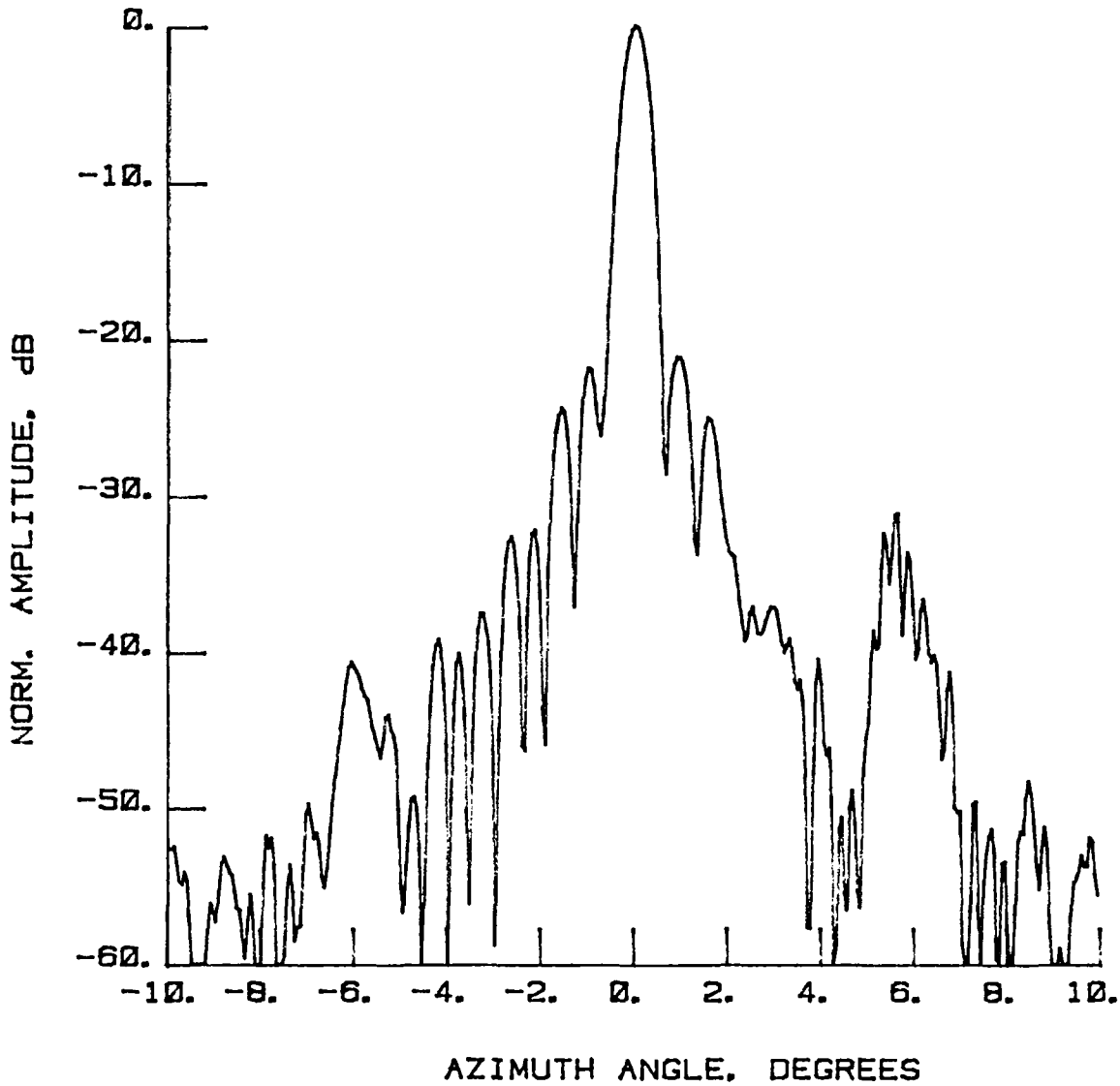

Figure 11 Test 1, 7.73 GHz, Co-Pol, E-Plane, Type 3

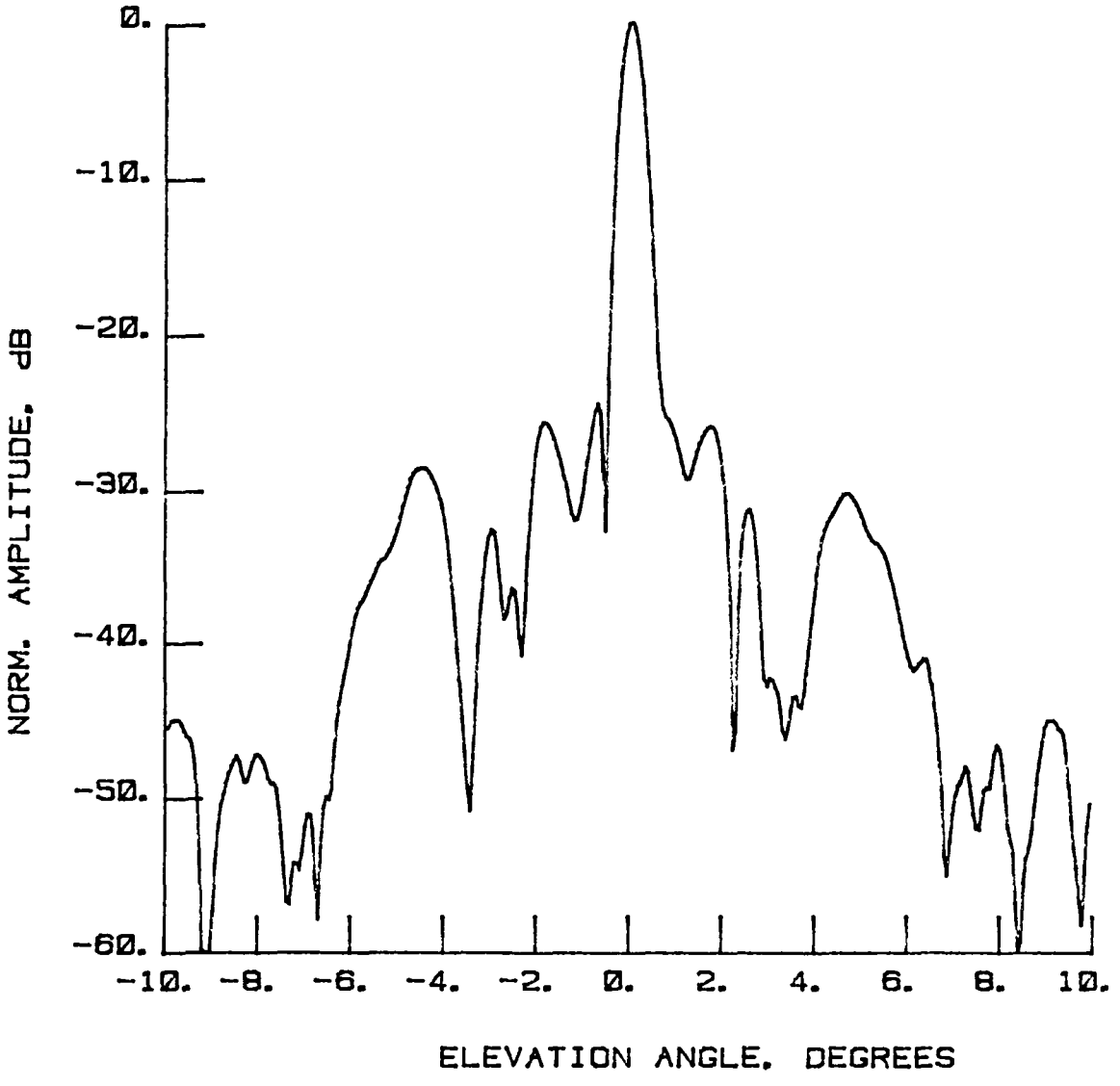

Figure 12 Test 1, 7.73 GHz, Co-Pol, H-Plane, Type 4

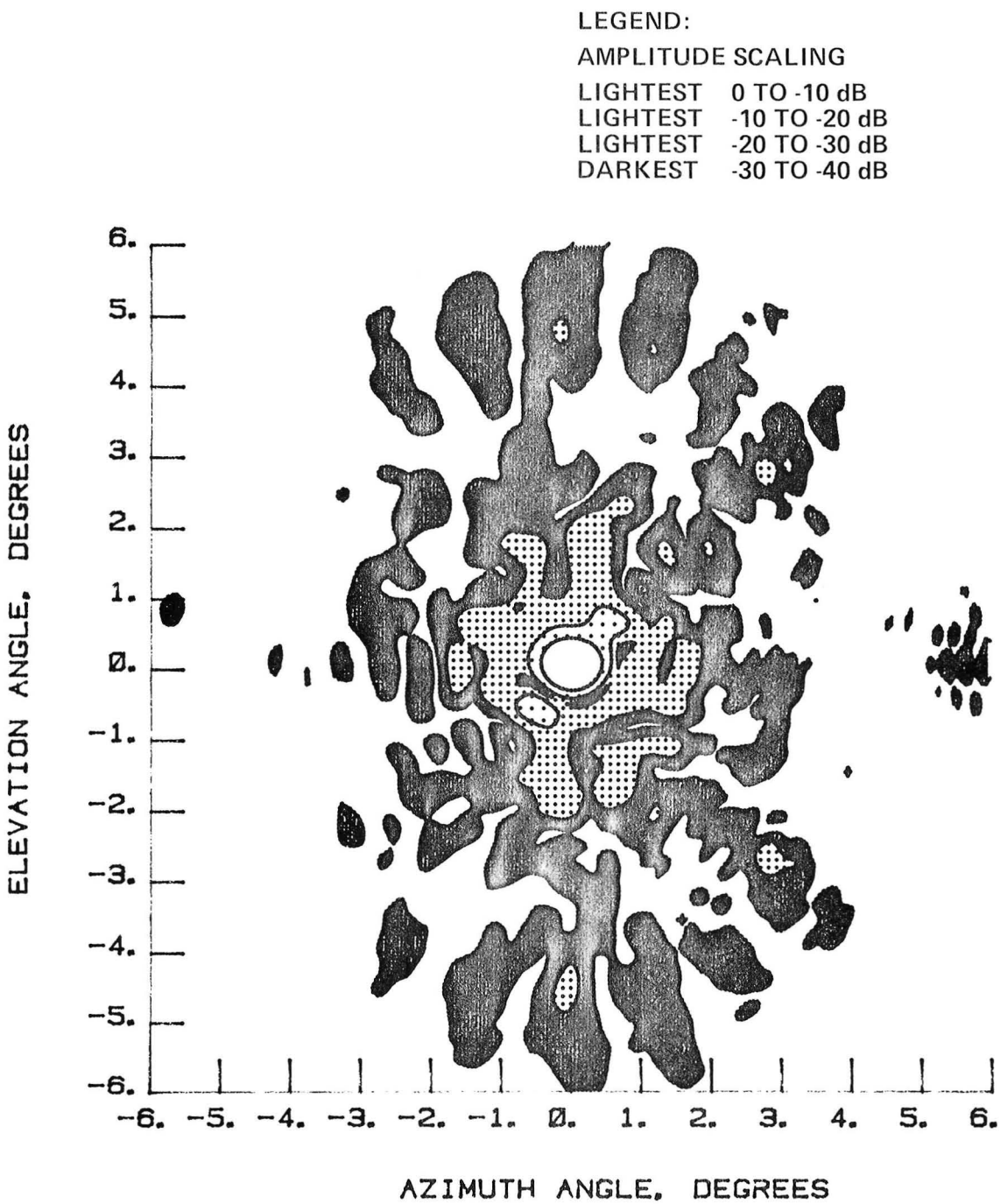

Figure 13 Test 1, 7.73 GHz, Co-Pol, Contour, Type 5

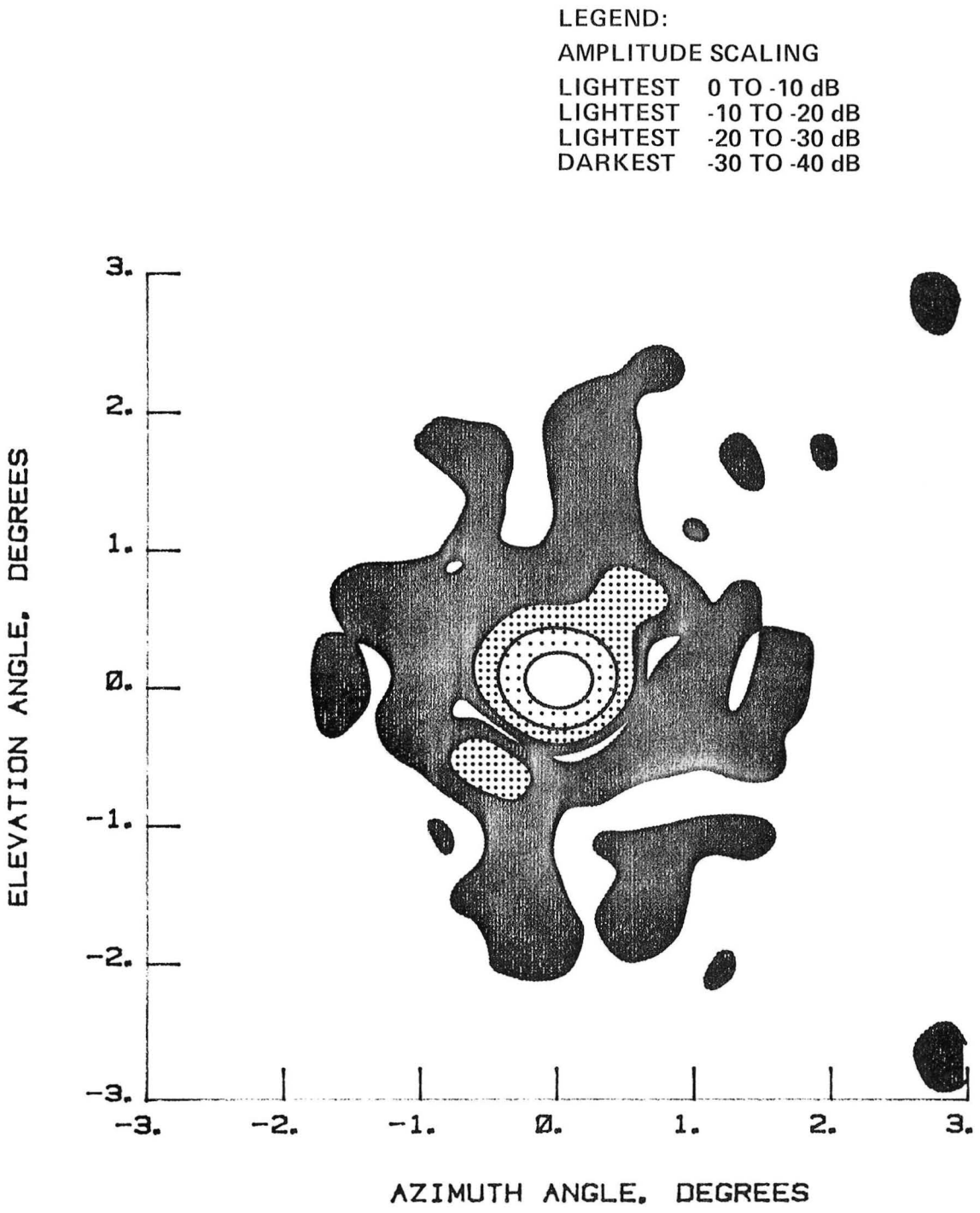

Figure 14 Test 1, 7.73 GHz, Co-Pol, Contour, Type 6

TEST IDENTIFICATION : LRCØ1

DATE : 17 SEPT. 1985

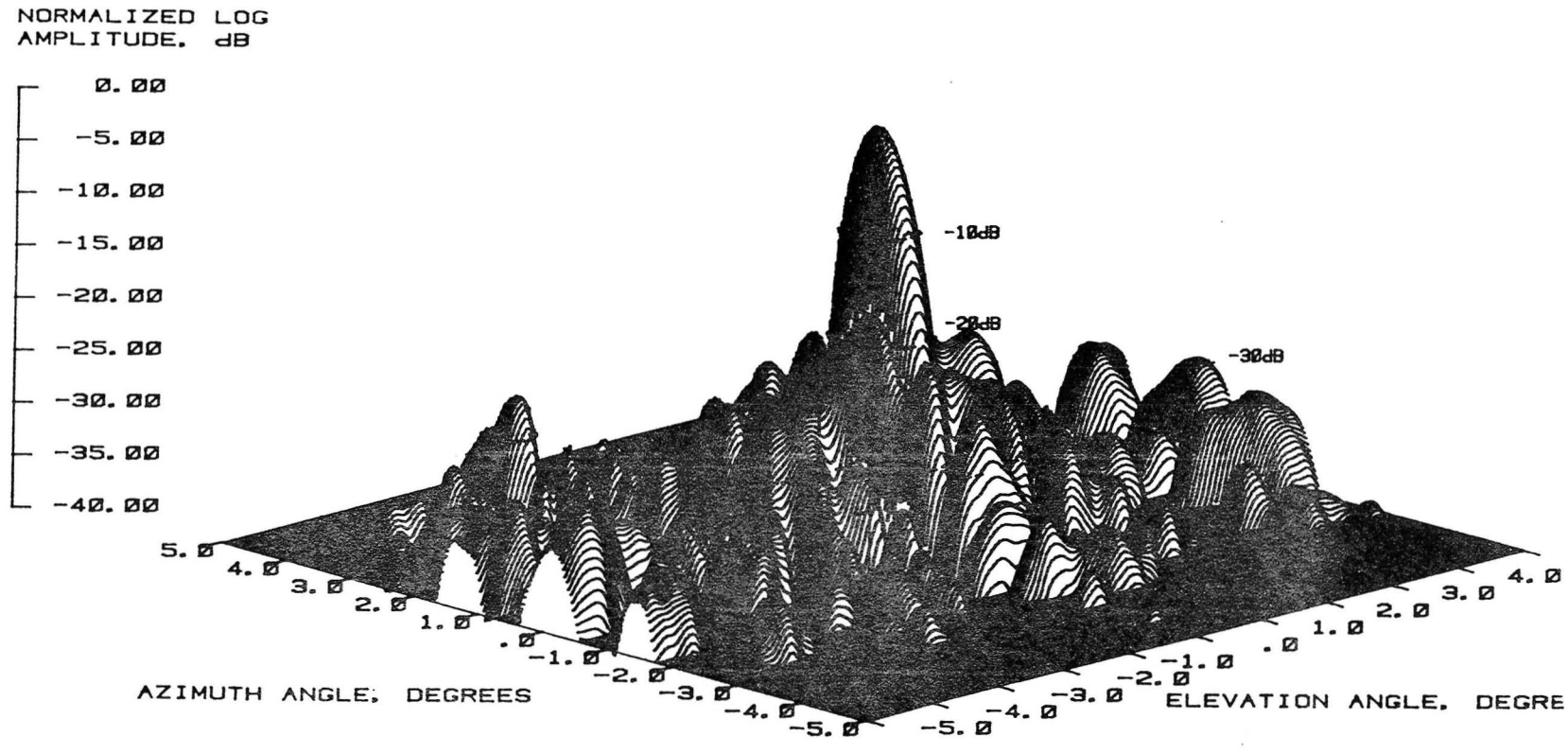

Figure 15 Test 1, 7.73 GHz, Co-Pol, 3-D, Type 7

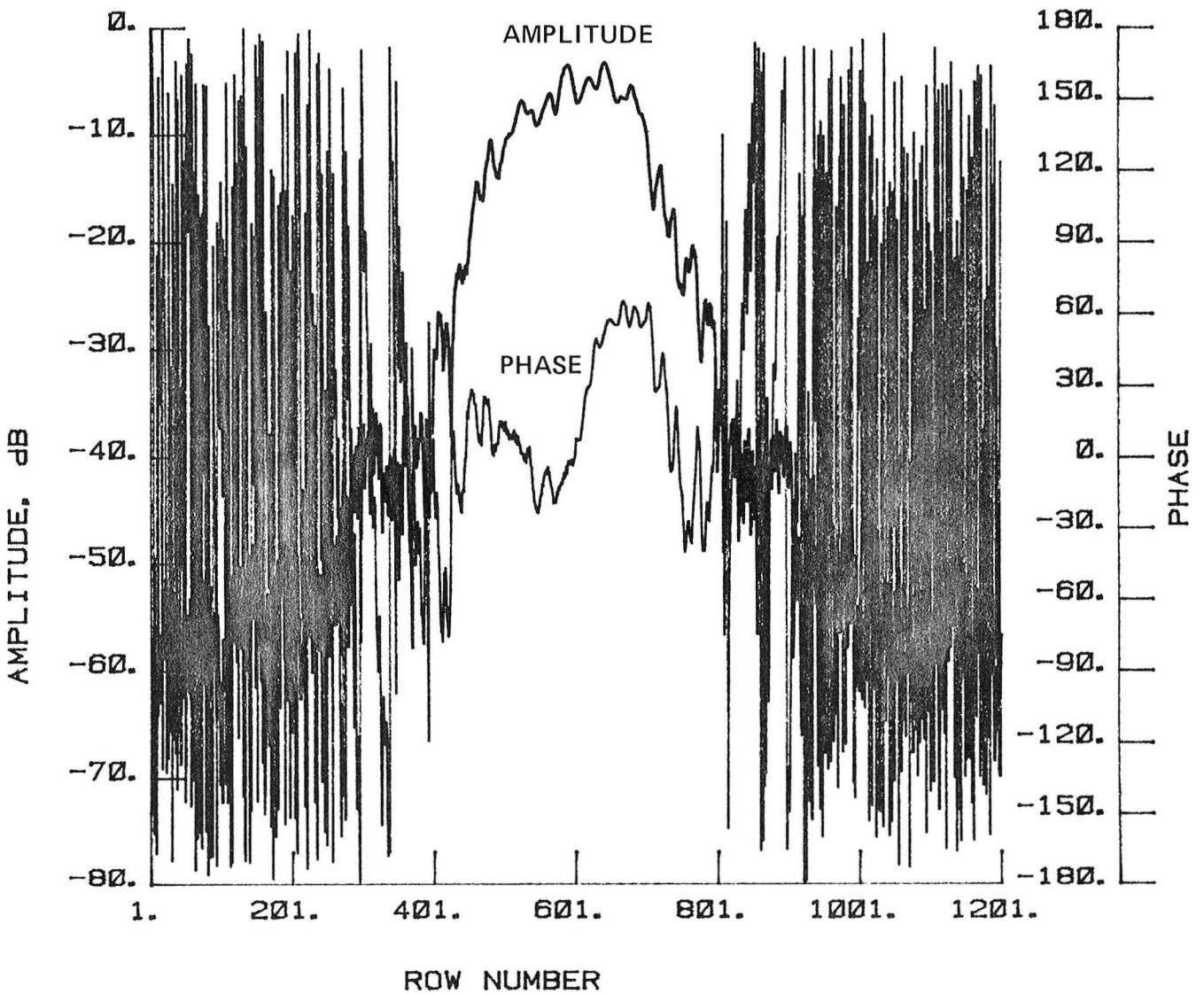

Figure 16 Test 1, 7.73 GHz, Co-Pol, H-Plane, Type 8

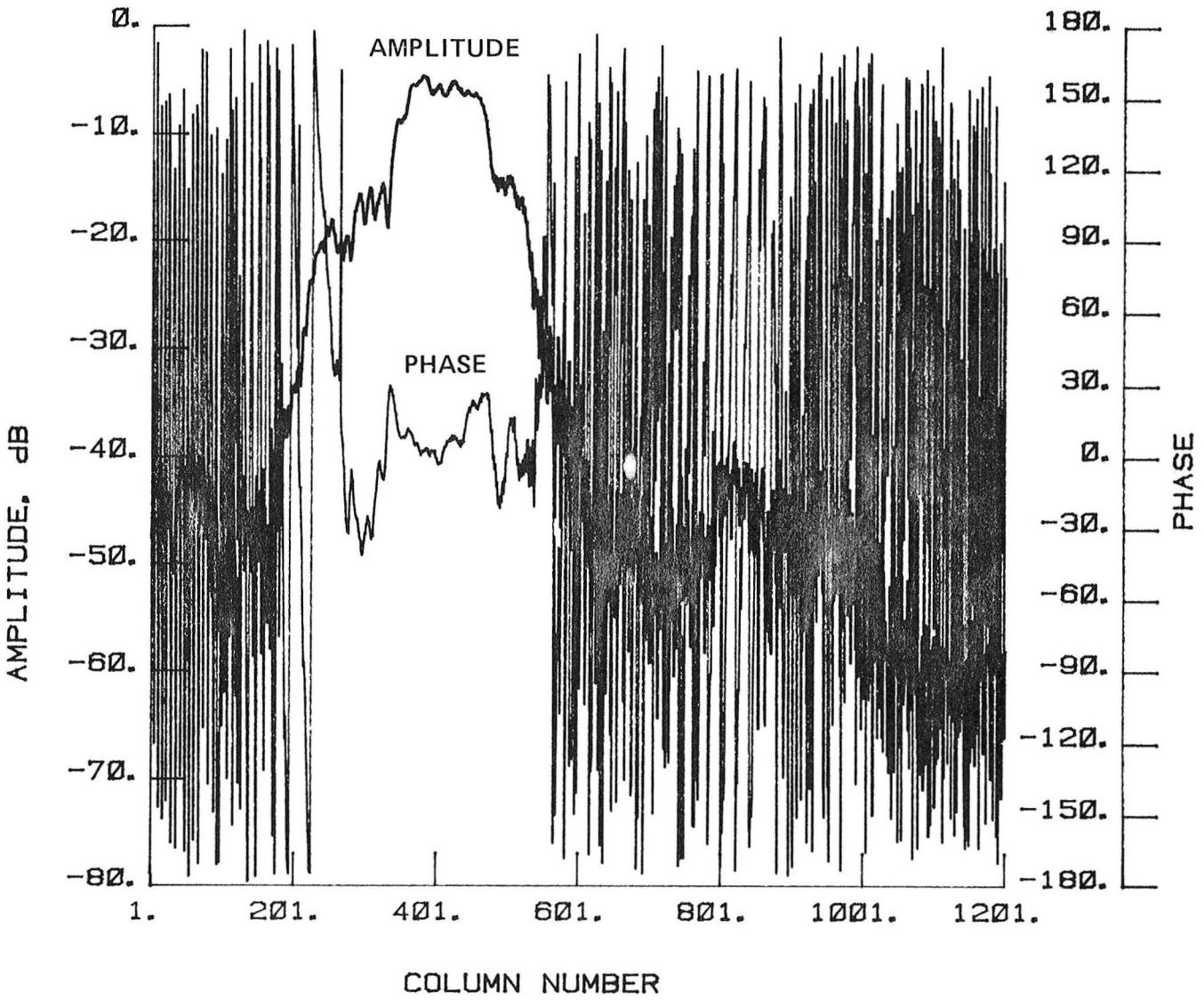

Figure 17 Test 1, 7.73 GHz, Co-Pol, E-Plane, Type 9

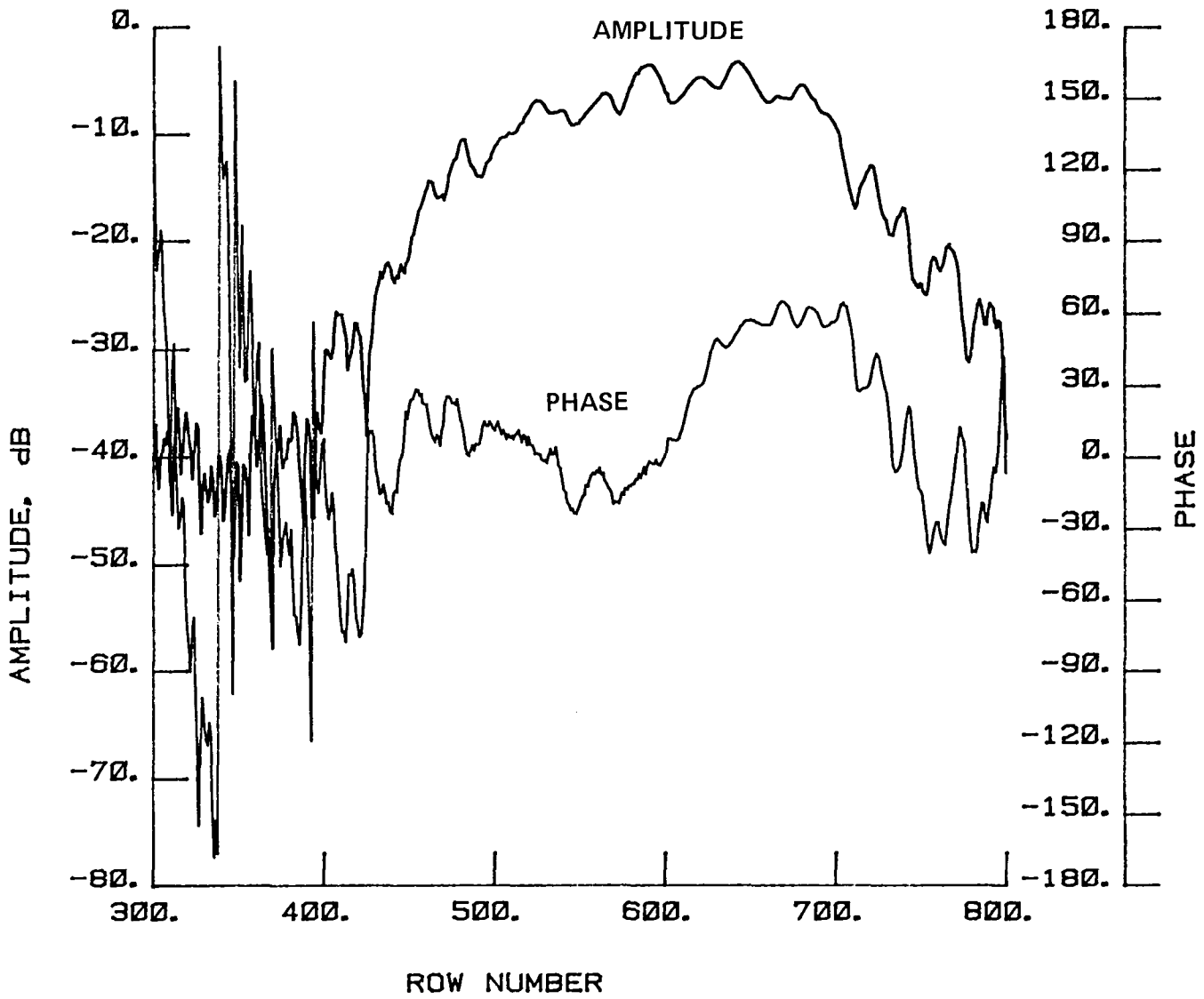

Figure 18 Test 1, 7.73 GHz, Co-Pol, H-Plane, Type 10

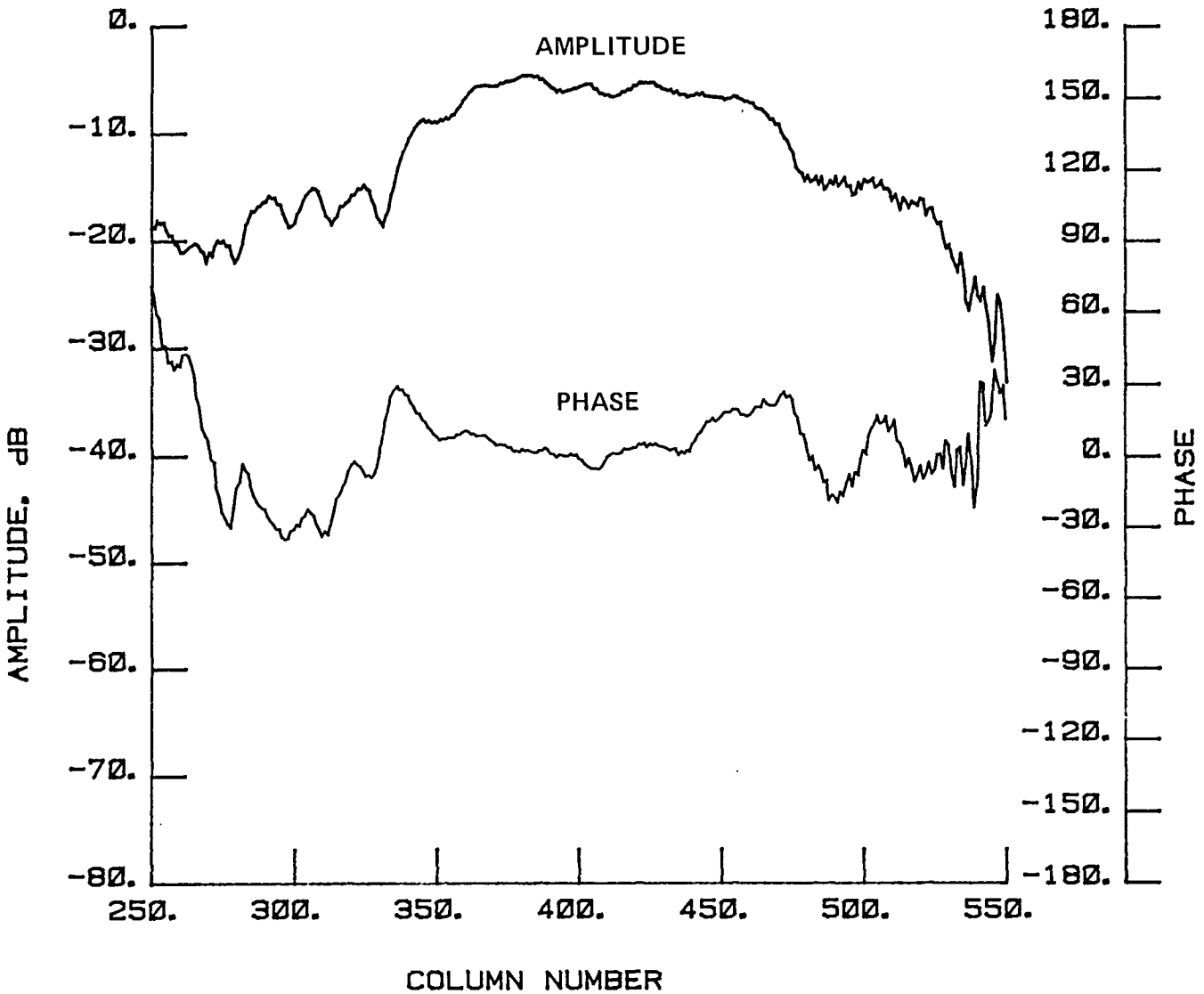

Figure 19 Test 1, 7.73 GHz, Co-Pol, E-Plane, Type 11

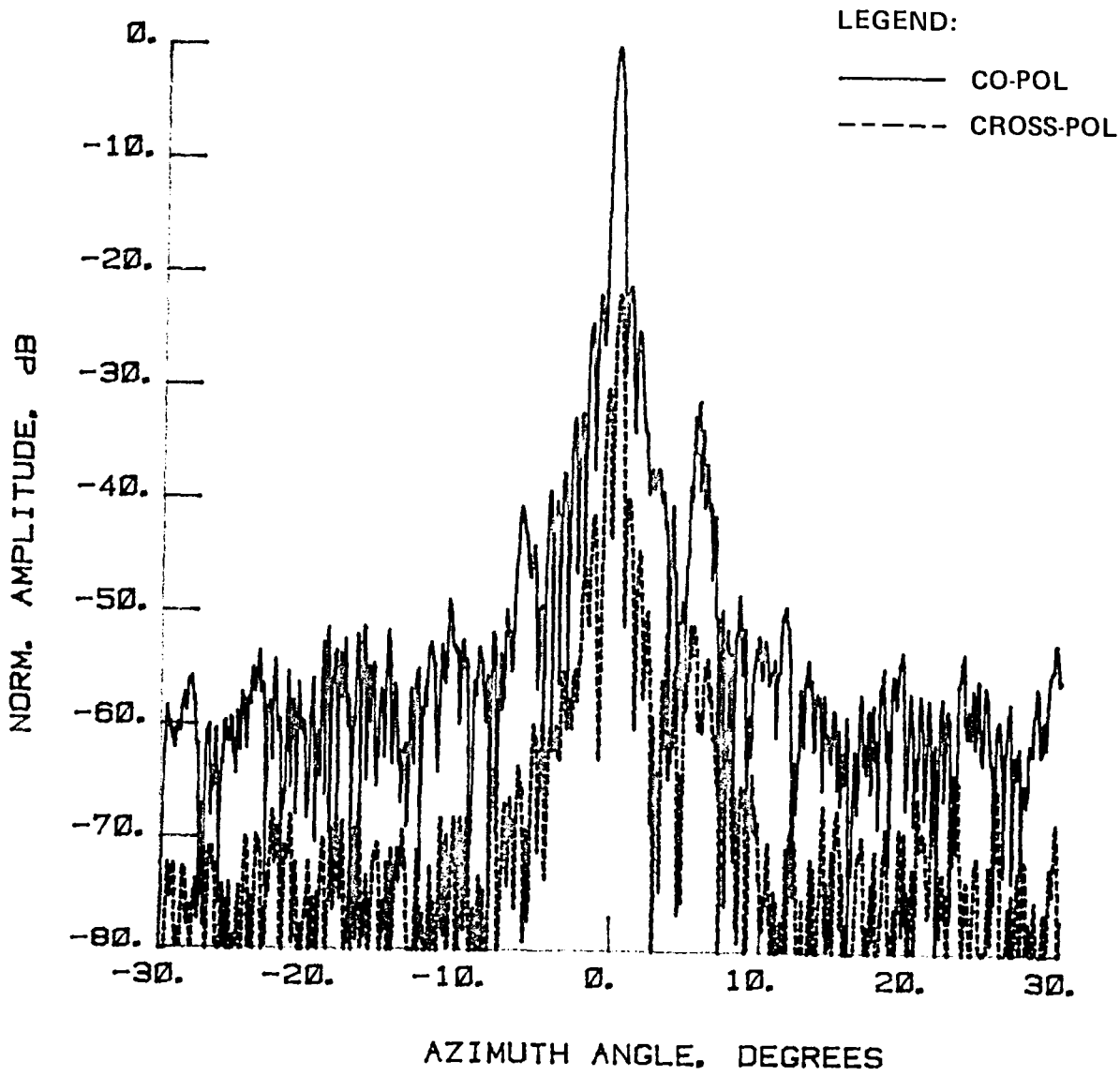

Figure 20 Test 2, 7.73 GHz, Cross-Pol, E-Plane, Type 12

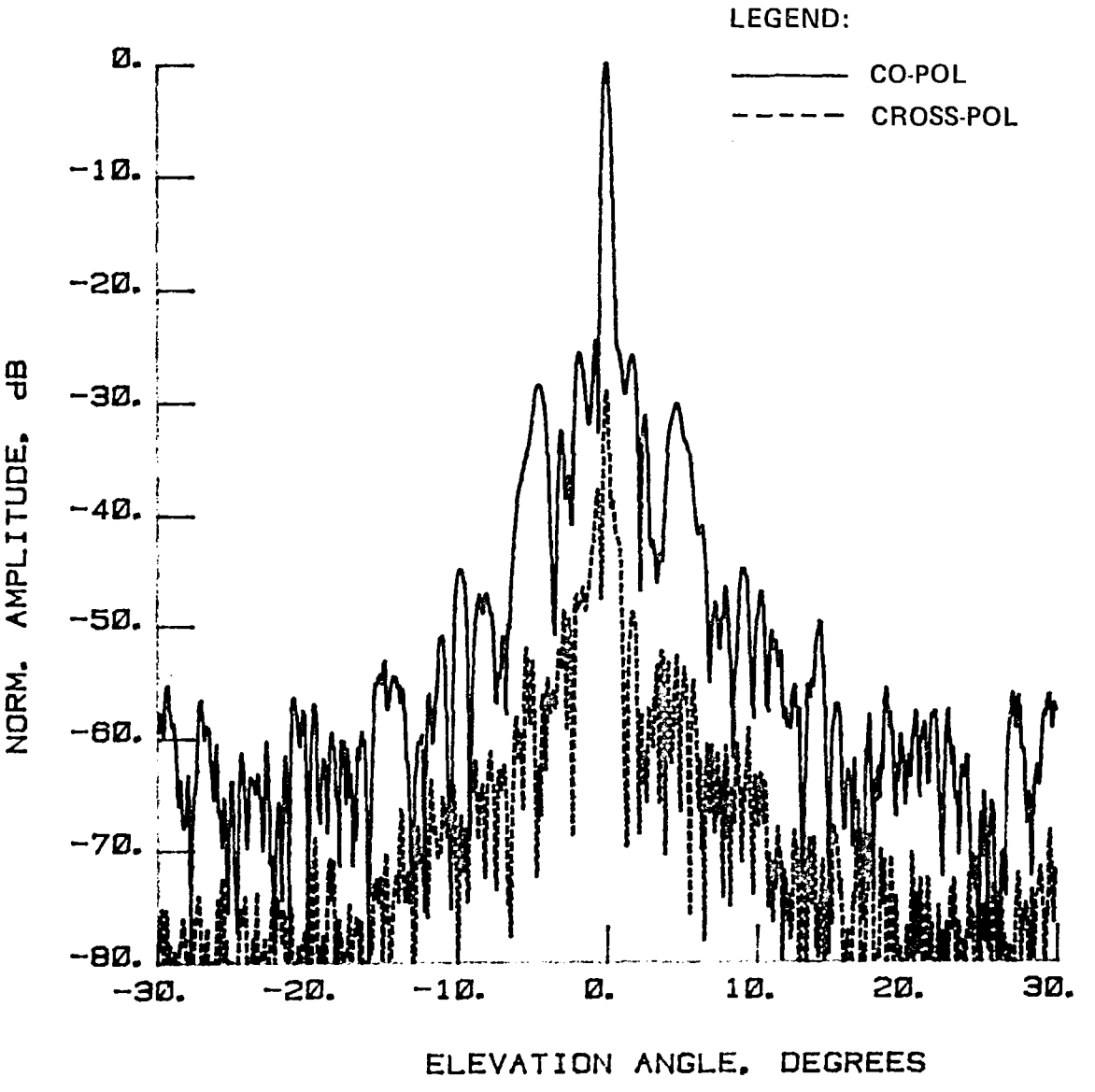

Figure 21 Test 2, 7.73 GHz, Cross-Pol, H-Plane, Type 13

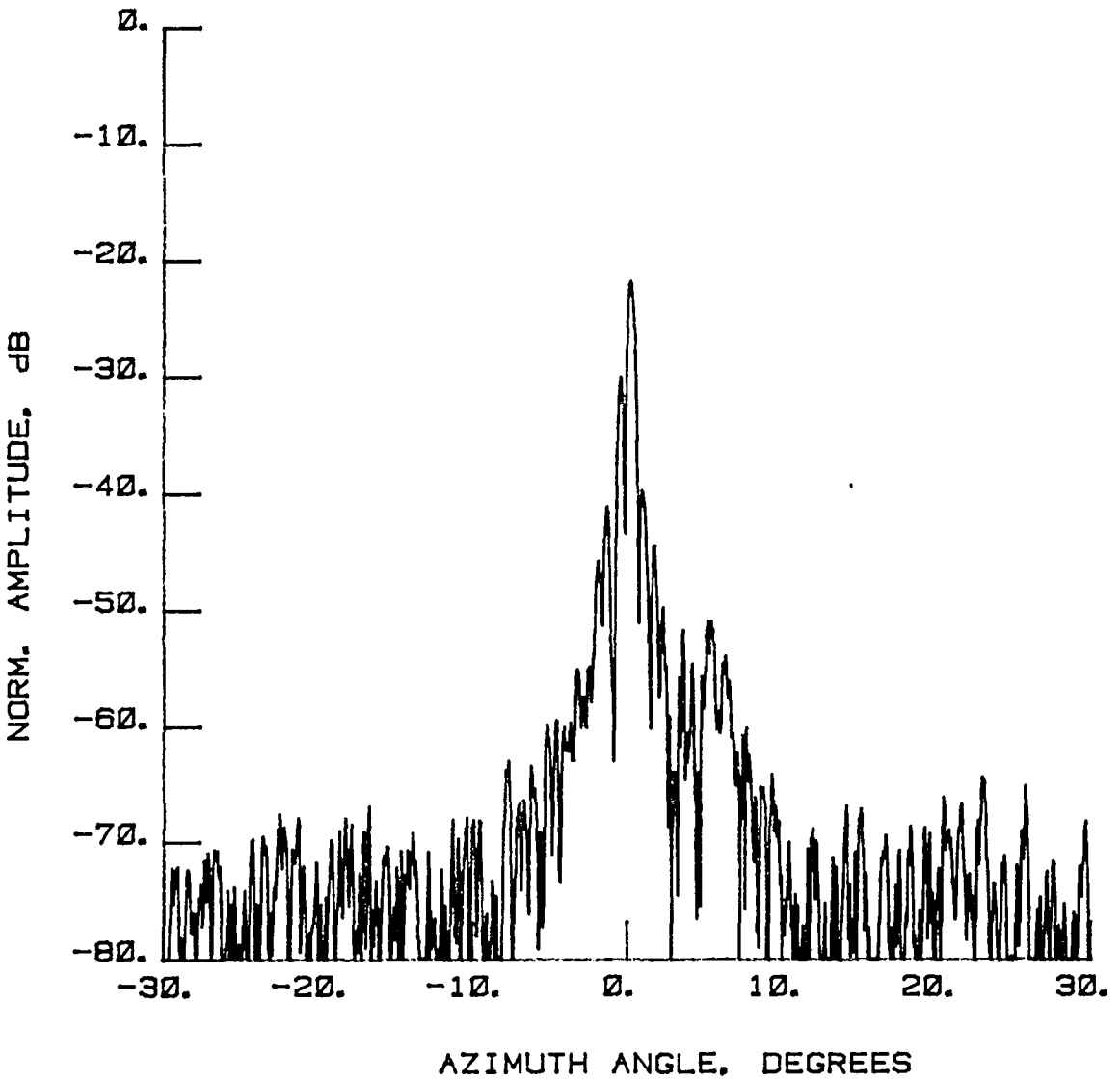

Figure 22 Test 2, 7.73 GHz, Cross-Pol, E-Plane, Type 14

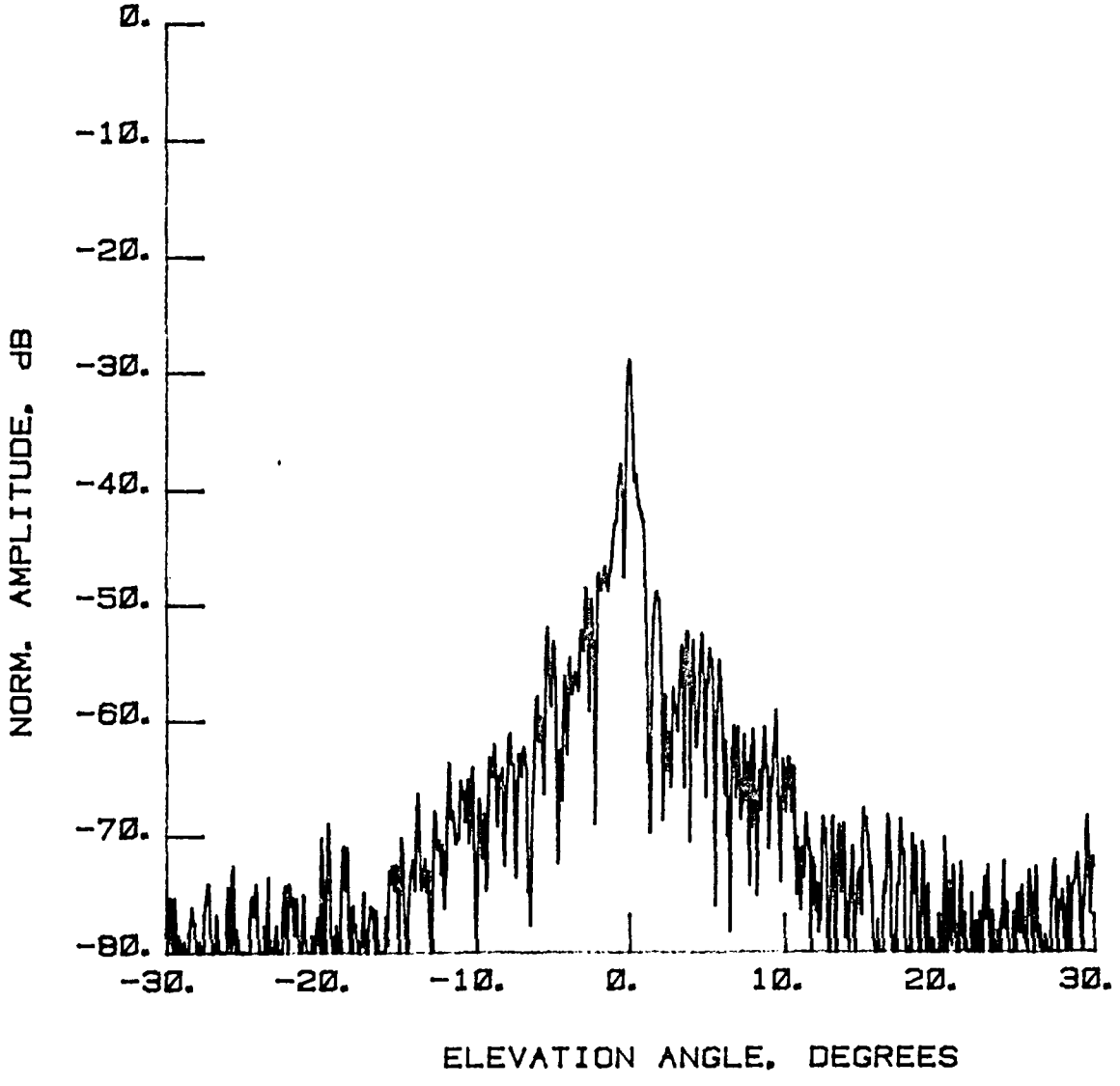

Figure 23 Test 2, 7.73 GHz, Cross-Pol, H-Plane, Type 15

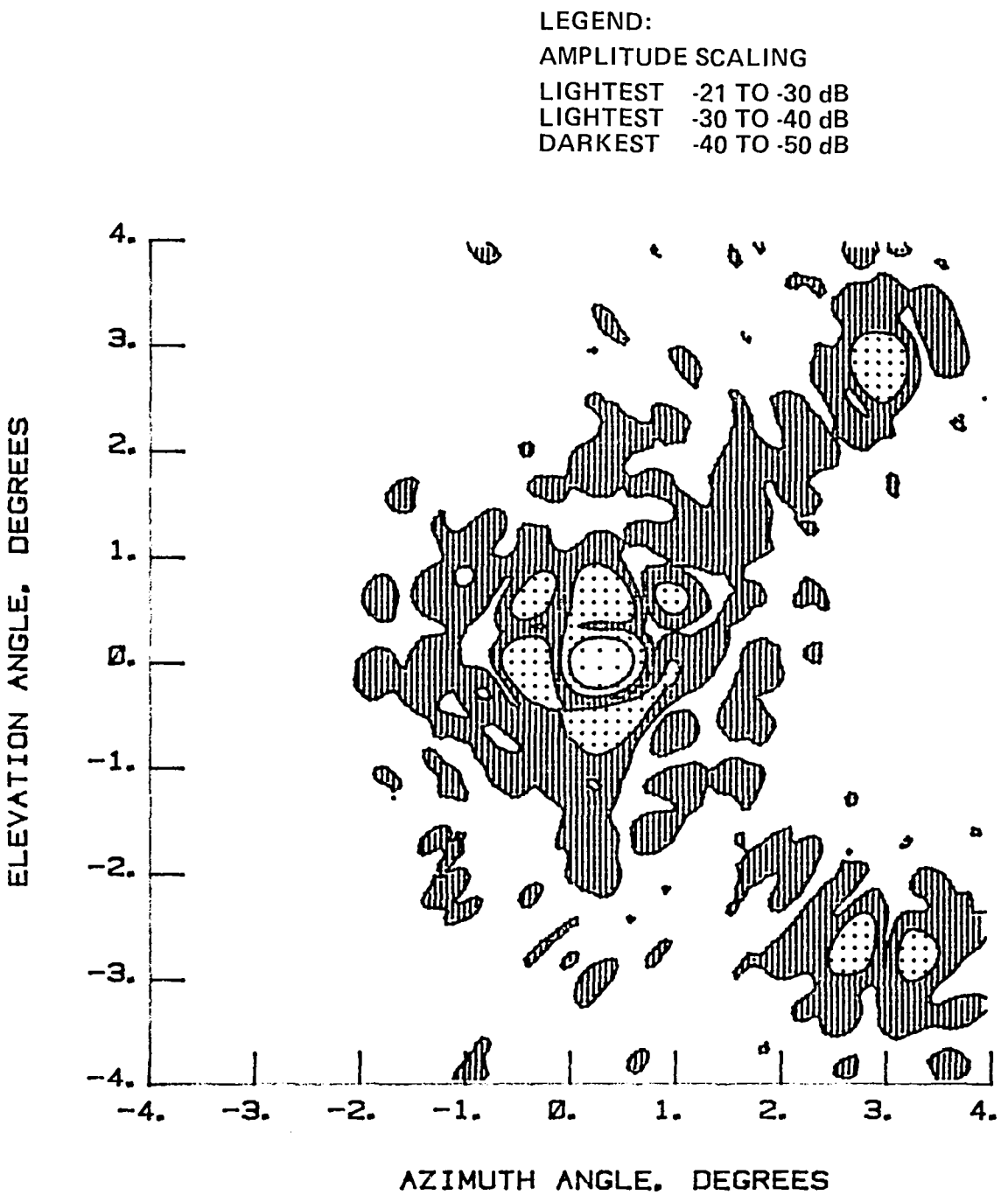

Figure 24 Test 2, 7.73 GHz, Cross-Pol, Contour, Type 16

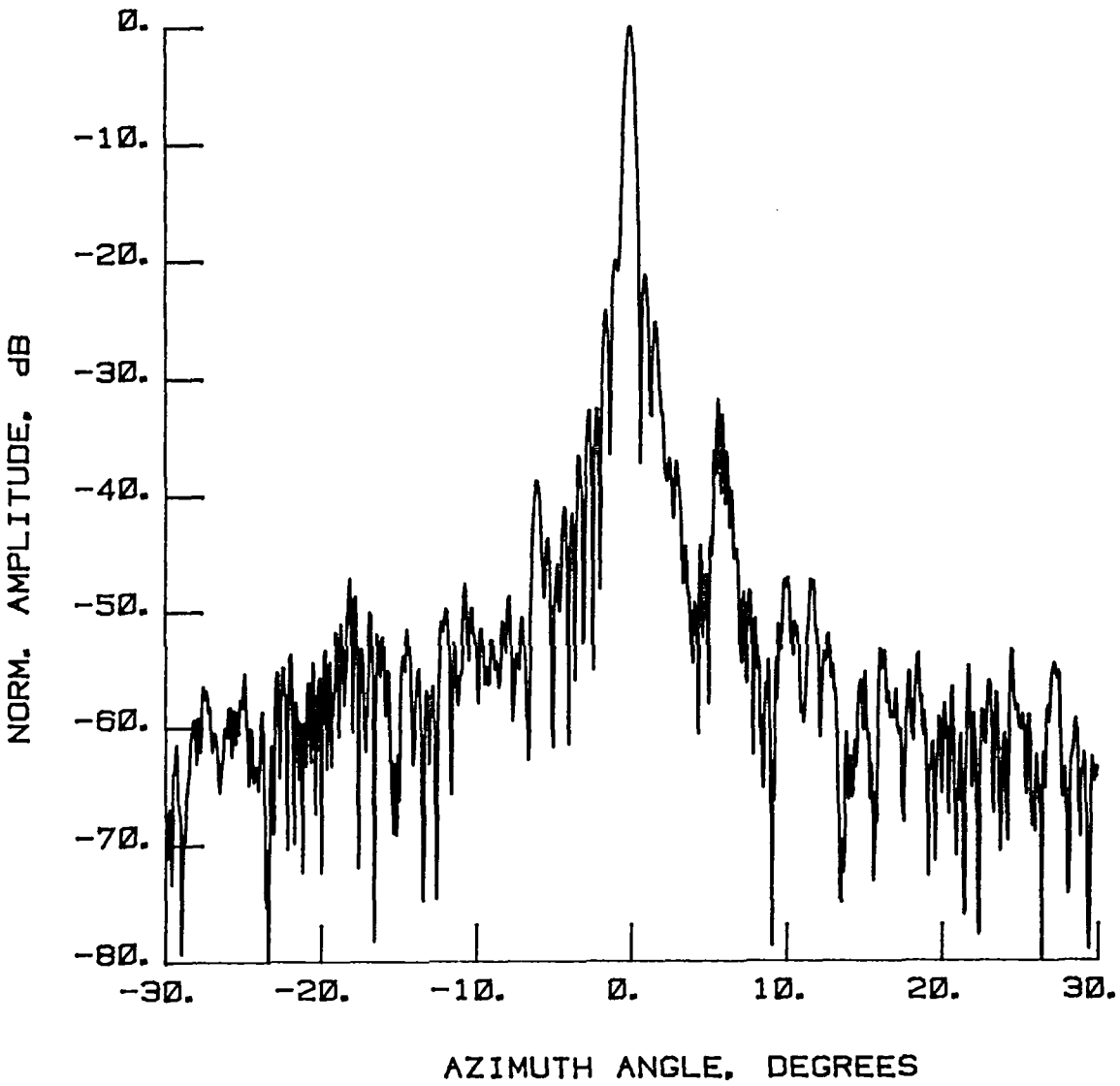

Figure 25 Test 3, 7.73 GHz, Co-Pol, E-Plane, Type 1

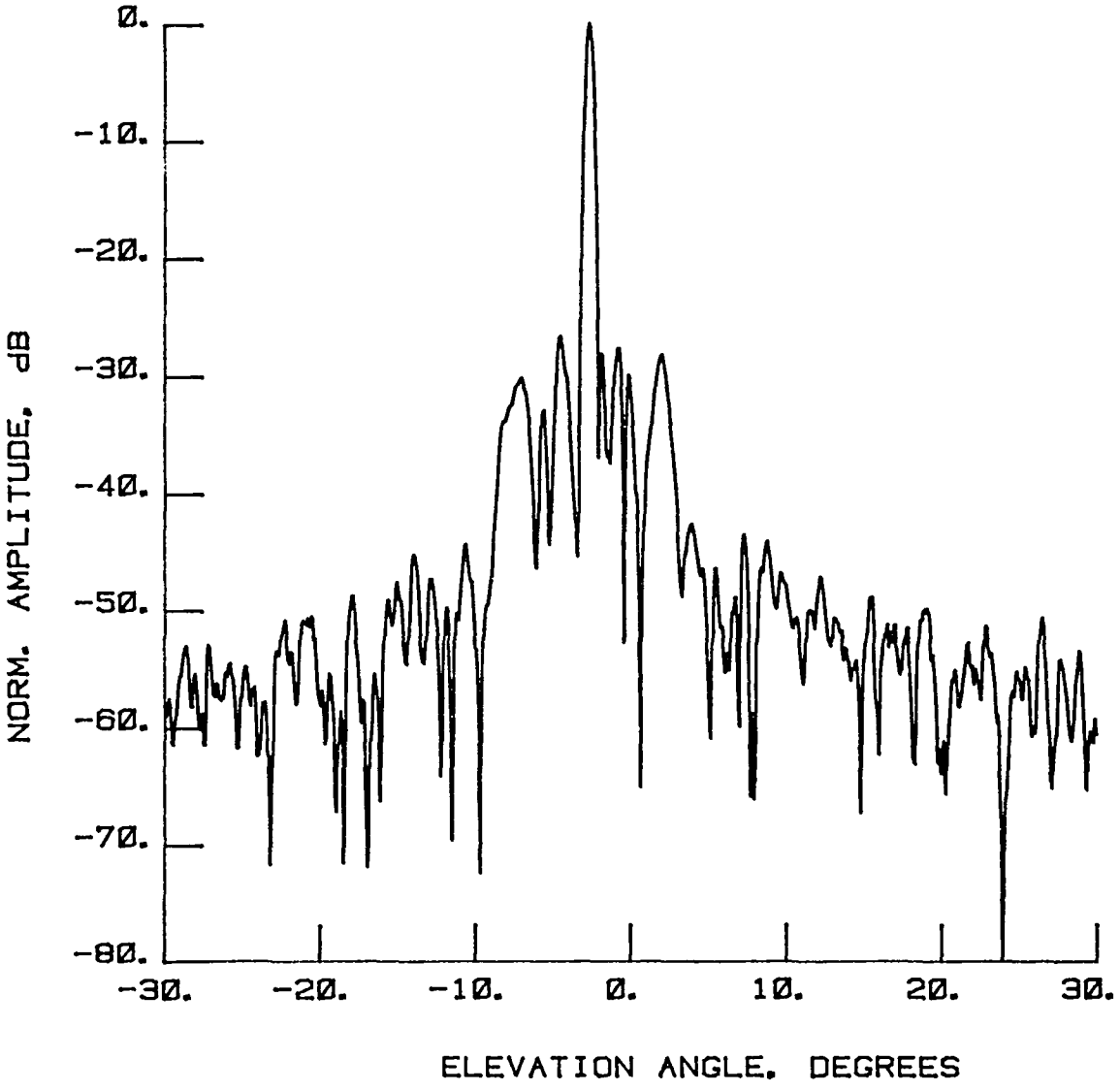

Figure 26 Test 3, 7.73 GHz, Co-Pol, H-Plane, Type 2

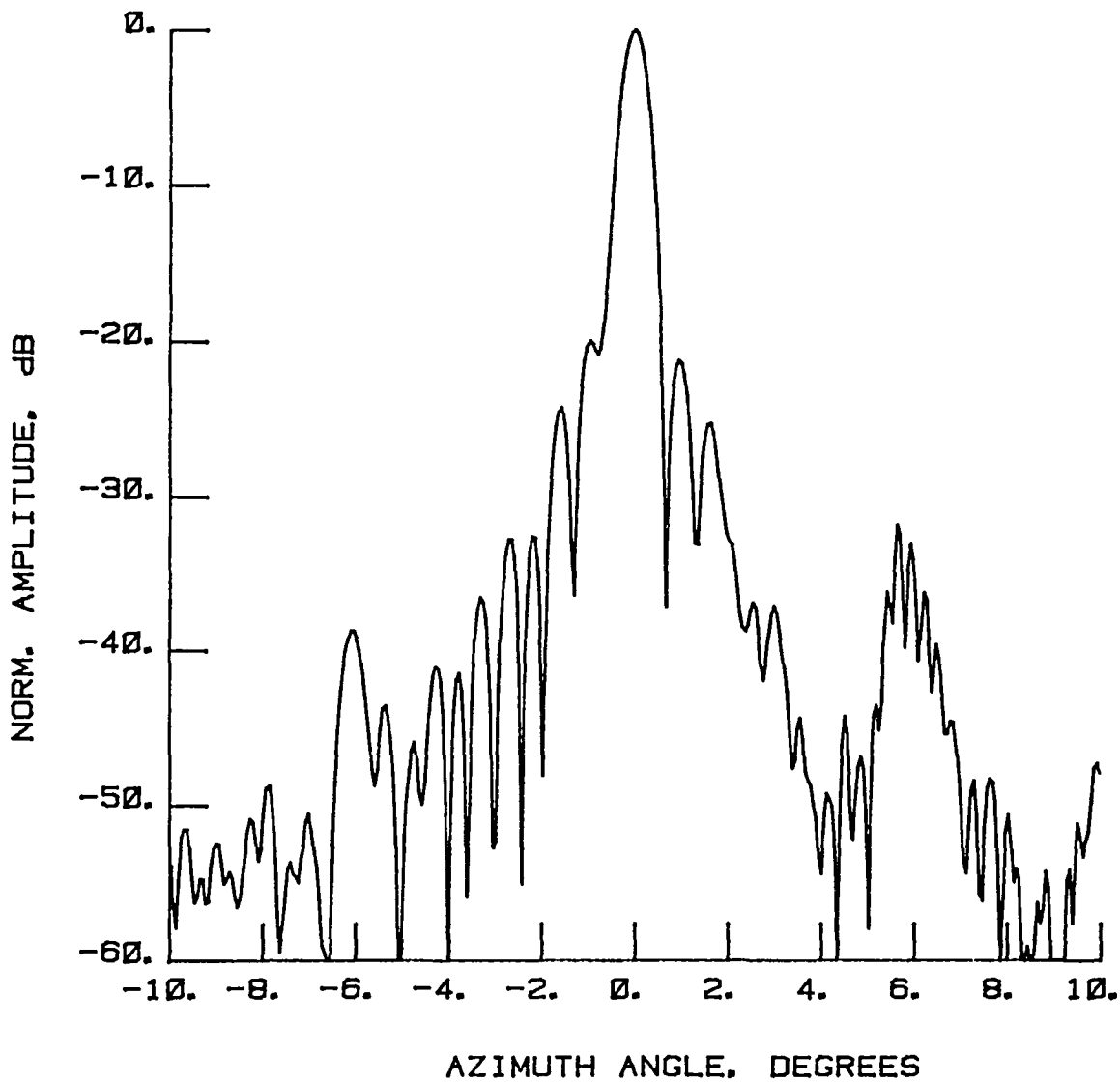

Figure 27 Test 3, 7.73 GHz, Co-Pol, E-Plane, Type 3

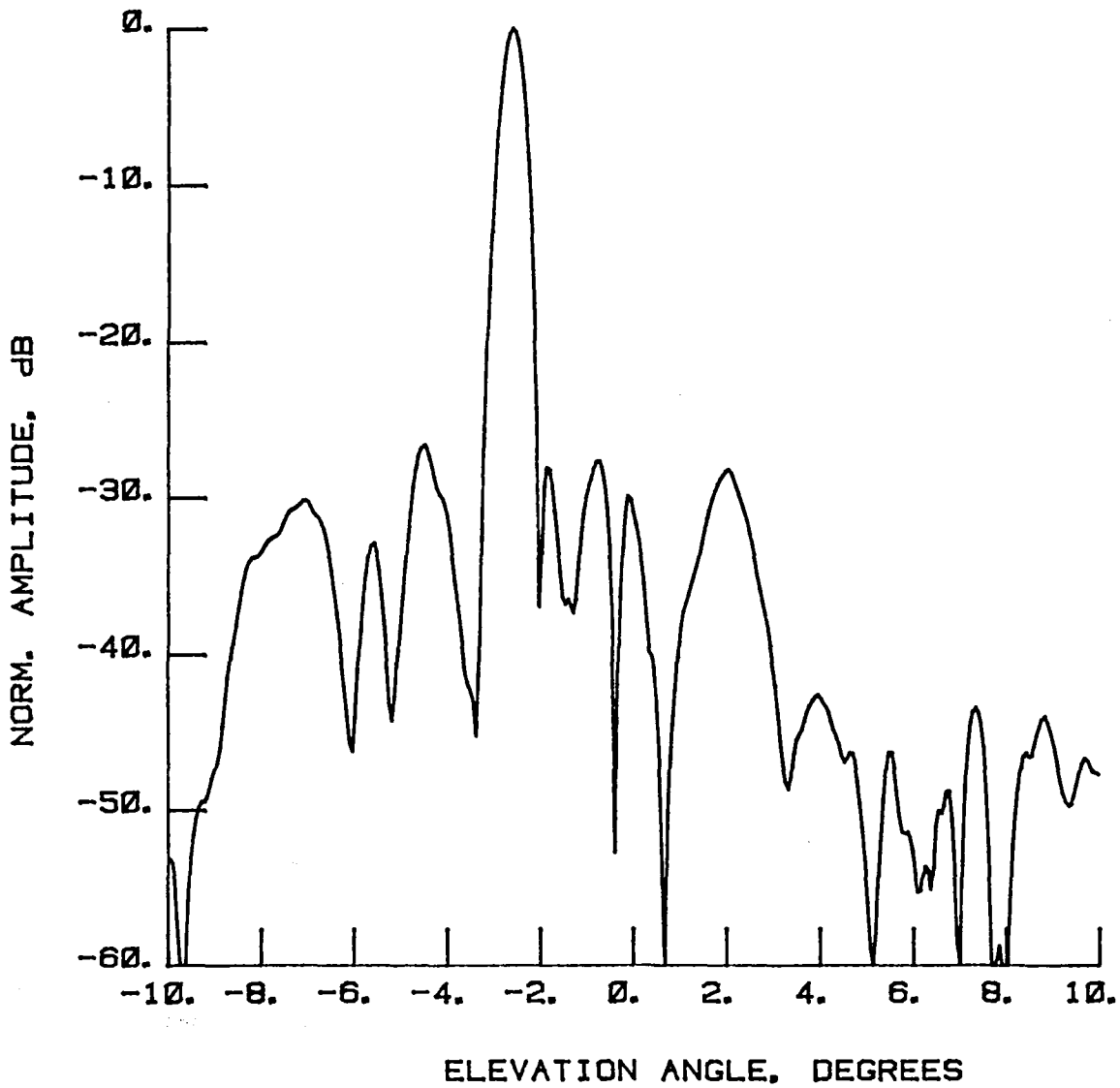

Figure 28 Test 3, 7.73 GHz, Co-Pol, H-Plane, Type 4

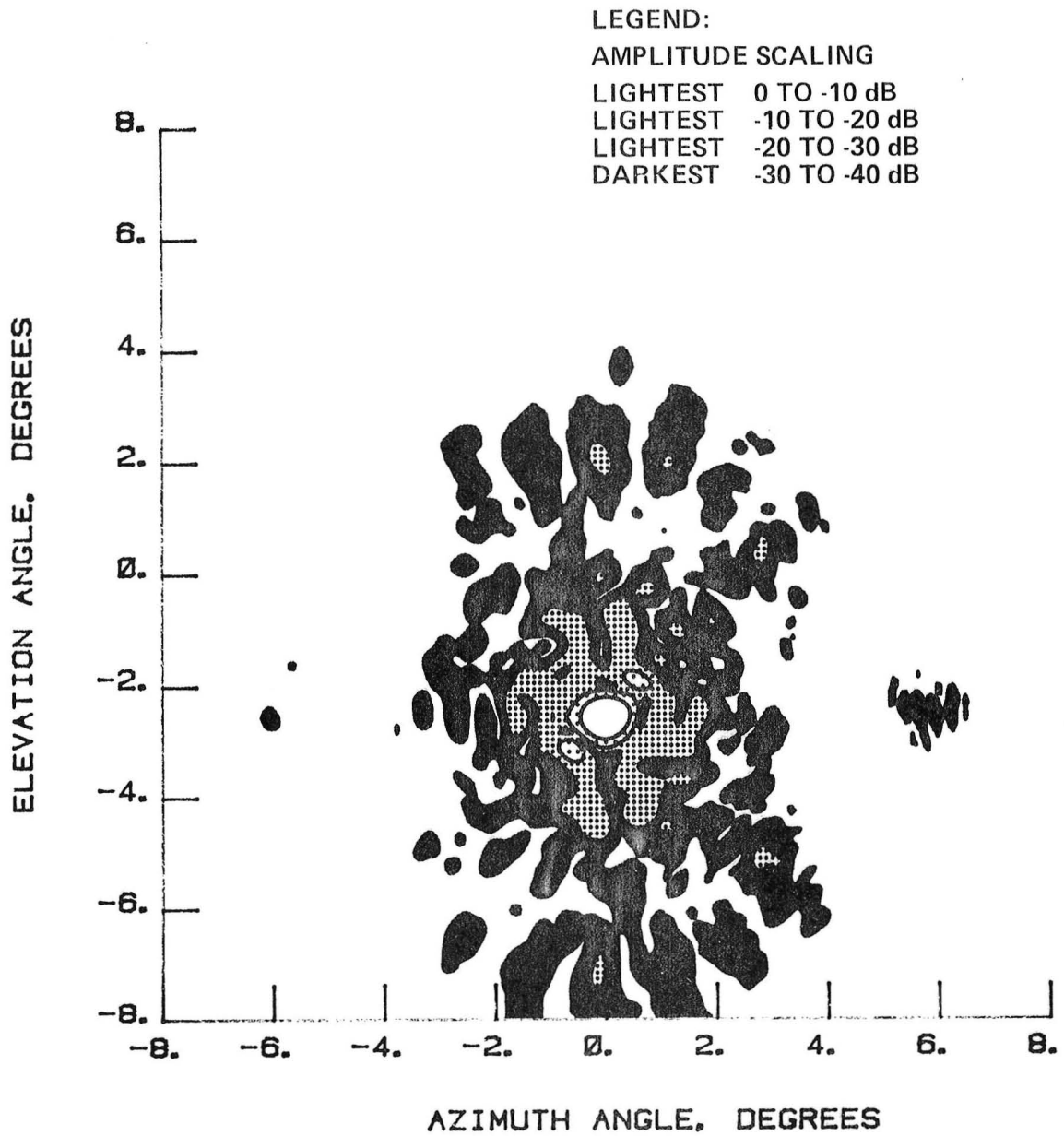

Figure 29 Test 3, 7.73 GHz, Co-Pol, Contour, Type 5

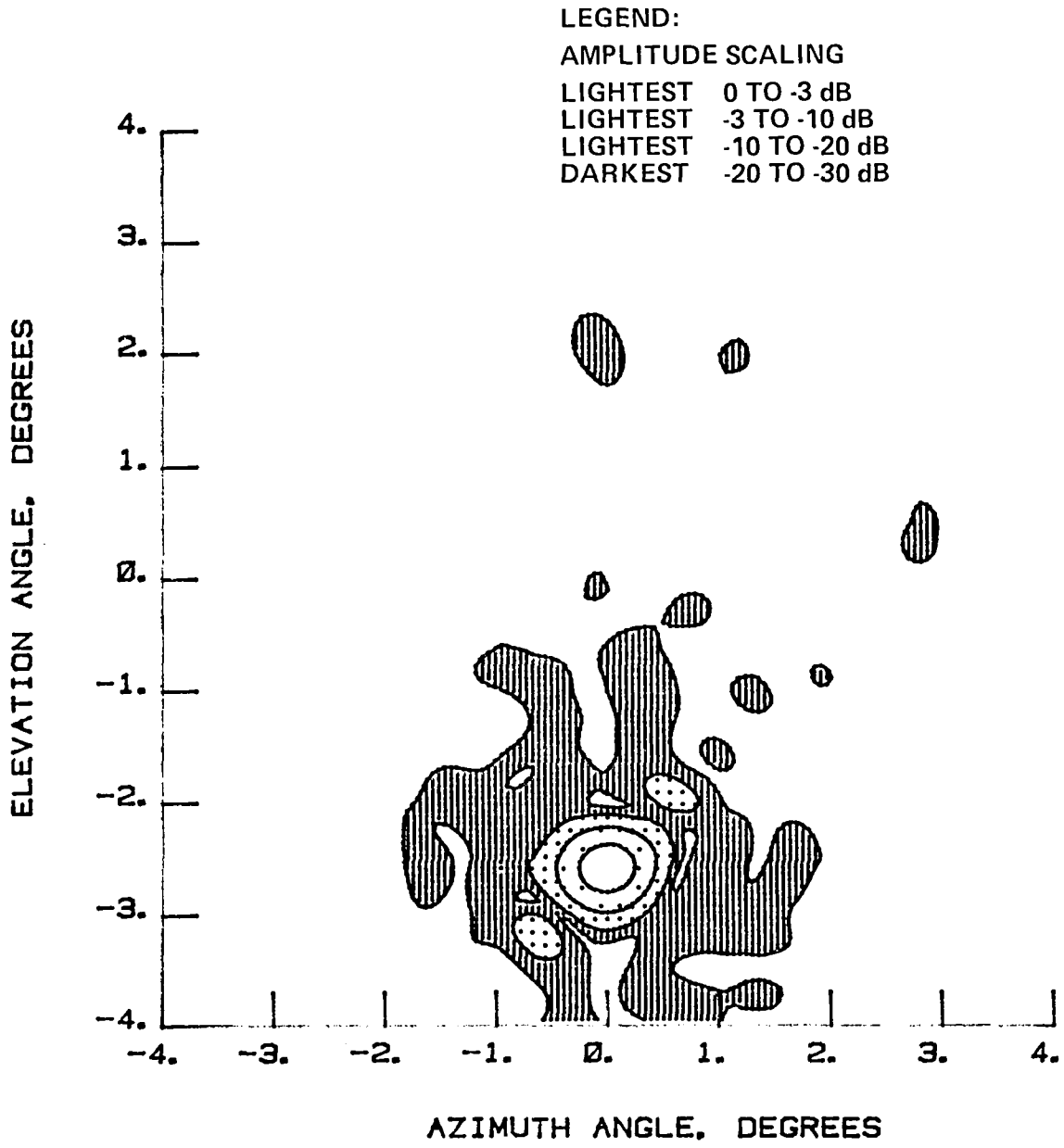

Figure 30 Test 3, 7.73 GHz, Co-Pol, Contour, Type 6

This Page Intentionally Left Blank

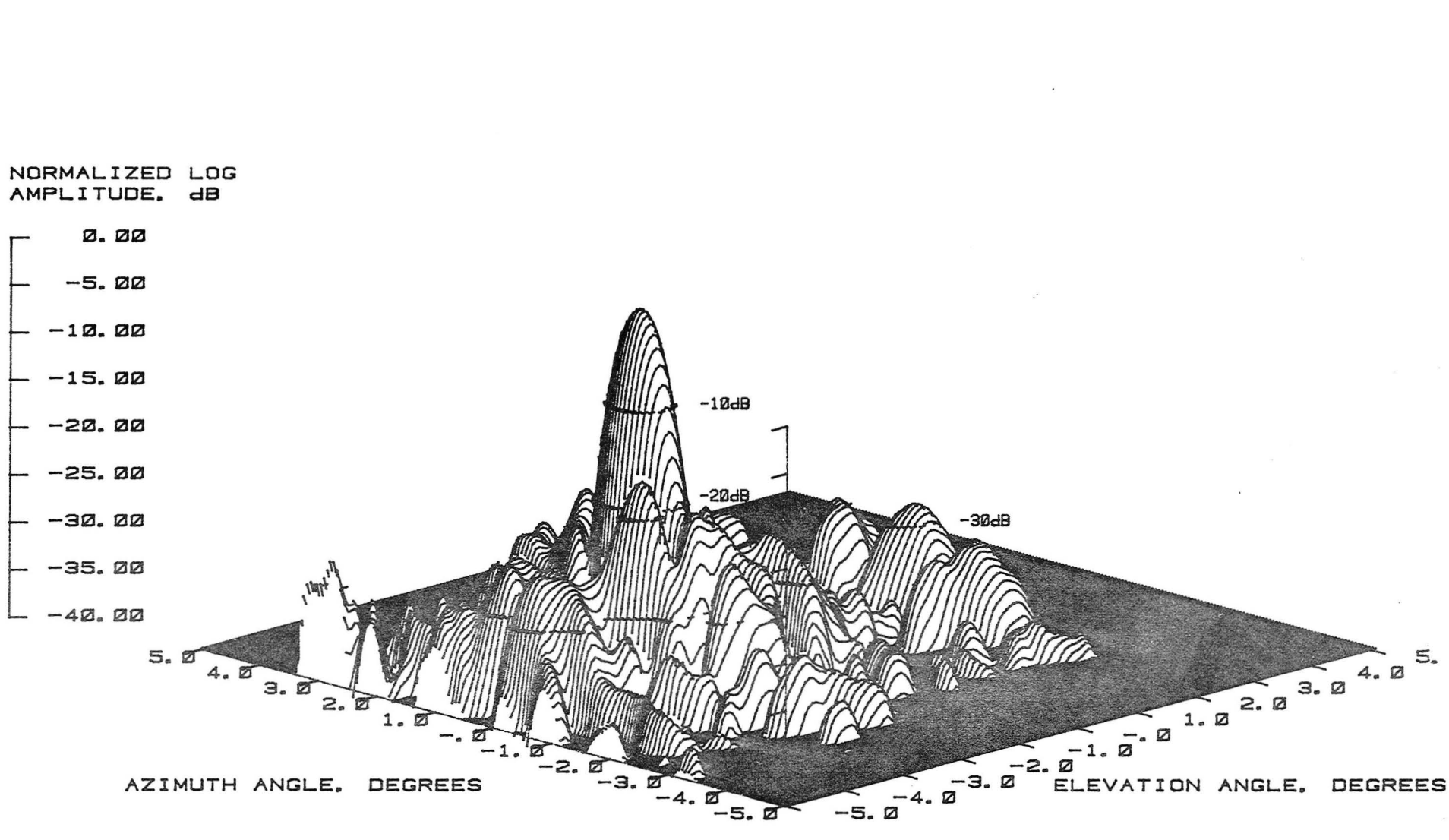

Figure 31 Test 3, 7.73 GHz, Co-Pol, 3-D, Type 7

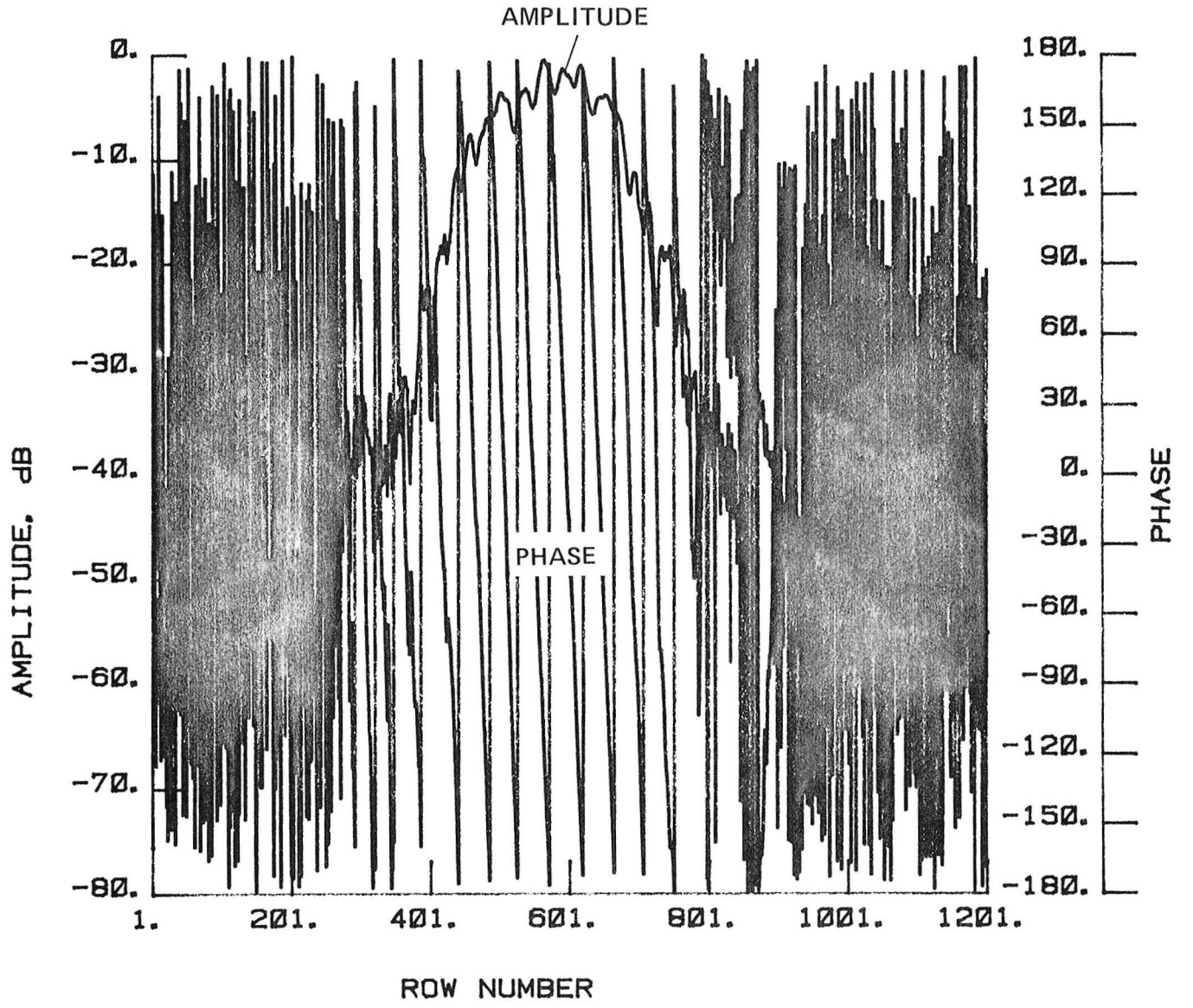

Figure 32 Test 3, 7.73 GHz, Co-Pol, H-Plane, Type 8

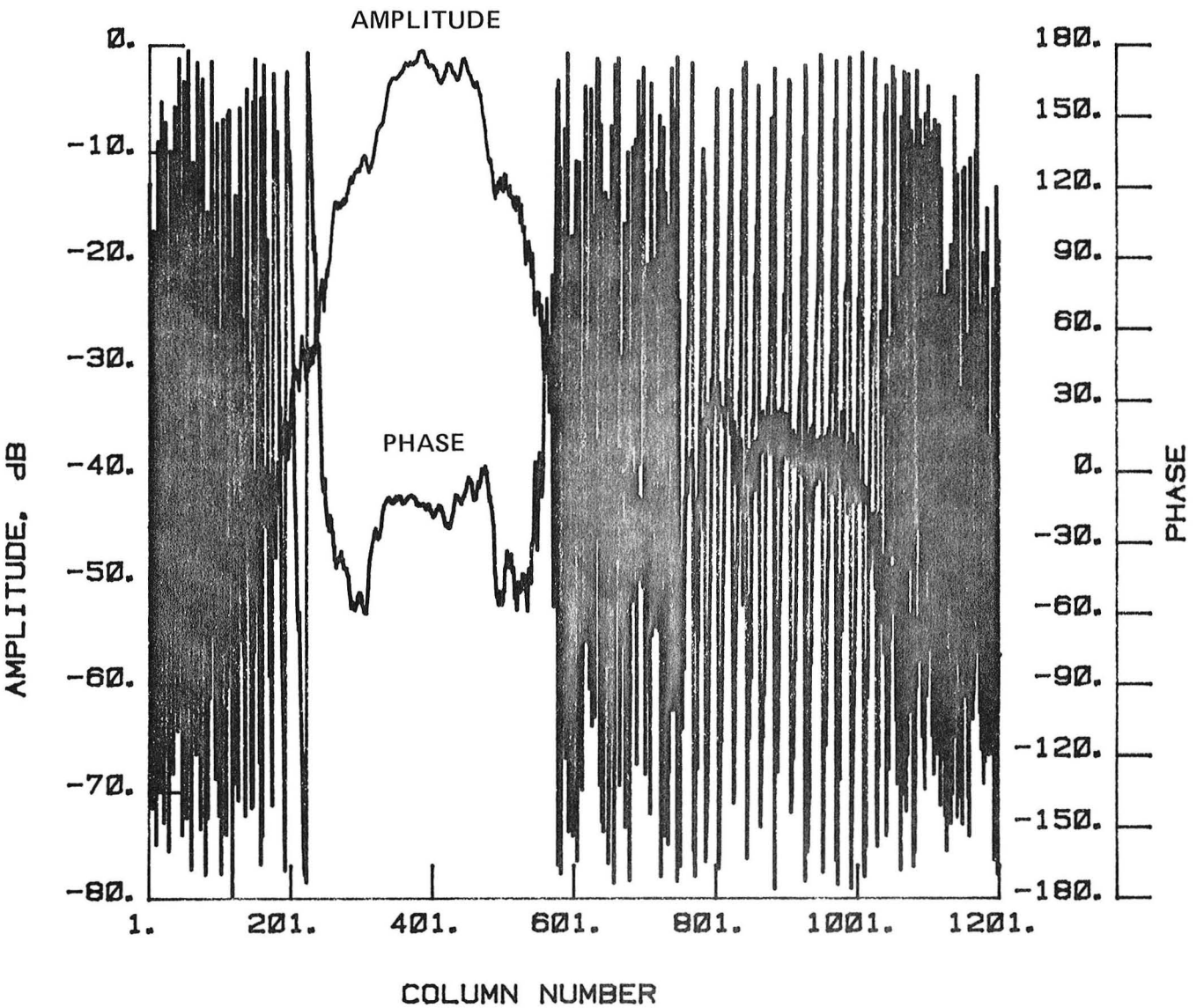

Figure 33 Test 3, 7.73 GHz, Co-Pol, E-Plane, Type 9

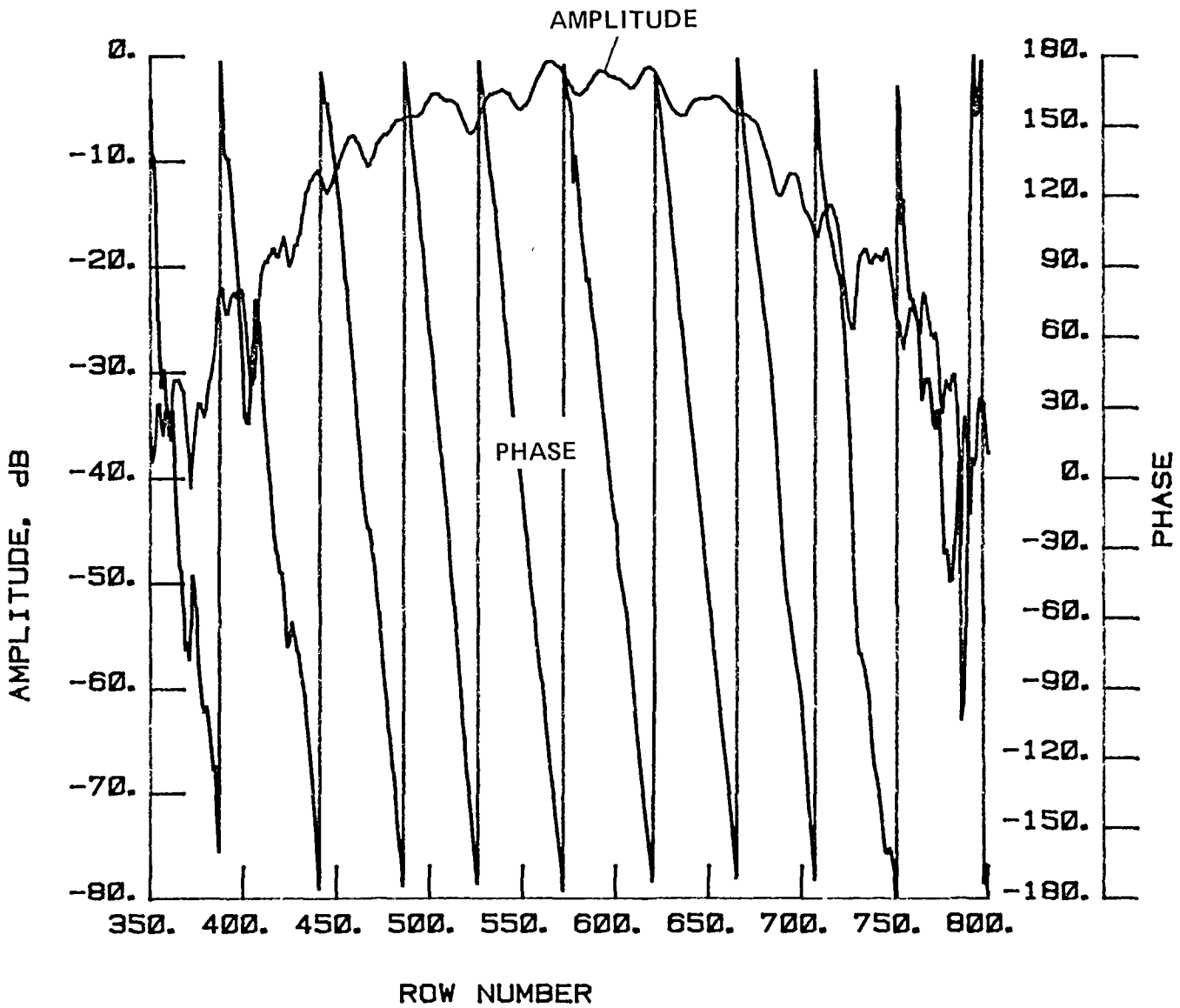

Figure 34 Test 3, 7.73 GHz, Co-Pol, H-Plane, Type 10

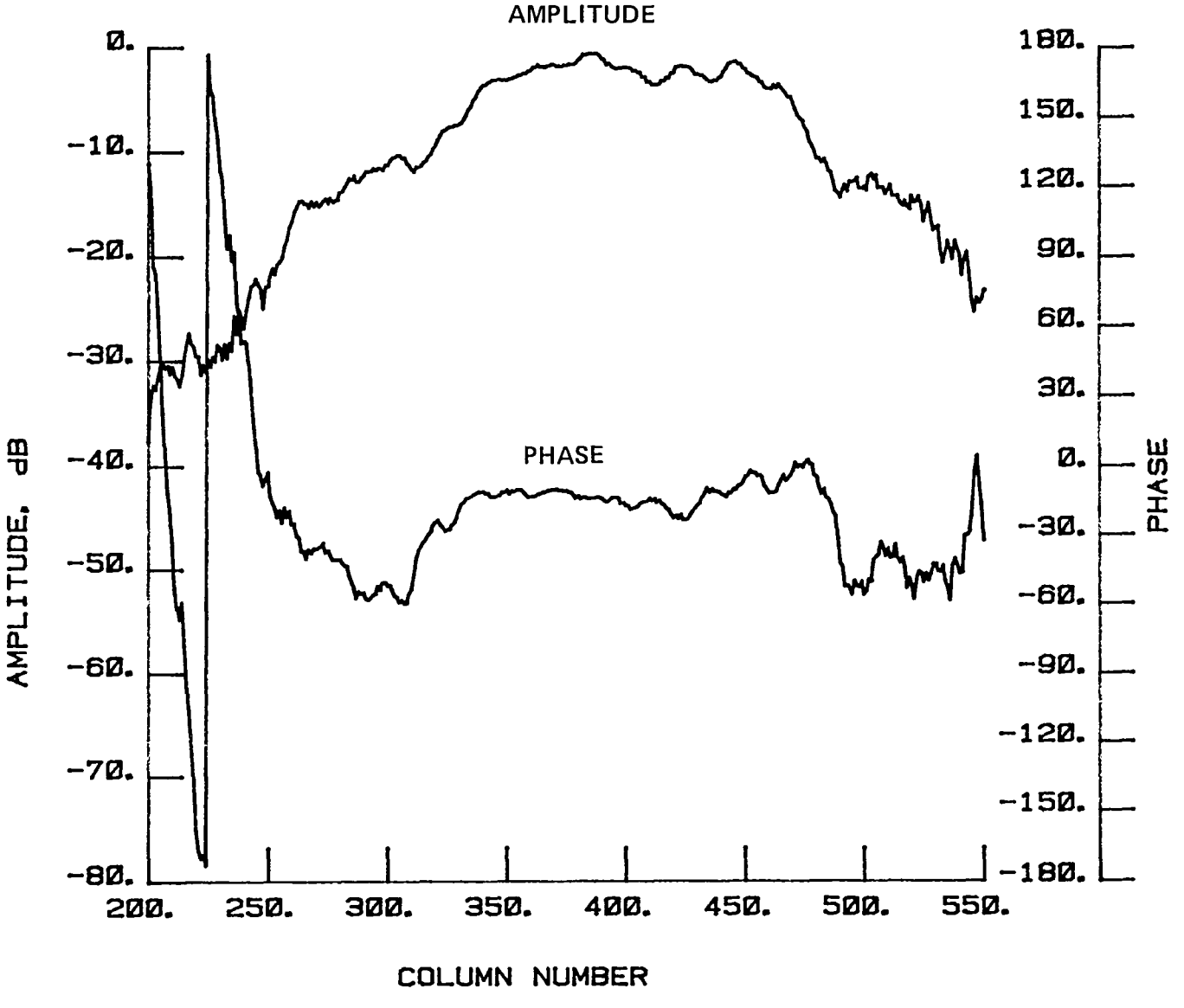

Figure 35 Test 3, 7.73 GHz, Co-Pol, E-Plane, Type 11

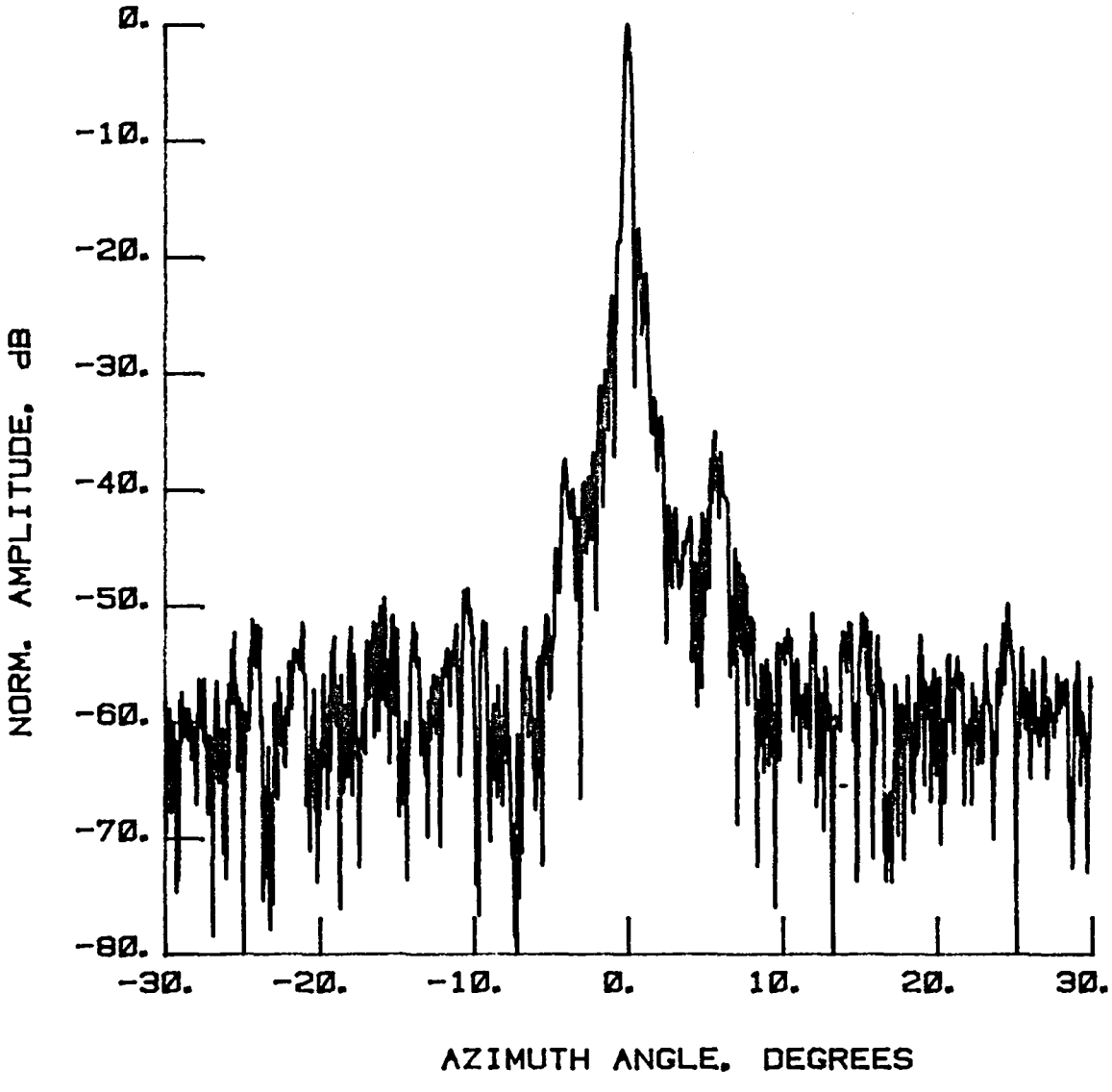

Figure 36 Test 4, 11.60 GHz, Co-Pol, E-Plane, Type 1

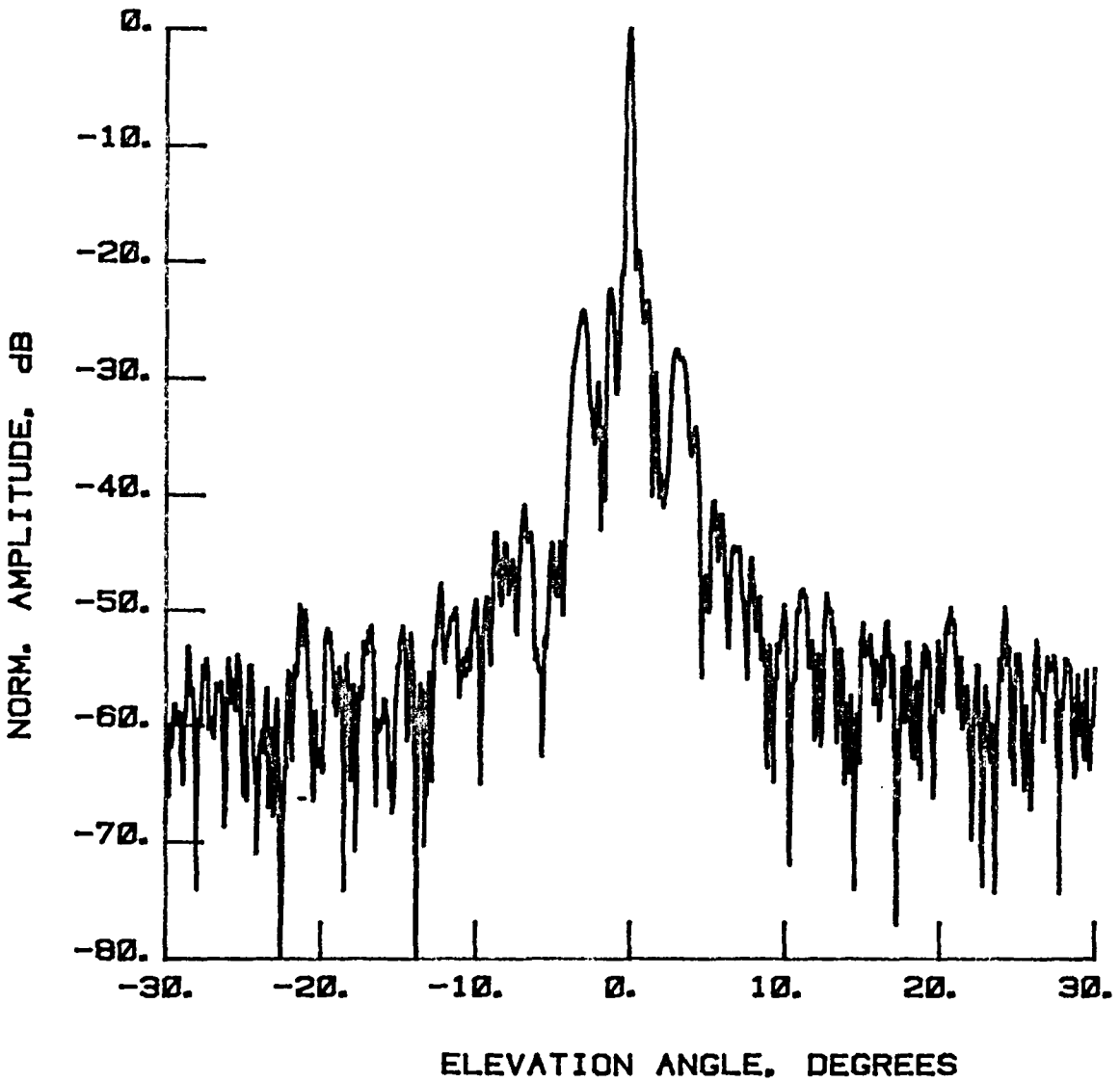

Figure 37 Test 4, 11.60 GHz, Co-Pol, H-Plane, Type 2

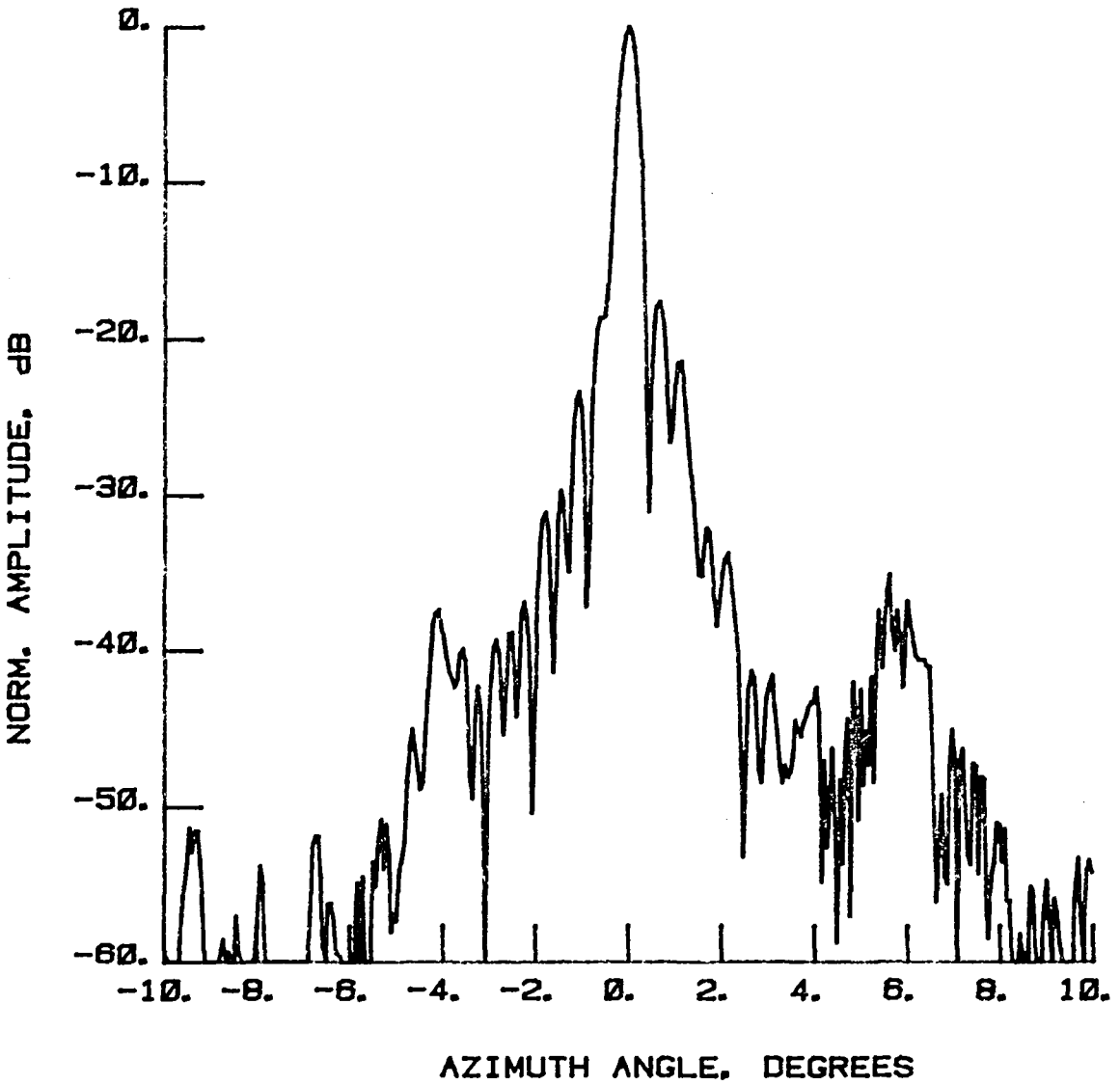

Figure 38 Test 4, 11.60 GHz, Co-Pol, E-Plane, Type 3

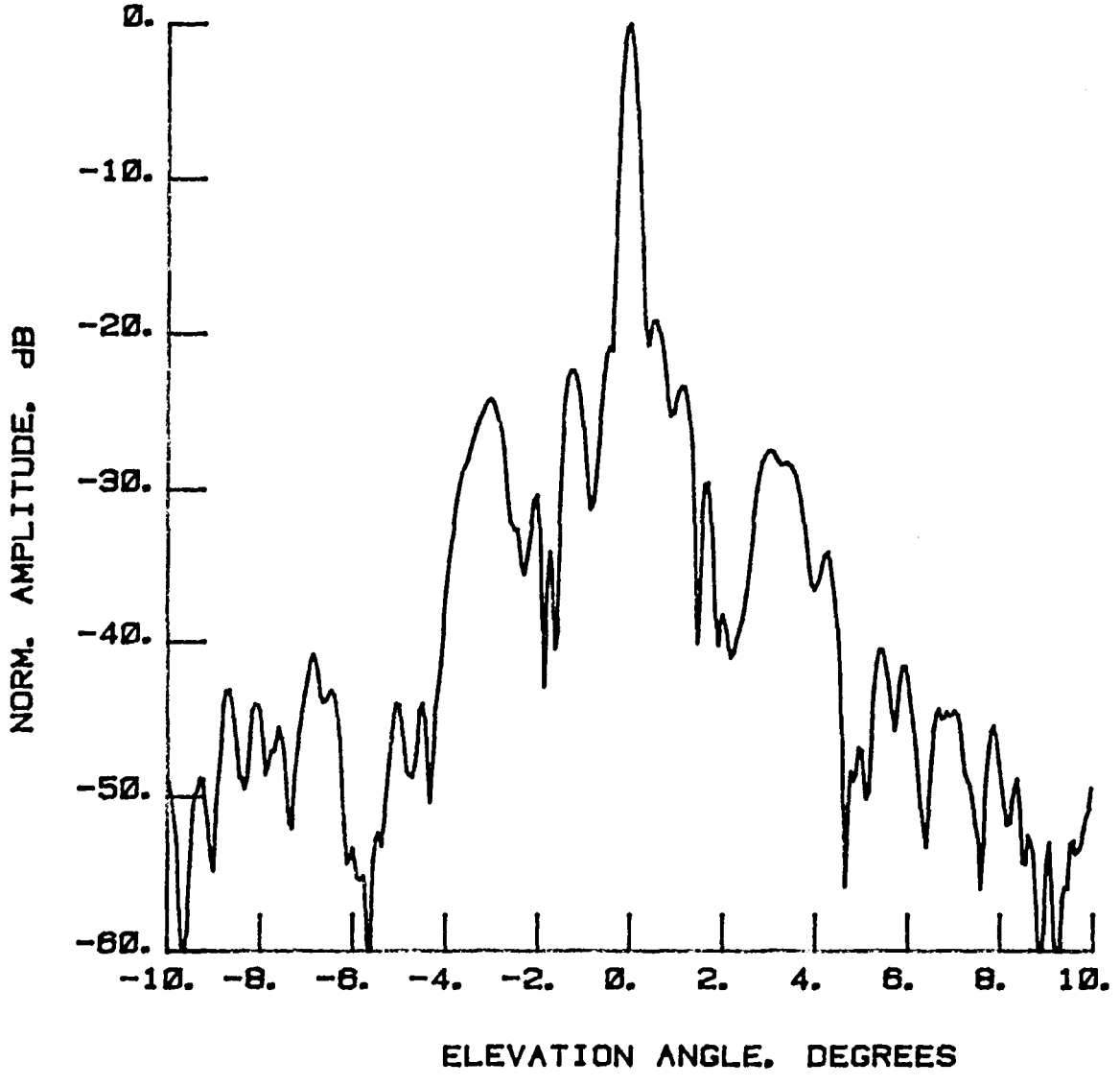

Figure 39 Test 4, 11.60 GHz, Co-Pol, H-Plane, Type 4

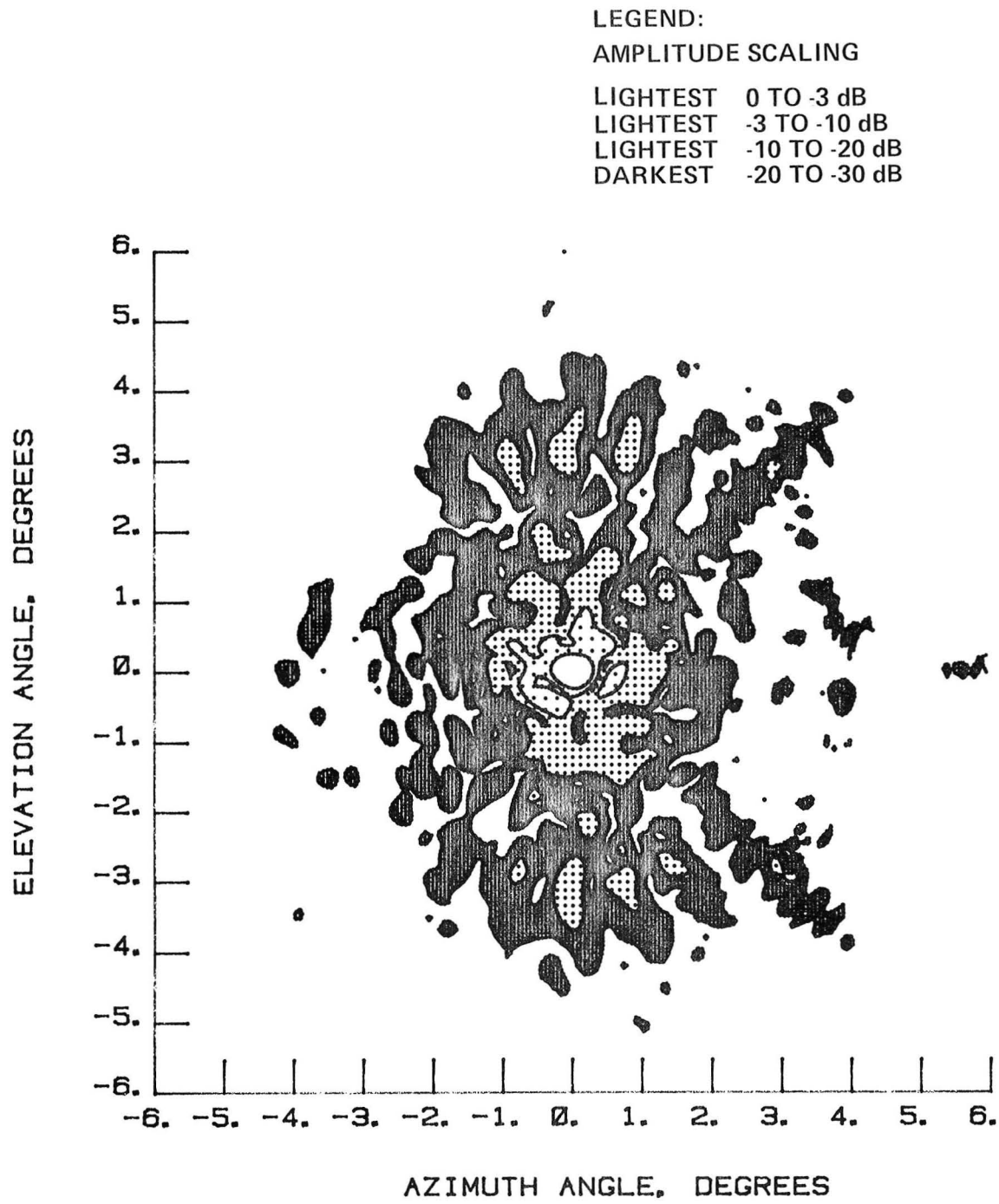

Figure 40 Test 4, 11.60 GHz, Co-Pol, Contour, Type 5

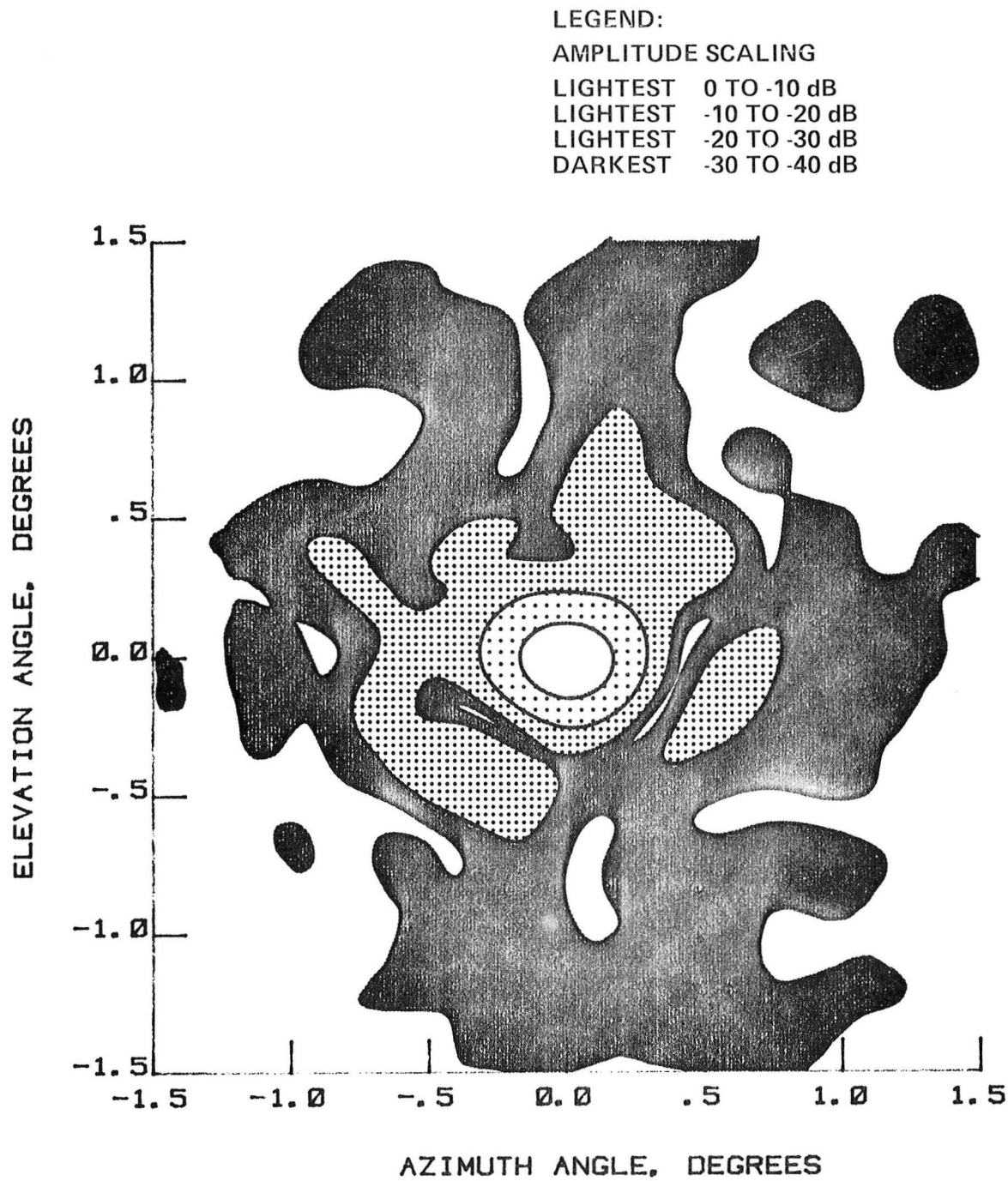

Figure 41 Test 4, 11.60 GHz, Co-Pol, Contour, Type 6

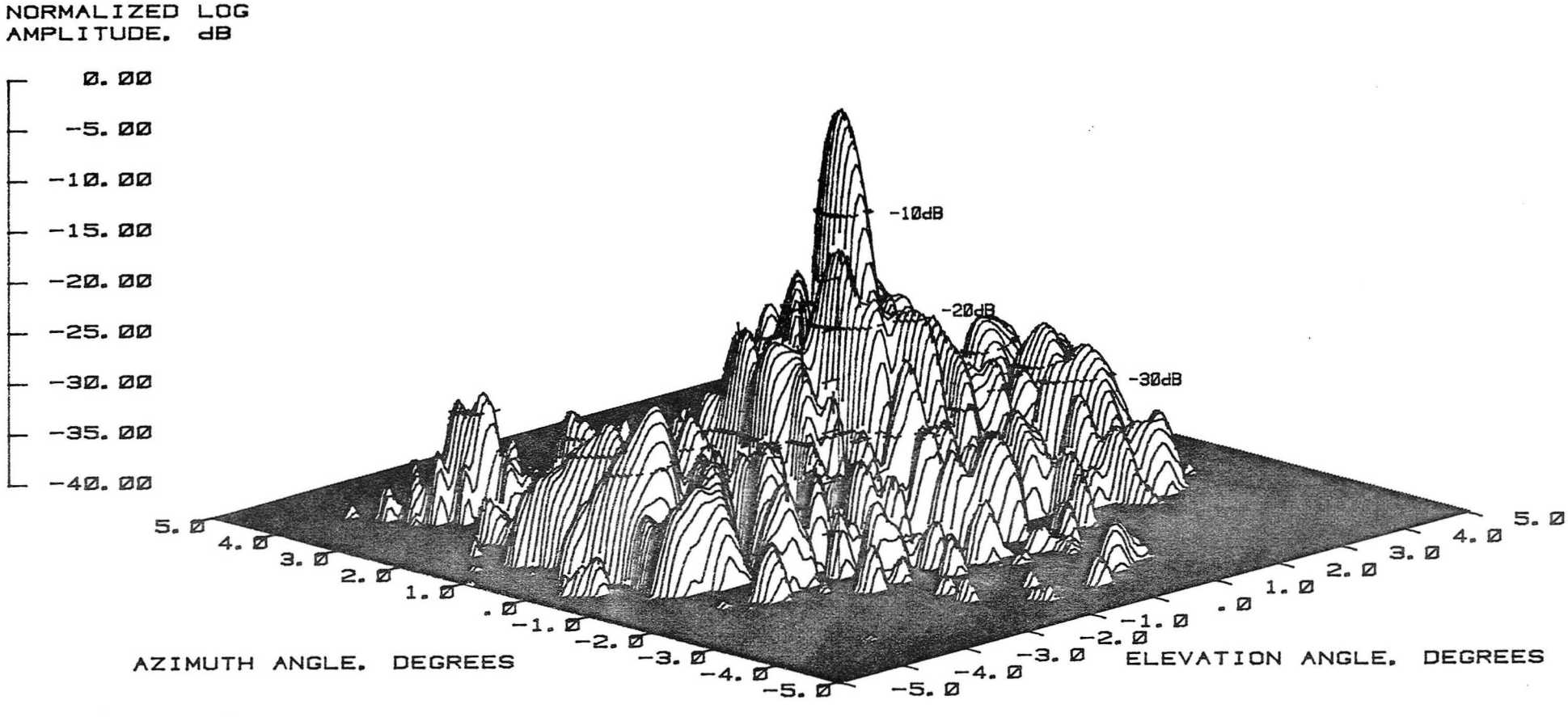

Figure 42 Test 4, 11.60 GHz, Co-Pol, 3-D, Type 7

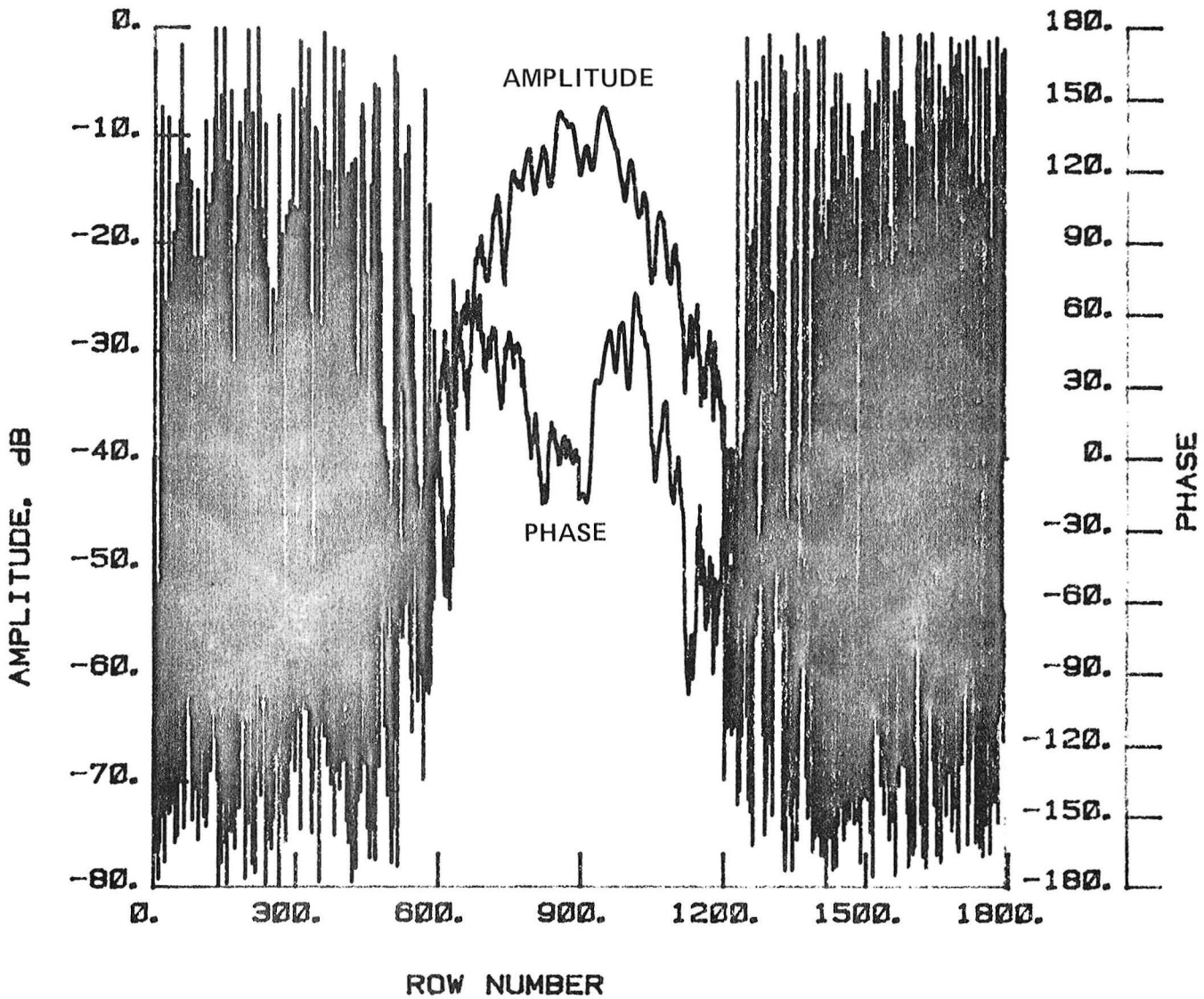

Figure 43 Test 4, 11.60 GHz, Co-Pol, H-Plane, Type 8

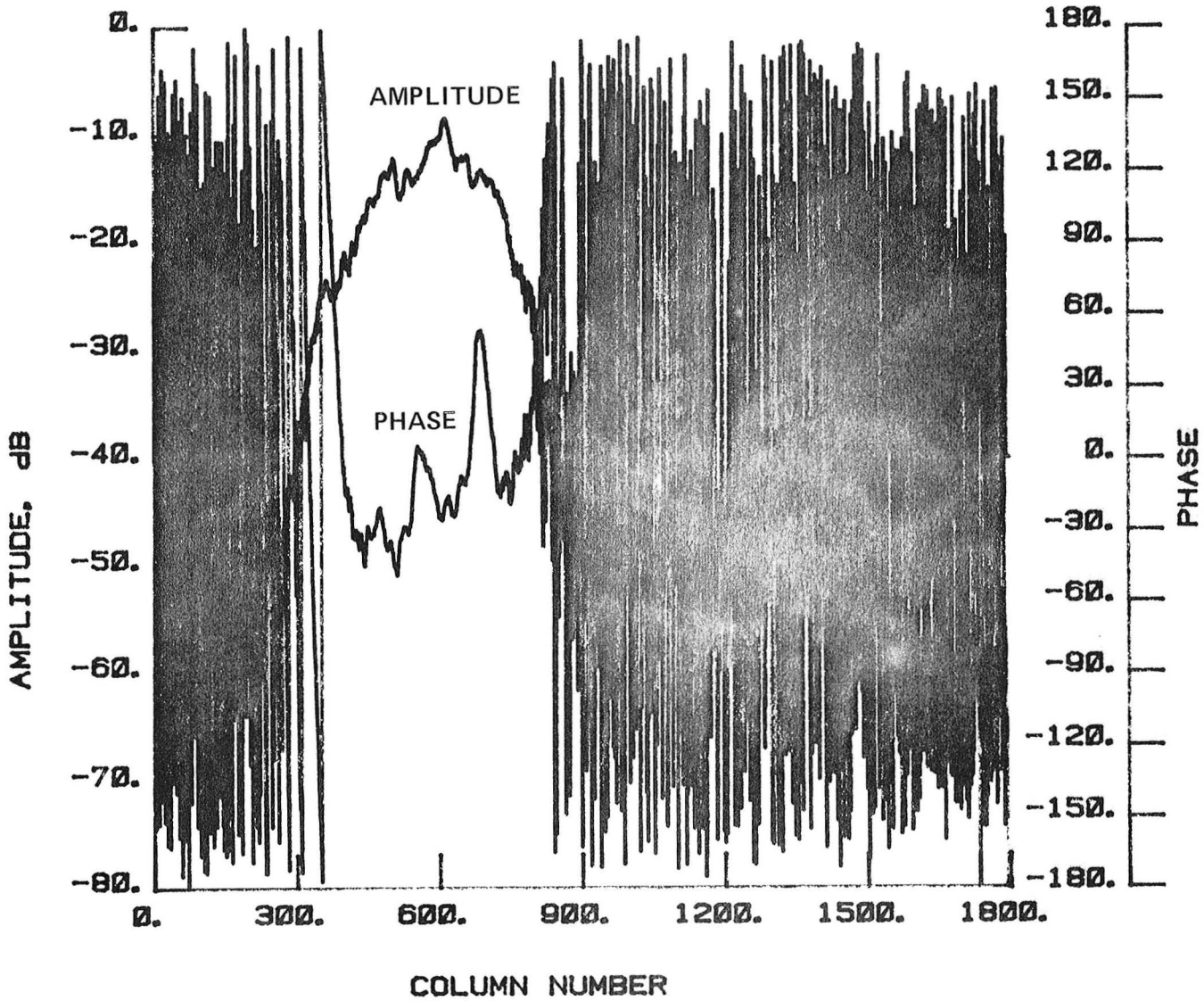

Figure 44 Test 4, 11.60 GHz, Co-Pol, E-Plane, Type 9

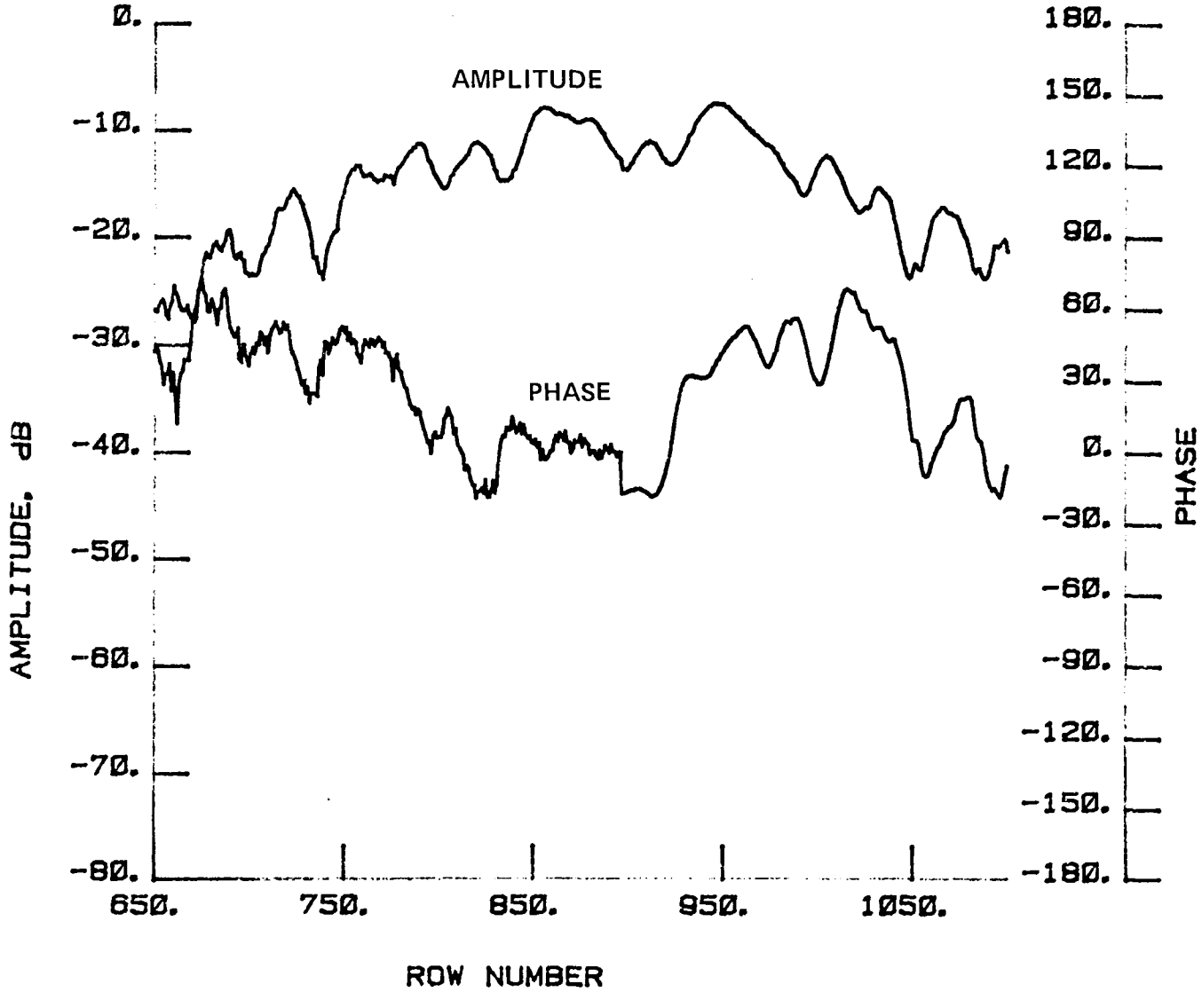

Figure 45 Test 4, 11.60 GHz, Co-Pol, H-Plane, Type 10

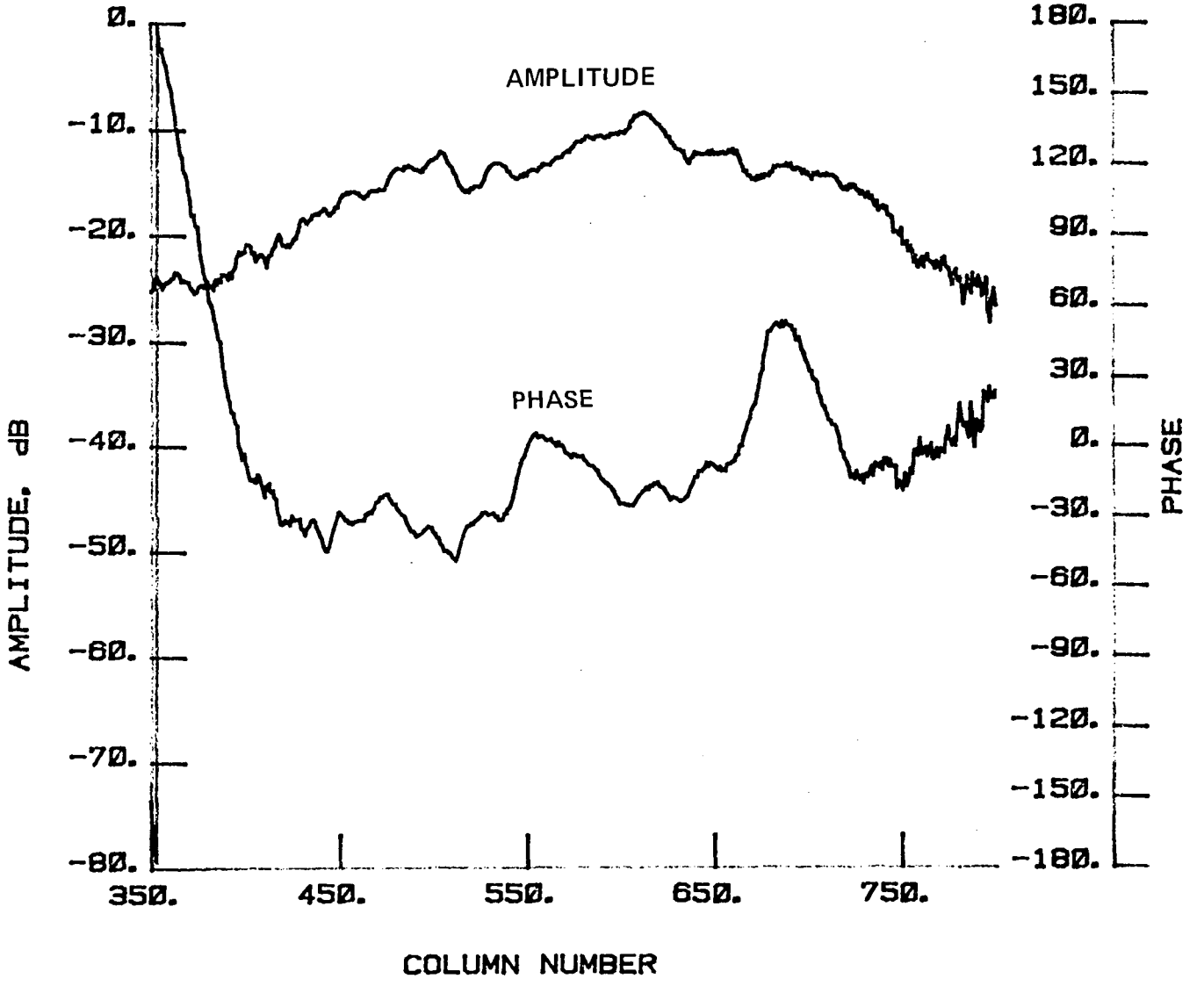

Figure 46 Test 4, 11.60 GHz, Co-Pol, E-Plane, Type 11

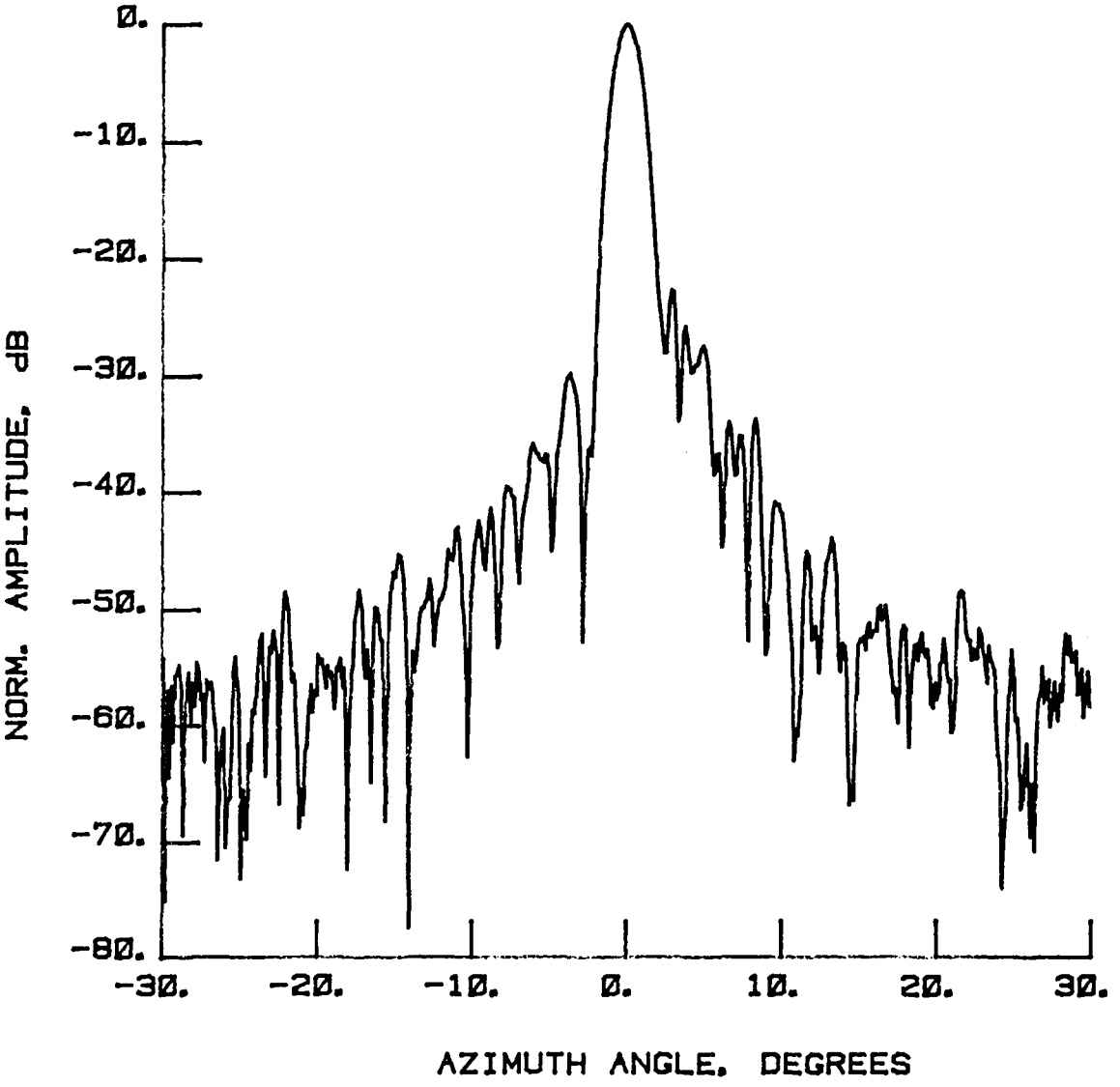

Figure 47 Test 5, 2.27 GHz, Co-Pol, E-Plane, Type 1

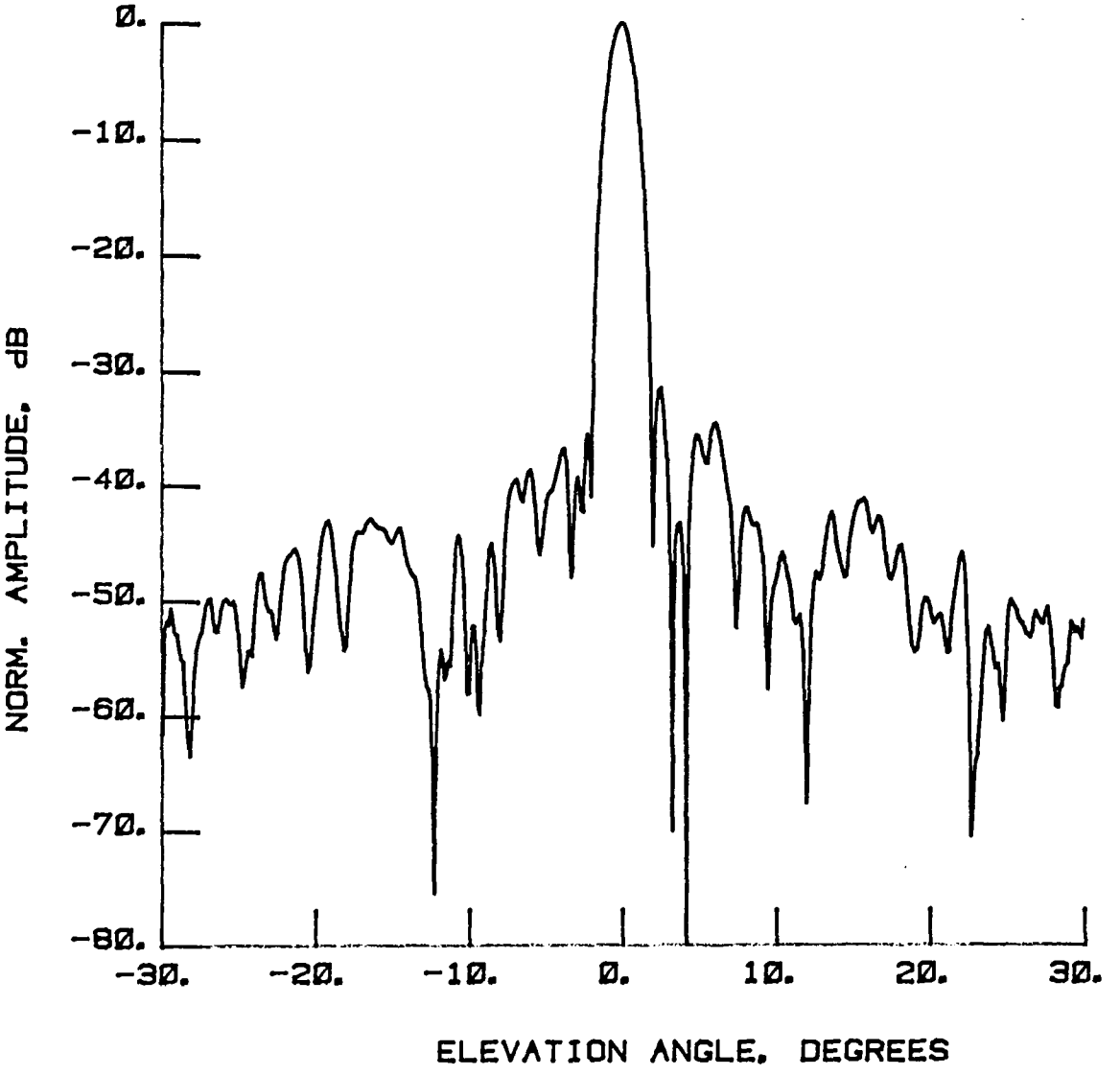

Figure 48 Test 5, 2.27 GHz, Co-Pol, H-Plane, Type 2

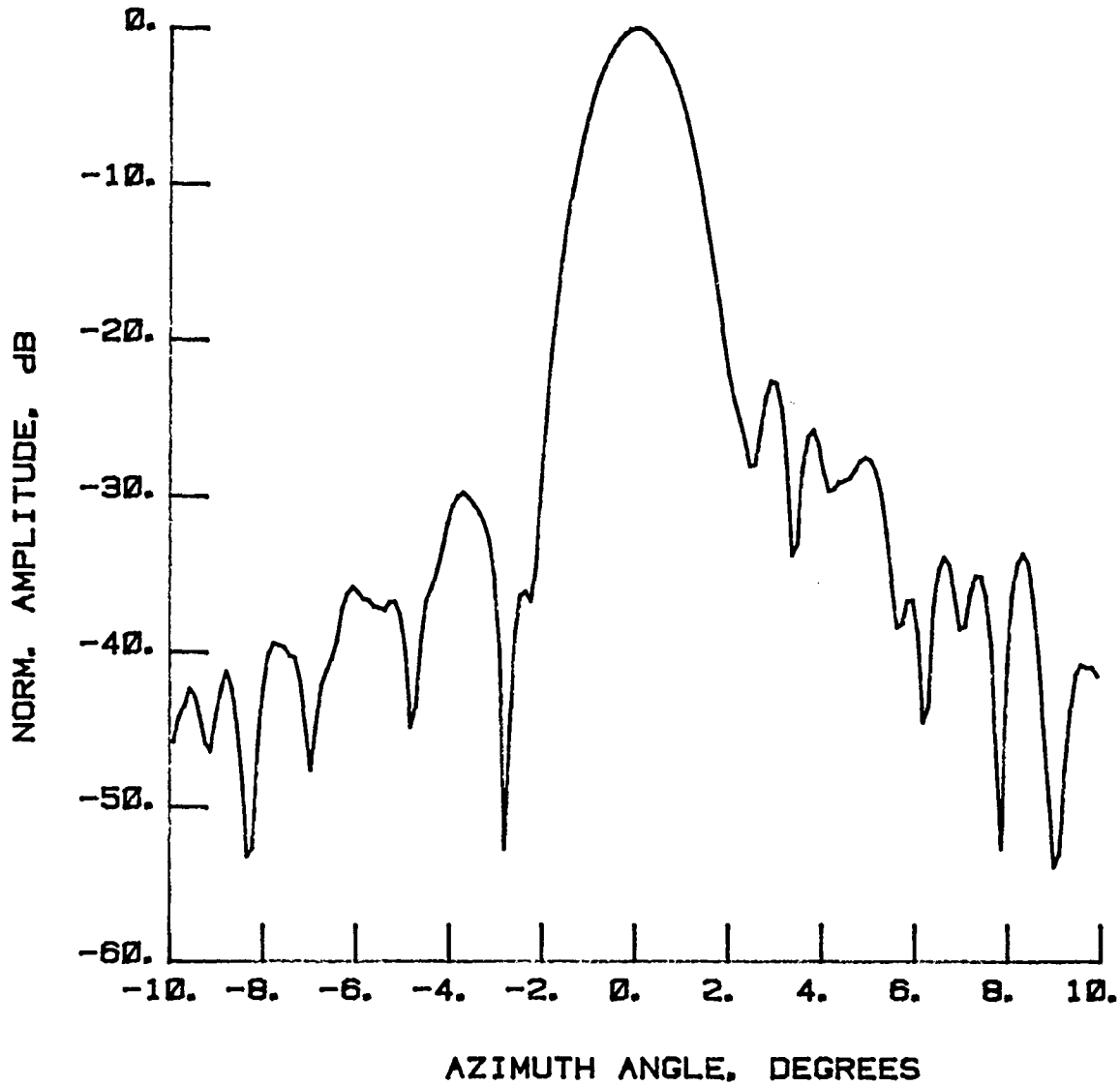

Figure 49 Test 5, 2.27 GHz, Co-Pol, E-Plane, Type 3

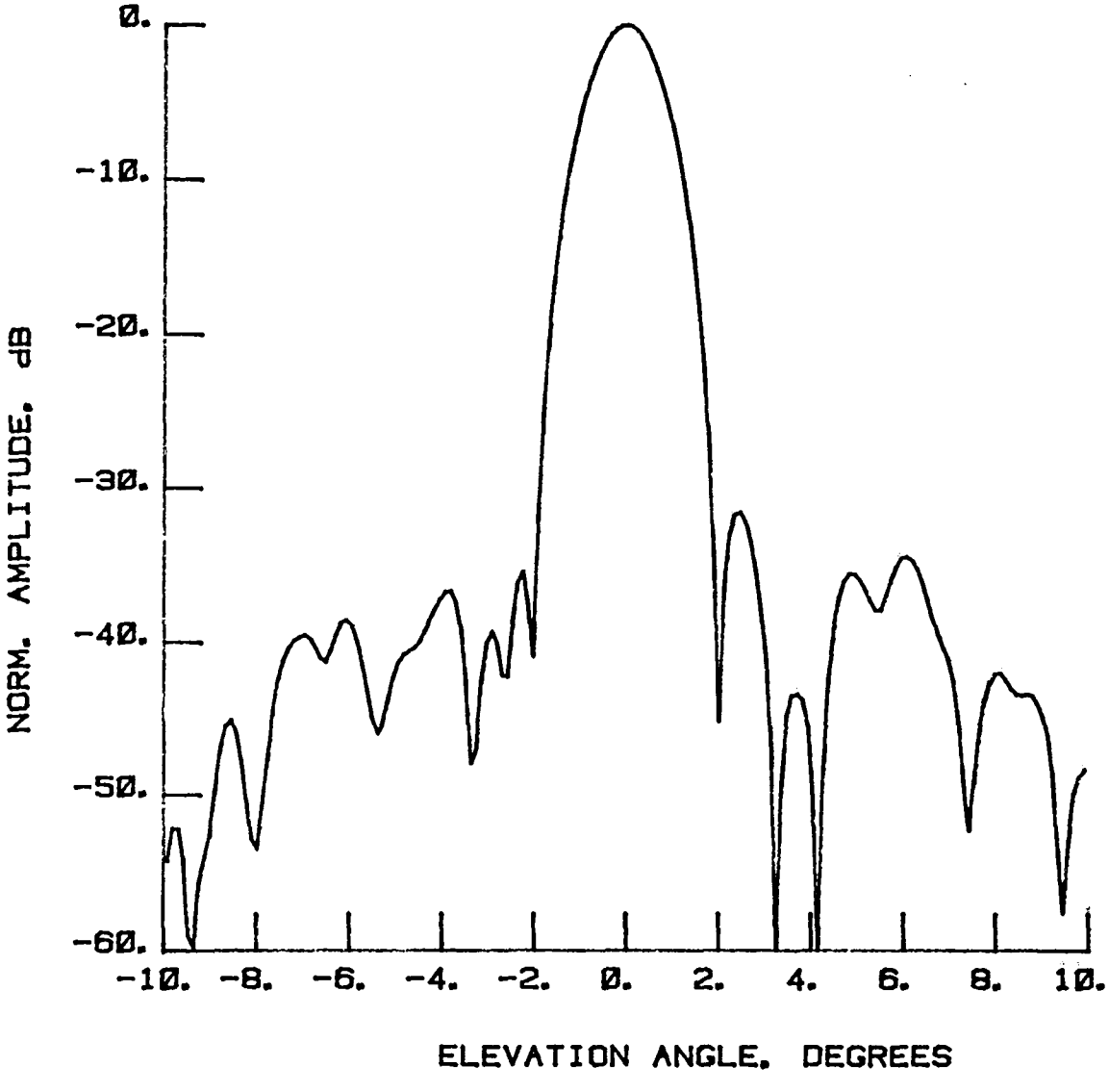

Figure 50 Test 5, 2.27 GHz, Co-Pol, H-Plane, Type 4

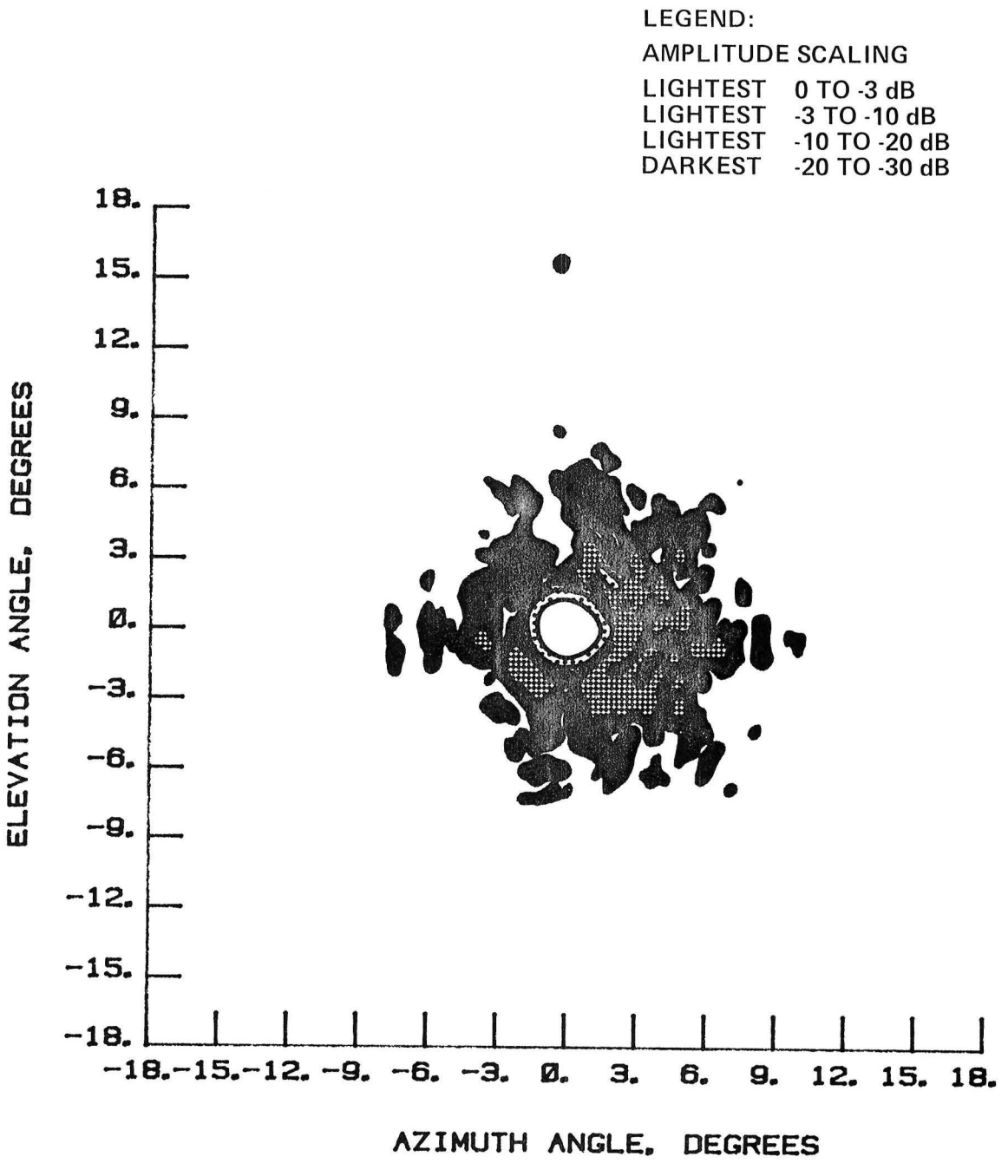

Figure 51 Test 5, 2.27 GHz, Co-Pol, Contour, Type 5

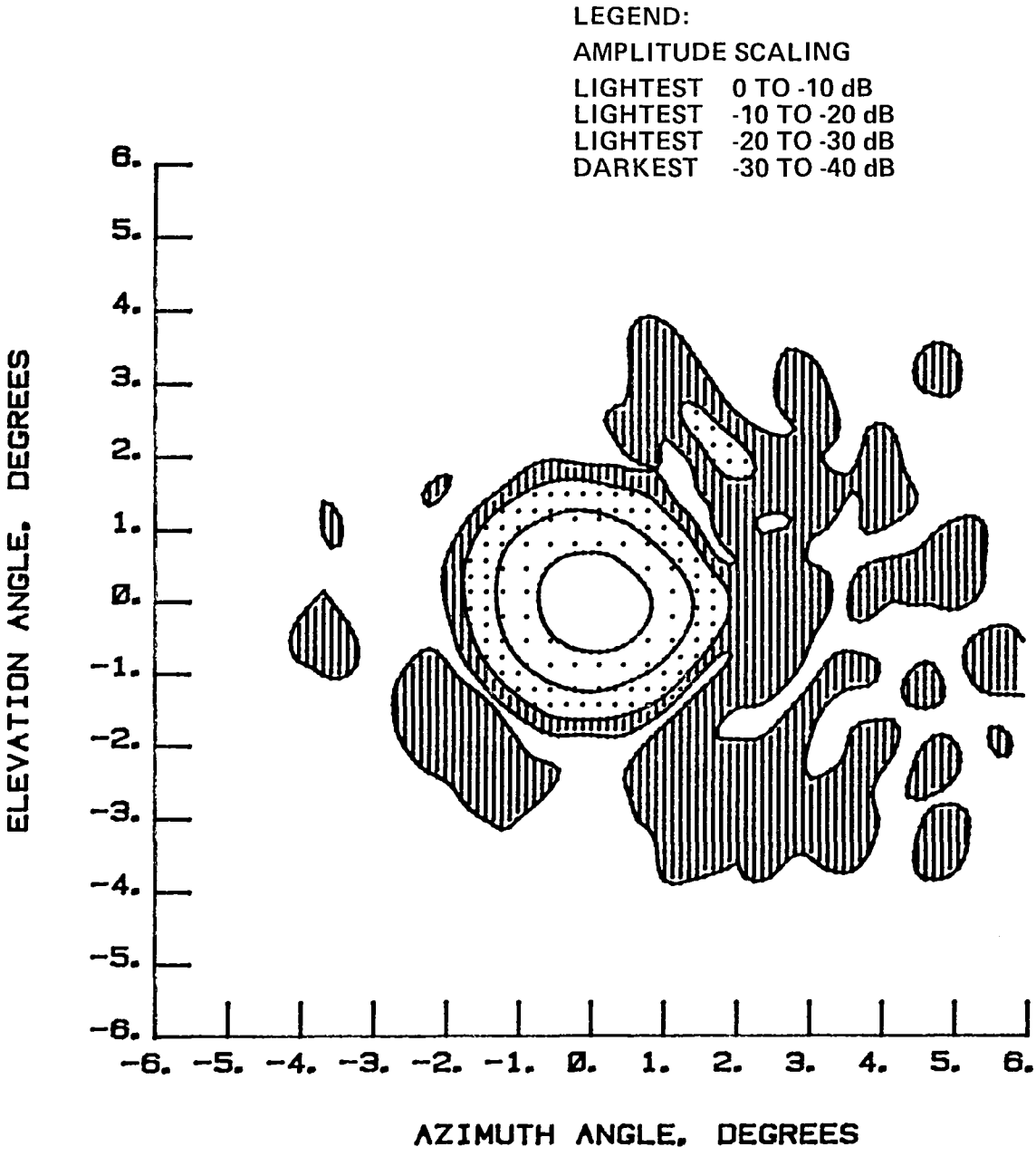

Figure 52 Test 5, 2.27 GHz, Co-Pol, Contour, Type 6

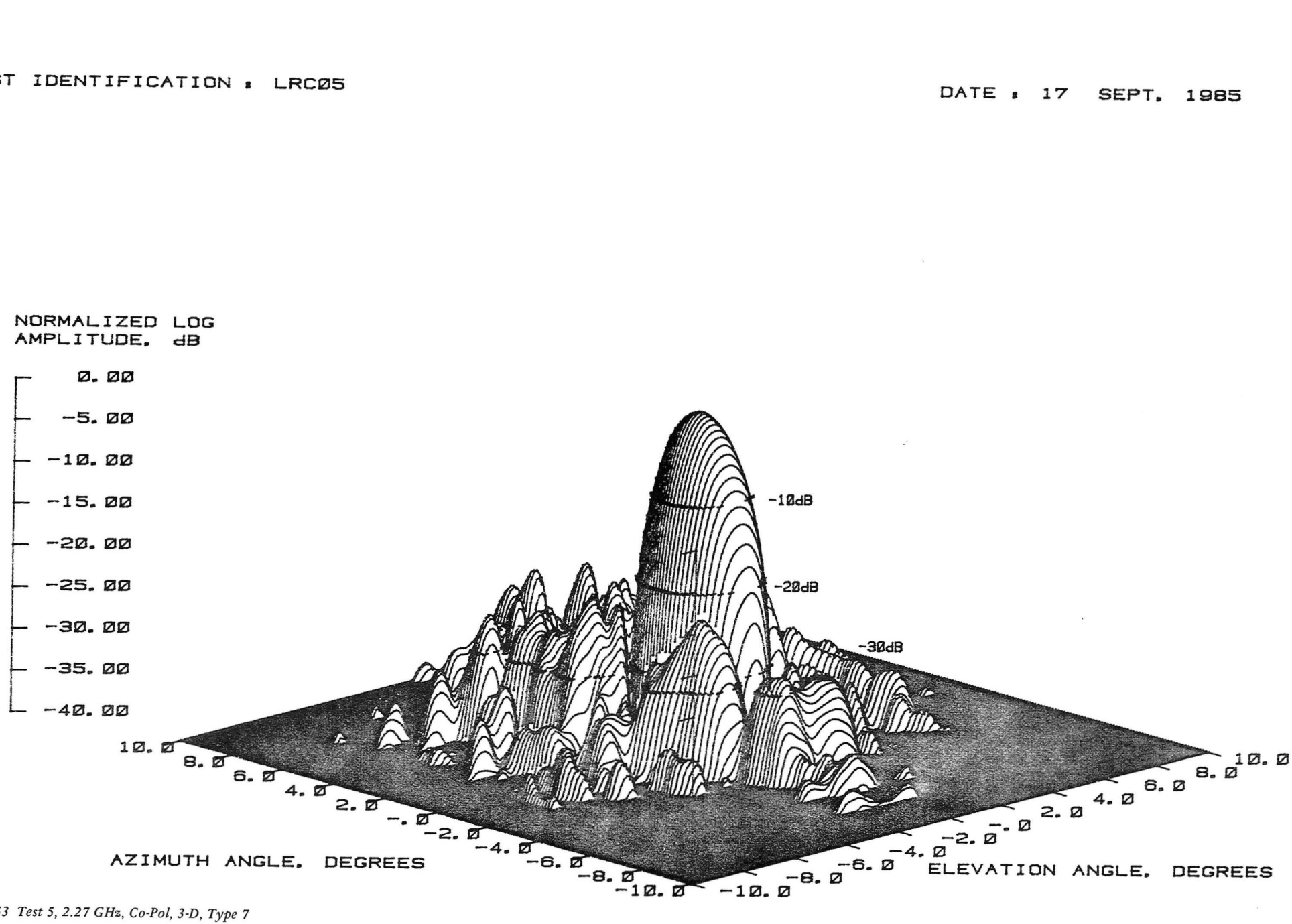

Figure 53 Test 5, 2.27 GHz, Co-Pol, 3-D, Type 7

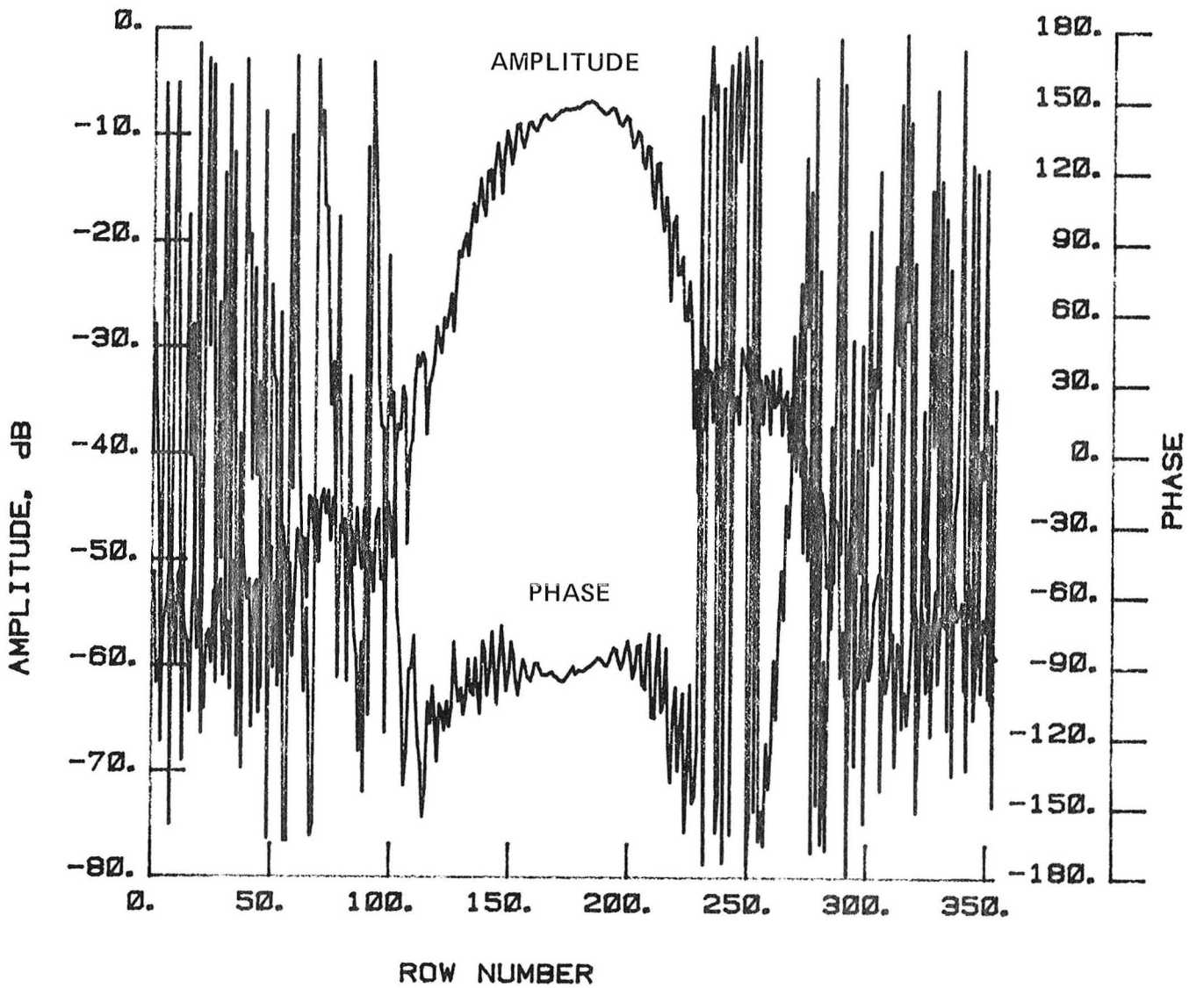

Figure 54 Test 5, 2.27 GHz, Co-Pol, H-Plane, Type 8

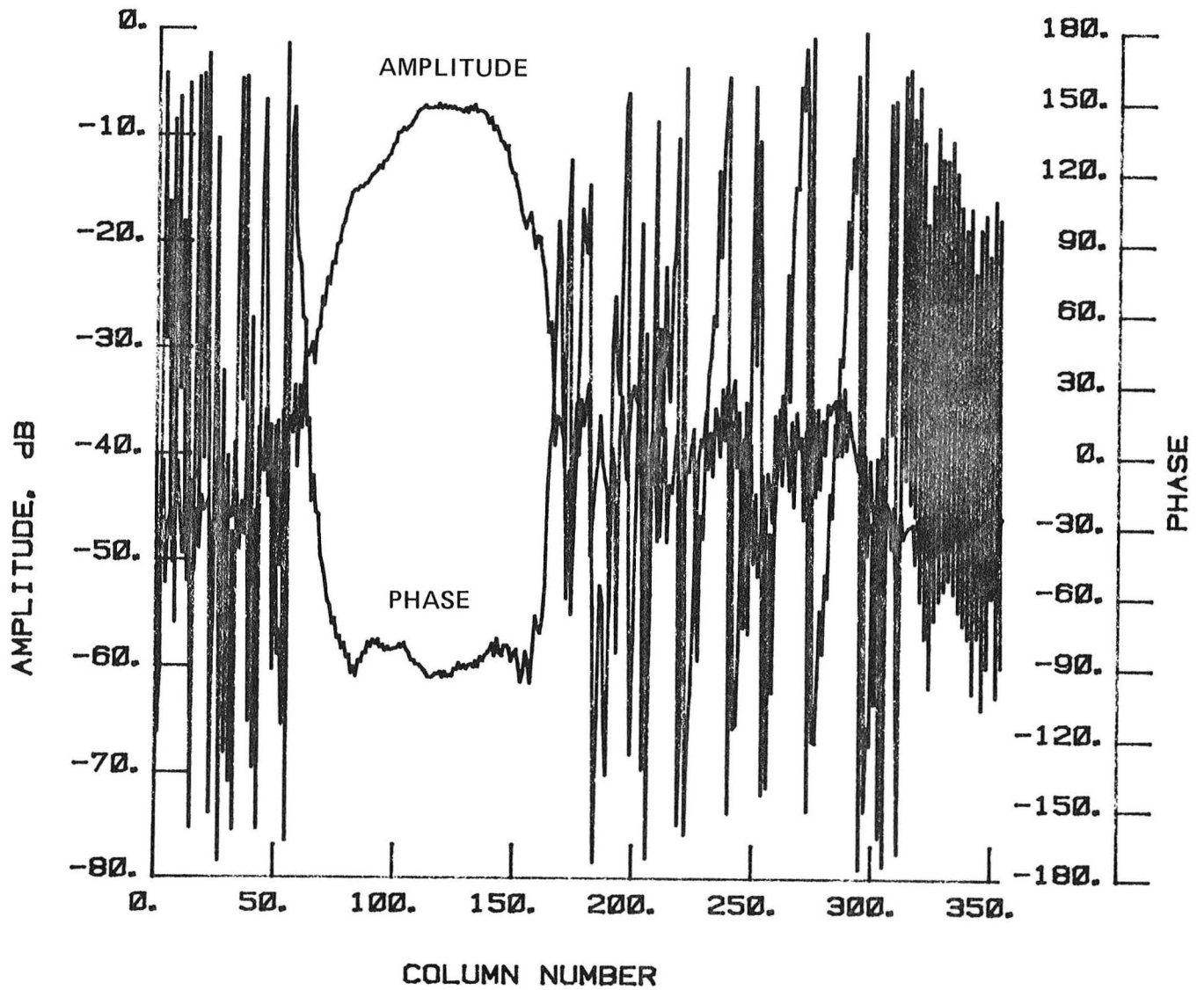

Figure 55 Test 5, 2.27 GHz, Co-Pol, E-Plane, Type 9

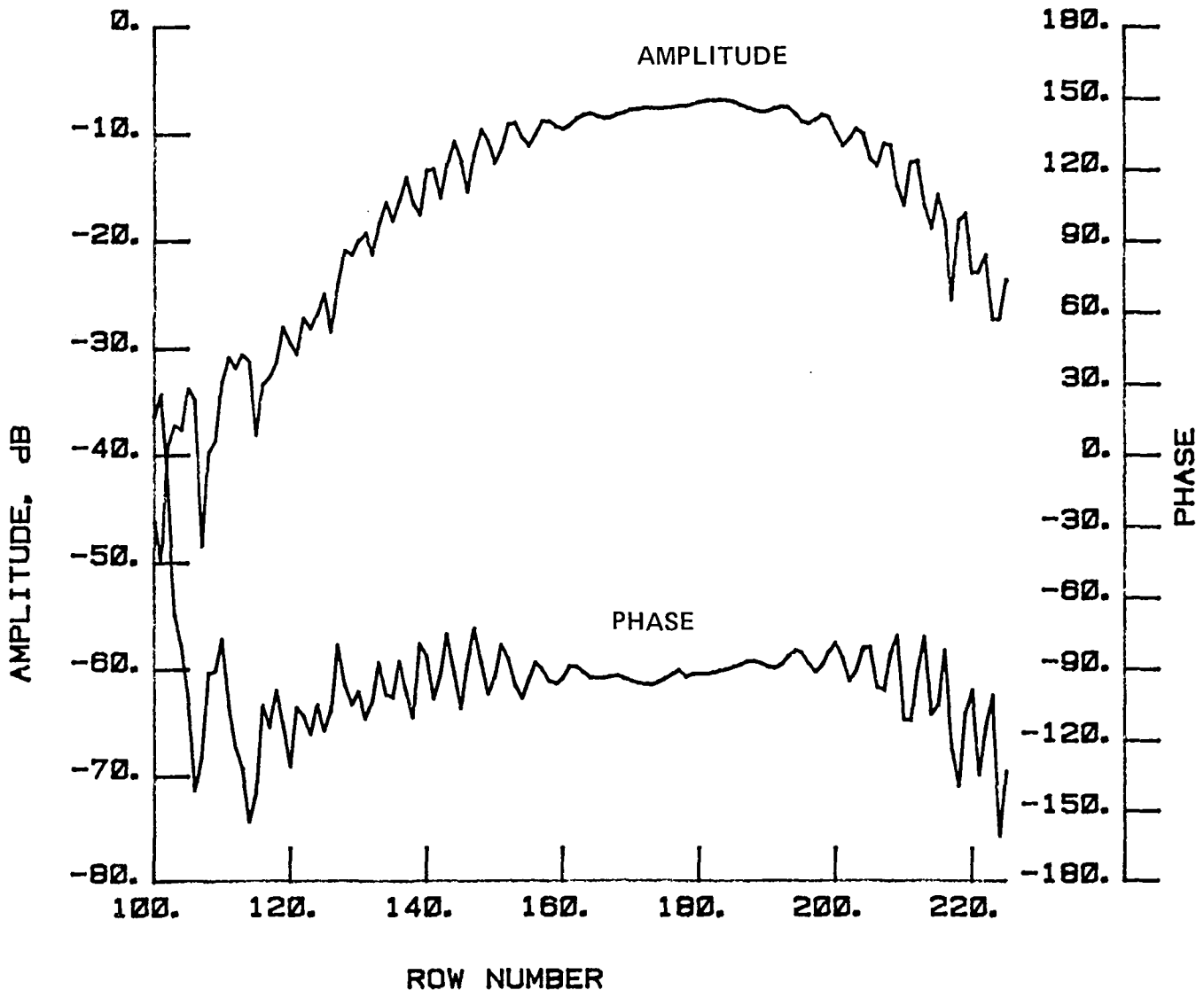

Figure 56 Test 5, 2.27 GHz, Co-Pol, H-Plane, Type 10

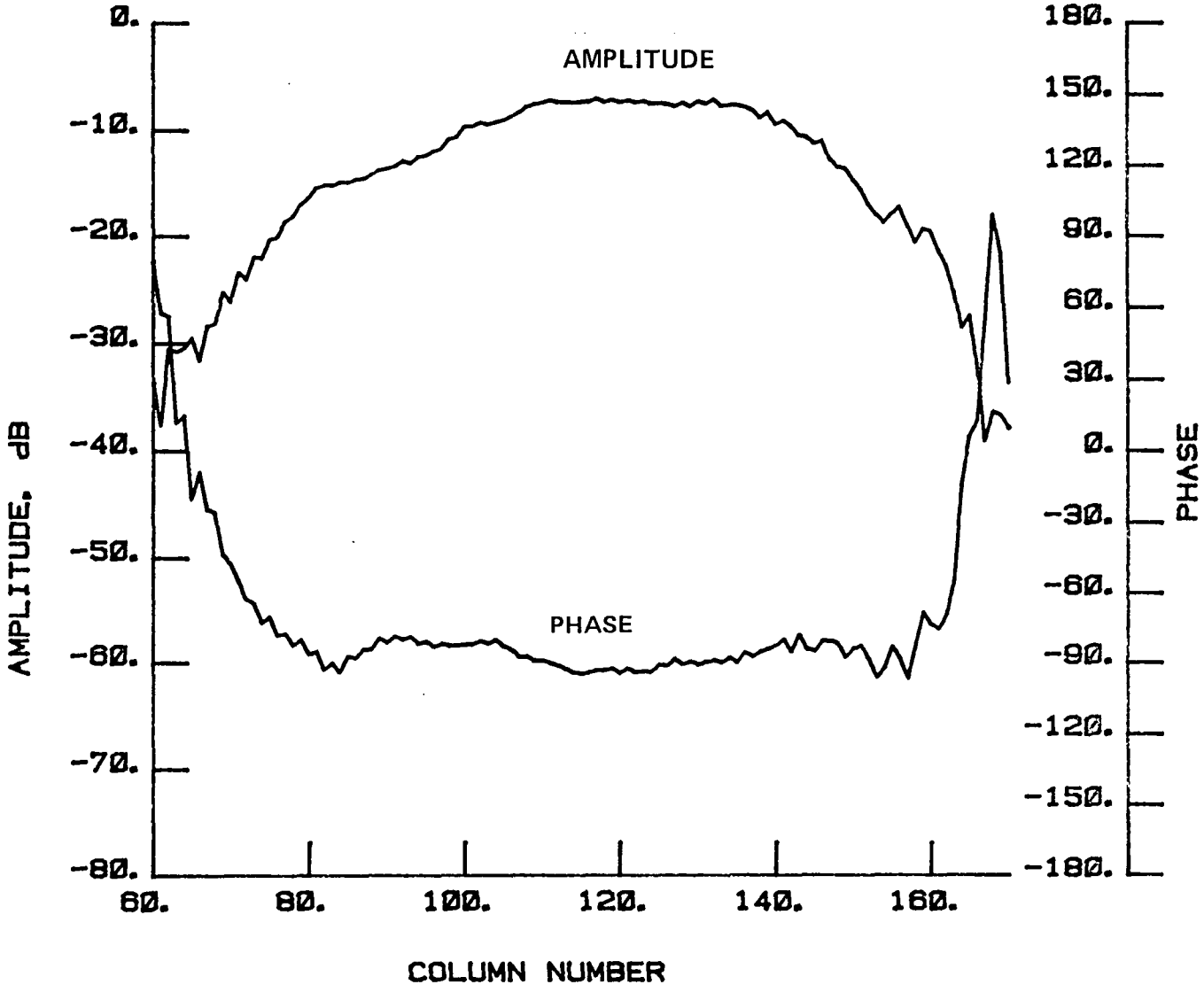

Figure 57 Test 5, 2.27 GHz, Co-Pol, E-Plane, Type 11

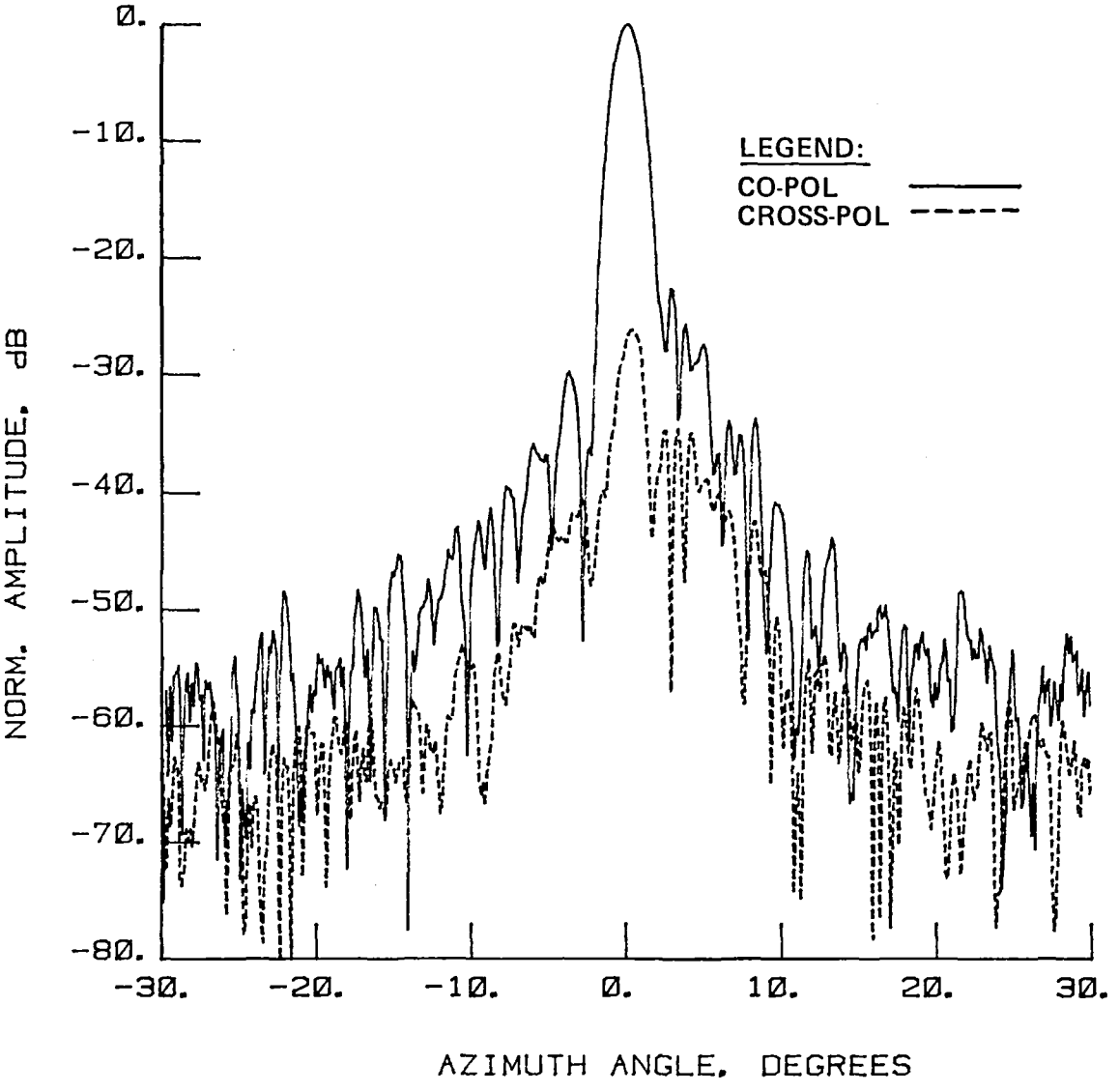

Figure 58 Test 6, 2.27 GHz, Cross-Pol, E-Plane, Type 12

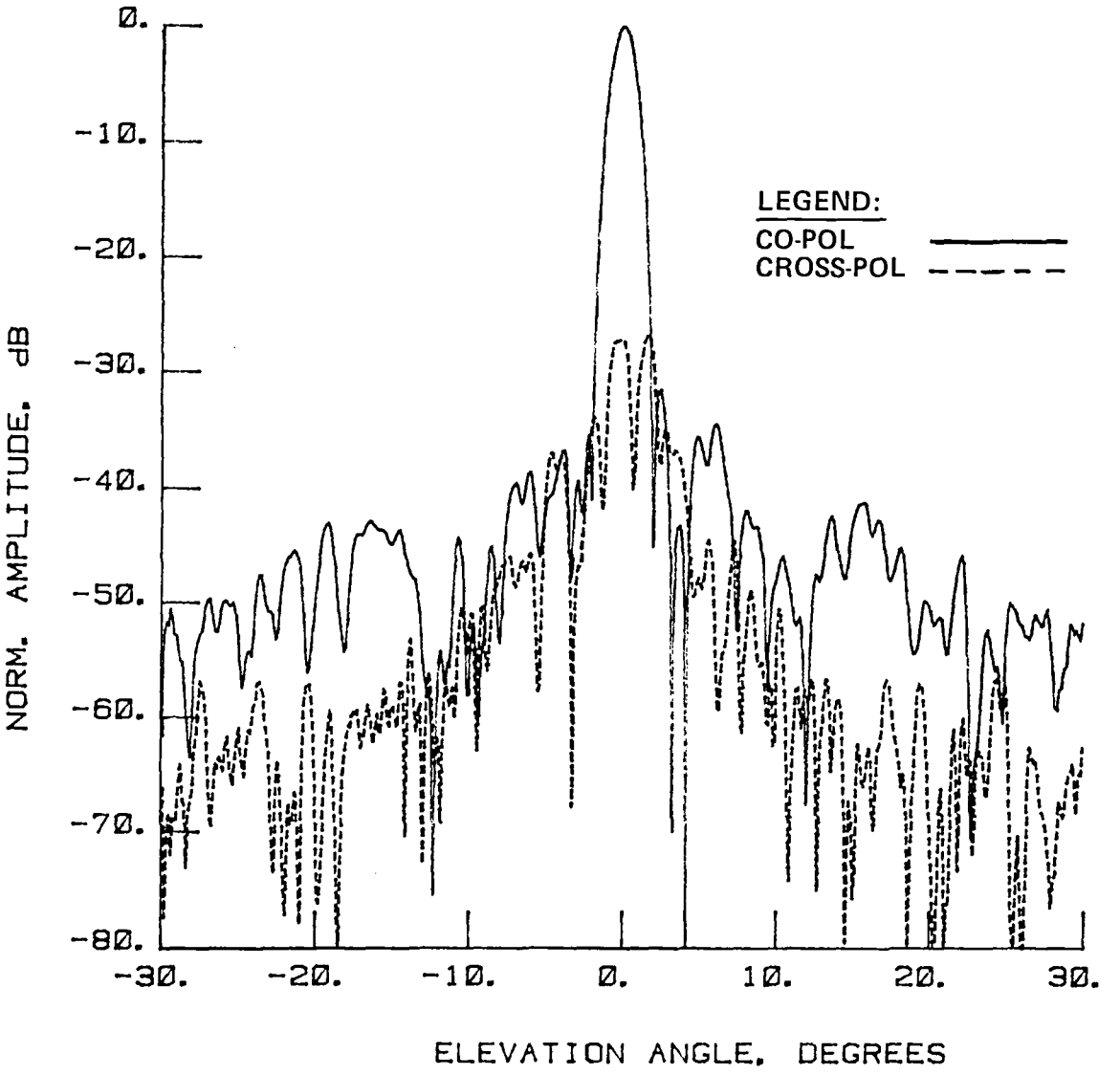

Figure 59 Test 6, 2.27 GHz, Cross-Pol, H-Plane, Type 13

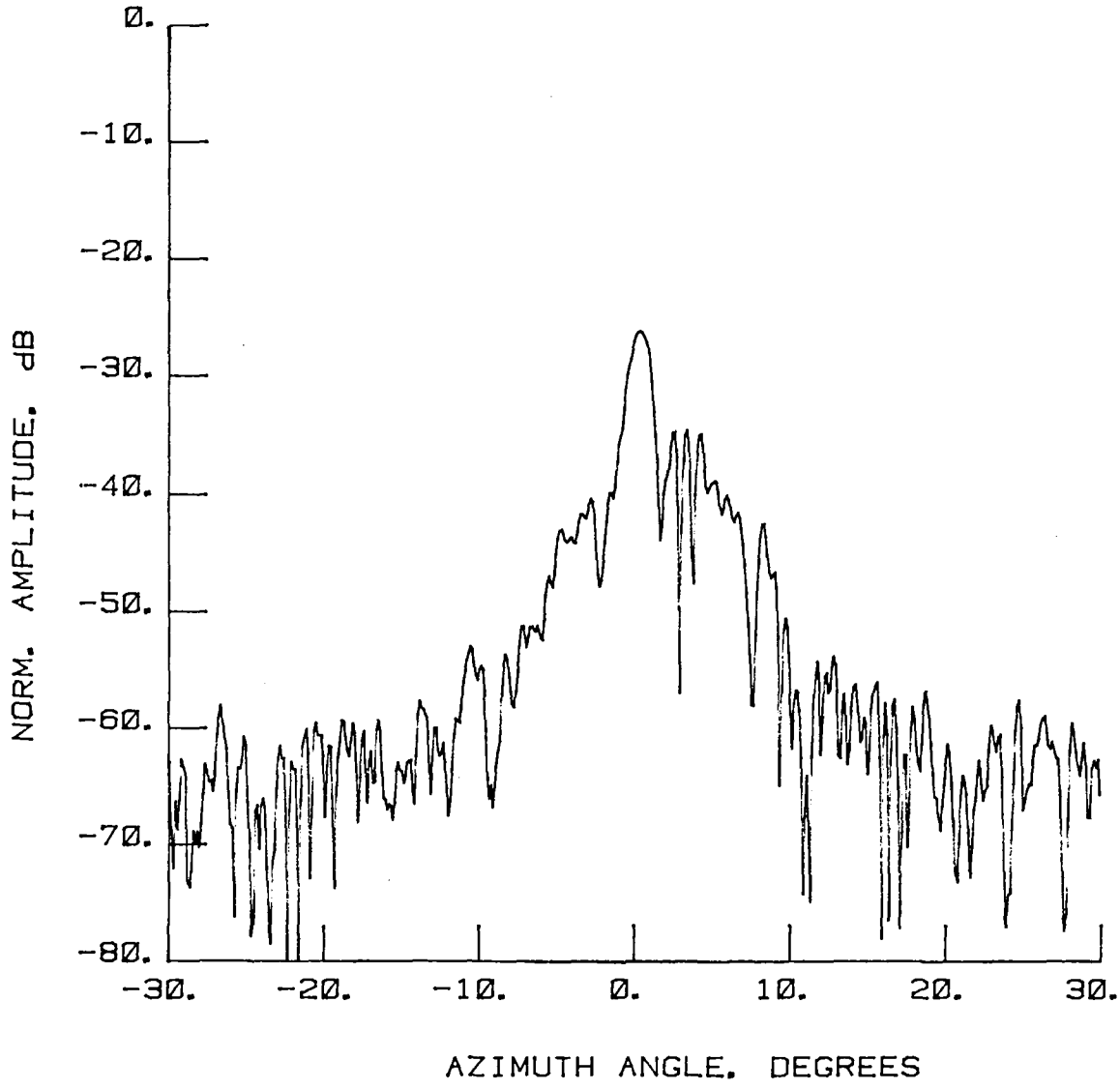

Figure 60 Test 6, 2.27 GHz, Cross-Pol, E-Plane, Type 14

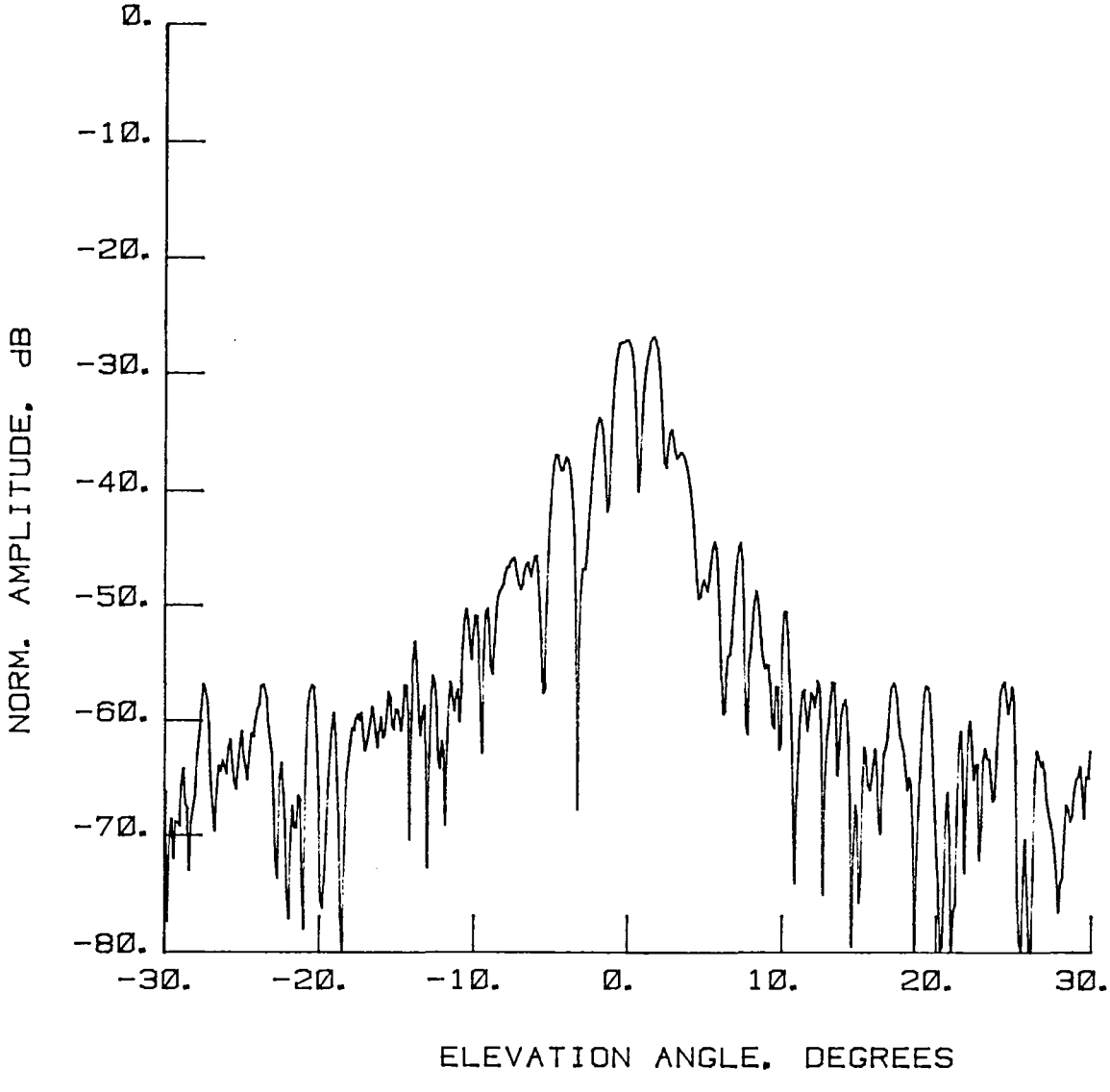

Figure 61 Test 6, 2.27 GHz, Cross-Pol, H-Plane, Type 15

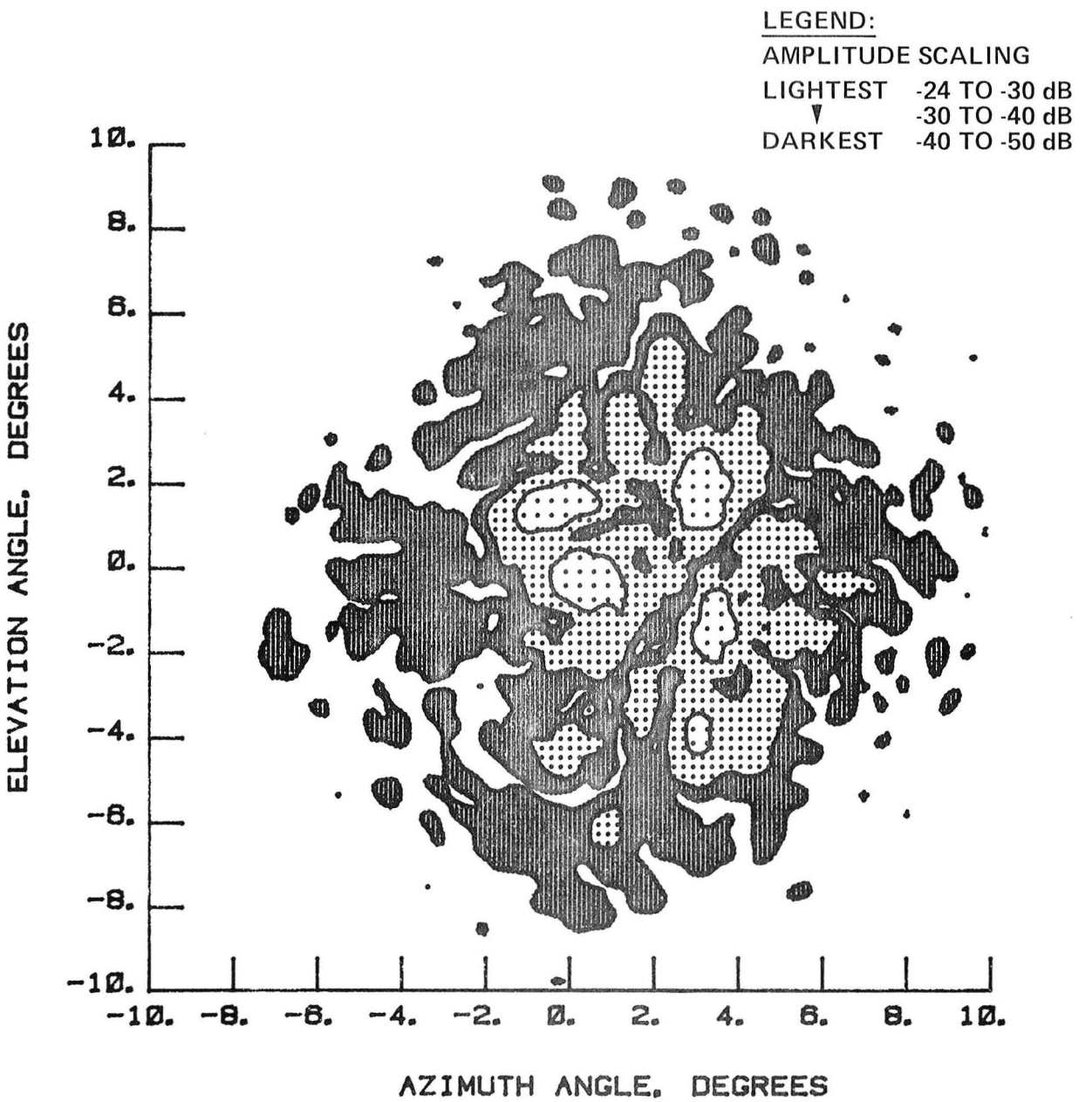

Figure 62 Test 6, 2.27 GHz, Cross-Pol, Contour, Type 16

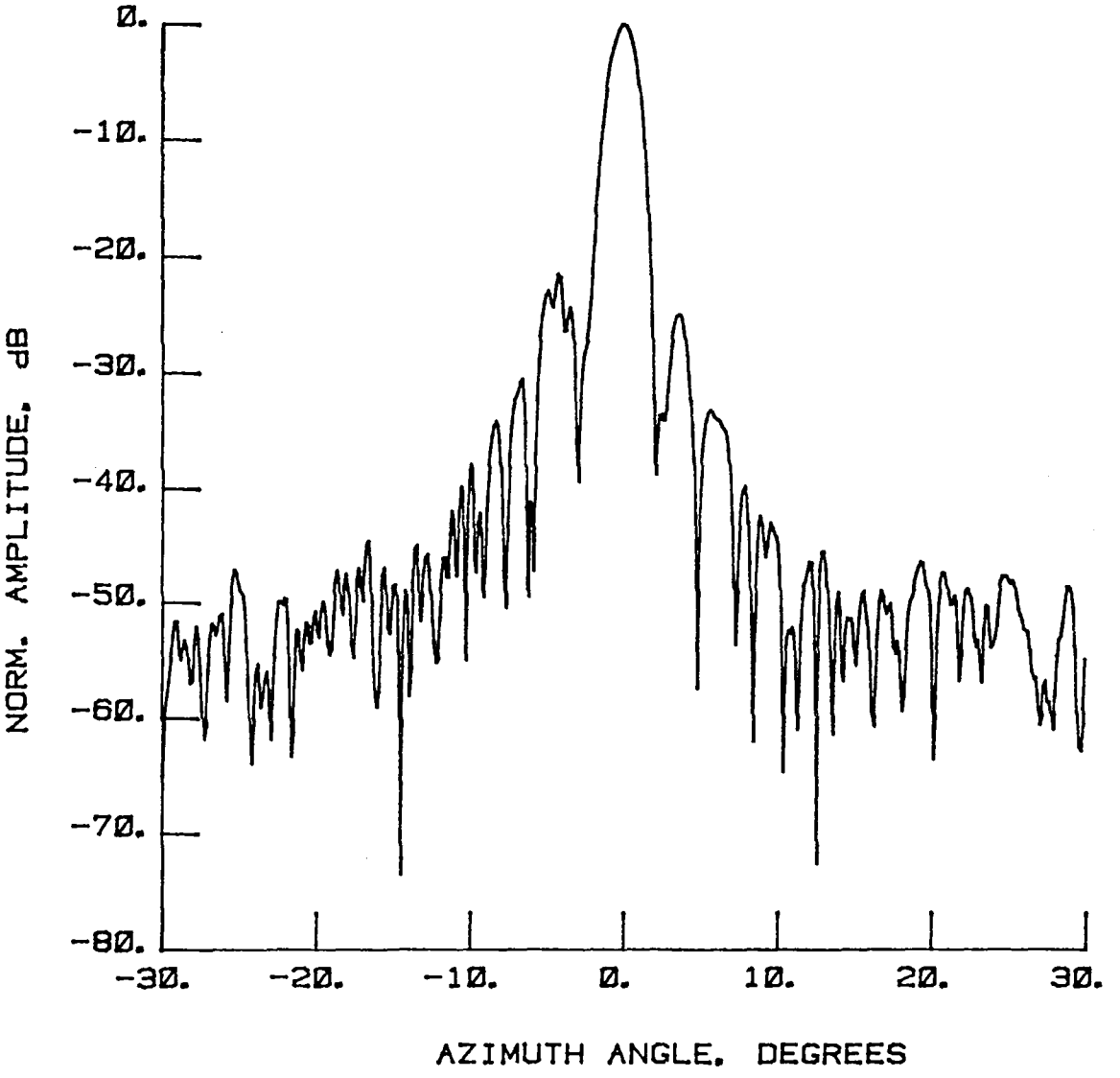

Figure 63 Test 7, 2.27 GHz, Co-Pol, E-Plane, Type 1

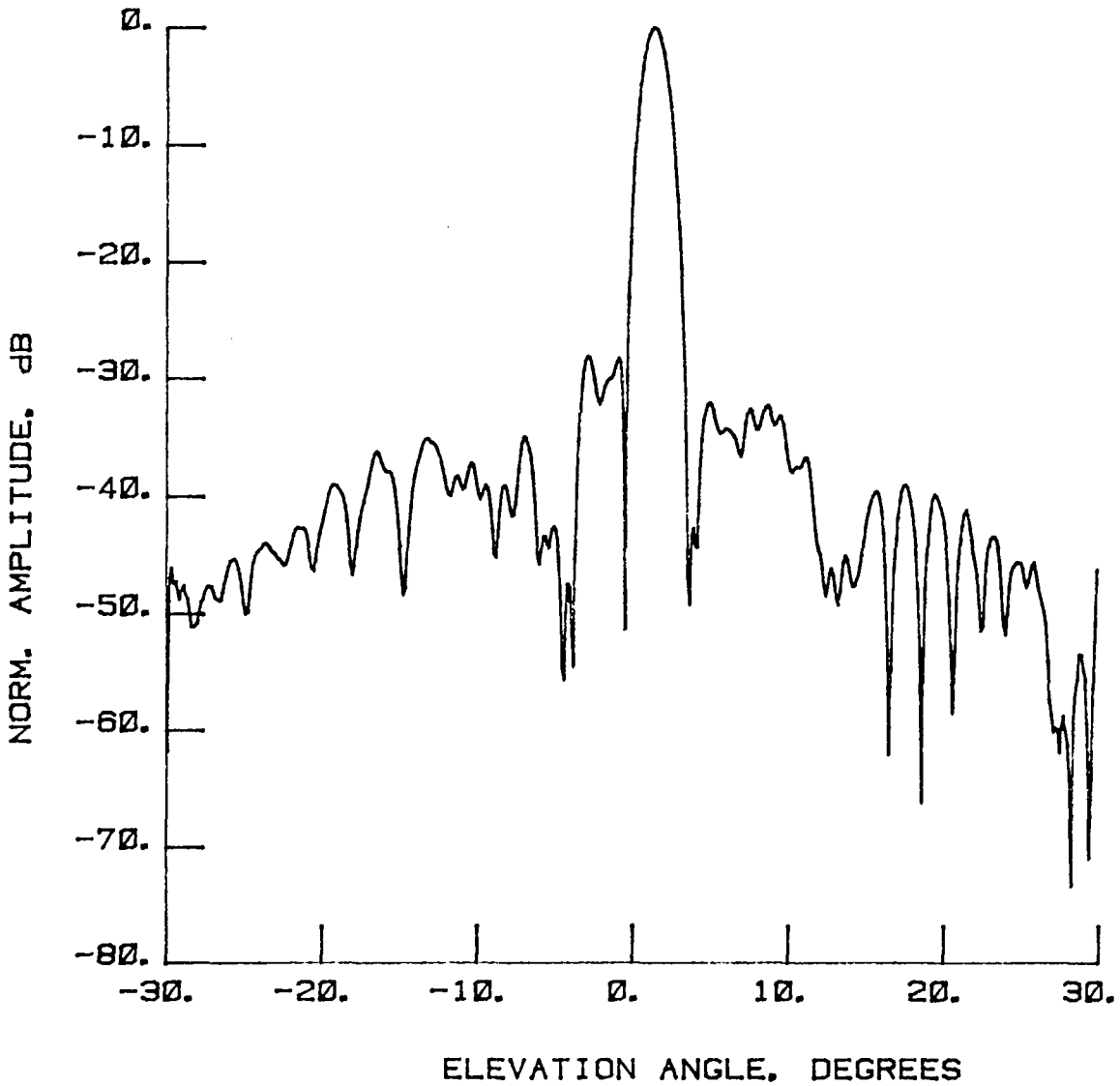

Figure 64 Test 7, 2.27 GHz, Co-Pol, H-Plane, Type 2

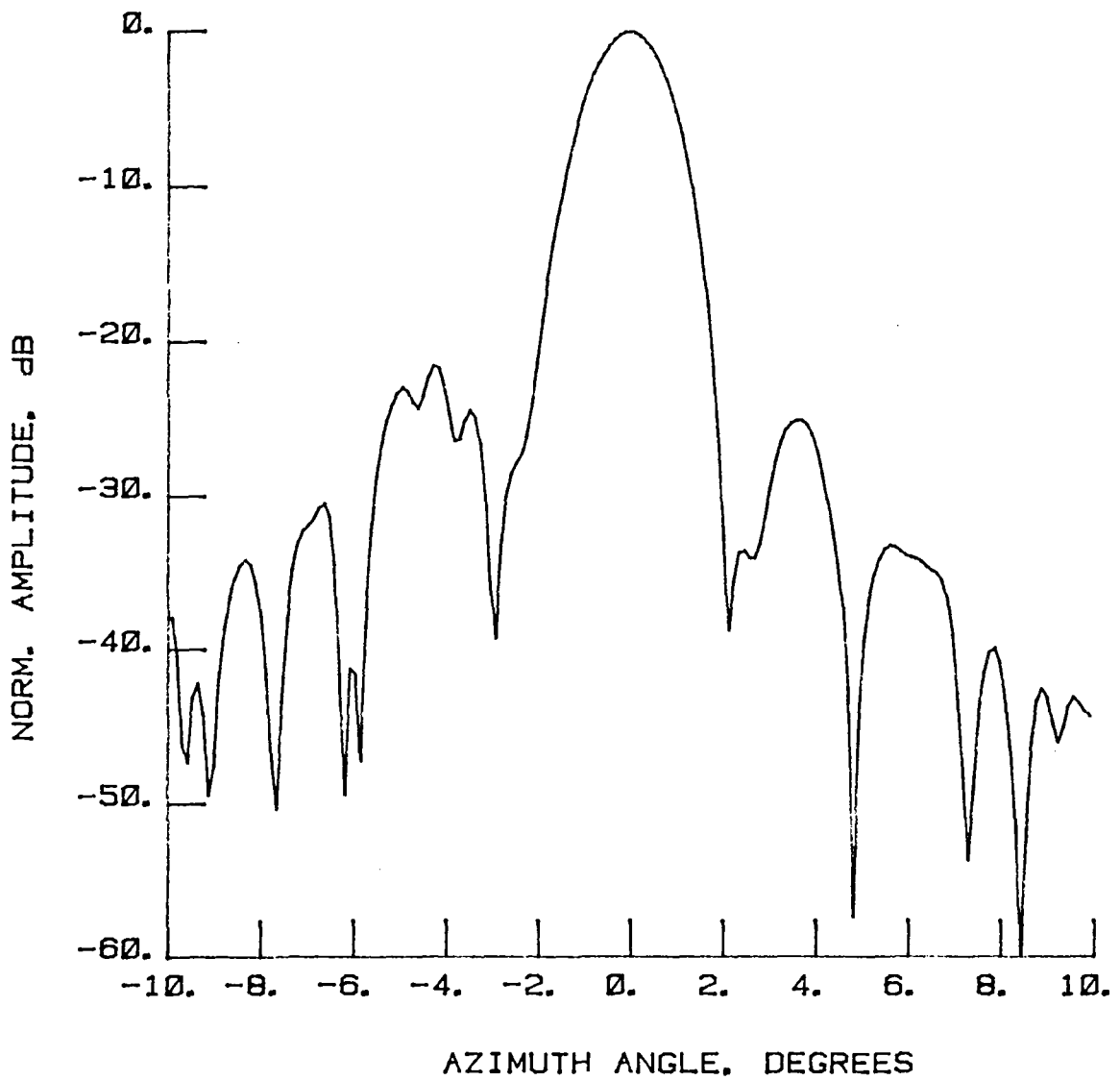

Figure 65 Test 7, 2.27 GHz, Co-Pol, E-Plane, Type 3

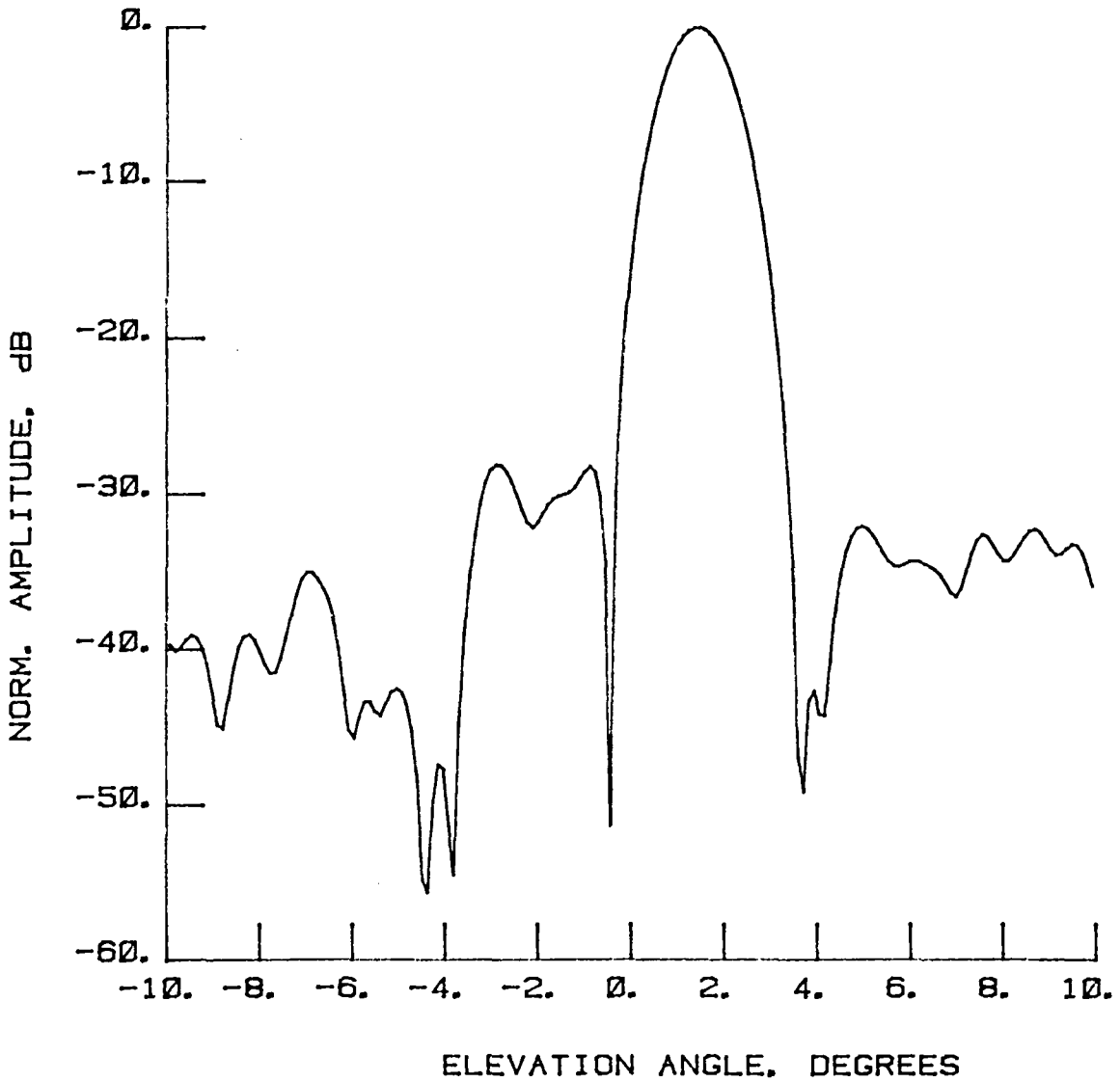

Figure 66 Test 7, 2.27 GHz, Co-Pol, H-Plane, Type 4

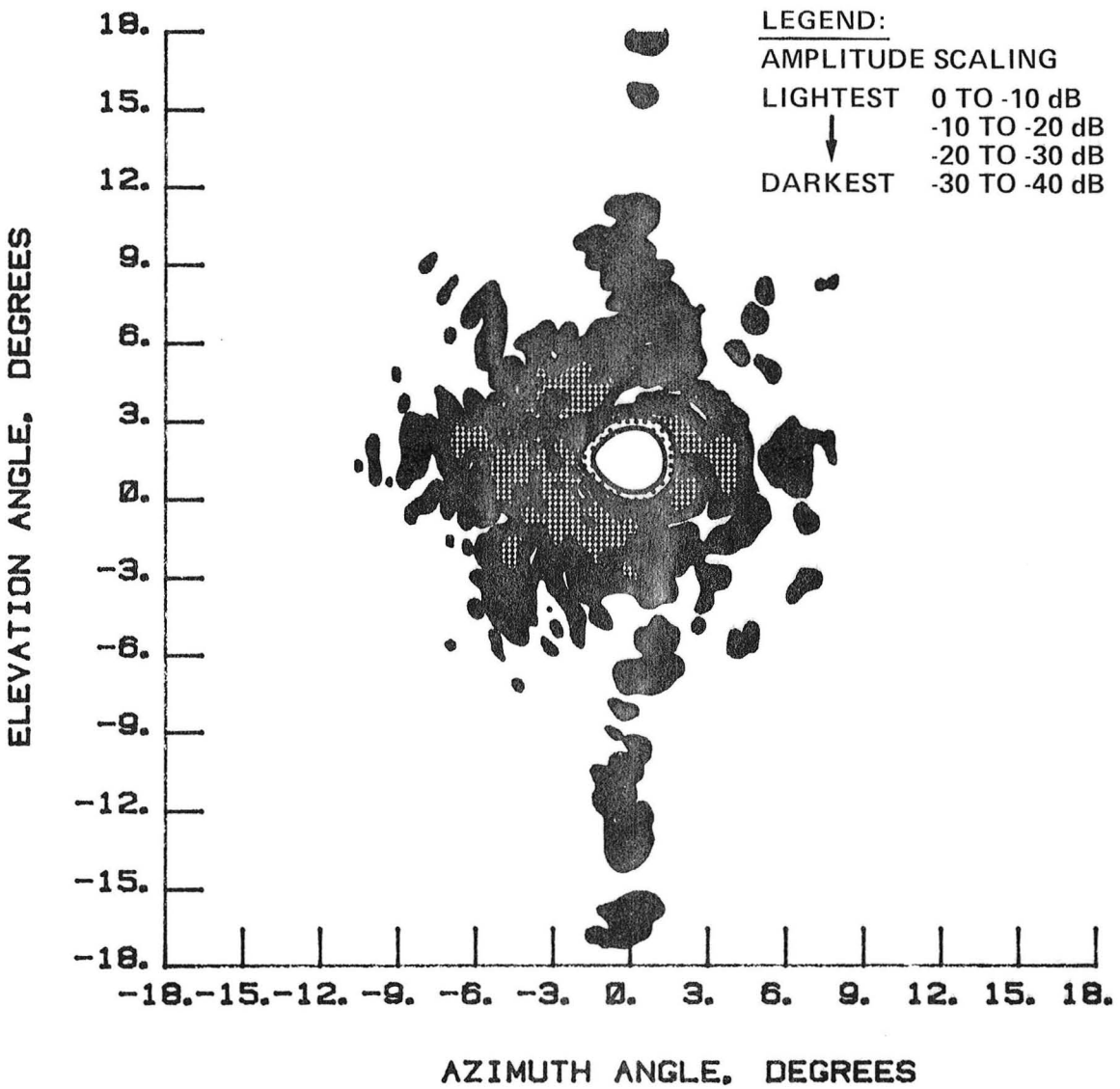

Figure 67 Test 7, 2.27 GHz, Co-Pol, Contour, Type 5

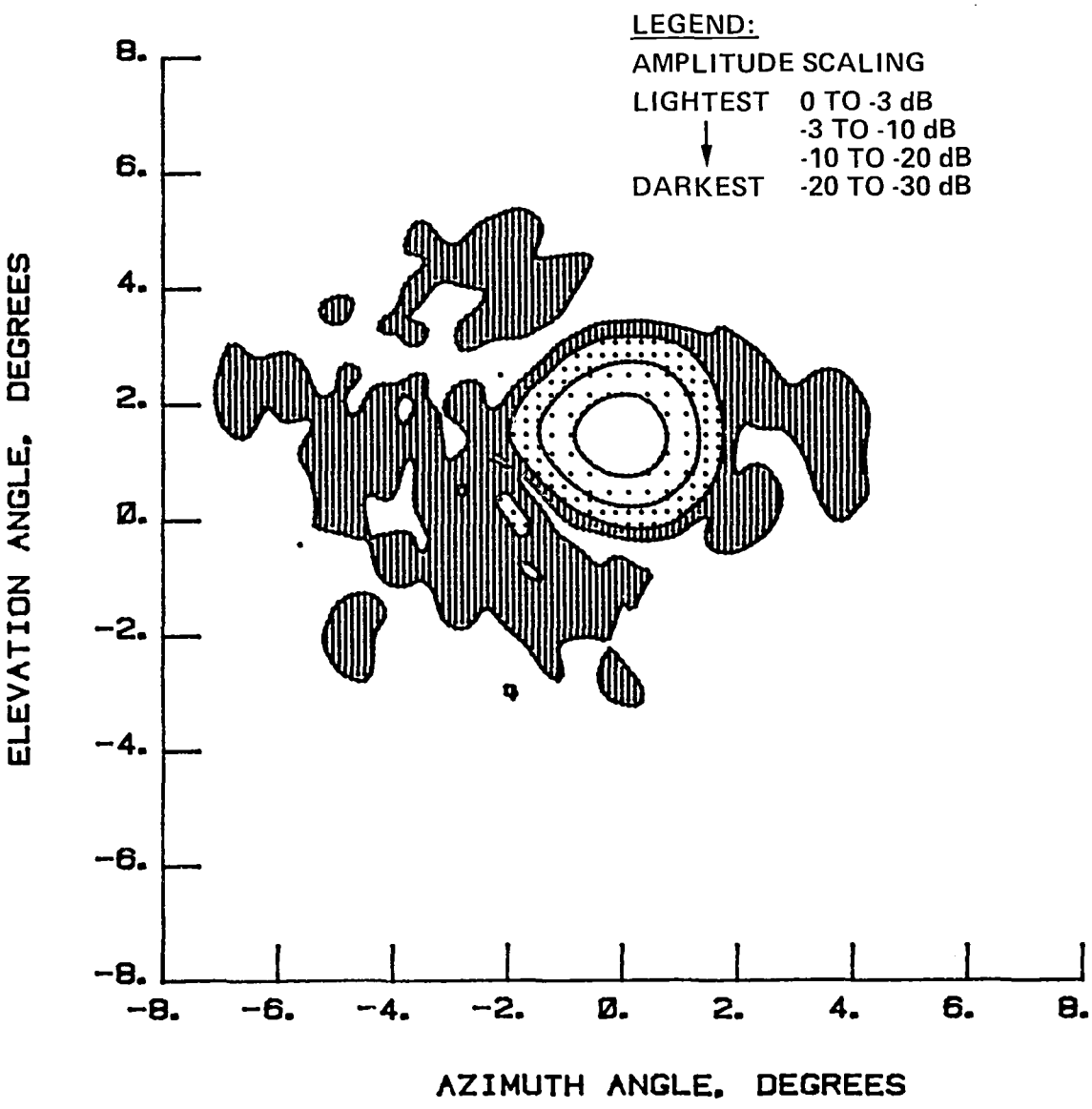

Figure 68 Test 7, 2.27 GHz, Co-Pol, Contour, Type 6

This Page Intentionally Left Blank

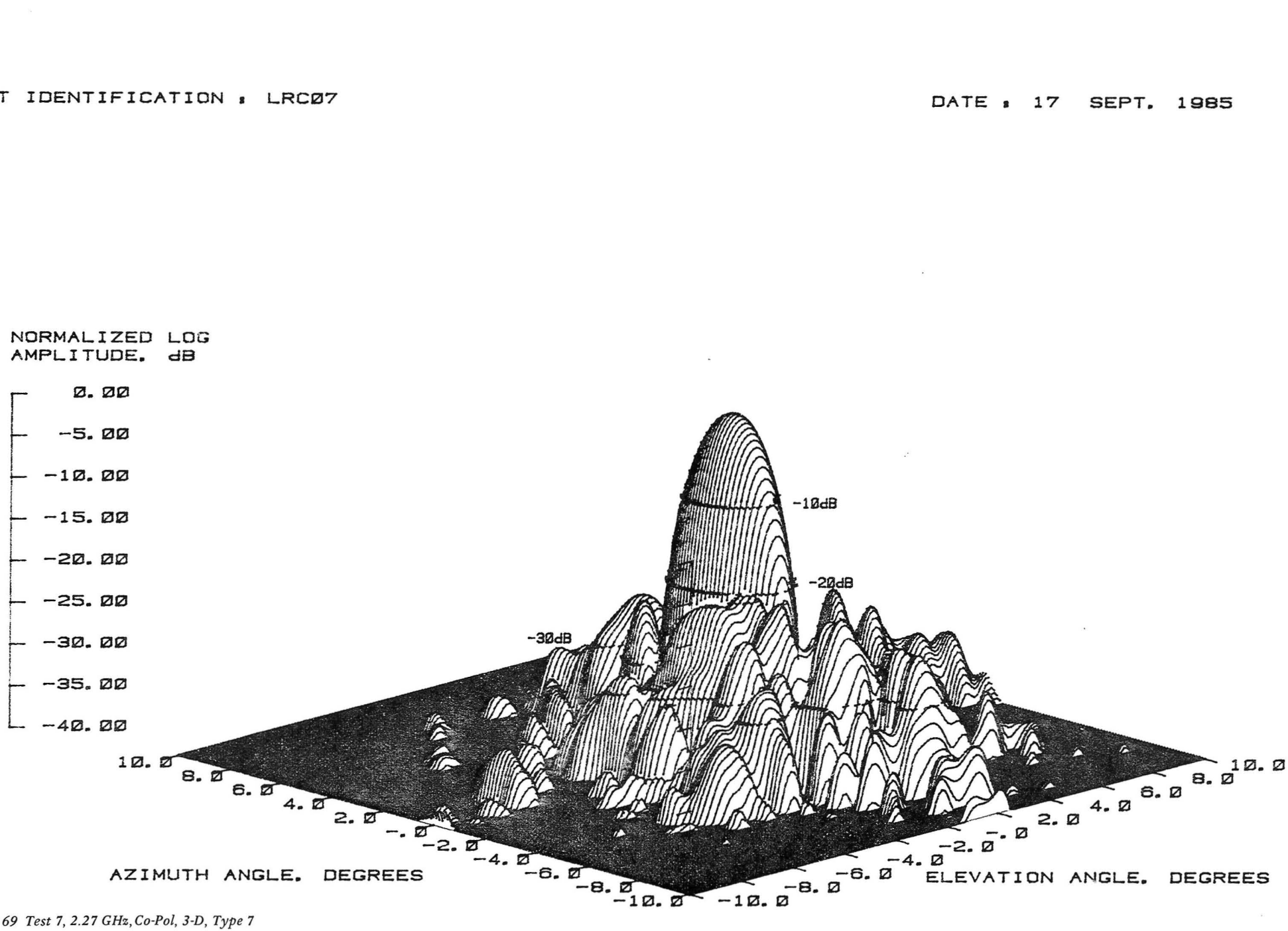

Figure 69 Test 7, 2.27 GHz, Co-Pol, 3-D, Type 7

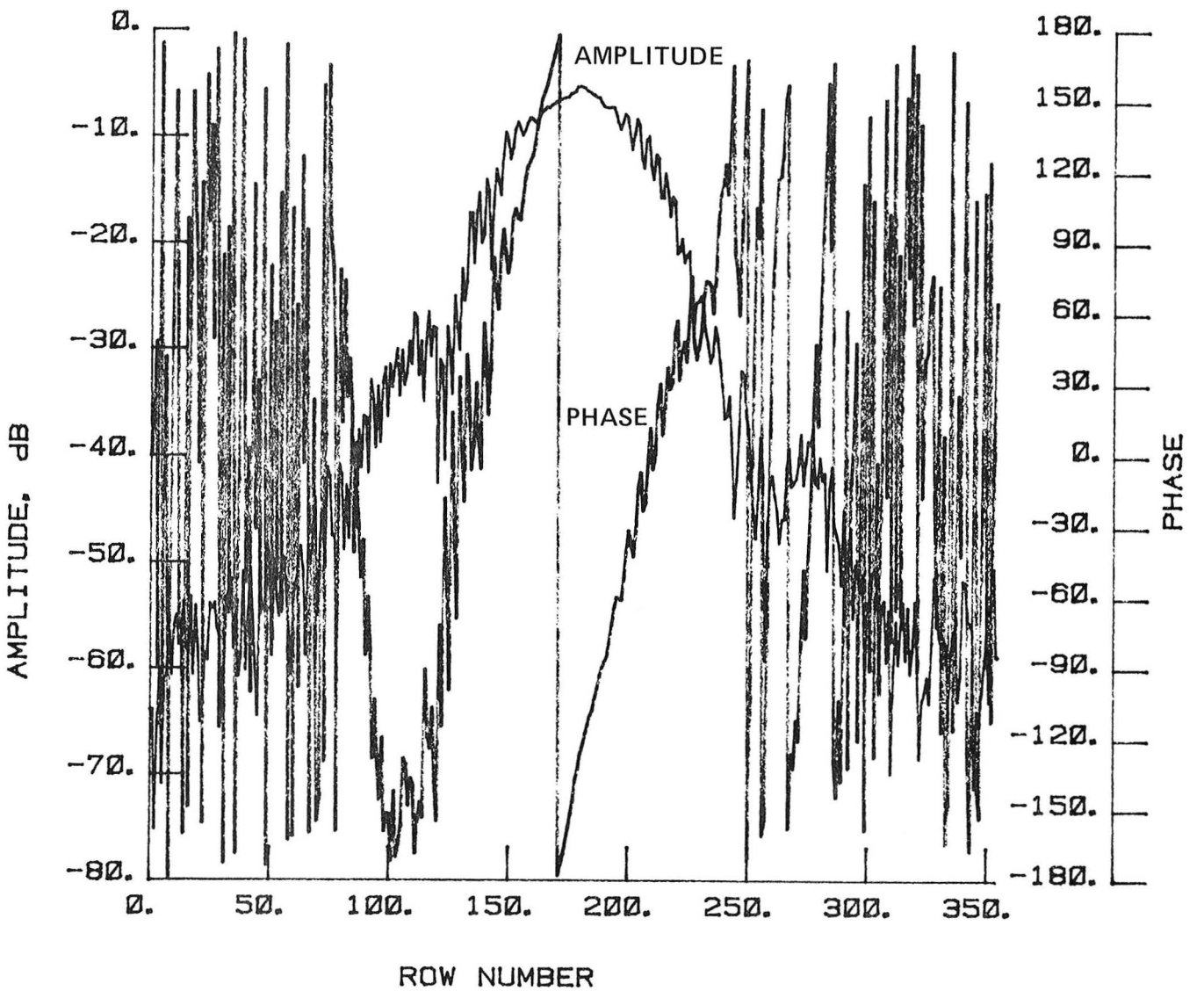

Figure 70 Test 7, 2.27 GHz, Co-Pol, H-Plane, Type 8

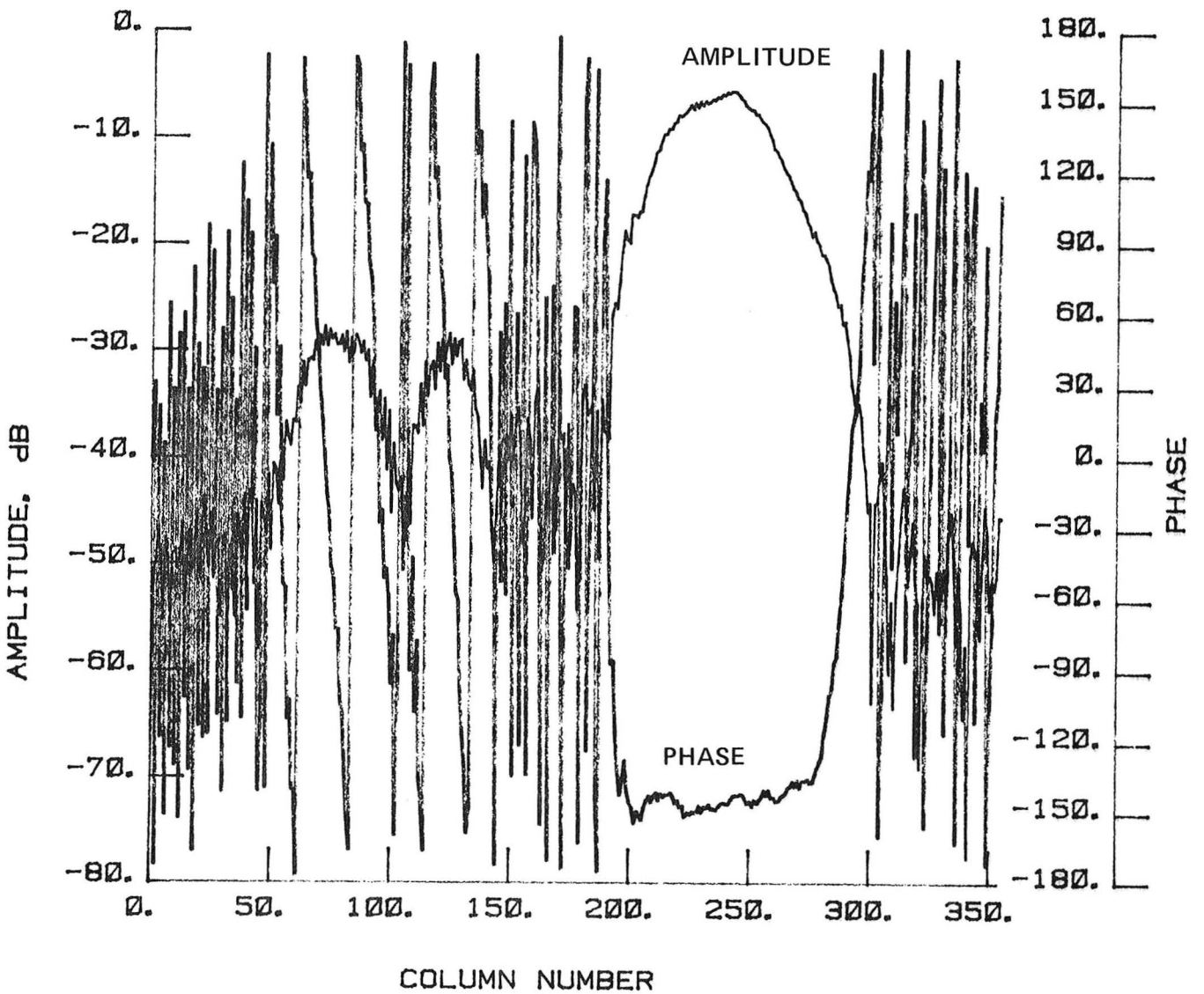

Figure 71 Test 7, 2.27 GHz, Co-Pol, E-Plane, Type 9

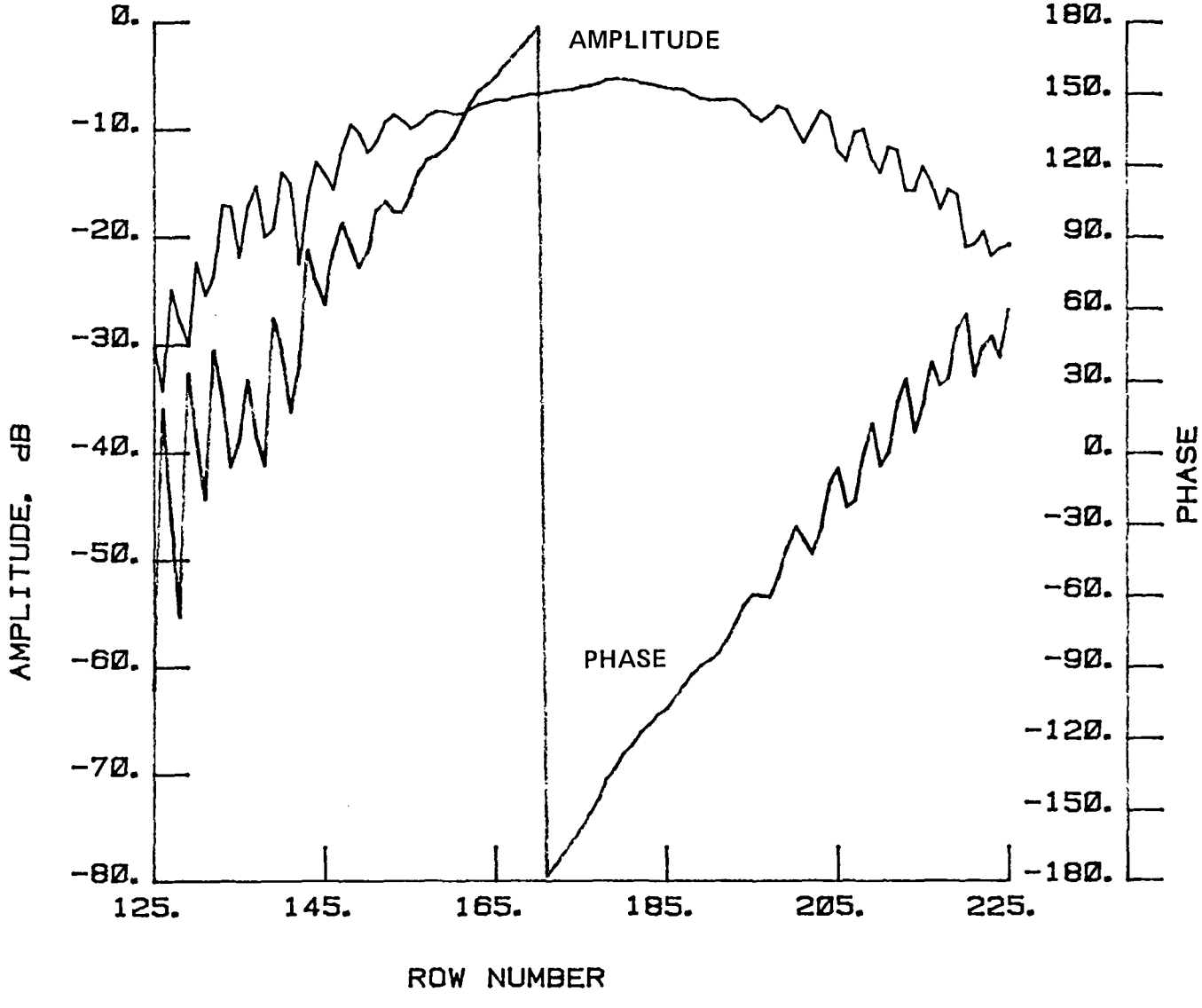

Figure 72 Test 7, 2.27 GHz, Co-Pol, H-Plane, Type 10

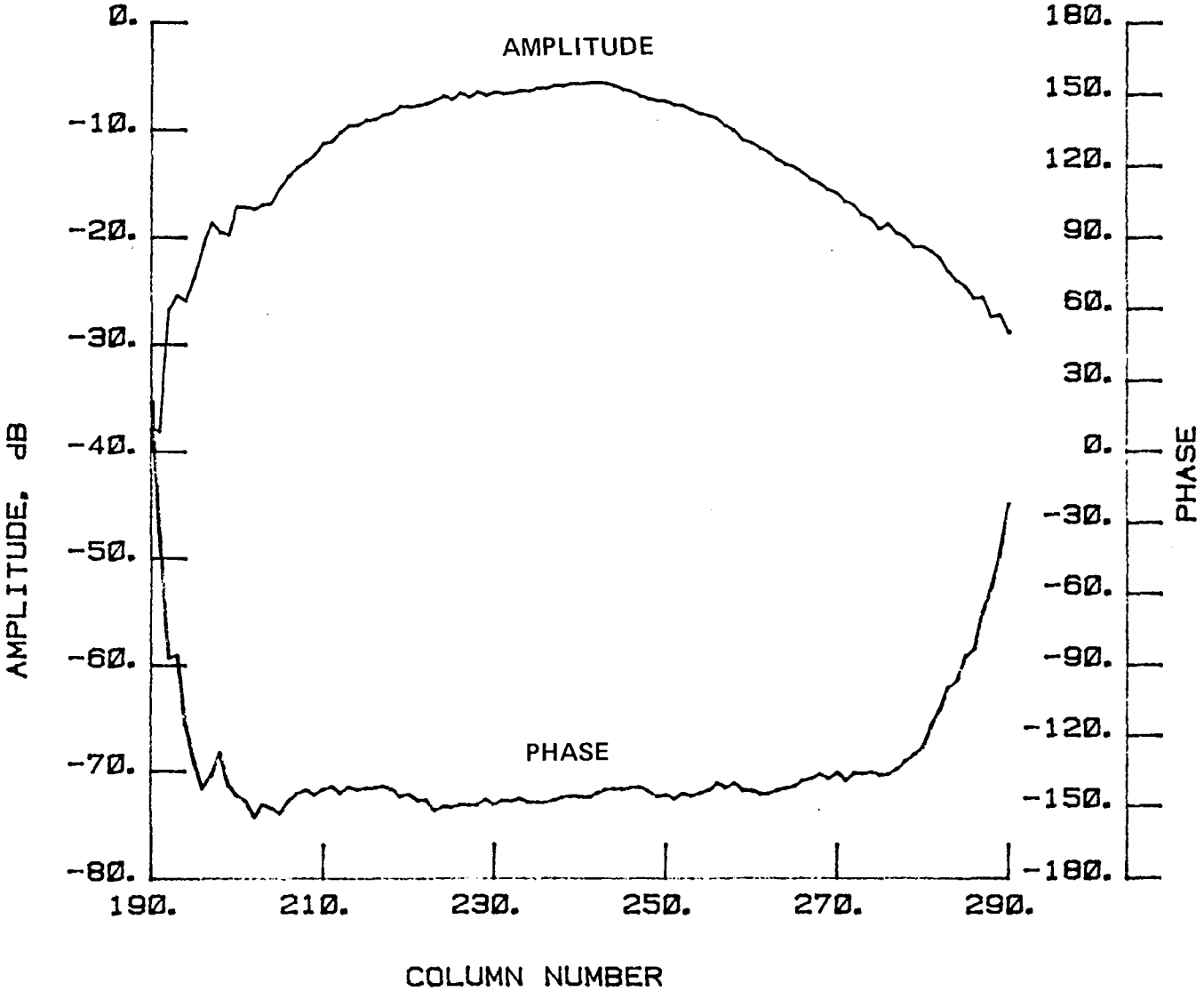

Figure 73 Test 7, 2.27 GHz, Co-Pol, E-Plane, Type 11

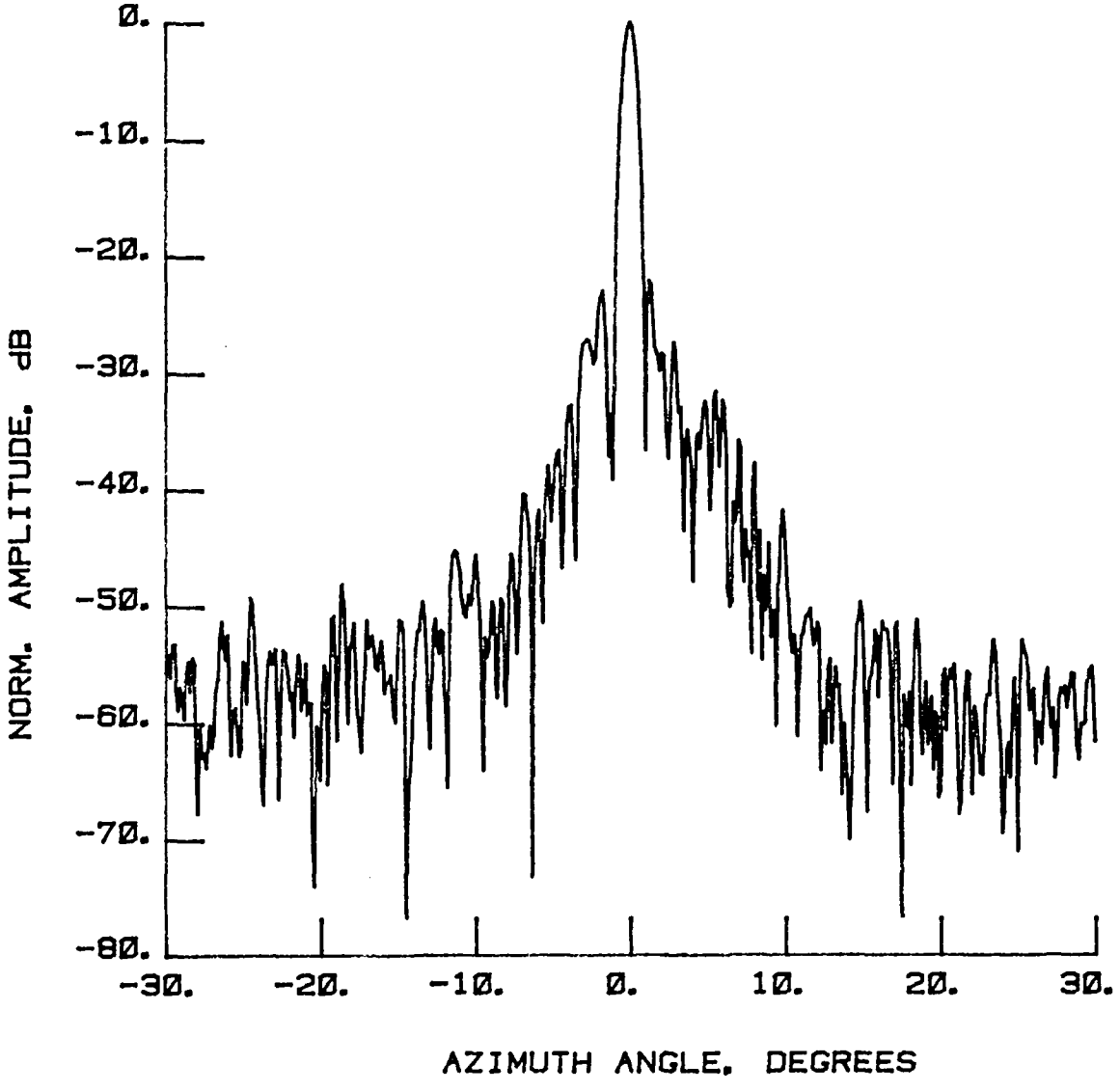

Figure 74 Test 12, 4.26 GHz, Co-Pol, E-Plane, Type 1

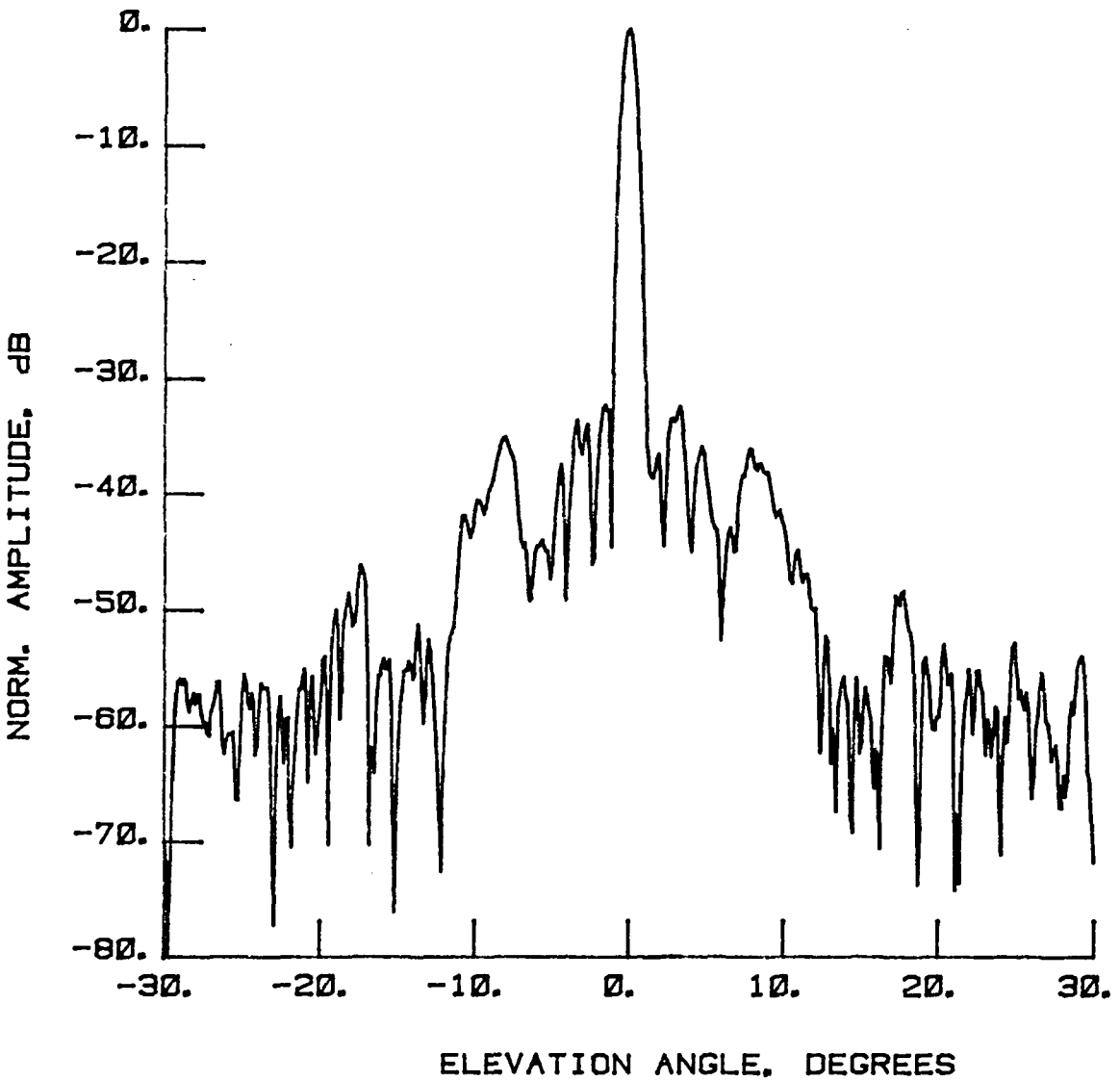

Figure 75 Test 12, 4.26 GHz, Co-Pol, H-Plane, Type 2

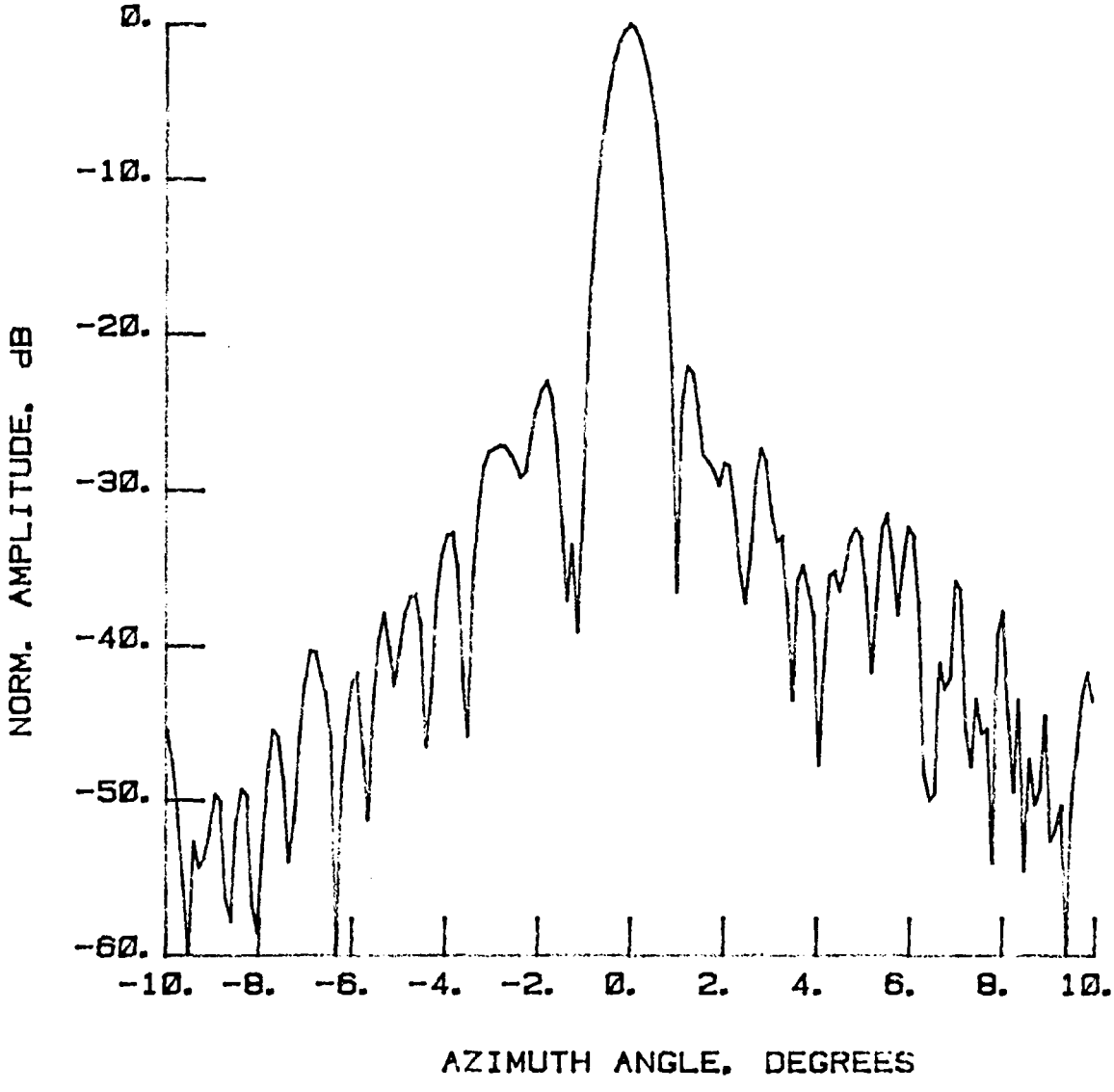

Figure 76 Test 12, 4.26 GHz, Co-Pol, E-Plane, Type 3

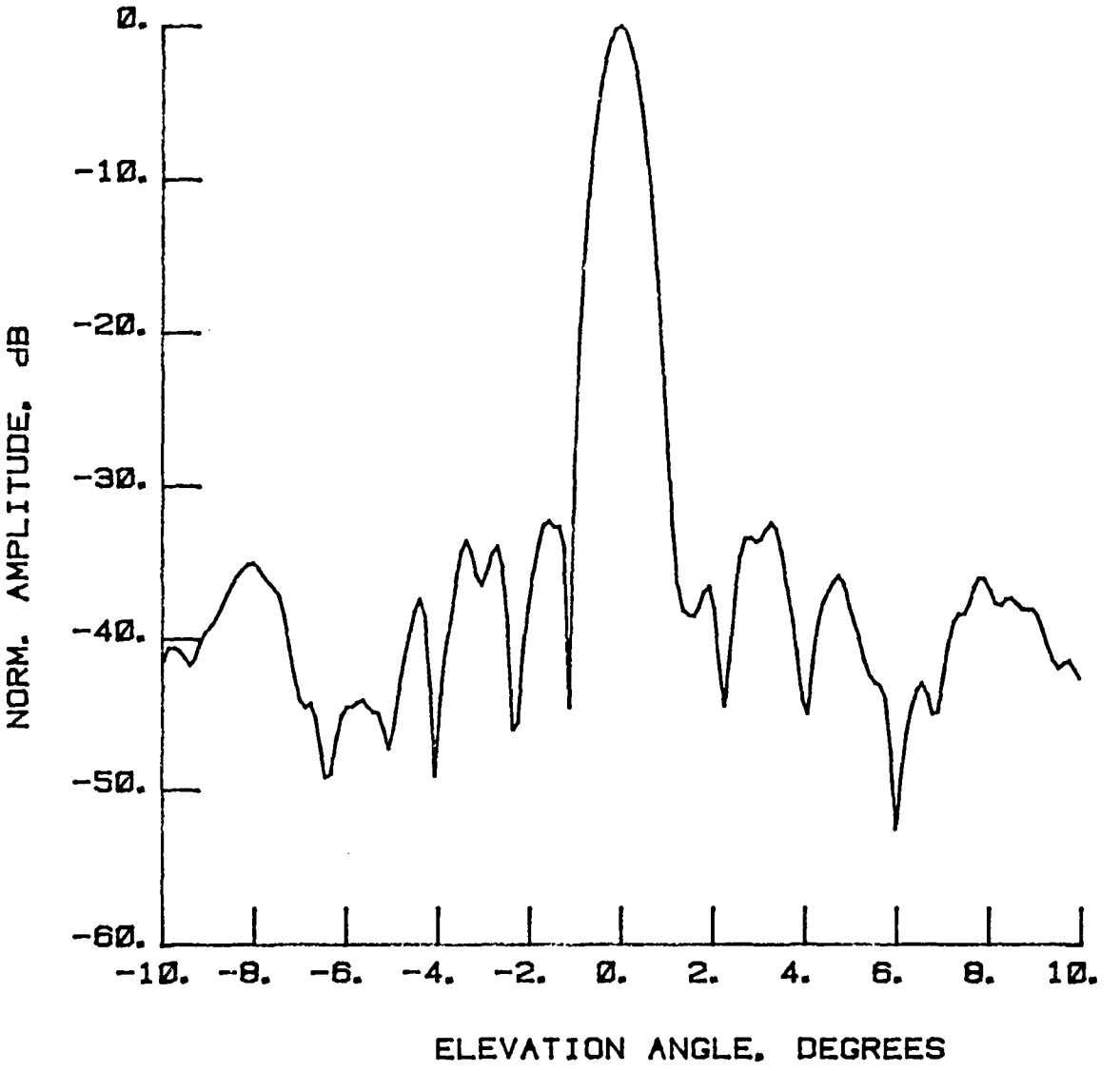

Figure 77 Test 12, 4.26 GHz, Co-Pol, H-Plane, Type 4

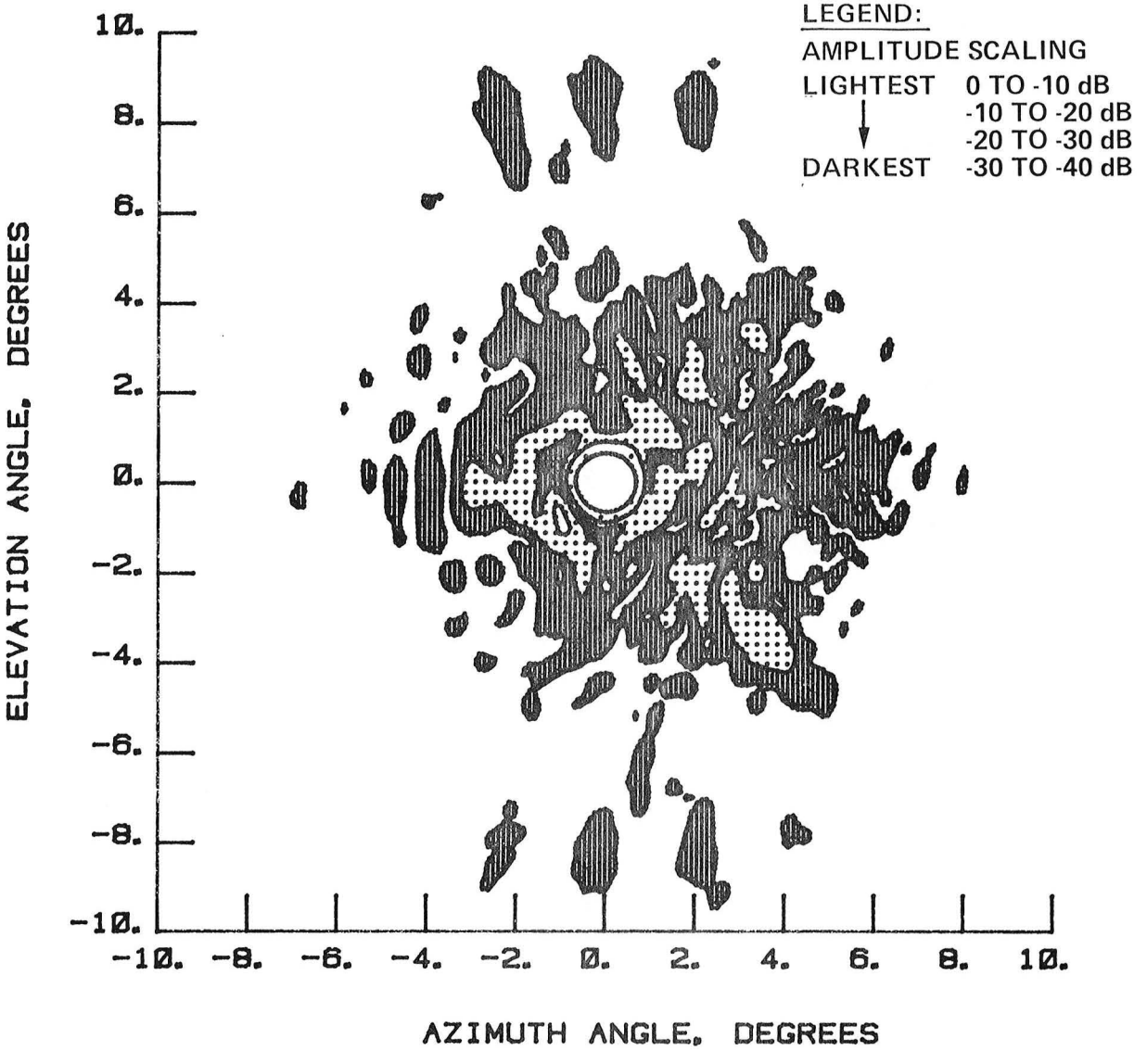

Figure 78 Test 12, 4.26 GHz, Co-Pol, Contour, Type 5

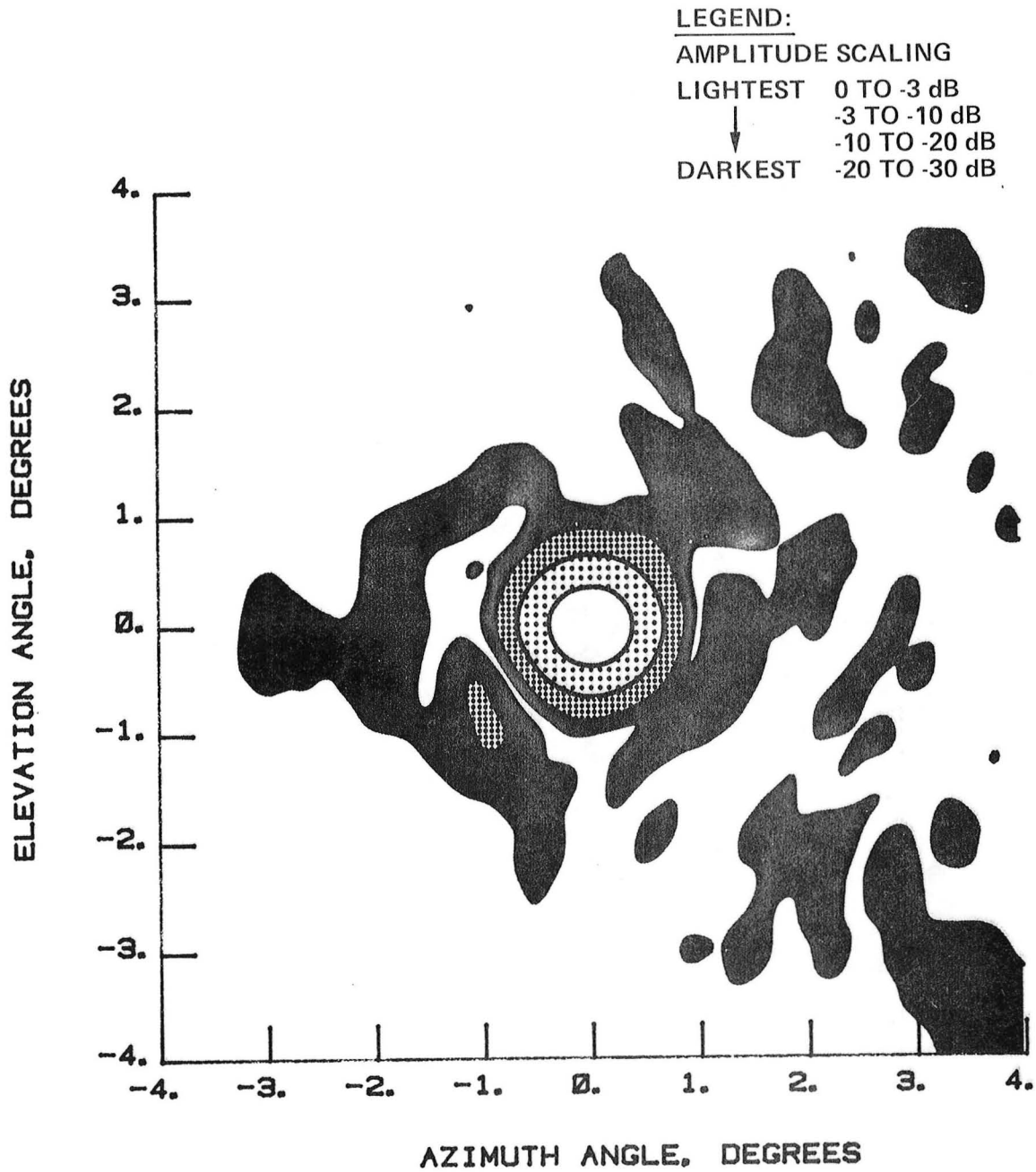

Figure 79 Test 12, 4.26 GHz, Co-Pol, Contour, Type 6

TEST IDENTIFICATION : LRC12

DATE : 18 SEPT. 1985

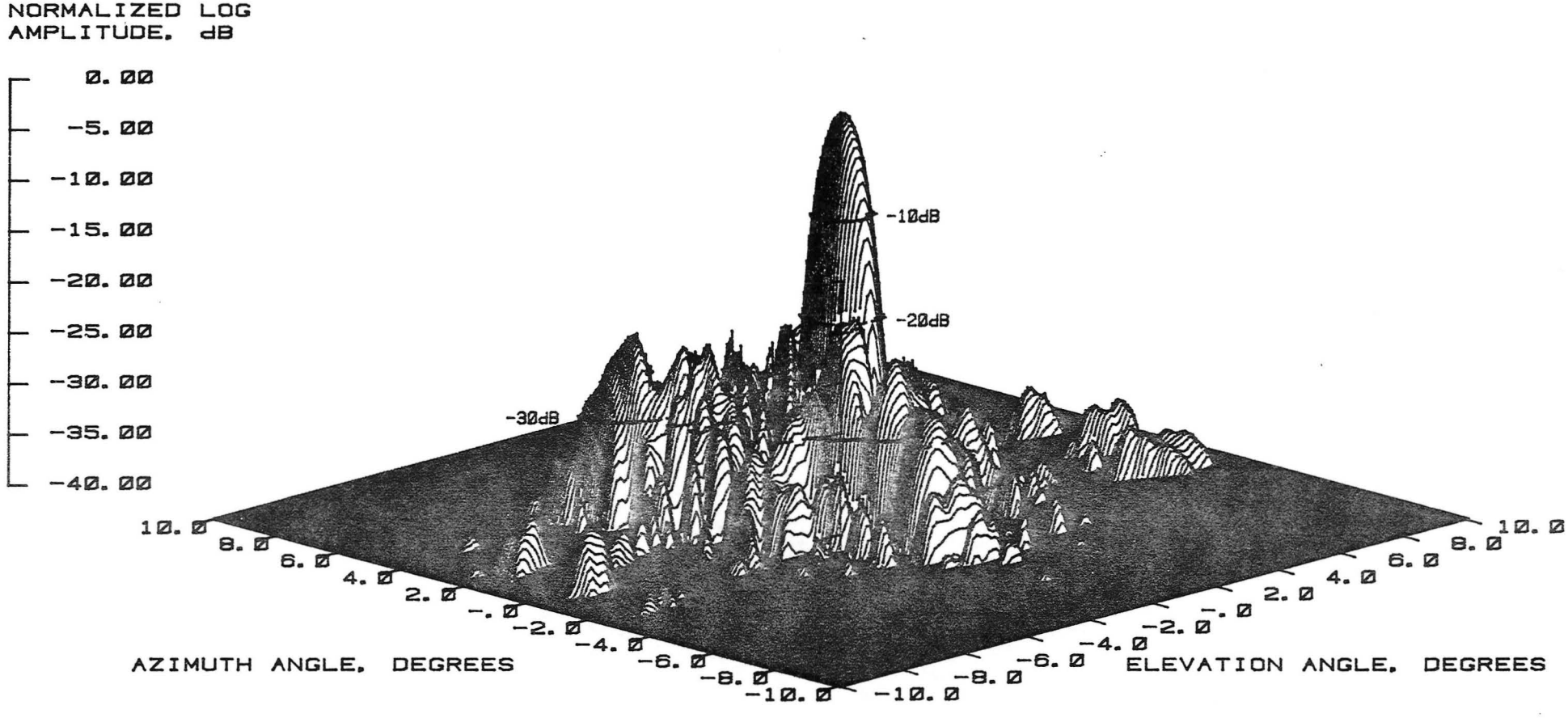

Figure 80 Test 12, 4.26 GHz, Co-Pol, 3-D, Type 7

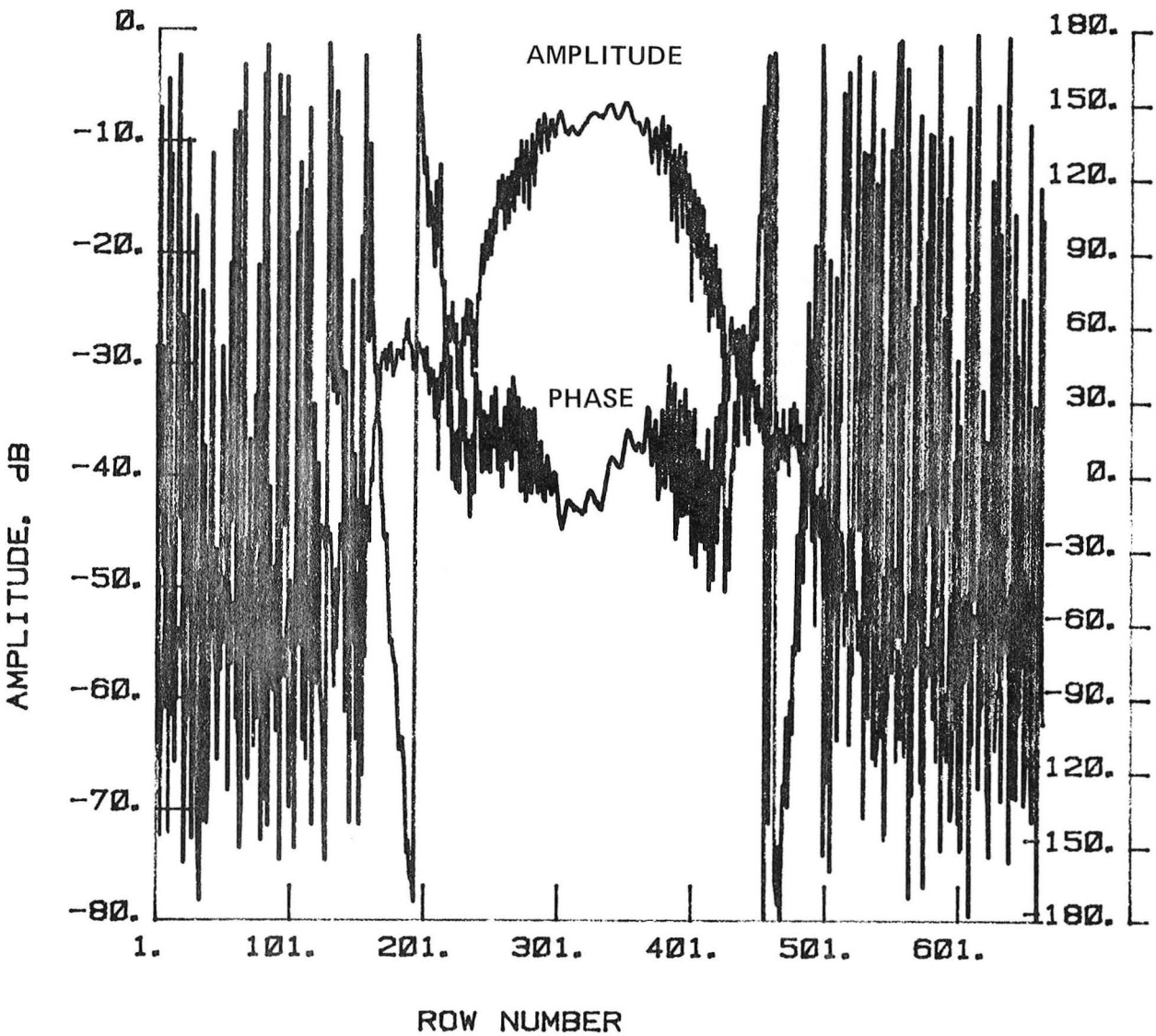

Figure 81 Test 12, 4.26 GHz, Co-Pol, H-Plane, Type 8

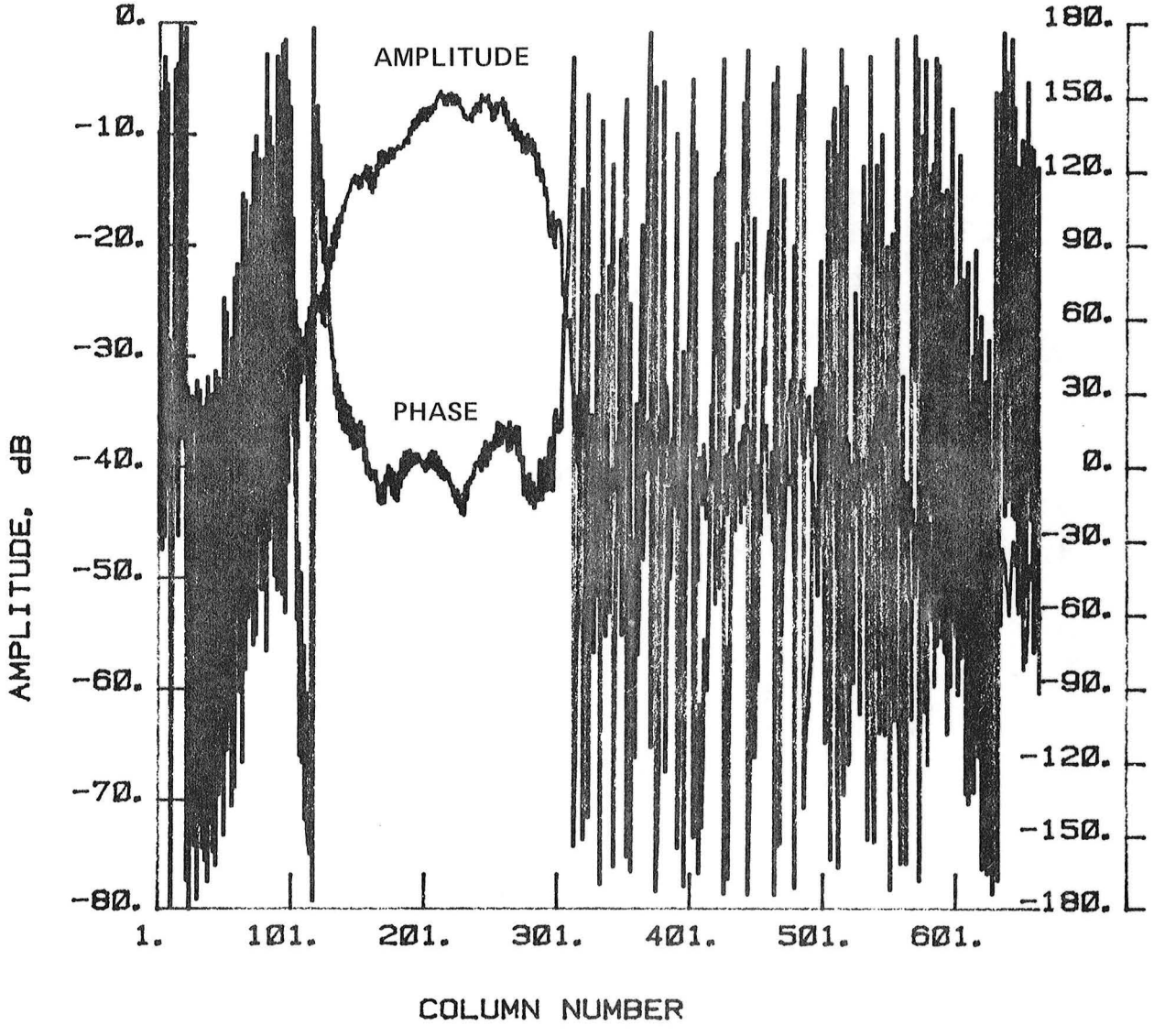

Figure 82 Test 12, 4.26 GHz, Co-Pol, E-Plane, Type 9

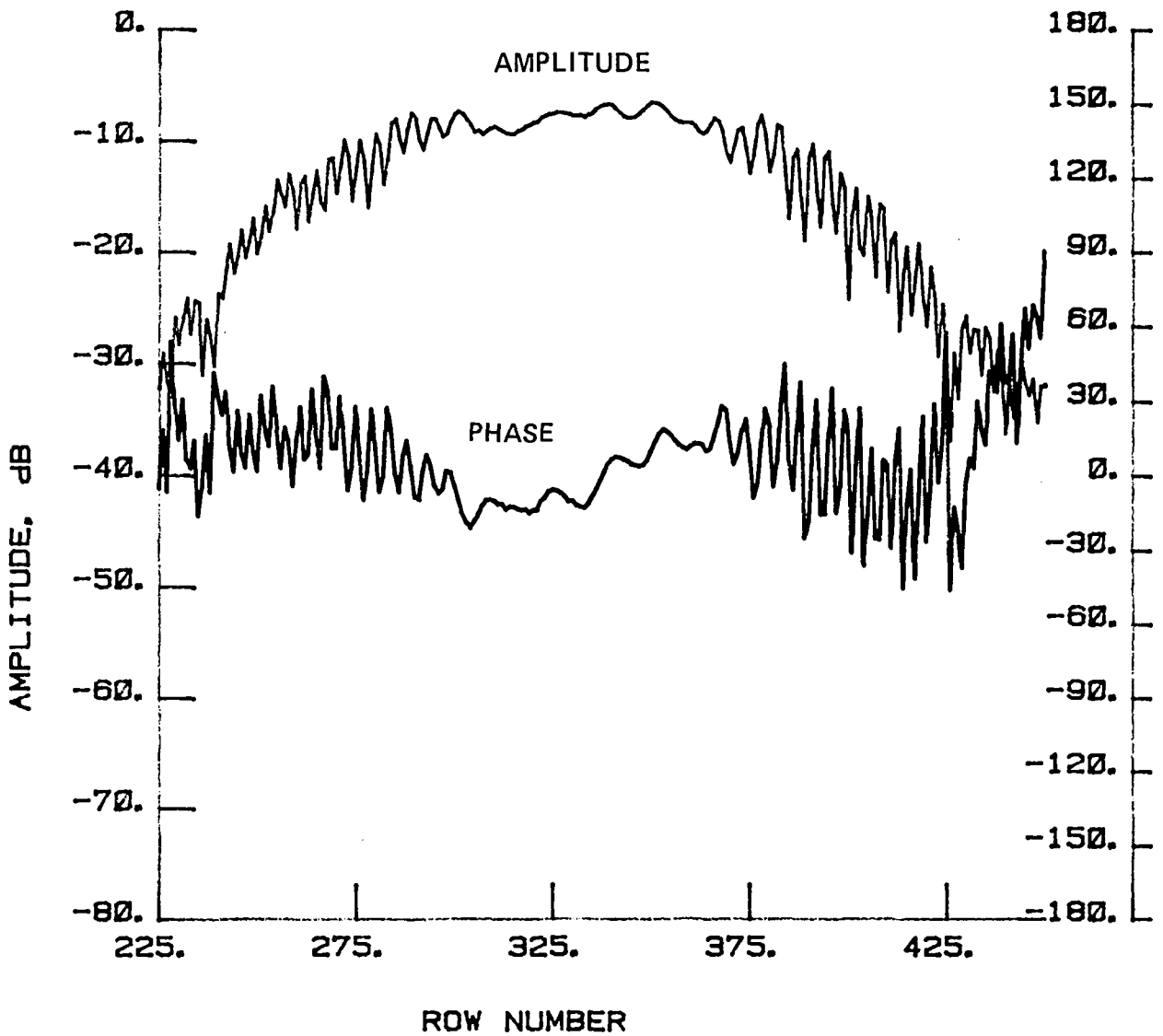

Figure 83 Test 12, 4.26 GHz, Co-Pol, H-Plane, Type 10

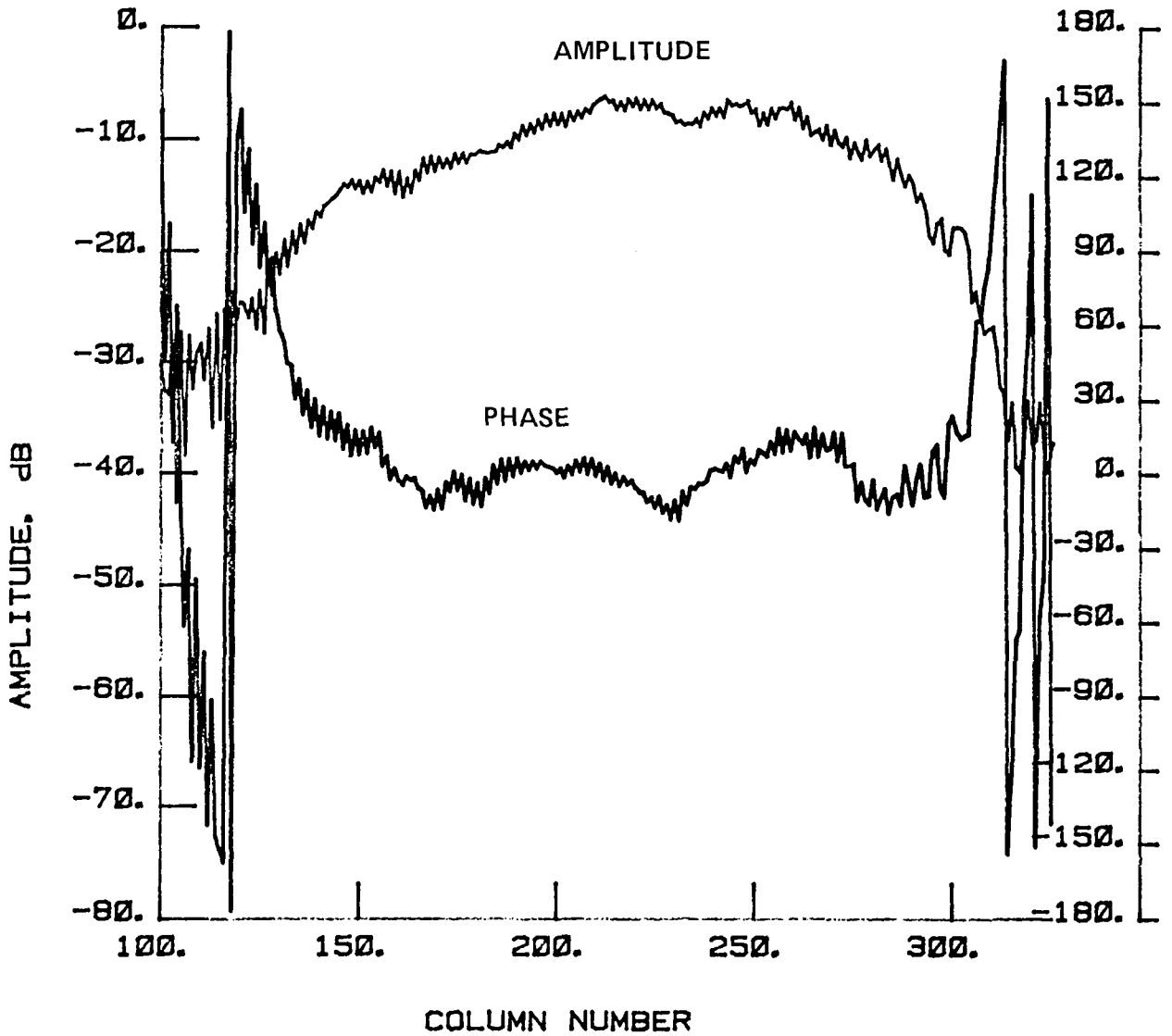

Figure 84 Test 12, 4.26 GHz, Co-Pol, E-Plane, Type 11

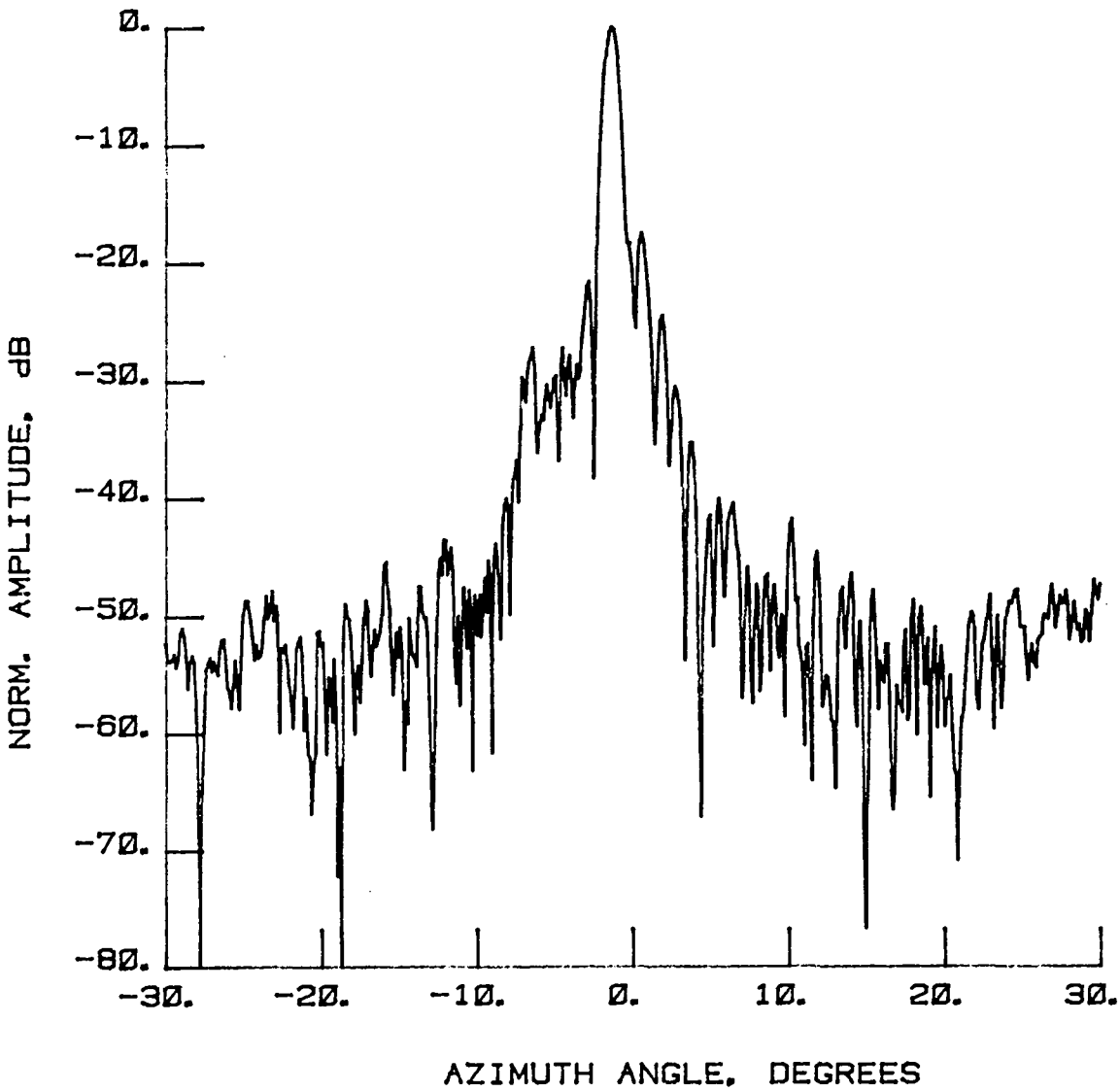

Figure 85 Test 13, 4.26 GHz, Co-Pol, E-Plane, Type 1

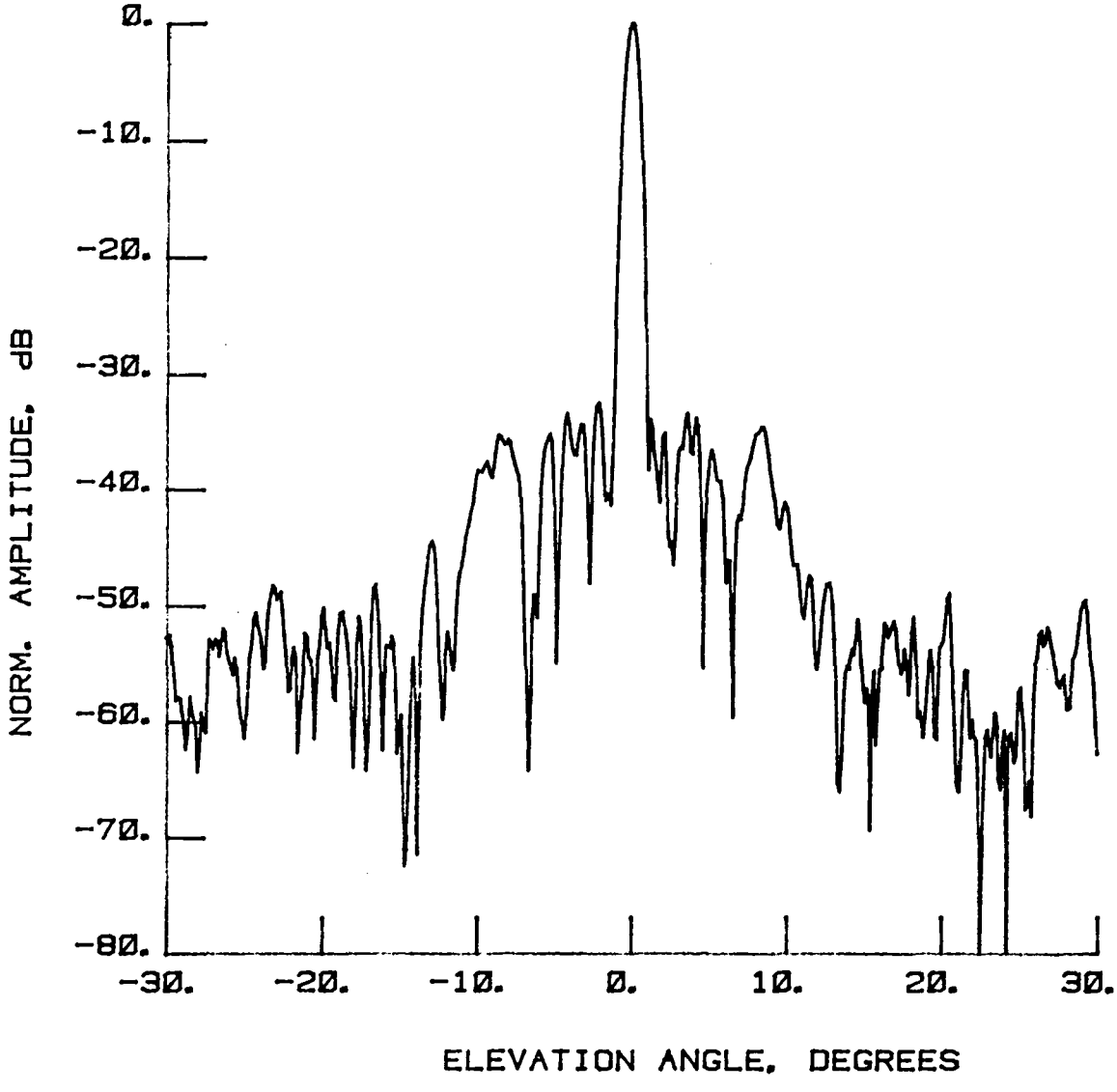

Figure 86 Test 13, 4.26 GHz, Co-Pol, H-Plane, Type 2

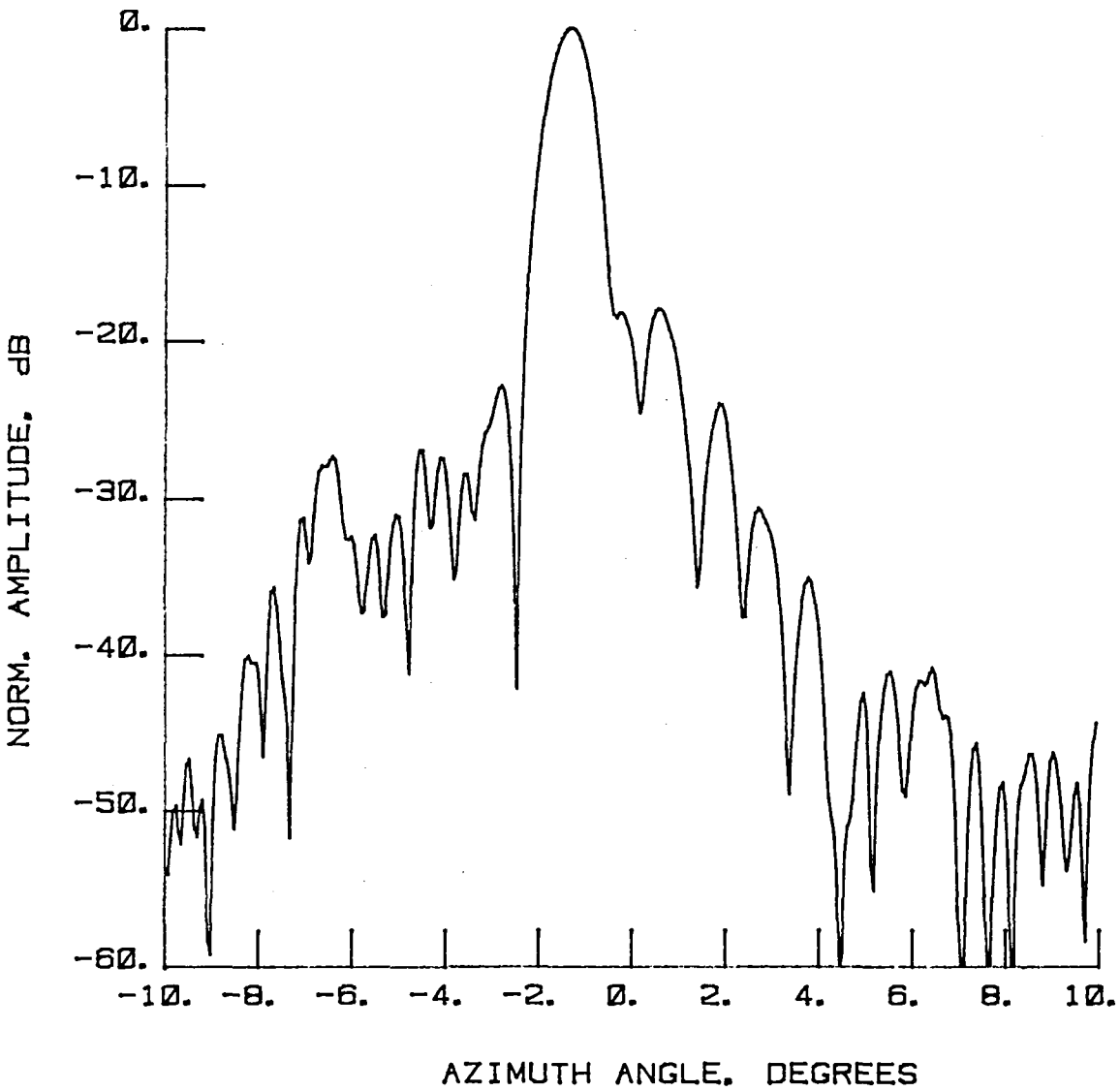

Figure 87 Test 13, 4.26 GHz, Co-Pol, E-Plane, Type 3

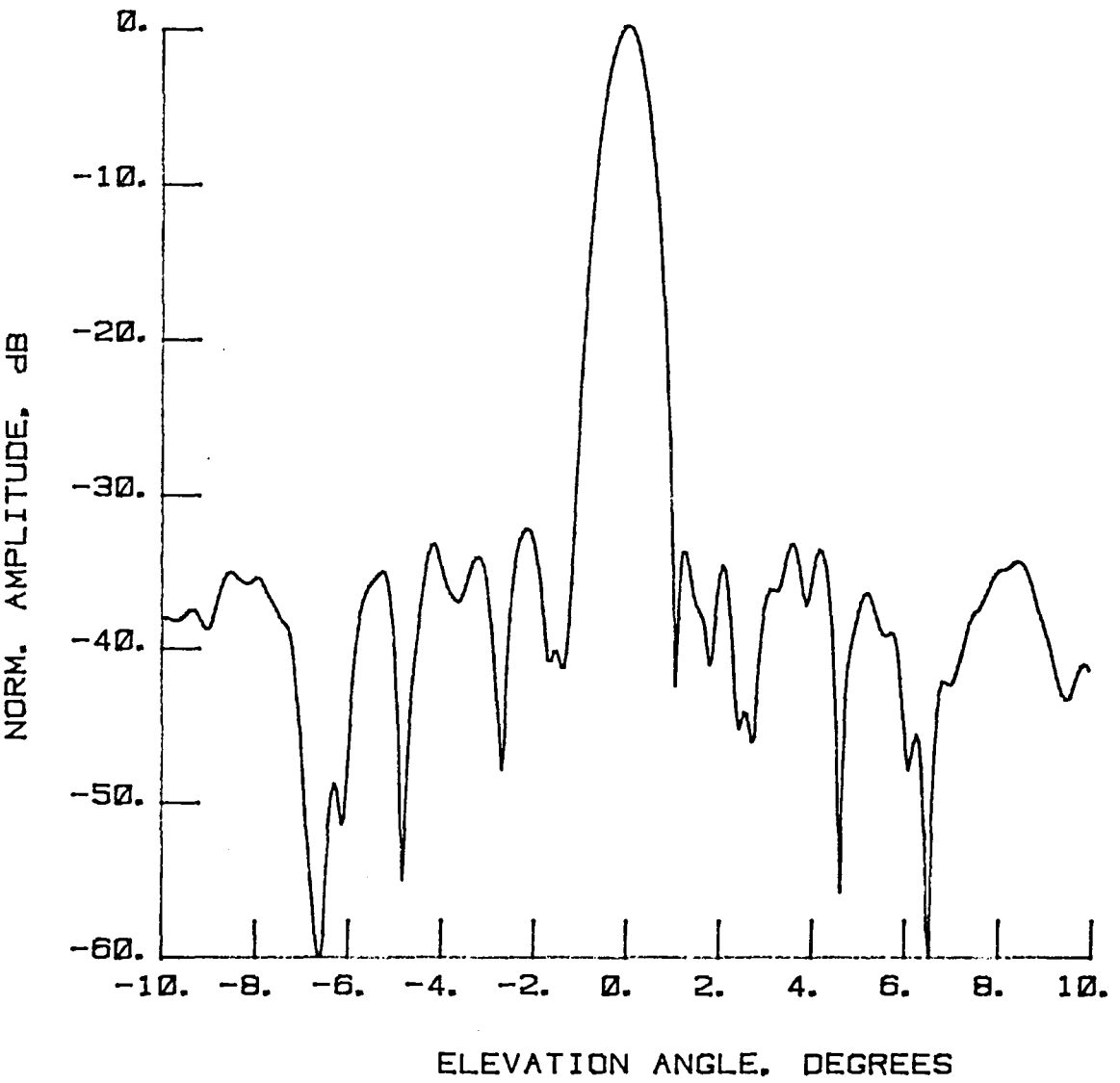

Figure 88 Test 13, 4.26 GHz, Co-Pol, H-Plane, Type 4

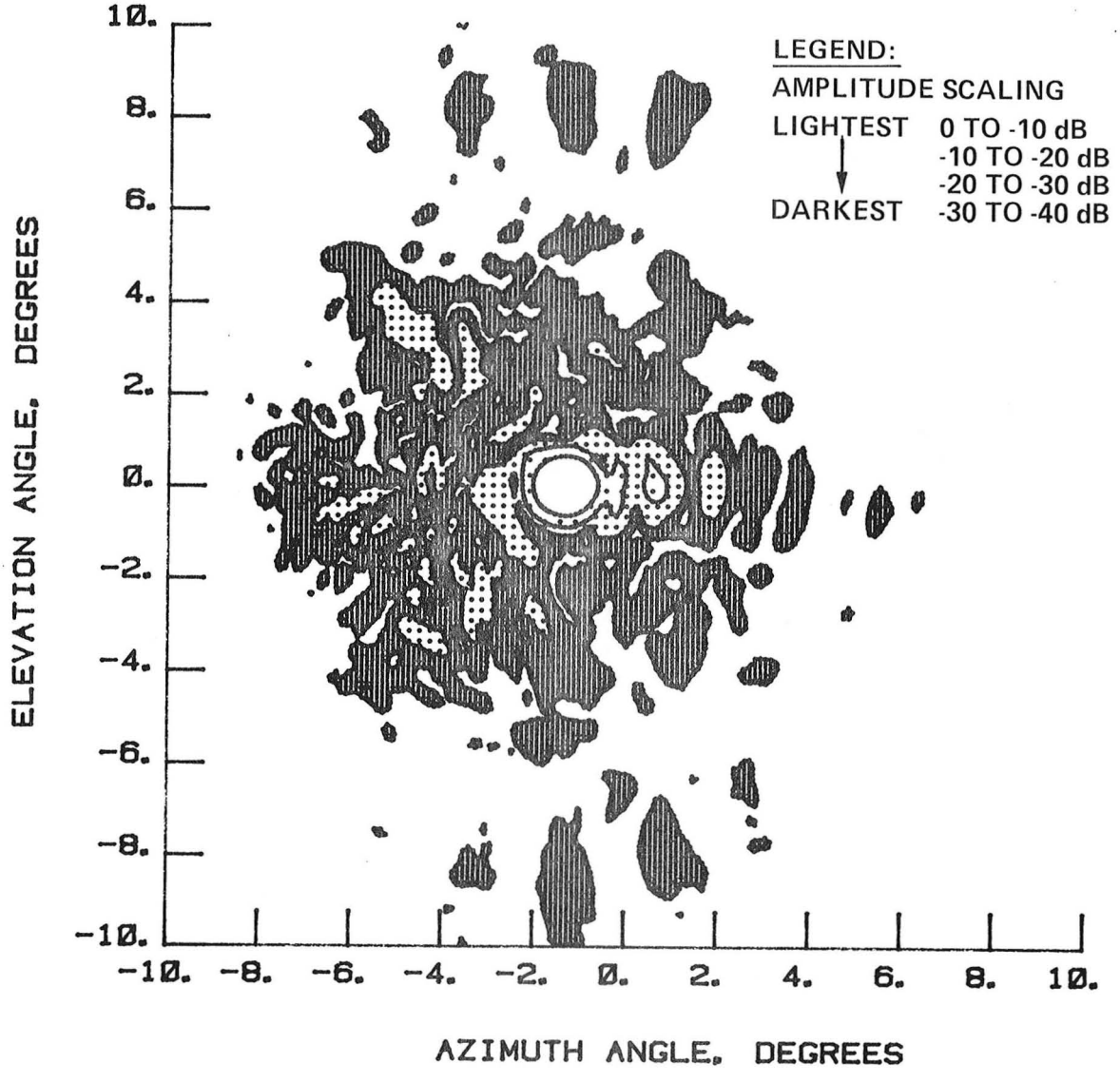

Figure 89 Test 13, 4.26 GHz, Co-Pol, Contour, Type 5

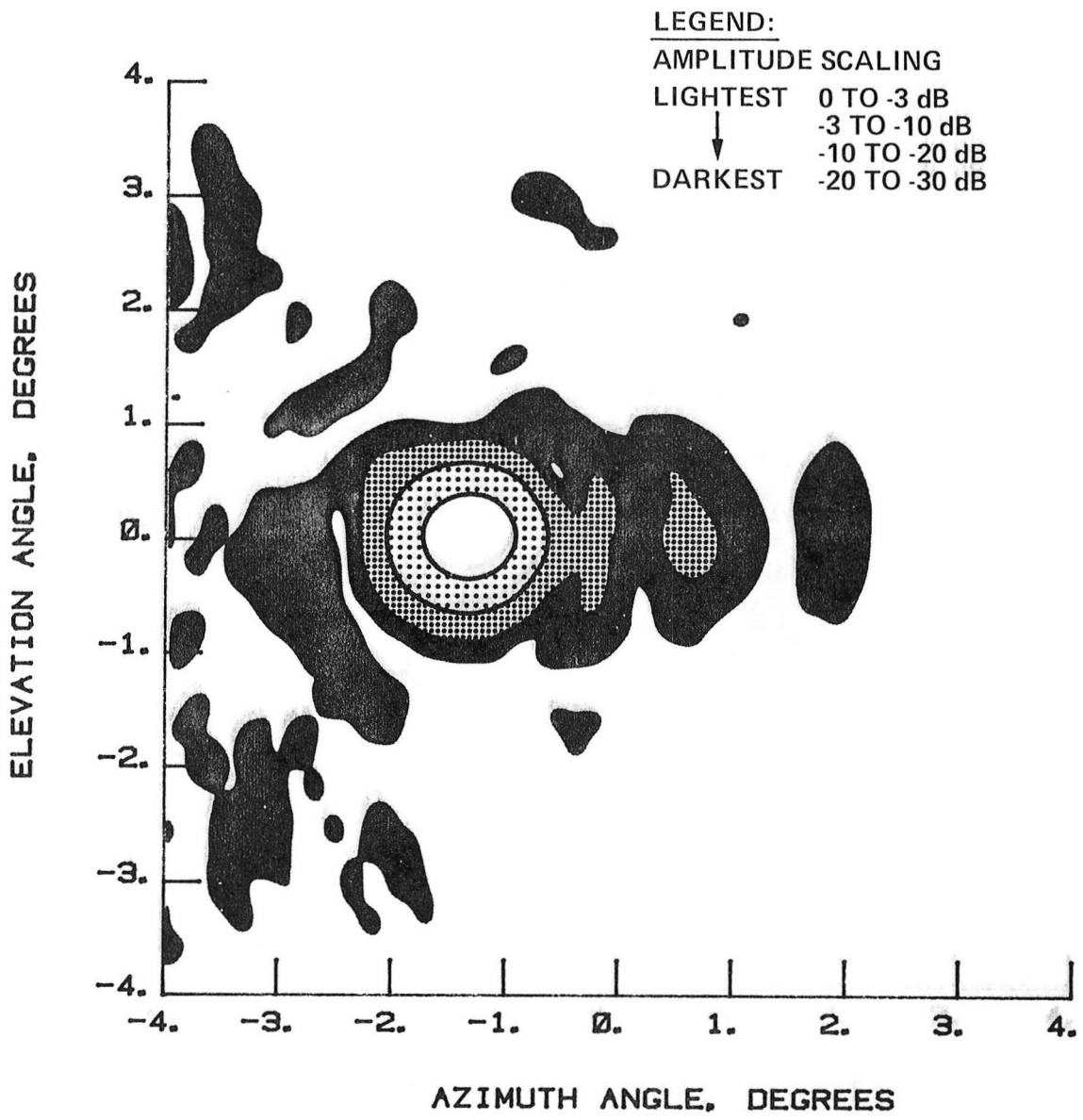

Figure 90 Test 13, 4.26 GHz, Co-Pol, Contour, Type 6

TEST IDENTIFICATION : LRC13/

DATE : 18 SEPT, 1985

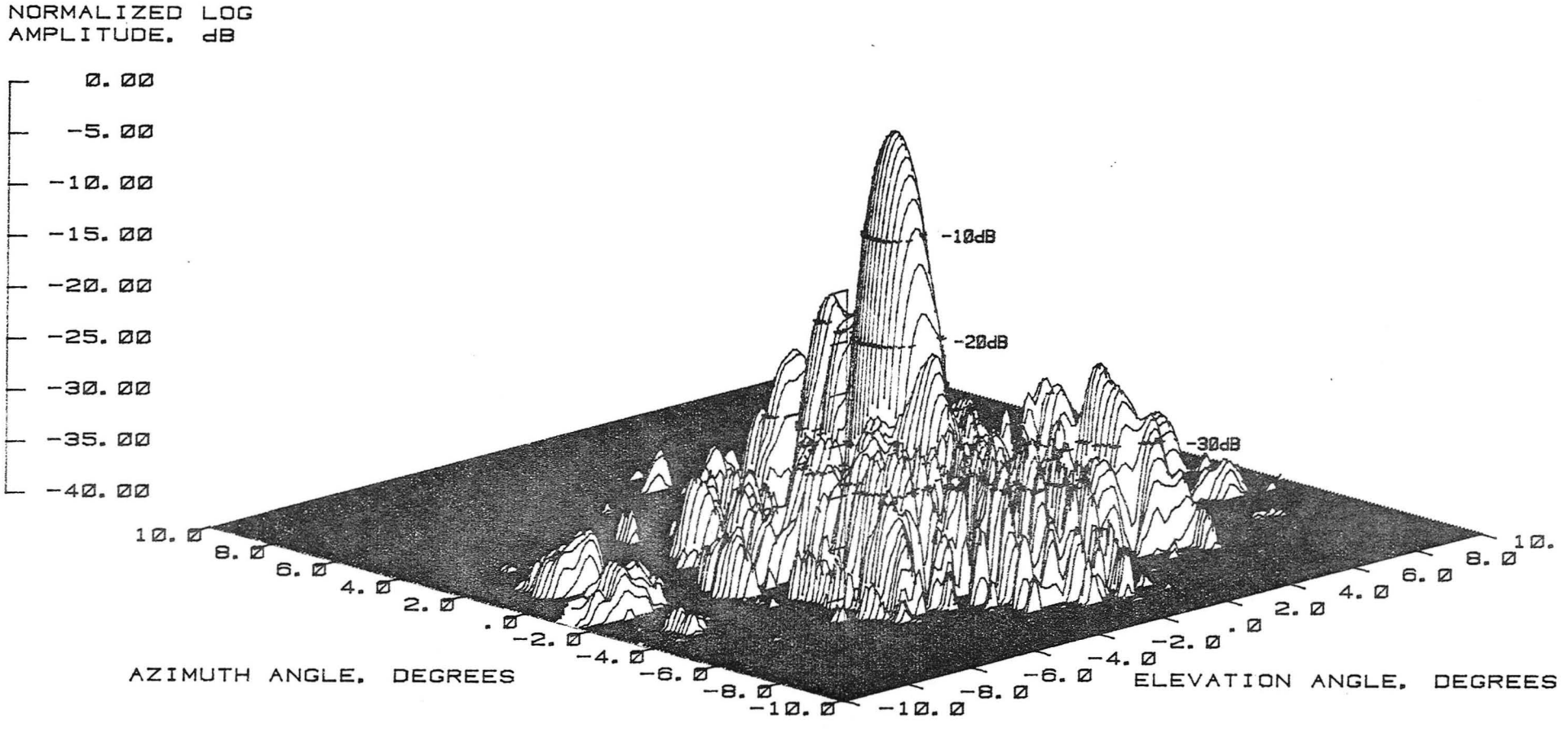

Figure 91 Test 13, 4.26 GHz, Co-Pol, 3-D, Type 7

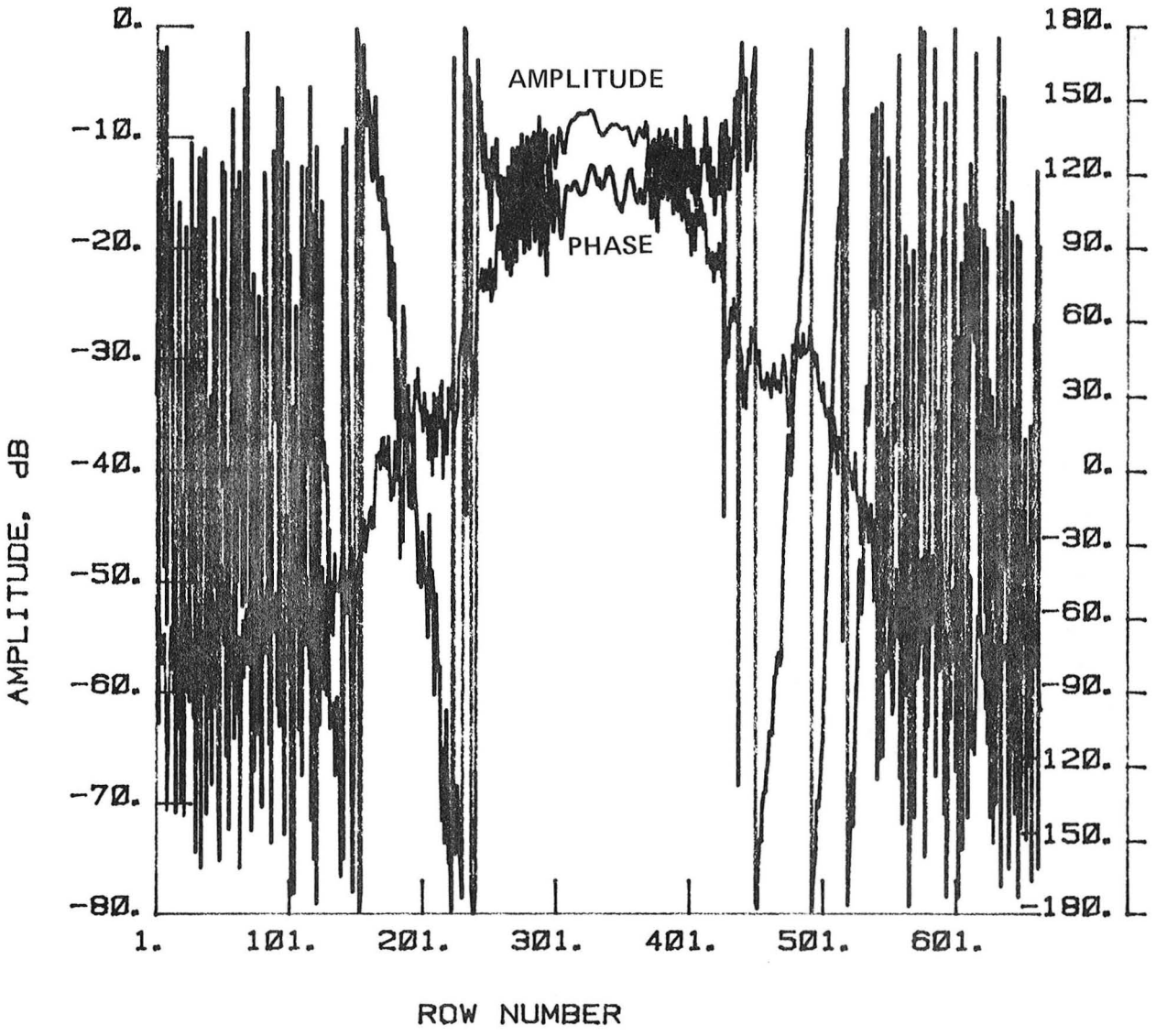

Figure 92 Test 13, 4.26 GHz, Co-Pol, H-Plane, Type 8

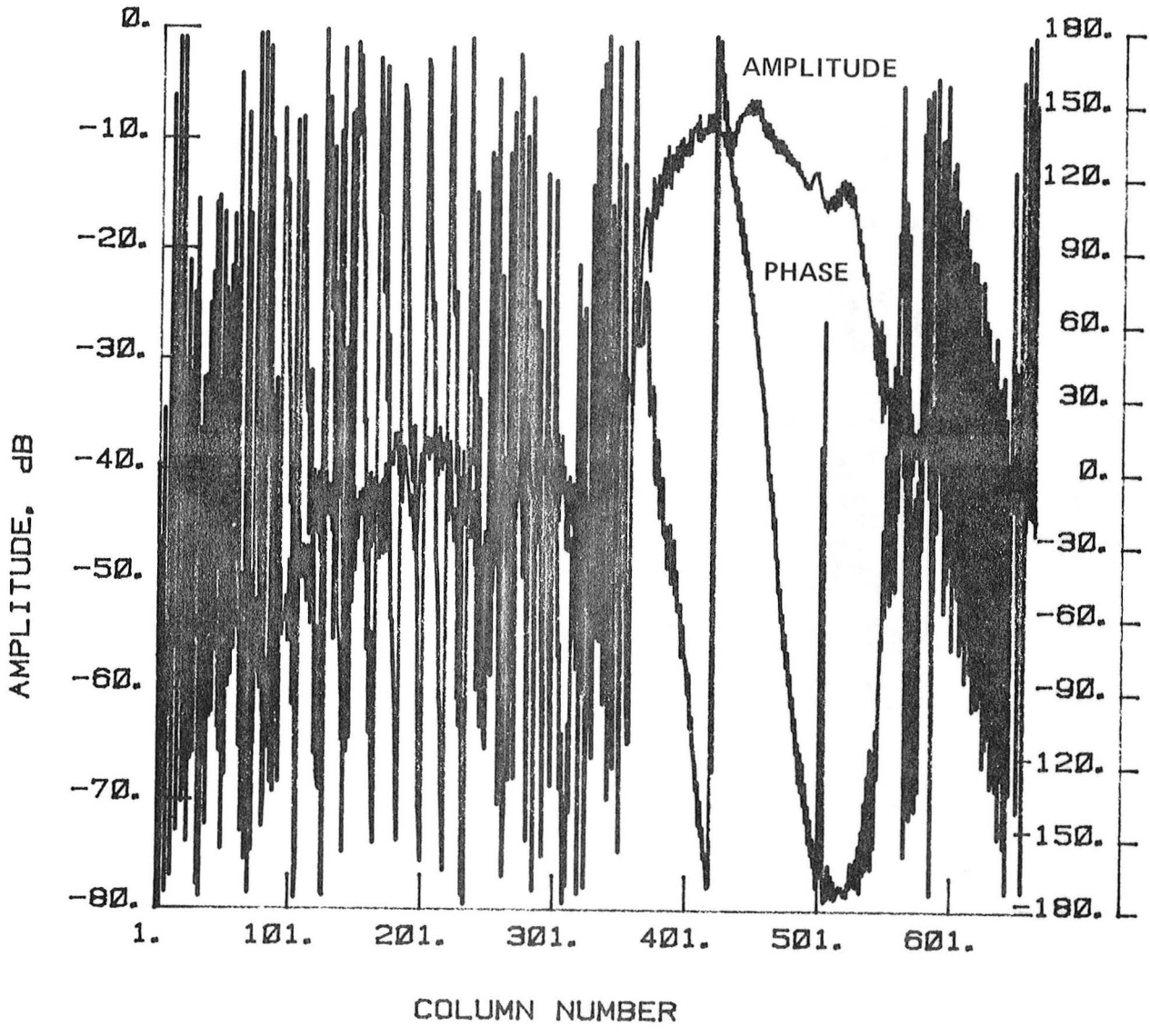

Figure 93 Test 13, 4.26 GHz, Co-Pol, E-Plane, Type 9

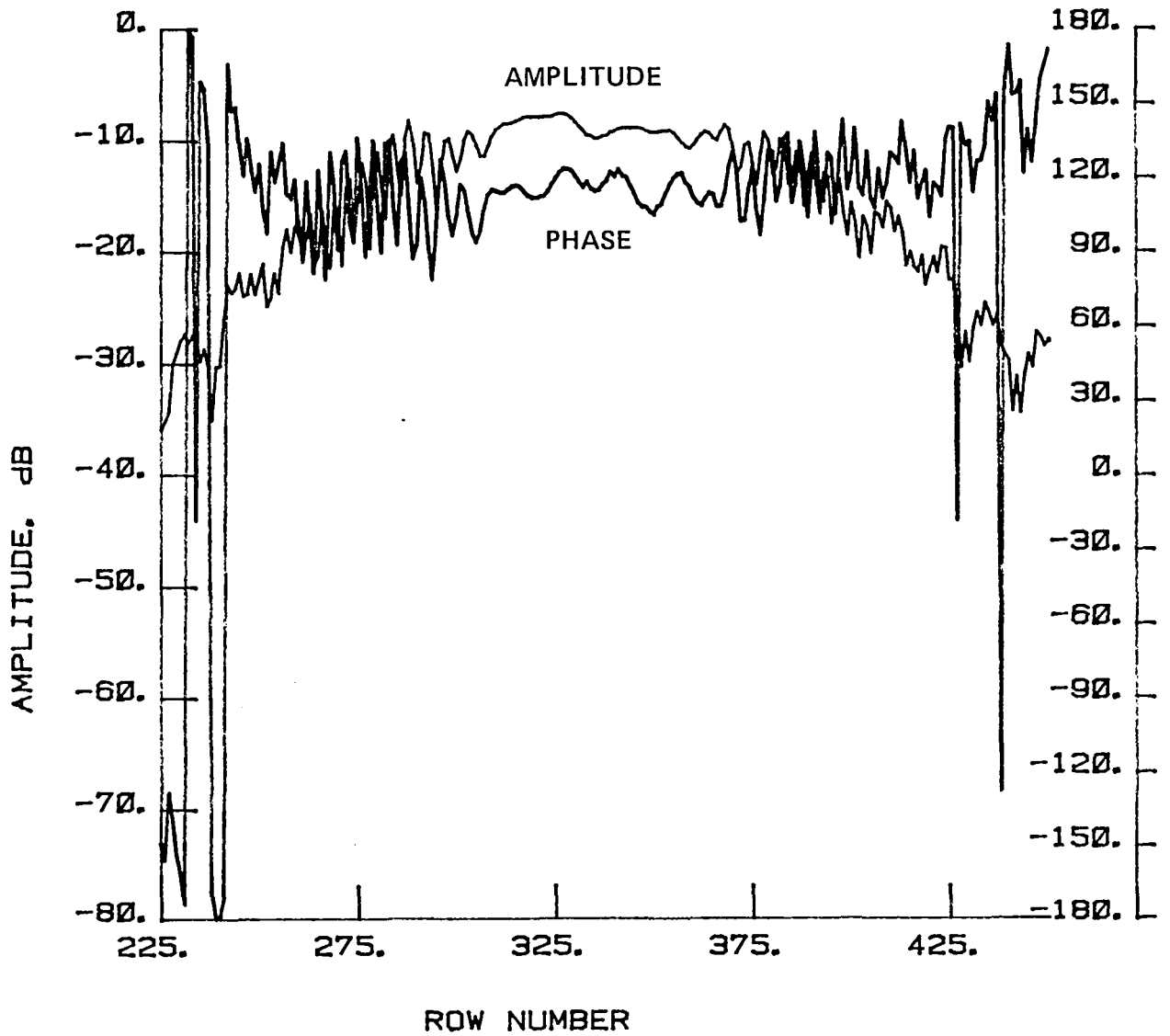

Figure 94 Test 13, 4.26 GHz, Co-Pol, H-Plane, Type 10

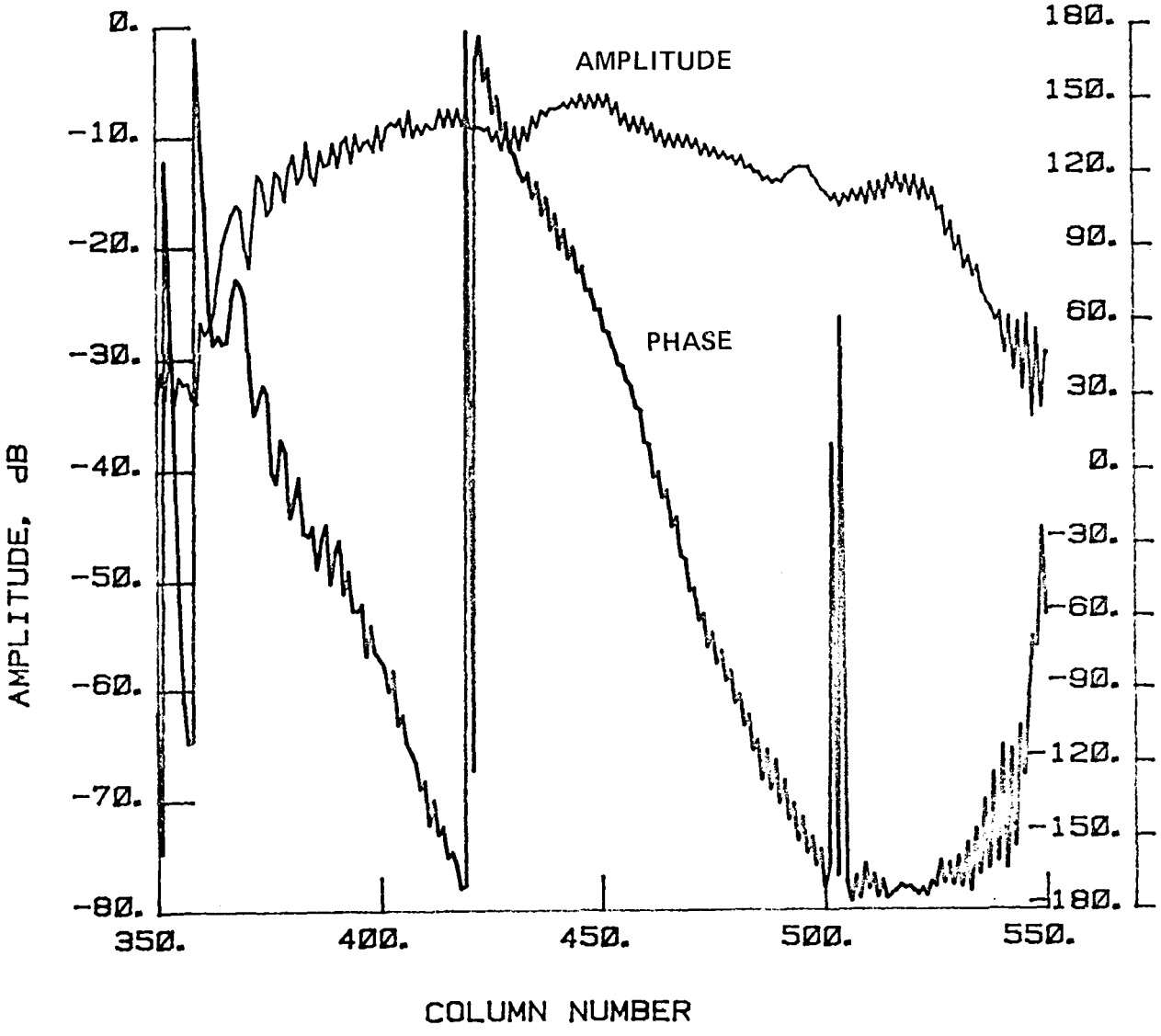

Figure 95 Test 13, 4.26 GHz, Co-Pol, E-Plane, Type 11

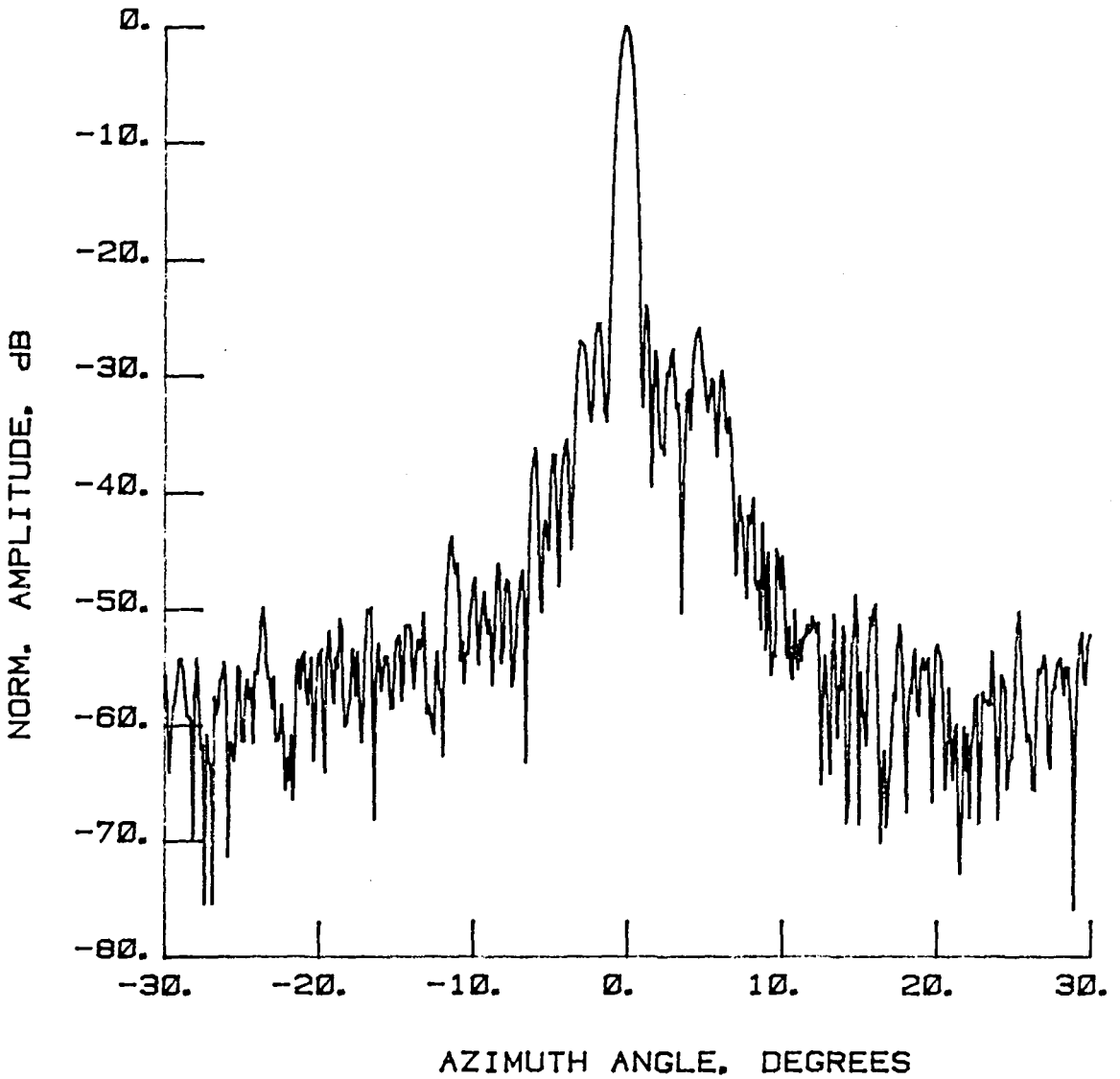

Figure 96 Test 14, 4.26 GHz, Co-Pol, E-Plane, Type 1

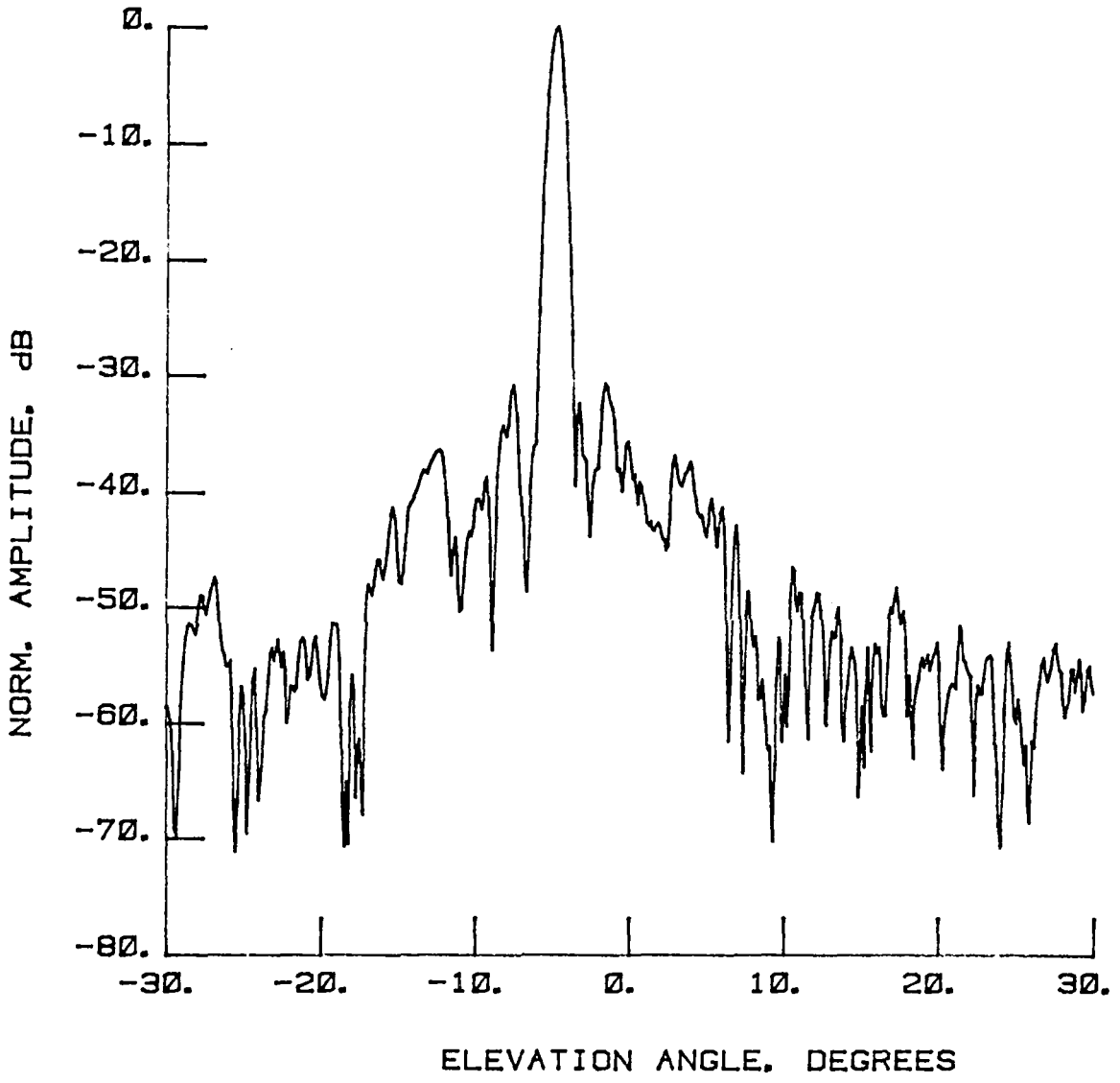

Figure 97 Test 14, 4.26 GHz, Co-Pol, H-Plane, Type 2

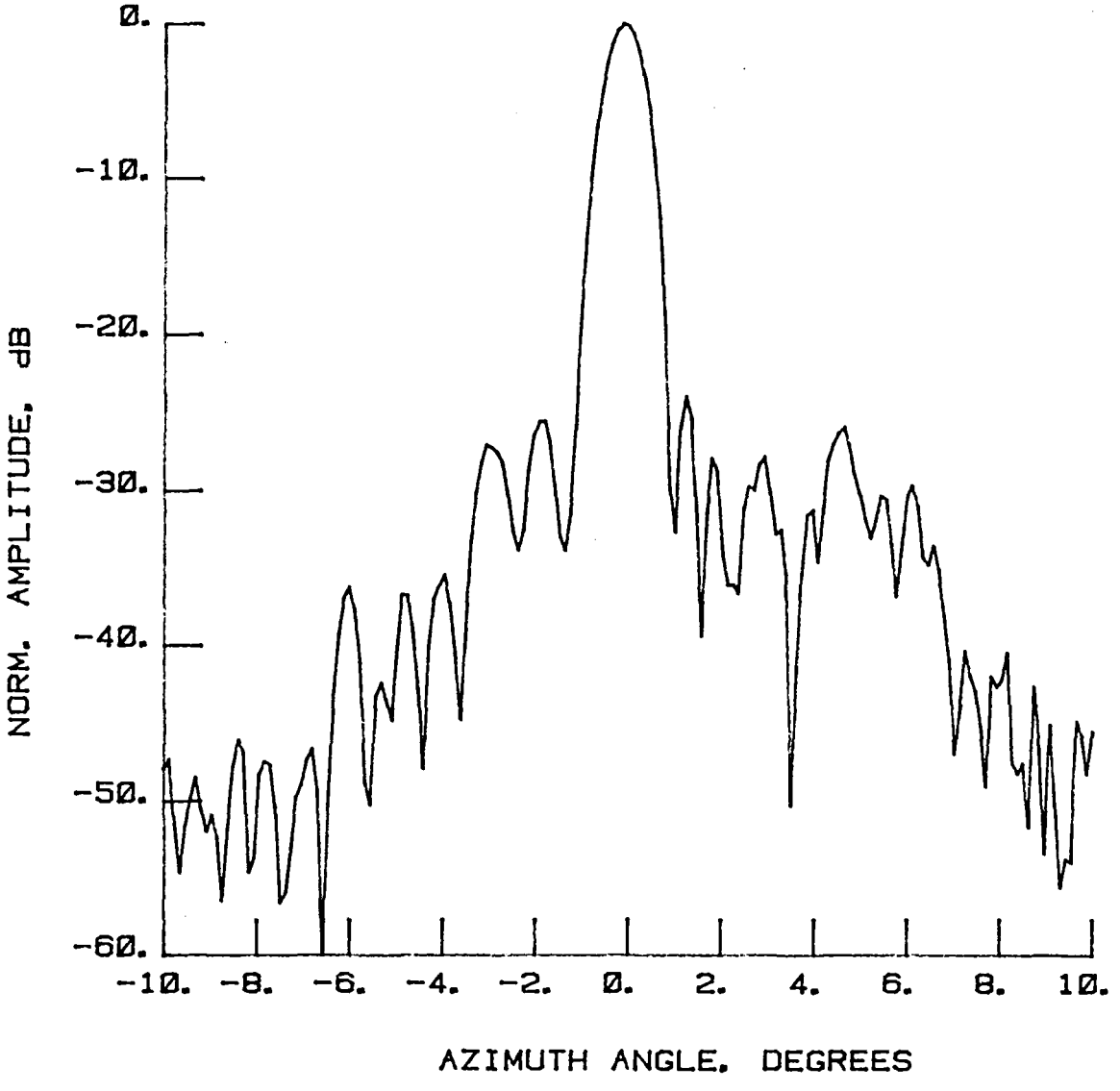

Figure 98 Test 14, 4.26 GHz, Co-Pol, E-Plane, Type 3

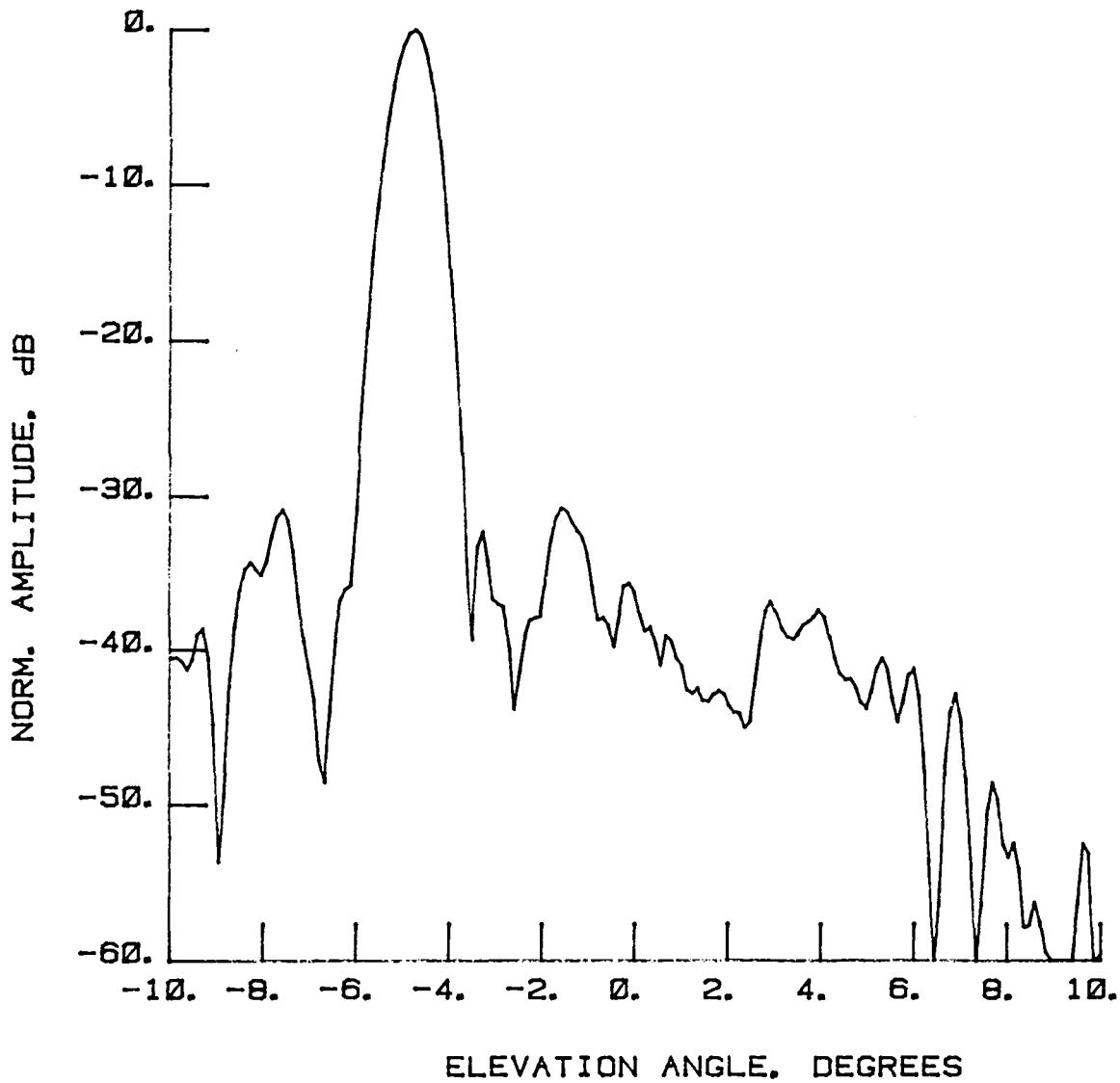

Figure 99 Test 14, 4.26 GHz, Co-Pol, H-Plane, Type 4

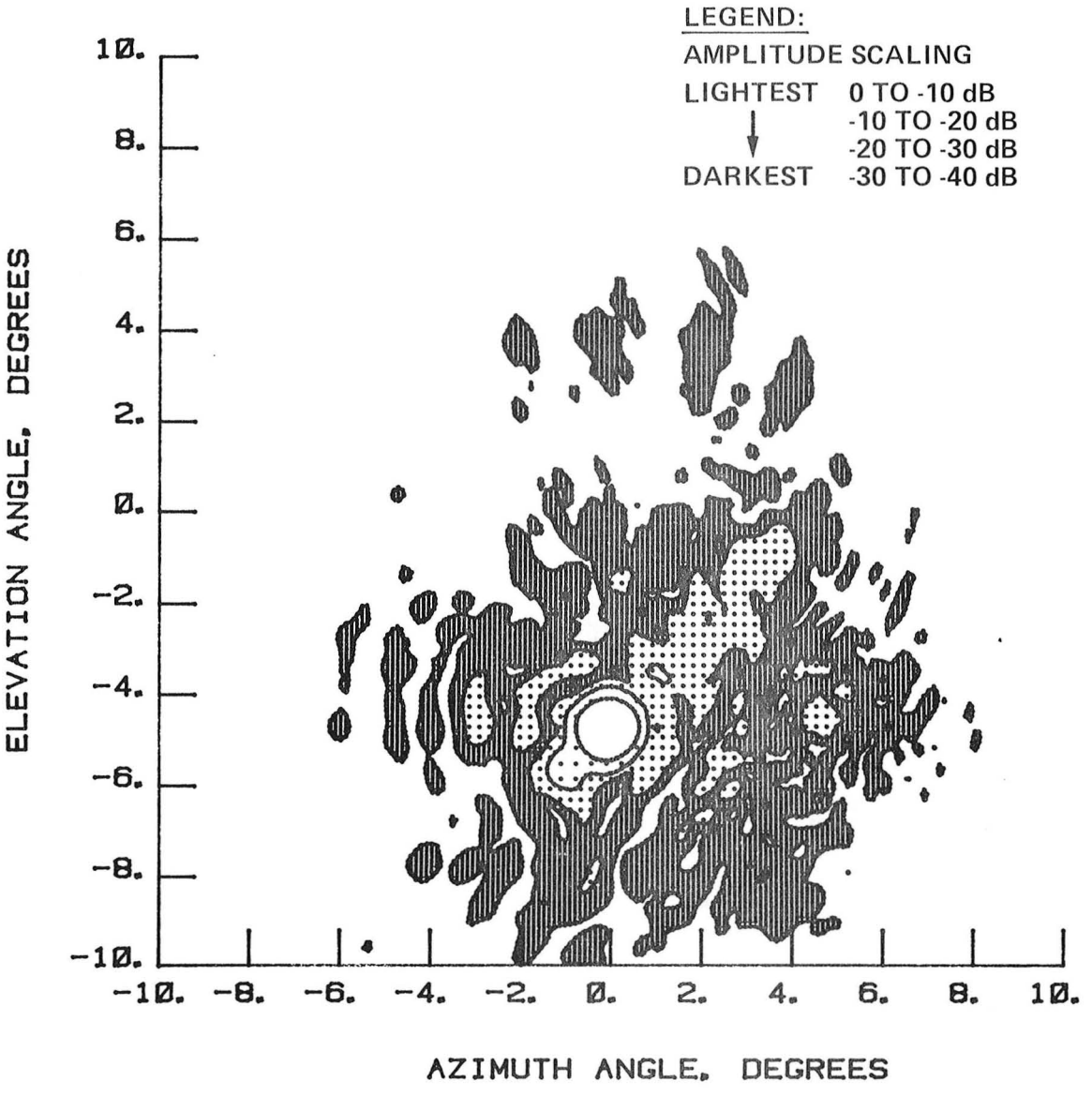

Figure 100 Test 14, 4.26 GHz, Co-Pol, Contour, Type 5

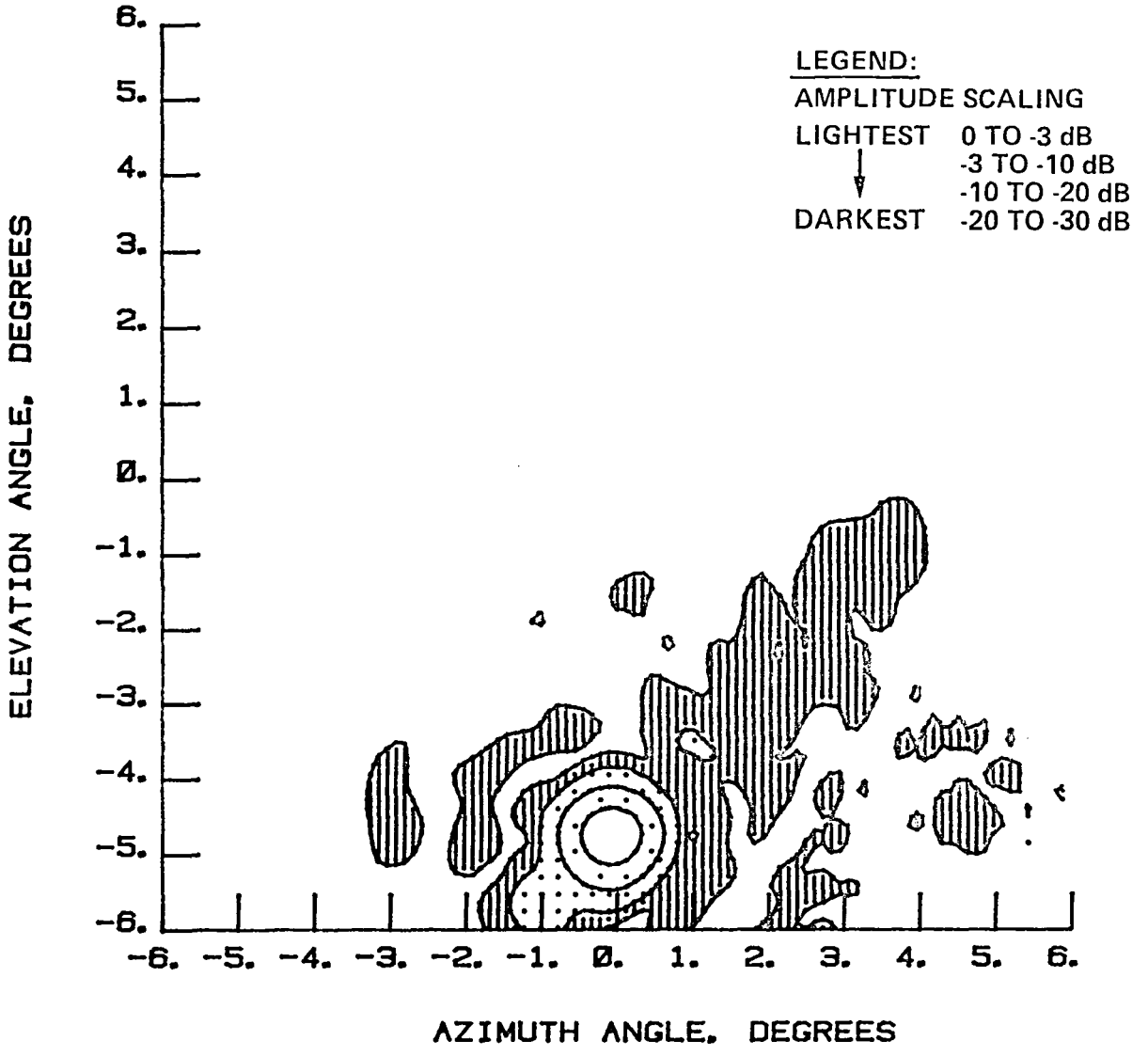

Figure 101. Test 14, 4.26 GHz, Co-Pol, Contour, Type 6

TEST IDENTIFICATION : LRC14/

DATE : 18 SEPT. 1985

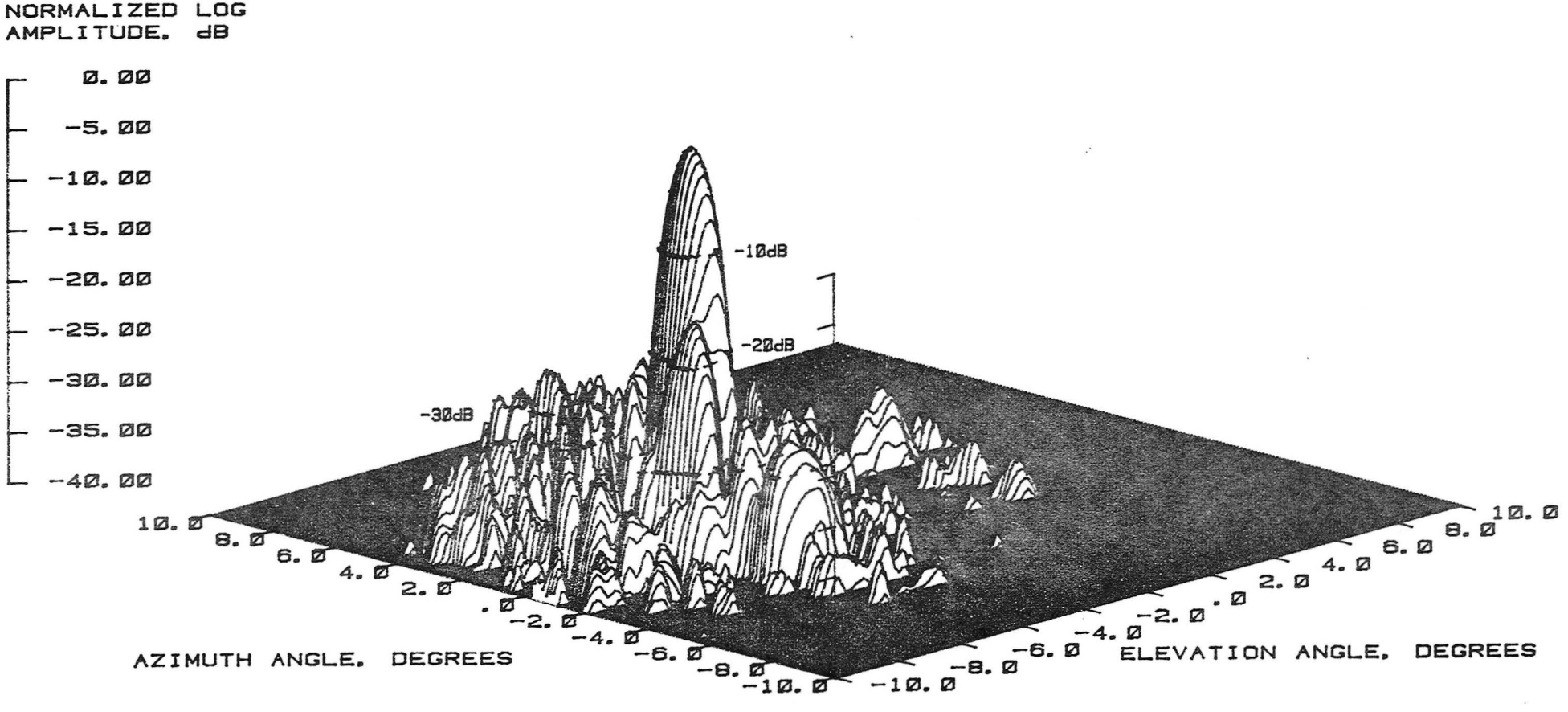

Figure 102 Test 14, 4.26 GHz, Co-Pol, 3-D, Type 7

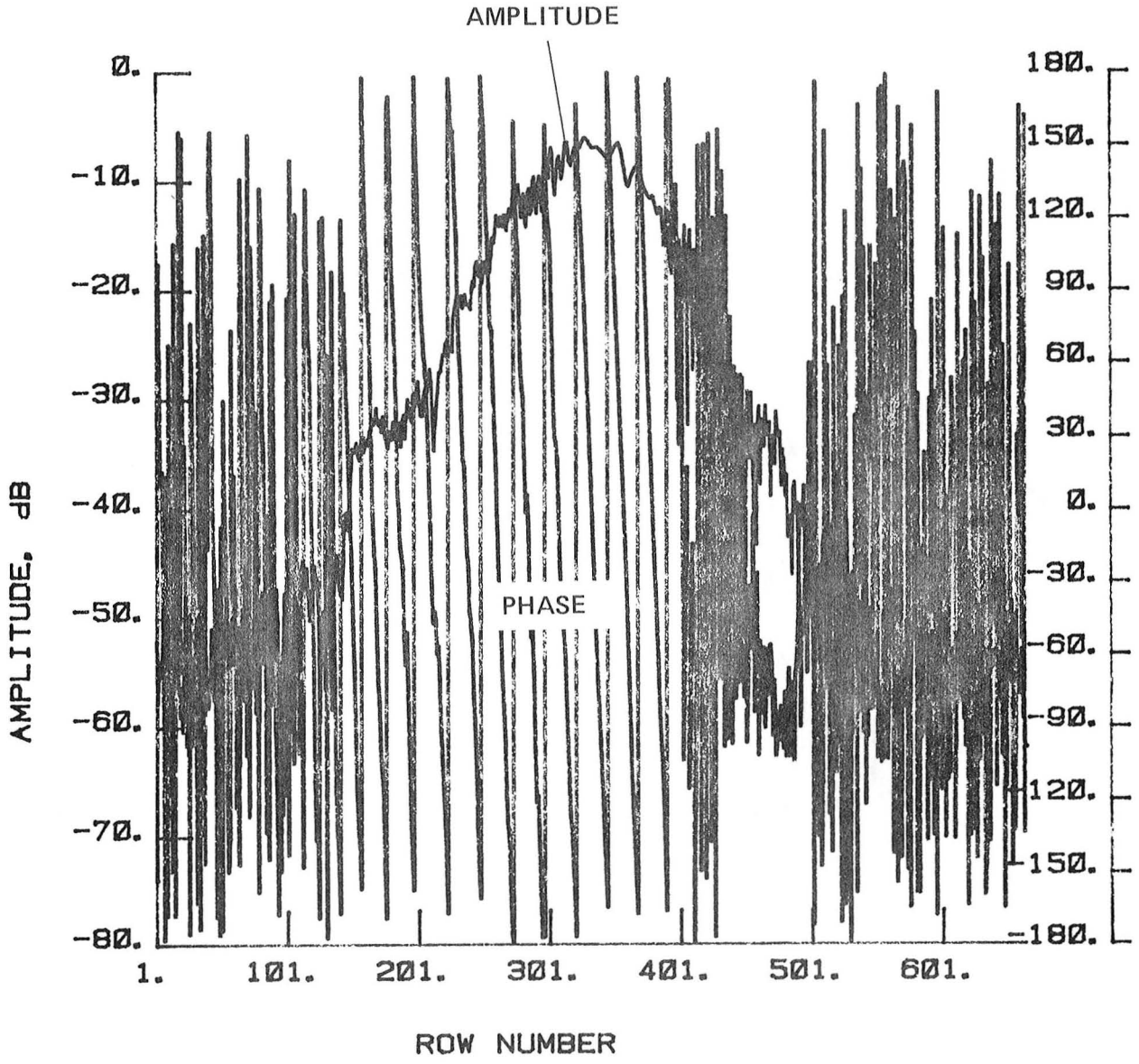

Figure 103 Test 14, 4.26 GHz, Co-Pol, H-Plane, Type 8

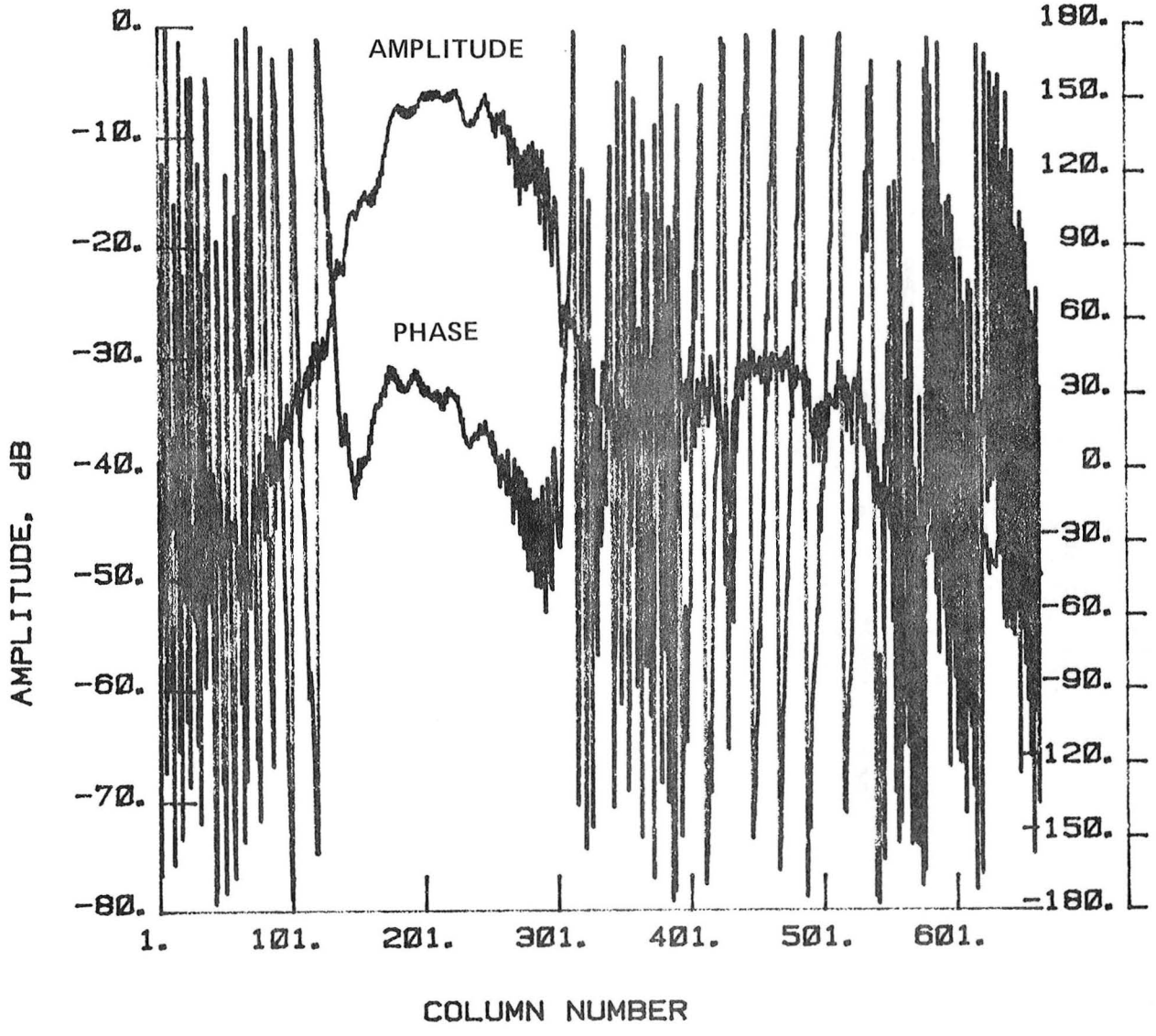

Figure 104 Test 14, 4.26 GHz, Co-Pol, E-Plane, Type 9

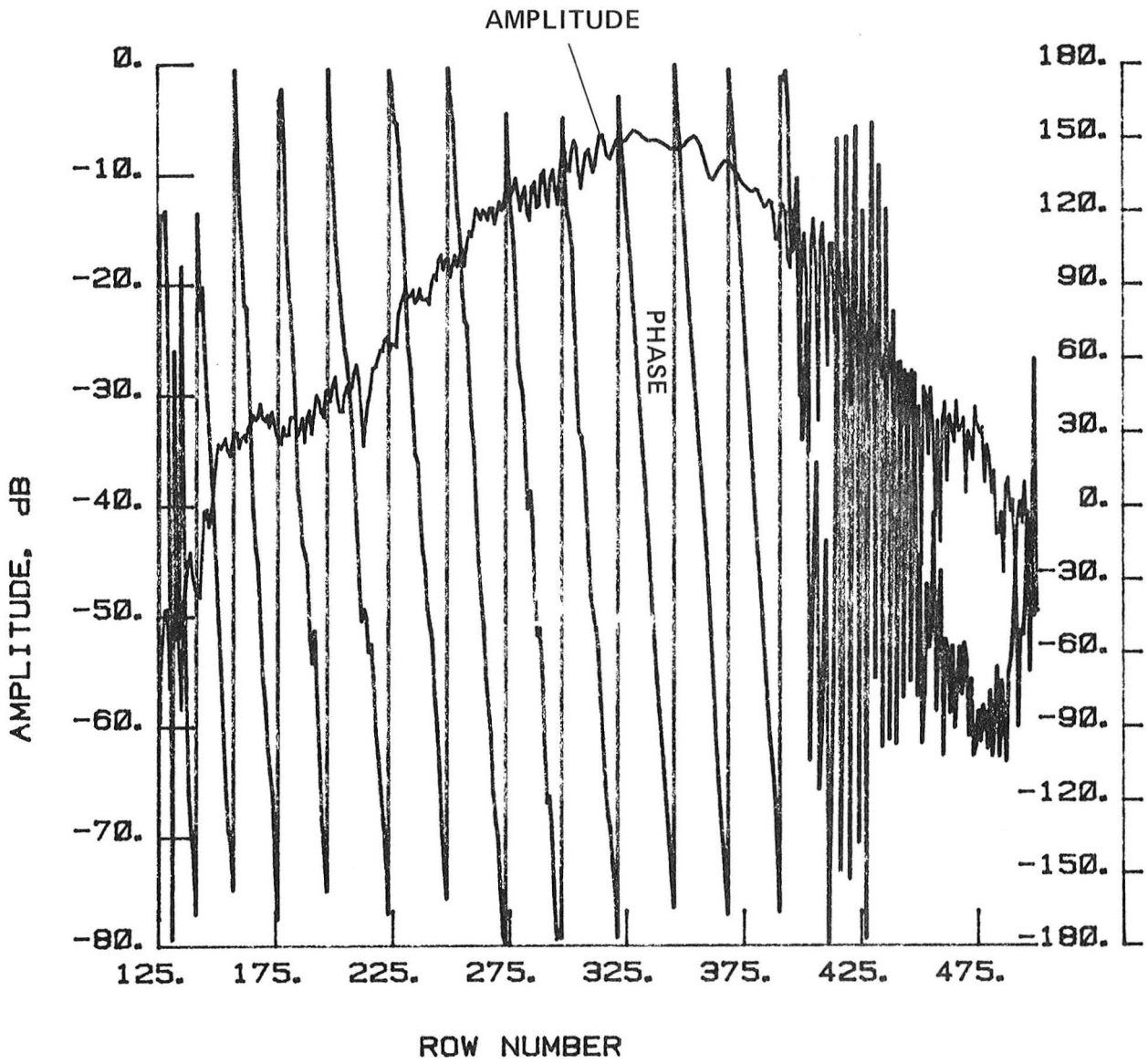

Figure 105 Test 14, 4.26 GHz, Co-Pol, H-Plane, Type 10

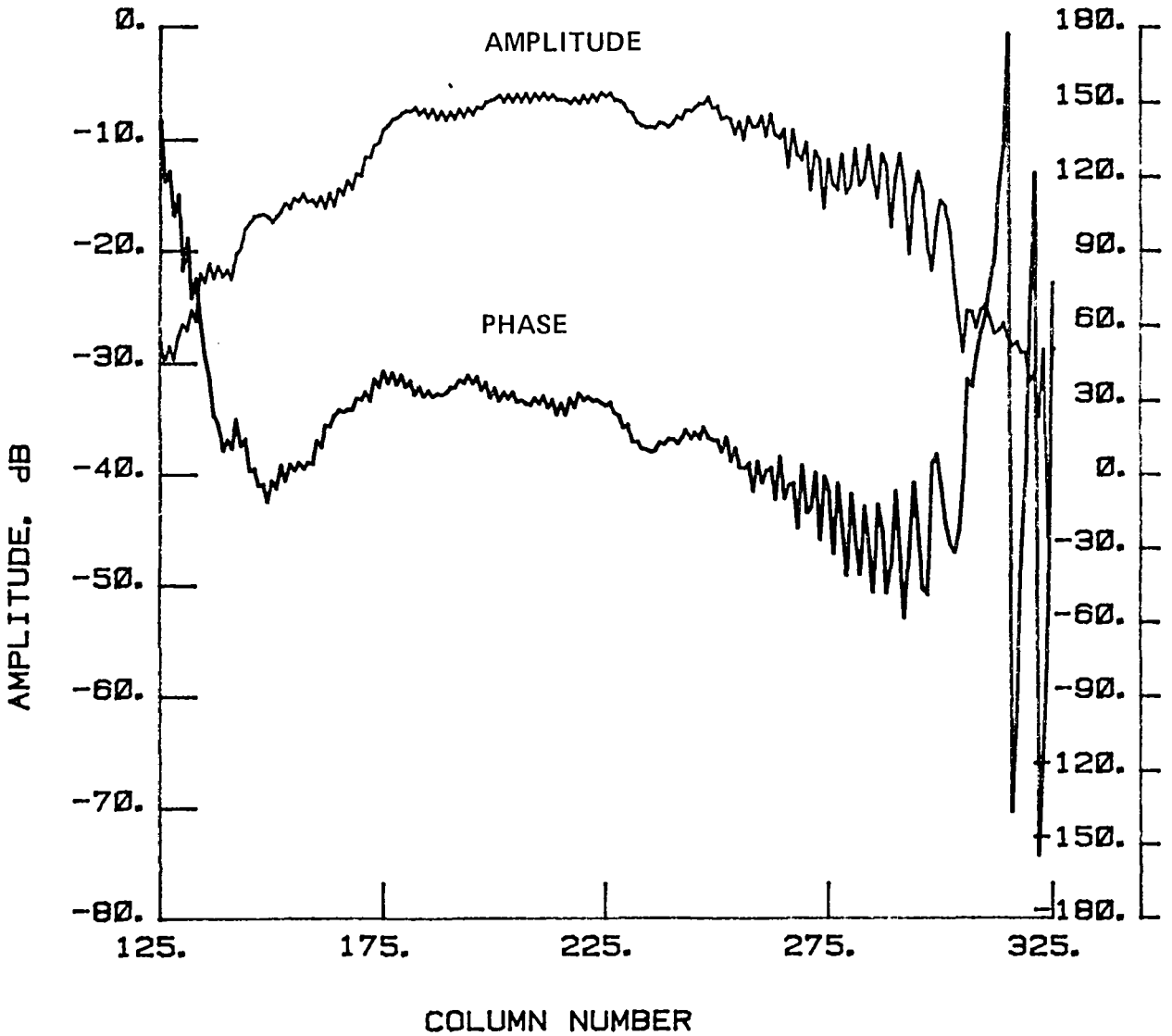

Figure 106 Test 14, 4.26 GHz, Co-Pol, E-Plane, Type 11

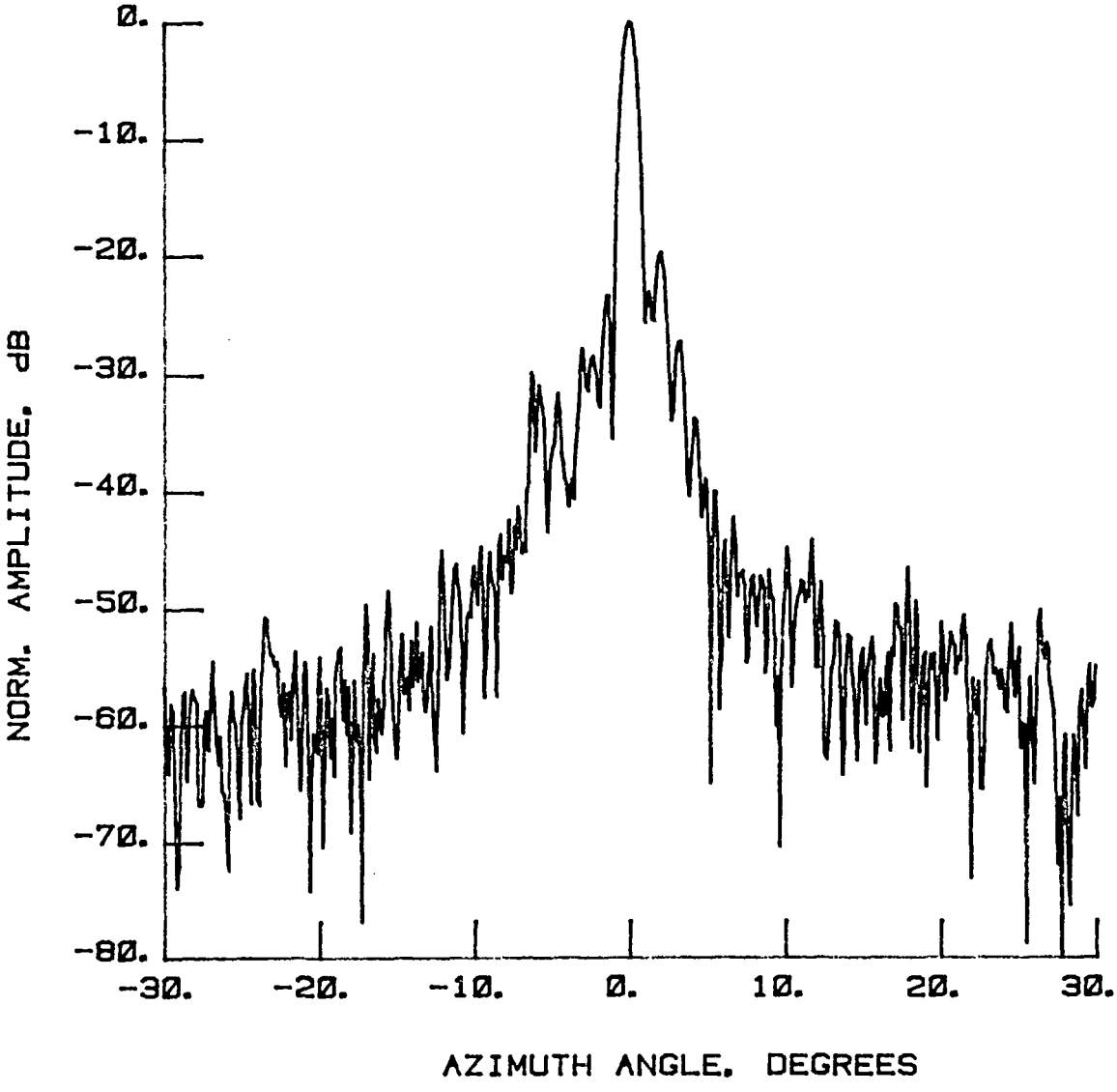

Figure 107 Test 15, 4.26 GHz, Co-Pol, E-Plane, Type 1

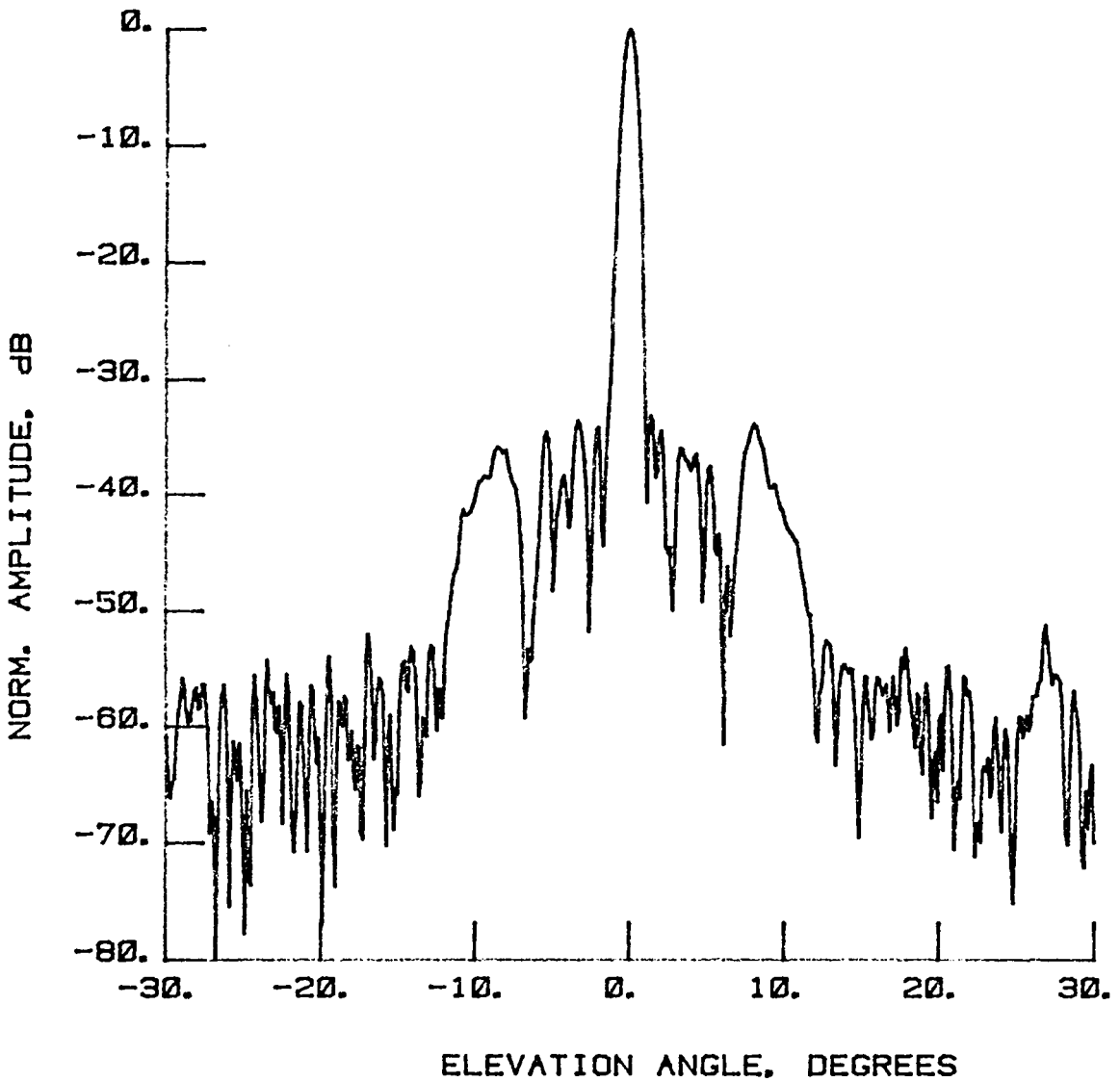

Figure 108 Test 15, 4.26 GHz, Co-Pol, H-Plane, Type 2

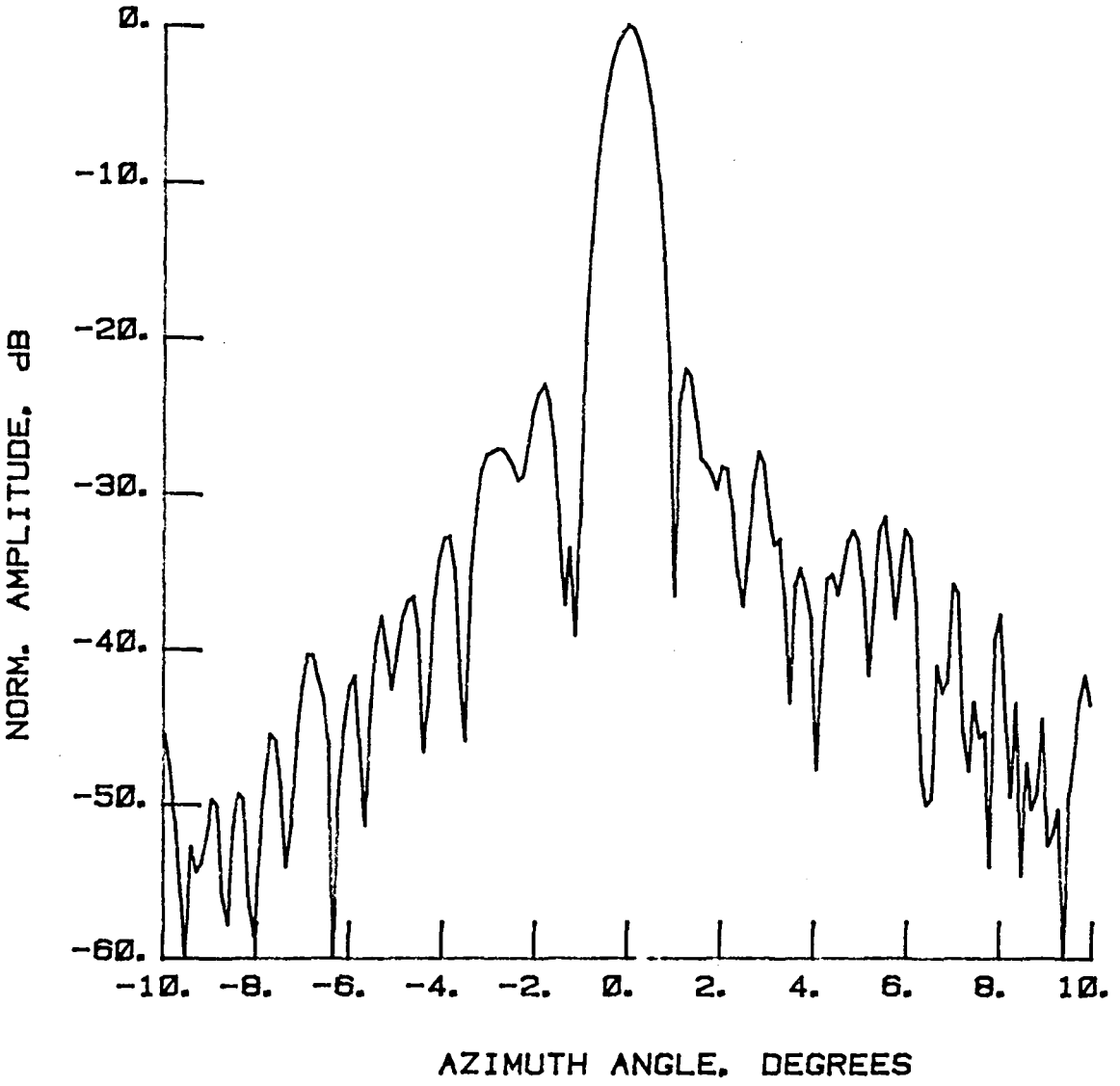

Figure 109 Test 15, 4.26 GHz, Co-Pol, E-Plane, Type 3

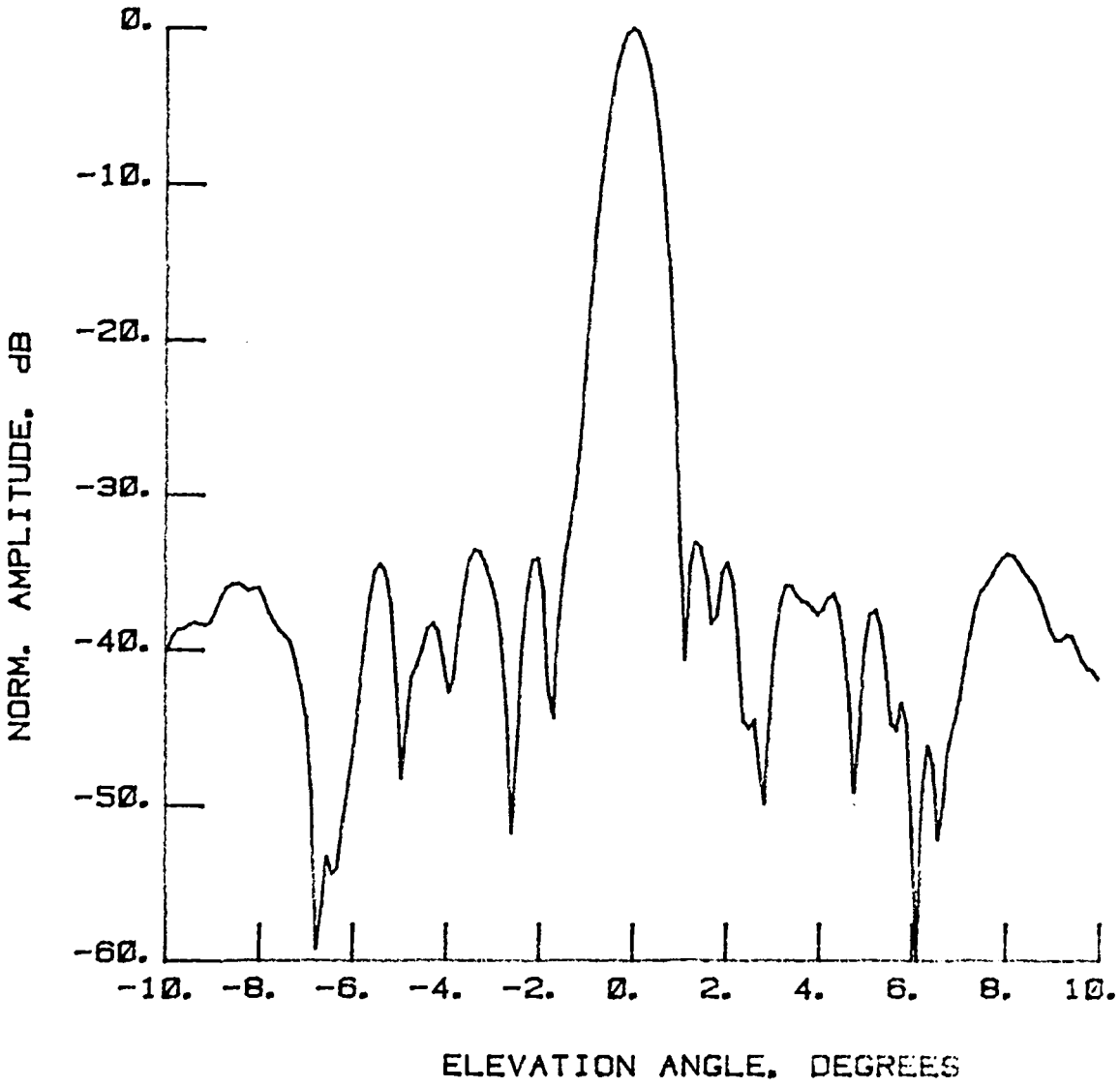

Figure 110 Test 15, 4.26 GHz, Co-Pol, H-Plane, Type 4

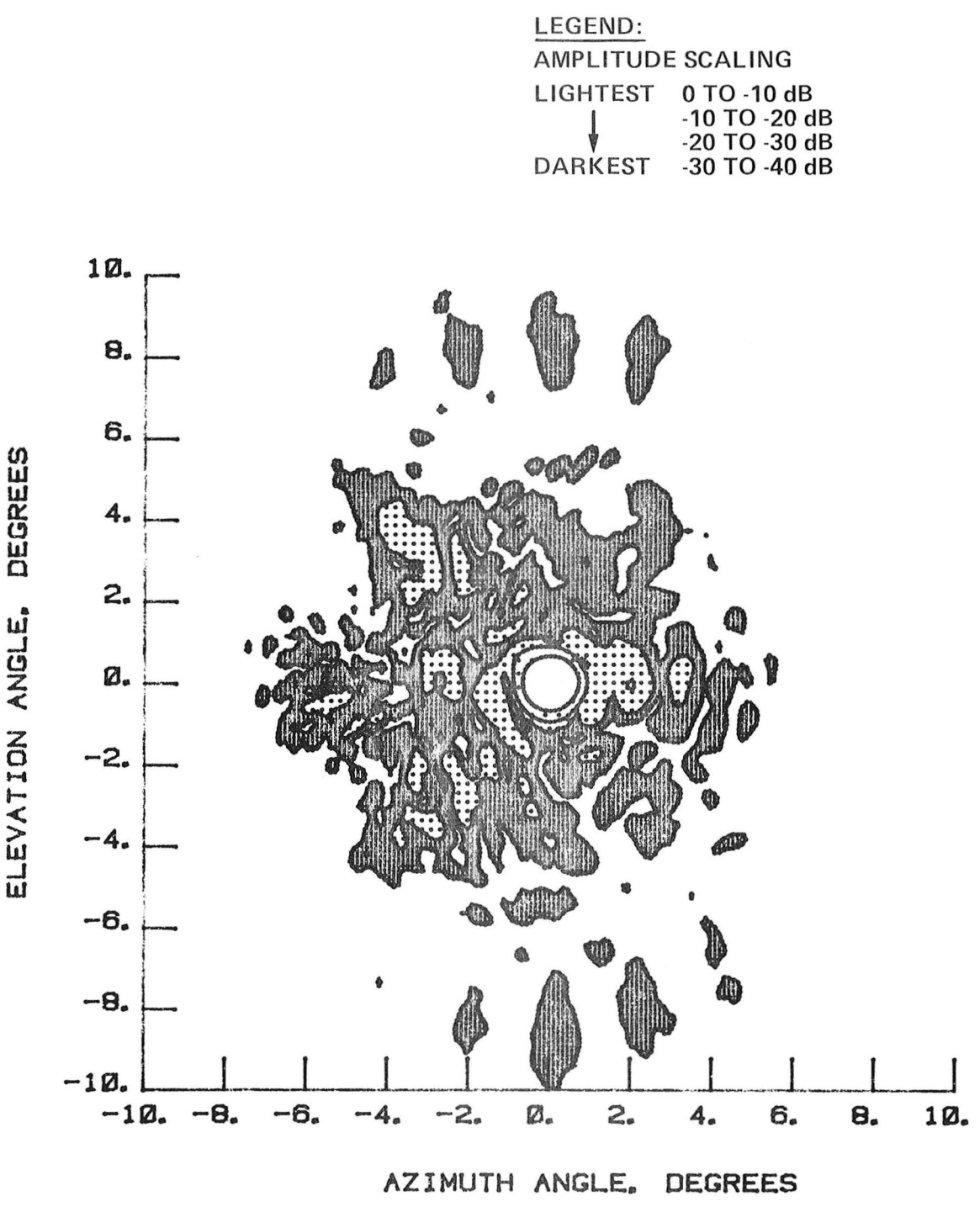

Figure 111 Test 15, 4.26 GHz, Co-Pol, Contour, Type 5

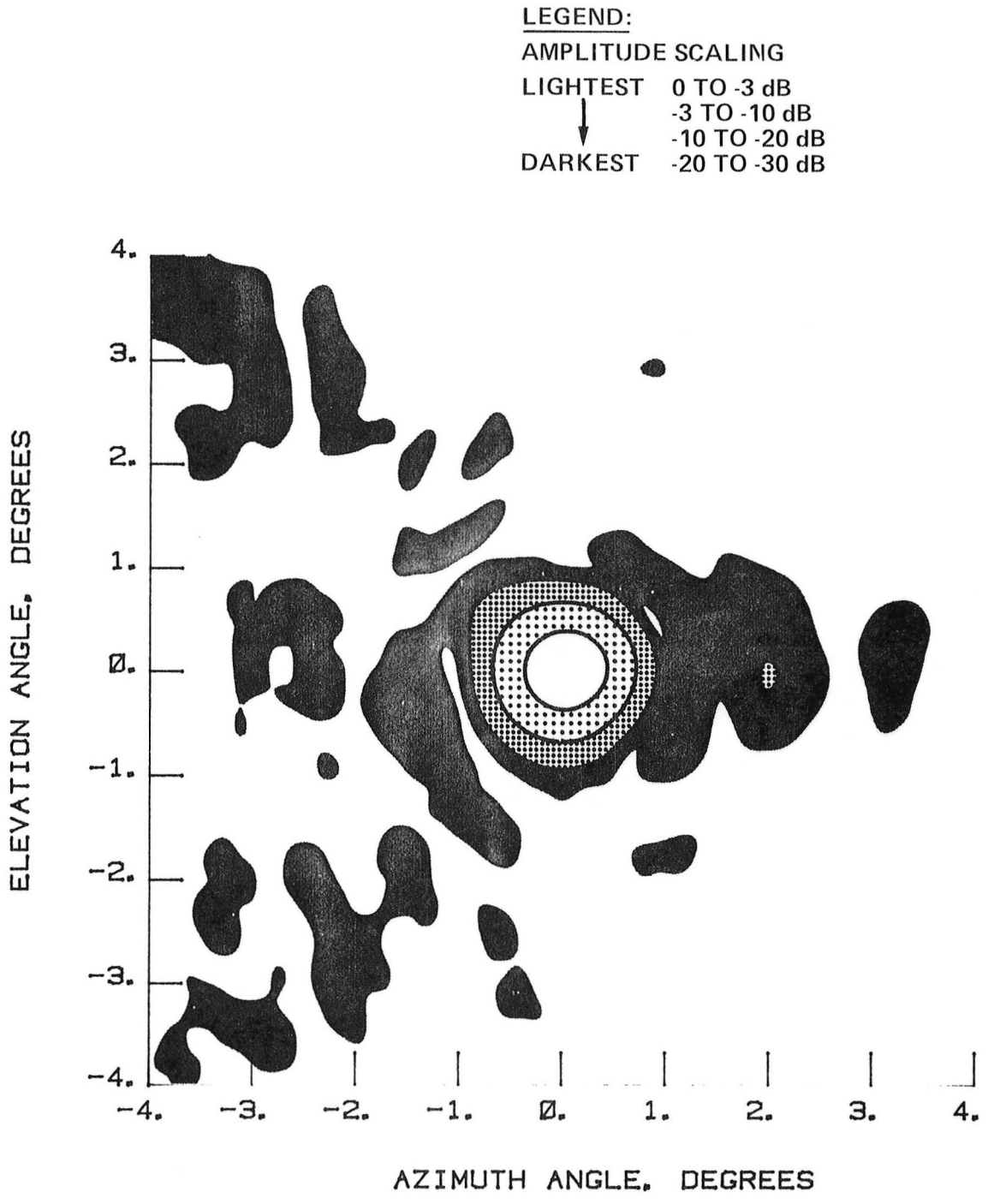

Figure 112 Test 15, 4.26 GHz, Co-Pol, Contour, Type 6

TEST IDENTIFICATION : LRC15/

DATE : 18 SEPT. 1985

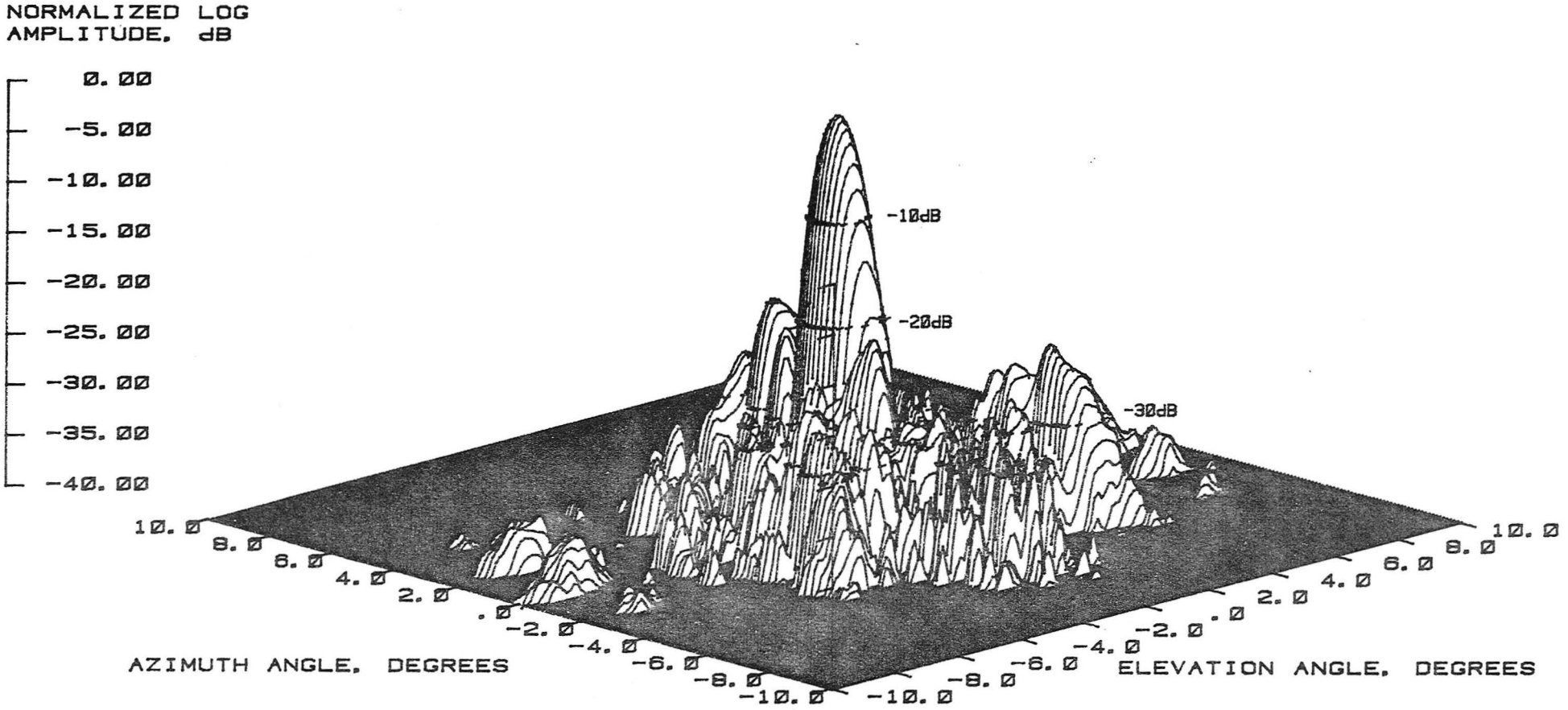

Figure 113 Test 15, 4.26 GHz, Co-Pol, 3-D, Type 7

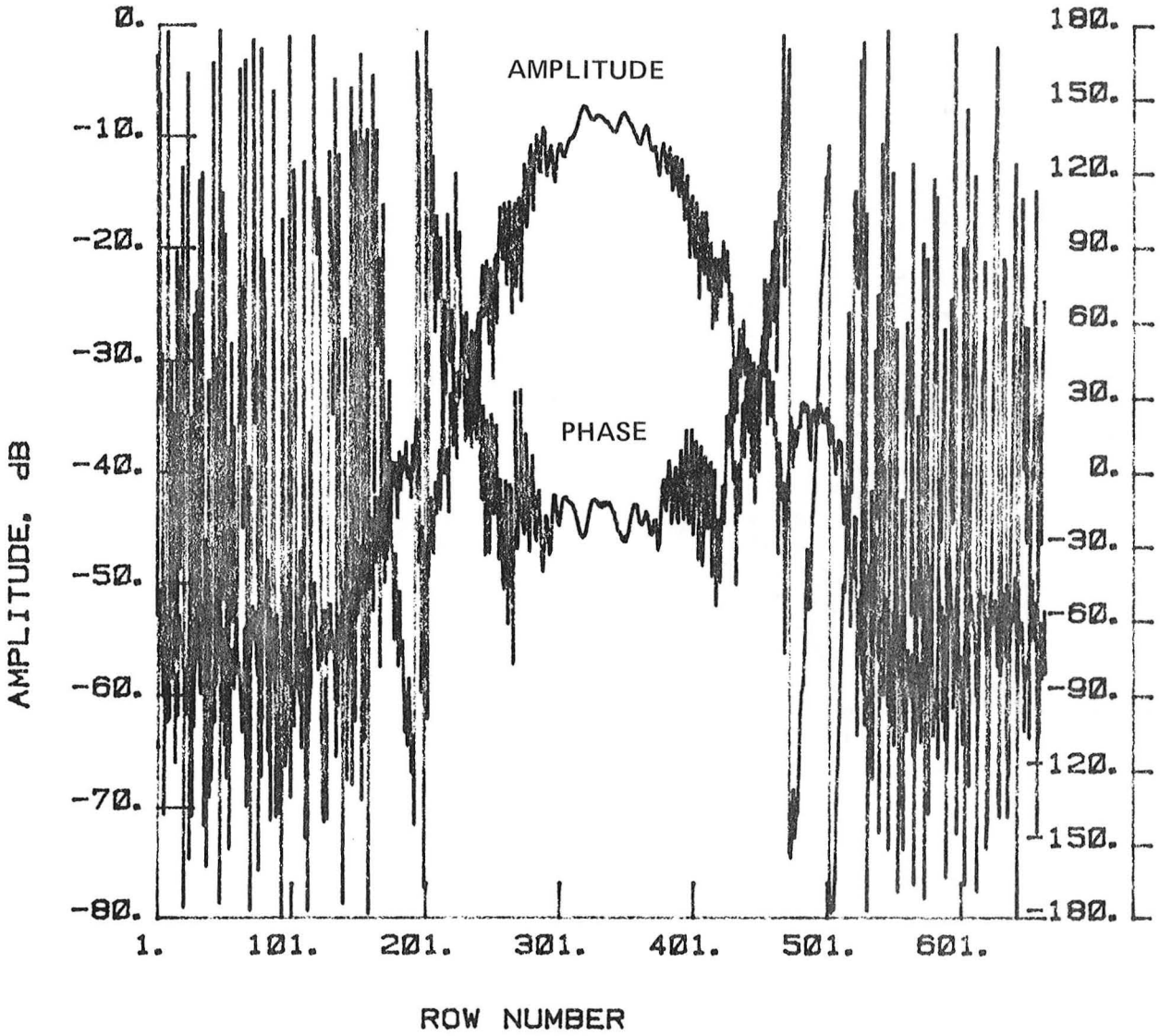

Figure 114 Test 15, 4.26 GHz, Co-Pol, H-Plane, Type 8

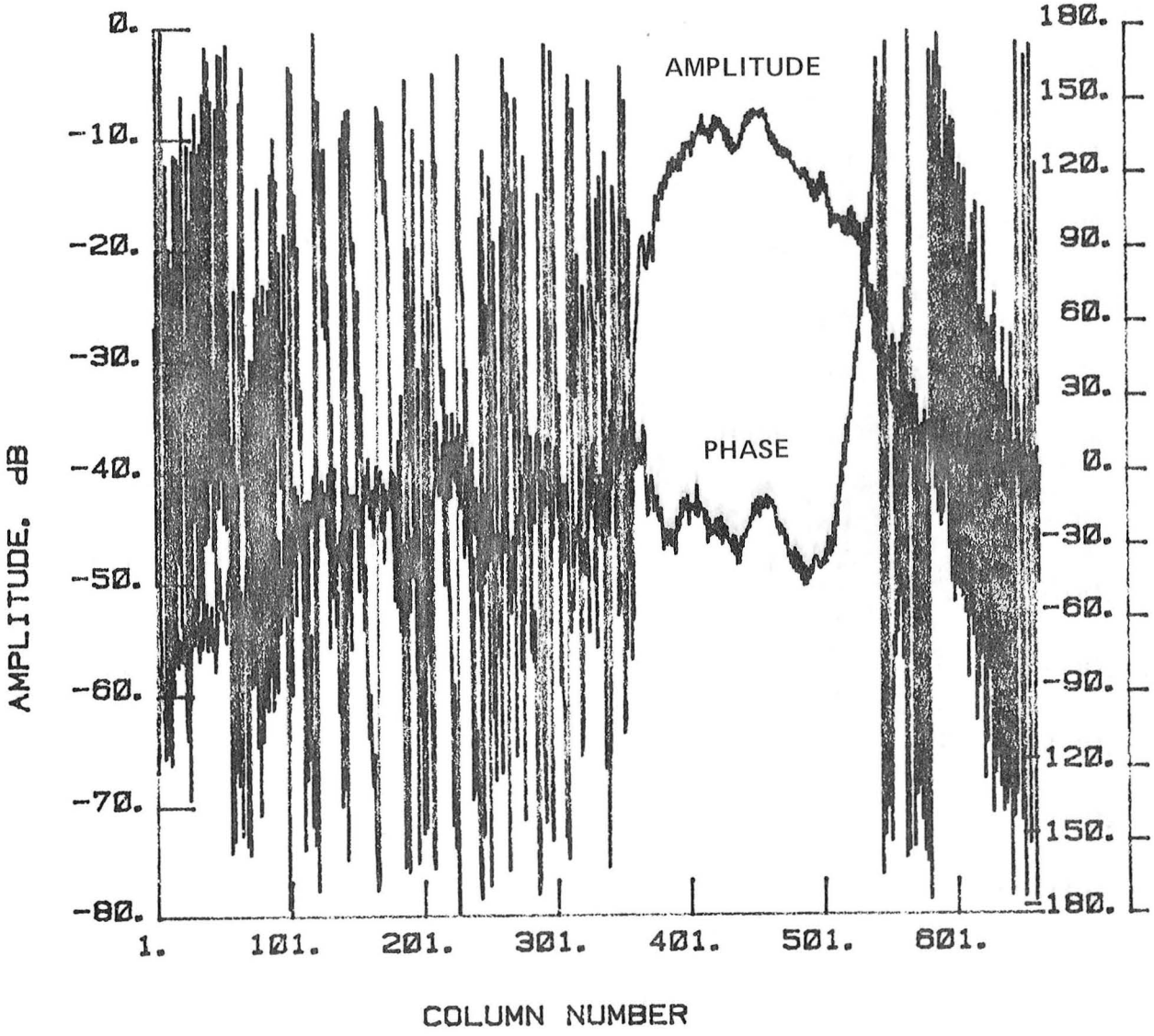

Figure 115 Test 15, 4.26 GHz, Co-Pol, E-Plane, Type 9

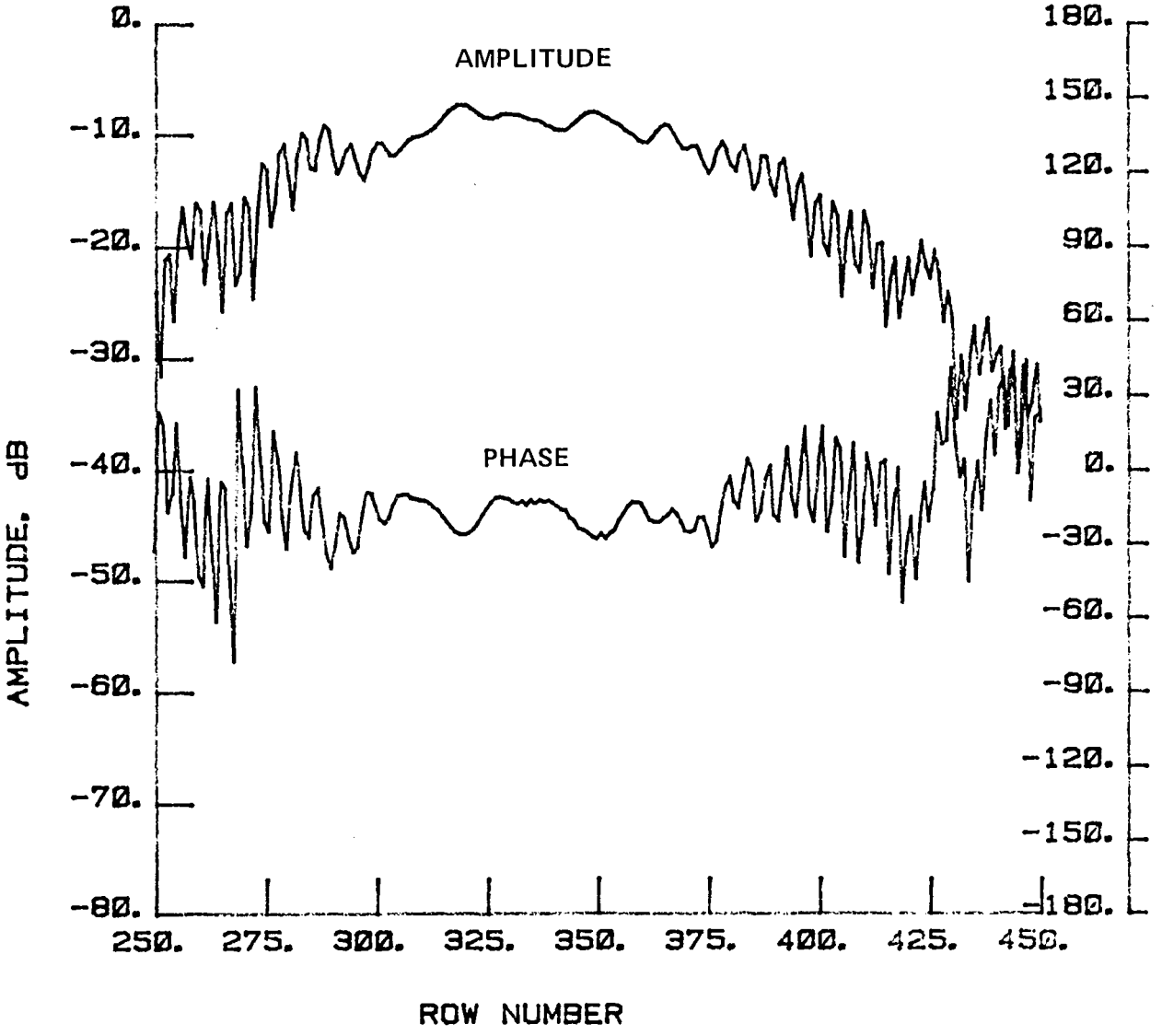

Figure 116 Test 15, 4.26 GHz, Co-Pol, H-Plane, Type 10

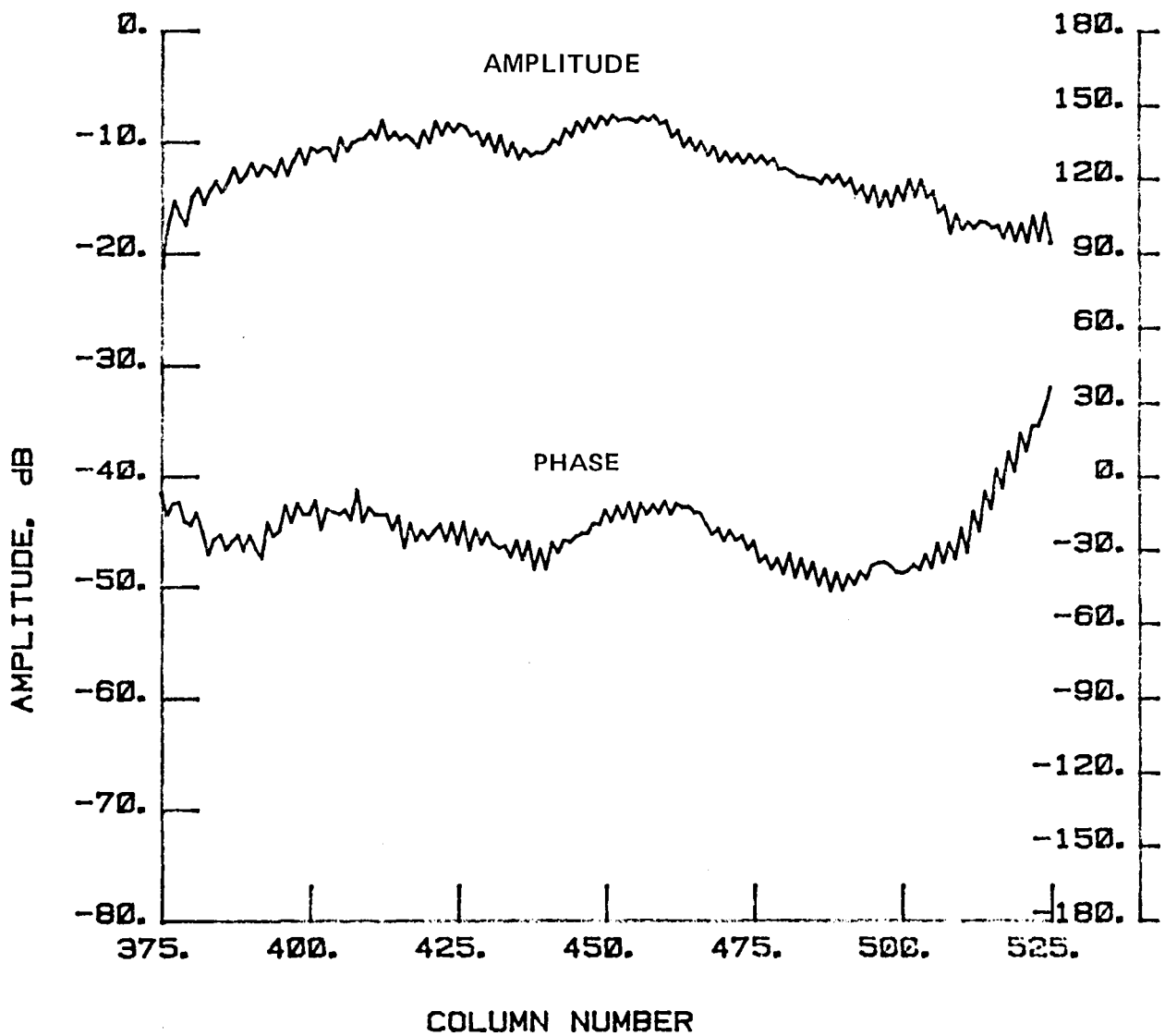

Figure 117 Test 15, 4.26 GHz, Co-Pol, E-Plane, Type 11

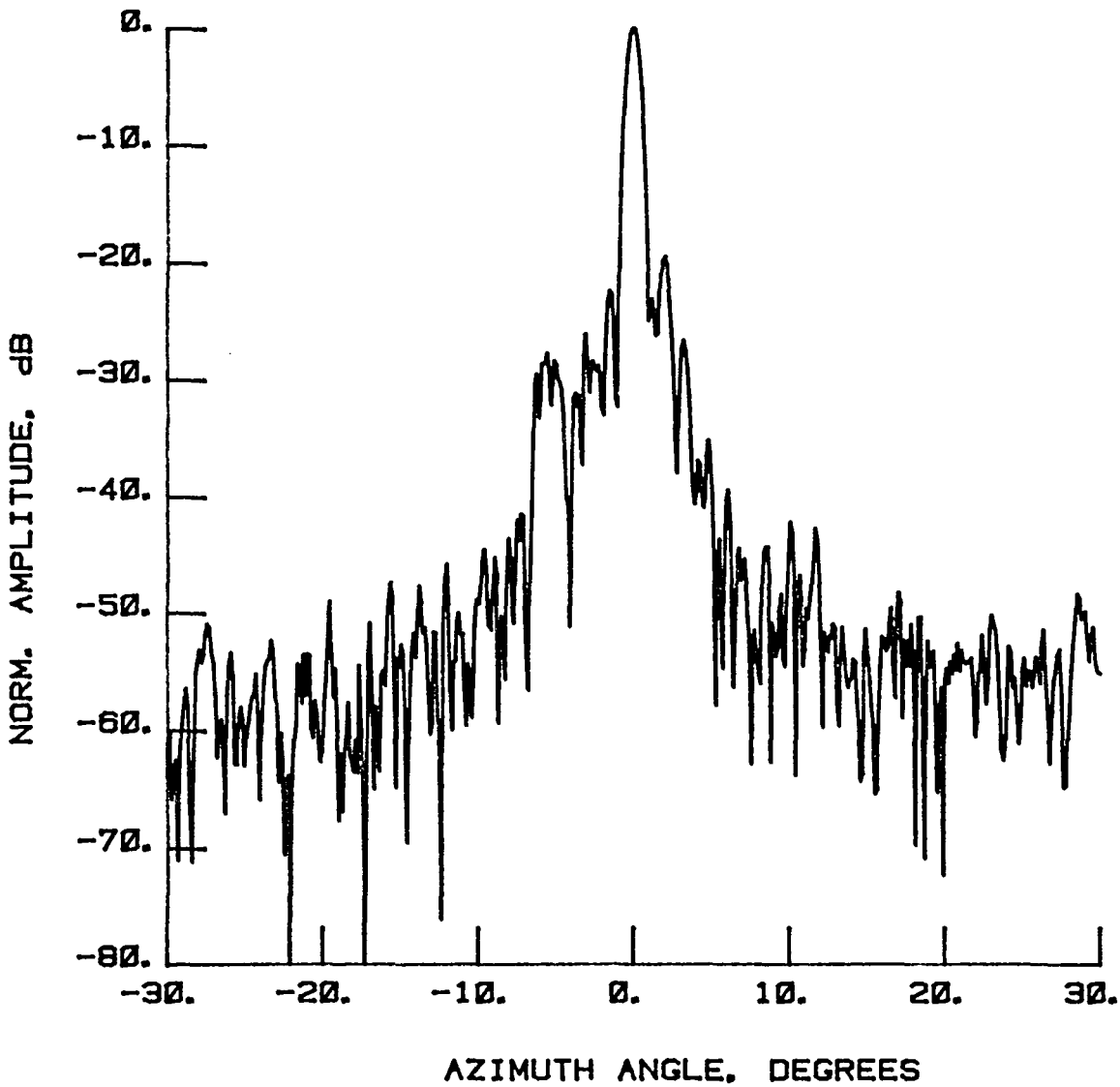

Figure 118 Test 16, 4.26 GHz, Co-Pol, E-Plane, Type 1

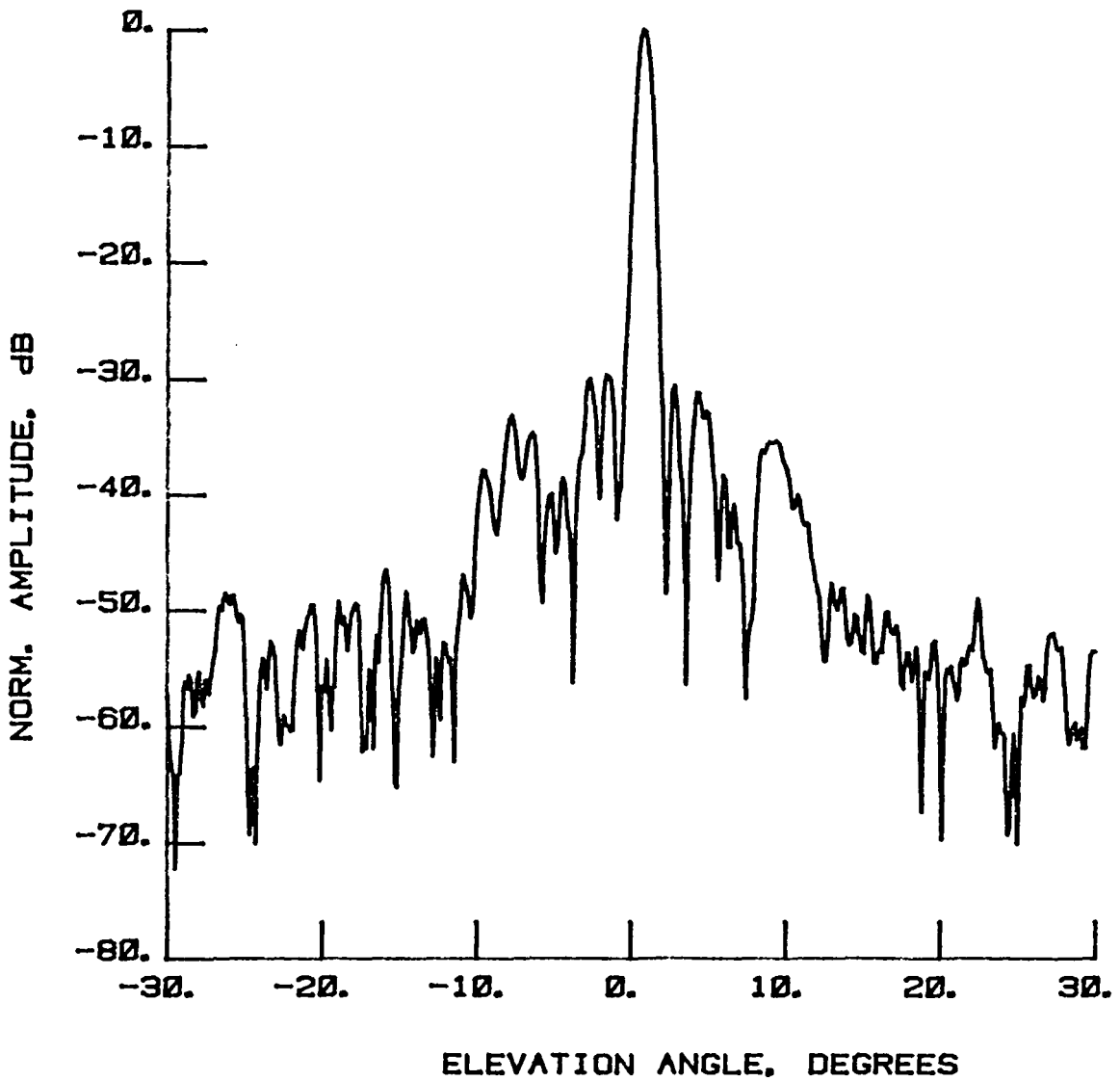

Figure 119 Test 16, 4.26 GHz, Co-Pol, H-Plane, Type 2

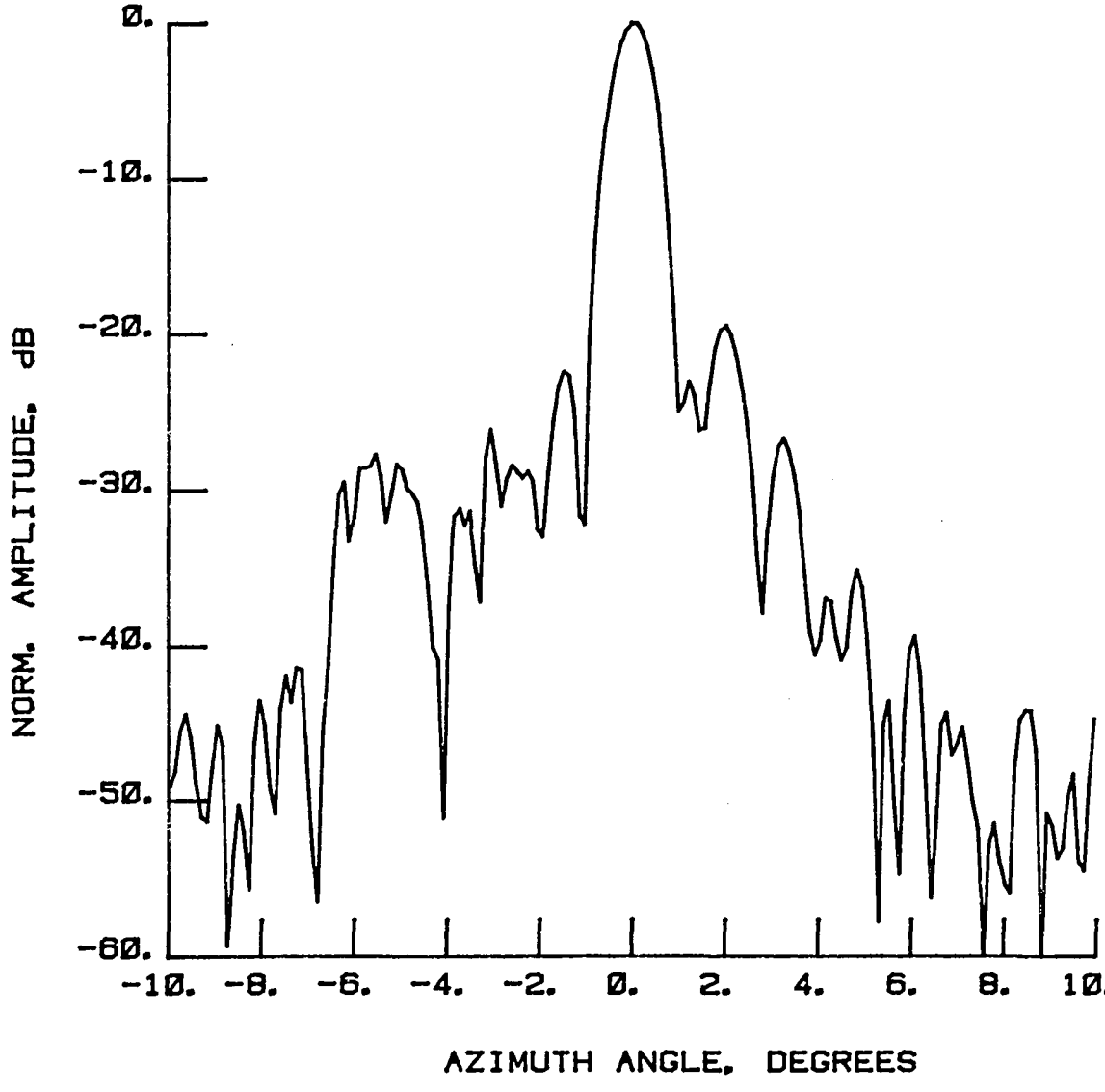

Figure 120 Test 16, 4.26 GHz, Co-Pol, E-Plane, Type 3

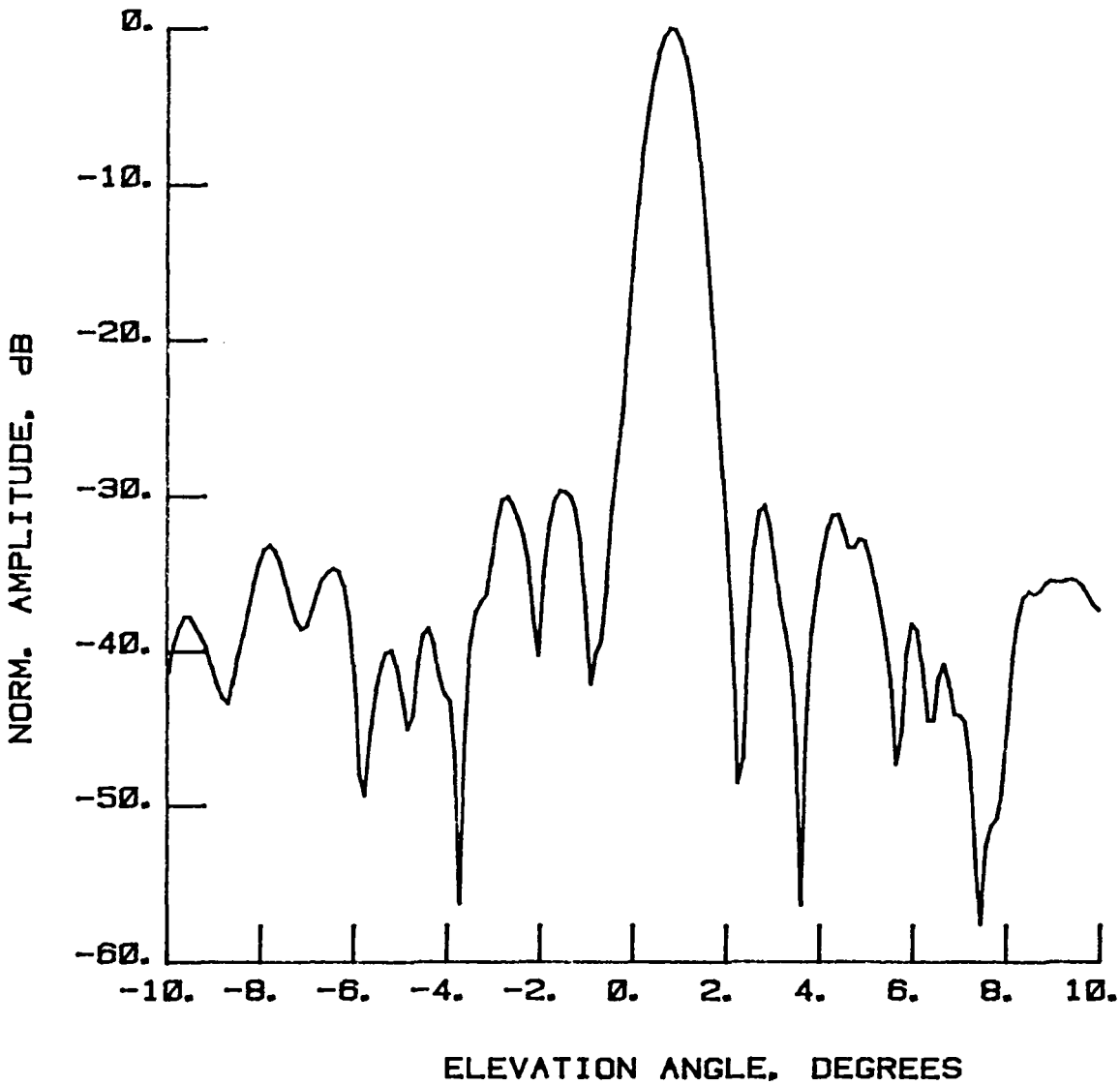

Figure 121 Test 16, 4.26 GHz, Co-Pol, H-Plane, Type 4

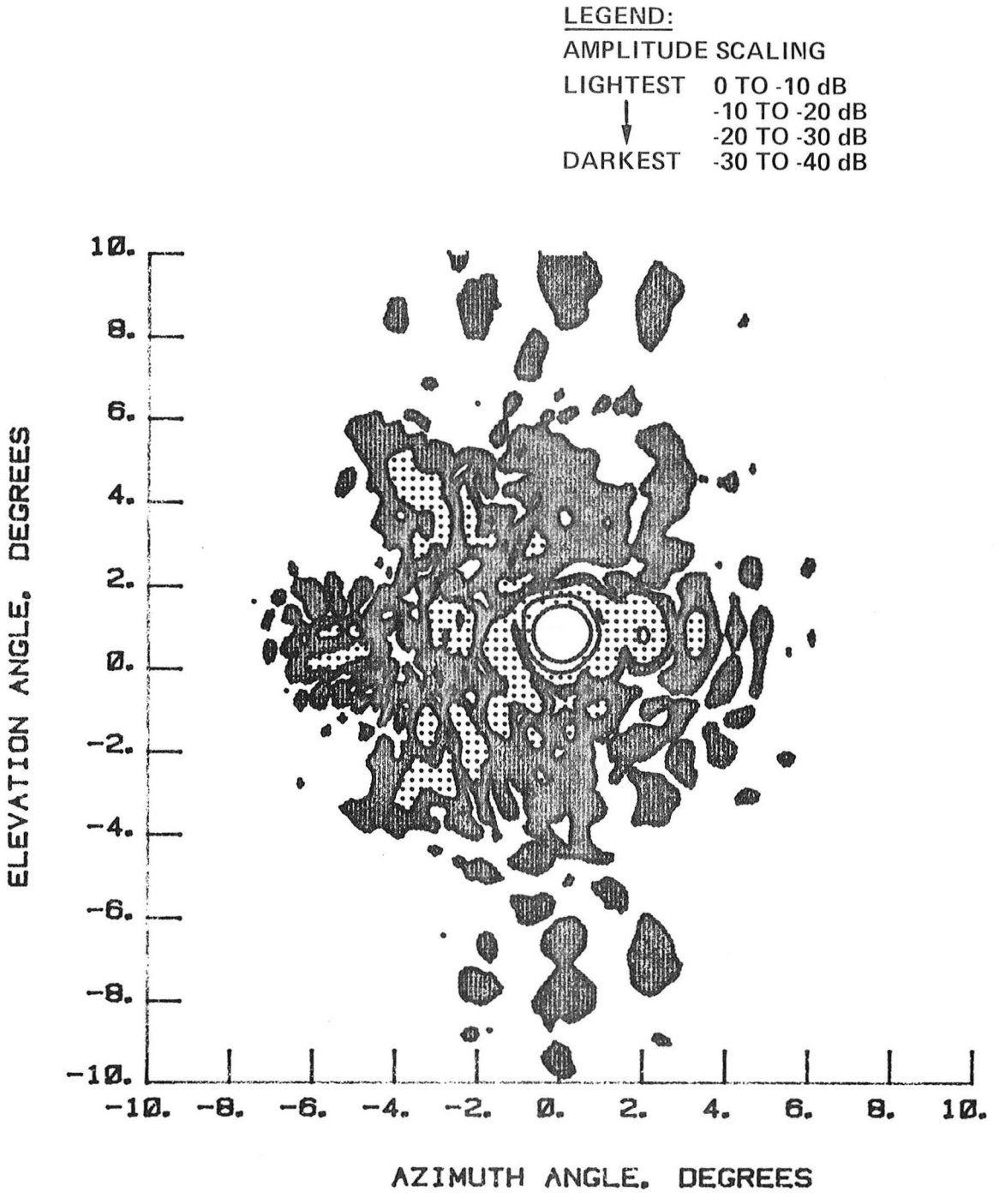

Figure 122 Test 16, 4.26 GHz, Co-Pol, Contour, Type 5

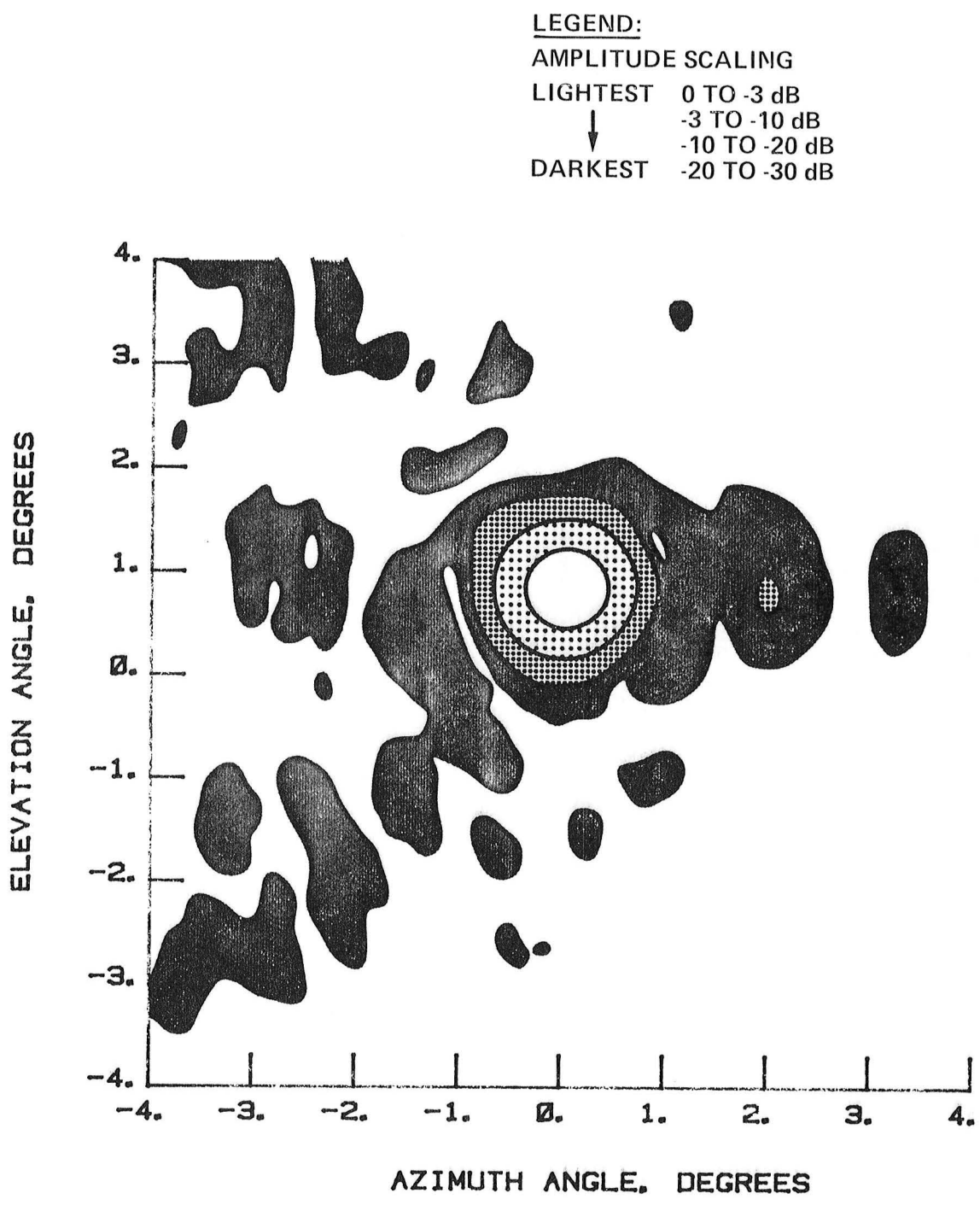

Figure 123 Test 16, 4.26 GHz, Co-Pol, Contour, Type 6

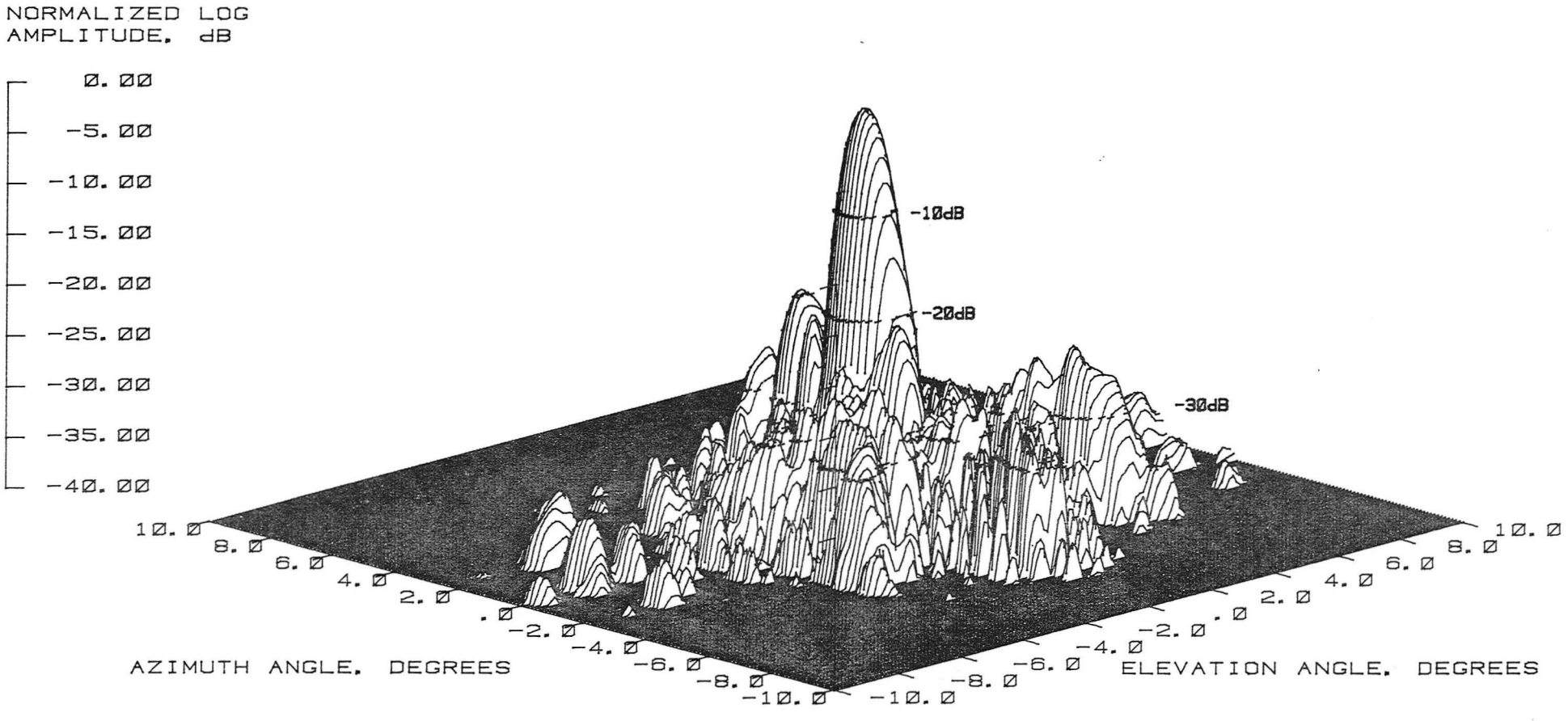

Figure 124 Test 16, 4.26 GHz, Co-Pol, 3-D, Type 7

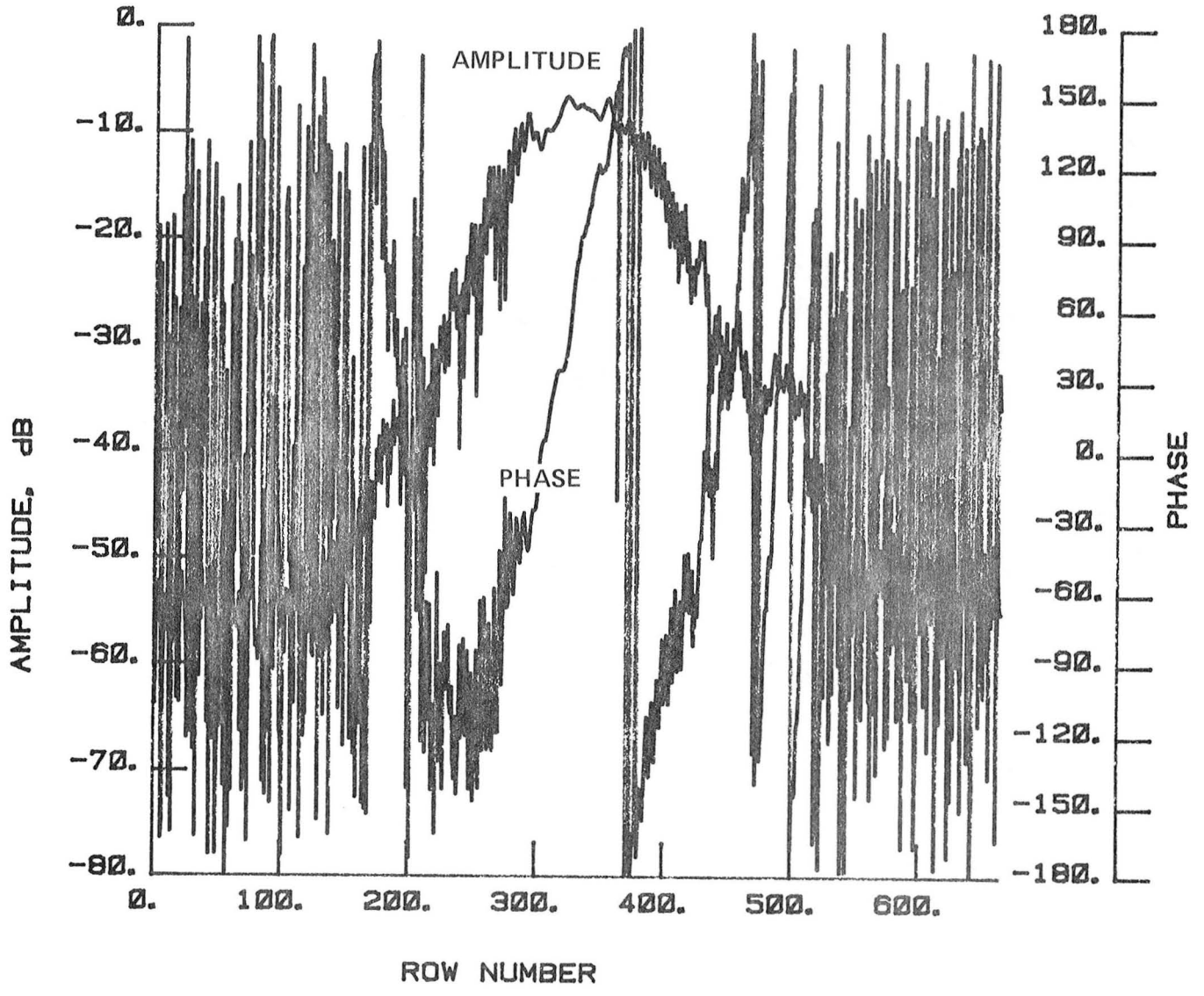

Figure 125 Test 16, 4.26 GHz, Co-Pol, H-Plane, Type 8

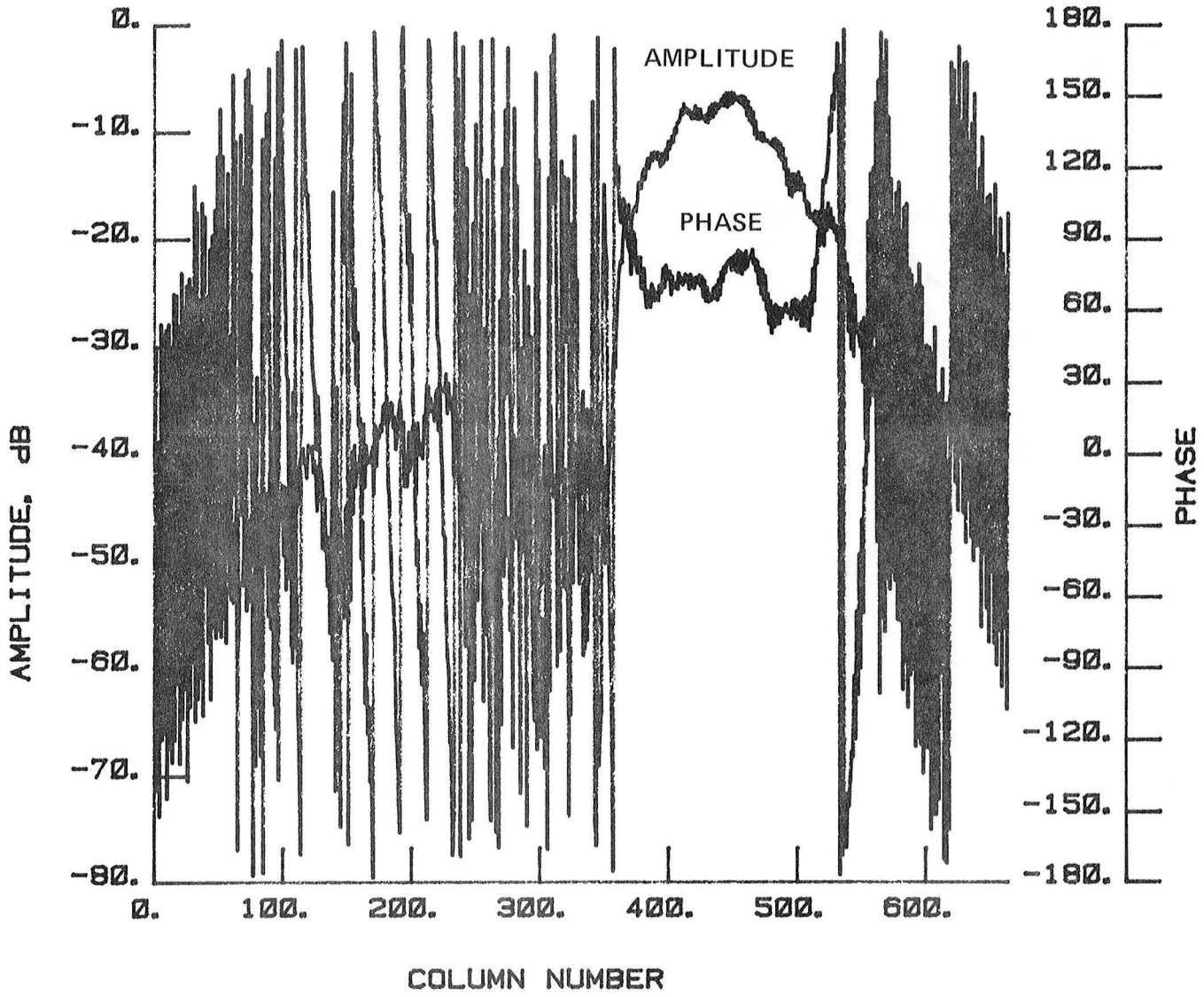

Figure 126 Test 16, 4.26 GHz, Co-Pol, E-Plane, Type 9

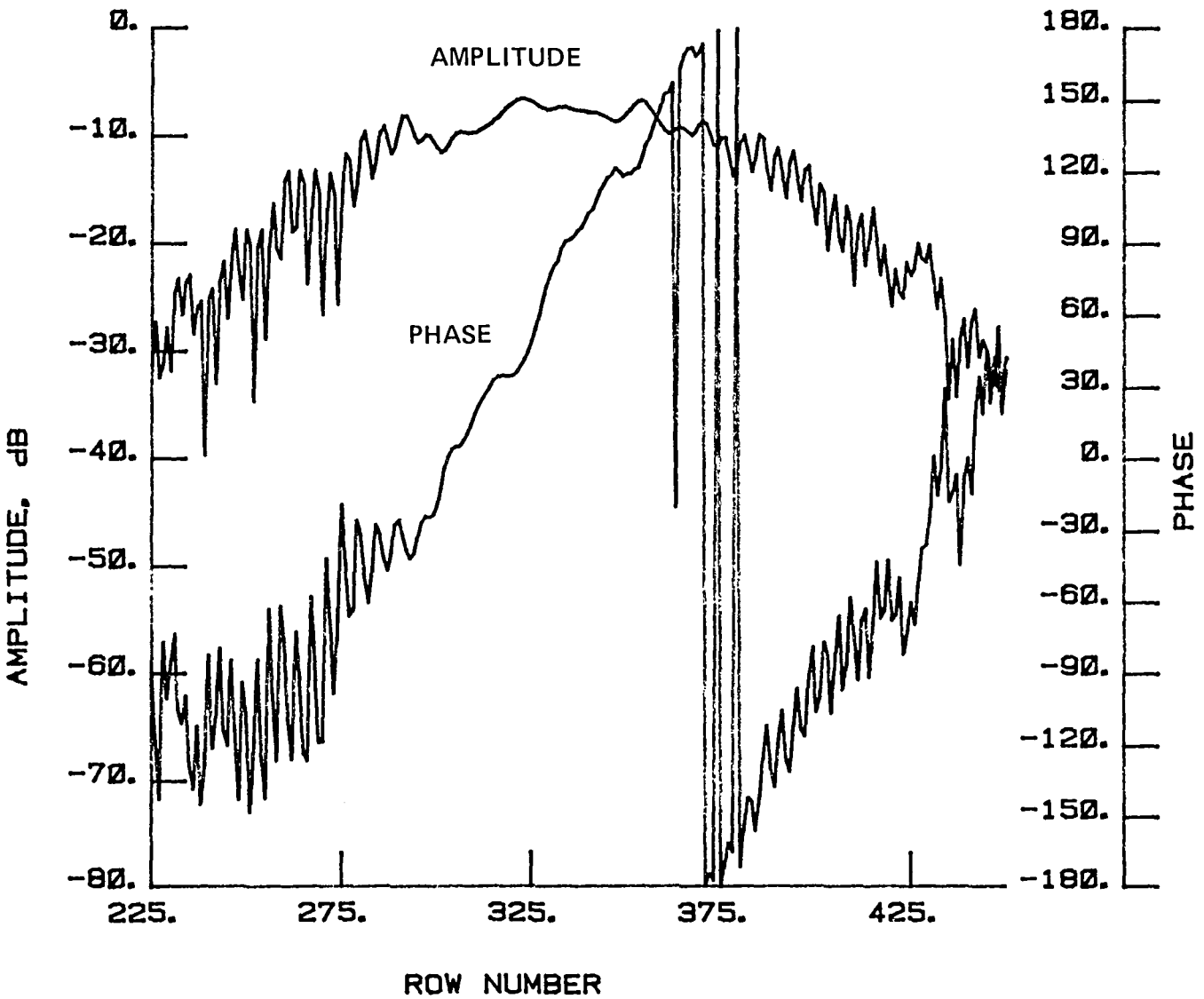

Figure 127 Test 16, 4.26 GHz, Co-Pol, H-Plane, Type 10

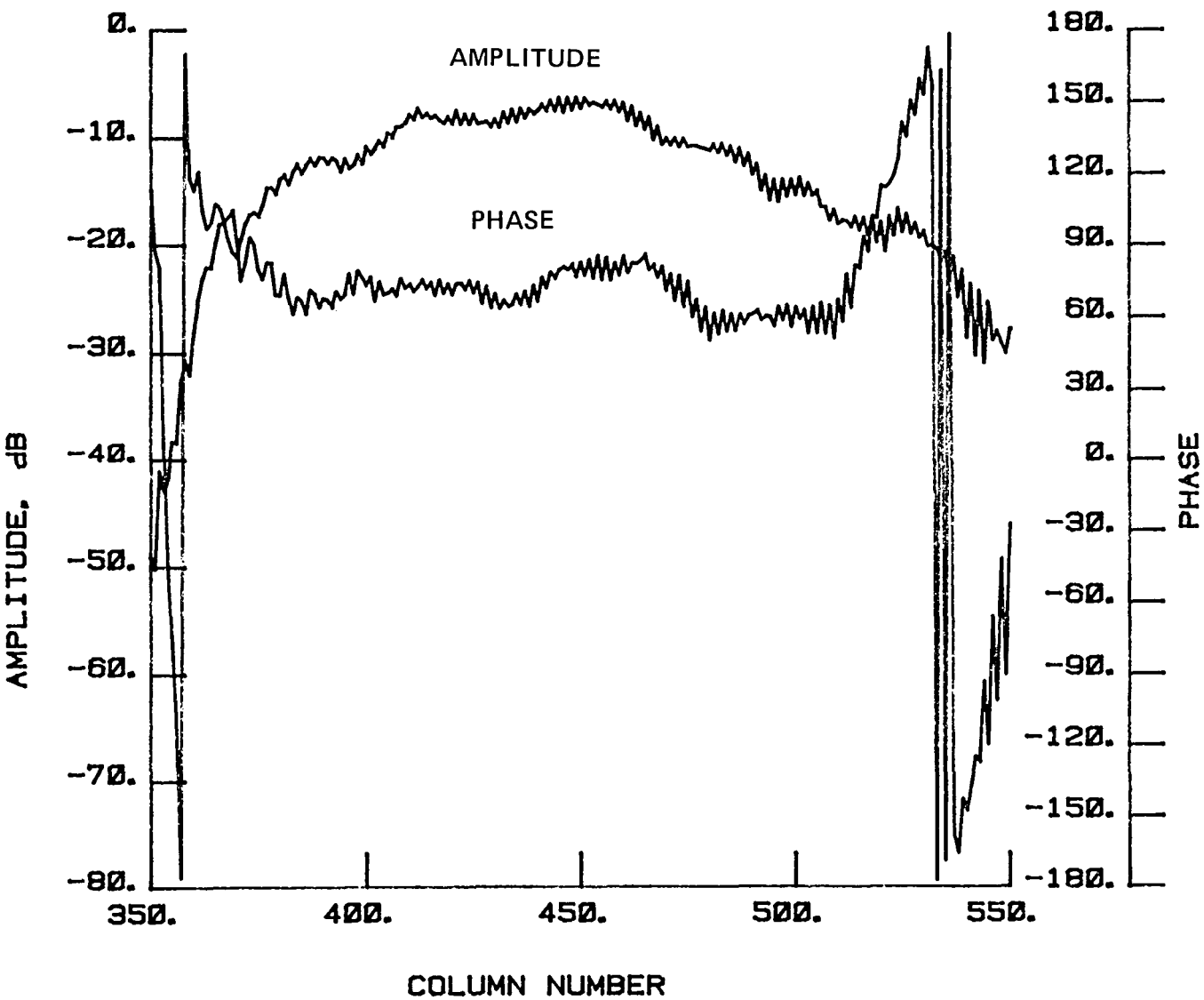

Figure 128 Test 16, 4.26 GHz, Co-Pol, E-Plane, Type 11

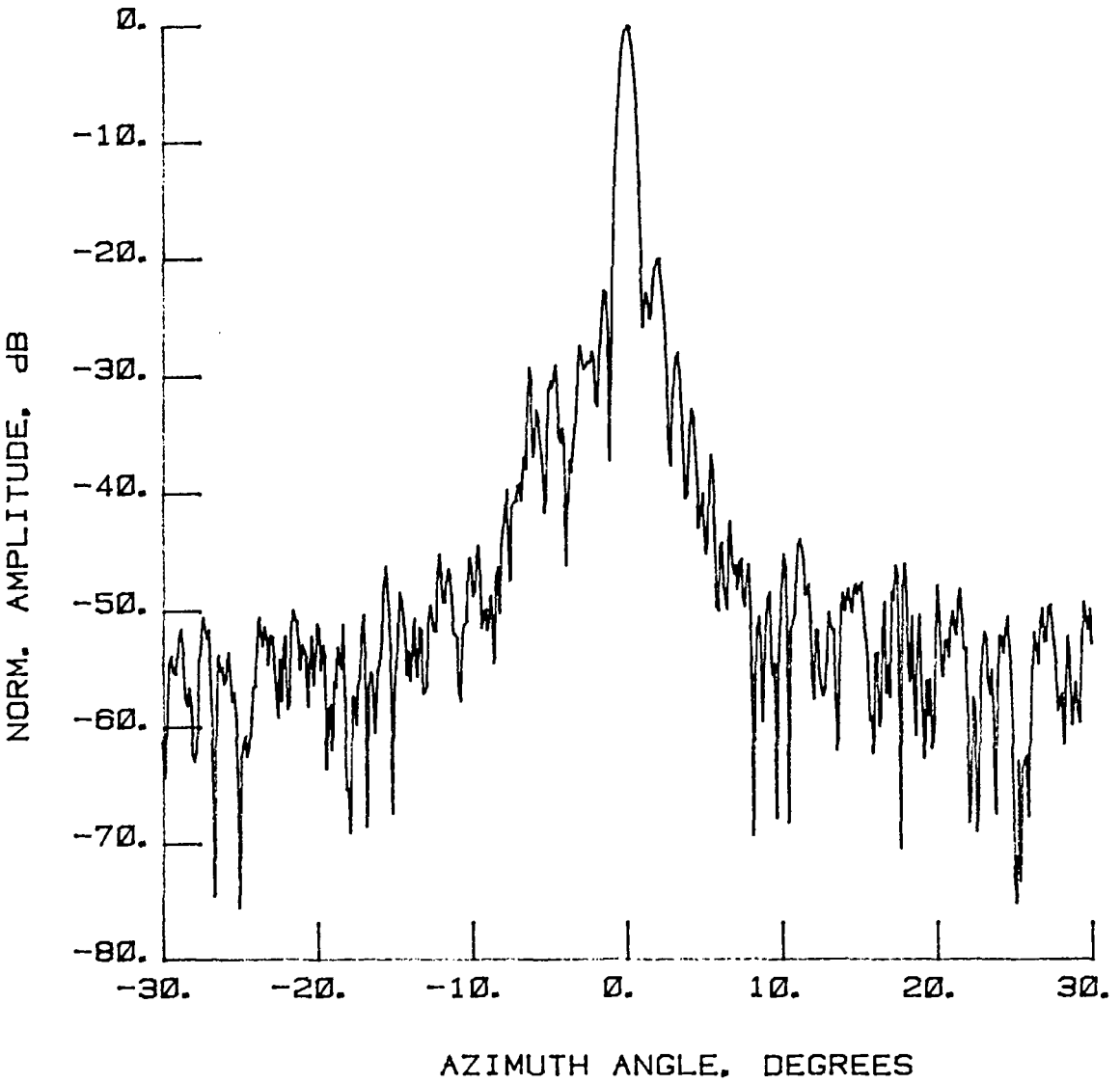

Figure 129 Test 17, 4.26 GHz, Co-Pol, E-Plane, Type 1

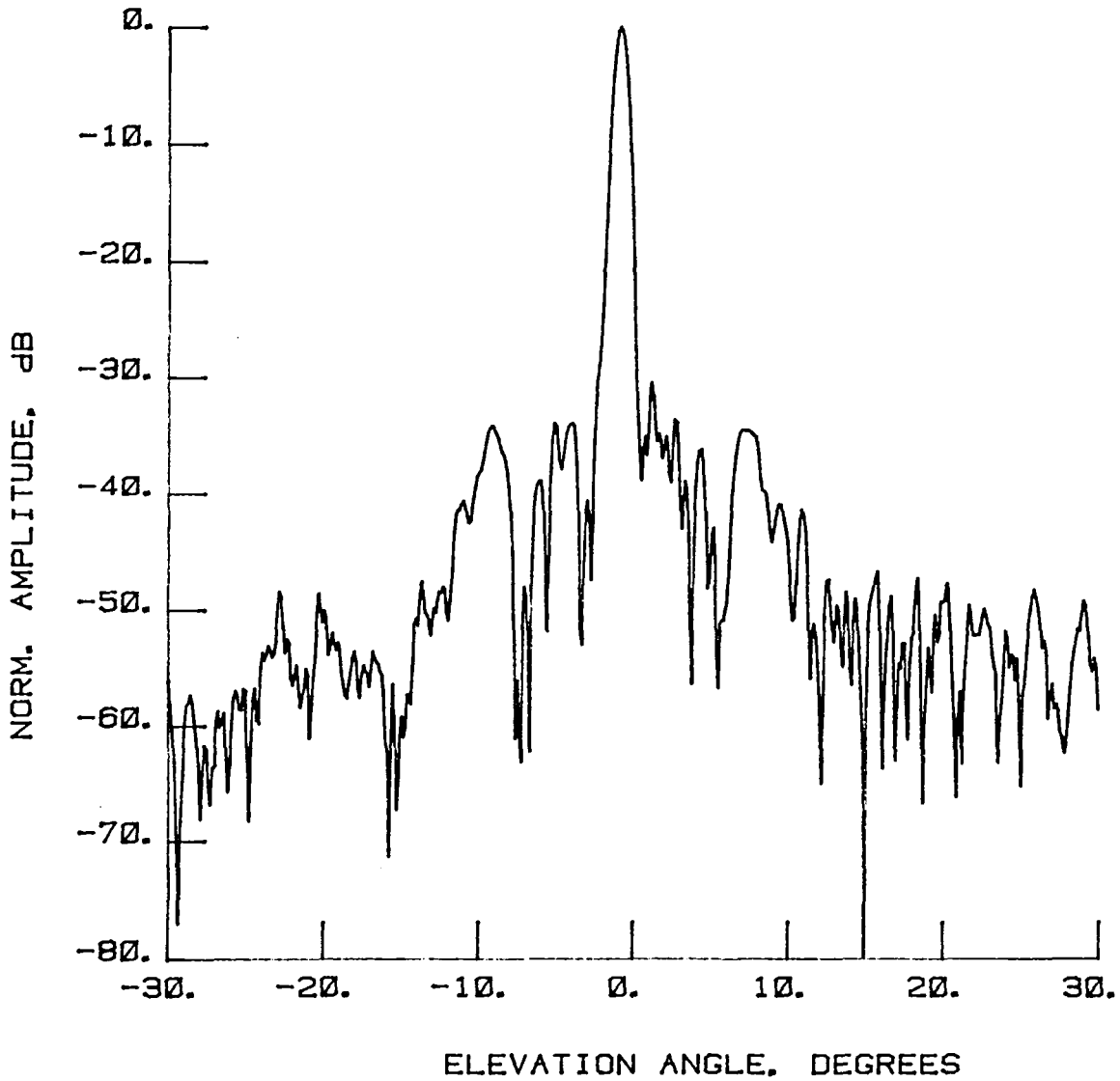

Figure 130 Test 17, 4.26 GHz, Co-Pol, H-Plane, Type 2

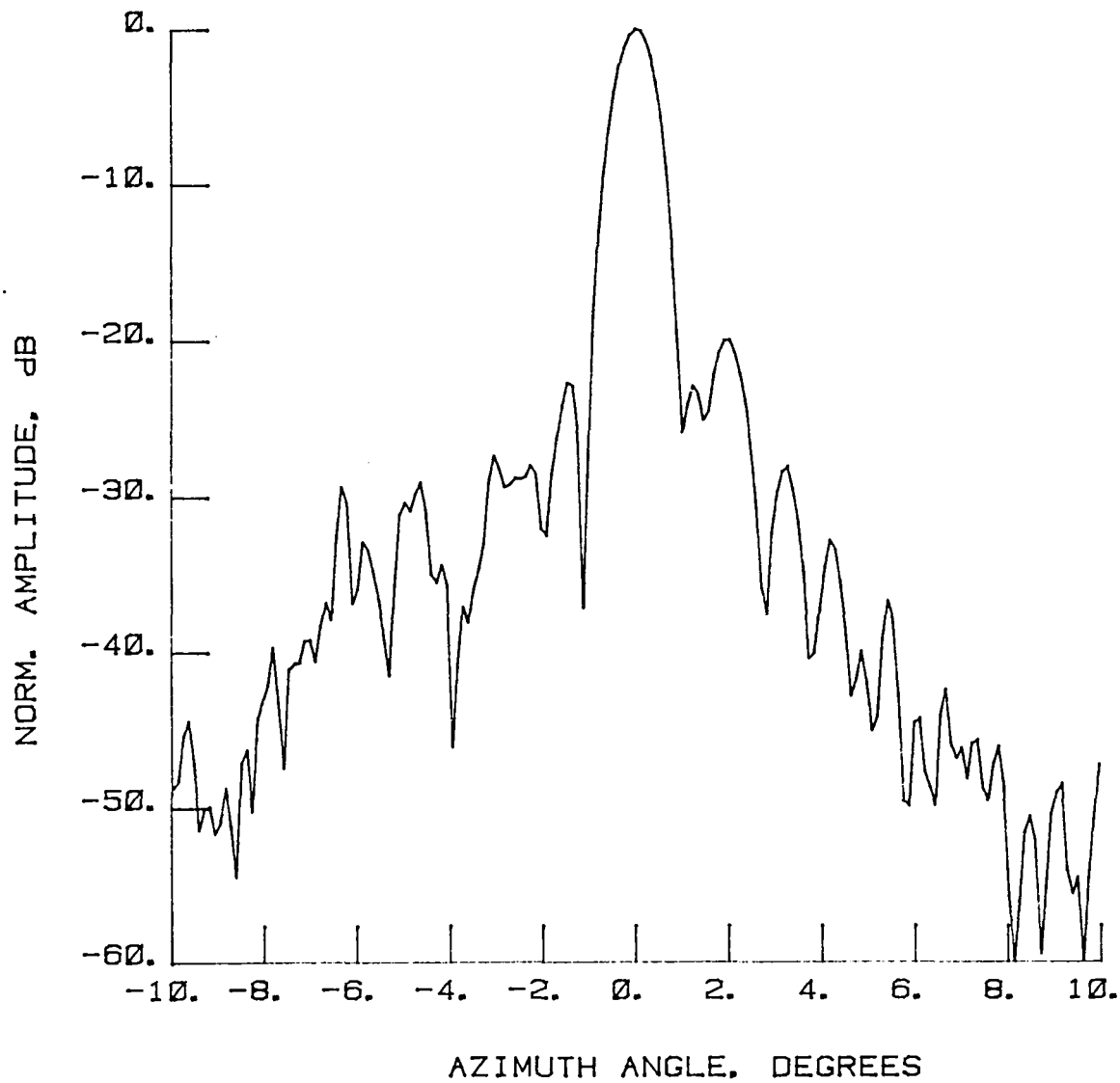

Figure 131 Test 17, 4.26 GHz, Co-Pol, E-Plane, Type 3

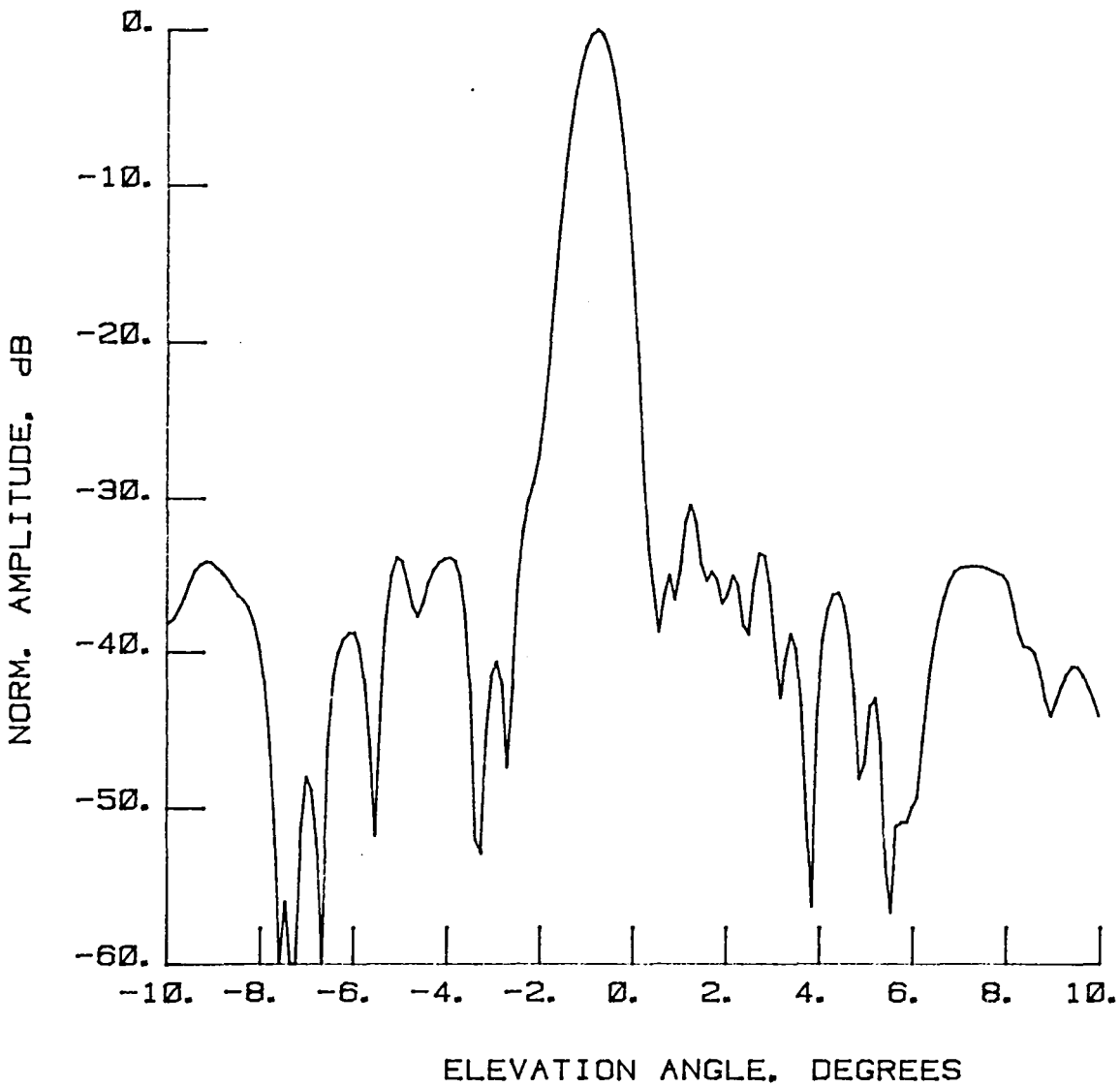

Figure 132 Test 17, 4.26 GHz, Co-Pol, H-Plane, Type 4

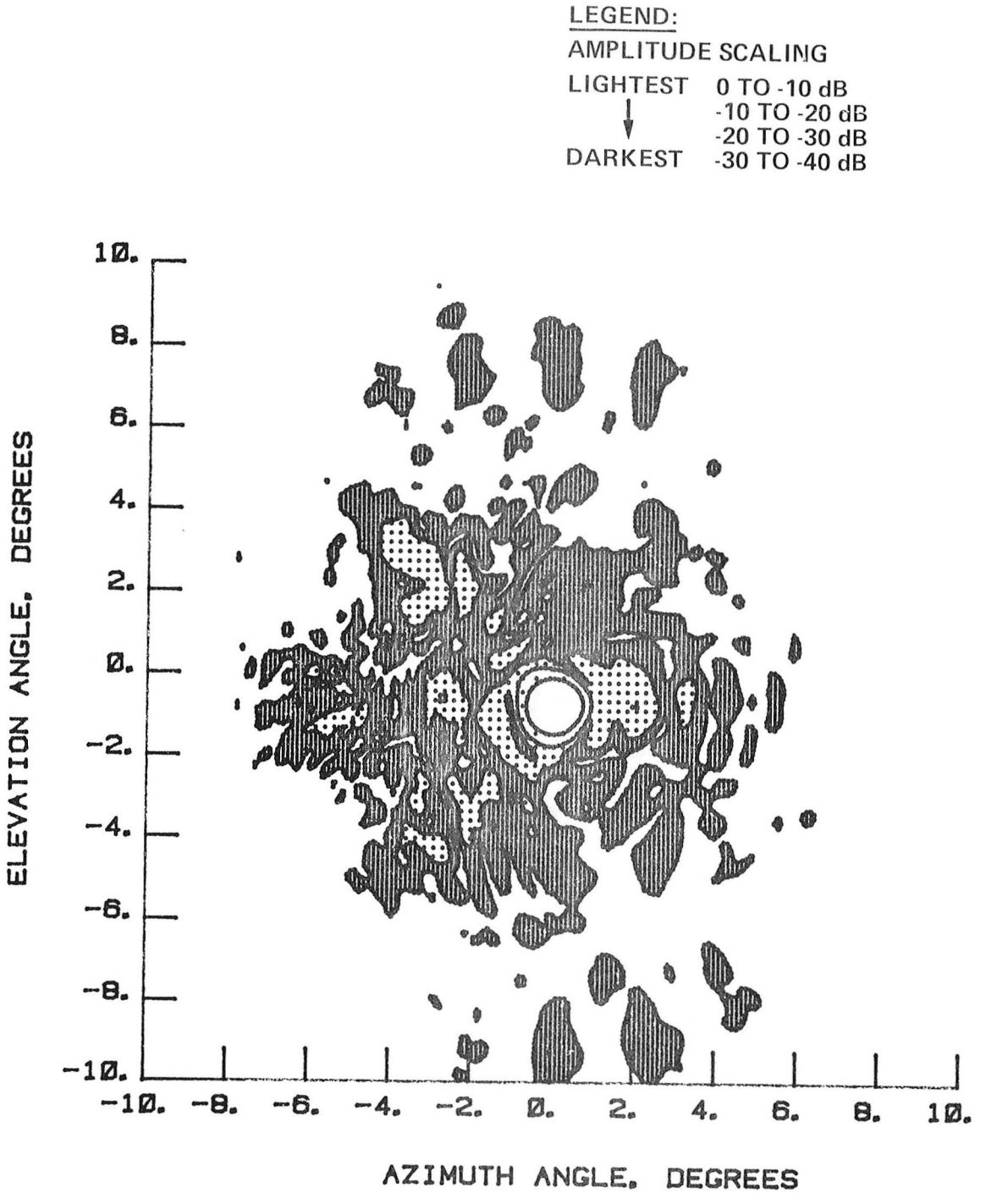

Figure 133 Test 17, 4.26 GHz, Co-Pol, Contour, Type 5

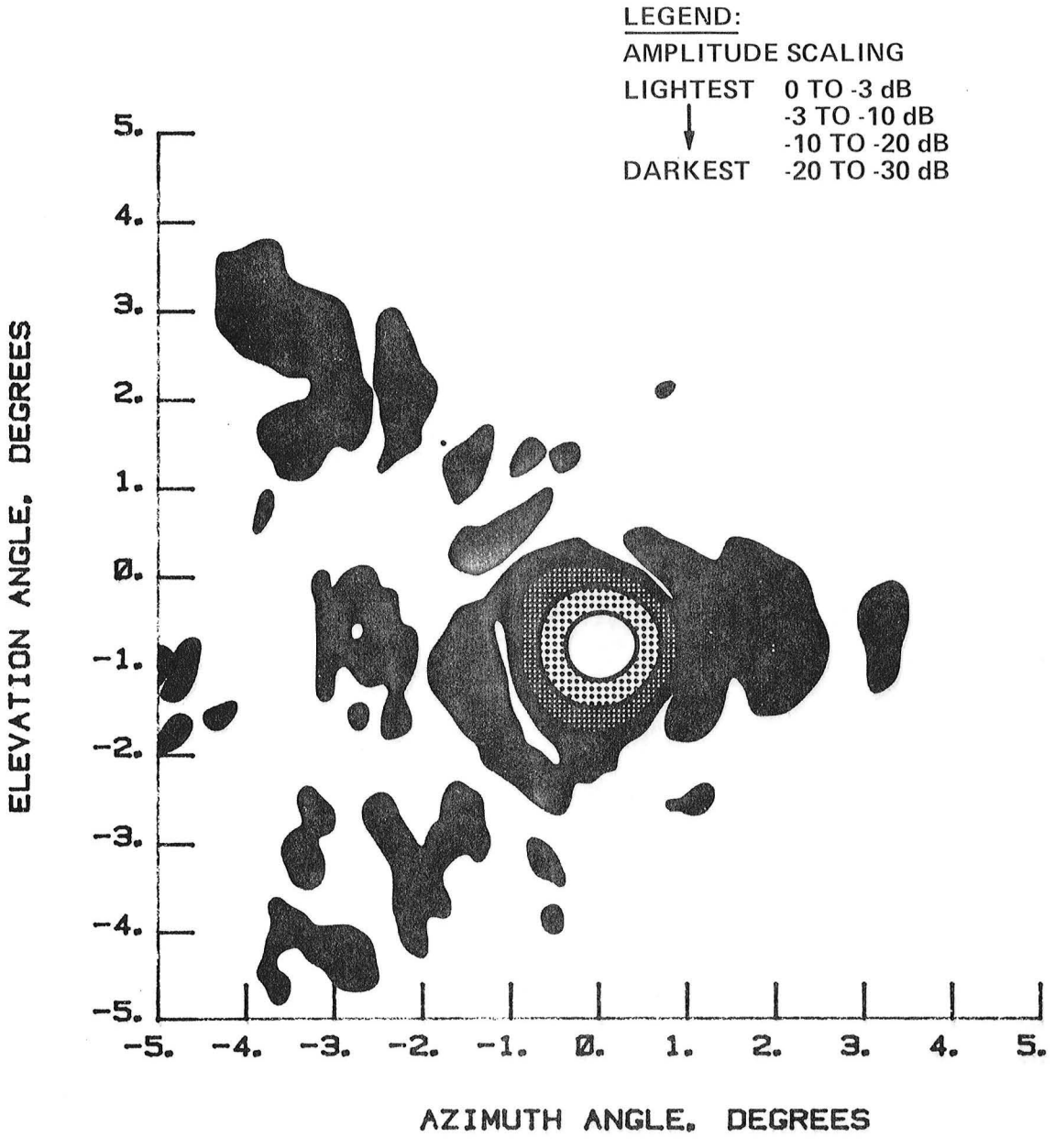

Figure 134 Test 17, 4.26 GHz, Co-Pol, Contour, Type 6

TEST IDENTIFICATION : LRC17/

DATE : 18 SEPT. 1985

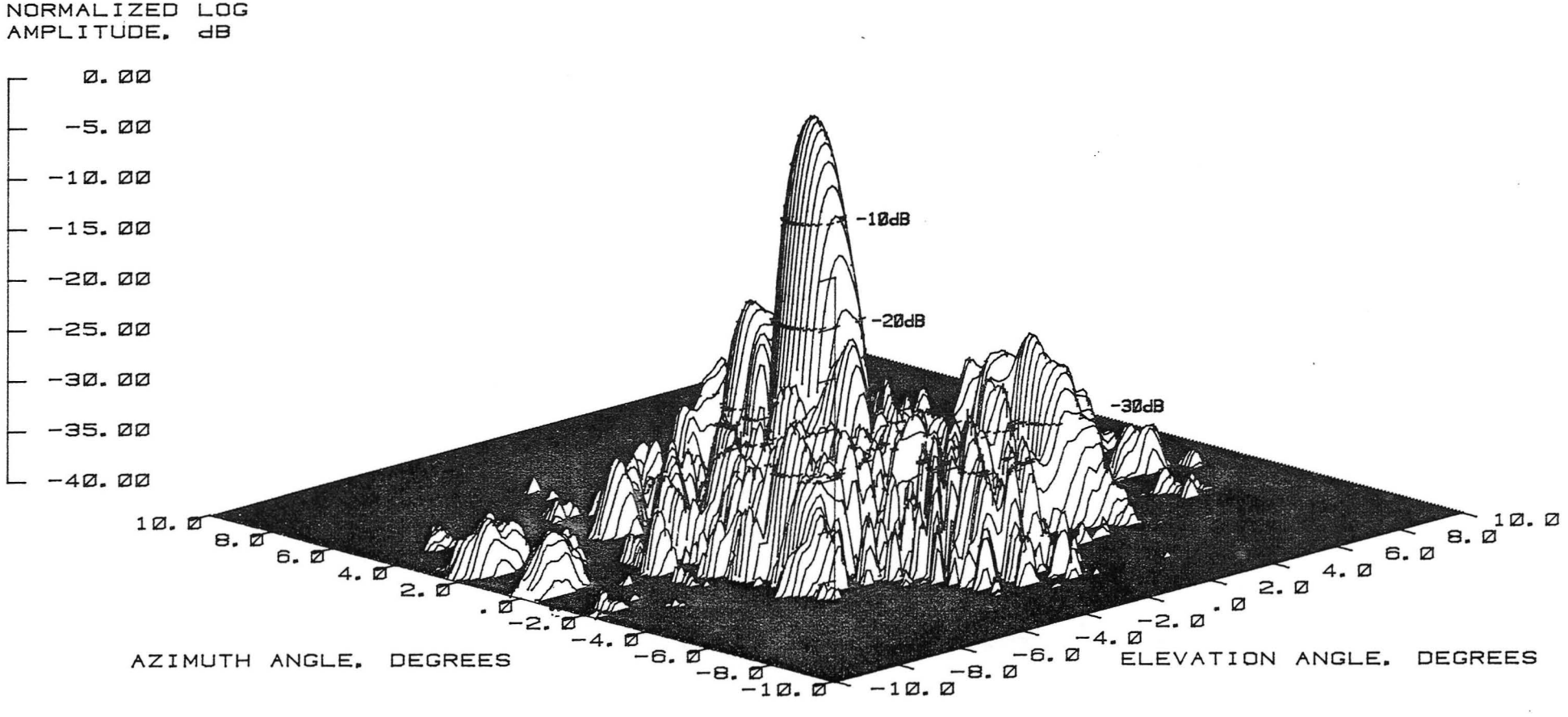

Figure 135 Test 17, 4.26 GHz, Co-Pol, 3-D, Type 7

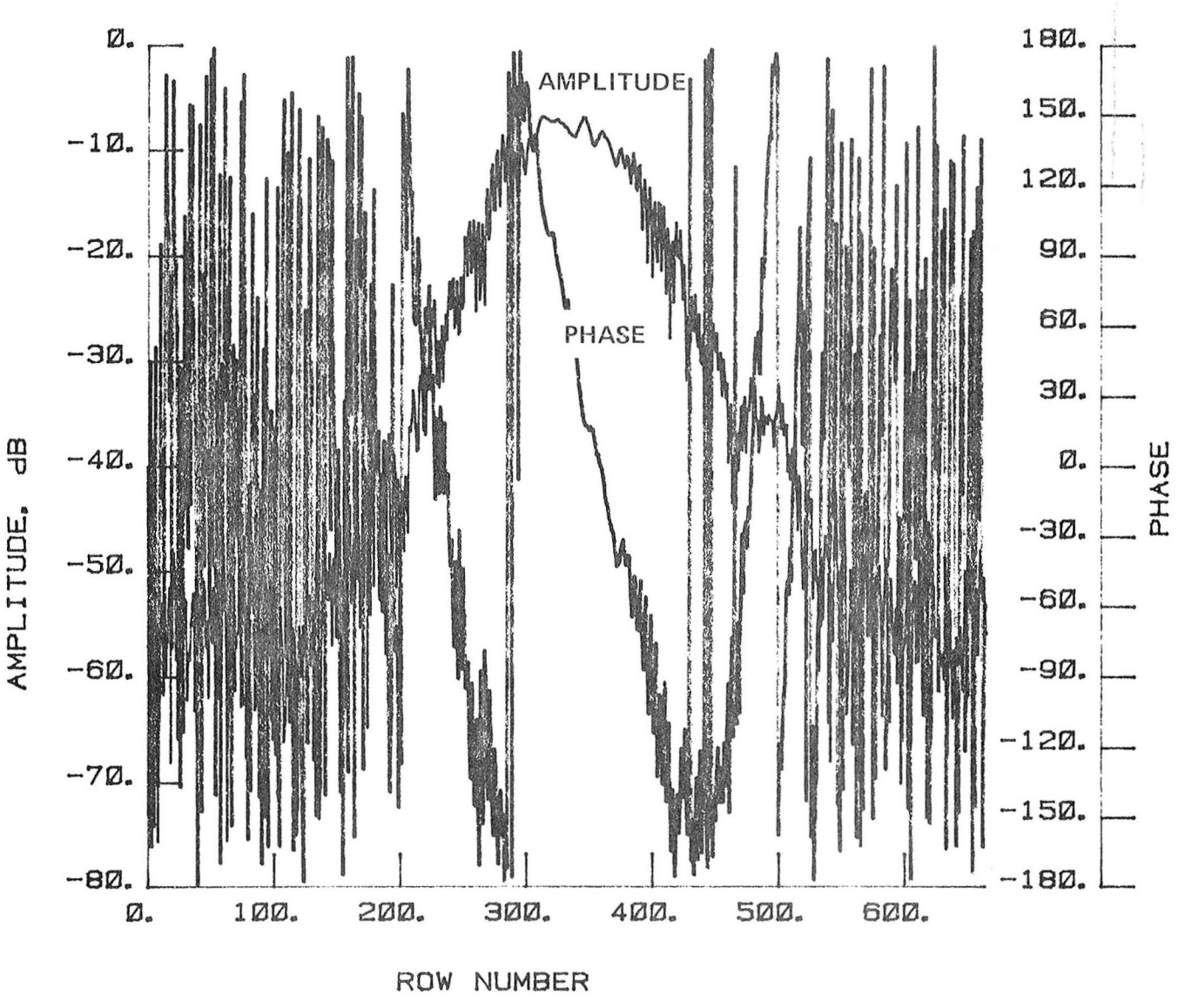

Figure 136 Test 17, 4.26 GHz, Co-Pol, H-Plane, Type 8

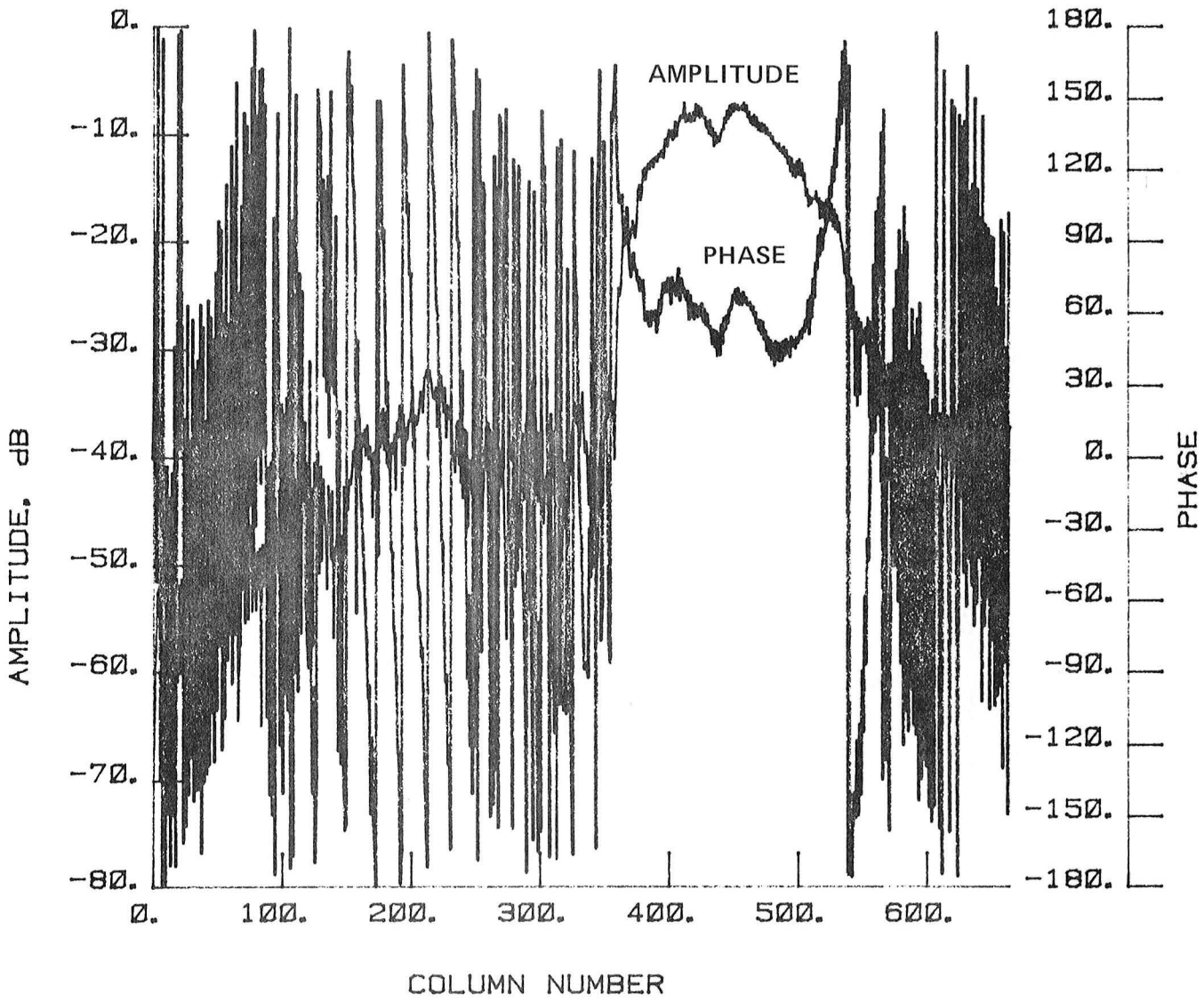

Figure 137 Test 17, 4.26 GHz, Co-Pol, E-Plane, Type 9

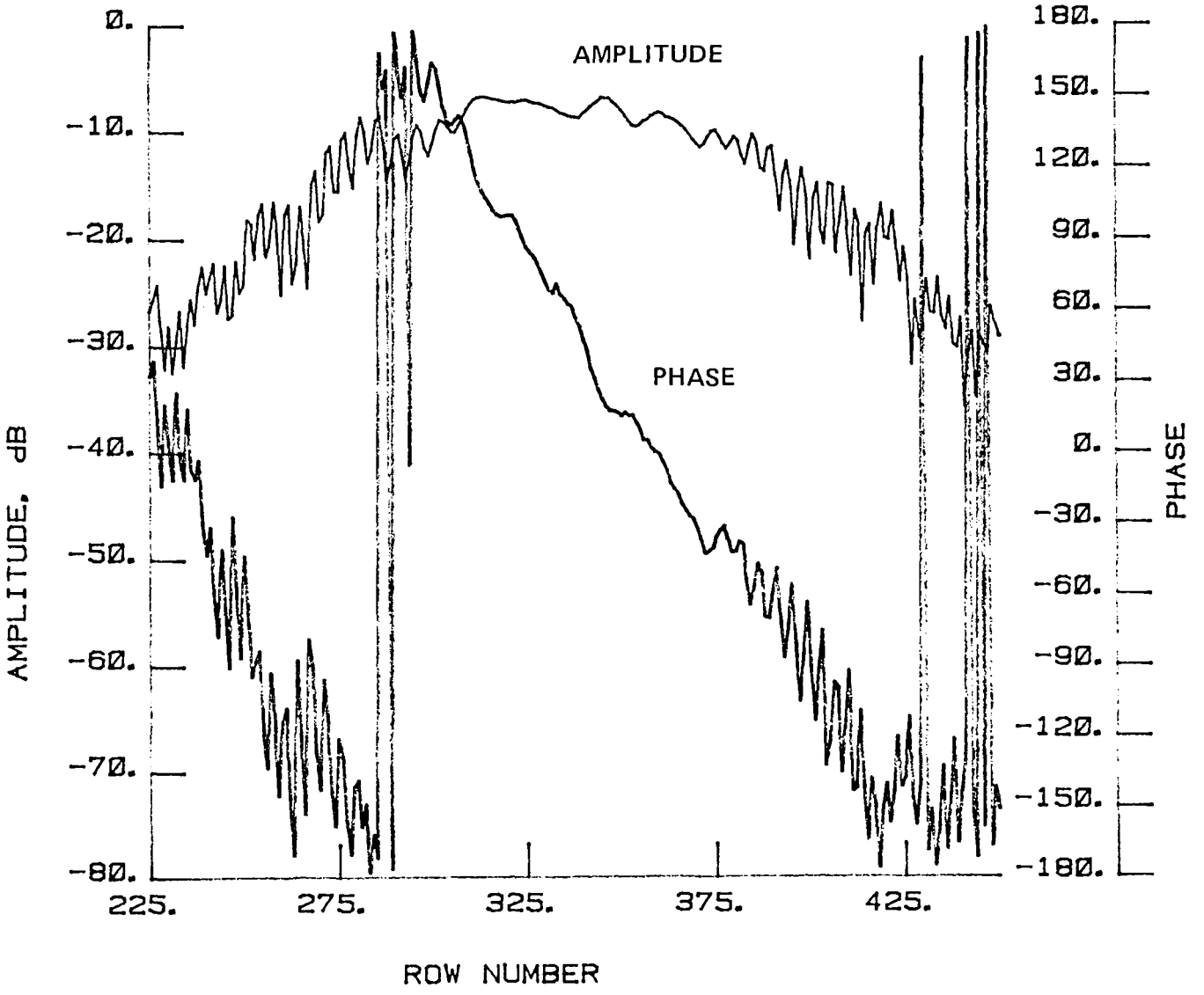

Figure 138 Test 17, 4.26 GHz, Co-Pol, H-Plane, Type 10

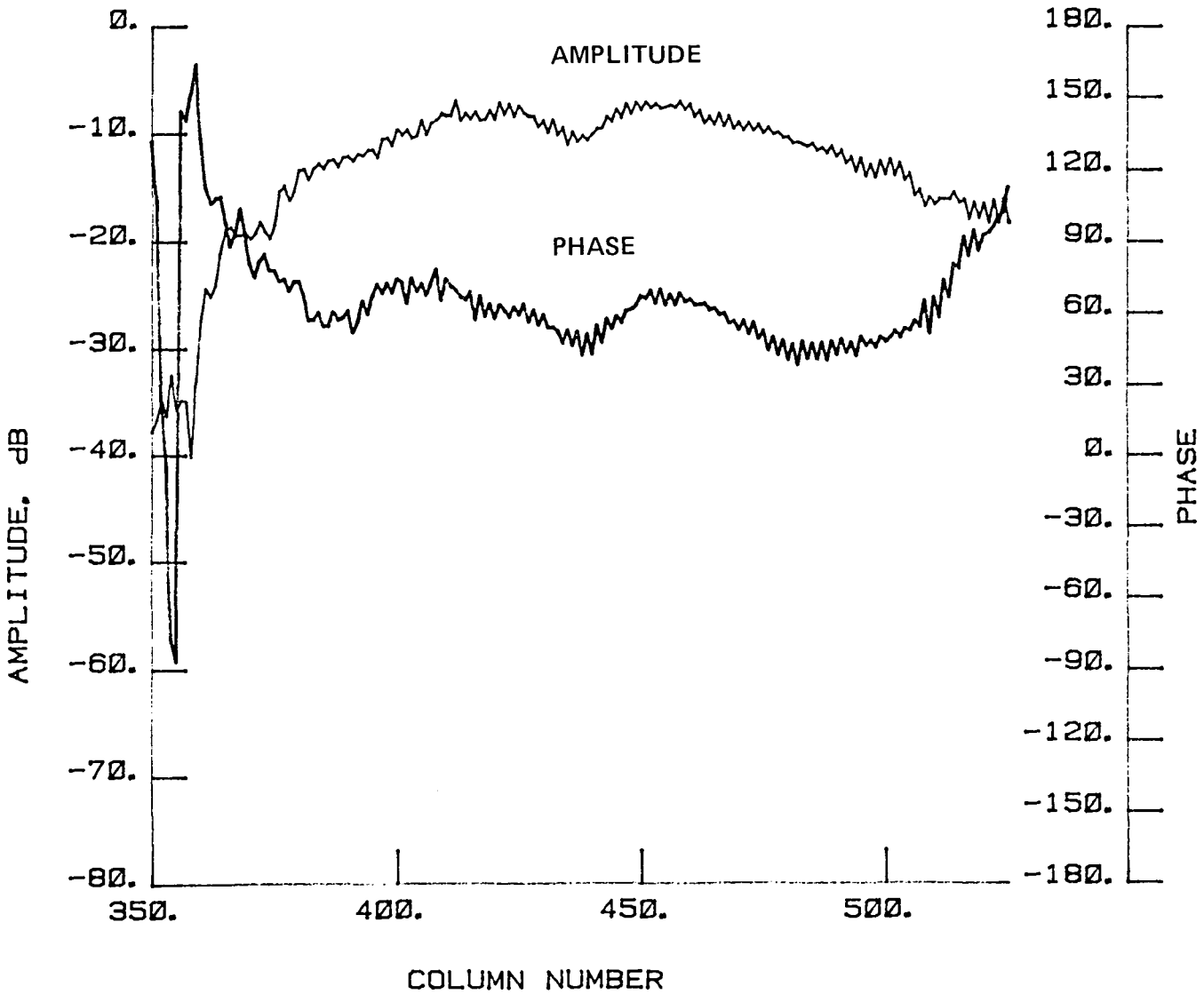

Figure 139 Test 17, 4.26 GHz, Co-Pol, E-Plane, Type 11

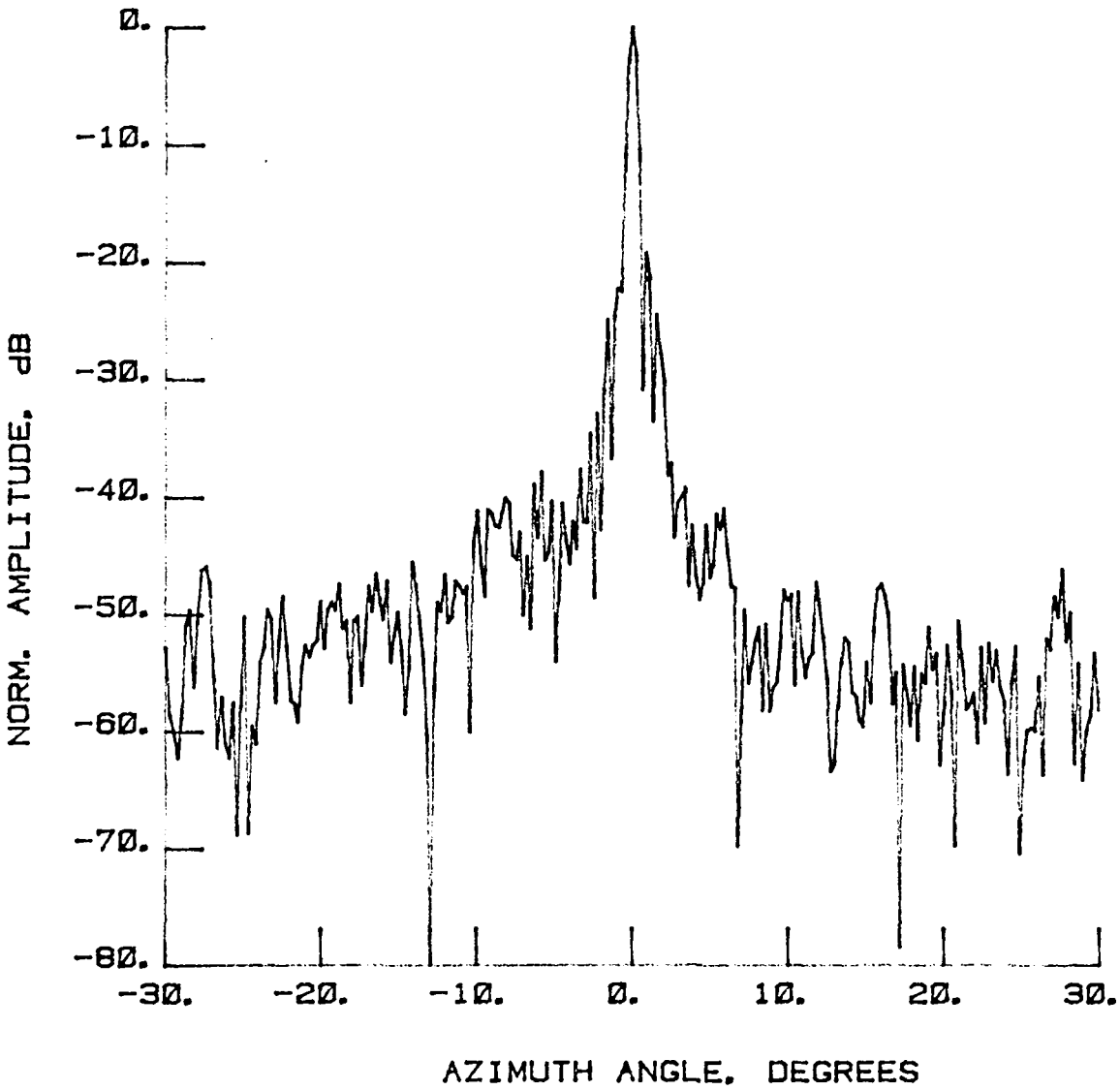

Figure 140 Test 18, 7.73 GHz, Co-Pol, E-Plane, Type 1

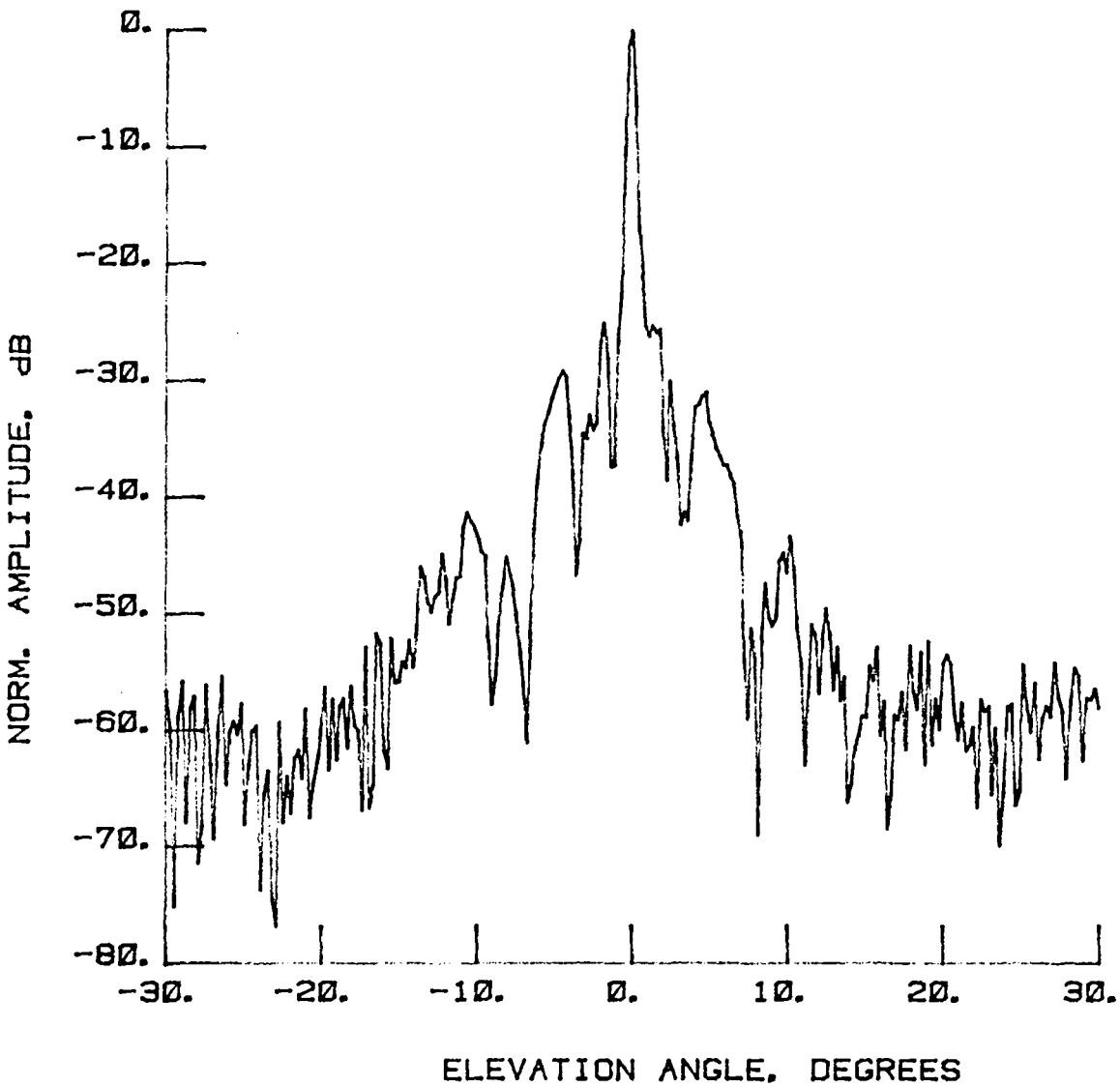

Figure 141 Test 18, 7.73 GHz, Co-Pol, H-Plane, Type 2

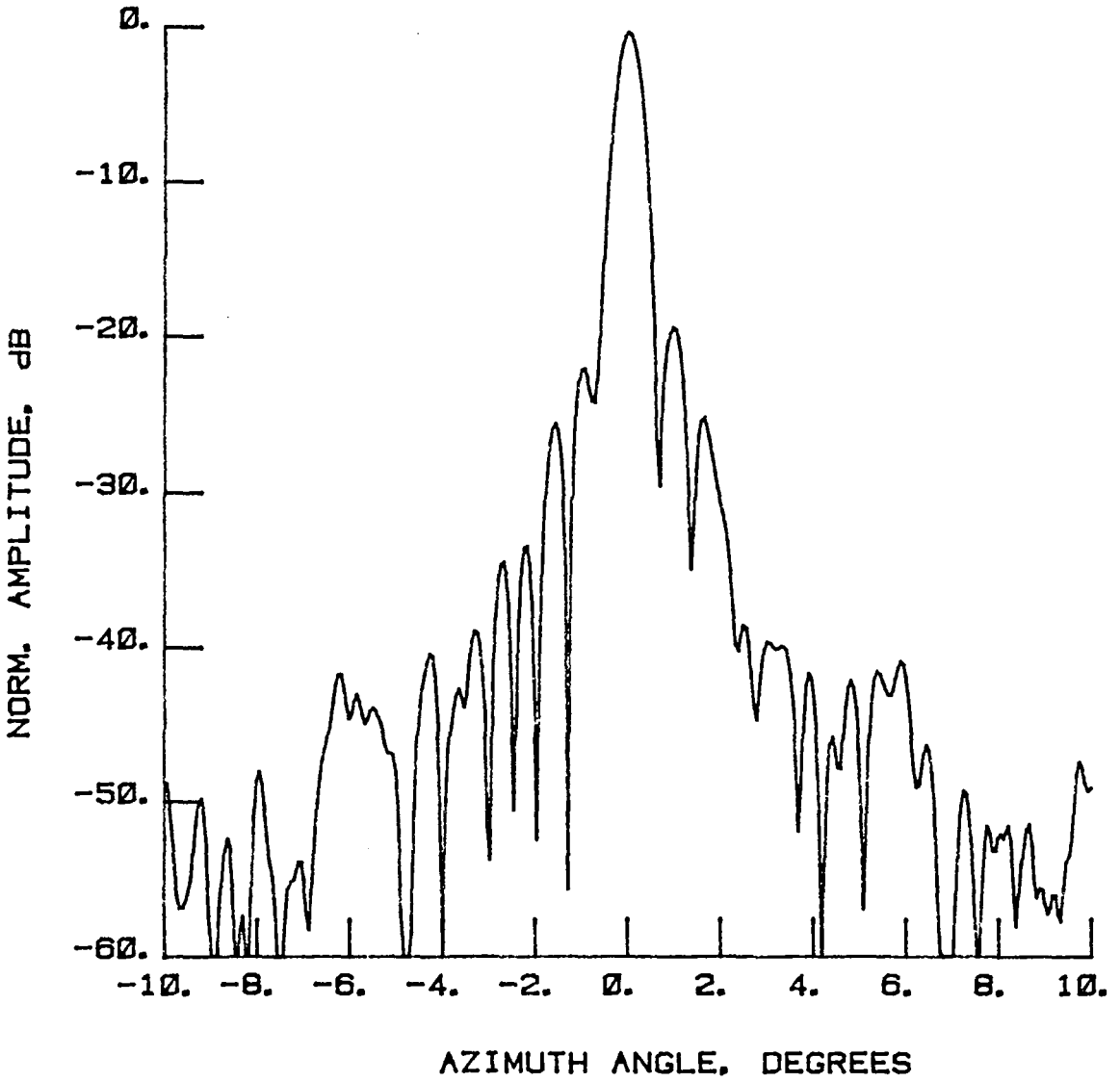

Figure 142 Test 18, 7.73 GHz, Co-Pol, E-Plane, Type 3

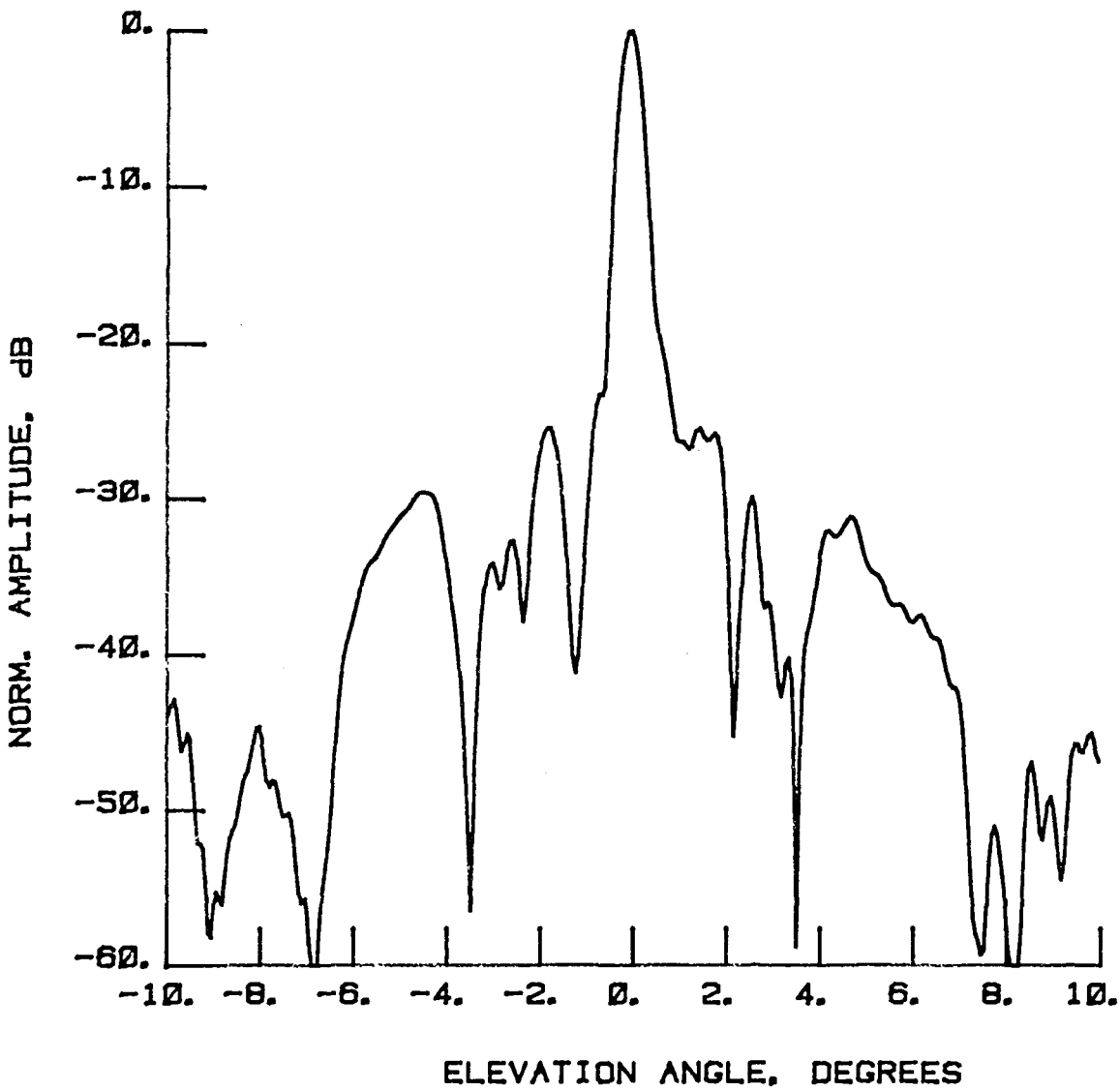

Figure 143 Test 18, 7.73 GHz, Co-Pol, H-Plane, Type 4

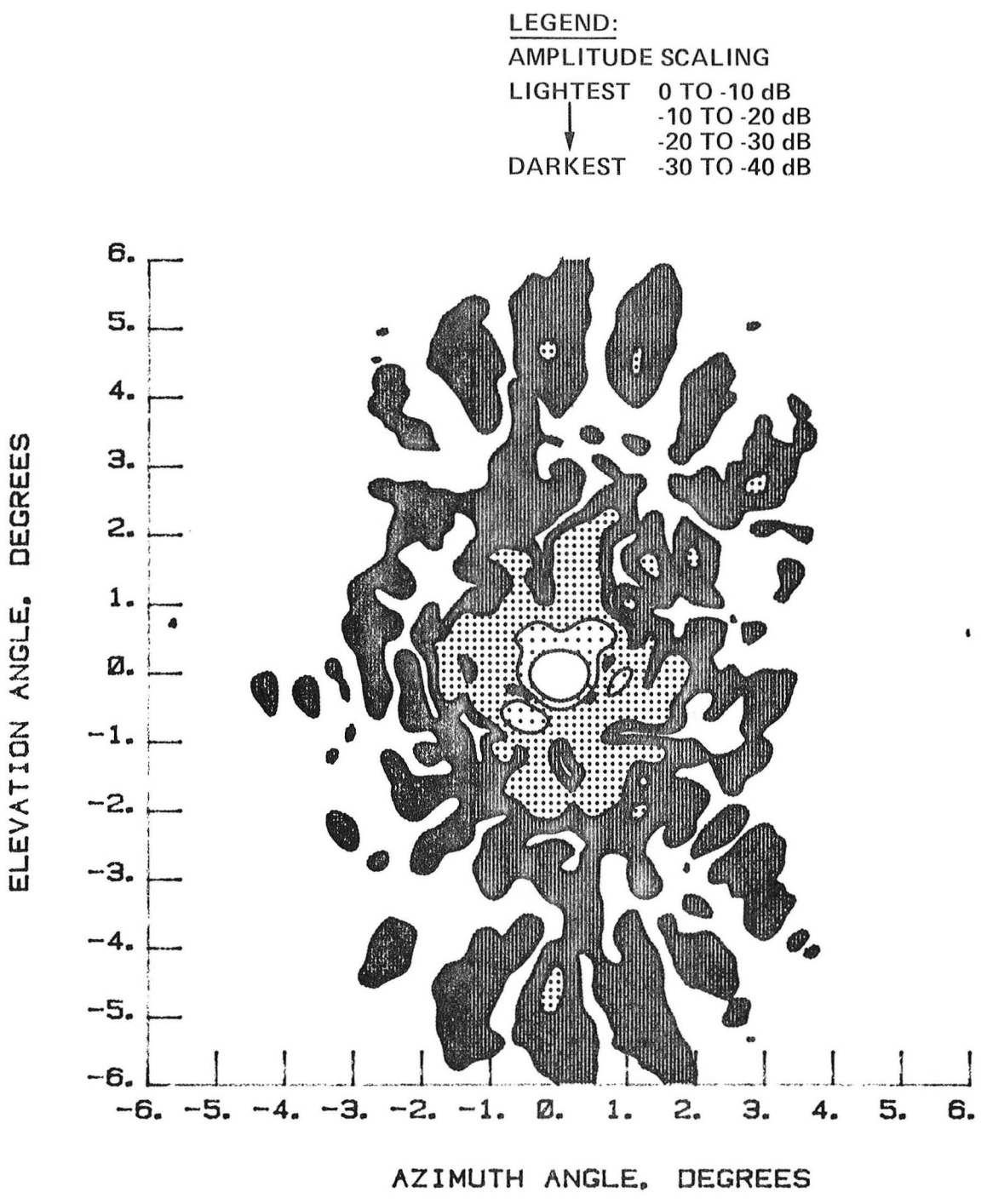

Figure 144 Test 18, 7.73 GHz, Co-Pol, Contour, Type 5

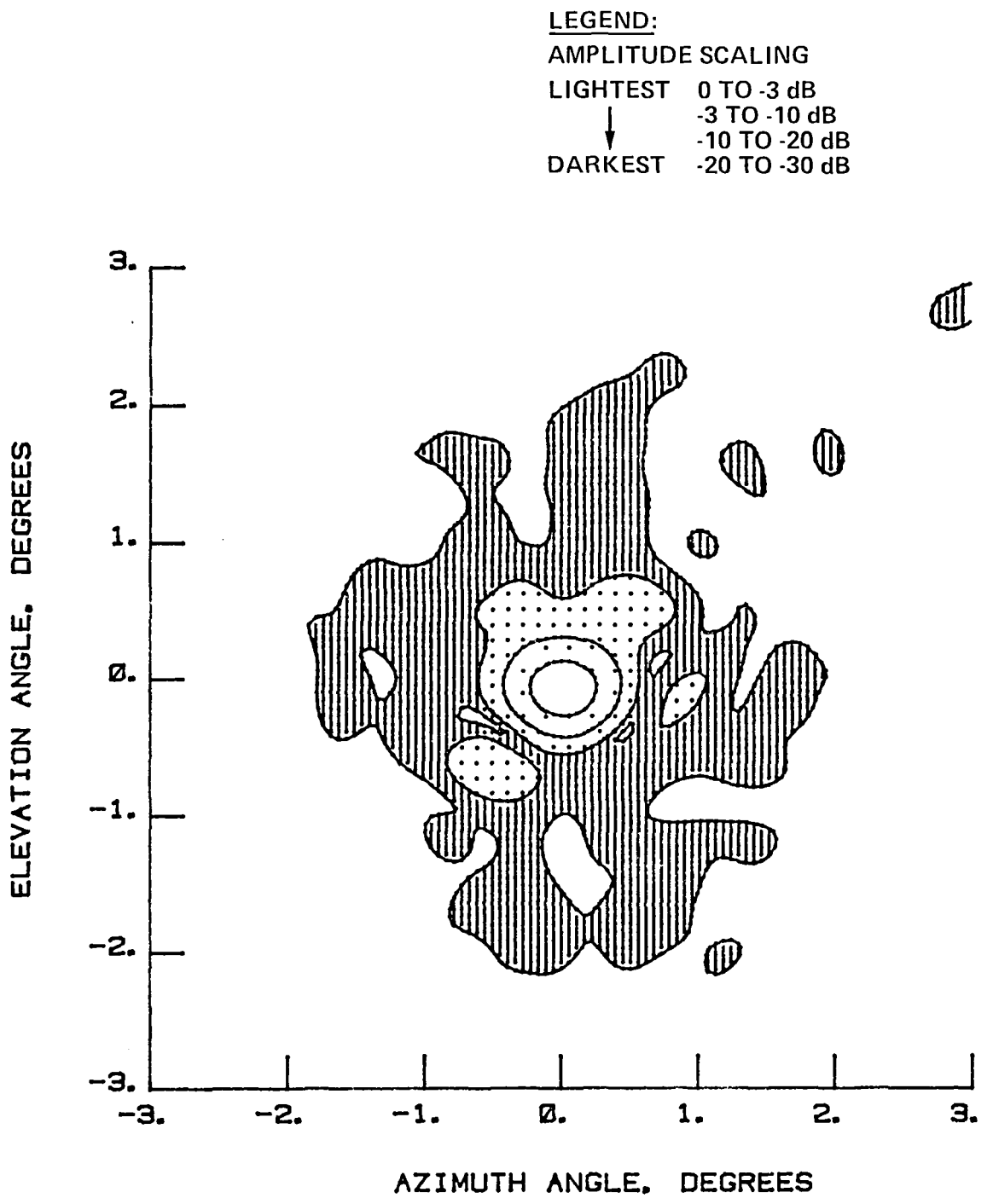

Figure 145 Test 18, 7.73 GHz, Co-Pol, Contour, Type 6

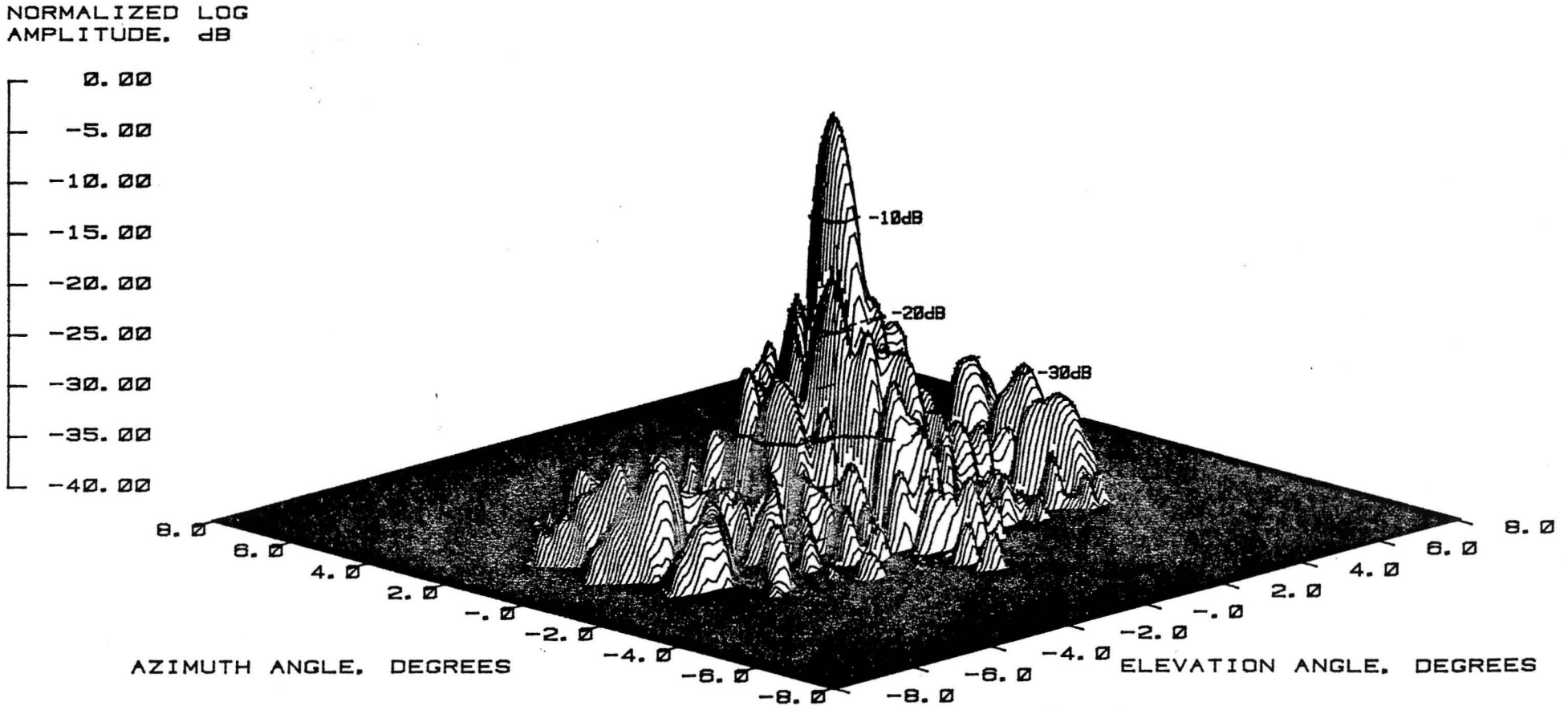

Figure 146 Test 18, 7.73 GHz, Co-Pol, 3-D, Type 7

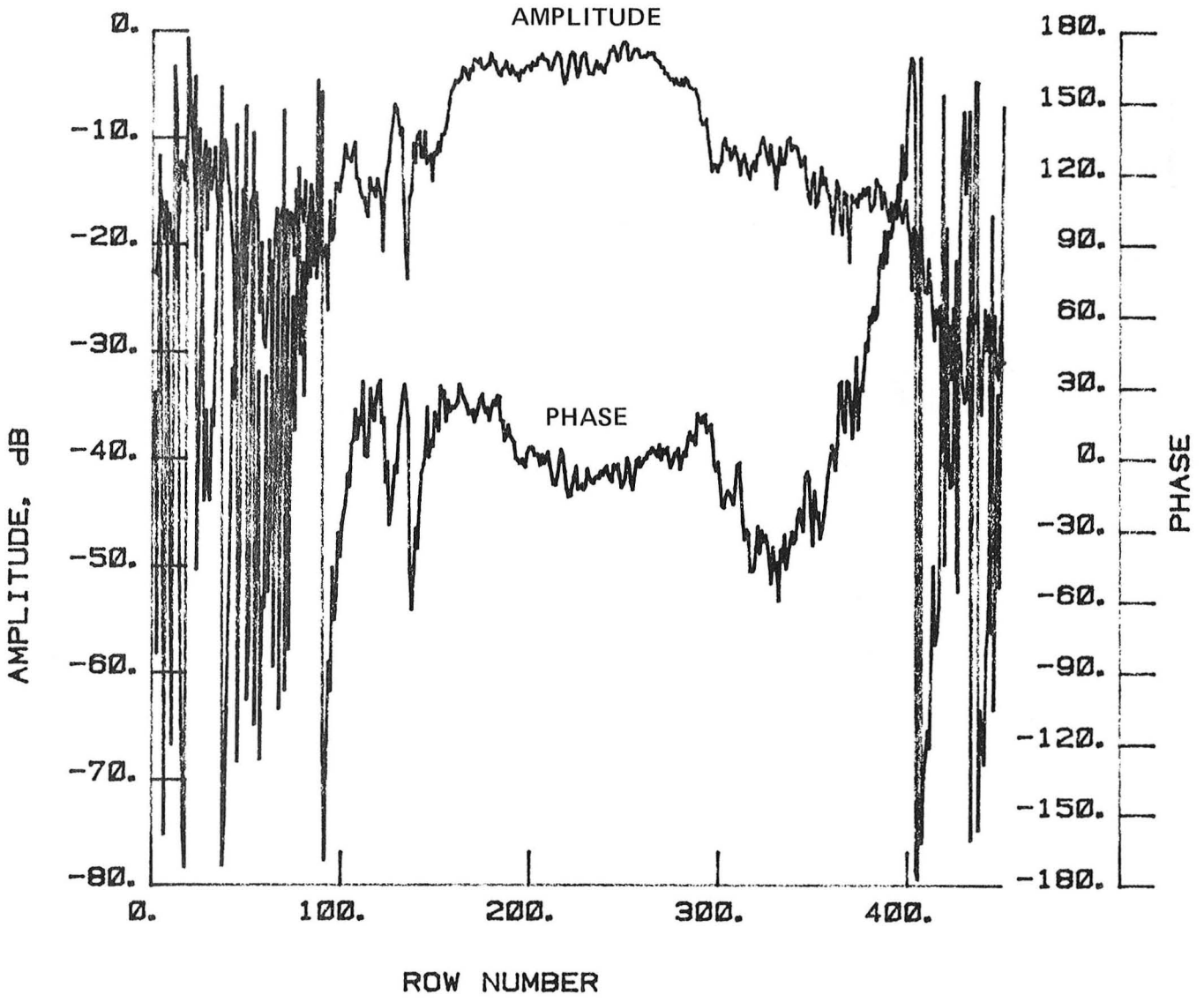

Figure 147 Test 18, 7.73 GHz, Co-Pol, H-Plane, Type 8

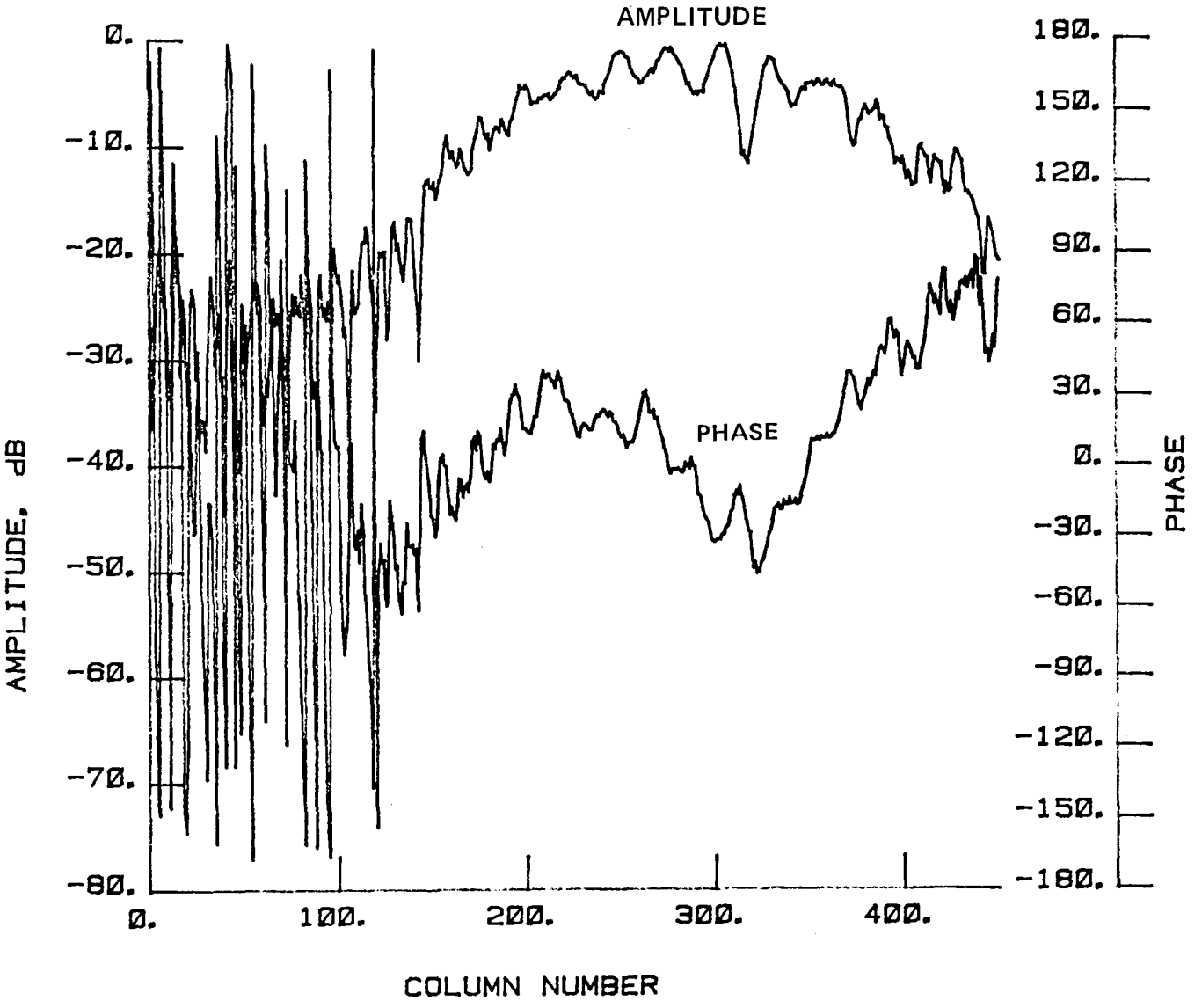

Figure 148 Test 18, 7.73 GHz, Co-Pol, E-Plane, Type 9

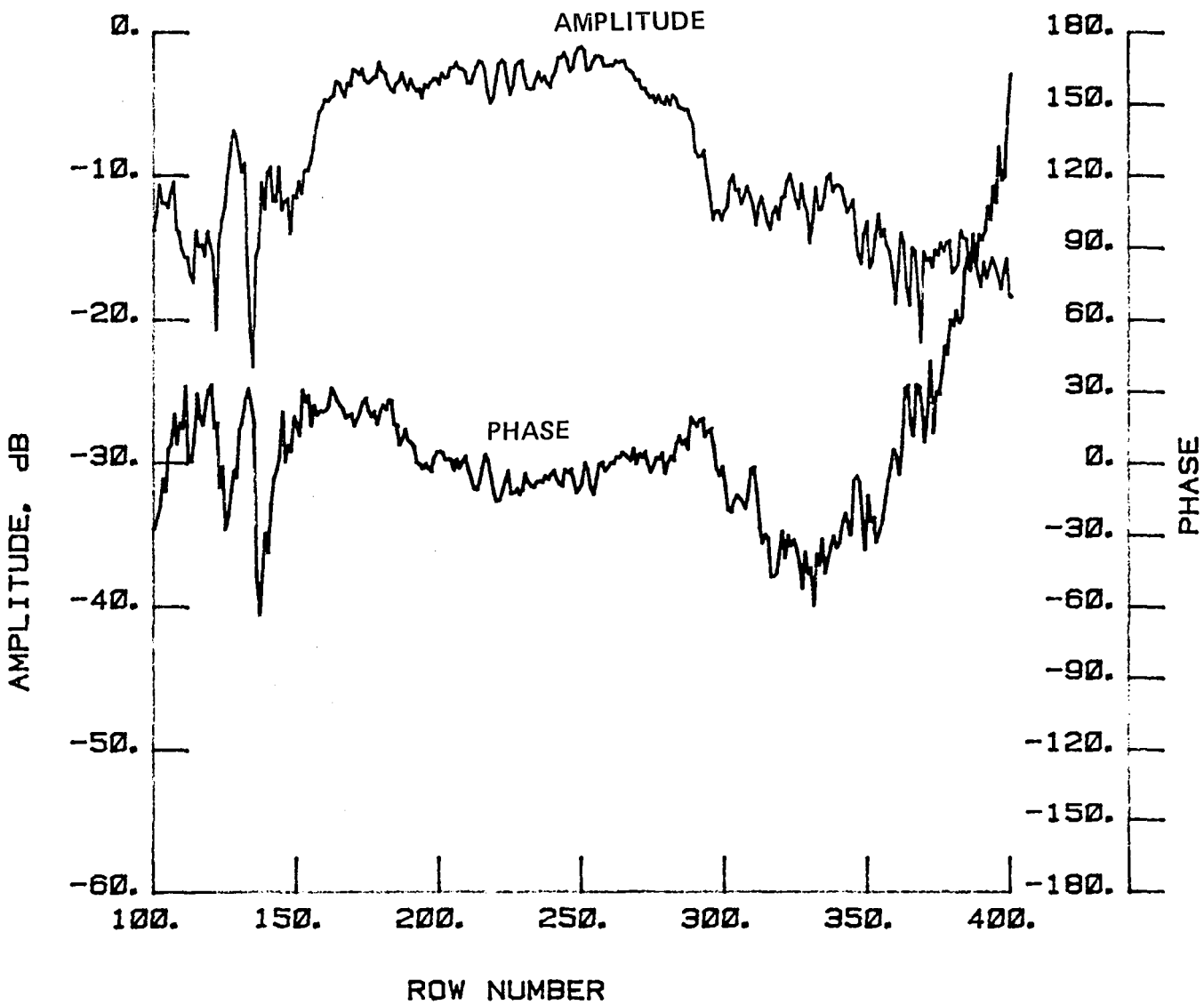

Figure 149 Test 18, 7.73 GHz, Co-Pol, H-Plane, Type 10

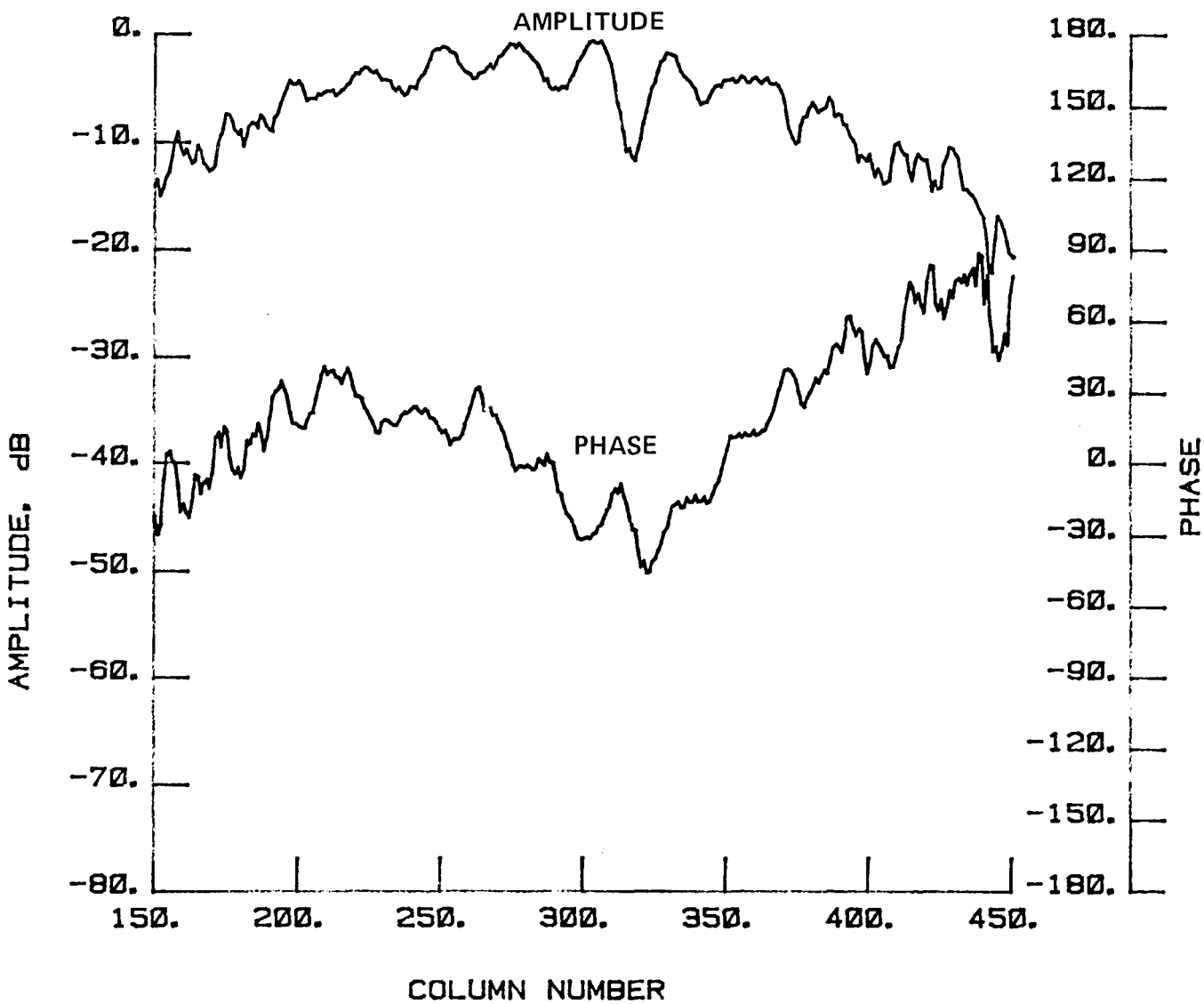

Figure 150 Test 18, 7.73 GHz, Co-Pol, E-Plane, Type 11

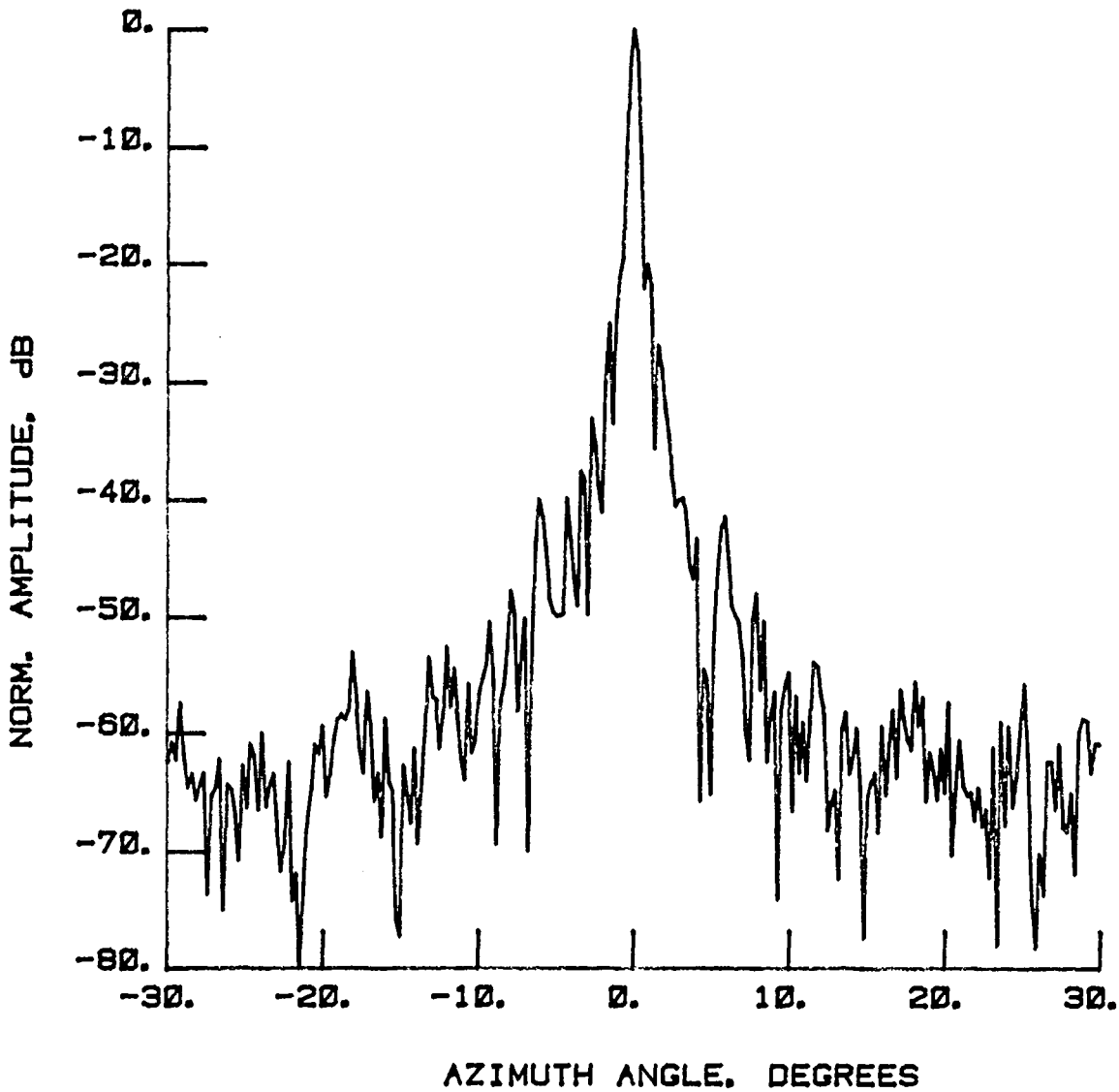

Figure 151 Test 19, 7.73 GHz, Co-Pol, E-Plane, Type 1

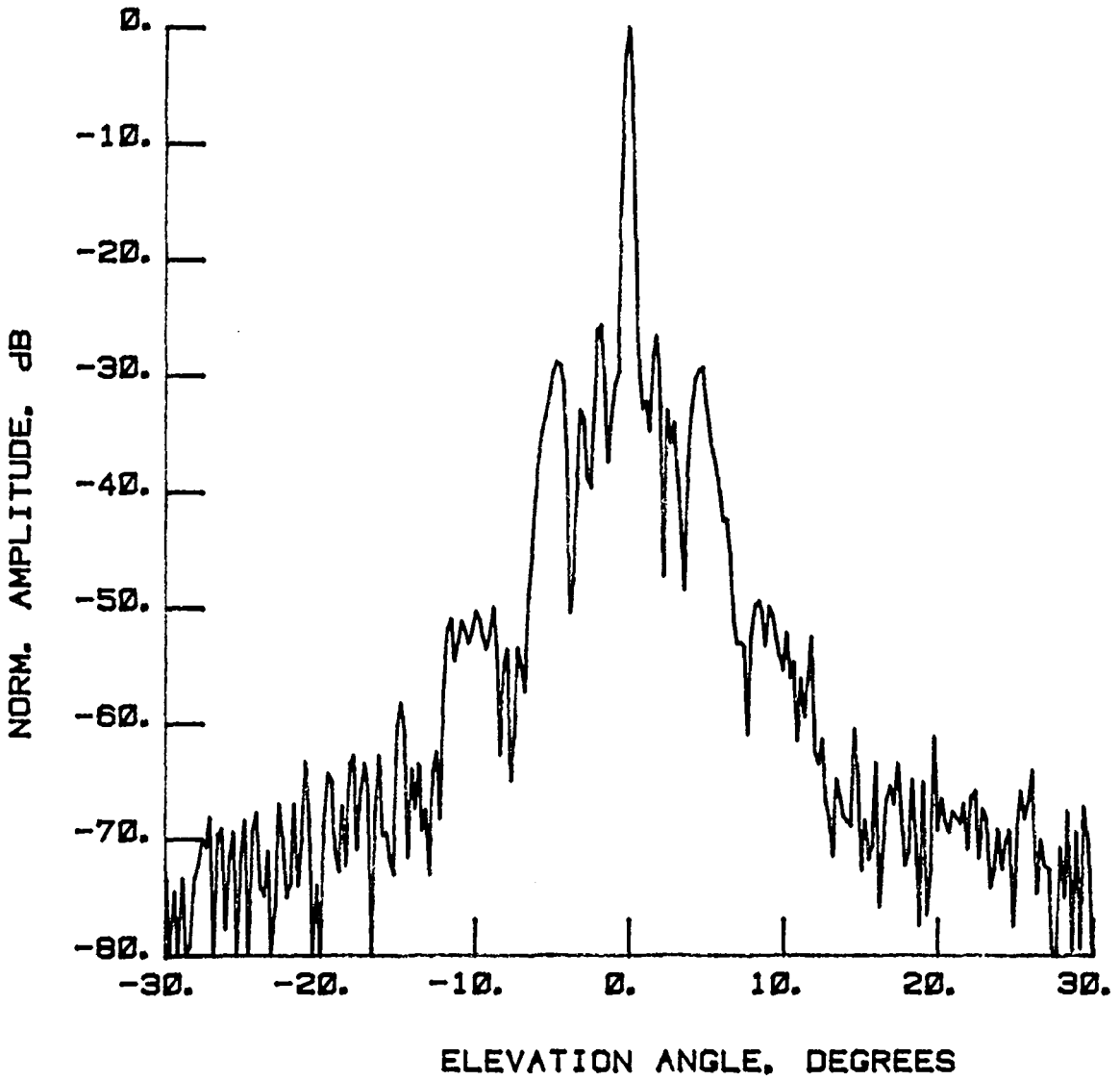

Figure 152 Test 19, 7.73 GHz, Co-Pol, H-Plane, Type 2

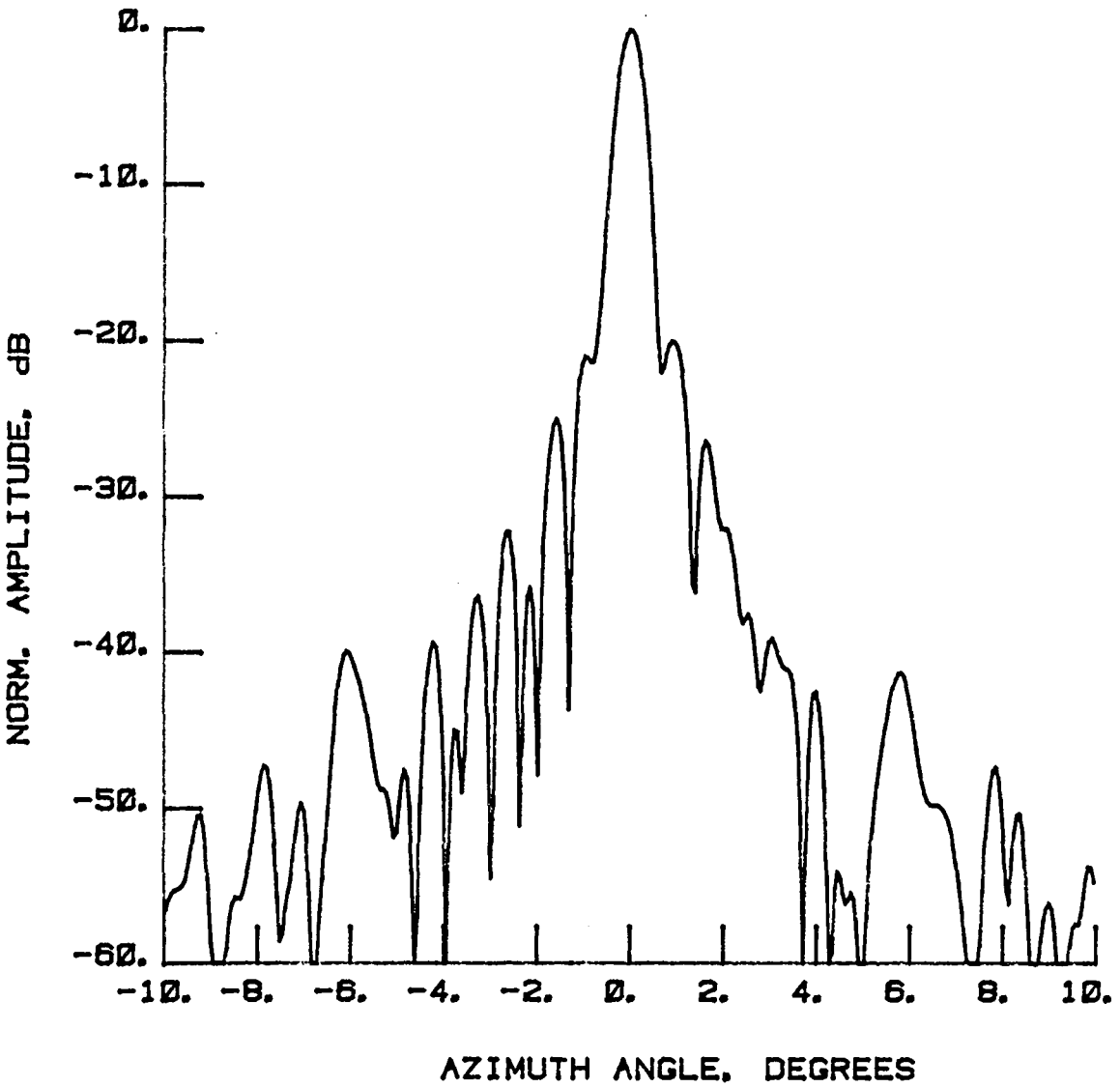

Figure 153 Test 19, 7.73 GHz, Co-Pol, E-Plane, Type 3

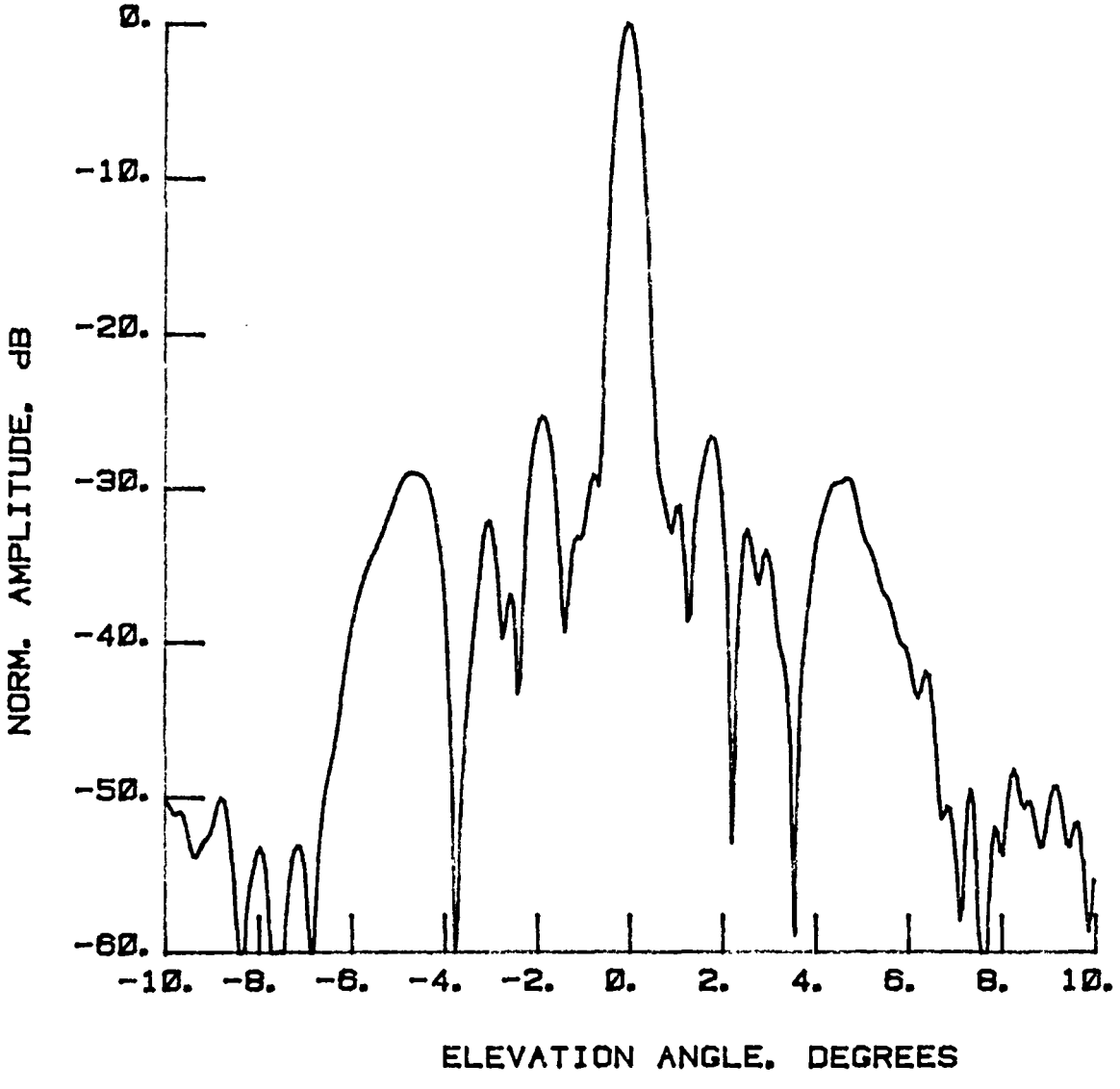

Figure 154 Test 19, 7.73 GHz, Co-Pol, H-Plane, Type 4

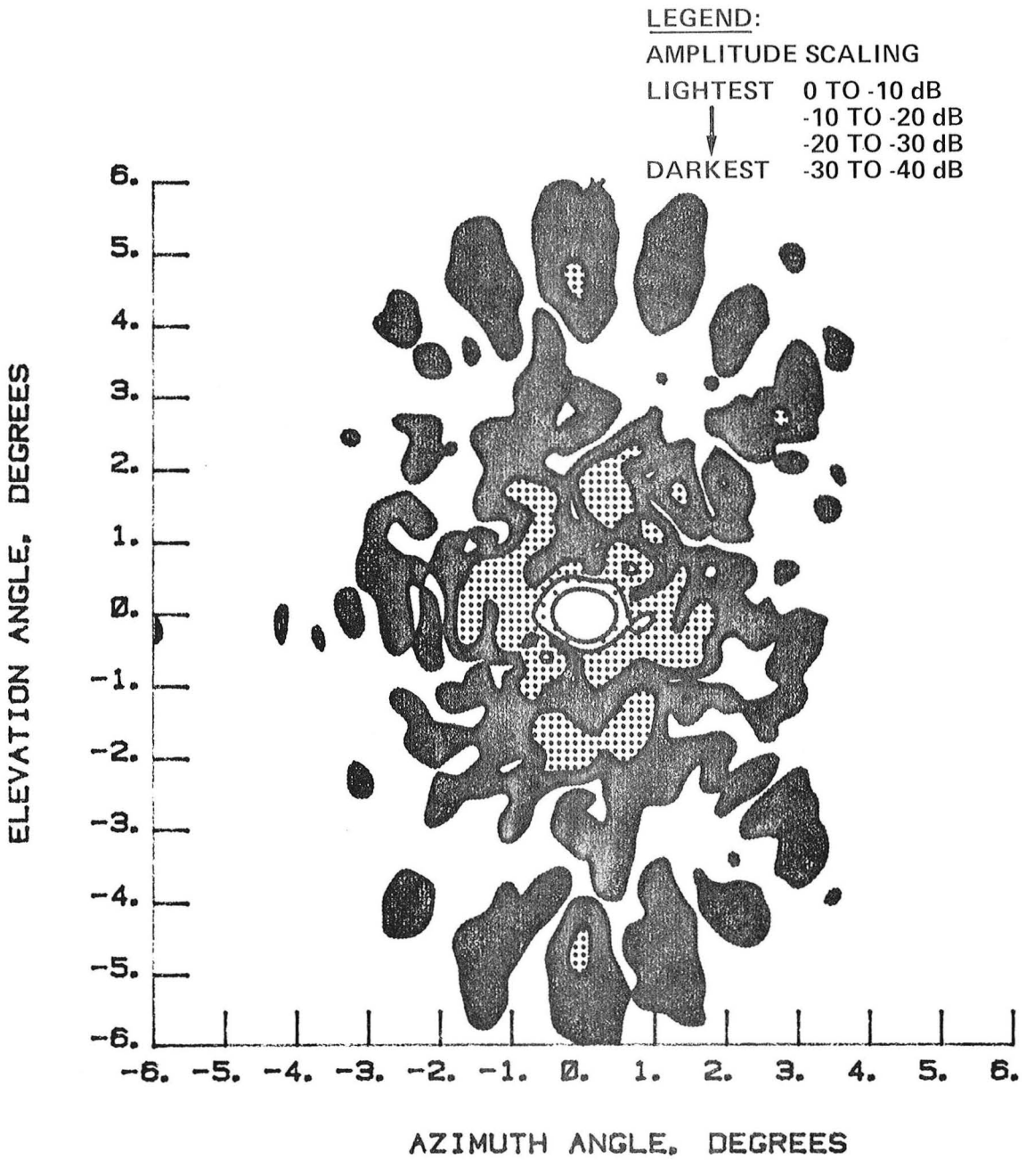

Figure 155 Test 19, 7.73 GHz, Co-Pol, Contour, Type 5

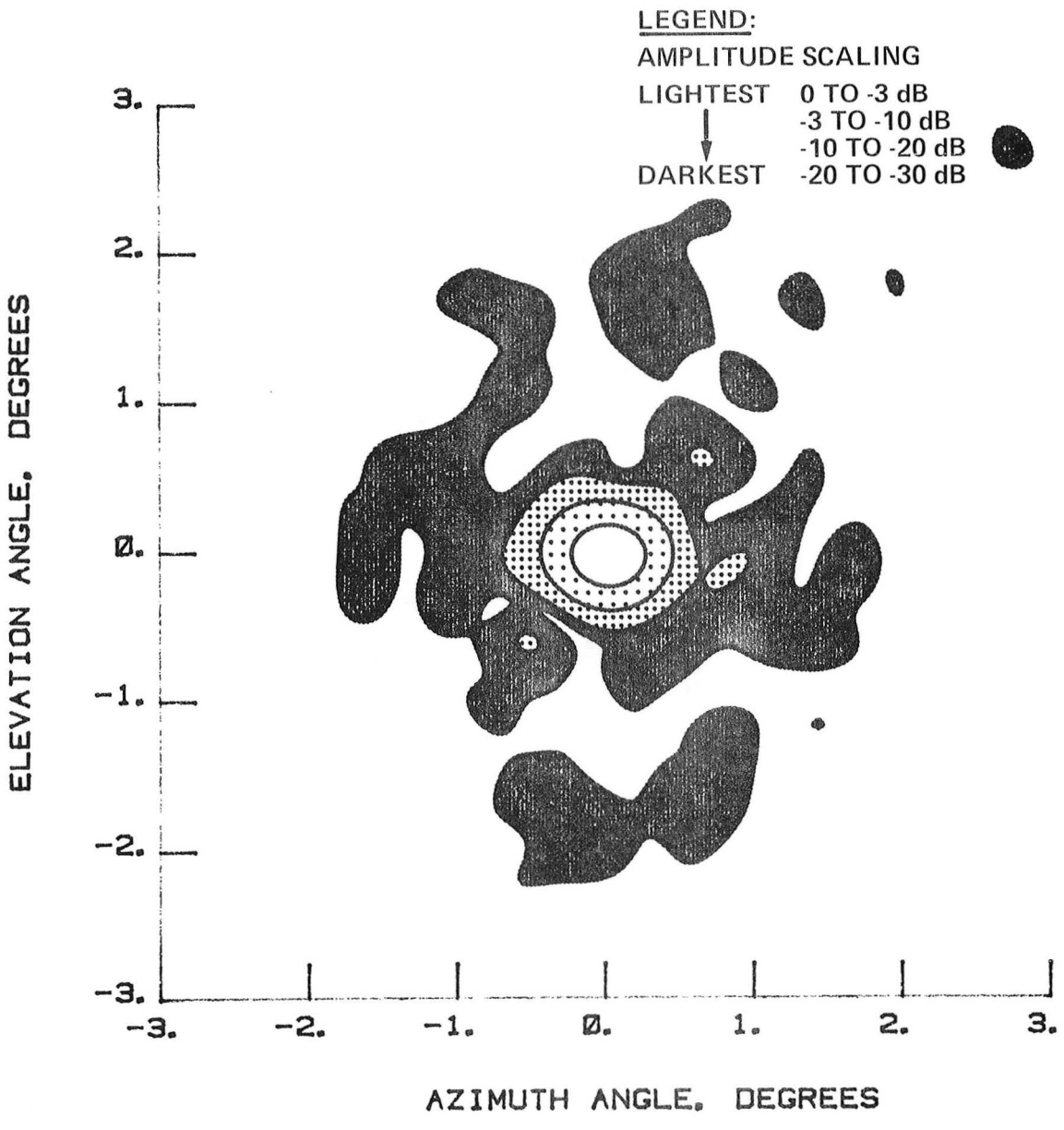

Figure 156 Test 19, 7.73 GHz, Co-Pol, Contour, Type 6

TEST IDENTIFICATION : LC19S

DATE : 18 SEPT. 1985

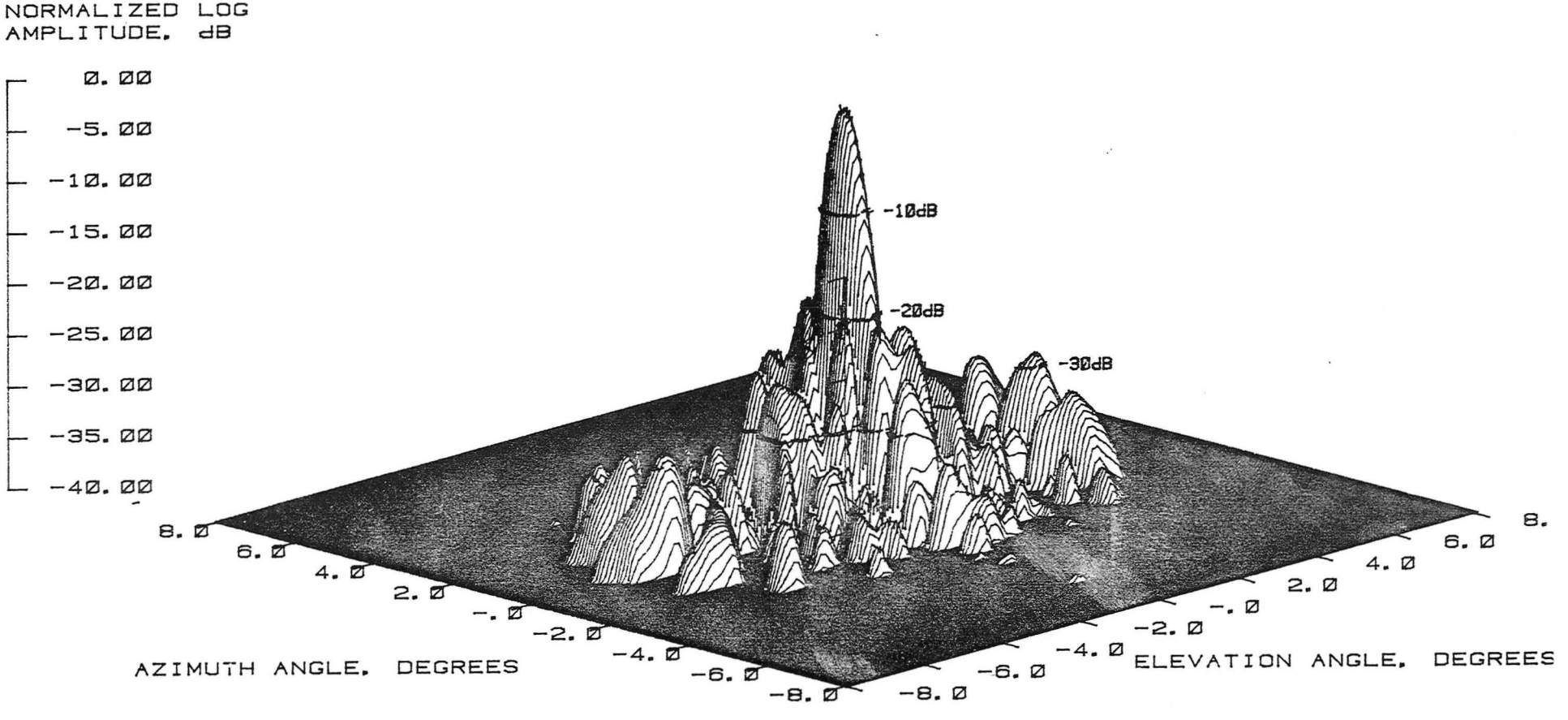

Figure 157 Test 19, 7.73 GHz, Co-Pol, 3-D, Type 7

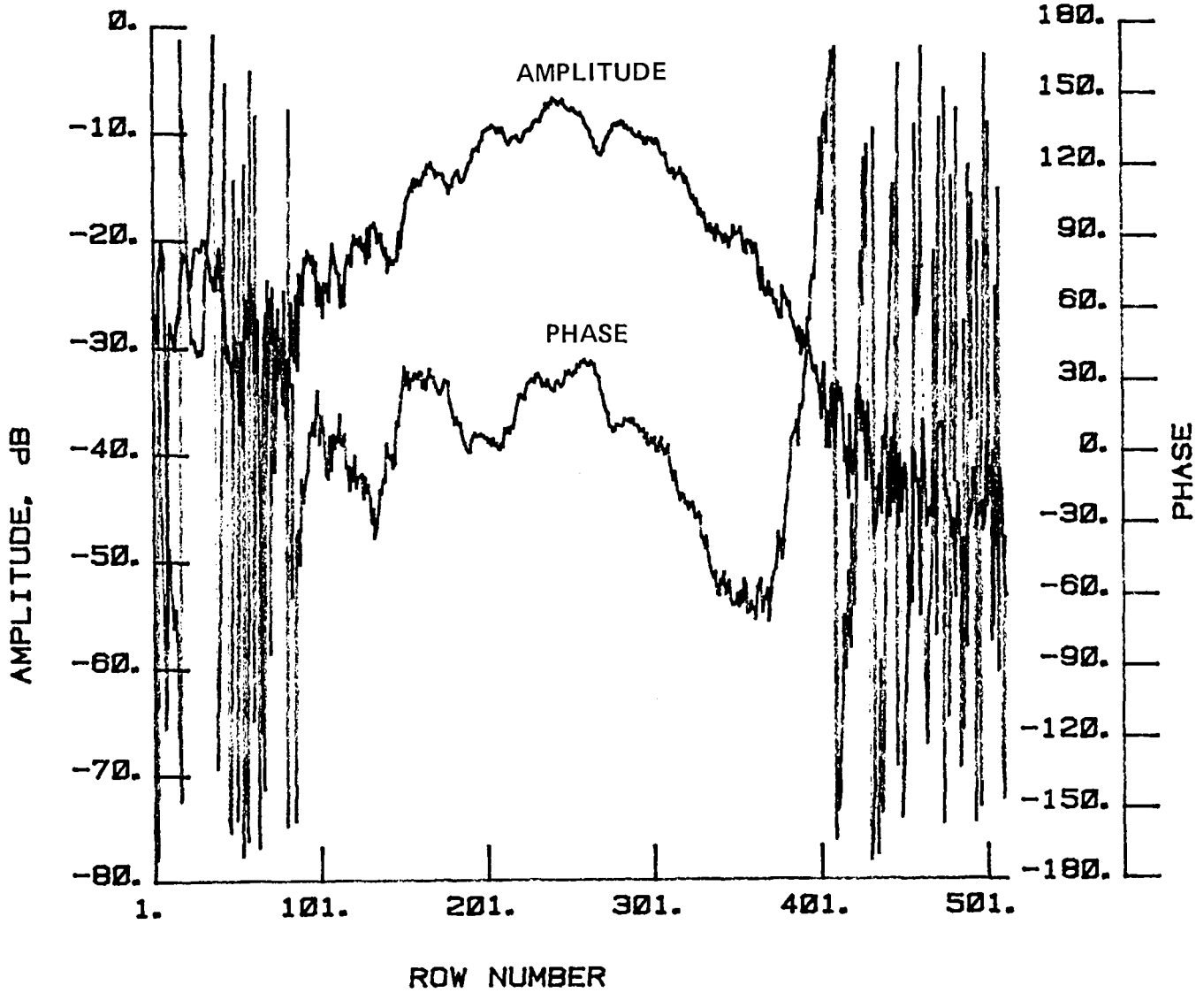

Figure 158 Test 19, 7.73 GHz, Co-Pol, H-Plane, Type 8

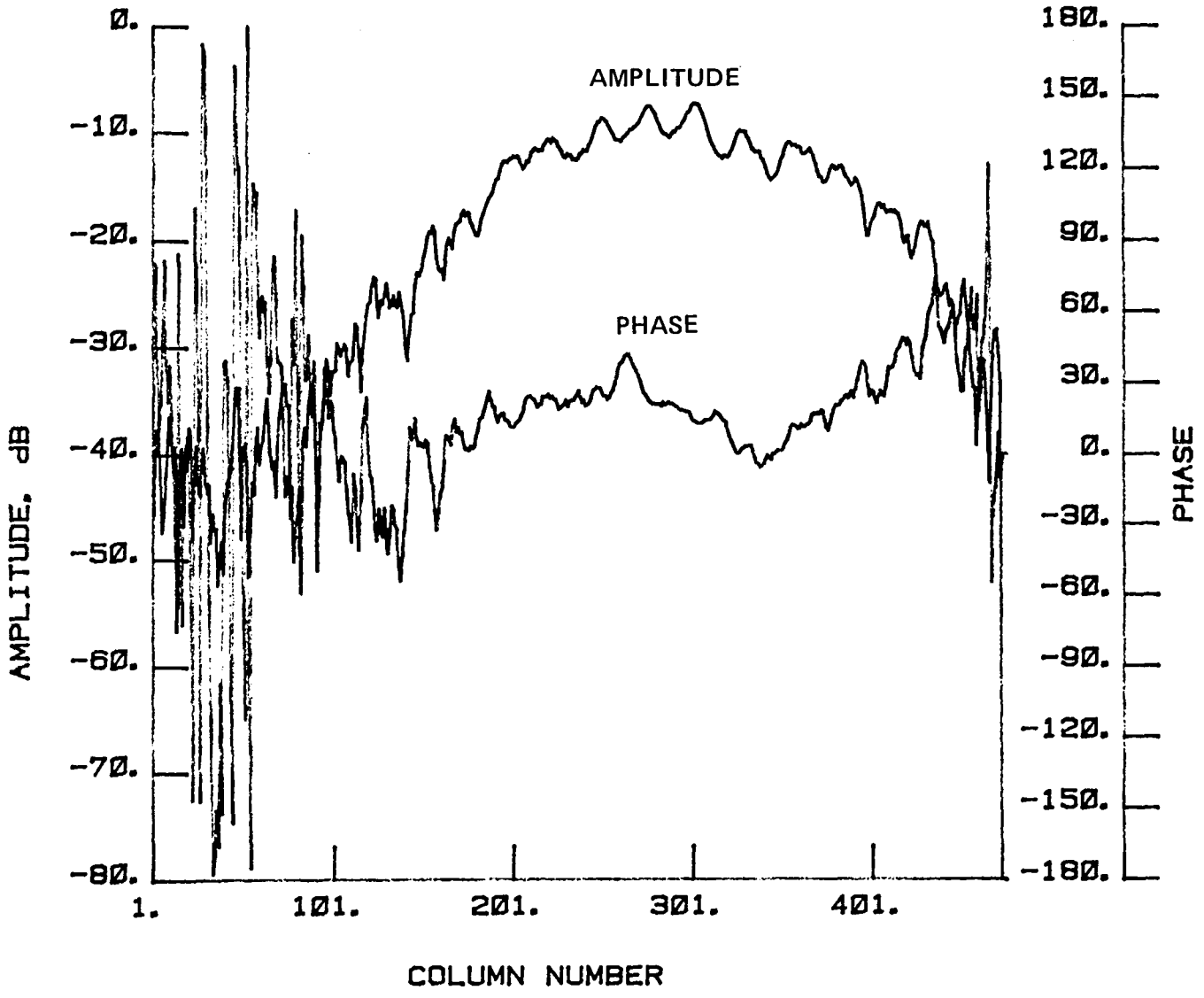

Figure 159 Test 19, 7.73 GHz, Co-Pol, E-Plane, Type 9

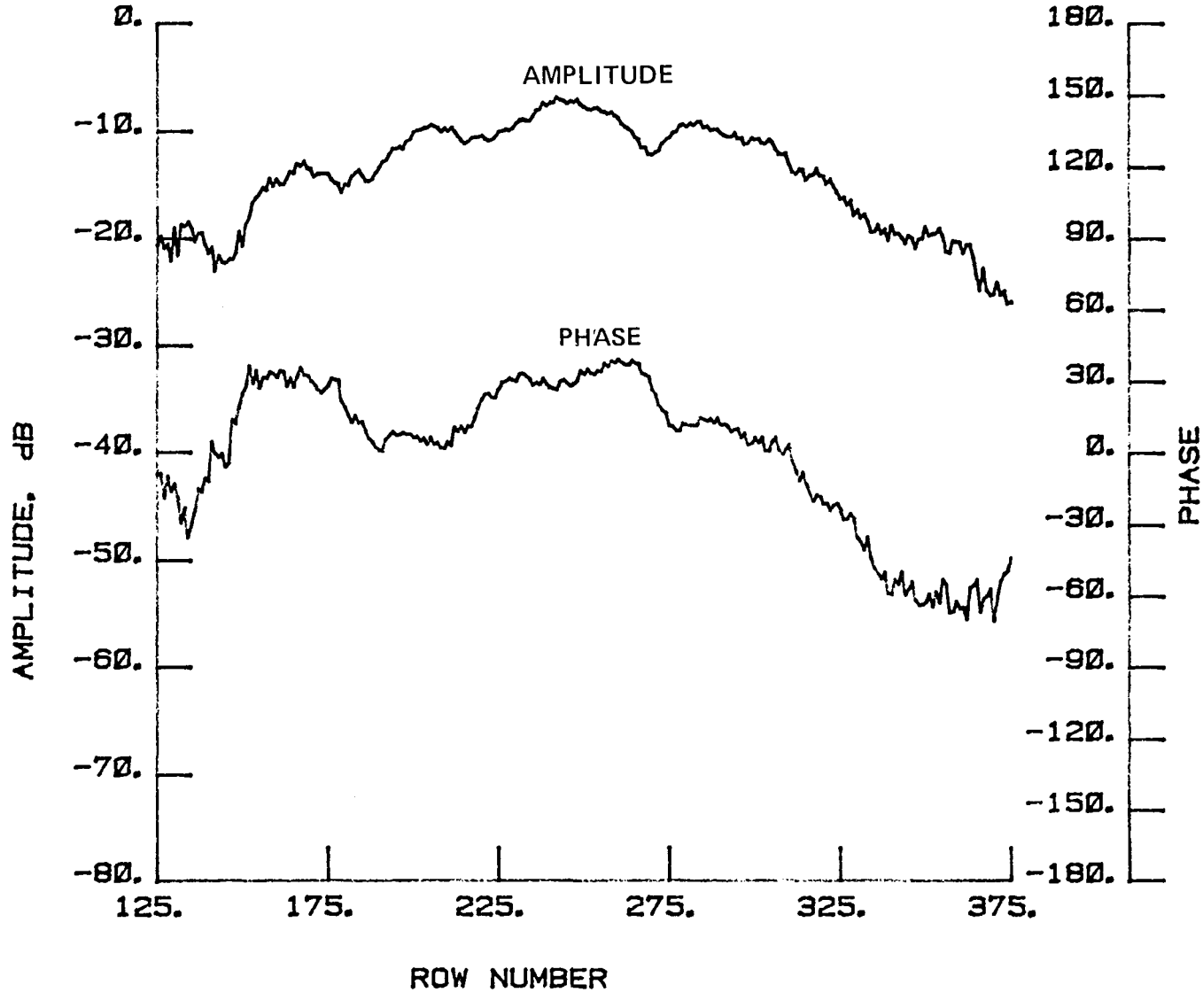

Test 160 Test 19, 7.73 GHz, Co-Pol, H-Plane, Type 10

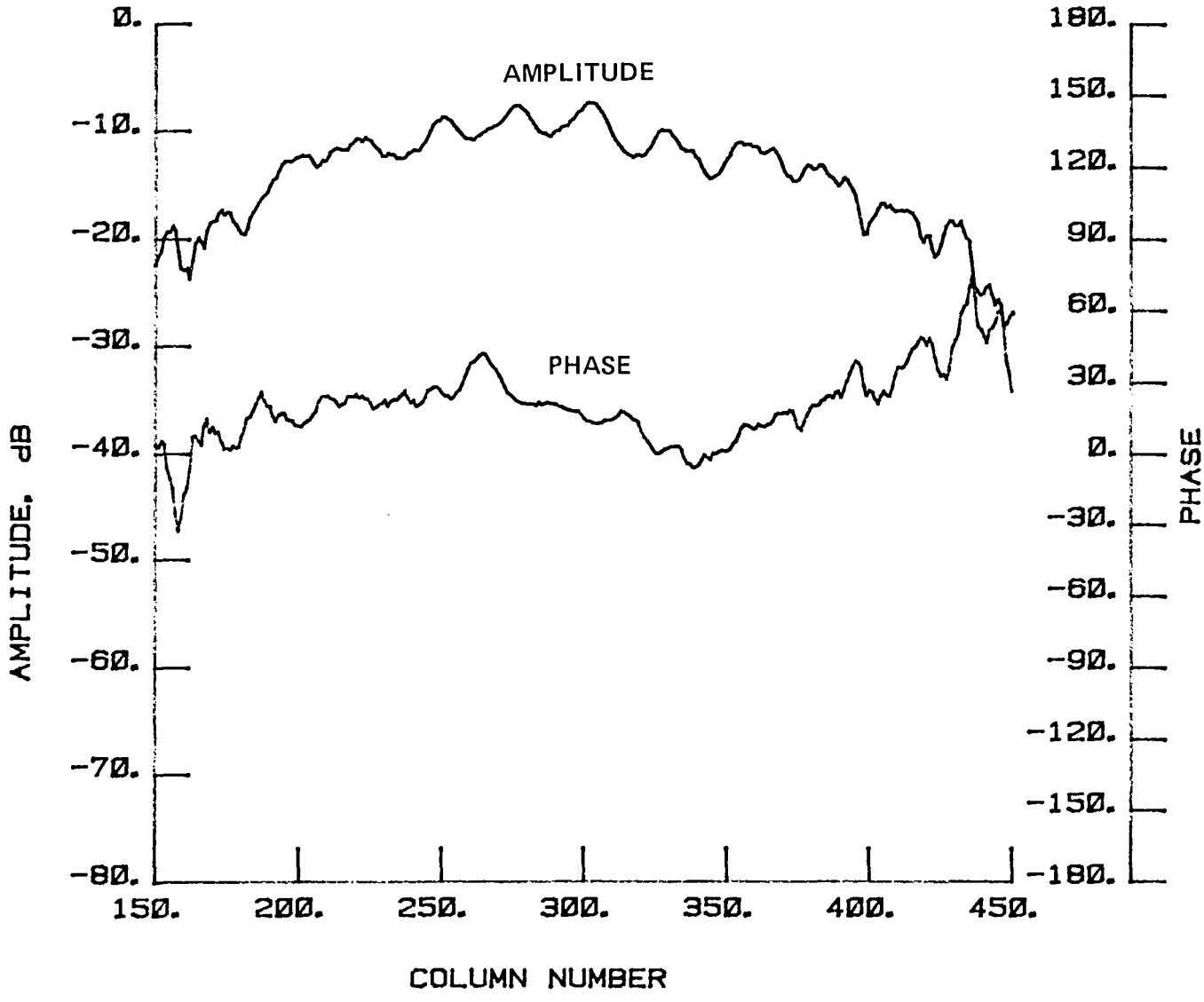

Figure 161 Test 19, 7.73 GHz, Co-Pol, E-Plane, Type 11

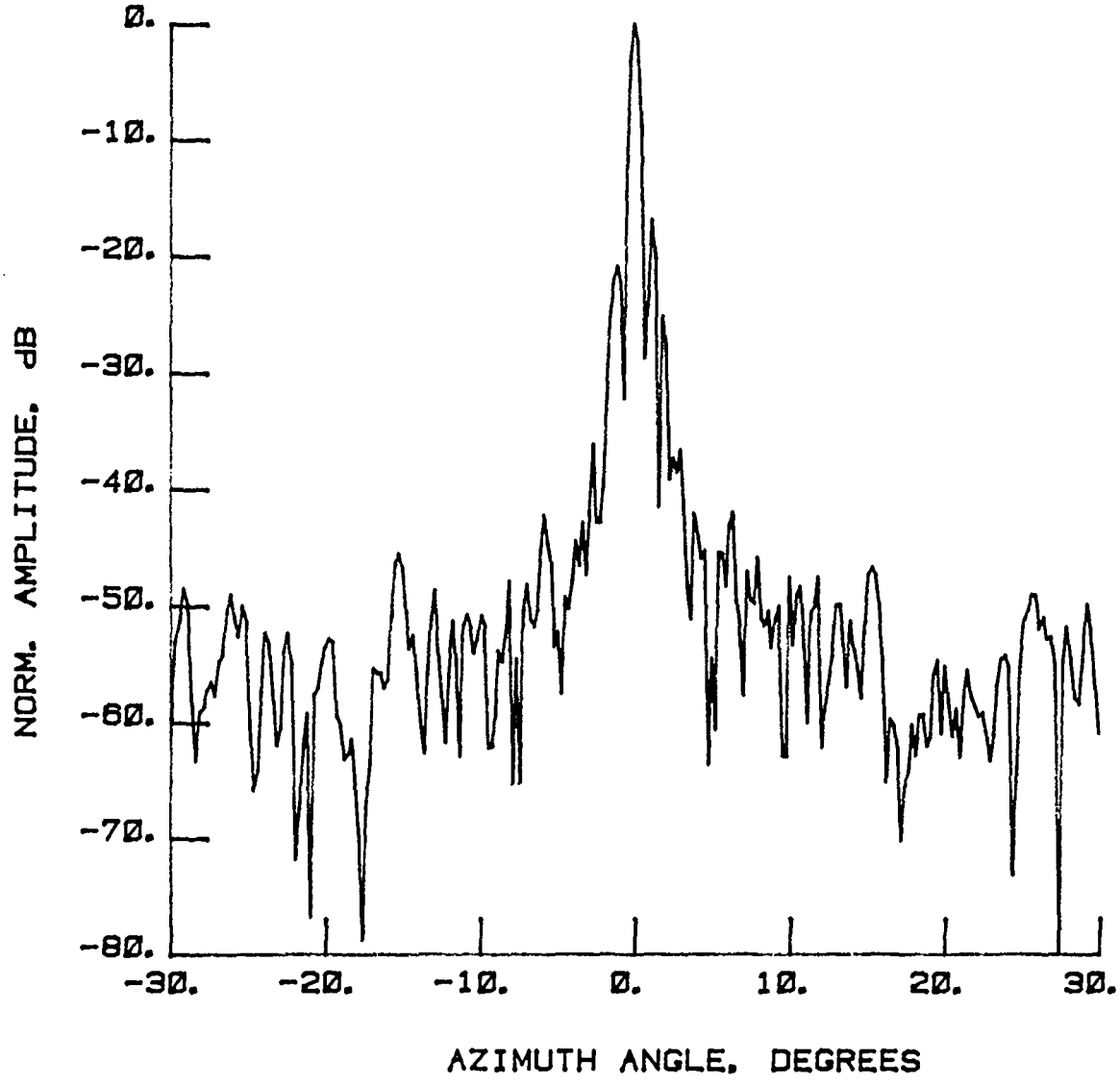

Figure 162 Test 20, 7.73 GHz, Co-Pol, E-Plane, Type 1

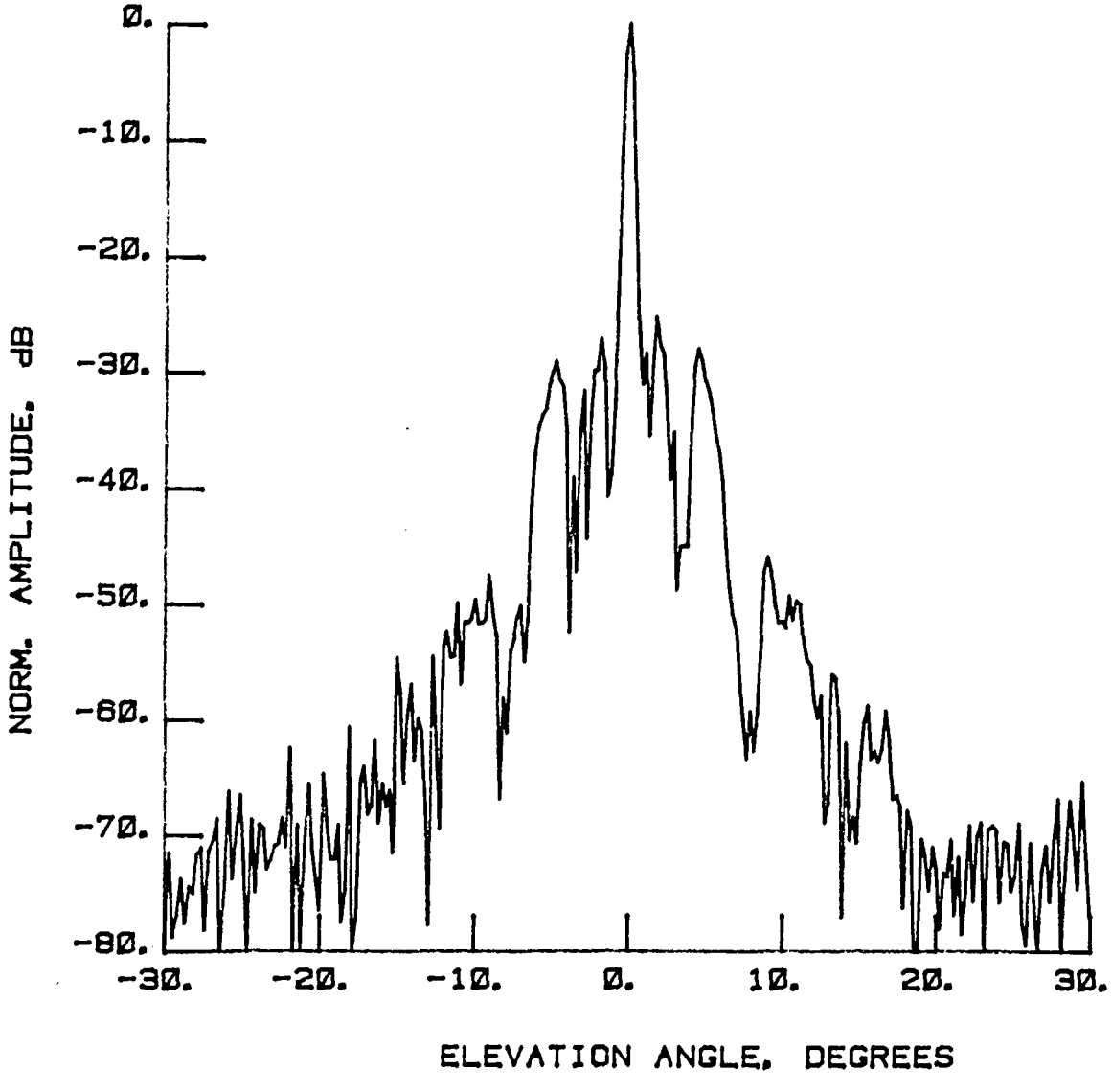

Figure 163 Test 20, 7.73 GHz, Co-Pol, H-Plane, Type 2

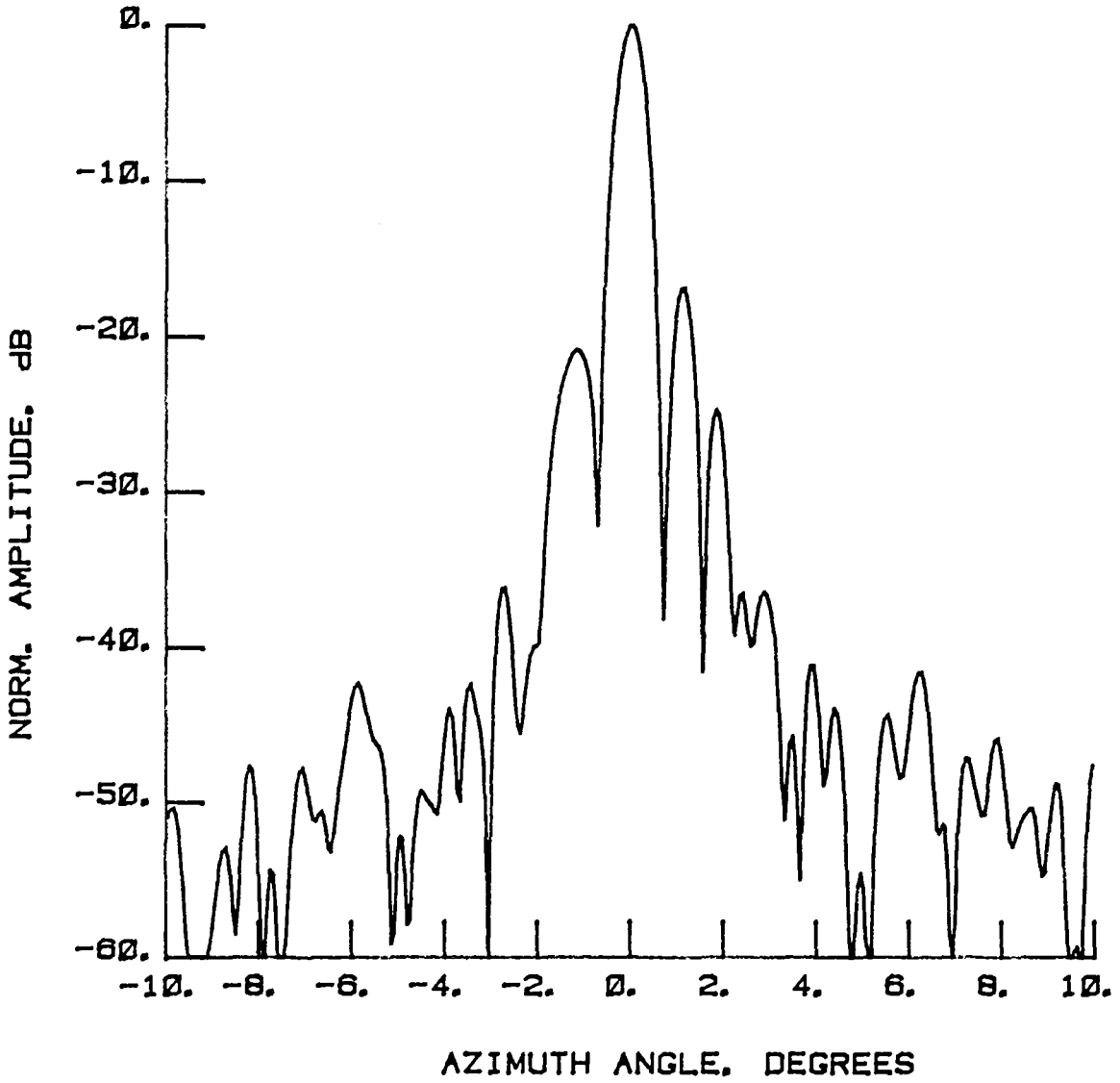

Figure 164 Test 20, 7.73 GHz, Co-Pol, E-Plane, Type 3

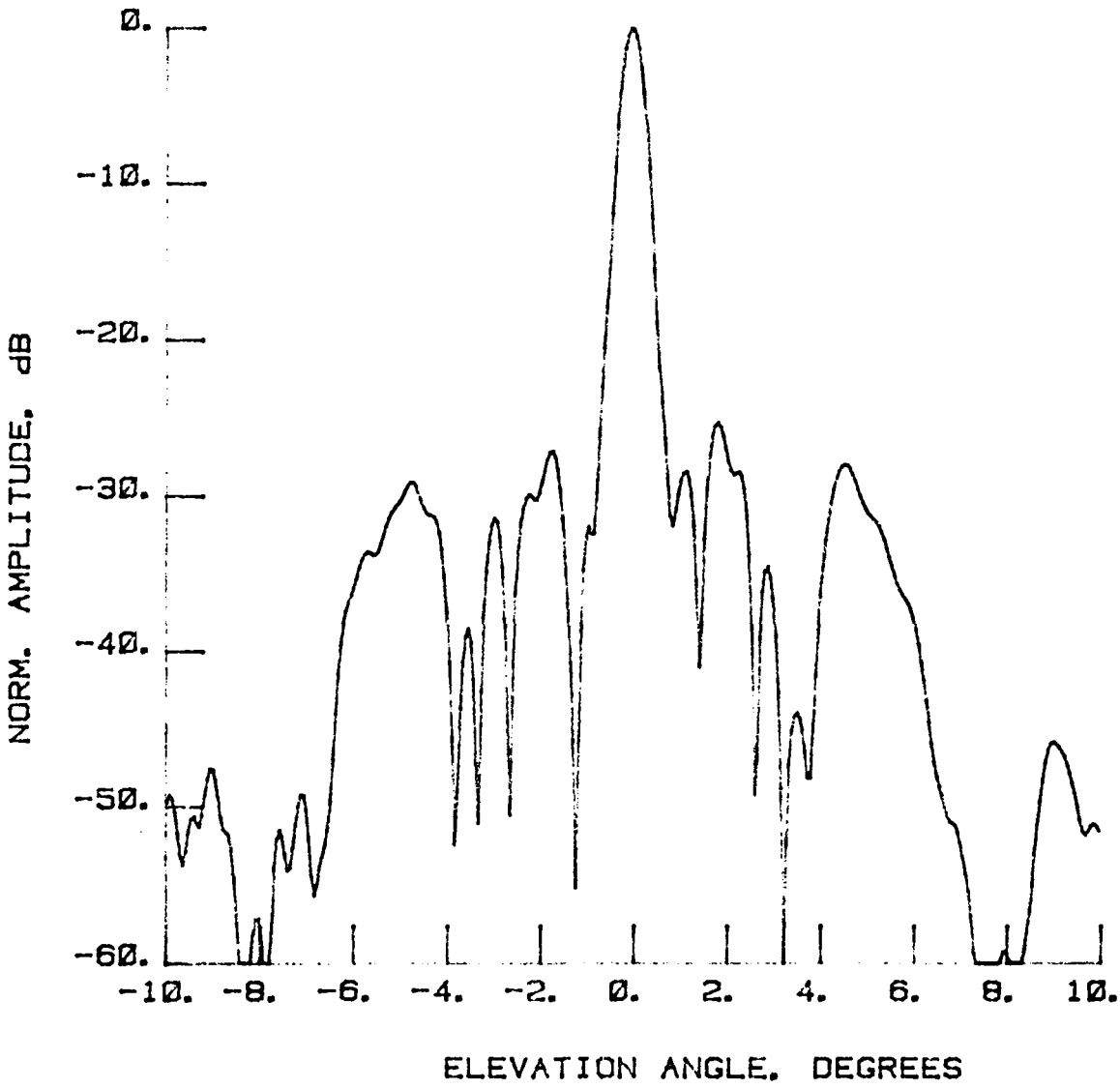

Figure 165 Test 20, 7.73 GHz, Co-Pol, H-Plane, Type 4

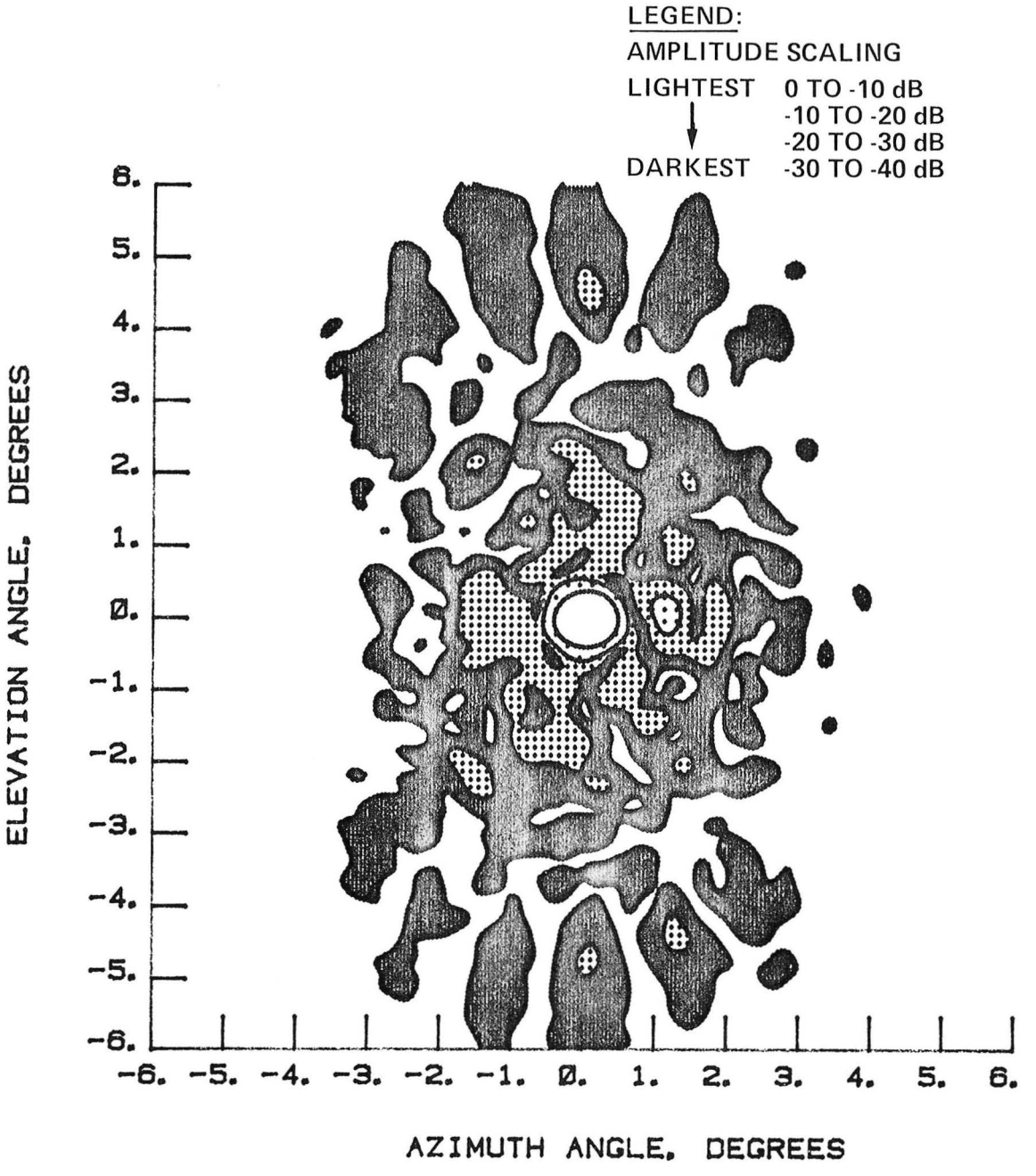

Figure 166 Test 20, 7.73 GHz, Co-Pol, Contour, Type 5

This Page Intentionally Left Blank

TEST IDENTIFICATION : LC20R

DATE : 18 SEPT. 1985

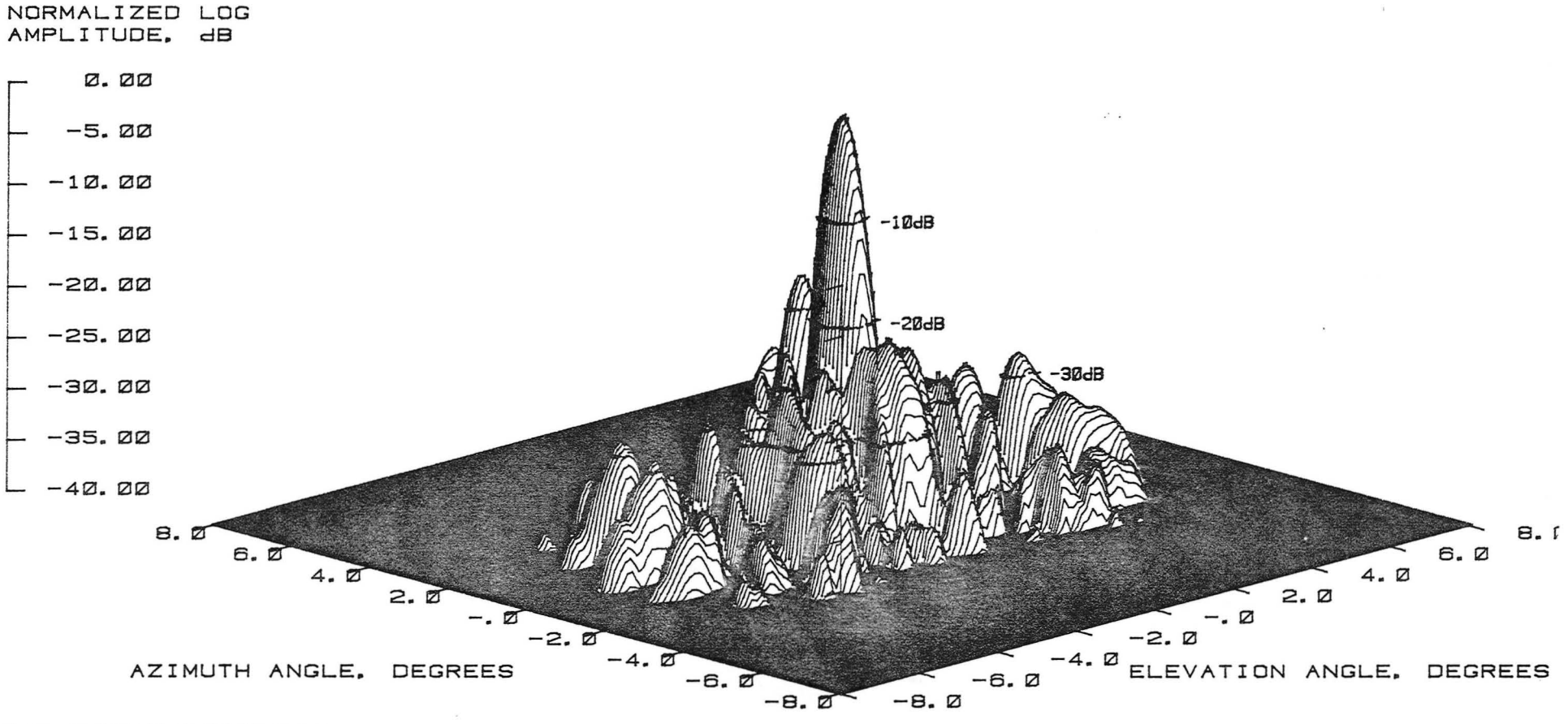

Figure 167 Test 20, 7.73 GHz, Co-Pol, 3-D, Type 7

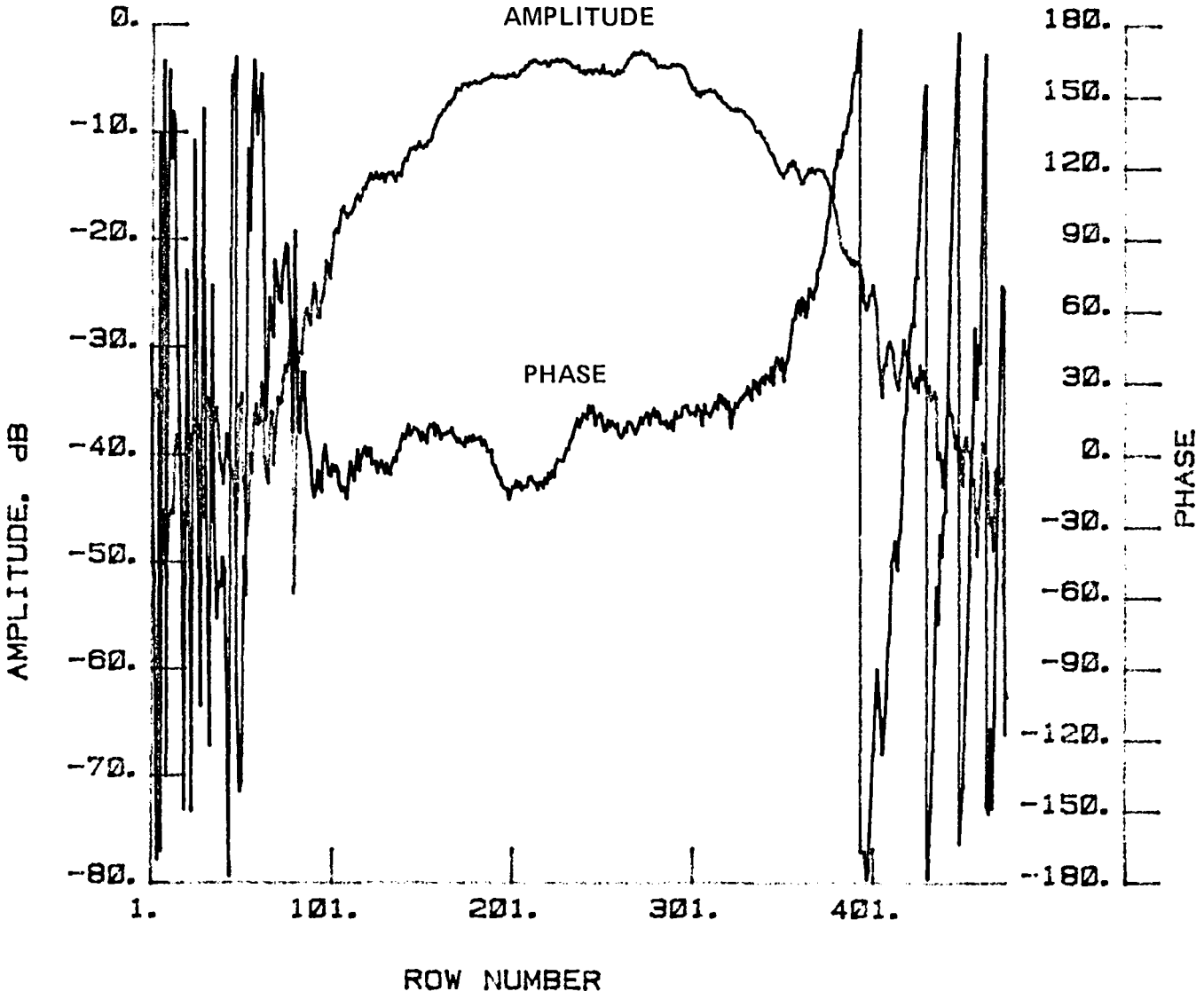

Figure 168 Test 20, 7.73 GHz, Co-Pol, H-Plane, Type 8

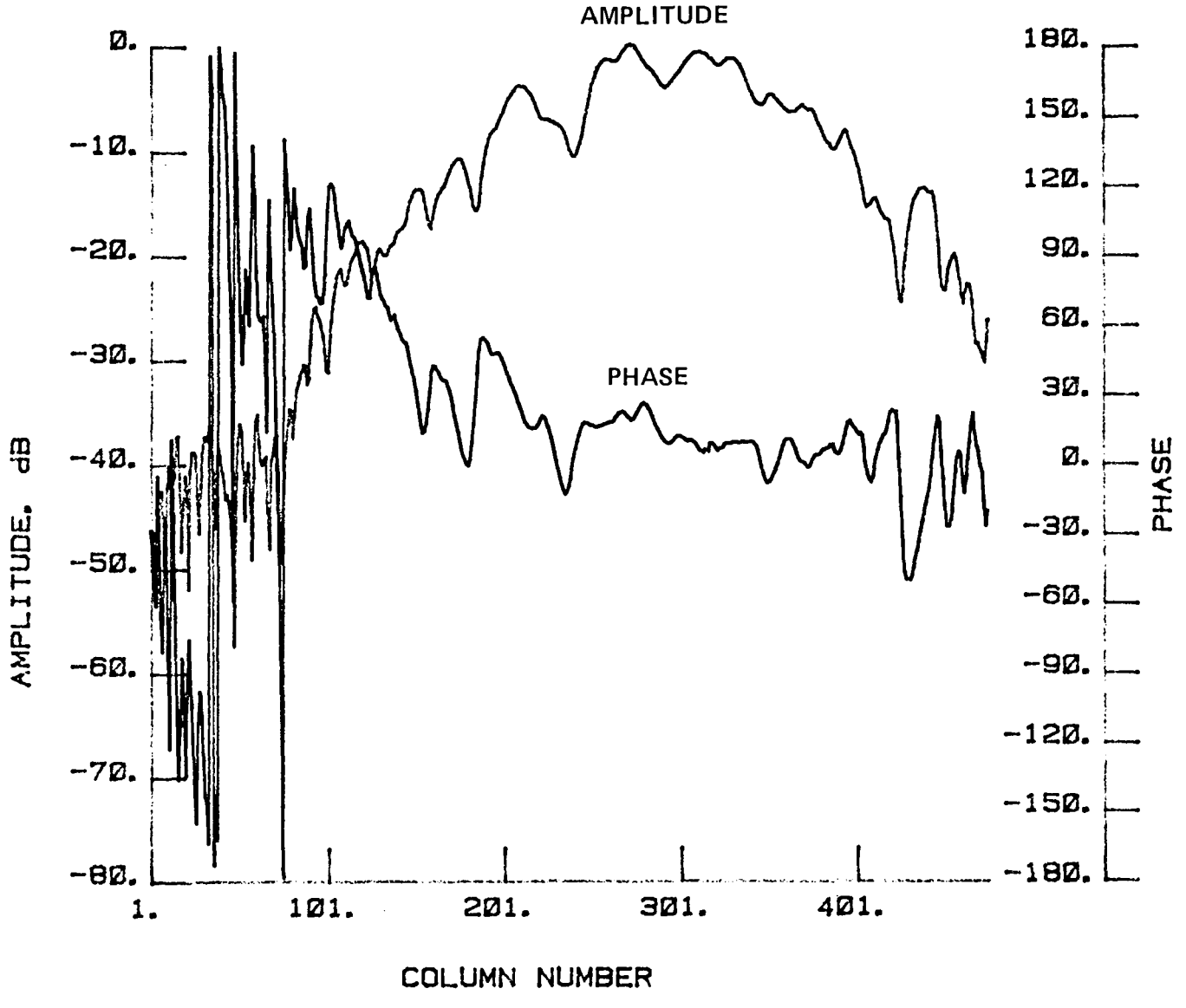

Figure 169 Test 20, 7.73 GHz, Co-Pol, E-Plane, Type 9

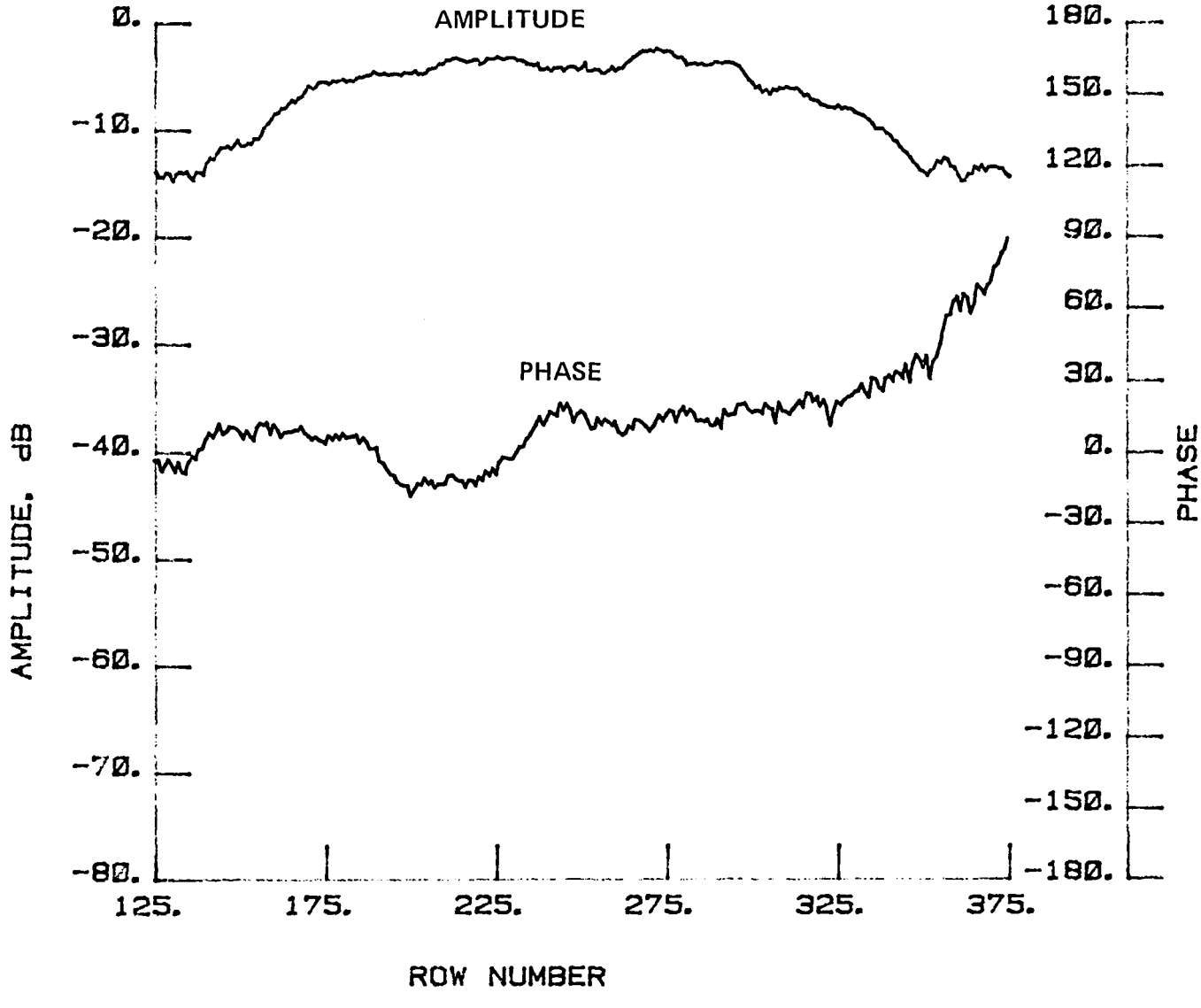

Figure 170 Test 20, 7.73 GHz, Co-Pol, H-Plane, Type 10

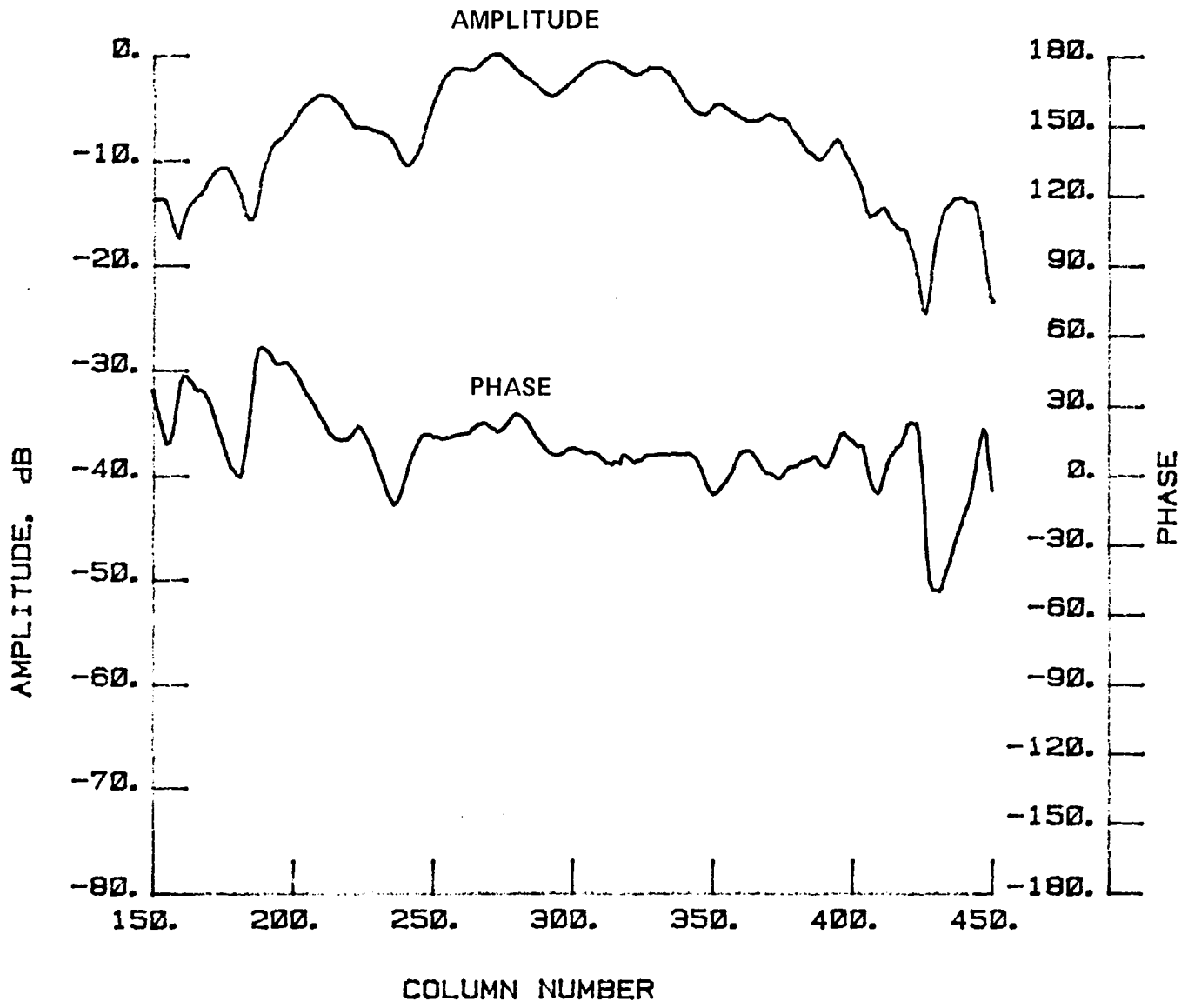

Figure 171 Test 20, 7.73 GHz, Co-Pol, E-Plane, Type 11

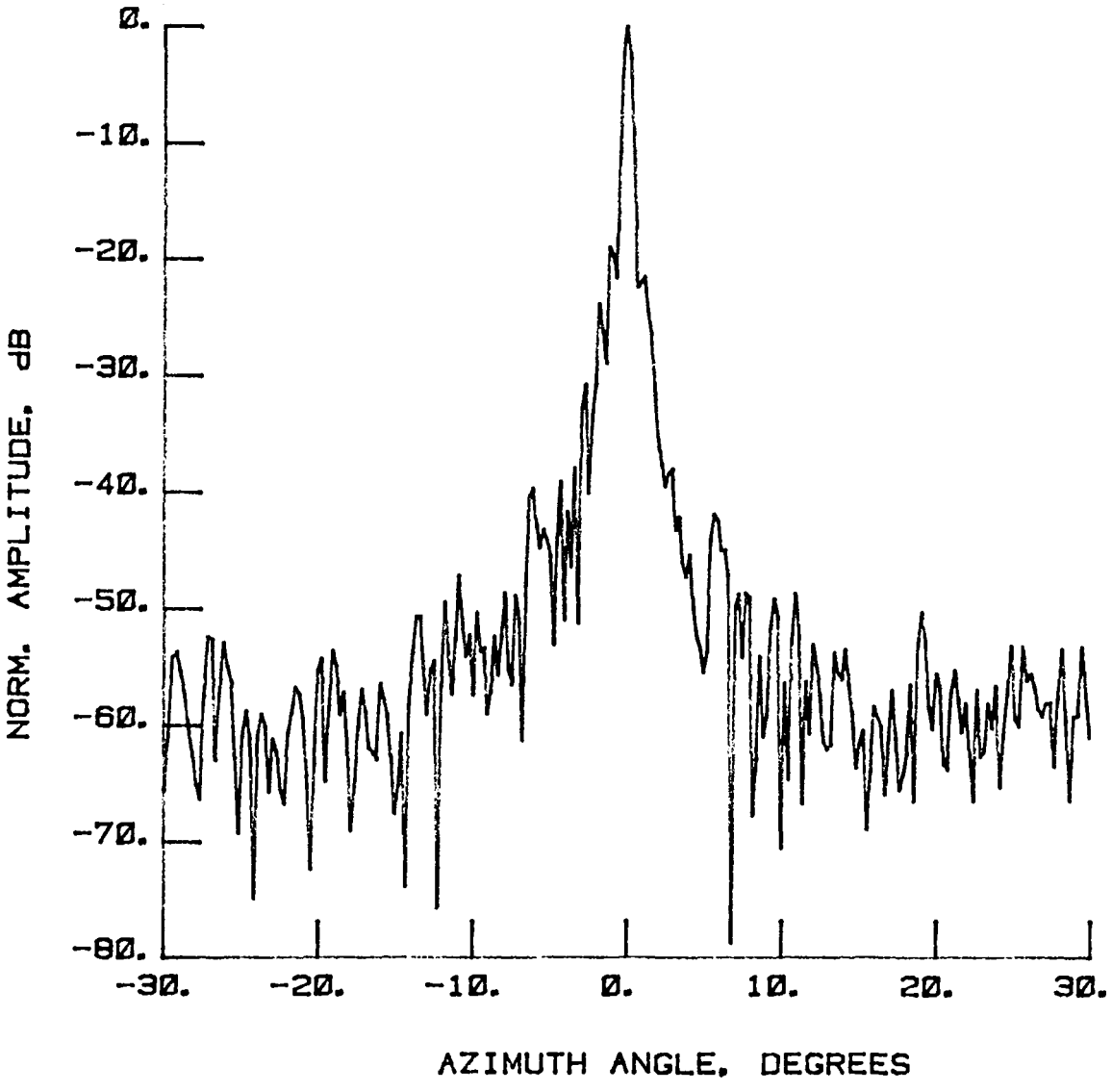

Figure 172 Test 21, 7.73 GHz, Co-Pol, E-Plane, Type 1

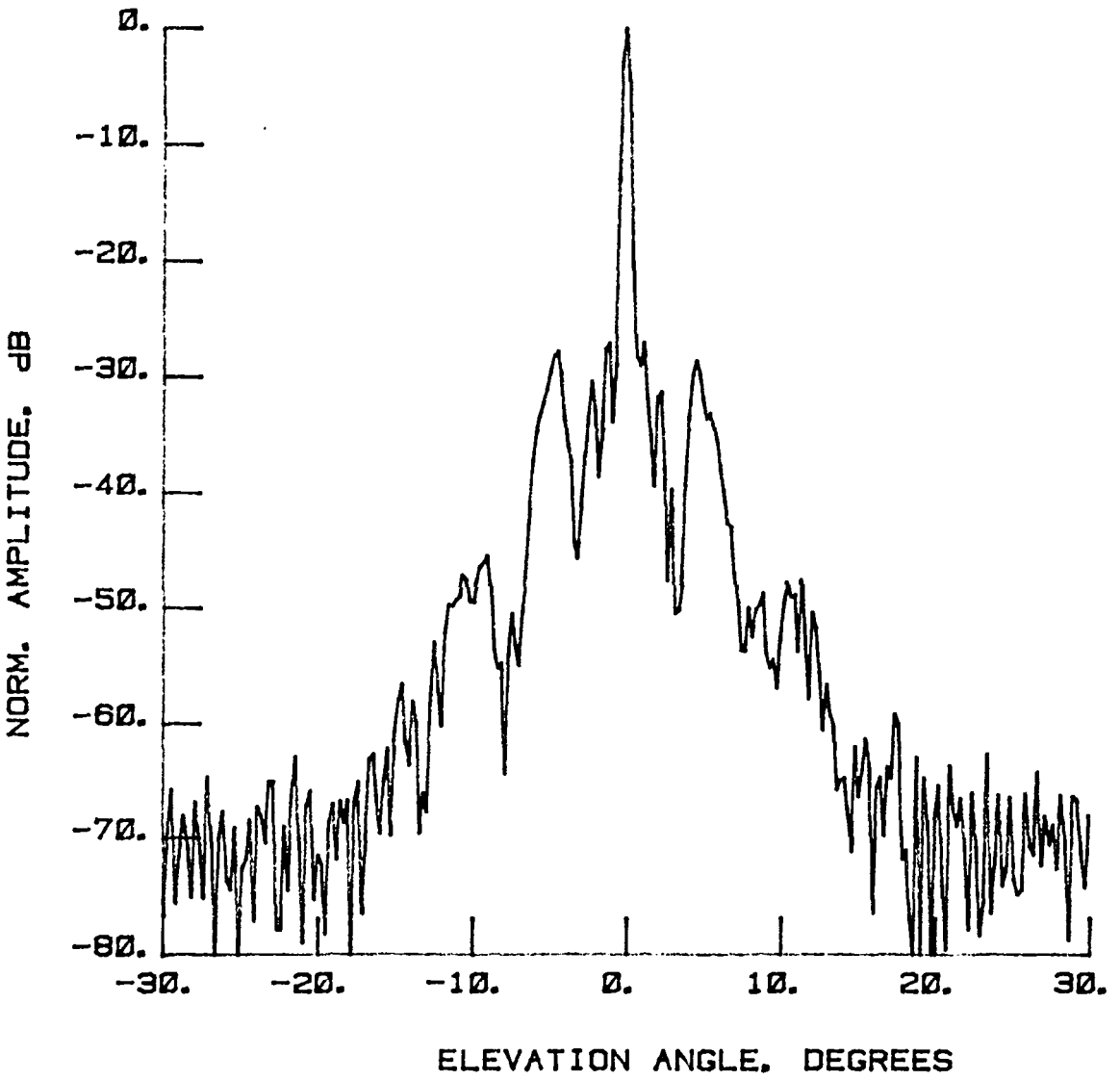

Figure 173 Test 21, 7.73 GHz, Co-Pol, H-Plane, Type 2

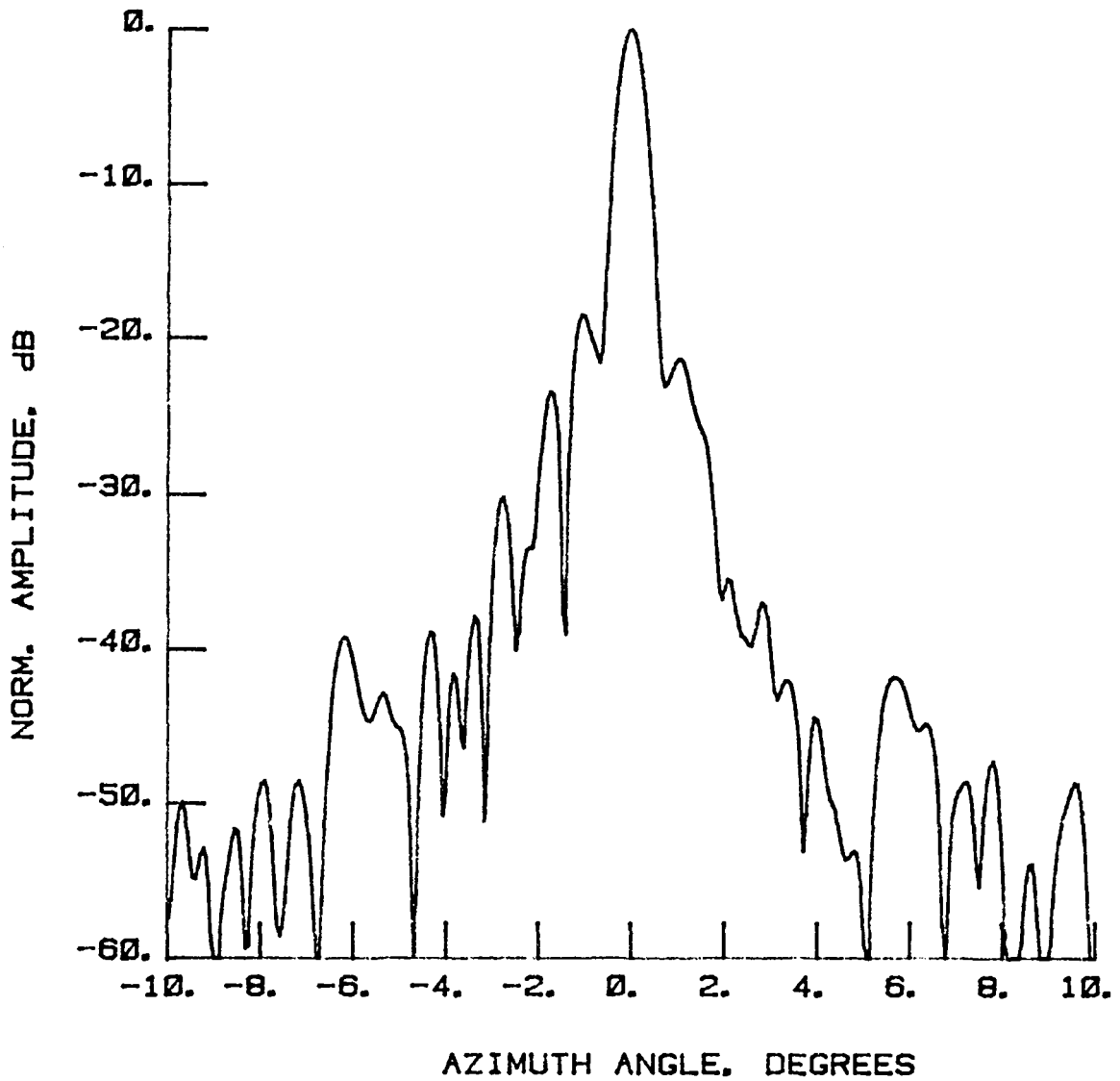

Figure 174 Test 21, 7.73 GHz, Co-Pol, E-Plane, Type 3

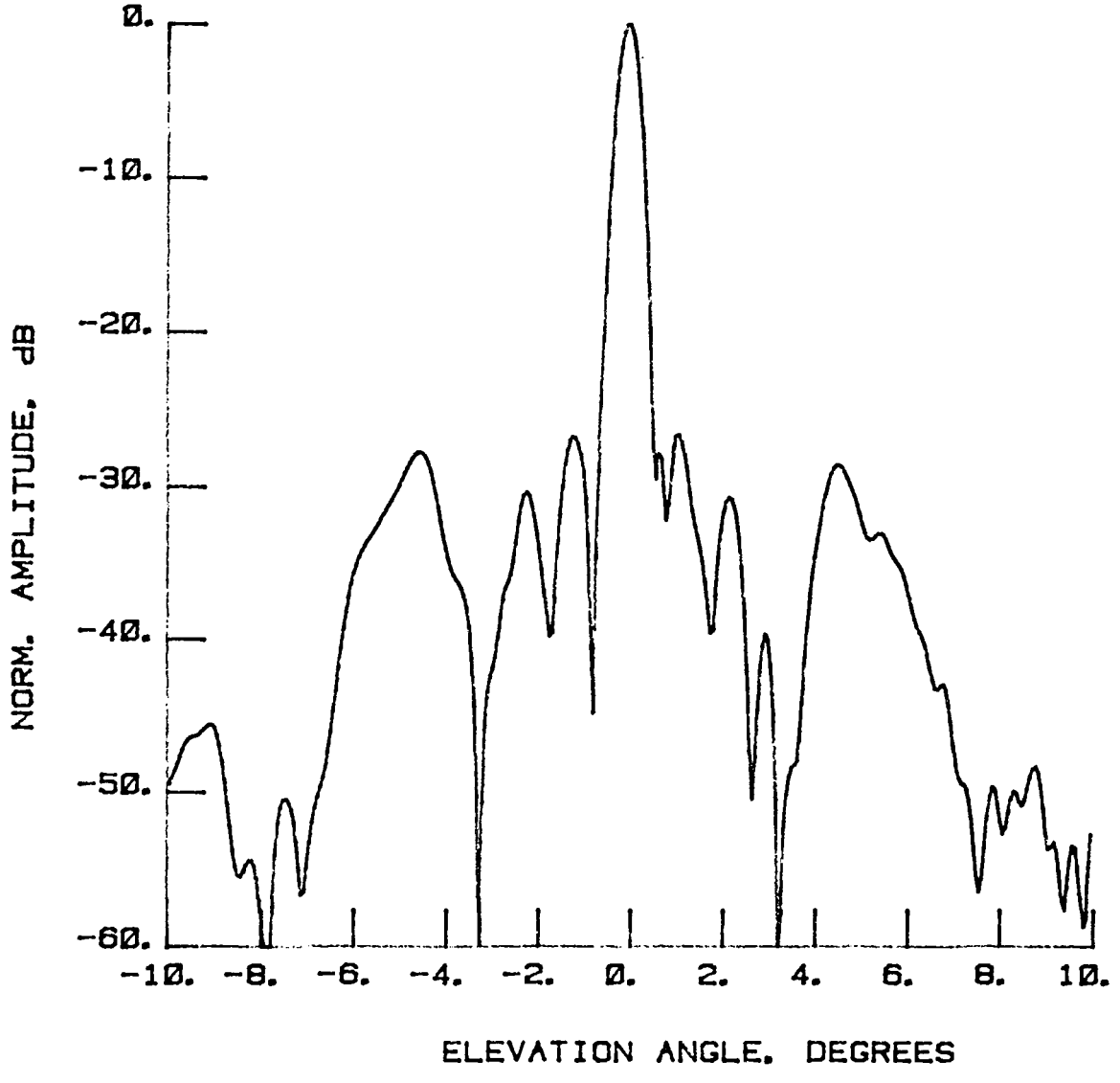

Figure 175 Test 21, 7.73 GHz, Co-Pol, H-Plane, Type 4

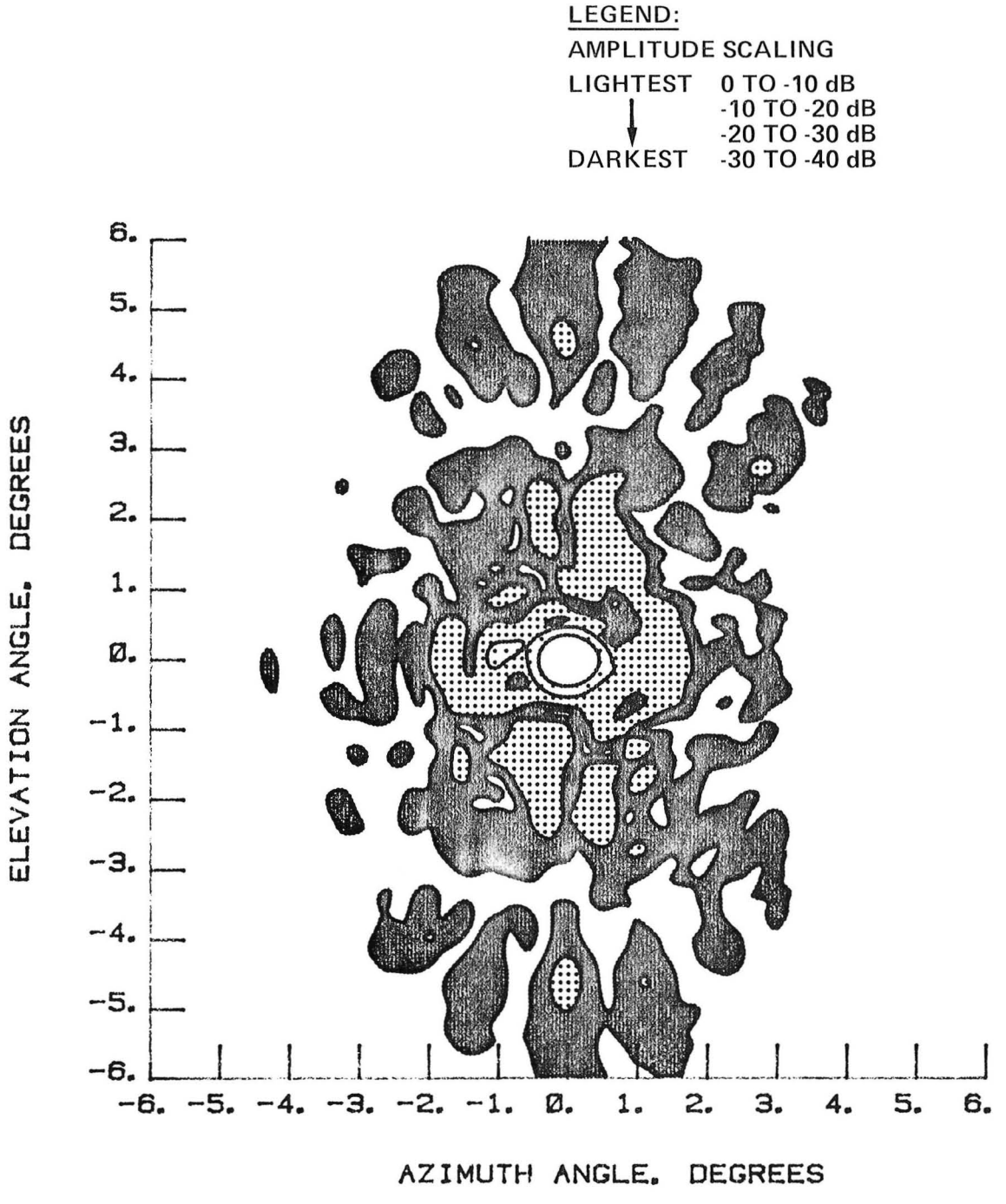

Figure 176 Test 21, 7.73 GHz, Co-Pol, Contour, Type 5

This Page Intentionally Left Blank

TEST IDENTIFICATION : LC21R

DATE : 18 SEPT. 1985

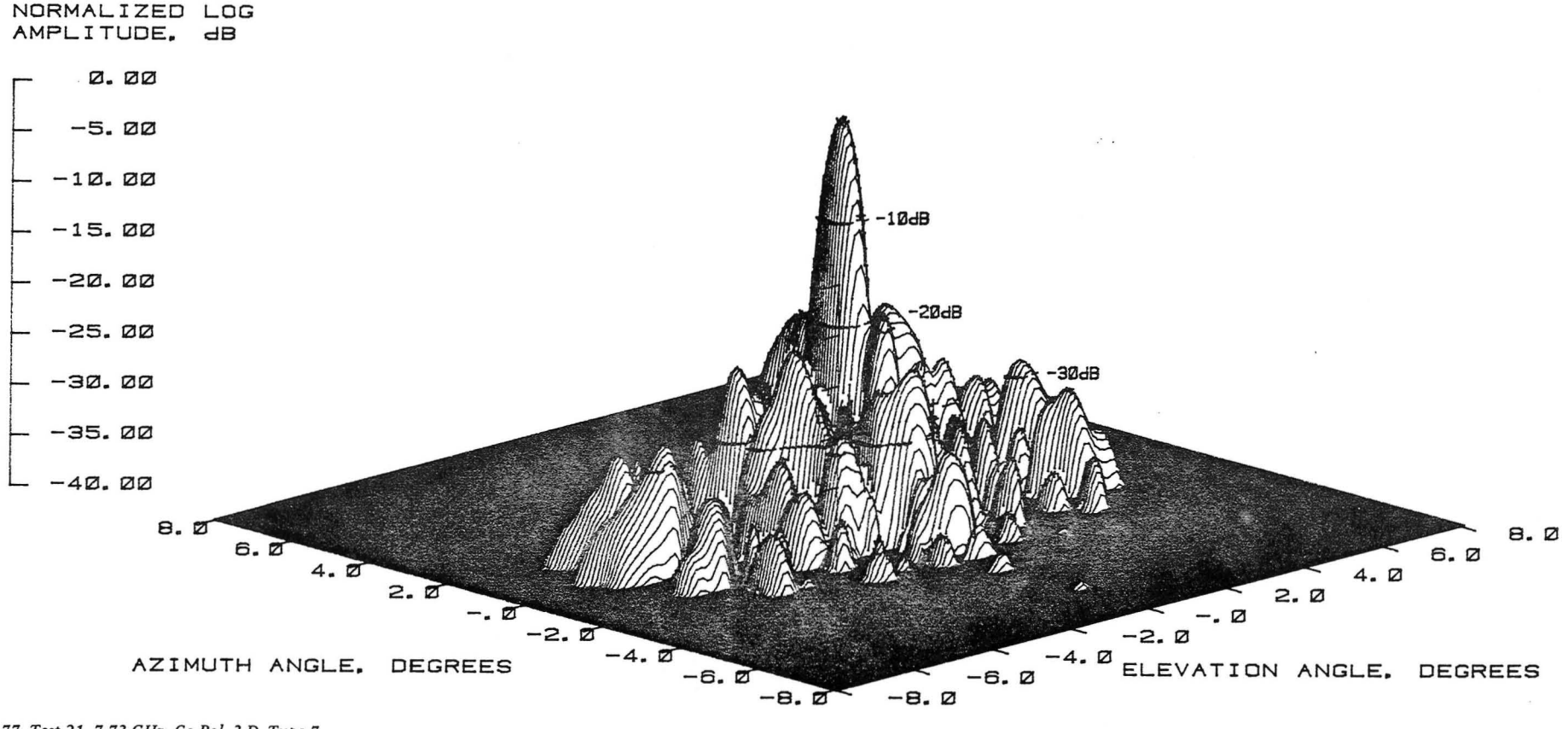

Figure 177 Test 21, 7.73 GHz, Co-Pol, 3-D, Type 7

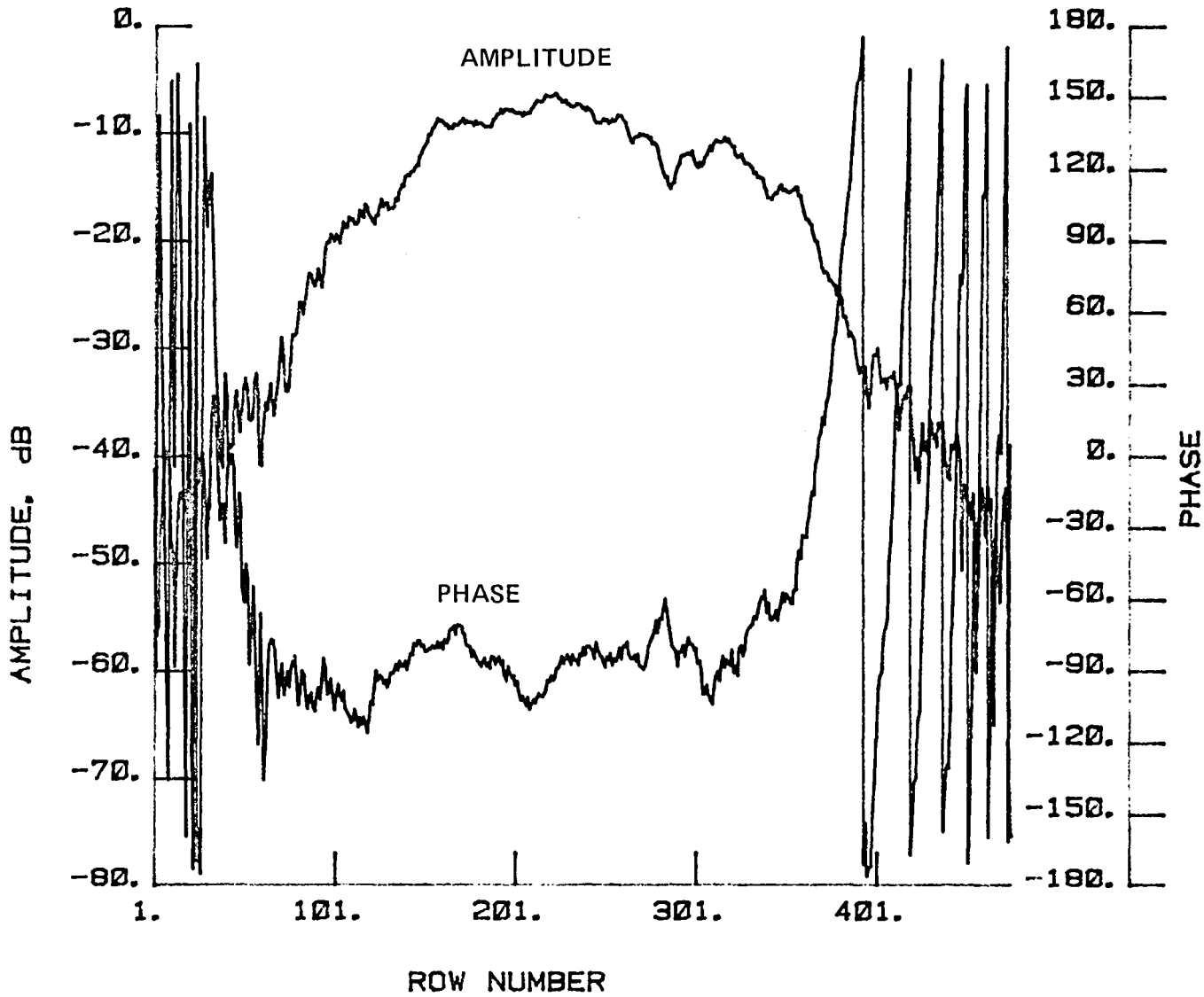

Figure 178 Test 21, 7.73 GHz, Co-Pol, H-Plane, Type 8

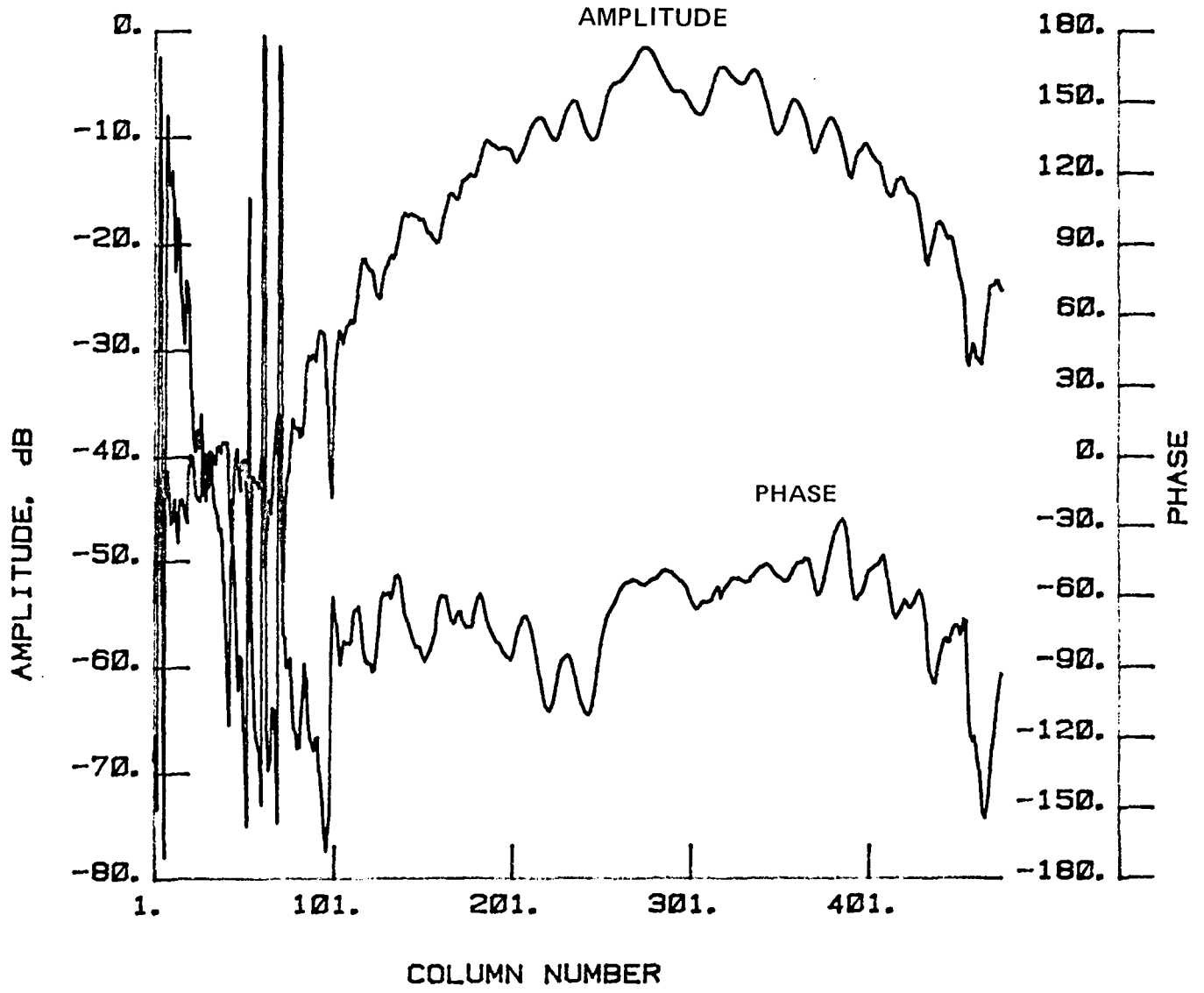

Figure 179 Test 21, 7.73 GHz, Co-Pol, E-Plane, Type 9

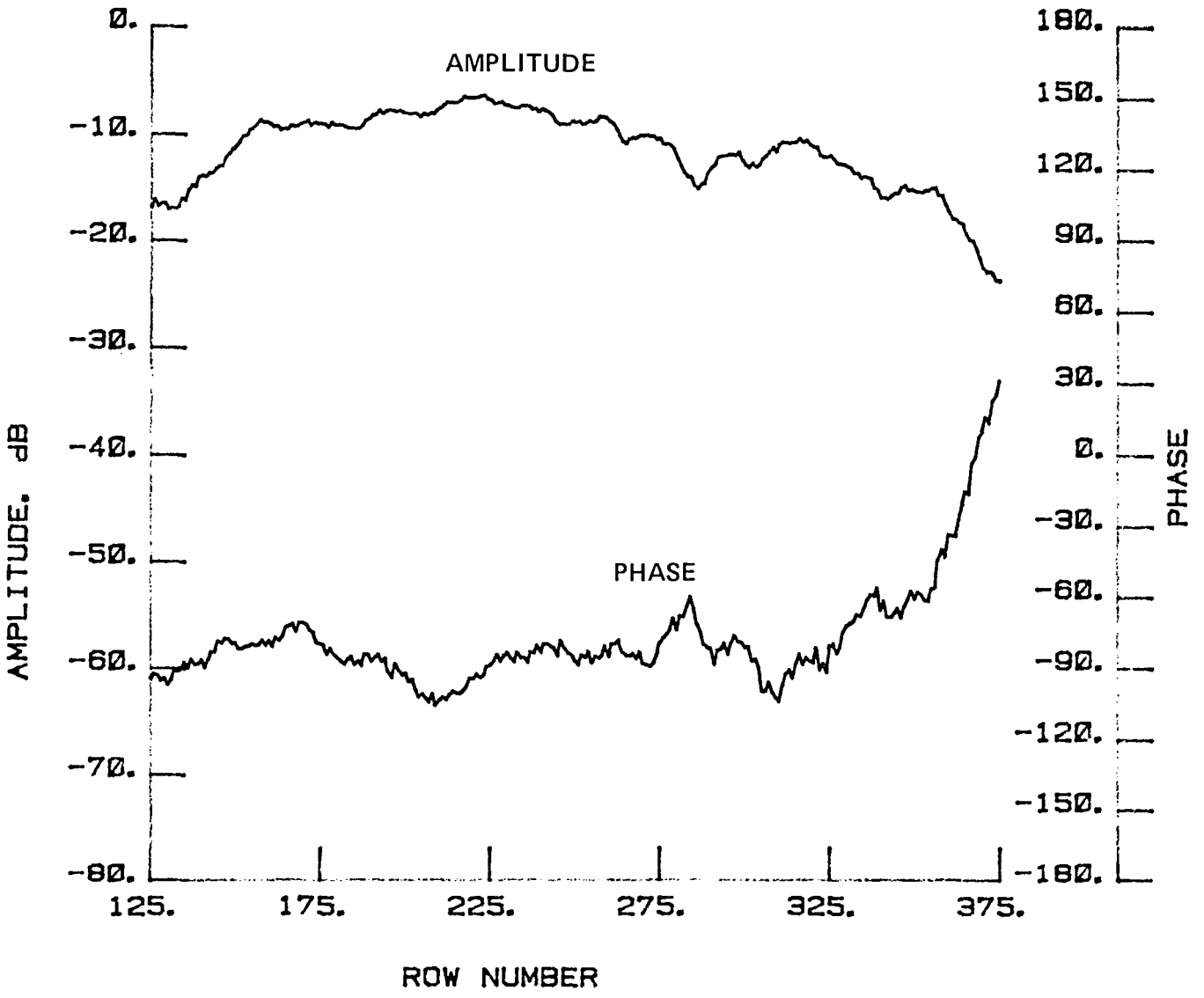

Figure 180 Test 21, 7.73 GHz, Co-Pol, H-Plane, Type 10

Figure 181 Test 21, 7.73 GHz, Co-Pol, E-Plane, Type 11

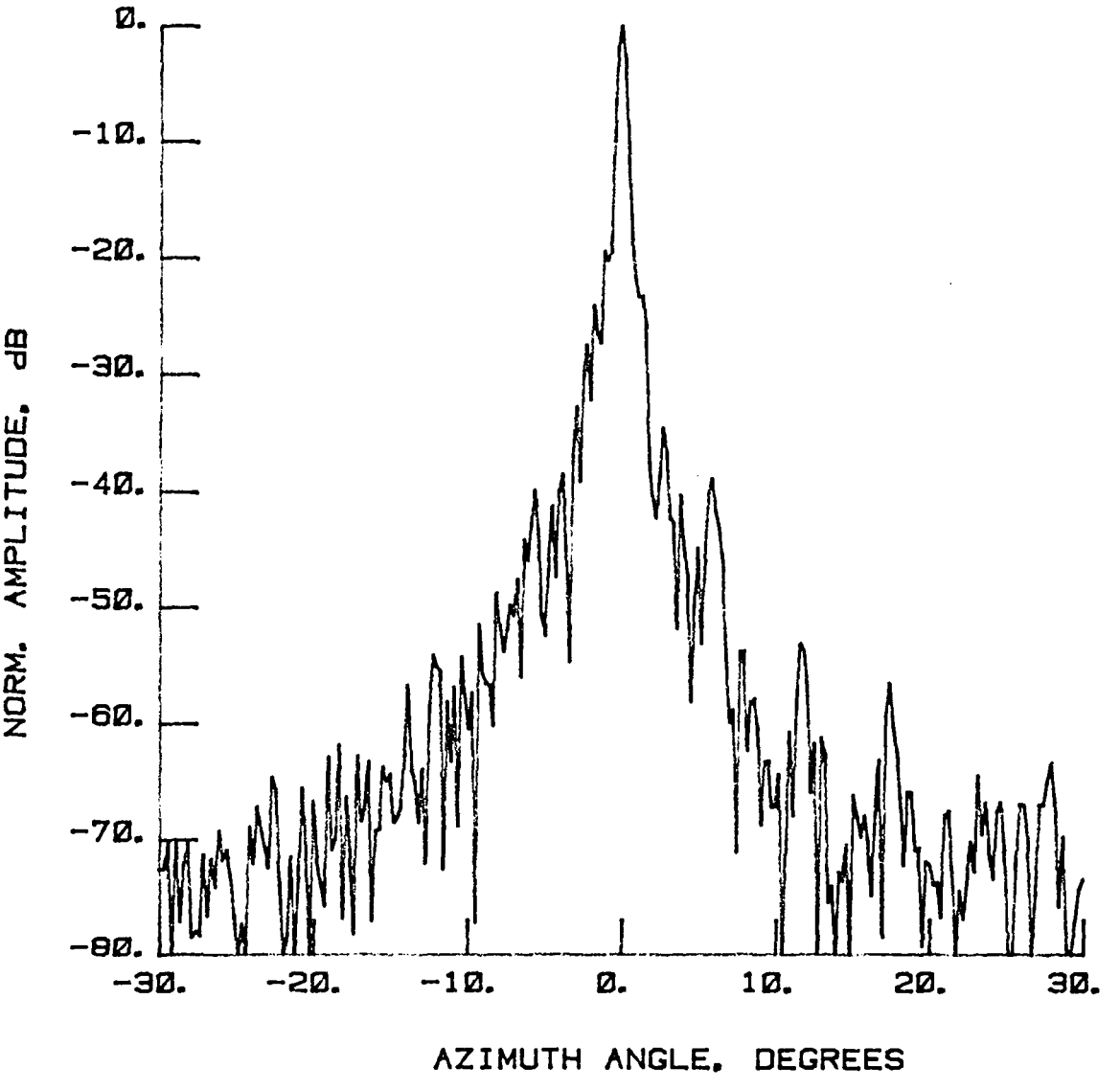

Figure 182 Test 22, 7.73 GHz, Co-Pol, E-Plane, Type 1

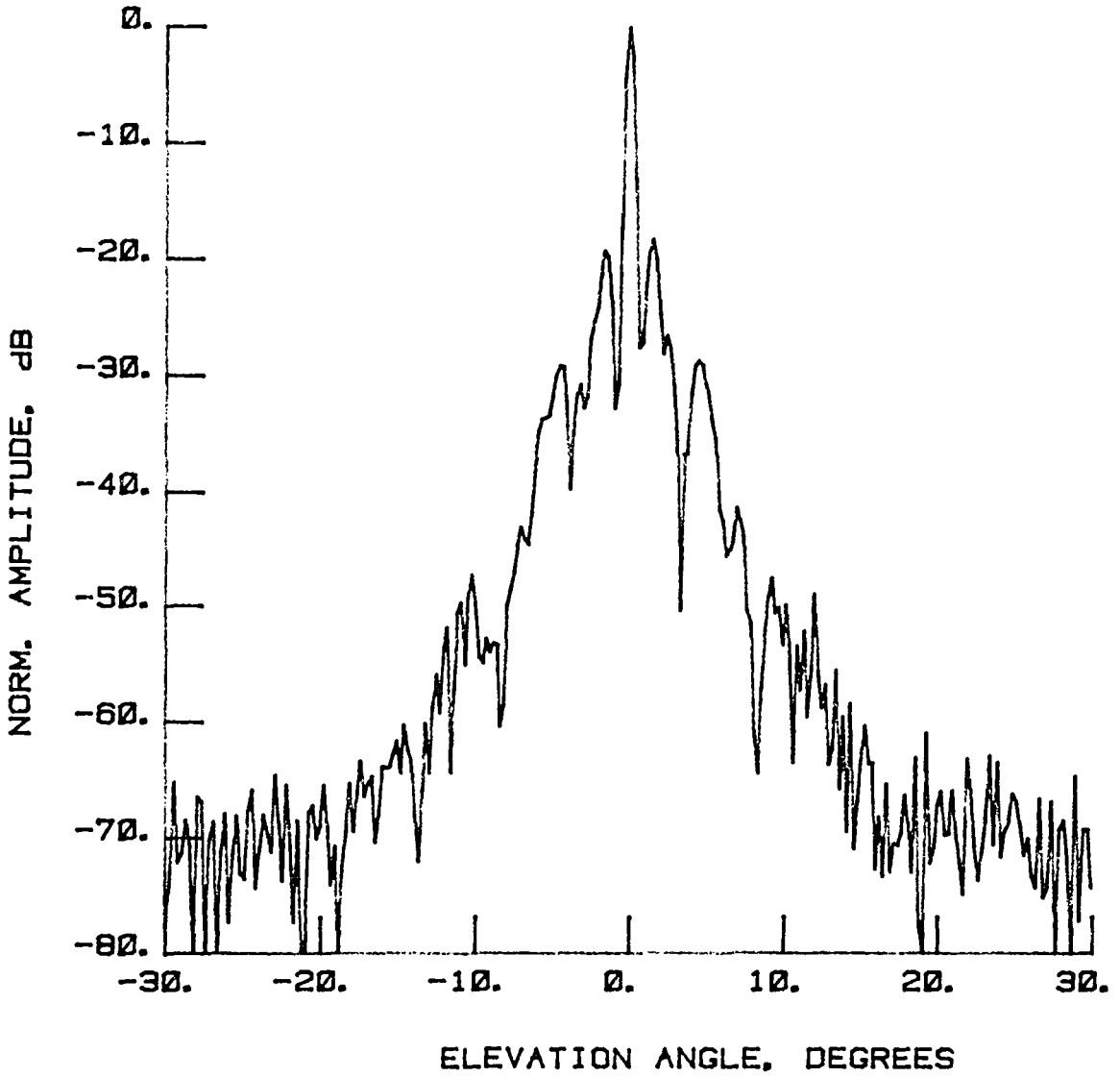

Figure 183 Test 22, 7.73 GHz, Co-Pol, H-Plane, Type 2

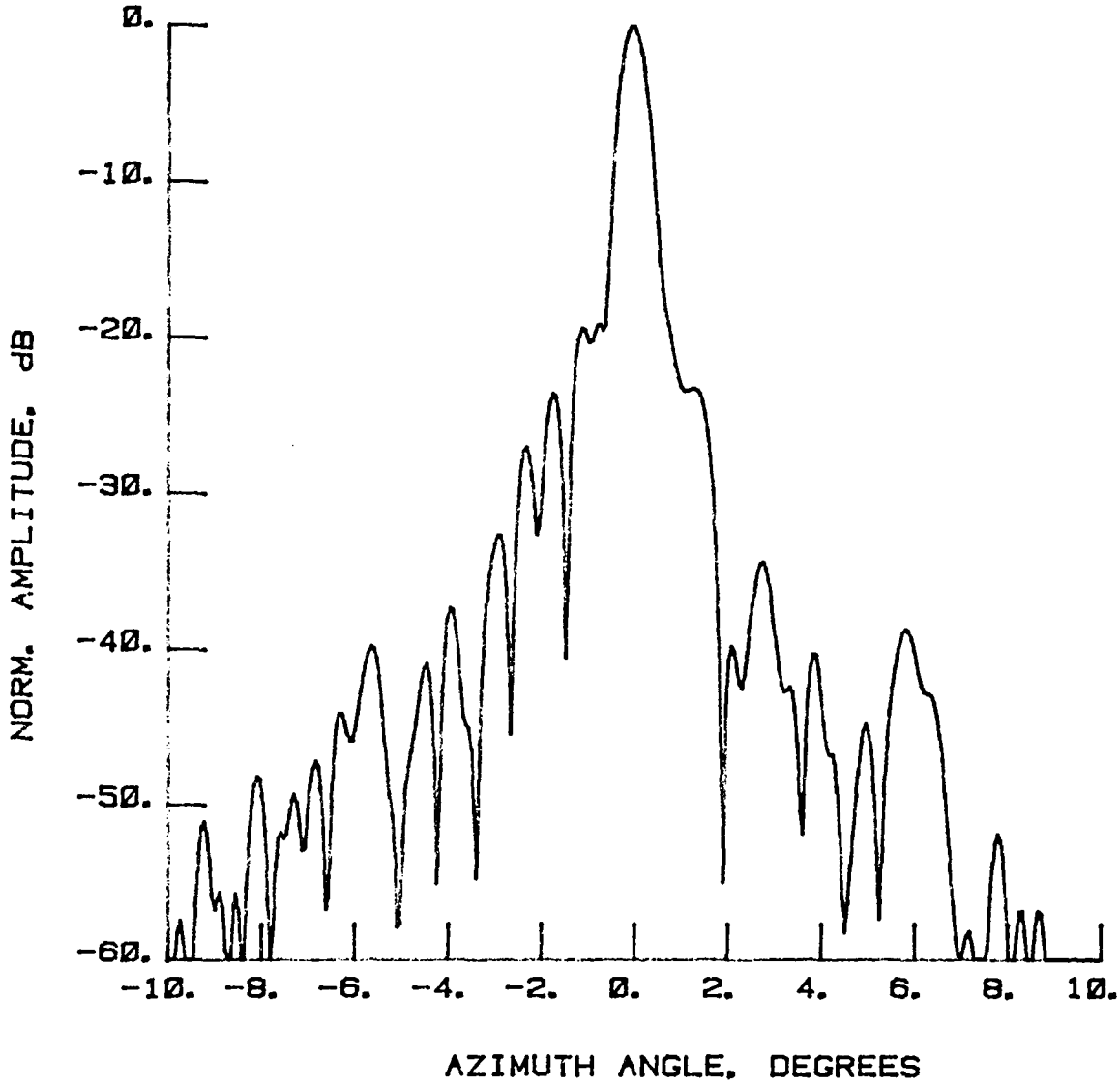

Figure 184 Test 22, 7.73 GHz, Co-Pol, E-Plane, Type 3

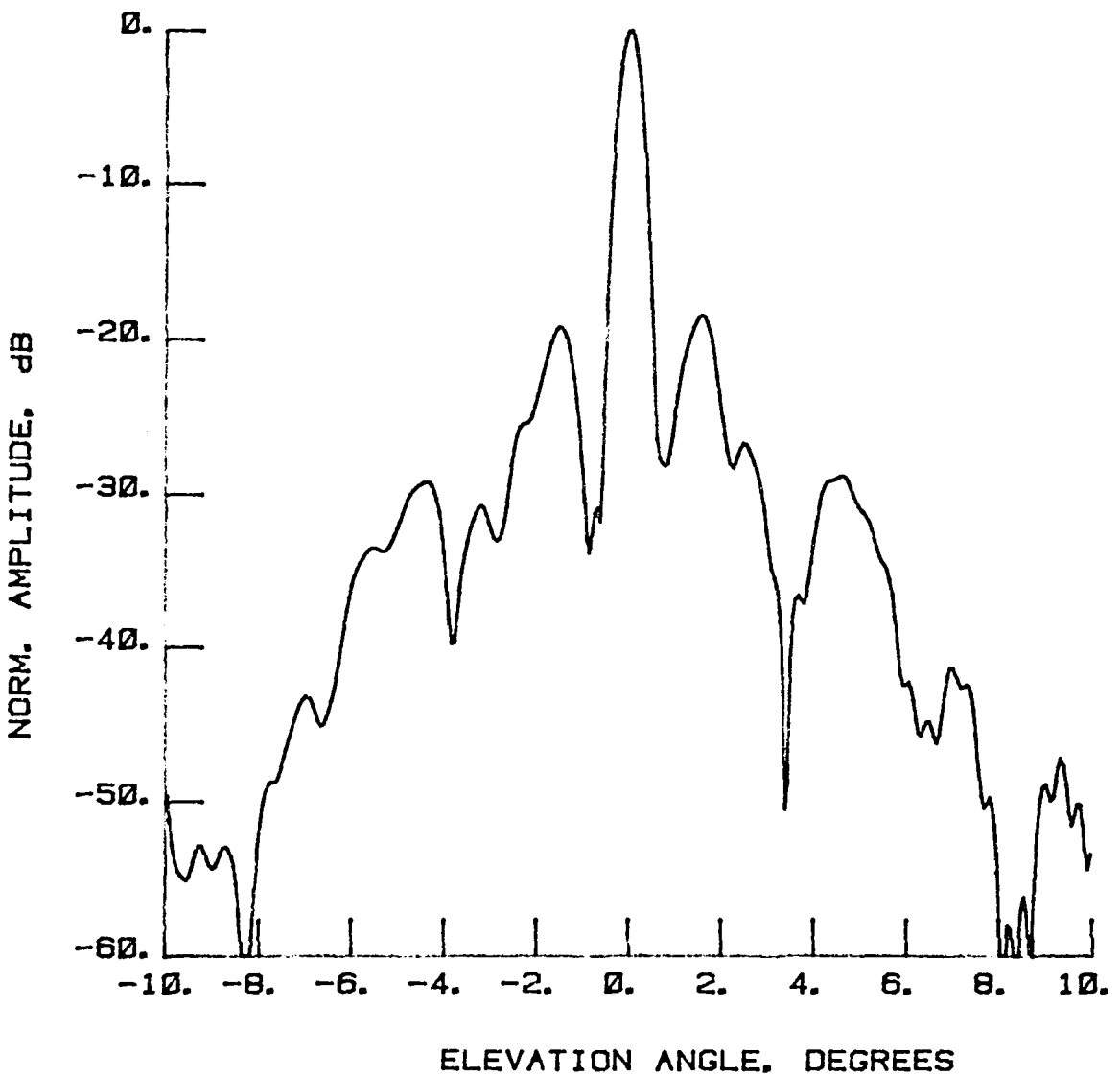

Figure 185 Test 22, 7.73 GHz, Co-Pol, H-Plane, Type 4

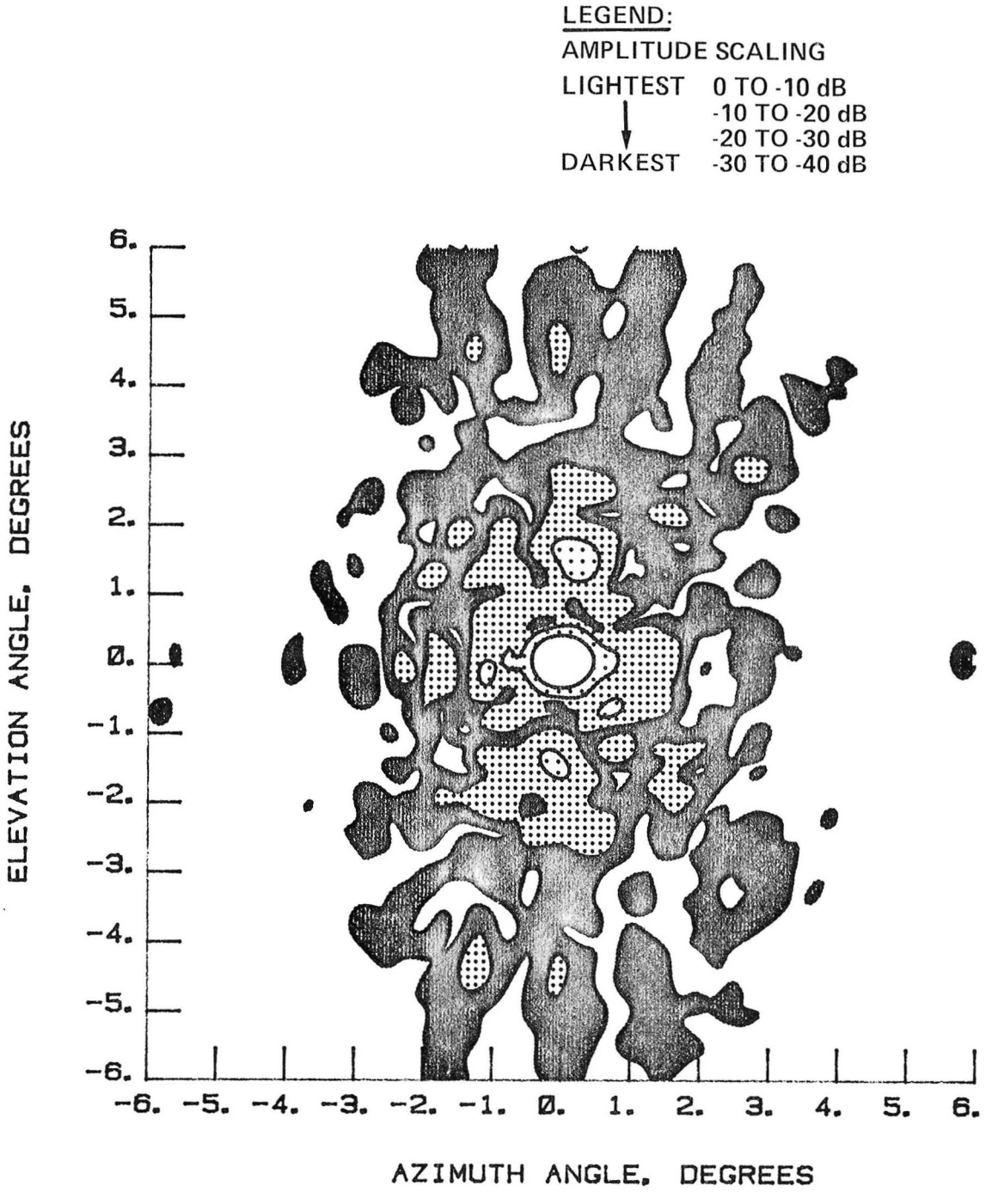

Figure 186 Test 22, 7.73 GHz, Co-Pol, Contour, Type 5

This Page Intentionally Left Blank

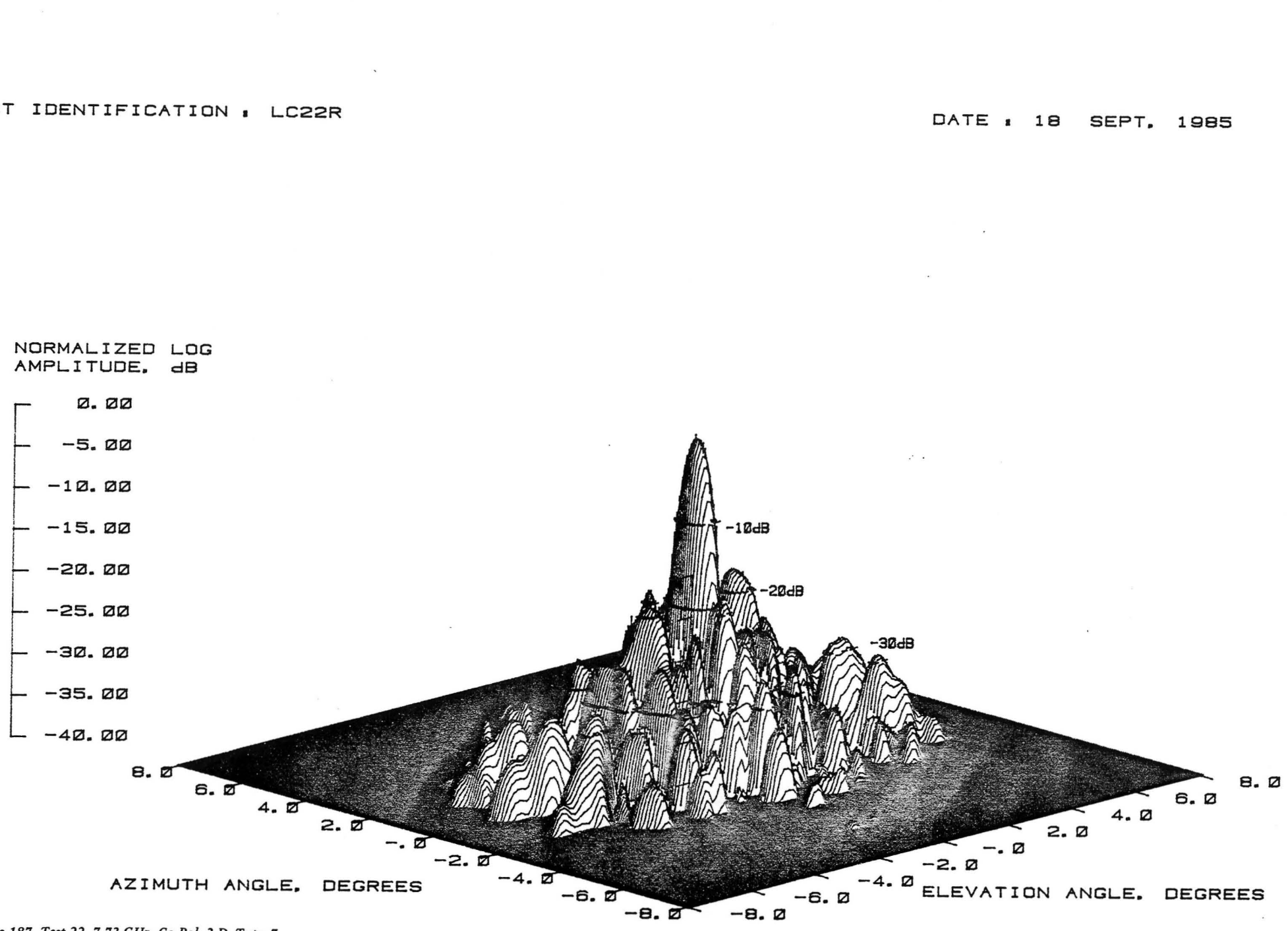

Figure 187 Test 22, 7.73 GHz, Co-Pol, 3-D, Type 7

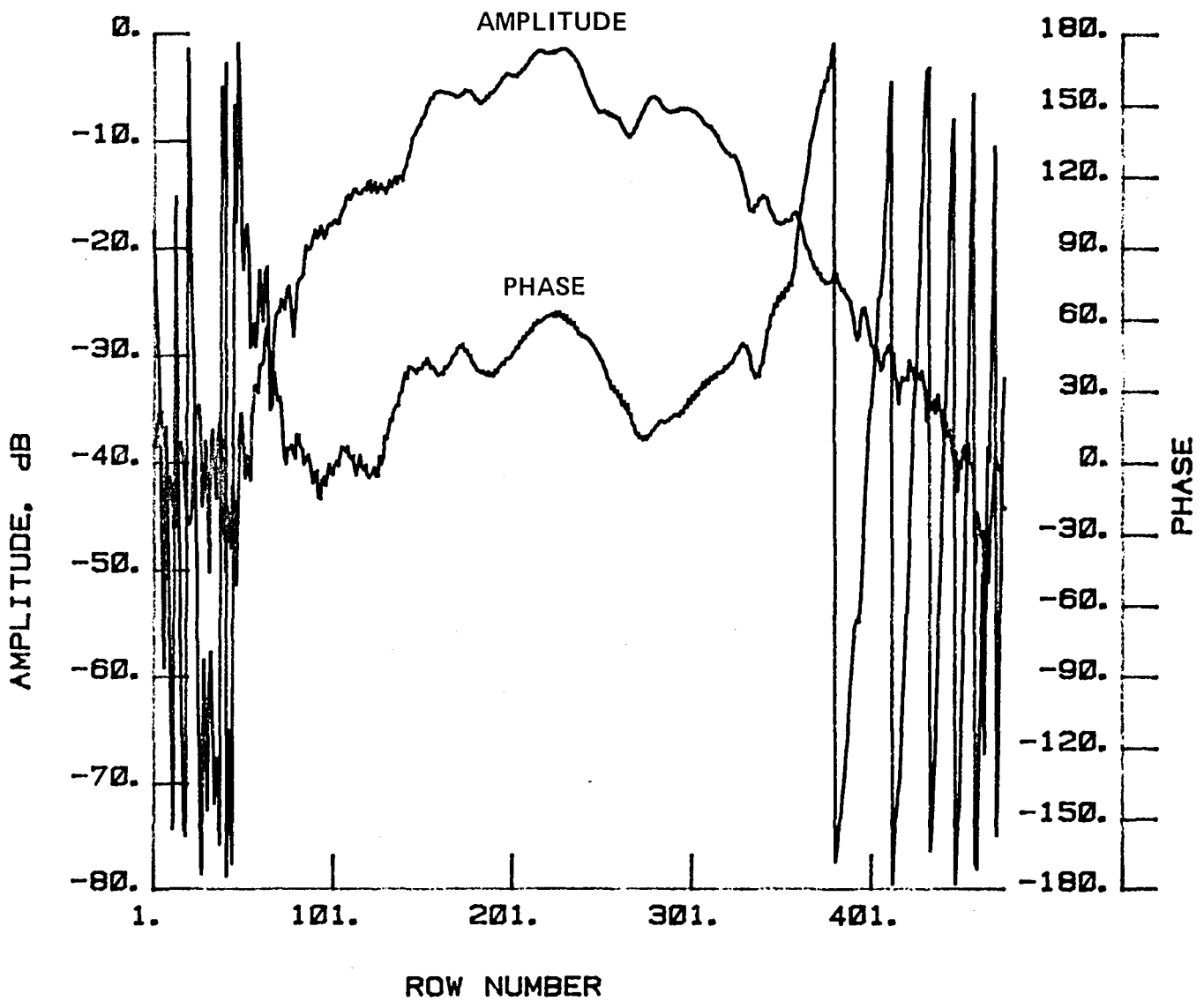

Figure 188 Test 22, 7.73 GHz, Co-Pol, H-Plane, Type 8

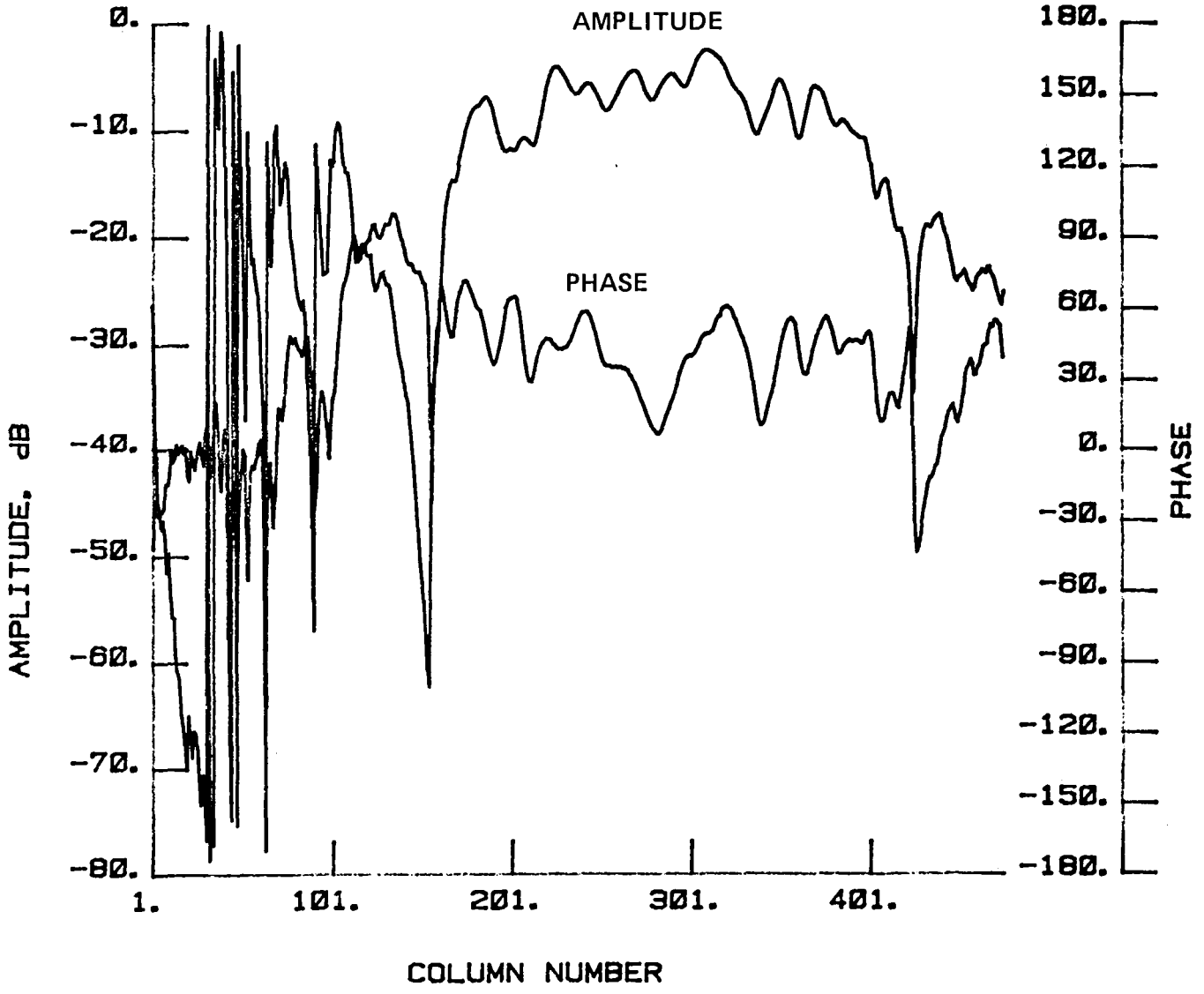

Figure 189 Test 22, 7.73 GHz, Co-Pol, E-Plane, Type 9

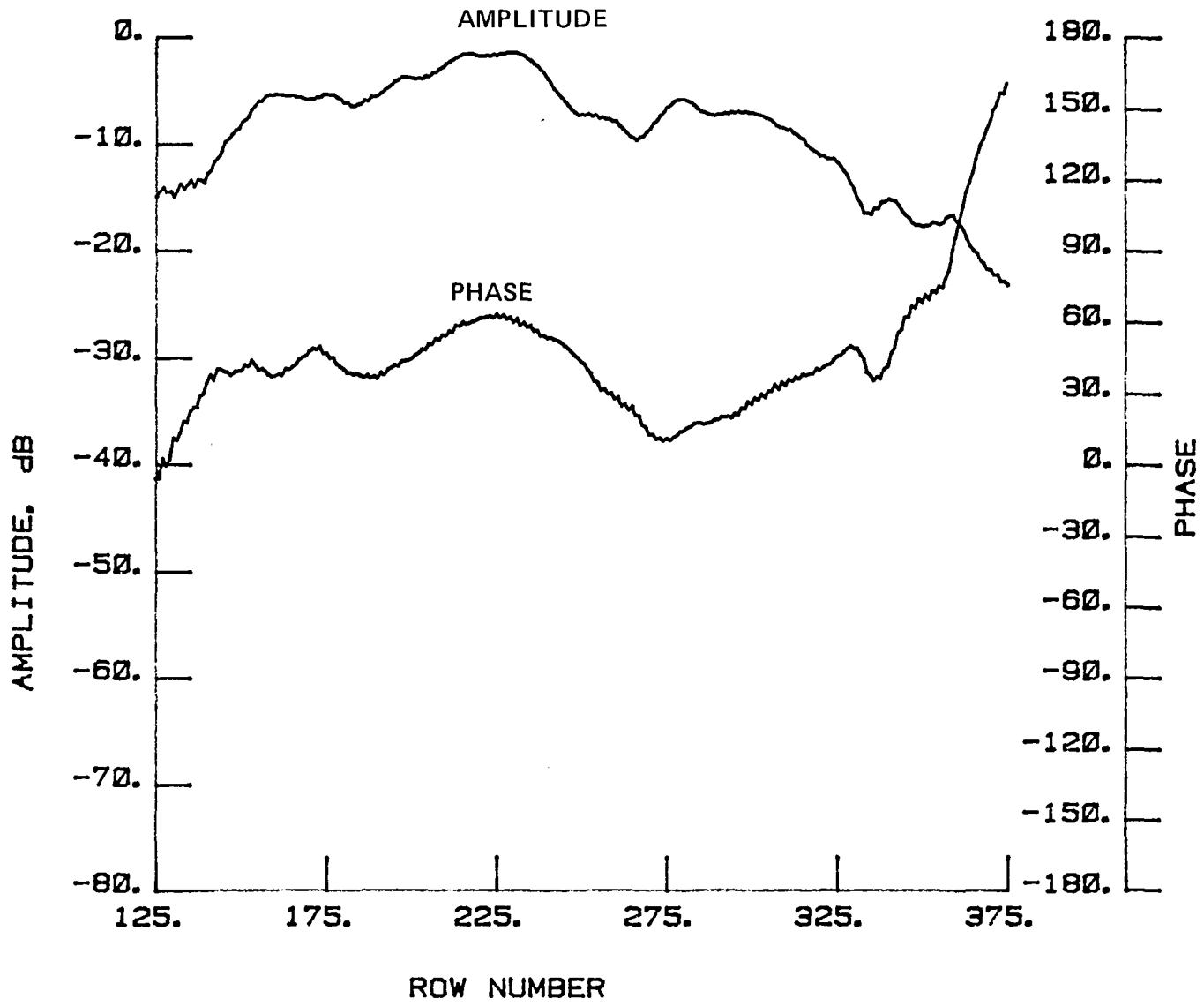

Figure 190 Test 22, 7.73 GHz, Co-Pol, H-Plane, Type 10

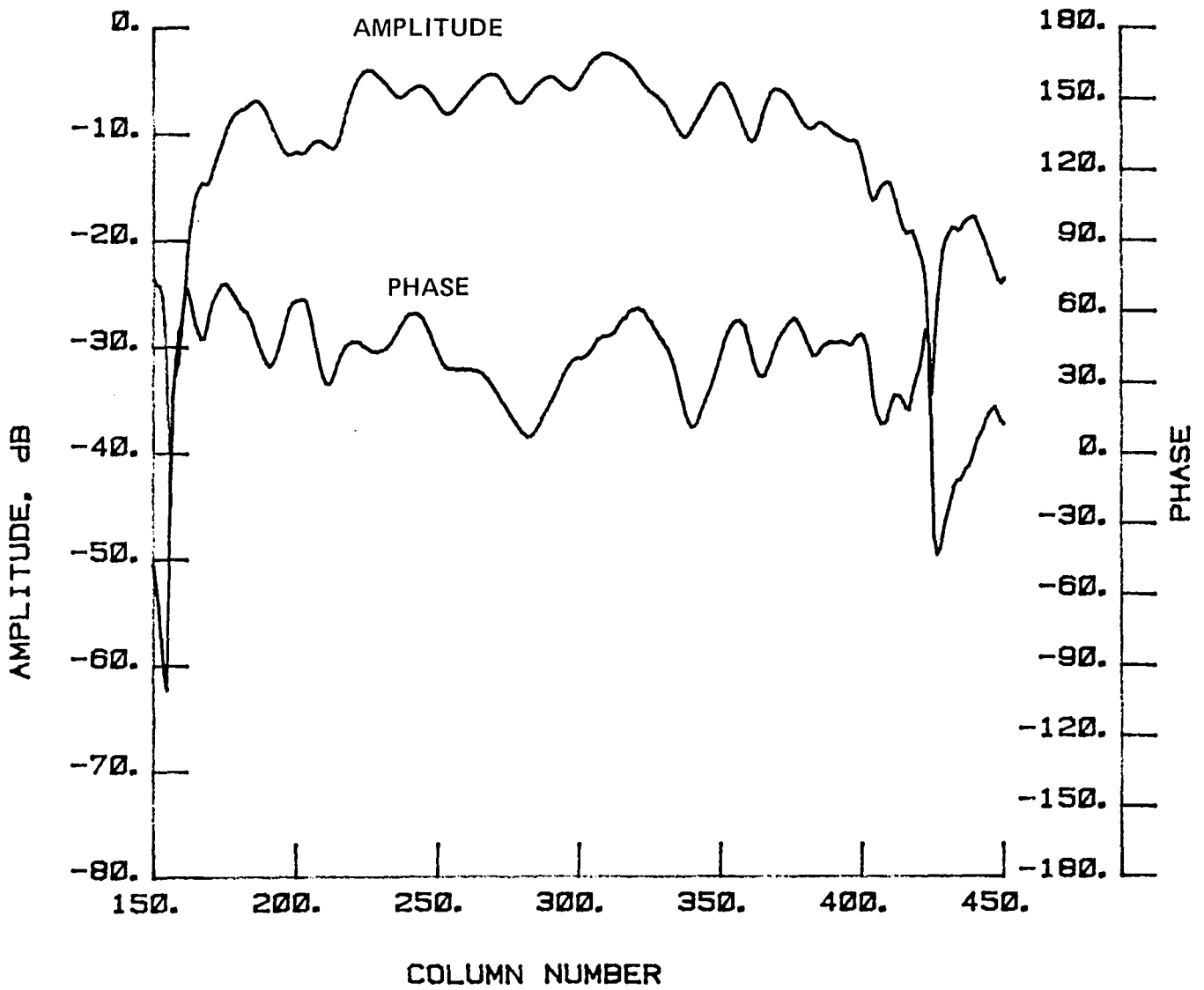

Figure 191 Test 22, 7.73 GHz, Co-Pol, E-Plane, Type 11

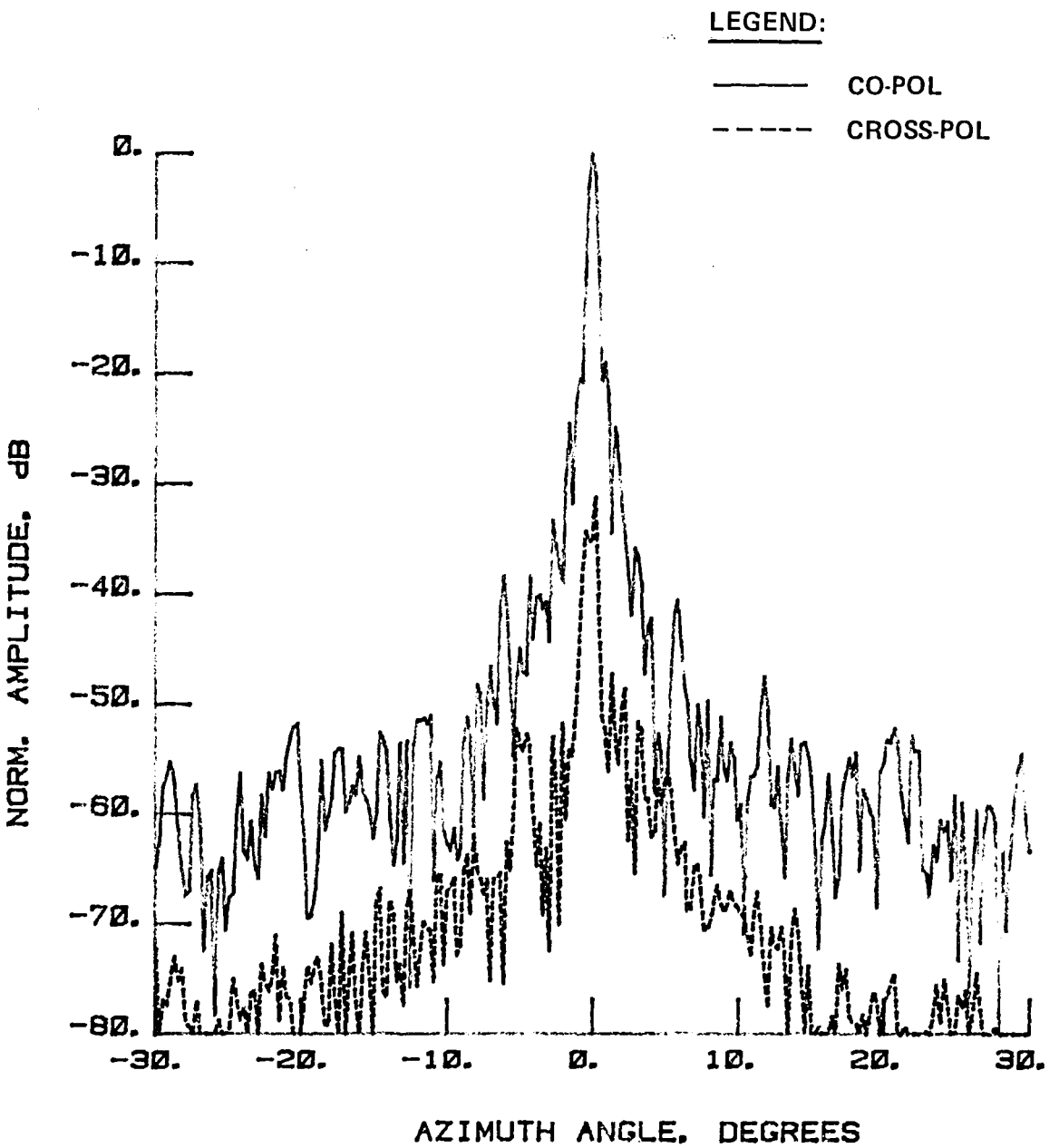

Figure 192 Test 23, 7.73 GHz, Cross-Pol, E-Plane, Type 12

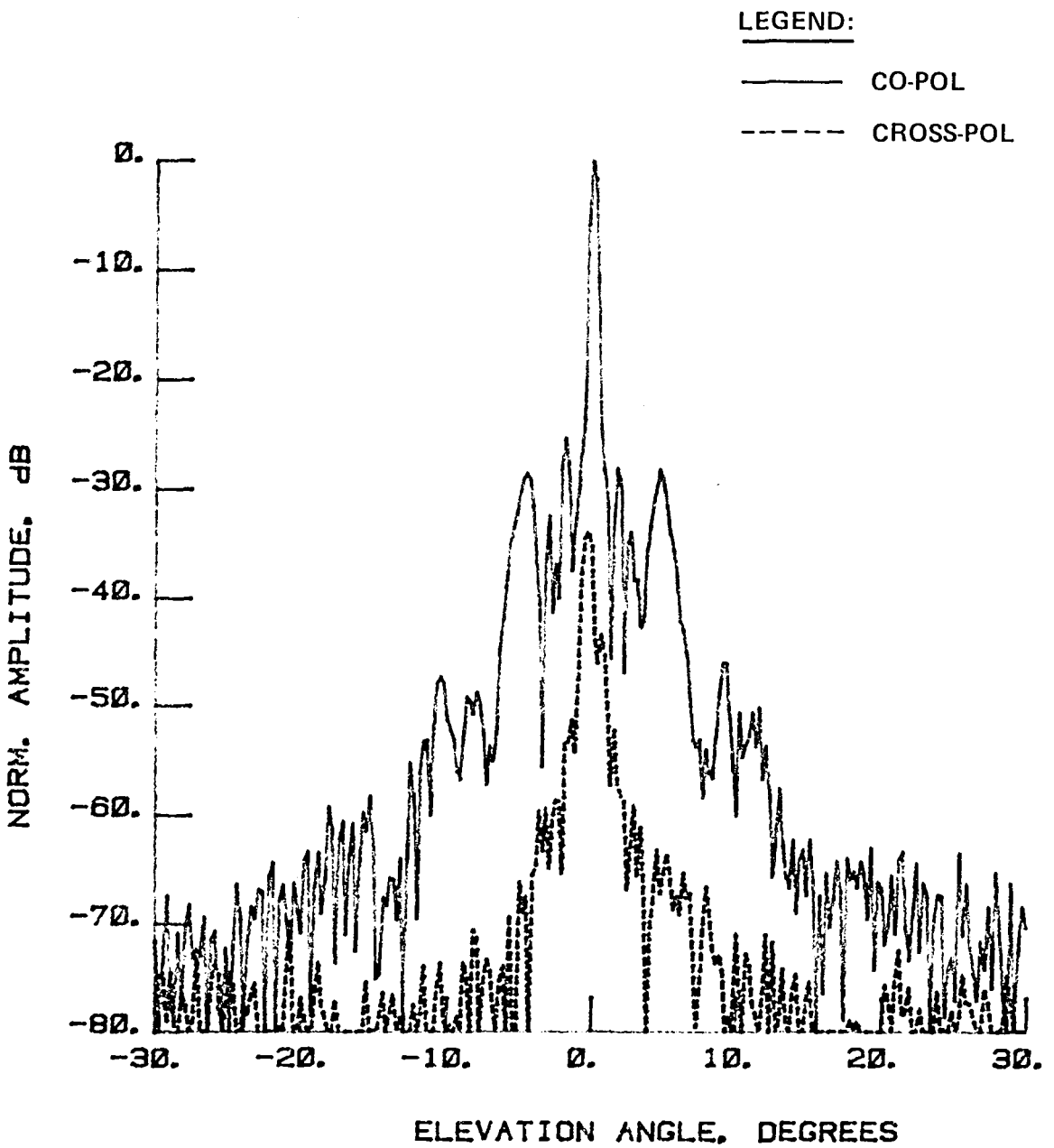

Figure 193 Test 23, 7.73 GHz, Cross-Pol, H-Plane, Type 13

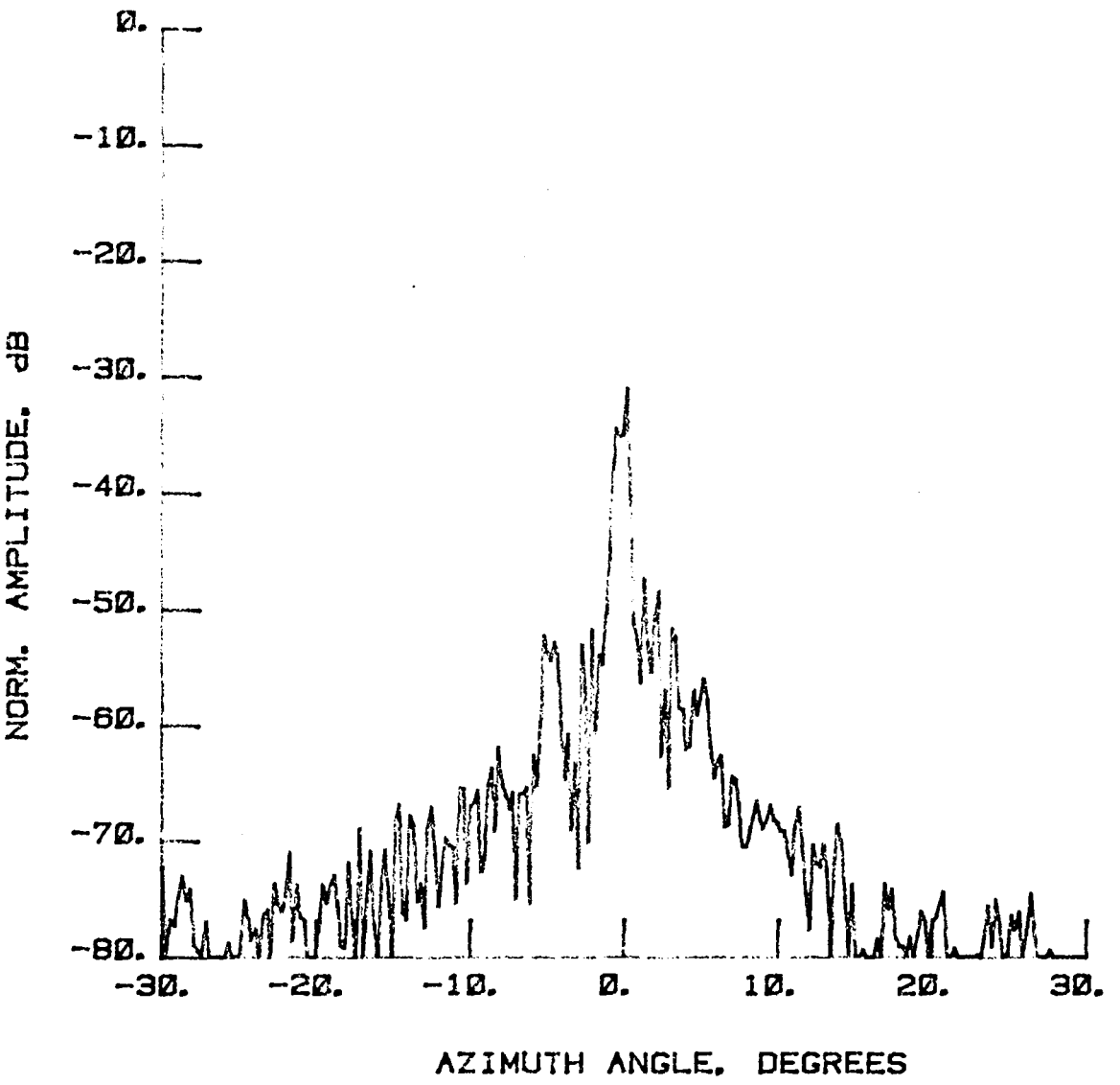

Figure 194 Test 23, 7.73 GHz, Cross-Pol, E-Plane, Type 14

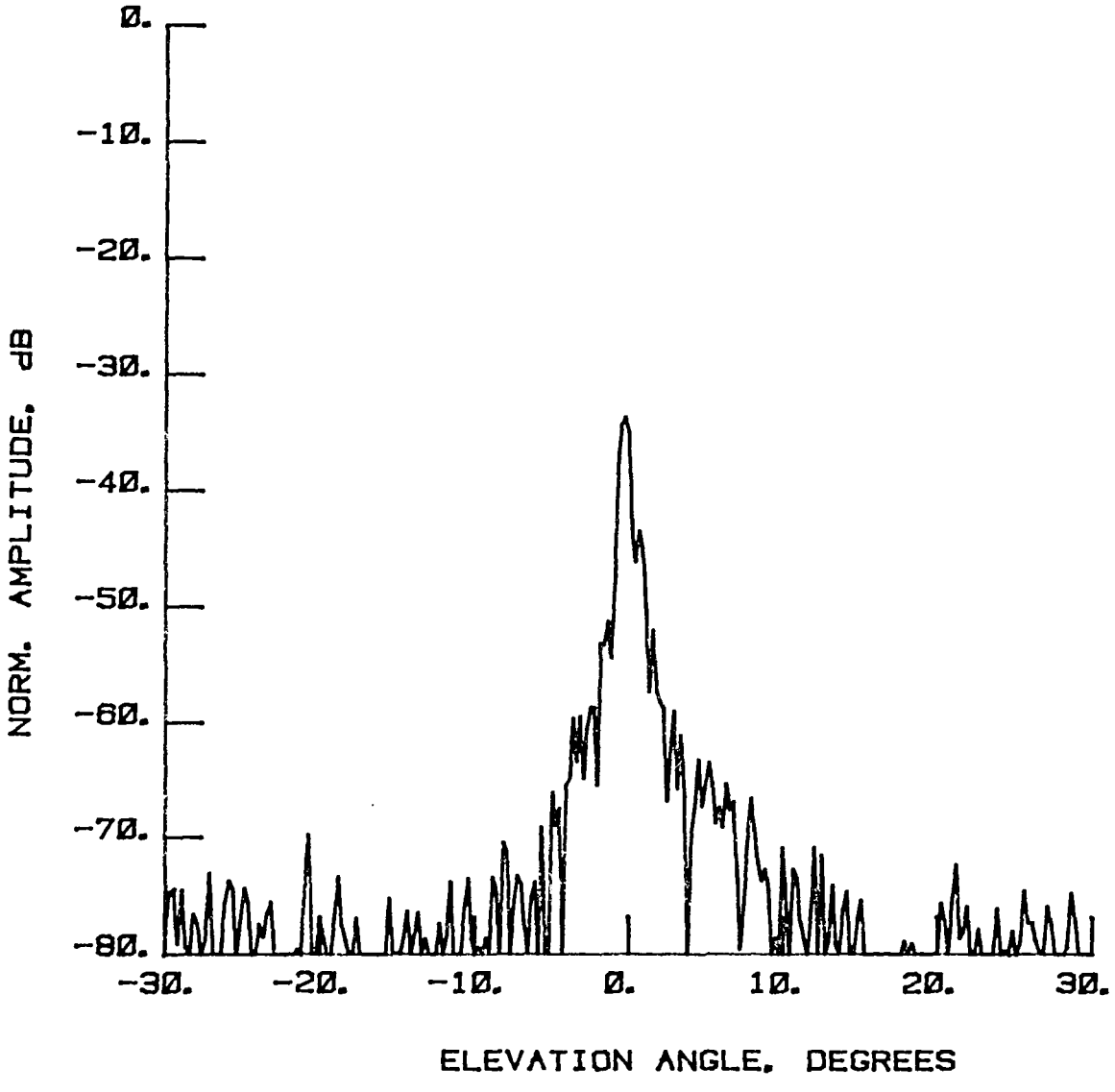

Figure 195 Test 23, 7.73 GHz, Cross-Pol, H-Plane, Type 15

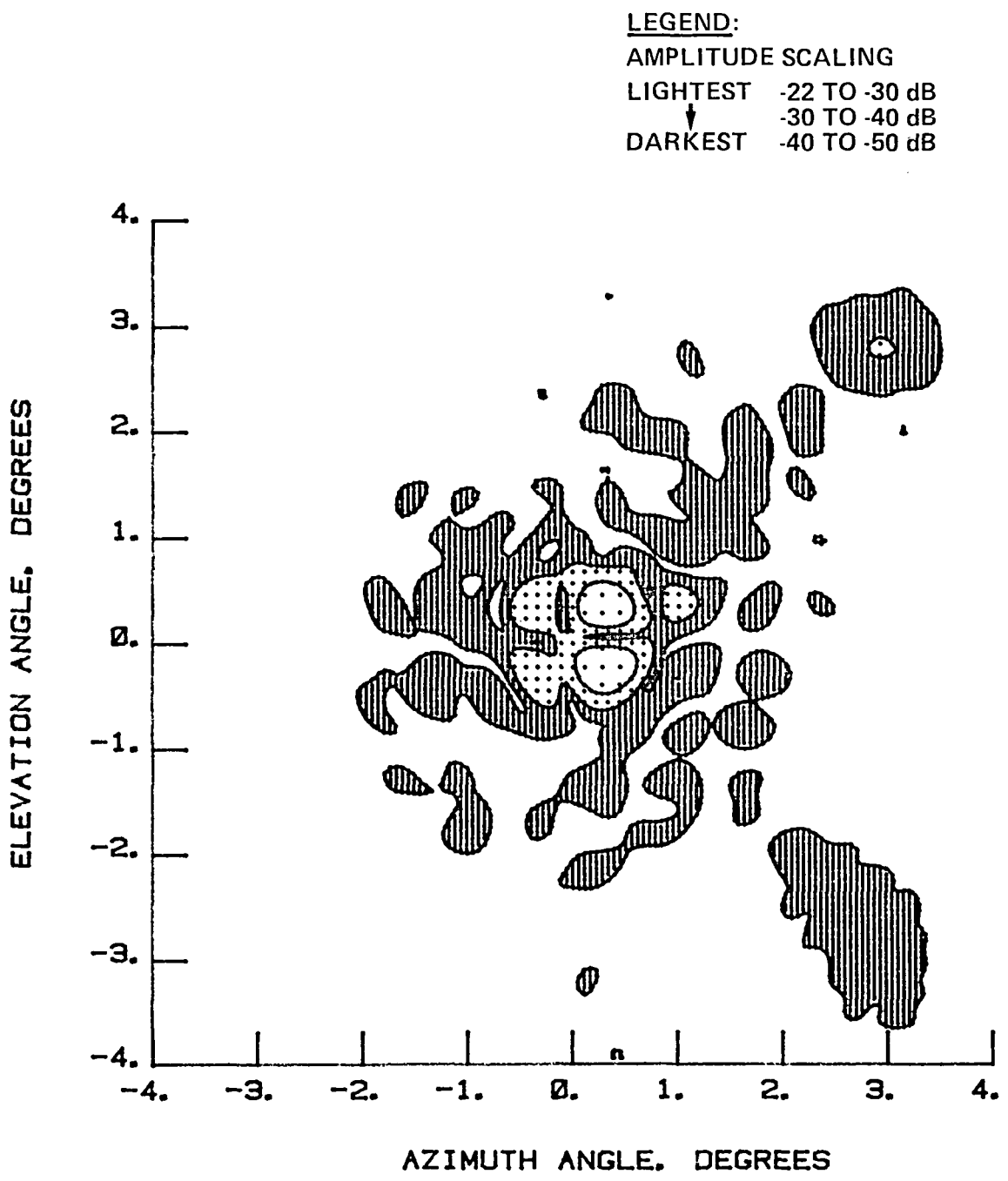

Figure 196 Test 23, 7.73 GHz, Cross-Pol, Contour, Type 16

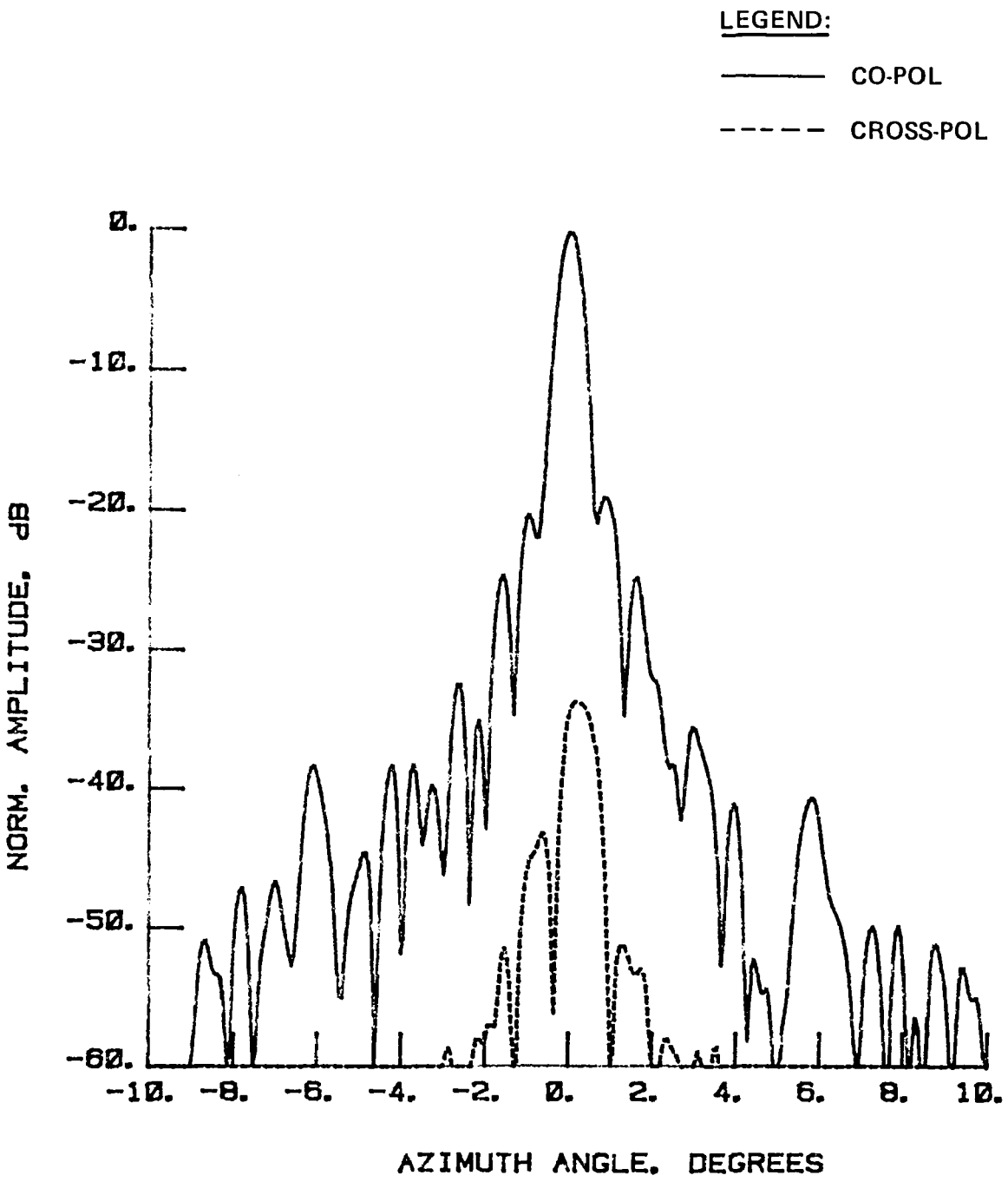

Figure 197 Test 23, 7.73 GHz, Cross-Pol, ±10° Scale, E-Plane Overlay through Peak Co-Pol (0, 0)

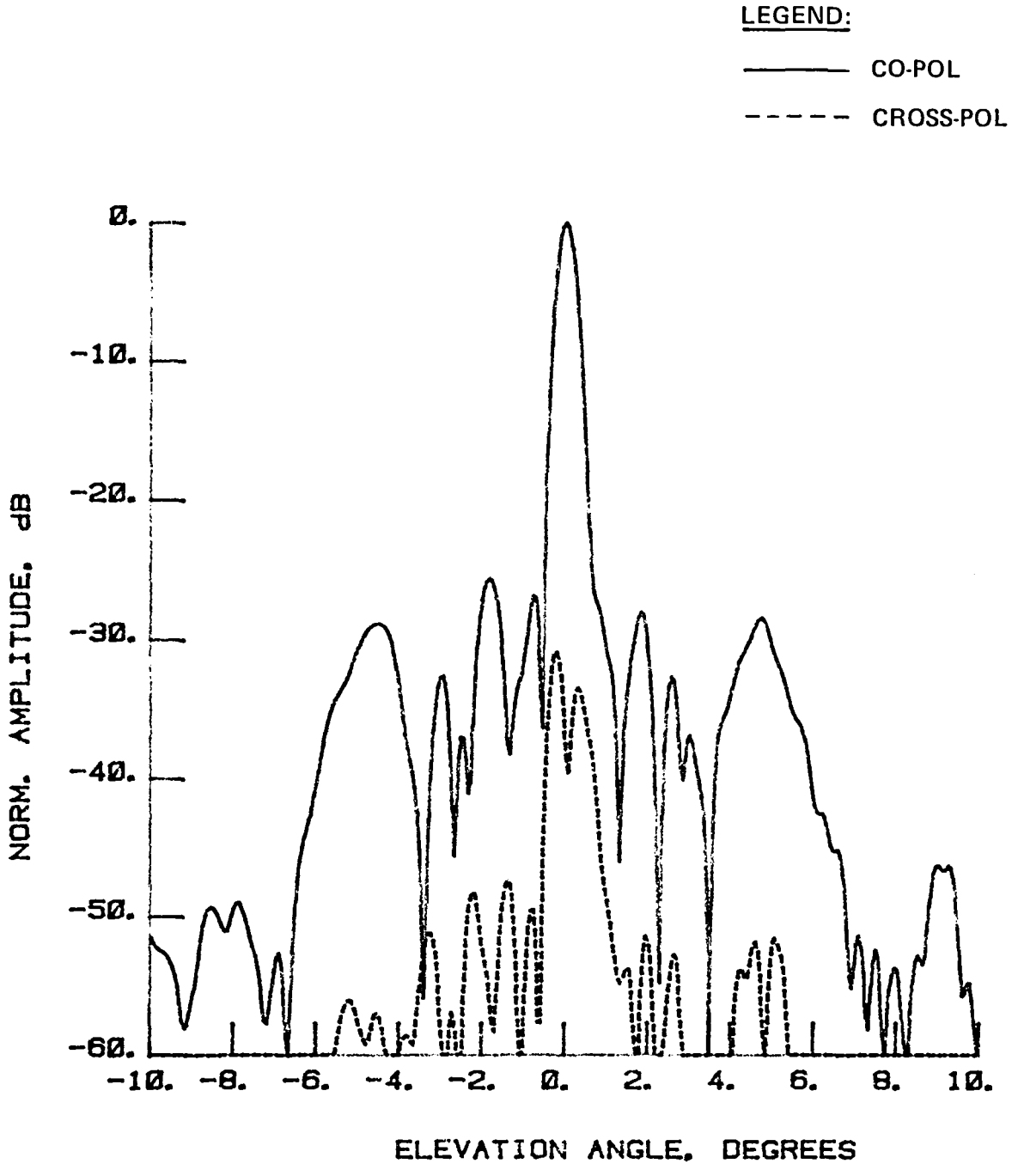

Figure 198 Test 23, 7.73 GHz, Cross-Pol, ±10° Scale, H-Plane, Overlay through Peak Co-Pol (0, 0)

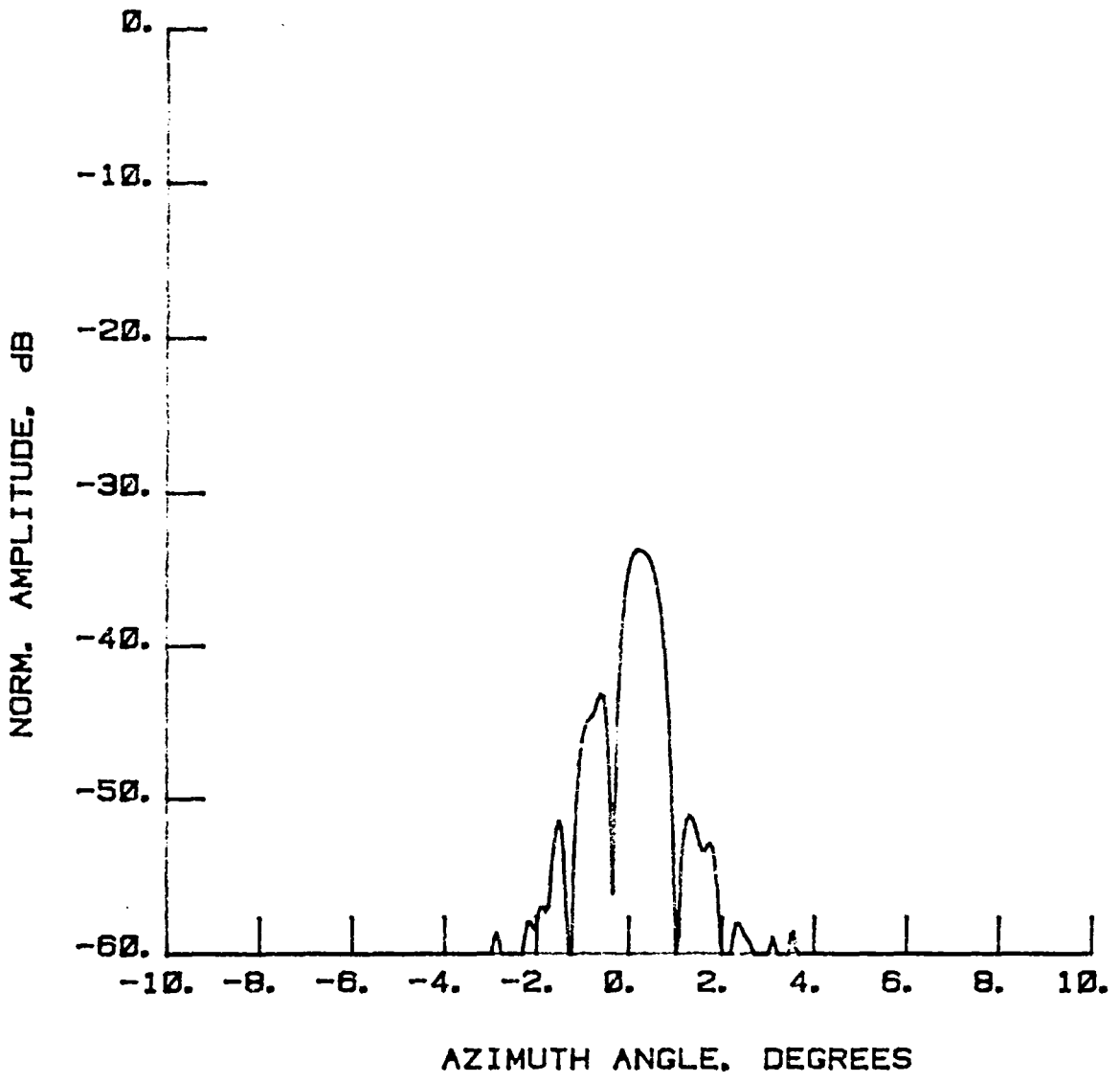

Figure 199

Test 23, 7.73 GHz, Cross-Pol, ±10° Scale, E-Plane of Cross-Pol through Peak Co-Pol (0, 0)

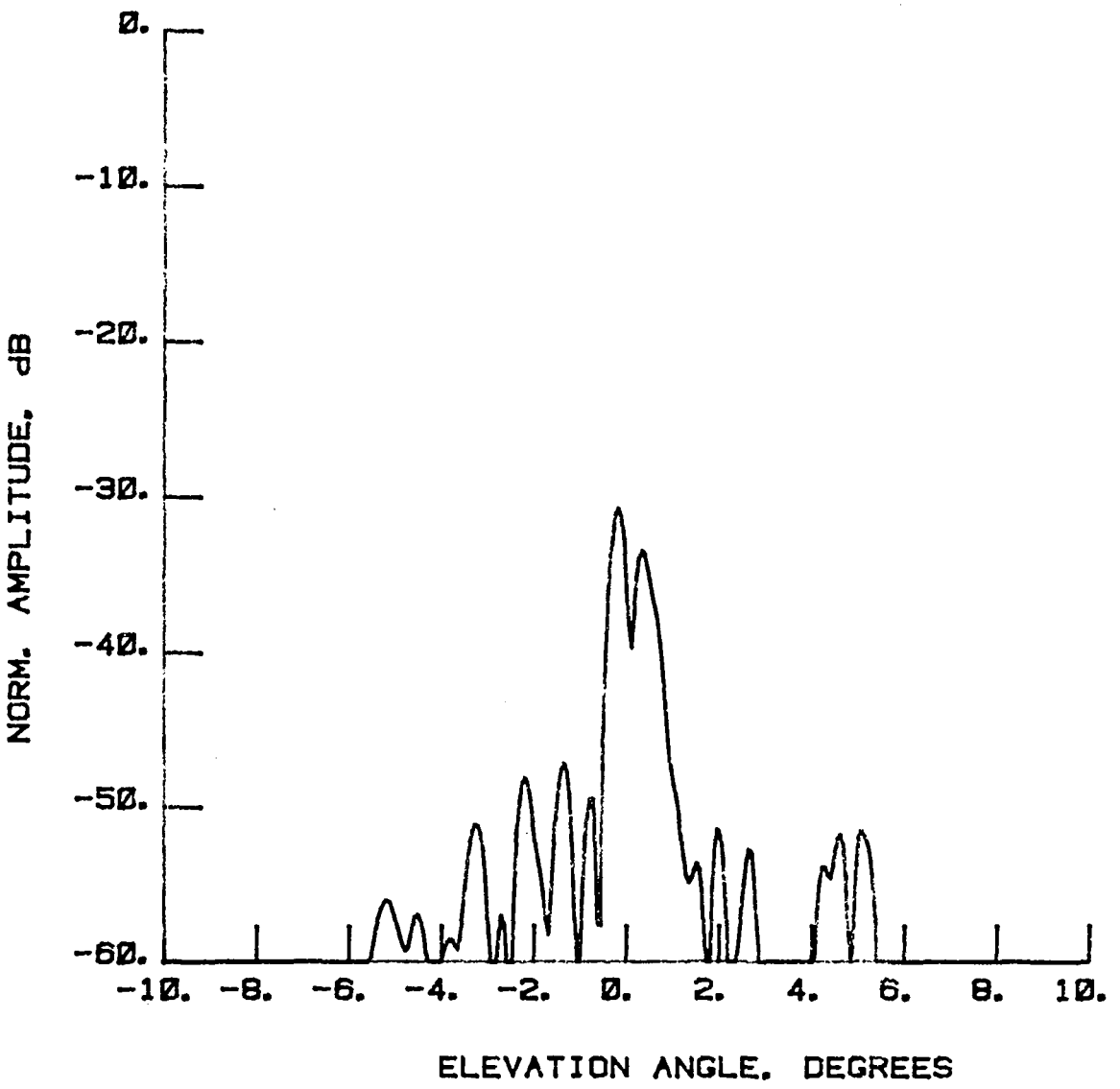

Figure 200

Test 23, 7.73 GHz, Cross-Pol, ±10° Scale, H-Plane of Cross-Pol through Peak Co-Pol (0, 0)

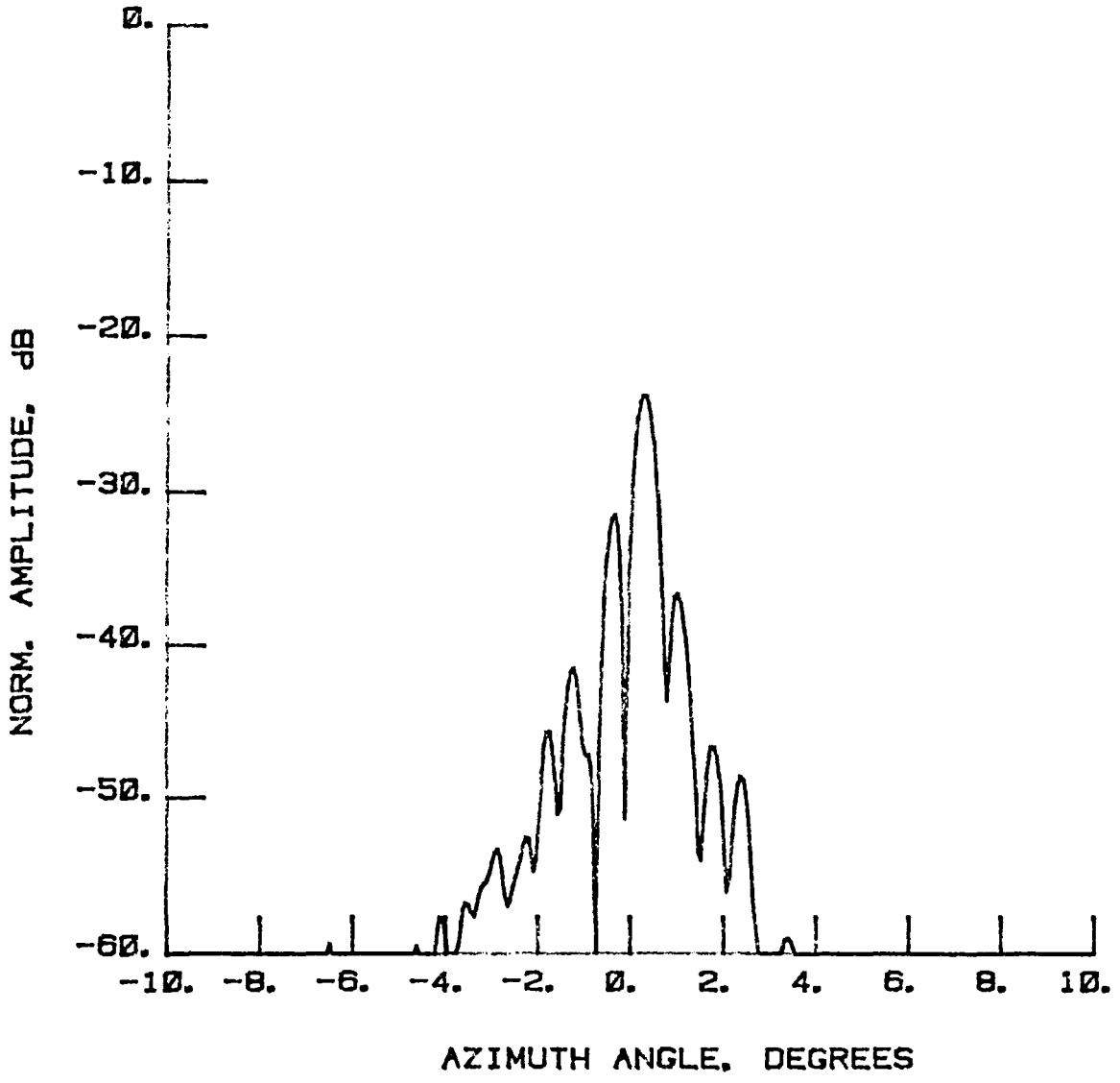

Figure 201

Test 23, 7.73 GHz, Cross-Pol, ±10° Scale, E-Plane of Cross-Pol through Peak Cross-Pol (0.28, 0.34)

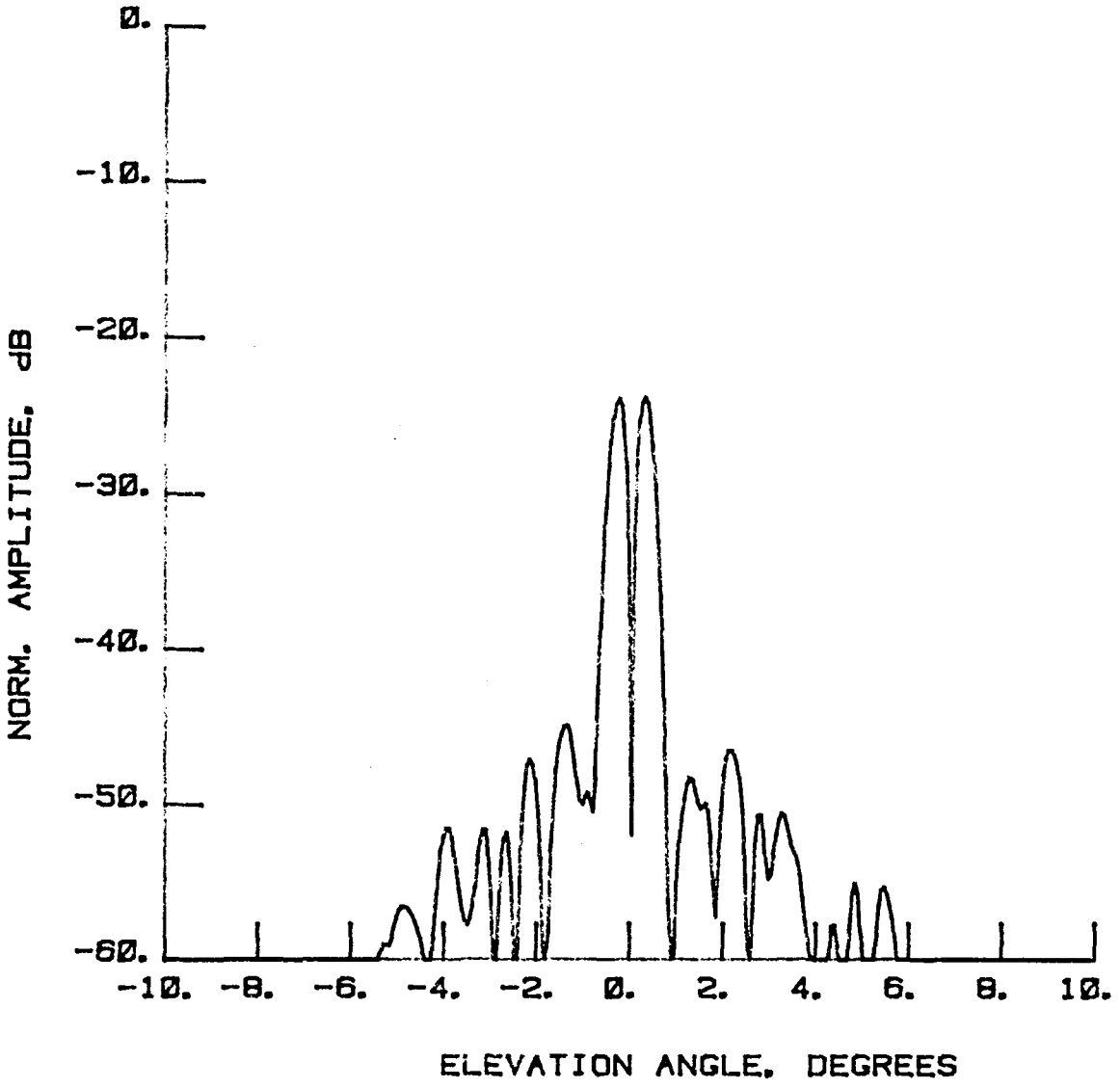

Figure 202

Test 23, 7.73 GHz, Cross-Pol, ±10° Scale, H-Plane of Cross-Pol through Peak Cross-Pol (0.28, 0.34)

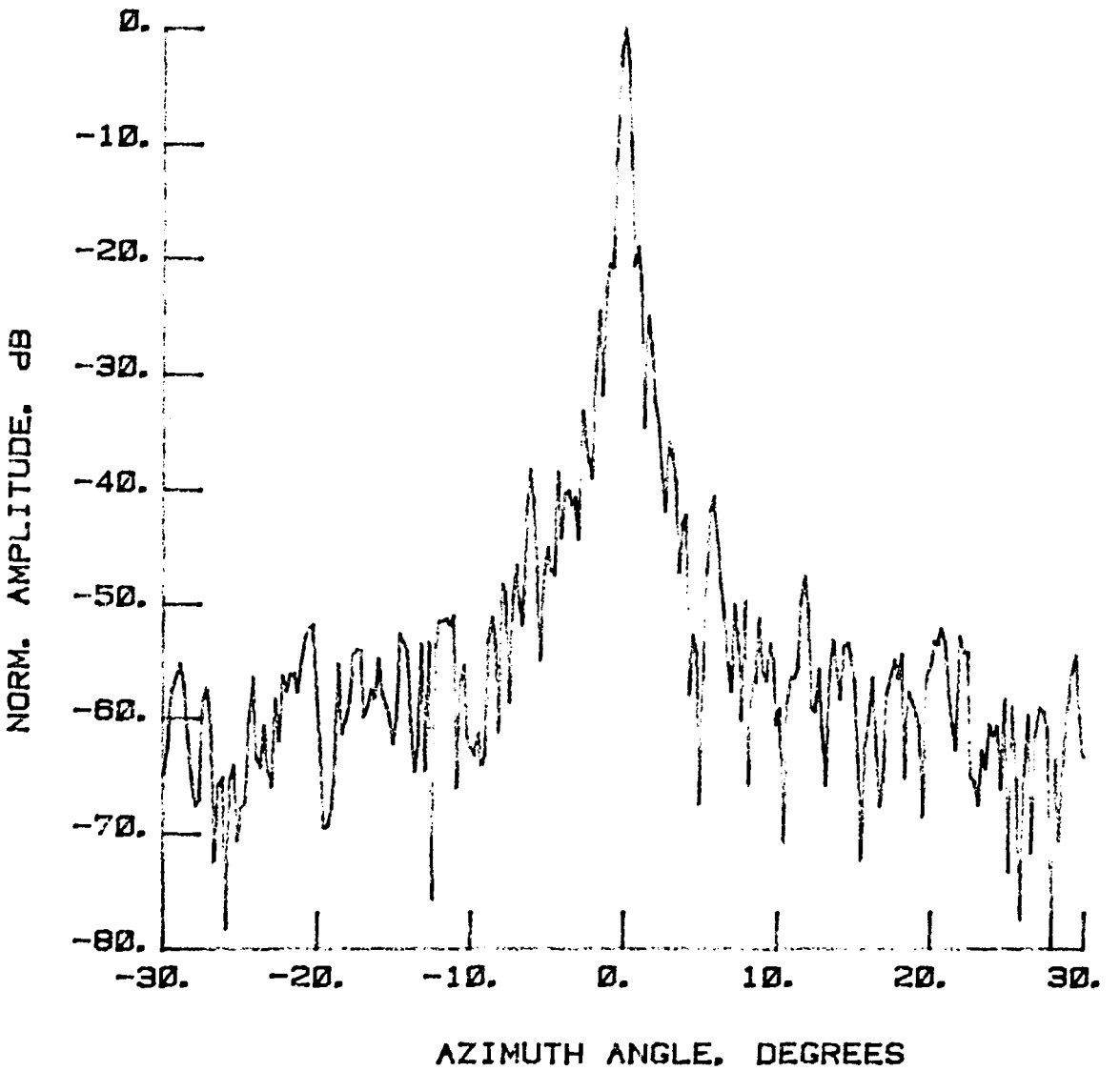

Figure 203 Test 24, 7.73 GHz, Co-Pol, E-Plane, Type 1

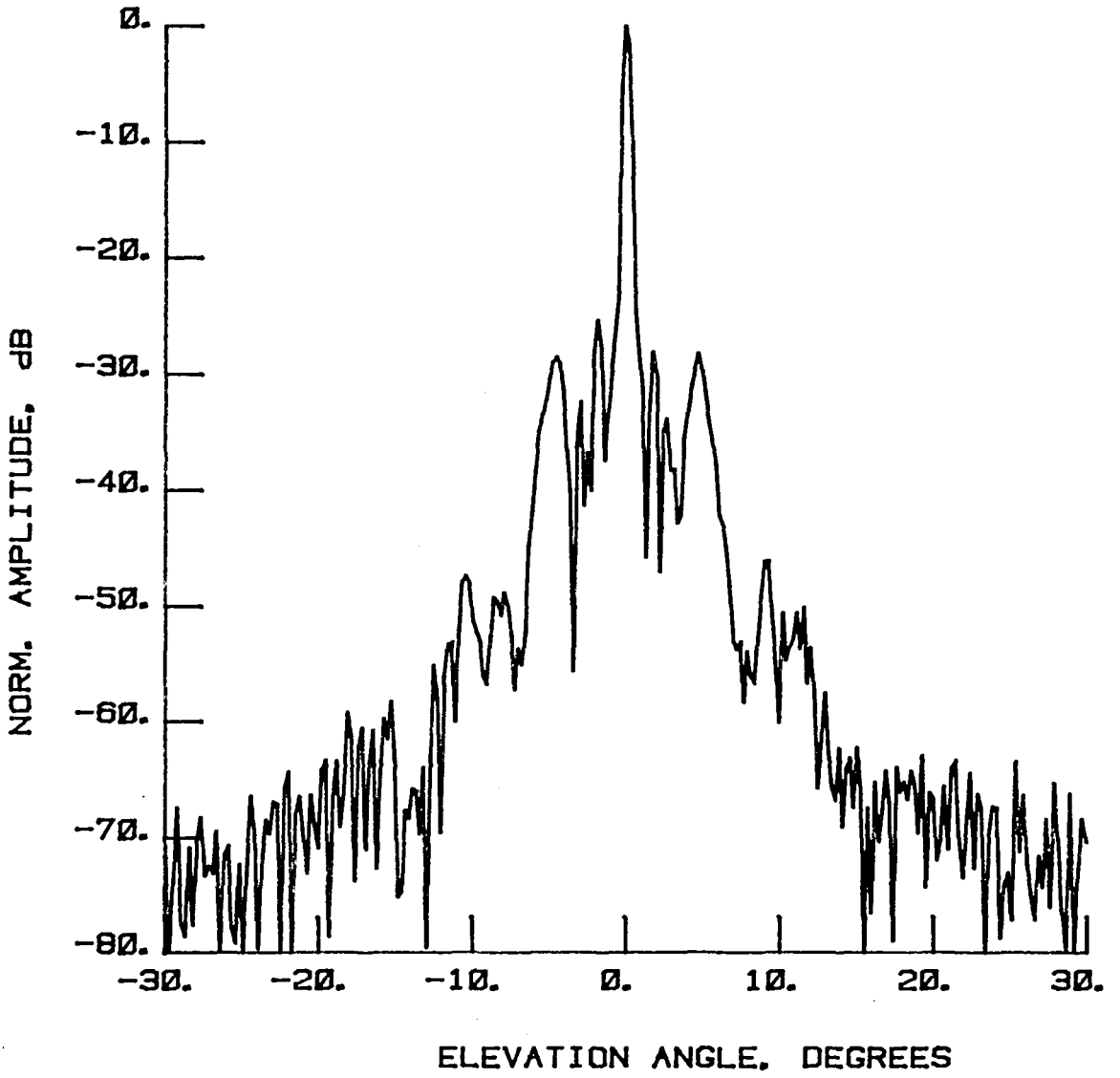

Figure 204 Test 24, 7.73 GHz, Co-Pol, H-Plane, Type 2

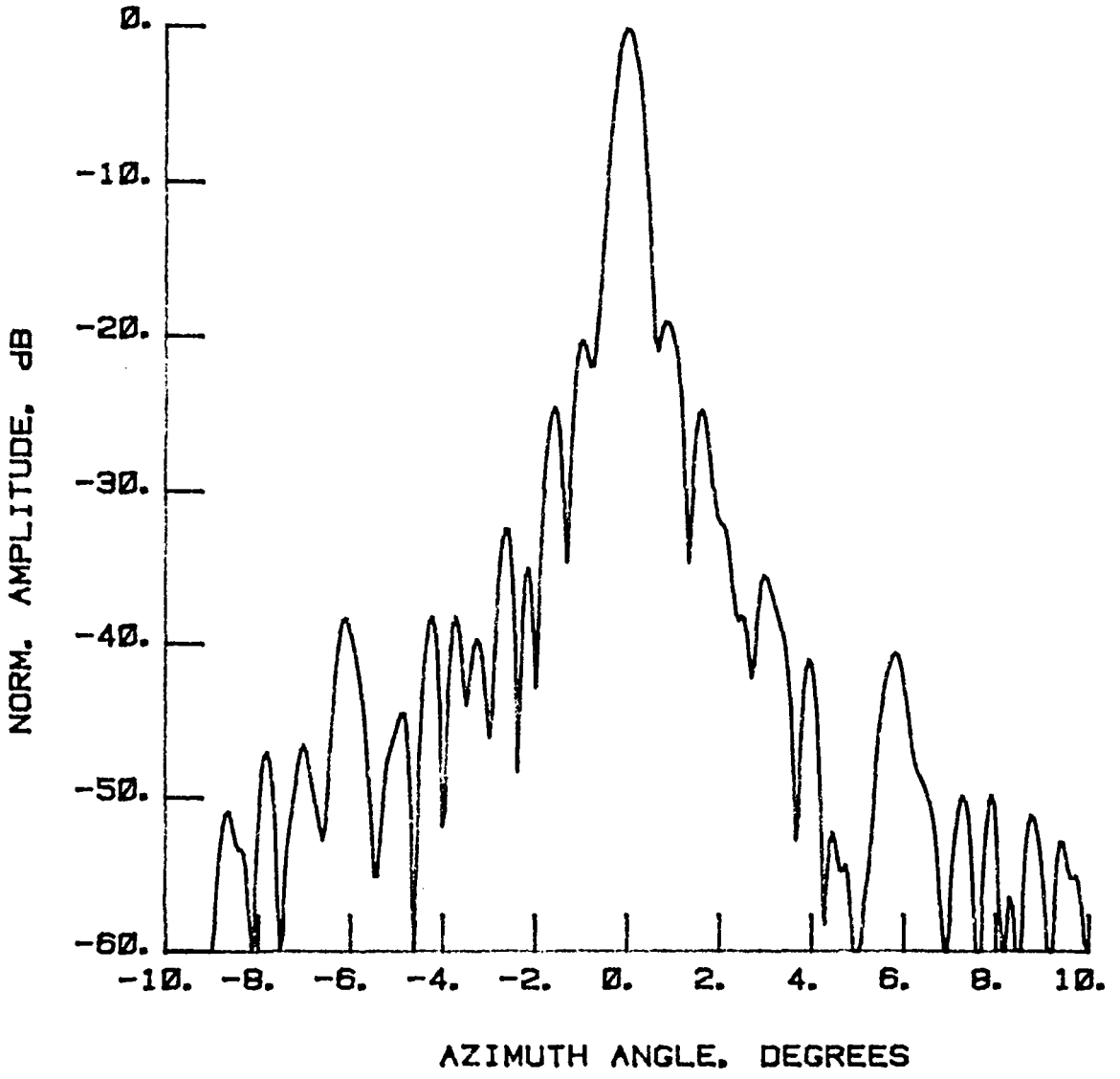

Figure 205 Test 24, 7.73 GHz, Co-Pol, E-Plane, Type 3

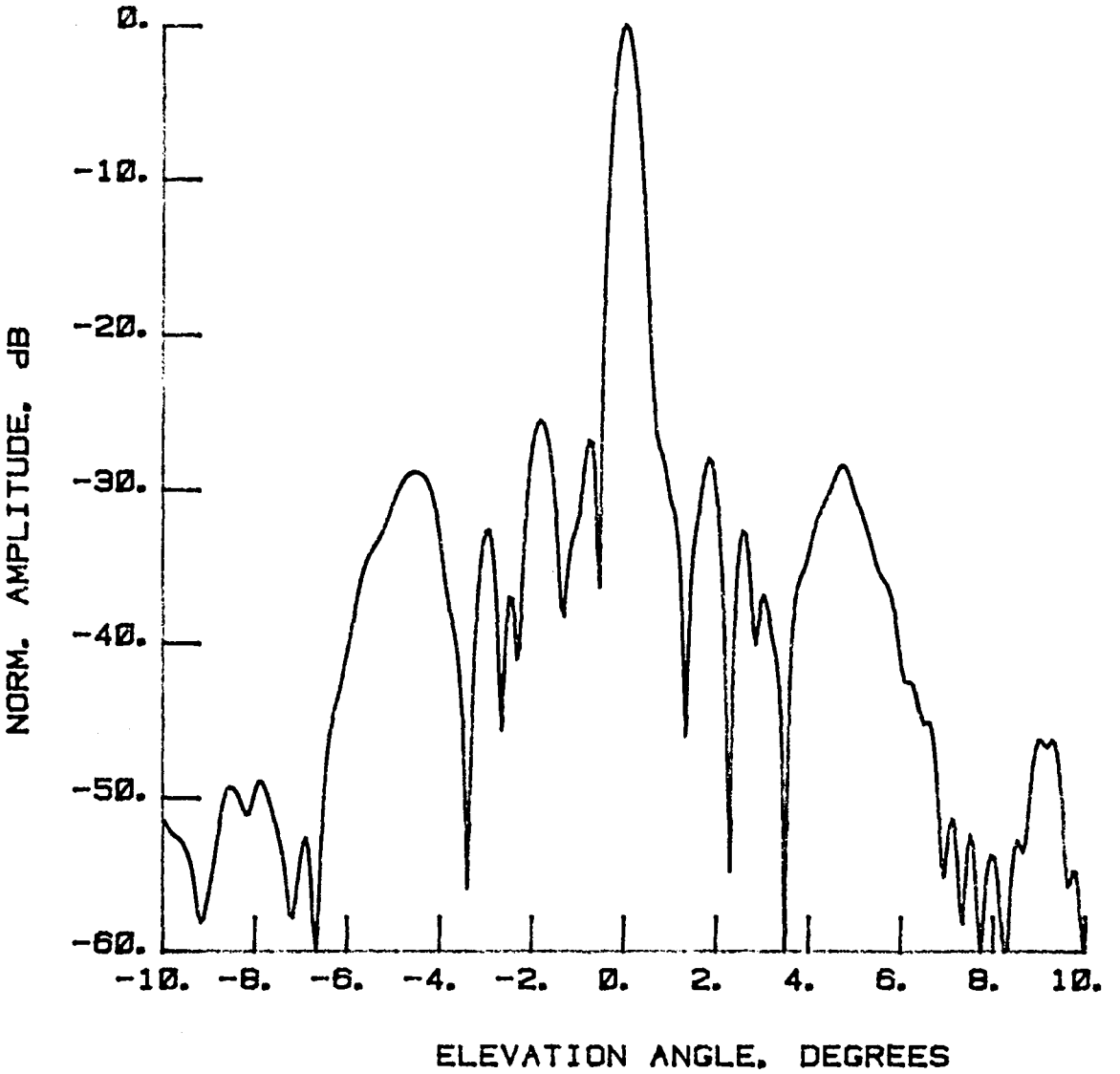

Figure 206 Test 24, 7.73 GHz, Co-Pol, H-Plane, Type 4

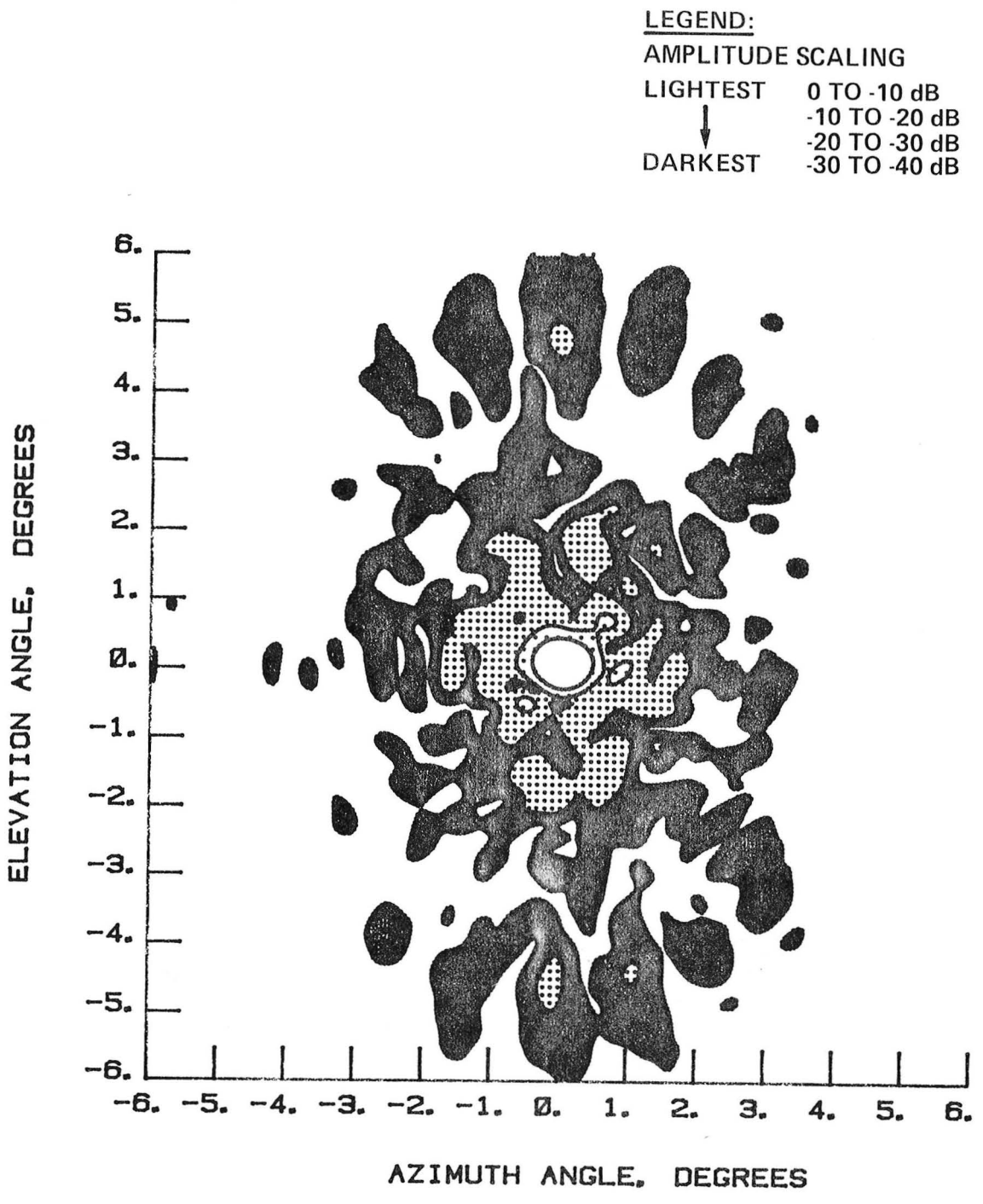

Figure 207 Test 24, 7.73 GHz, Co-Pol, Contour, Type 5

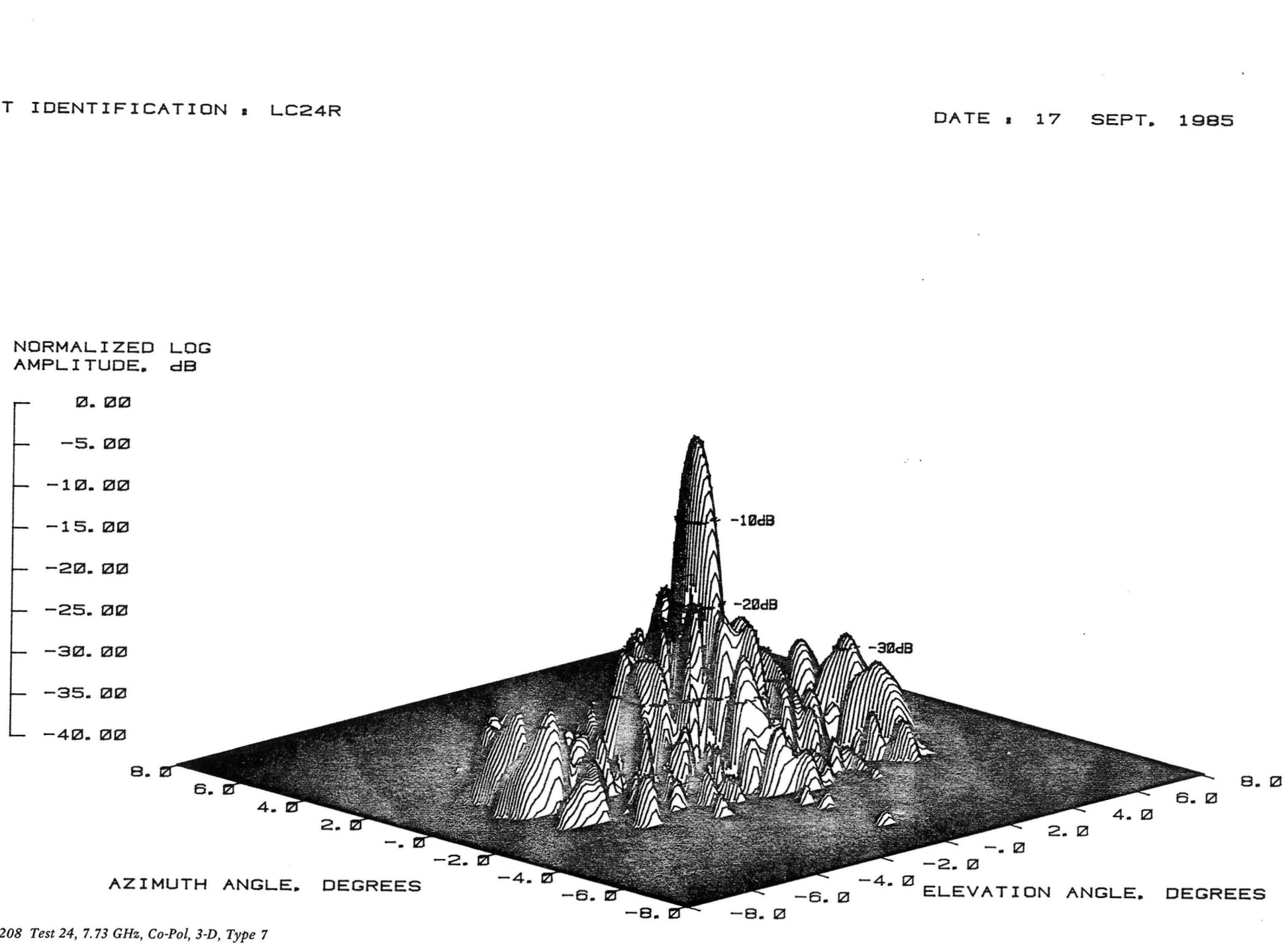

Figure 208 Test 24, 7.73 GHz, Co-Pol, 3-D, Type 7

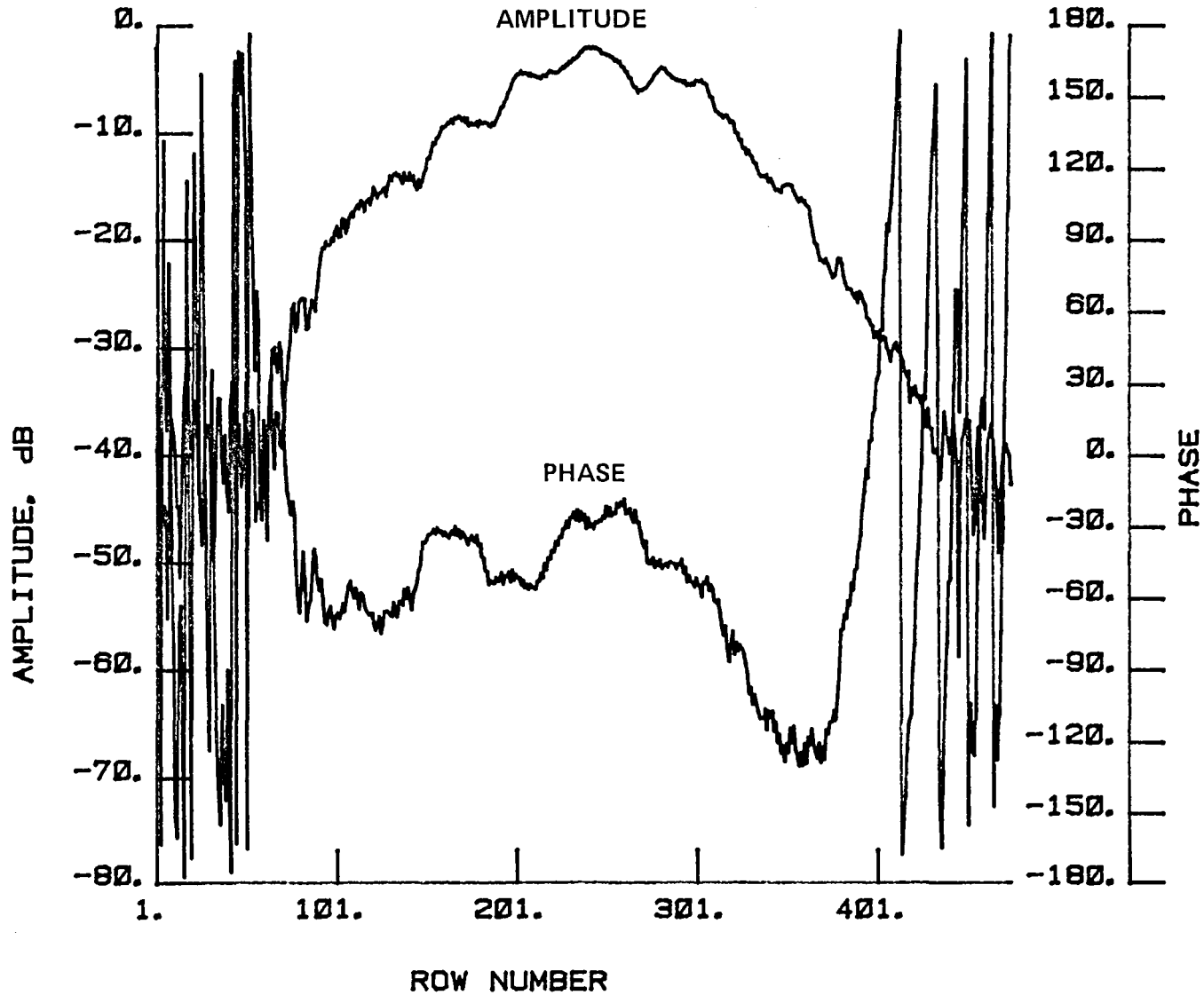

Figure 209 Test 24, 7.73 GHz, Co-Pol, H-Plane, Type 8

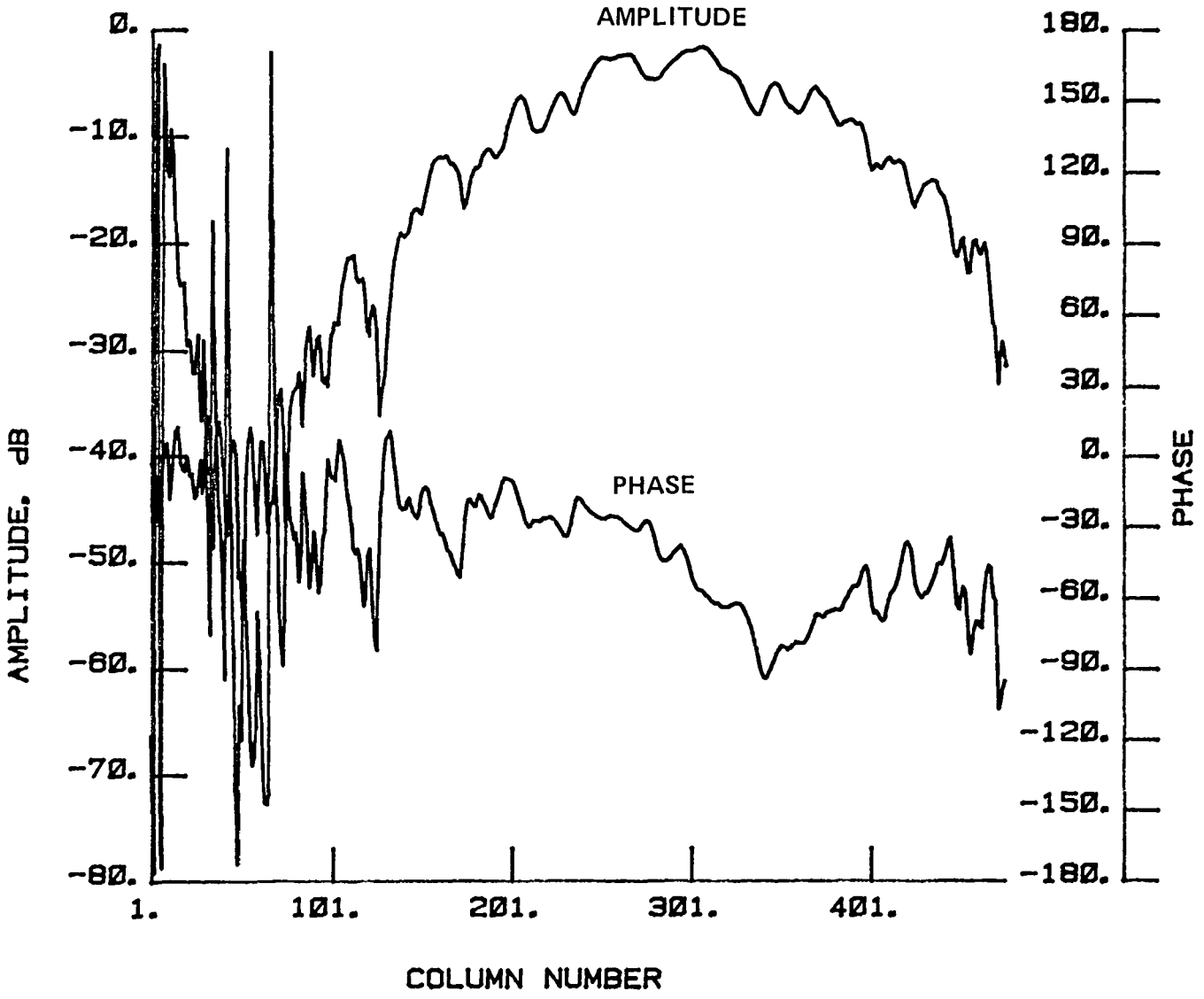

Figure 210 Test 24, 7.73 GHz, Co-Pol, E-Plane, Type 9

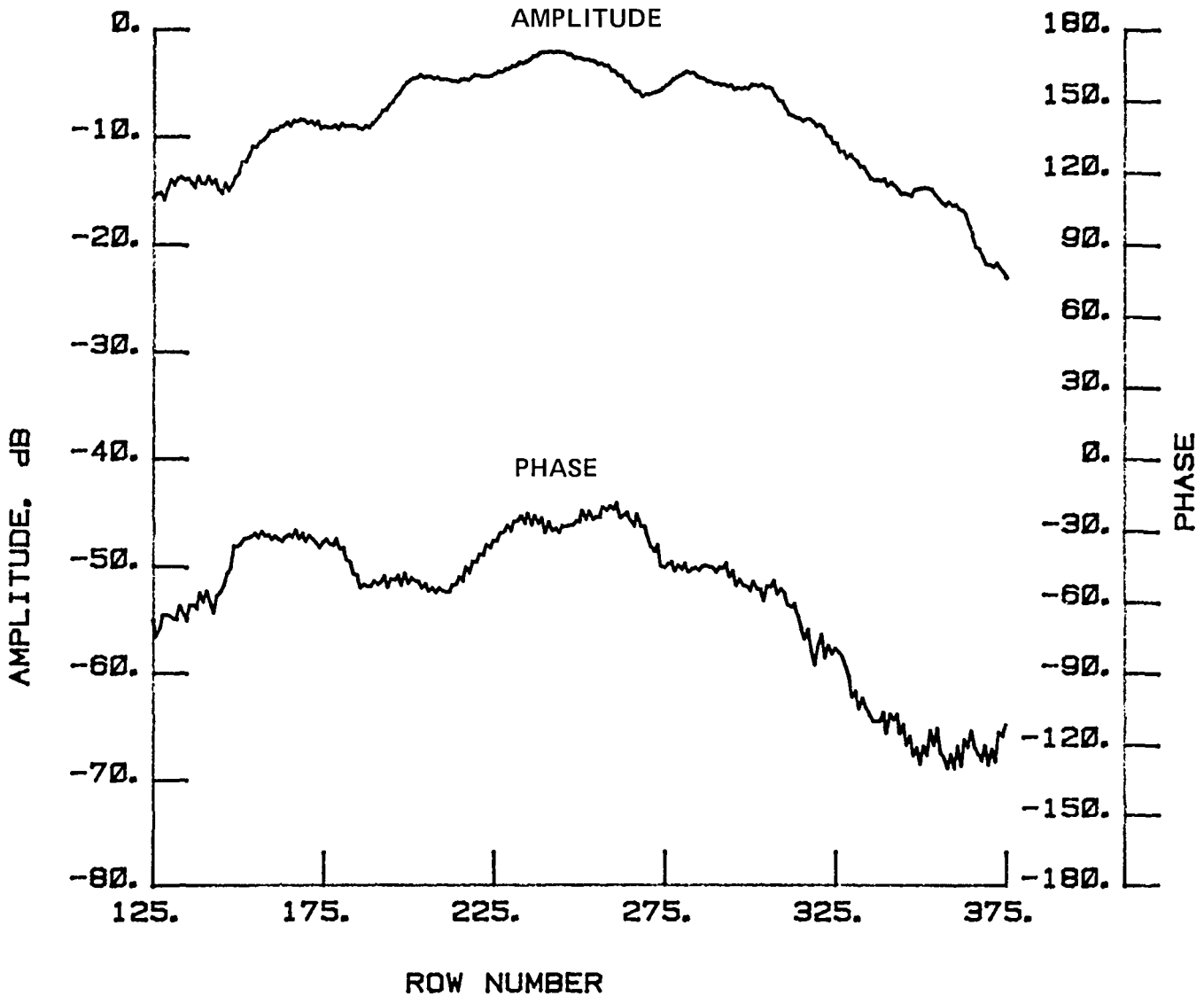

Figure 211 Test 24, 7.73 GHz, Co-Pol, H-Plane, Type 10

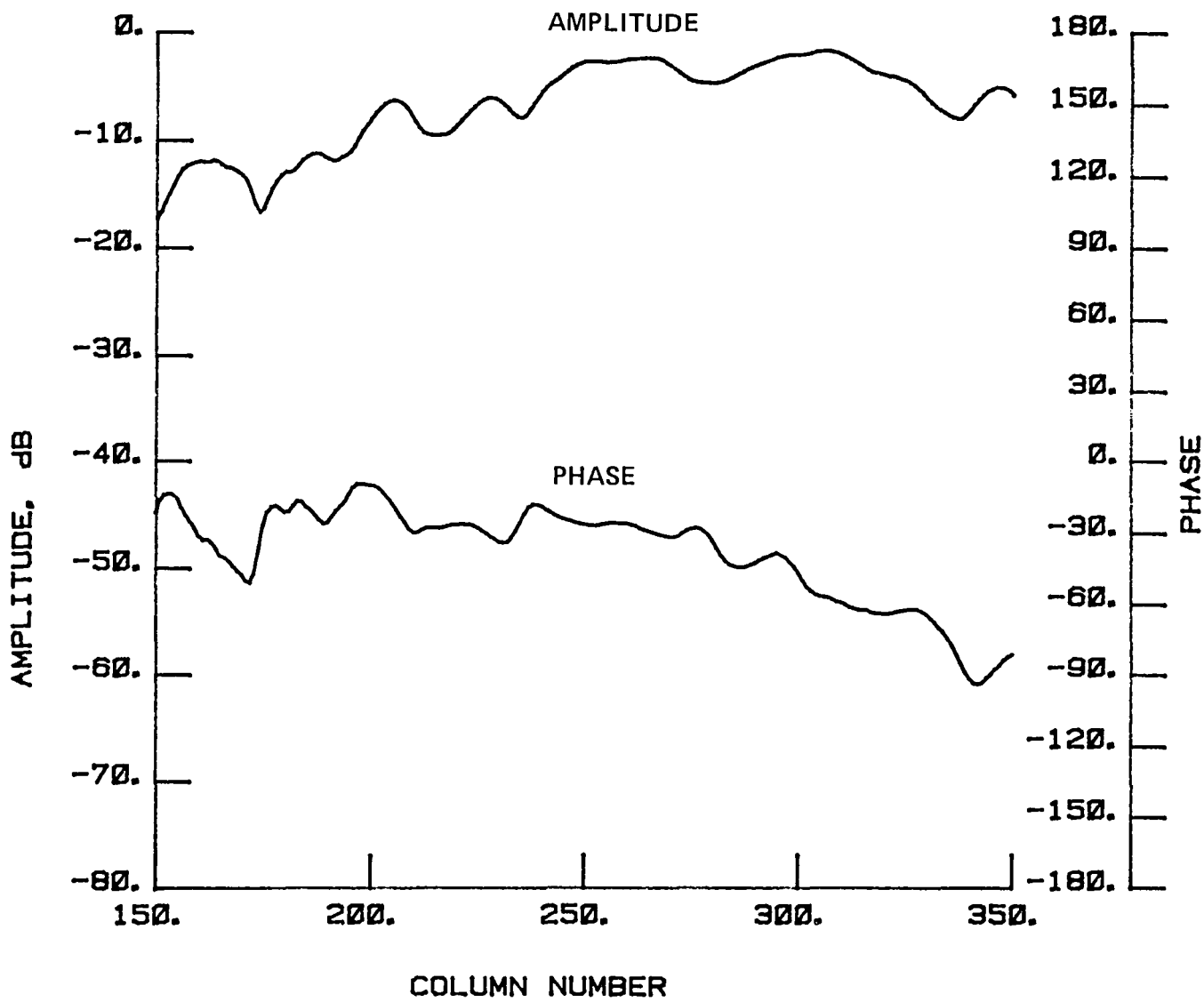

Figure 212 Test 24, 7.73 GHz, Co-Pol, E-Plane, Type 11

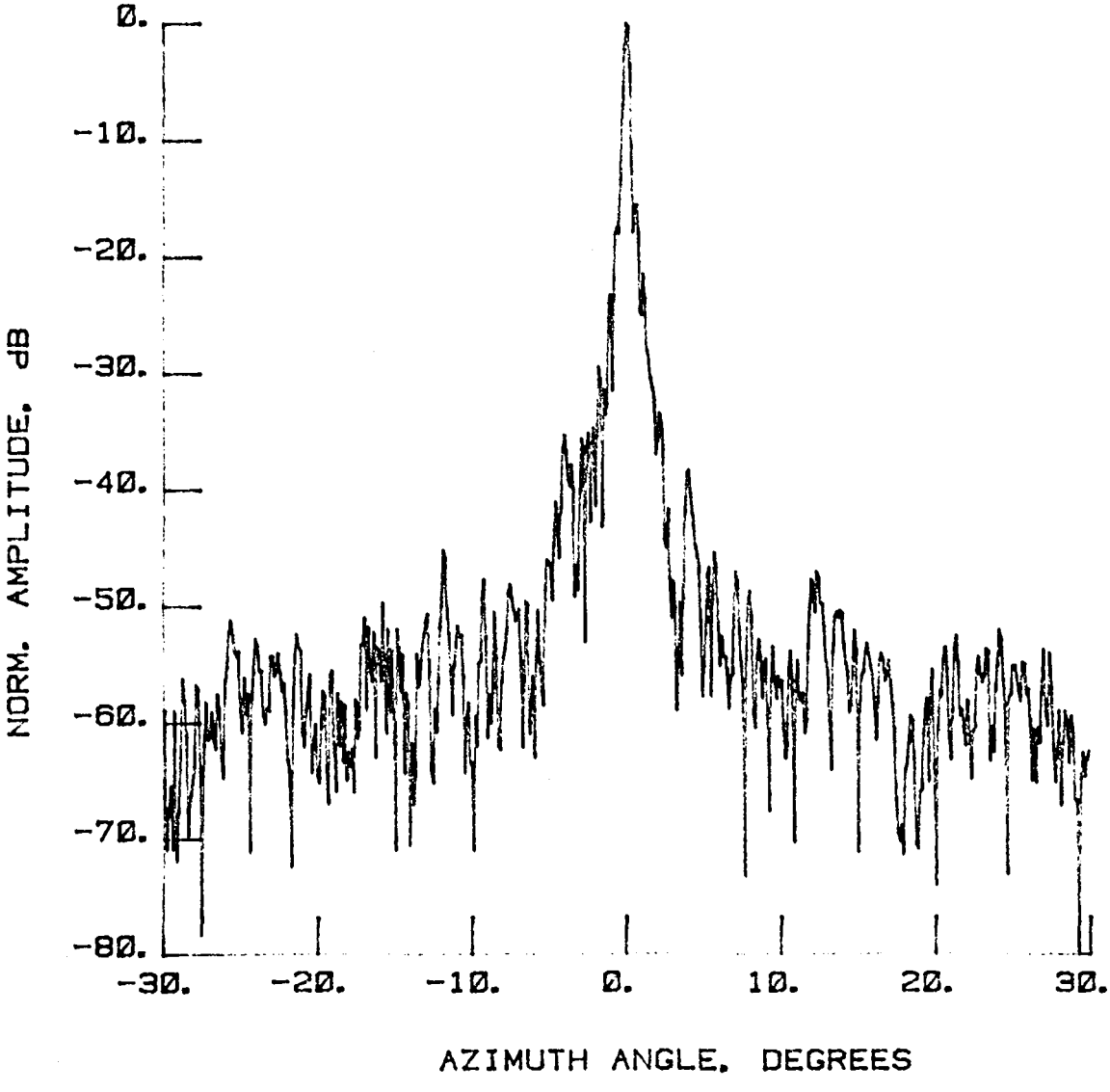

Figure 213 Test 25, 11.60 GHz, Co-Pol, E-Plane, Type 1

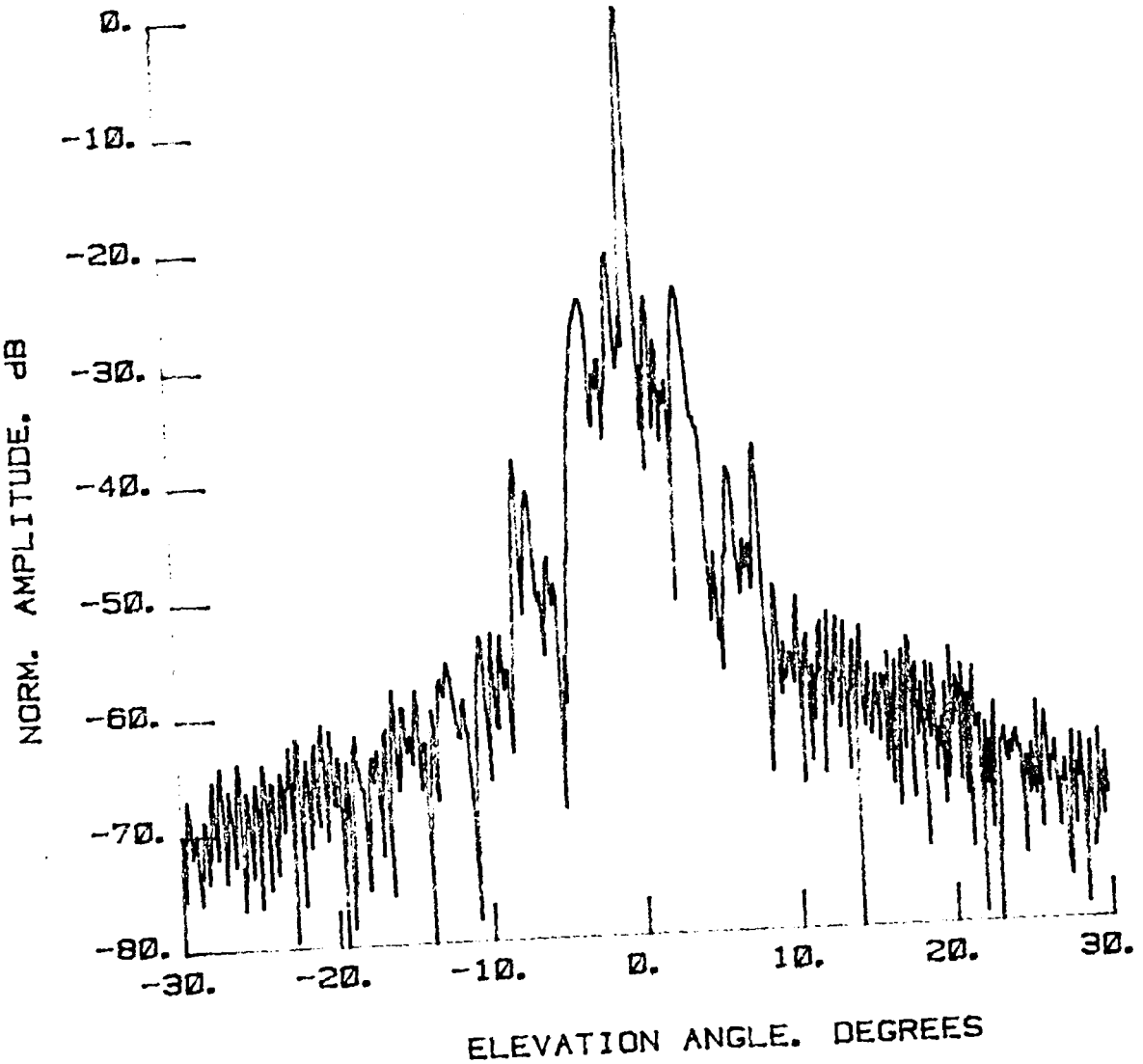

Figure 214 Test 25, 11.60 GHz, Co-Pol, H-Plane, Type 2

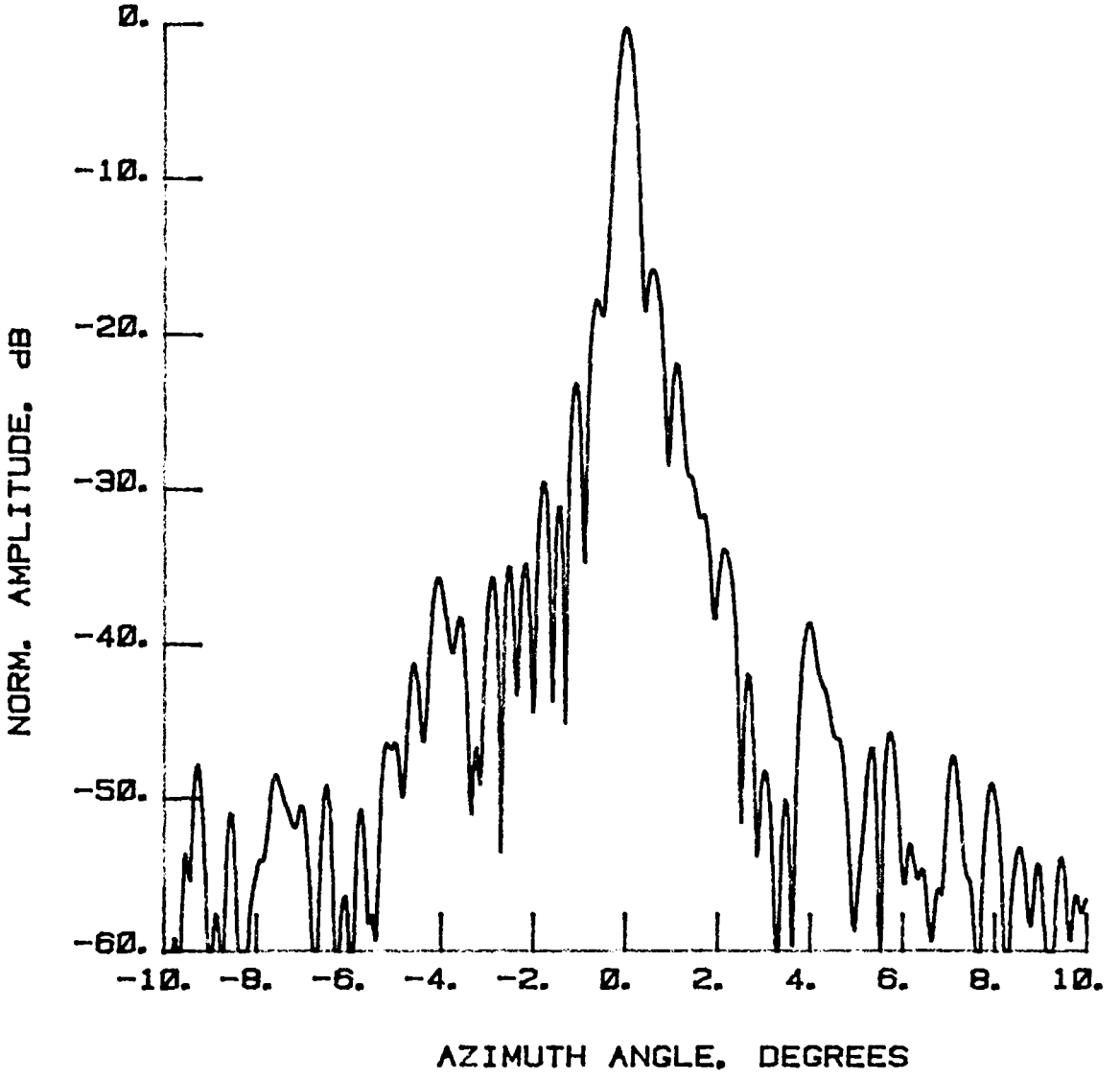

Figure 215 Test 25, 11.60 GHz, Co-Pol, E-Plane, Type 3

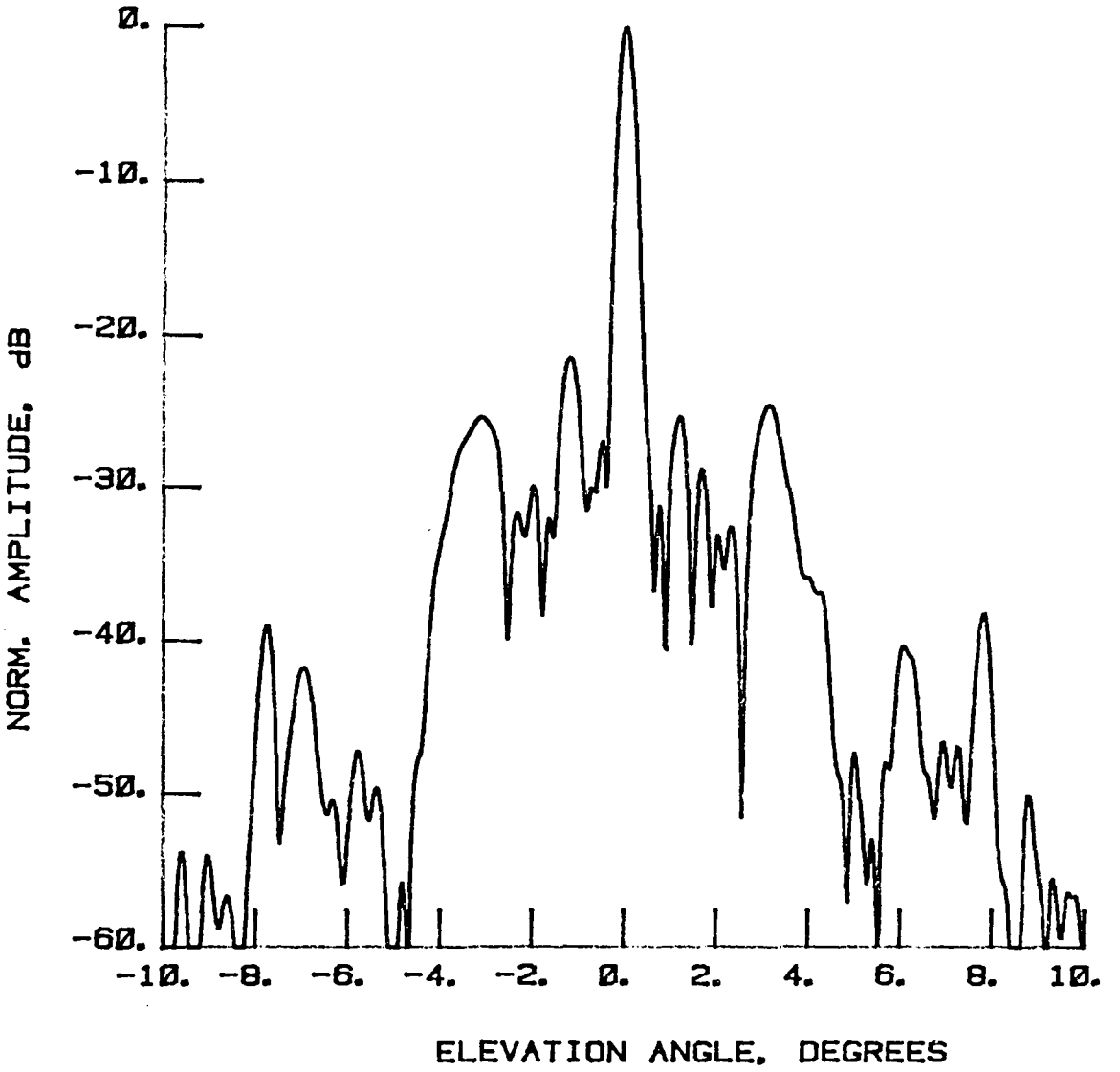

Figure 216 Test 25, 11.60 GHz, Co-Pol, H-Plane, Type 4

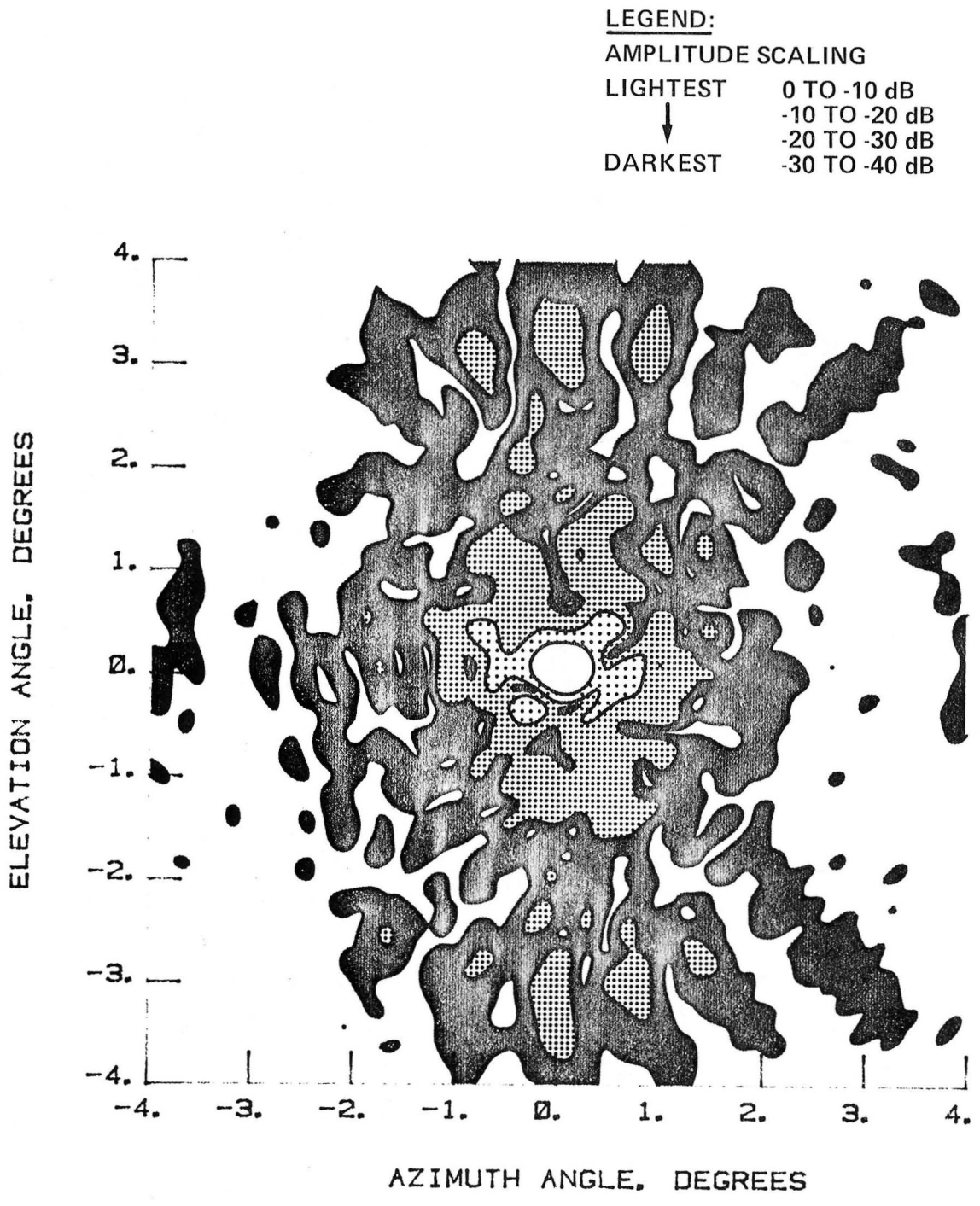

Figure 217 Test 25, 11.60 GHz, Co-Pol, Contour, Type 5

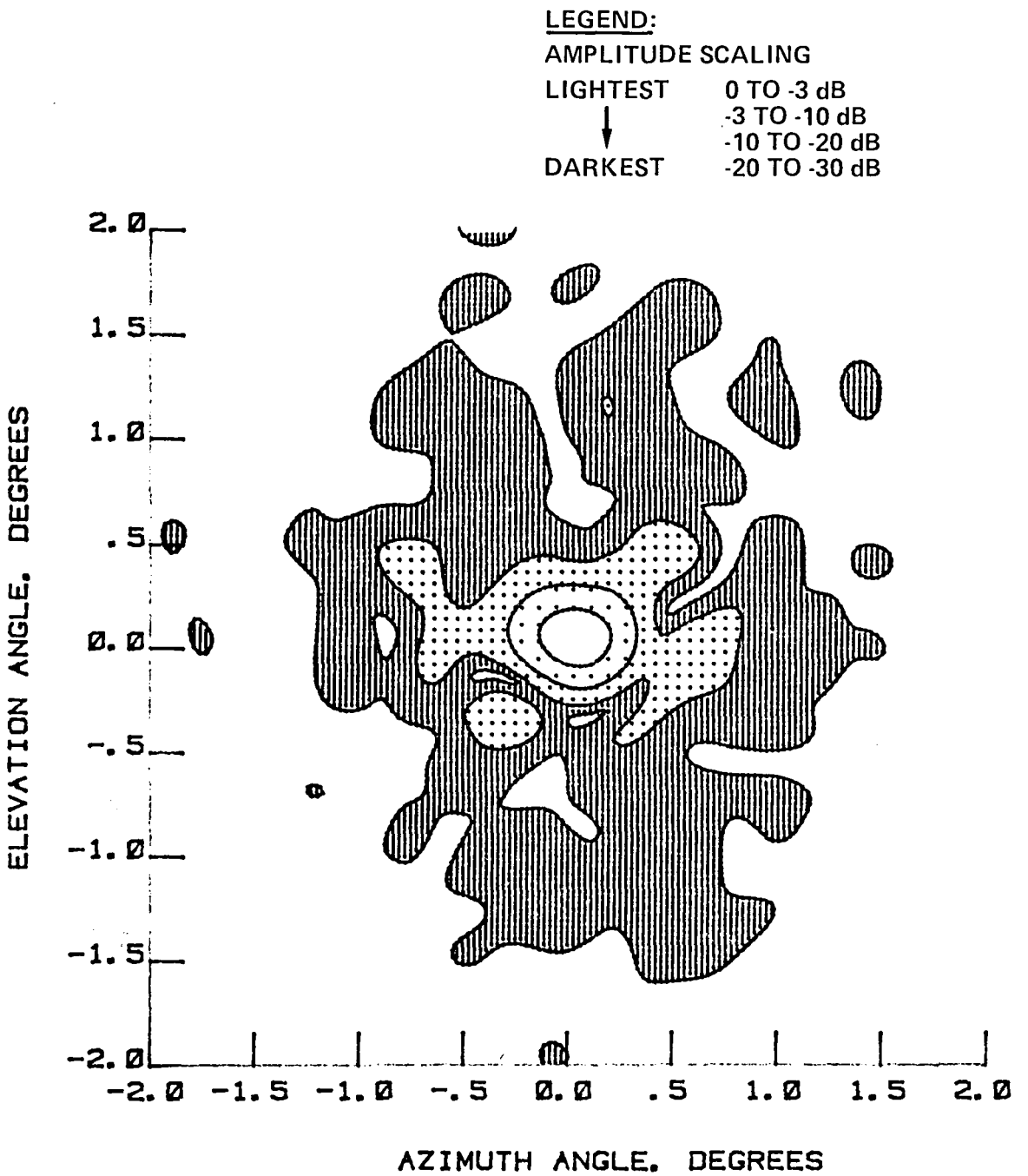

Figure 218 Test 25, 11.60 GHz, Co-Pol, Contour, Type 6

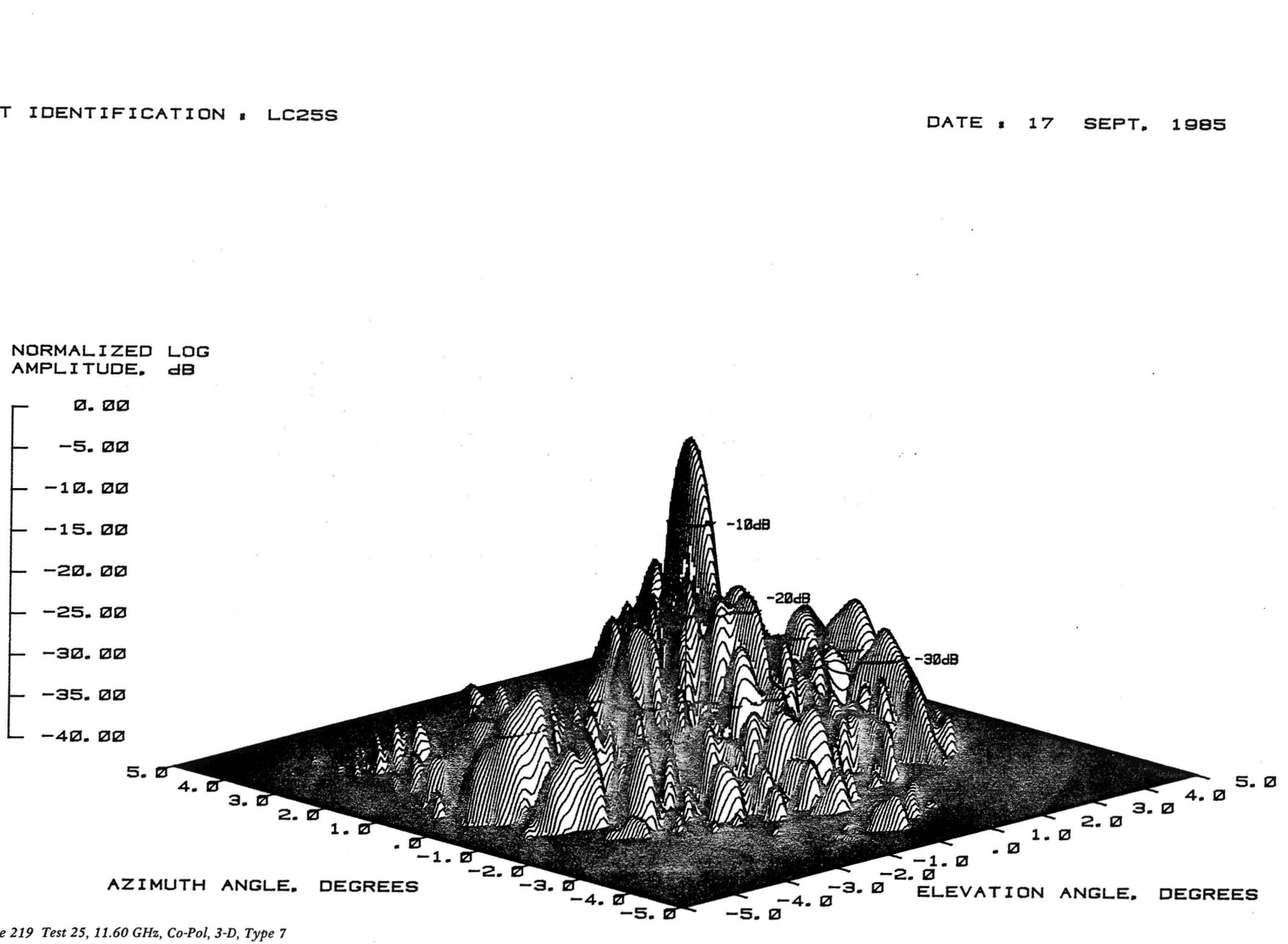

Figure 219 Test 25, 11.60 GHz, Co-Pol, 3-D, Type 7

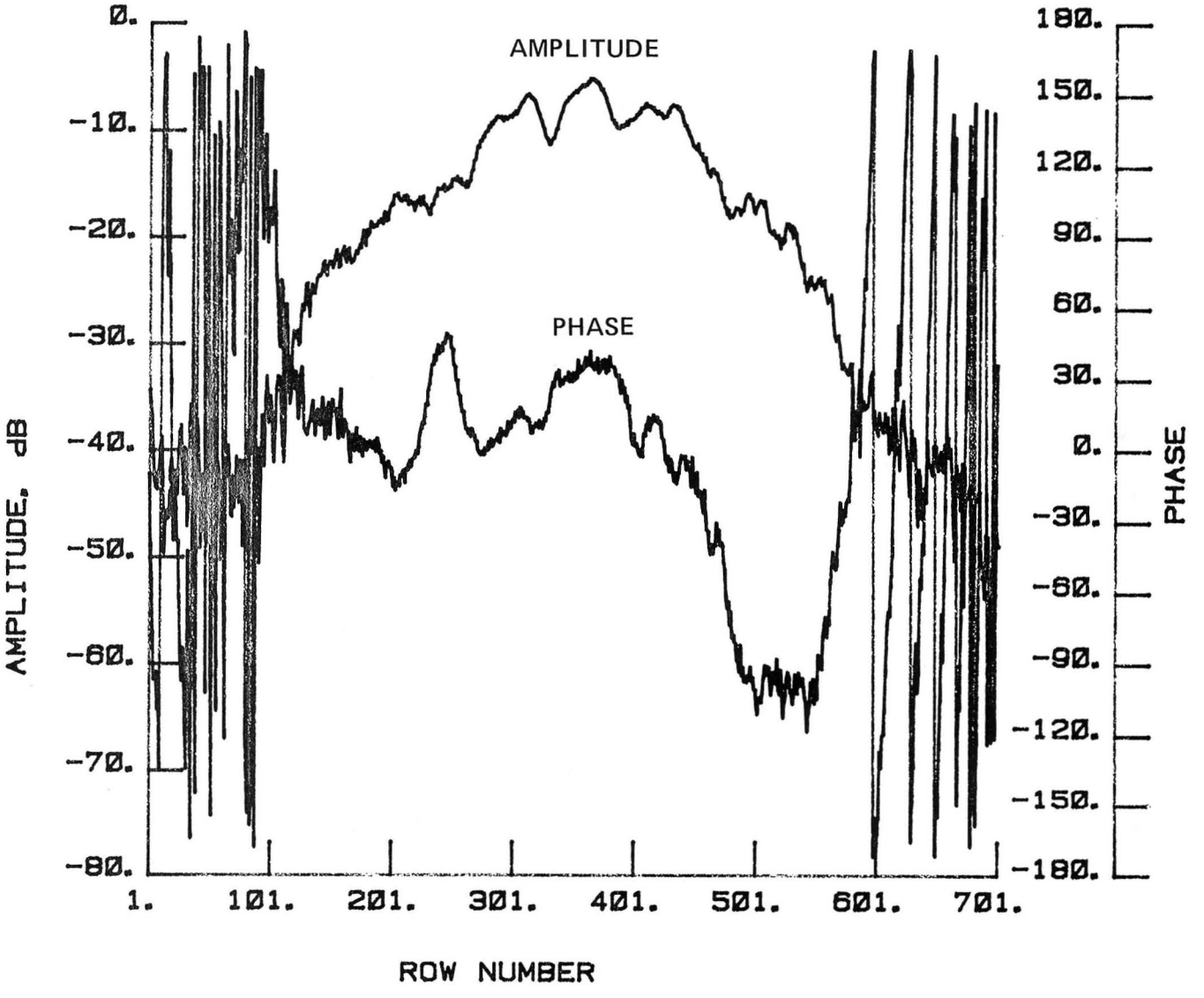

Figure 220 Test 25, 11.60 GHz, Co-Pol, H-Plane, Type 8

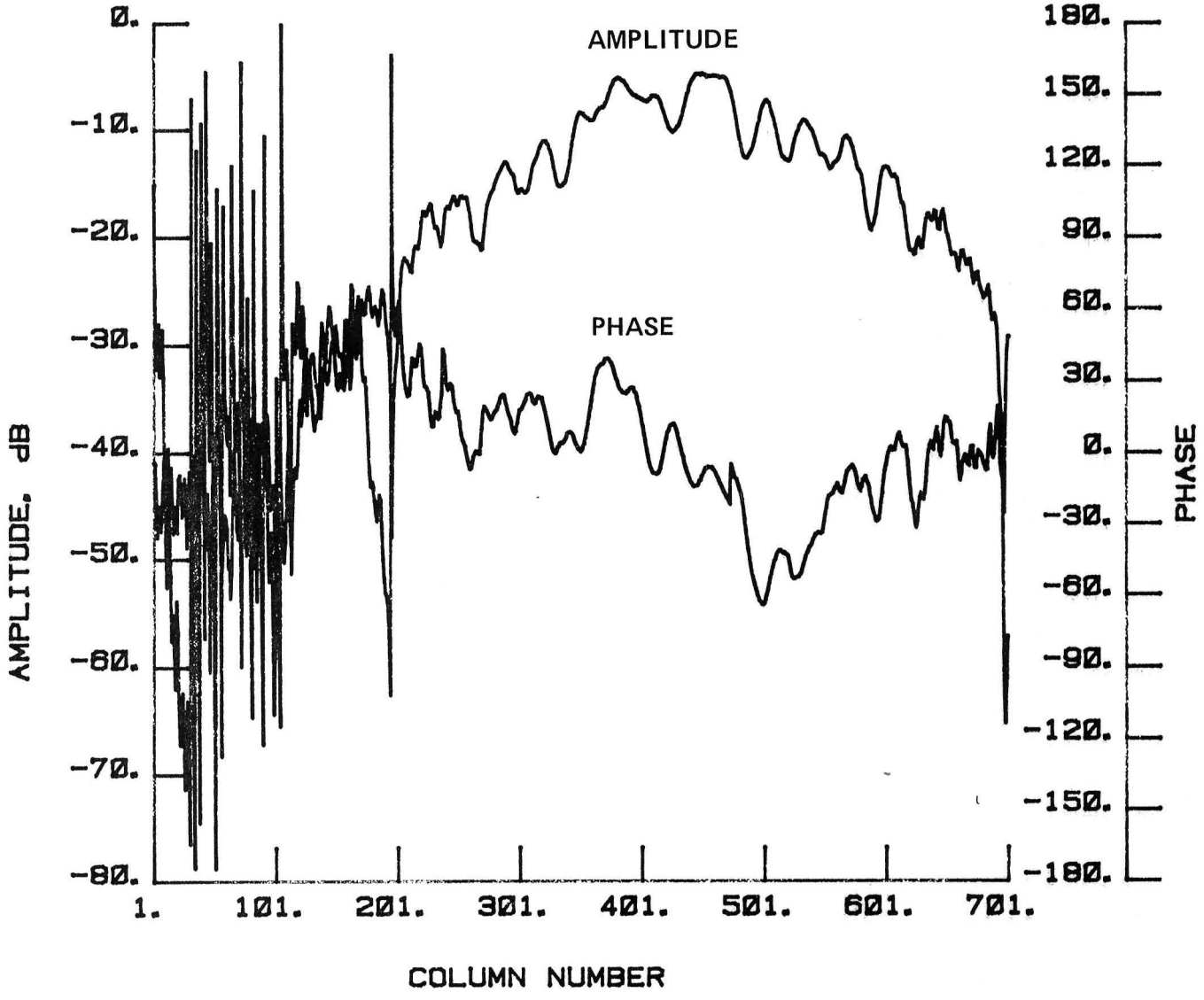

Figure 221 Test 25, 11.60 GHz, Co-Pol, E-Plane, Type 9

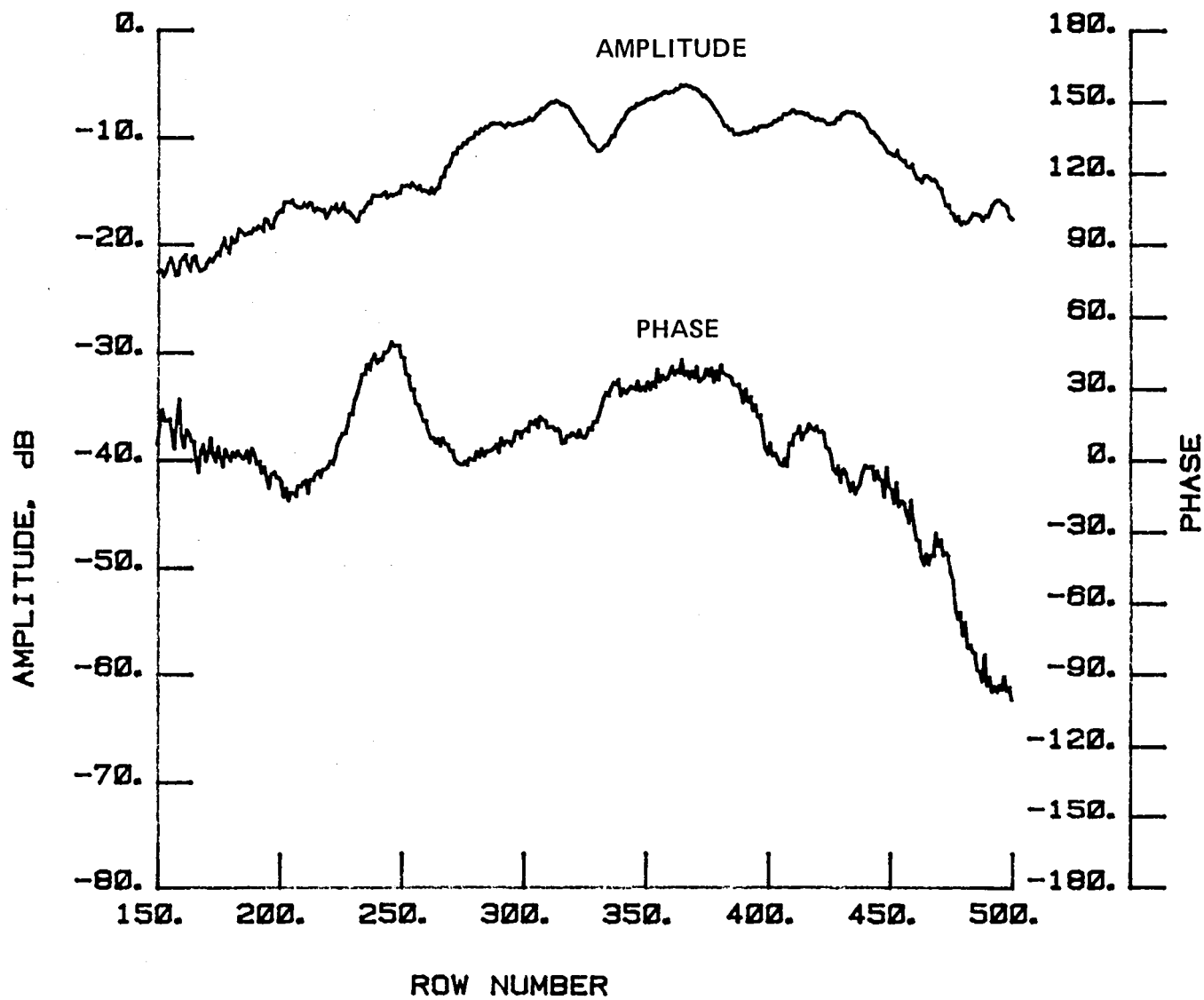

Figure 222 Test 25, 11.60 GHz, Co-Pol, H-Plane, Type 10

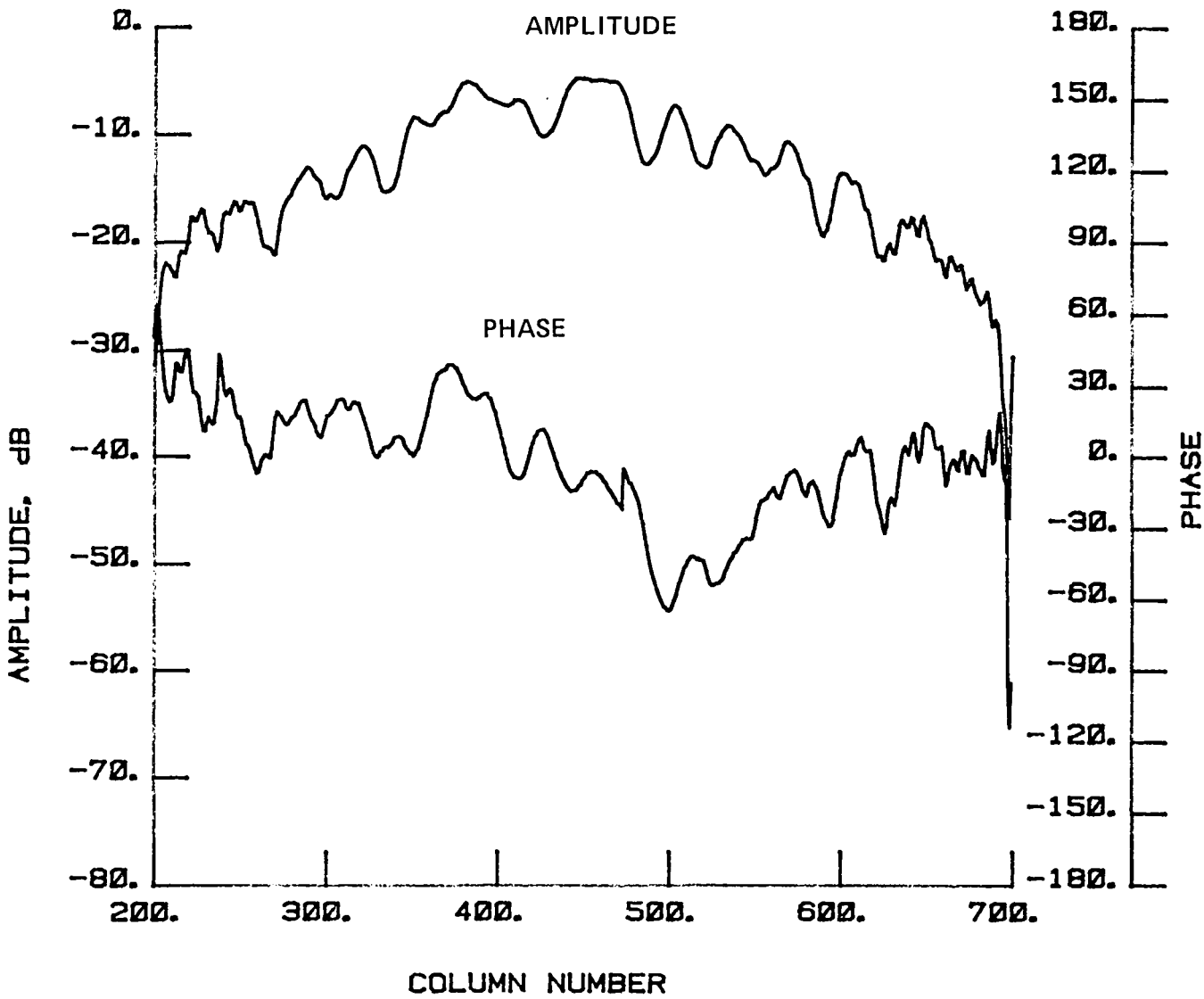

Figure 223 Test 25, 11.60 GHz, Co-Pol, E-Plane, Type 11

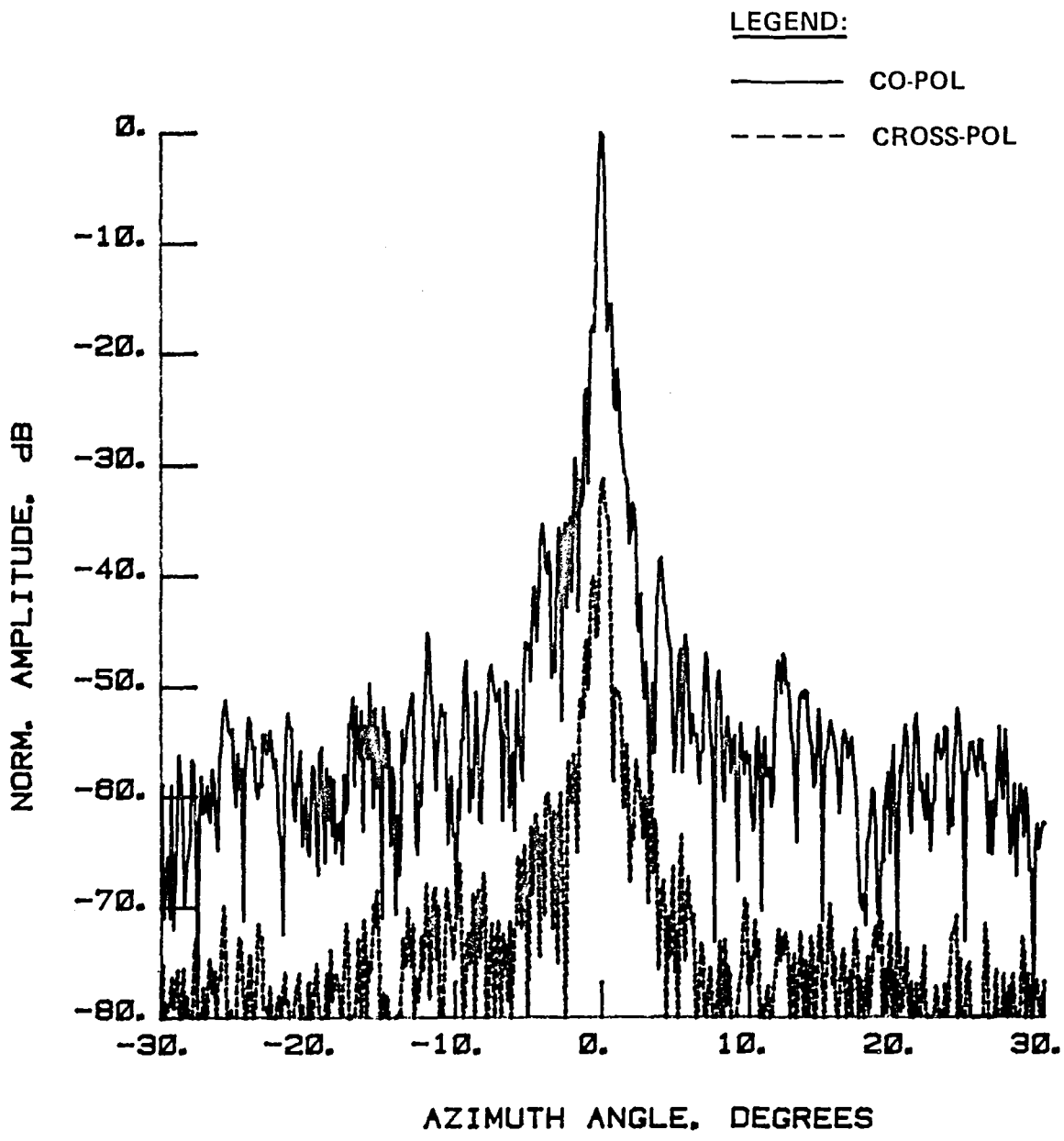

Figure 224 Test 26, 11.60 GHz, Cross-Pol, E-Plane, Type 12

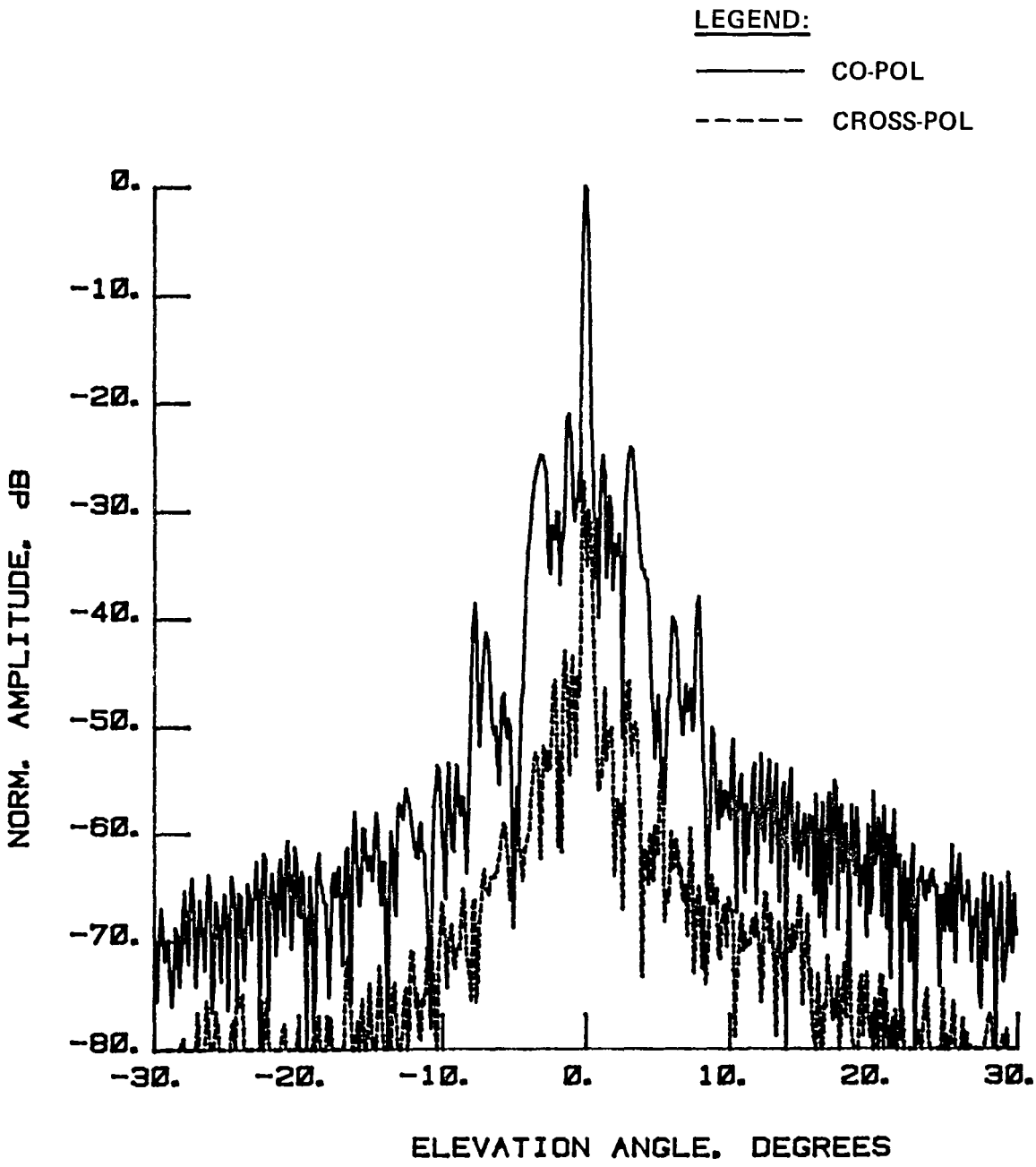

Figure 225 Test 26, 11.60 GHz, Cross-Pol, H-Plane, Type 13

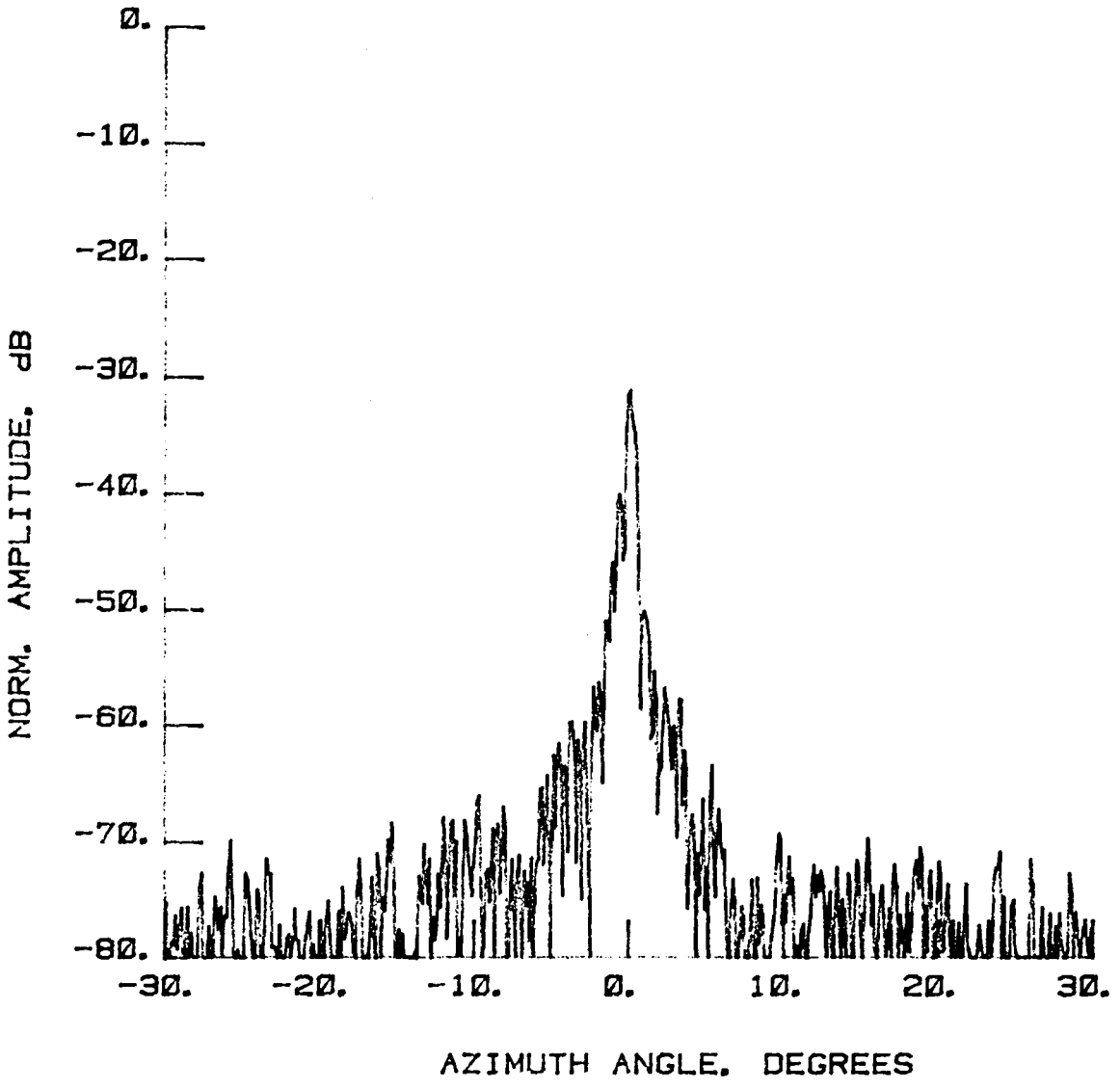

Figure 226 Test 26, 11.60 GHz, Cross-Pol, E-Plane, Type 14

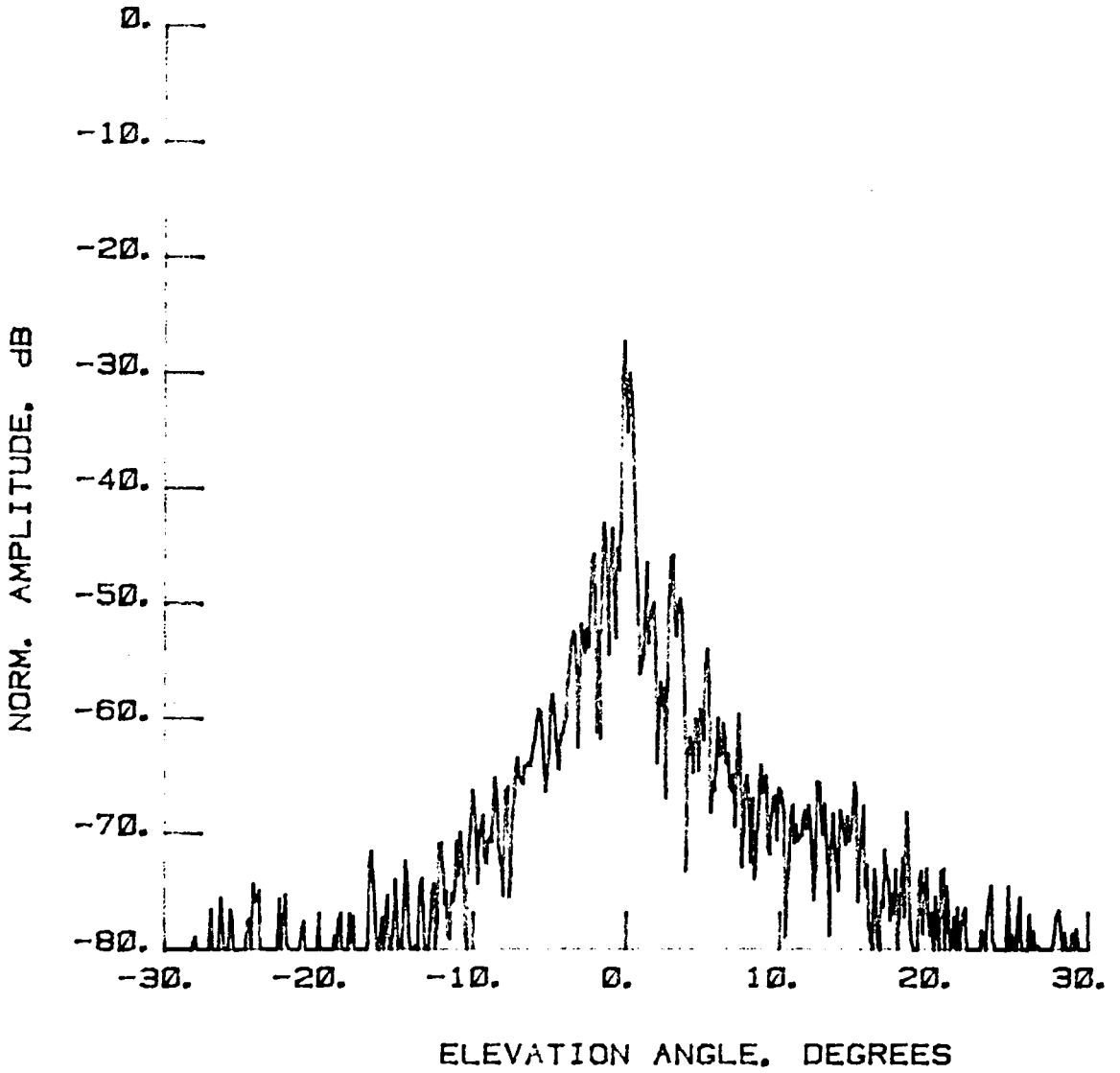

Figure 227 Test 26, 11.60 GHz, Cross-Pol, H-Plane, Type 15

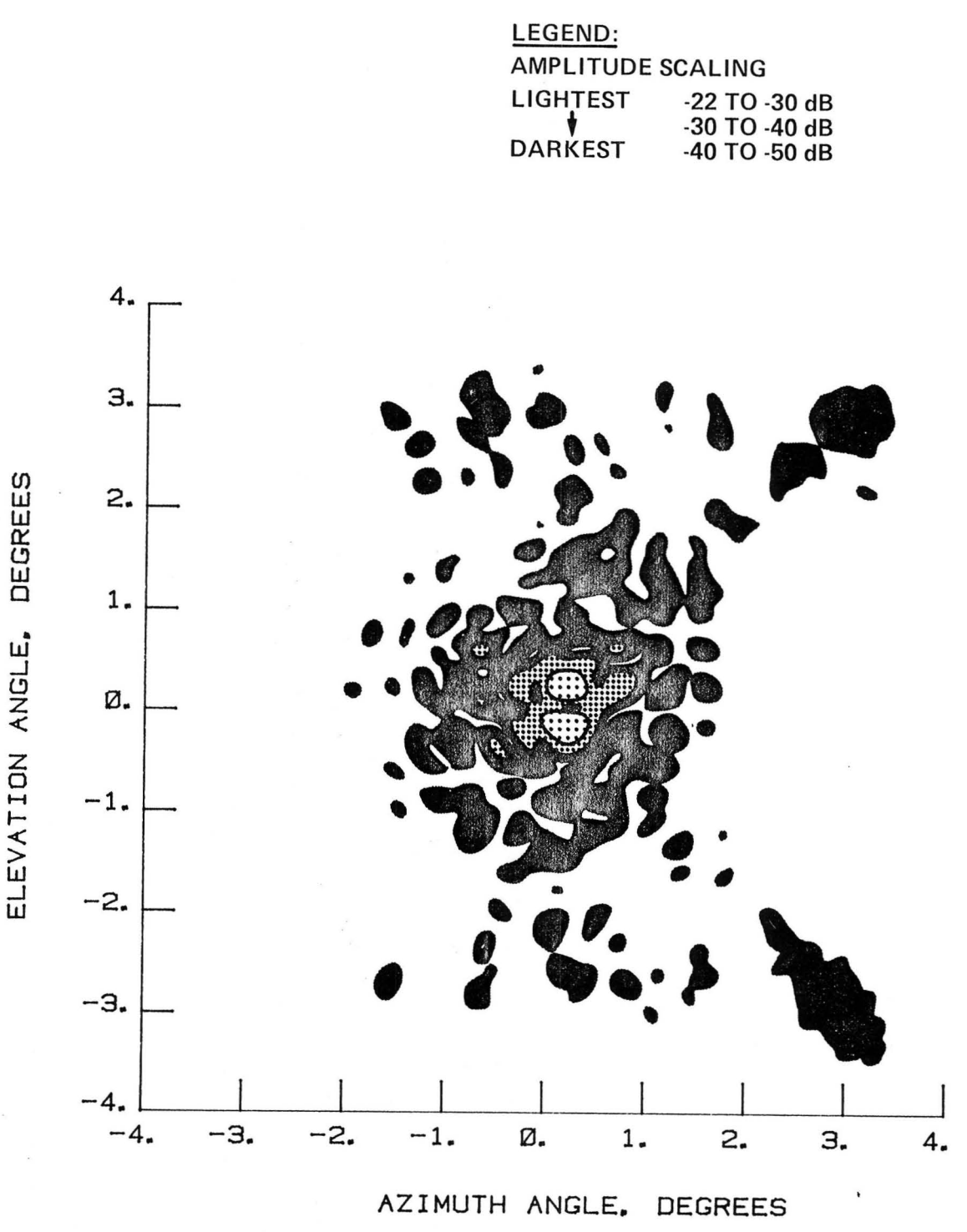

Figure 228 Test 26, 11.60 GHz, Cross-Pol, Contour, Type 16

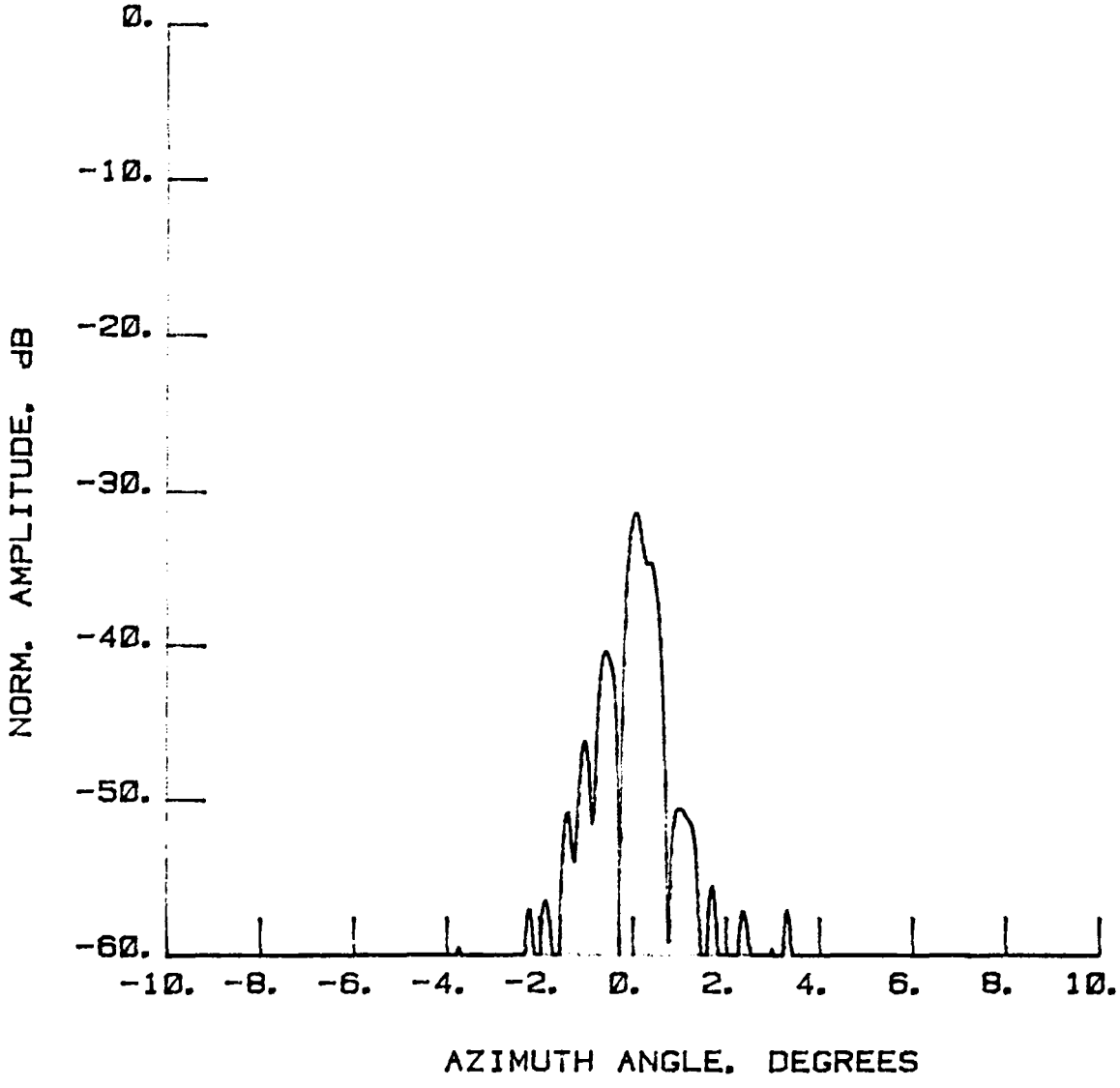

Figure 229

Test 26, 11.60 GHz, Cross-Pol, ±10° Scale, E-Plane of Cross-Pol through Peak Co-Pol (0, 0)

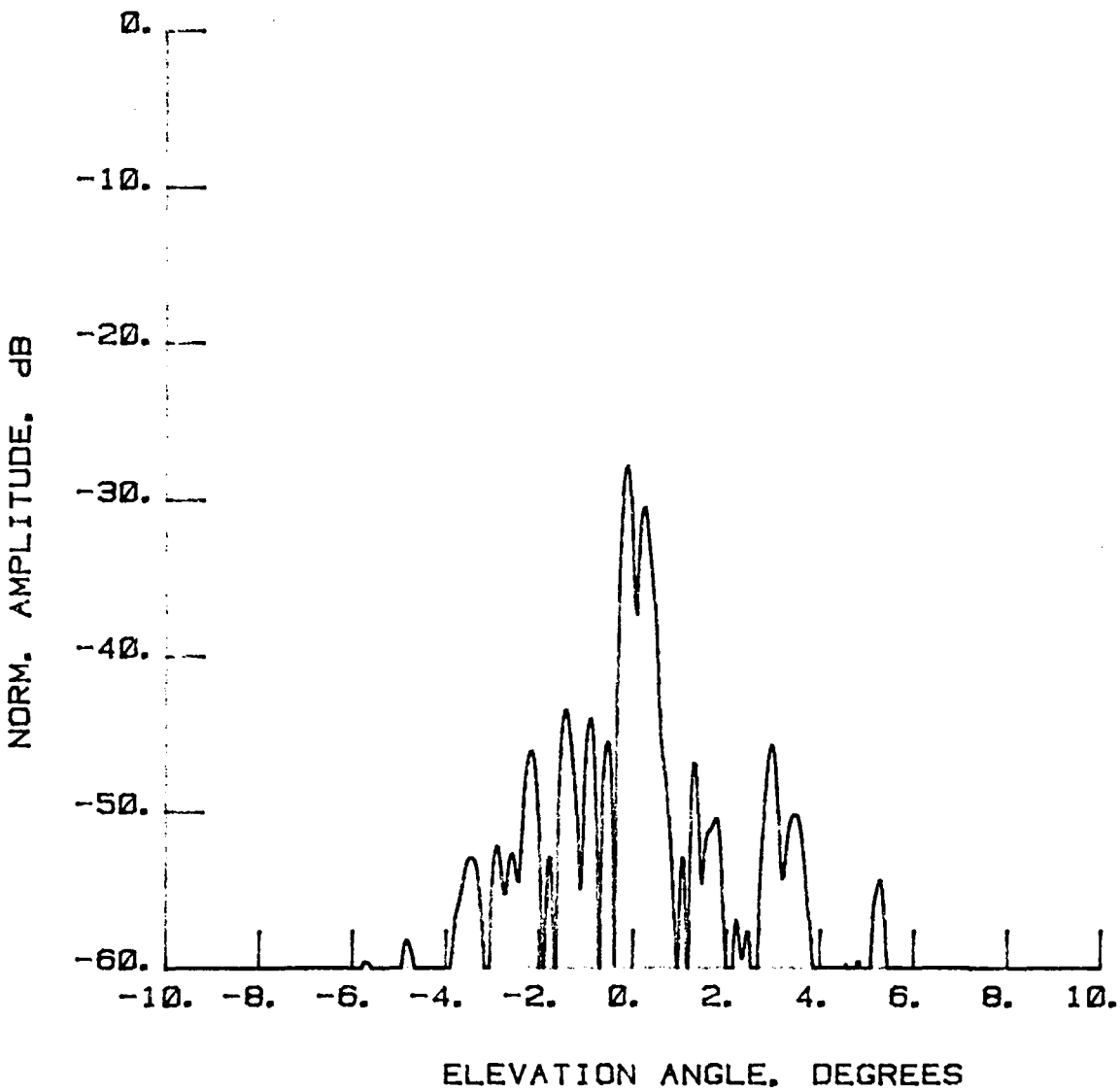

Figure 230

Test 26, 11.60 GHz, Cross-Pol, ±10° Scale, H-Plane of Cross-Pol through Peak Co-Pol (0, 0)

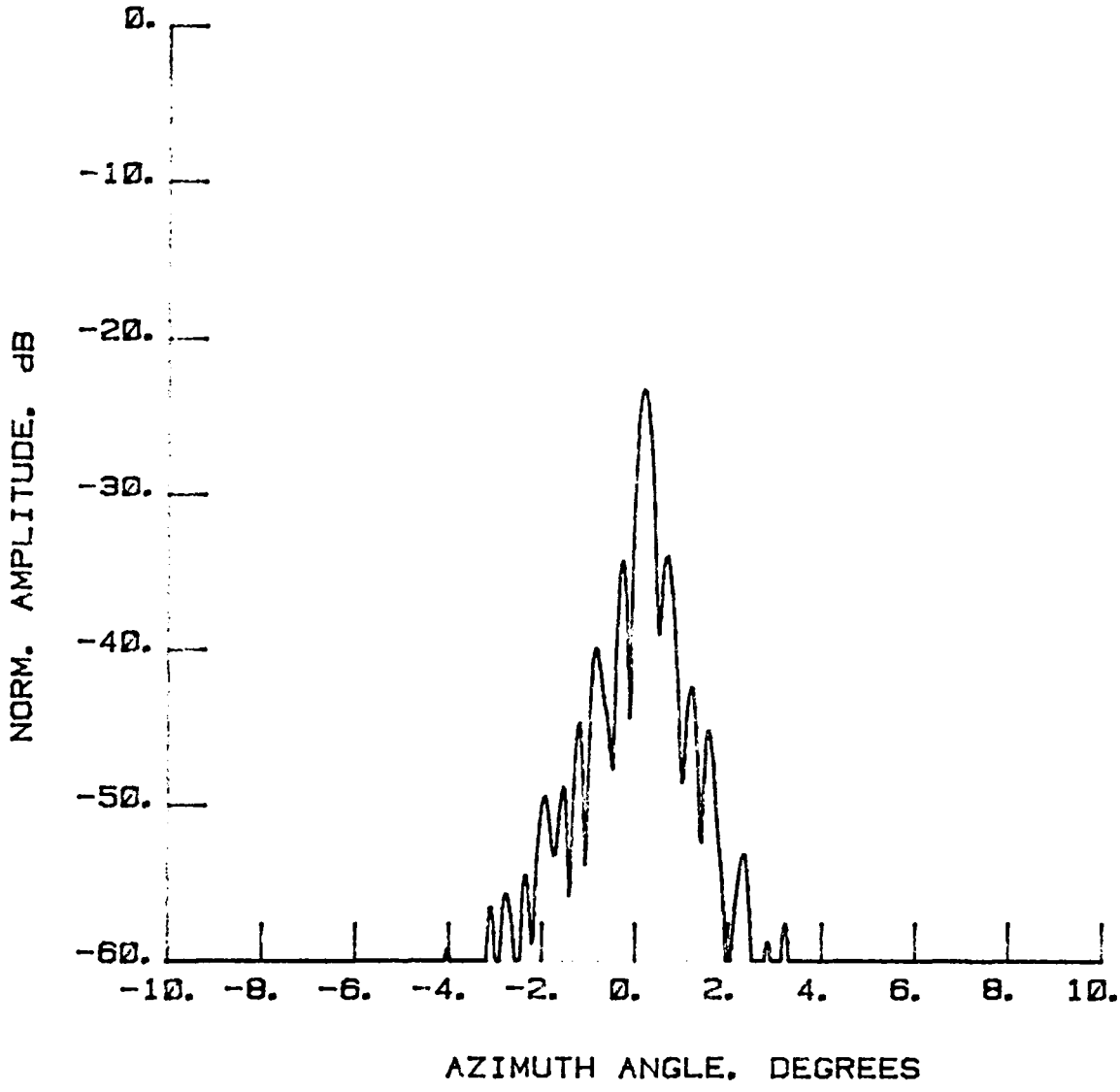

Figure 231

Test 26, 11.60 GHz, Cross-Pol, ±10° Scale, E-Plane of Cross-Pol through Peak Cross-Pol (0.20, 0.22)

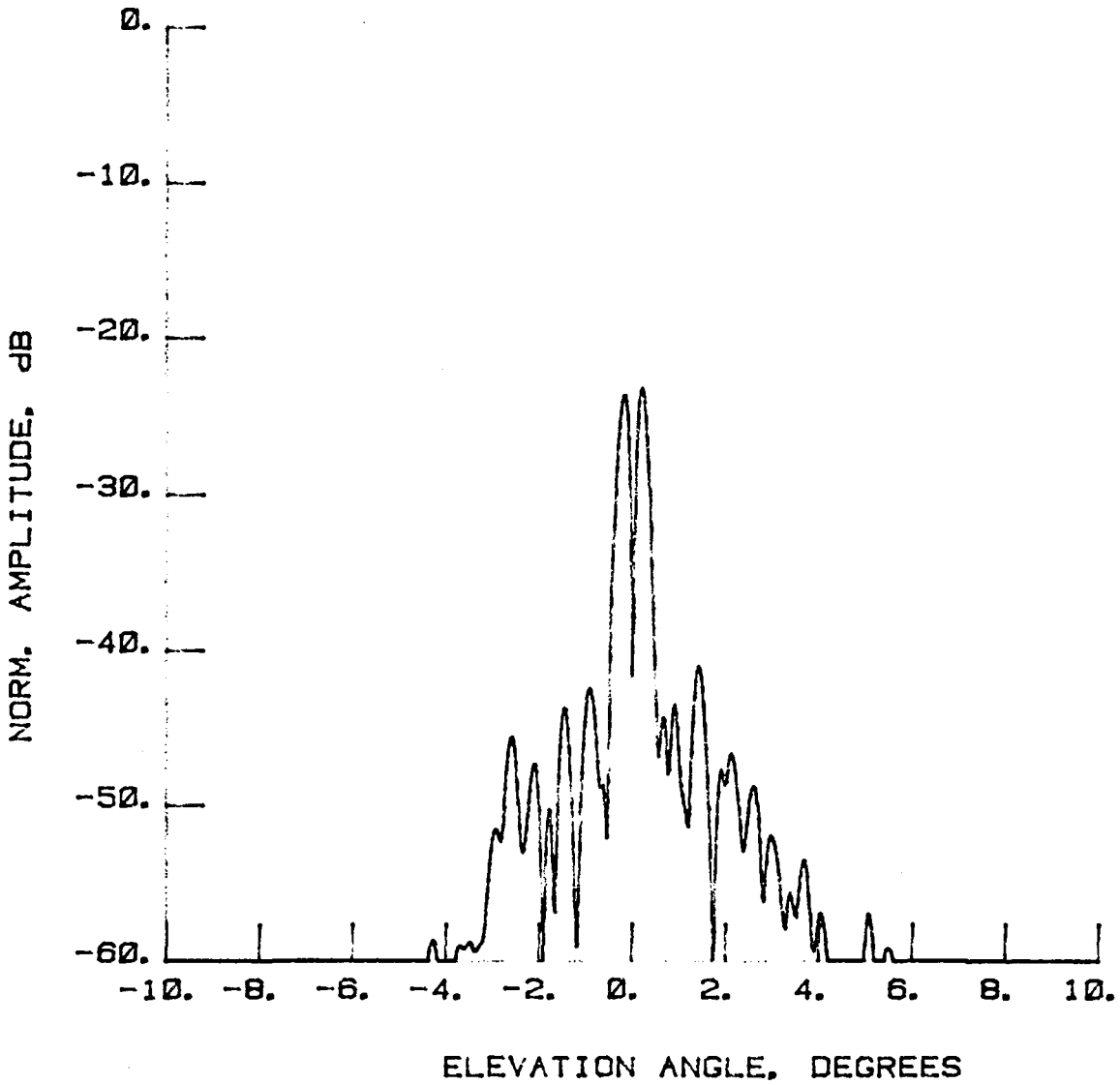

Figure 232

Test 26, 11.60 GHz, Cross-Pol, ±10° Scale, H-Plane of Cross-Pol through Peak Cross-Pol (0.20, 0.22)

This Page Intentionally Left Blank

5.0 ANTENNA GAIN/BEAMWIDTH

For these two measures of antenna performance it is important to realize that the hoop column antenna in this program has been configured for quad aperture operation. The reflecting surface has been contoured to form four focal points in a single structure. During most of the measurements, one quadrant (labeled Quadrant 4) was used extensively; however, all quadrants were tested to some extent.

The gain values listed in this section are the true antenna gain in dBi, not to be confused with or interpreted as directivity. Of the various parameters measured in a near-field system, accurate antenna gain is the most difficult to measure, primarily because of its inherent sensitivity to impedance match and to reflections within the probe circuitry. Because the probe radiation pattern is relatively wide, reflection external to the probe can also produce significant errors. In the measurements that follow, great care has been taken to produce accurate, state-of-the-art results.

Table 5.1 lists the antenna gain and maximum first sidelobe level versus test number for the LaRC tests. The accuracy of the gain measurements throughout the program was consistent with the error analysis in Volume I. The values given for gain are peak values in dBi for both the co- and cross-polarized field components.

In Table 5.2, the gain and beamwidth in the two principal planes has been tabulated for each frequency for the co-polarized field component. The primary error source in beamwidth is the resolution of the far-field data (density of the data points). For this report the error is within $\pm 2\%$ of the true value.

Table 5-1 Antenna Gain and Maximum First Sidelobe Level for Each Test

Test	Frequency, GHz	Gain dBi	Polarization (Co & Cross)	Maximum First Sidelobe Level, dB
1	7.73	50.86	Co	-15.8
2	7.73	26.85	Cross	
3	7.73	51.52	Co	-16.0
4	11.60	53.85	Co	-11.9
5	2.27	39.65	Co	-19.5
6	2.27	15.43	Cross	
7	2.27	39.35	Co	-19.4
12	4.26	45.57	Co	-18.4
13	4.26	45.03	Co	-16.9
14	4.26	44.75	Co	-18.2
15	4.26	45.07	Co	-19.0
16	4.26	44.91	Co	-17.5
17	4.26	44.91	Co	-19.5
18*	7.73		Co	-14.9
19*	7.73		Co	-19.4
21*	7.73		Co	-16.5
22*	7.73		Co	-18.0
24*	7.73		Co	-15.4
25*	11.60		Co	-15.5

*Gain not measured.

Table 5-2 Antenna Gain and Beamwidth for Each Test Frequency

Frequency, GHz	Gain, dBi	E-Plane, °	H-Plane, °
2.27	39.65	1.55	1.30
4.26	45.57	0.78	0.73
7.73	50.86	0.43	0.50
11.60	53.85	0.29	0.35

6.0 SUMMARY AND CONCLUSIONS

The series of tests performed on the HCA is extensive and demonstrates that an extremely high degree of accuracy in the near- and far-field patterns has been achieved in a large scale system. The tests also demonstrate that high performance has been achieved in the HCA. As stated in Volume I, the following conclusions are the most significant:

- Antenna performance is high.
- First sidelobes are dependent on the quality of the reflecting surface. A -18 dB relative to the main beam peak is typical at 7.73 GHz.
- Mechanical oscillations within the hoop column structure appear as errors in the wide-angle, low-level sidelobes and contribute little or no error to the main beam or principal sidelobes.
- Pattern distortion resulting from beam steering is minimal.
- Lobes generated by the parasitic apertures are minimal.
- Cross-polarized far-field radiation occurs at low levels typical of a quality antenna system.

For the measurement system the following conclusions are of importance:

- Accuracy has been achieved over wide dynamic ranges in the far-field in a large scale system.
- Measurement stability/repeatability over extended periods has been achieved.
- Accurate gain measurements have been made.
- Near-field diagnoses have been demonstrated as powerful tools in optimizing antenna performance. The phase maps presented in Volume I using near-field measurements can shape mesh surfaces.

Standard Bibliographic Page

1. Report No.	2. Government Accession No.	3. Recipient's Catalog No.
NASA CR-178060		

4. Title and Subtitle	5. Report Date
Near-Field Testing of the 15-Meter Model of the Hoop-Column Antenna, Volume II - Near- and Far-Field Plots for the LaRC Feeds	March 1986
	6. Performing Organization Code
7. Author(s)	8. Performing Organization Report No.
John Hoover, Neill Kefauver, Tom Cencich, and Jim Osborn	MCR-85-640
9. Performing Organization Name and Address	10. Work Unit No.
Martin Marietta Denver Aerospace P.O. Box 179 Denver, CO 80201	11. Contract or Grant No. NAS1-18016
12. Sponsoring Agency Name and Address	13. Type of Report and Period Covered
National Aeronautics and Space Administration Washington, DC 20546	Contractor Report
	14. Sponsoring Agency Code 506-58-23-01

15. Supplementary Notes

Technical Monitor--Lyle C. Schroeder, NASA Langley Research Center
Hampton, VA 23665-5225

16. Abstract

This report documents the technical results from near-field testing of the 15-meter model of the hoop column antenna at the Martin Marietta Denver Aerospace facility. The antenna consists of a deployable central column and a 15-meter hoop, stiffened by cables into a structure with a high tolerance repeatable surface and offset feed location. The surface has been configured to have four offset parabolic apertures, each about 6 meters in diameter, and is made of gold plated molybdenum wire mesh. Pattern measurements were made with feed systems radiating at frequencies of 7.73, 11.60, 2.27, 2.225, and 4.26 (all in GHz). This report (Volume II) gives the detailed patterns measured with the LaRC feeds (7.73, 11.60, 2.27, and 4.26 GHz). Volume I covers the testing from an overall viewpoint and contains information of generalized interest for testing large antennas, including the deployment of the antenna in the Martin Facility and the measurements to determine mechanical stability and trueness of the reflector surface, the test program outline, and a synopsis of antenna electromagnetic performance. A detailed listing of the antenna patterns are provided for the 2.225 Ghz feed in Volume III of this report.

17. Key Words (Suggested by Authors(s))	18. Distribution Statement
Large space deployable antenna Near field antenna patterns Cable stiffened hoop/column Quad aperture, offset feeds	Unclassified-Unlimited Subject Category 15

19. Security Classif.(of this report)	20. Security Classif.(of this page)	21. No. of Pages	22. Price
Unclassified	Unclassified	281	A13

For sale by the National Technical Information Service, Springfield, Virginia 22161